https://theses.gla.ac.uk/

Theses Digitisation:

https://www.gla.ac.uk/myglasgow/research/enlighten/theses/digitisation/

This is a digitised version of the original print thesis.

Copyright and moral rights for this work are retained by the author

A copy can be downloaded for personal non-commercial research or study, without prior permission or charge

This work cannot be reproduced or quoted extensively from without first obtaining permission in writing from the author

The content must not be changed in any way or sold commercially in any format or medium without the formal permission of the author

When referring to this work, full bibliographic details including the author, title, awarding institution and date of the thesis must be given

Enlighten: Theses
https://theses.gla.ac.uk/
research-enlighten@glasgow.ac.uk

ON THE INTERPRETATION OF POLARIMETRIC OBSERVATIONS OF CLOSE BINARY STARS

by

Colin Aspin B.Sc. M.Sc.

Thesis

submitted to the

University of Glasgow

for the degree of

Ph.D.

Department of Astronomy,
The University,
Glasgow G12 8QQ

March 1981

ProQuest Number: 10800601

All rights reserved

INFORMATION TO ALL USERS
The quality of this reproduction is dependent upon the quality of the copy submitted.

In the unlikely event that the author did not send a complete manuscript
and there are missing pages, these will be noted. Also, if material had to be removed,
a note will indicate the deletion.

ProQuest 10800601

Published by ProQuest LLC (2018). Copyright of the Dissertation is held by the Author.

All rights reserved.
This work is protected against unauthorized copying under Title 17, United States Code
Microform Edition © ProQuest LLC.

ProQuest LLC.
789 East Eisenhower Parkway
P.O. Box 1346
Ann Arbor, MI 48106 – 1346

Thesis
6350
Copy 1

GLASGOW
UNIVERSITY
LIBRARY

to my Mother and Father,
in gratitude for everything.

Preface.

Questions concerning the nature of binary star systems have been asked for many decades. The advent of photoelectric techniques of measuring the amount of light from a particular object enabled a great step to be taken in the understanding of these celestial bodies. Photometry when combined with spectroscopic observations have given an increasing insight into the relationship between the two stellar components and in recent times have made possible the discovery of the interaction of the stars in the form of mass transfer, exchange and accretion, by such phenomena as gas streams, disks and wakes. However many discoveries still await an independent confirmation. The application of other equally sophisticated techniques to the study of binary systems was investigated.

Polarimetric detectors were developed to measure small polarizations of light from single stars, caused by the interstellar medium, to a high accuracy. Eventually these instruments were turned to binary systems in the hope that previously predicted phenomena may be observable and hence contribute to the knowledge of the stellar systems.

It is to the interpretation of the detected polarimetric behaviour in certain binaries that this thesis is directed. The development of a simple, herein called 'canonical', model predicting phase locked variations in the linear polarization of the light from particular close binaries is followed and extended in numerous ways to enable a statistically rigorous

evaluation of the compatibility of the model and observational data. A major contribution to the study of close binaries is that the model described here (developed initially by Brown McLean and Emslie 1978) enables an independent determination of the orbital inclination of the system directly from the observed polarimetric variations. The accuracy of such a determination is investigated fully in the presence of noise on the observations and the predicted inclination is critically compared with those values obtained from photometric and spectroscopic analyses in the light of detailed numerical and analytic testing of the model fit. All data currently available (post 1975) that is of a suitable form (i.e. published fully) is re-analysed using the canonical model and plans for future observing of suitable binaries are related (suitable in the sense of not blatently violating the assumptions of the model a priori).

The work presented here has been carried out in cooperation with Drs. J. C. Brown and J. F. L. Simmons. The relative contribution to the work of each chapter/paper is indicated by the ordering of the authorship on the papers detailed below.

Certain chapters of this thesis have been published (or are in the process of being published), the titles and authorship of which are given below together with the chapter number concerned.

Paper 1 : ' Critique of the Polarimetric Nature of Cygnus X-1' Simmons, Aspin and Brown (1980) (Chapter 2).

Paper 2 : 'Polarimetric Accuracy Required for the Determination of Binary Star Inclinations' Aspin, Simmons and Brown (1981) (Chapter 3)

Paper 3 : 'High Inclination Bias in Polarimetric Binary Diagnostics' Simmons, Aspin and Brown (1981) (Chapter 4) - in press

Paper 4 : 'Reappraisal of the Polarimetric Data for 7 Binaries' Aspin and Simmons (1981) (Chapter 5) - in press

Paper 5 : 'Analysis of Polarimetric Observations of Binaries at Unequal Phase Intervals' Aspin,Simmons and Brown (1981) (Chapter 8 and further work) in preparation.

Paper 6 : 'The Effect of Orbital Eccentricity on Polarimetric Binary Diagnostics' Brown,Aspin,Simmons and McLean (1981) (Chapter 6) - in press

Paper 7 : 'Polarimetric modelling of HD50896' McLean and Aspin (1981) - in preparation.

We conclude this thesis with a summary of future work involving observations and theoretical development of the canonical model and its diagnostic capabilities.

I acknowledge the financial support of the S.R.C. for 2 years of the research project and Mr. and Mrs. R. Aspin for the remaining period.

I wish to extend my thanks to Drs. J.C. Brown and J.F.L.Simmons for their invaluable guidance and assistance during the three years of may research in Glasgow.and for many stimulating and fruitful discussions. I also wish to thank Mrs. L.Williamson for deciphering my scrawl and providing the typed copy of the thesis. I extend my thanks also to Dr.I.W. Walker for many hours of faultless tabulating and together with Mr.H.E.Schwarz and Mr. R.C. Fyvie for making Room 409 a place to remember.....

CONTENTS

ON THE INTERPRETATION OF POLARIMETRIC OBSERVATIONS OF CLOSE BINARY STARS

by

Colin Aspin B.Sc. M.Sc.

Thesis

submitted to the

University of Glasgow

for the degree of

Ph.D.

SUMMARY

Department of Astronomy,
The University,
Glasgow G12 8QQ

March 1981

SUMMARY

Over the last few years the problem of determining orbital and physical parameters of close binaries has become paramount in interpreting the complex nature of these systems. Photometry and spectroscopy have in many cases combined to give reasonably accurate values of such parameters as the binary inclination and orbital eccentricity. In some cases however the two methods have provided conflicting values of the inclination i, for example, and it remains to obtain independent estimates to confirm or not the previous values.

The development of techniques to interpret the variable linear polarization observed in certain binaries has proceeded hand in hand with the improvement of observational techniques and the continuing discovery of new 'polarimetric binaries'. A relatively simple model was presented by Brown,McLean and Emslie (1978) whereby the variation inpolarization of the light from binaries is caused by the orbital motion of a scattering region situated within the system and corotating with it. This scattering region is assumed optically thin and under the corotation assumption to be in a circular orbit about the primary star. The behaviour of the polarization is phase locked to the orbital period of the system and variation occurs , in the general case at both the first and second harmonic of that period (i.e. at the period itself and half that period). If the scattering region is of a form symmetric about the orbital plane of the system then the polarization has a second harmonic structure only (i.e. it varies a half the binary period) and produces a double looped ellipse figure in the Q,U plane.

In this thesis we extend this simple, and hence 'canonical' model to enable an optimum set of the model parameters to be

obtained in the presence of noisy data. The optimum inclination i_{opt} is found when the χ^2 statistic is minimized and an error or uncertainty in this value is estimated by forming a Relative Confidence Interval at a particular (i.e. chosen) significance level. This model optimization technique is then applied to Cygnus X-1 data with the result that the uncertainty in i_{opt} is significantly larger than previous estimates. (cf. Chapter 2)

A thorough statistical and numerical analysis of the determination of inclinations by this method is undertaken in Chapter 3 and Chapter 4 where we establish the severe nature of the bias of the inclination estimator in the canonical model and show that a high degree of accuracy is needed in polarimetric measurements before reasonable (i.e. $\pm 5^{\circ}$) Confidence Intervals on i are established.

In Chapter 5 we reanalyse the available data for seven binaries (Algol, AO Cas, HD47129, Ori E (B and U filter data), u Her, U Sge and V444 Cygni) and show that the previous confidence in the values of the inclination i estimated from such analyses was misleading and that by the optimization technique of Chapter 2 a wide range of inclinations would equally well fit the data at the significance level chosen (10% sig.). We also discuss in this Chapter the determination of other parameters from polarimetric observations (namely the number of scatterers inthe scattering region, the scatterer (i.e. electron) density and in the case of systems with gas streams the mass transfer rate between the two stars).

Chapters 6and 7 deal with the generalization of the model to take into account the effect of orbital eccentricity of the scattering region and a calculation of the expected polarization from an accretion disk ar wake respectively.

Chapter 8 again generalizes the canonical model ,this time to

enable analysis of data taken at uneqiual phase intervals. In the previous optimization of Chapter 2 the model was developed to produce best fit values of the free parameters from equally spaced observations. This new general analysis now allows the analysis of sections of data, not covering the complete phase range. This would allow treatment of perhaps out-of-eclipse data only for eclipsing binaries or a sequentaal analysis of data sectioned into small groups froma complete data set and hence giving a more flexible range of possible ways of treating the data.

This new optimization technique is applied to the data mentioned above in three different ways (i.e. all the data, out-of-eclipse data and sectioned data) in Chapter 9. Chapter 10 consists of the application of the various optimization techniques outlined in the previous Chapters to the B,U and G filter of HD50896 provided by McLean (1980).

Throughout this thesis we have frequently noted that the analyses and techniques developed herein will only be fully testable when new data taken in the way outlined in Chapter 8, has been acquired. The data used in the Chapters mentioned above are from binary systems that do not correspond entirely to the type we would generally expect to analyse with the canonical model. New data of such systems would prove the ultimate test for the procedures related in this thesis.

Polarimetric Definitions

Summarized here for convenience are the definitions units and notation required for the description of the linear polarization state of light.

Consider the output signal from a polarimeter. This would consist of a sinusoid with maximum and minimum intensity over the variation of I_{max} and I_{min} respectively. The total change in intensity $dI = I_{max} - I_{min}$ and is equal to I_p the intensity of the polarized component of the electro-magnetic radiation detected. If we take I_u as the intensity of the unpolarized component of the radiation so that $I_{tot} = I_u + I_p$, where I_{tot} is the total intensity then the degree of polarization of the light is p and equals :

$$p = \frac{I_p}{I_p + I_u} = \frac{(p_x^2 + p_y^2)^{\frac{1}{2}}}{I_{tot}}$$

also

$$p = \frac{I_{max} - I_{min}}{I_{max} + I_{min}}$$

where p_x and p_y are the unormalized Stokes parameters describing the linear polarization.

The quantities Q and U are here defined as the normalized Stokes parameters i.e. $Q = p_x/I_{tot}$ and $U = p_y/I_{tot}$.

The polarization state of light is generally described by the quantities Q,U or p,θ where θ is the position angle of the polarization in the equatorial coordinate system . $\theta = 0^o$ implies a preferential direction of the E vector North or South and $\theta = 45^o$ implies a preferential direction NE or SW etc.).

We also have the relation:

$$Q = p\cos 2\theta$$

and $$U = p\sin 2\theta$$

to relate the two sets of quantities.
p is often called the degree of polarization with the percentage polarization being signified by $P = p.100\ \%$. p is generally in units of magnitude. Hence, for example, if $p = .0001$ mag. as is reasonable for close binaries then $P = .01\%$.

We generally refer to (Q,U) as the normalized Stokes parameters describing the polarzation state throughout this thesis.

1. POLARIMETRIC OBSERVATIONS OF BINARIES AND THEIR INTERPRETATION

1.1 Introduction

Investigation of the nature of close binary systems has traditionally taken the form of spectroscopic and photometric observations over long intervals of time (i.e. many orbital cycles). This has led to the estimation of certain binary parameters (within the limits of the model used) to a high degree of accuracy (i.e. photometry light curves have indicated $i = 83^{\circ} \pm 2^{\circ}$ for Algol (Soderhjelm 1980)). The values of these parameters, which include the stellar masses, and relative luminosities, the separation of the stars, and their orbital period and inclination, are however sometimes controversial. It is then desirable to obtain an independant evaluation of the parameters concerned to either confirm or disprove the previous results. In the case of eclipsing binaries, the margin of error in model parameters is narrowed by the physical presence of the eclipse for not only does the inclination i have to be greater than a certain minimum value to obtain an eclipse but the eclipse provides us with a scan across the stellar disk. Even in this case however there may be significant uncertainty in estimating i or parameters dependant on it (Budding 1980). The masses of the binary components, for example, are generally obtained from spectroscopy. The radial velocity curves for the system are used to give a value to the mass function (Batten 1973) defined by $f(m_1,m_2,i) = m_2^3 \sin^3 i/(m_1+m_2)^2$. Consequently the masses deduced are severely dependent on the value adopted for i. In Figure (1.1) this dependence is illustrated for the X-ray binary system Cygnus X-1. We plot the primary component mass (m_1) versus the secondary mass (m_2) for four different inclinations at constant f(m) using Bolton's (1972) value of the mass function, namely $f(m) = 0.18$.

One can see immediately that for any assumed value of m_1 the range of possible m_2 values is large. If we take $m_1 \approx 20\ m_{\odot}$ as normal for the observed 09·7 Iab spectral type then m_2 can take any mass in the range $5\ m_{\odot} \gtrsim m_2 \gtrsim 15\ m_{\odot}$ for inclinations $30^{\circ} \gtrsim i \gtrsim 70^{\circ}$ making further discussion of its nature (i.e. black hole or neutron star) inconclusive. The transition from a neutron star to a black hole secondary is an ill-defined concept. Various estimates of the maximum

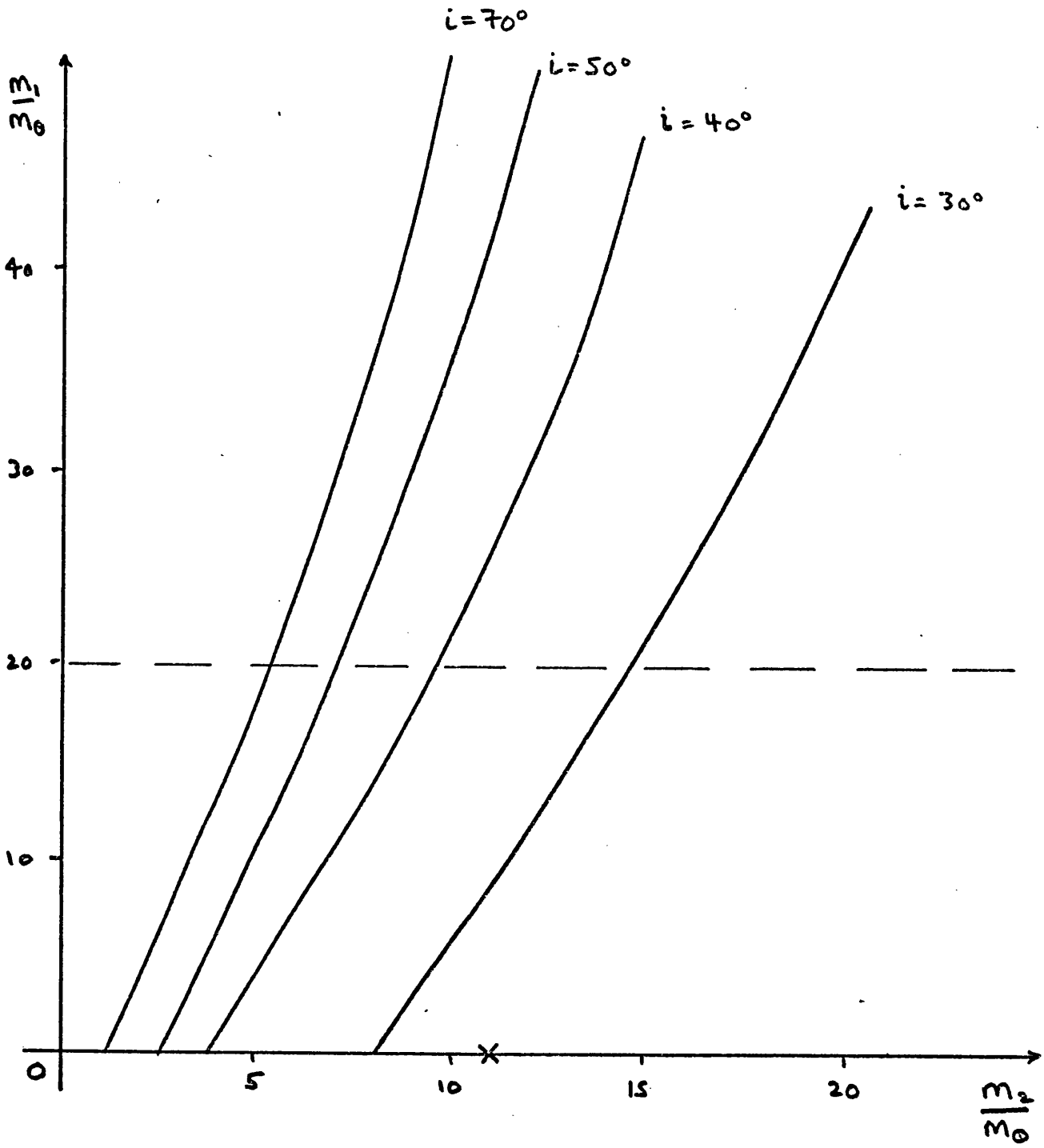

Figure 1.1 - Graph of the variation of the mass of the secondary star in Cygnus X-1 with that of the primary component for a Mass function of 0.18 (Bolton 1972). The X on the abscissa marks the maximum mass of a neutron star with rapid rotation and an arbitrary equation of state (Hegyi 1977). If one assumes $m_1 = 20\ M_\odot$ (dashed line) then the range of possible m_2 values when inclinations 70° to 30° are considered is from A($5M_\odot$) to B($15M_\odot$).

mass of a neutron star have been proposed($m_{max} \sim 0.7\ m_\odot$ - Opperheim and Volkoff (1939); $m_{max} \sim 1.86\ m_\odot$ - Bethe and Johnson (1959); $m_{max} \sim 2.7\ m_\odot$ - Pandharipande, Pines and Smith (1976)) and to some extent depend on the equation of state assumed for the neutron star. An arbitrary equation of state, with rapid rotation of the object, is seen to give an upper limit of this mass $m_{max} \sim 12\ m_\odot$ (Hegyi 1977) although this is by no means certain. It is sometimes possible to rule out certain ranges of inclination by the presence or absence of eclipses. Cygnus X-1 does not show eclipse behaviour in either its optical or X-ray light curve, the former of which is dominated by ellipsoidal variations (Cherepashchuk et al., 1972, Walker 1972, Lester et al., 1973). (Second order light variations (Hutchings 1974) are caused by a slight eccentricity of the orbit of the system). Depending on the radius one assumes for the optical star a limit on i can be obtained above which eclipses would occur. Bolton (1975) has found this to be $i \sim 60^\circ$ using the light curve synthesis program of Wilson and Devinney (1971). This value still leaves, however, a large range of possible inclinations, even assuming that the radius value and secondary mass value used in the estimation are correct. The maximum value of Bolton (1975) is much higher than the reported 'best fit' value from light curve analyses of Hutchings (1974b) which indicates $i = 30^\circ \pm 2^\circ$. This latter value assumes, however, that the primary star fills its Roche lobe which may not be the case. A method of obtaining i, and other binary parameters, without assuming parameter values such as the stellar radii, mass etc. would allow additional light to be shed on the problem. An independent method for close binary diagnostics was proposed by Brown, McLean and Emslie (1978). The method involves the modelling of polarimetric variation observed in the light of certain binary systems. A restricted formulation of this idea has also presented, independently, by Rudy and Kemp (1978). This idea of studying binaries polarimetrically is not new and dates back to Shakhovskoi (1968) who observed β Lyrae polarimetrically (cf. Section 1.2). The possibility of determining binary inclinations from these observations has however, only recently been developed in the above two papers. A check on the values of i by a method independent of photometry /spectroscopy would be

invaluable in confirming (or otherwise) the other determinations and could add substantial weight to both the above alternative methods. The purpose of this introduction is to summarize the observations and theories of polarimetric variability relating to the production of such phenomena leading up to the two papers mentioned above, as well as later observations and theories included for comparisons.

Only in the last decade has the use of polarimetry been widely accepted as a powerful additional diagnostic technique in certain astrophysical fields. The first broad band polarimetric measurements of stellar objects occurred in the late 1940's. Hall (1949) and Hiltner (1949) discovered that many stars showed strong polarization which was concluded as due to the polarizing effect of the interstellar medium. The mechanism responsible for the polarization is now thought to be scattering of starlight on aligned dust/gas particles, with the aligning mechanism being associated with the interstellar (galactic) magnetic field. In a subsequent study of this by Gehrels (1960) the wavelength dependence of the interstellar polarization was discussed and more recently, Kemp (1972) and Martin, Illing and Angel (1972) observed for the first time the circular polarization effects of the interstellar medium. The polarization was assumed interstellar in origin because (a) it was seen to be independent of the physical properties of the stellar objects observed and (b) there was a correlation between interstellar absorption lines and bands in spectra with the amount of polarization (Serkowski 1961). The polarization was seen to be larger for more distant stars in low galactic latitudes (more interstellar medium between us and the star).

The idea that binary systems may intrinsically polarize their own radiation was first considered in 1934. In a paper in Nature by Öhman (1934) the possibility of intrinsic polarization manifesting itself in the profiles of particular spectral lines was proposed. Observations of β Lyrae were presented consisting of spectra taken in polarized light. β Lyrae became the centre of much research in years to come. We now consider β Lyrae in detail as an example of earlier observational work and modelling techniques.

1.2 β Lyrae

Öhman's suggestion that intrinsic polarization effects may be evident in spectral line profiles was based on early work (Öhman 1929). He there considered possible objects that might show polarization of fluorescence radiation. A mechanism that could be responsible for the polarization effects in the lines was proposed by Wood et al (1928). In that paper they discussed the nature of the production of polarized light by fluorescence or resonance. The latter of these, resonance radiation is the result of natural spontaneous radiative decay (i.e. without outside stimulus: collisions or further photon absorption) from an excited state to a lower energy level. The resulting photon of emission due to the transition is of the same wavelength as the originally absorbed photon but it is not simply reradiated in the direction of incidence. The process is that of scattering of light by the atom and has a polarizing effect on the emitted radiation. Fluorescence is slightly different with the excited atom being excited to a yet higher state, before eventually returning to its original configuration. Öhman suggested that fluorescence (or resonance) should cause polarization effects in spectral lines ($H\gamma$ and D_2 - sodium) of certain astronomical objects such as stars with non-spherical shape, such that polarization from different parts of the object do not cancel. This would be the case for a spherically shaped object since no prefered plane of polarization would exist. Lyot (1934) observed this effect in solar prominences. Experiments by Öhman (1929) indicated that if hydrogen or sodium were excited by plane polarized light and observed perpendicular to the electric vector of this incident radiation the resultant $H\gamma$ (or Sodium D_2) fluorescence would have a polarization of $\sim$ 90% (16% for D_2). Heisenberg (1925) had shown theoretically that the Zeeman effect predicted a similar polarizing effect but with $\sim$ 100% polarization for $H\gamma$ and 60% for D_2 sodium. Since $H\gamma$ line produced reasonable agreement between Öhman's earlier measurements (Öhman 1929) and theory it was used by Öhman in his observations of β Lyrae. He took 117 spectrograms over 118 nights on the 40 inch reflector of the Stockholm observatory. Spectra were taken with different slit orientations (corresponding to different polarimetric analyser positions w.r.t. the incident light). The

precise instrumental arrangement is described in Öhman (1928). Using 3 dispersions (9, 23, 27 Å/mm at Hγ - the dispersion depending on the wavelength considered) and scanning the resultant spectra with a self-recording micro photometer he found the faint polarization effect of the fluorescence radiation in Hγ with no clear effect in other lines. The line profiles were seen to be deeper and broader on the violet side of the line for some images (those corresponding to particular slit positions - unstated). No polarization effects were observed near minimum light (phase - 0.0) but effects were seen during nearly all other phases including secondary eclipse (phase - 0.5). Both the plane and degree of polarization were found to vary over phase with a period of $\sim$ 103 days. This period however was not established over a long enough timescale to make its presence undeniable. The polarization effects were concluded as arising from the B9 star (primary) but the origin of the oscillatory polarization effect in the absorption line was undetermined. The next reported polarimetric observations of β Lyrae appeared some 28 years later. Shakhovskoi (1962) then presented observations taken on the 40 cm double astrograph (plate observations) of the Crimean Astrophysical Observatory. With 90 observations covering some 40 nights he found that the polarization (before subtraction of the interstellar component) was dependent on the phase of the binary. The observations, made with no filter and therefore covering a broad band of plate sensitivity, were seen to be approximately repeatable in later spectrophotometrically established orbital cycles. The procedure of establishing the 'real' variability and removing random observational errors and fluctuations was to calculate a mean curve over the whole observing period. This, in effect, is folding and binning the observations on an a priori established period,(a technique we will frequently encounter in this thesis). Each mean point was formed from observations whose phase was less than 0·032 apart. The observed Stokes parameters (Q,U) were averaged forming the mean value for each bin $(\bar{Q},\bar{U})$. From these the degree of polarization $\bar{p}$ and the position angle of the preferential plane of variation of the electric vector $\bar{\theta}$ measured relative to the instrumental reference system, were calculated using the relations:

$$\bar{p} = (\bar{Q}^2 + \bar{U}^2)^{\frac{1}{2}} \quad \text{and} \quad \bar{\theta} = \tfrac{1}{2} \tan^{-1} \left(\frac{\bar{U}}{\bar{Q}}\right)$$

Both $\bar{Q}$ and $\bar{U}$ are normalized separately.

The binary elements used for the phase reduction were those of Nekrasova and Polosukhina (1960) i.e. JD 2436406·409 + $12^{d}.94251E$. The residuals between $(\bar{Q}, \bar{U})$ and (Q,U) for each bin were used to calculate the observational error σ , defined as

$$\sigma^2 = \frac{1}{N} \sum_{i=0}^{N-1} \frac{1}{(2n-1)} \sum_{j=0}^{n-1} (Q_j - \bar{Q}_i)^2 + (U_j - \bar{U}_i)^2 \qquad (1.1)$$

where N = the number of mean points (bins)
and n = the number of observations per bin.
and for the observations presented took the value $\sim 0.16\%$.
This value was compared to similar qualities calculated from observations of standard polarimetric stars (Shakhovskoi and Dimov 1962) and it was concluded that most of the difference between individual observations and mean points was due to observational error indicating that the mean curves were acceptable. The resultant $\bar{p}$ and $\bar{\theta}$ variations with phase Φ and light curve variations are shown in Figure (1.2). Shakhovskoi's (1962) interpretation of the observations was that the polarization observed was a combination of interstellar (time independent) and intrinsic from the binary. This latter component varied in both magnitude and direction with orbital phase and was interpreted as probably being caused by scattering on gaseous material in the system. The interstellar polarization was found to be $p_I \sim 0{\cdot}7\%$ and $\theta_I \sim 158^{\circ}$ which did not contradict Hall's (1958) values for that region of sky. Besides investigating scattering in gaseous material as a mechanism for the variability Shakhovskoi also considered other processes producing asymmetric geometries e.g. photospheric scattering, with the integrated light of the system showing a variable polarized component at times of eclipse, and scattering of light in a 'hotspot' heated by reflection of radiation from the hotter star by the cooler star envelope (The so called 'reflection effect'). Both mechanisms were ruled out as contributions to the intrinsic polarization by observational evidence namely the variable polarization outside eclipse and the sharp fluctuations seen at phases $\Phi \sim 0{\cdot}4$ and $0{\cdot}9$. These two mechanisms mentioned above will be dealt with in Chapter 1.6. Shakhovskoi noted that possible minor fluctuations ($\sim 0{\cdot}1\%$) may well be contributions from either (or both) of these effects.

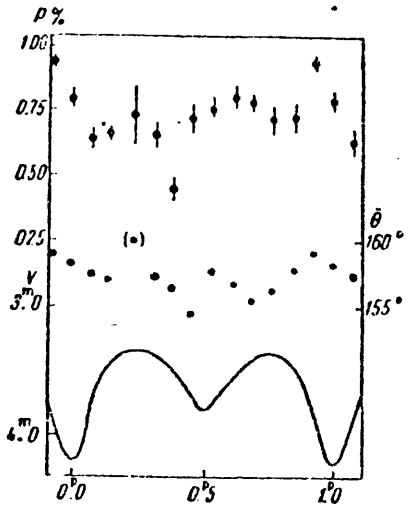

Figure 1.2 - Binned (mean)curves of linear polarization and position angle vs phase and total light variations for β Lyrae (after Shakhovskoi 1962)

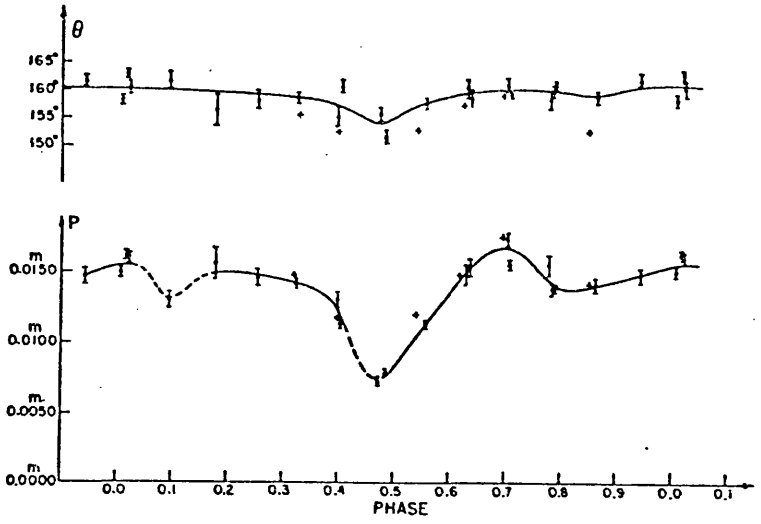

Figure 1.3 - Polarization and position angle variations in the V band for β Lyrae (after Appenzeller 1965)

The conclusion that gaseous material present in the system may be the main cause of intrinsic polarization was supported by earlier evidence (Struve and Wade 1960). Features in the helium emission line profiles had been observed at various phases and Shakhovskoi concluded that they originated in a gas stream/envelope in the binary. This material would scatter light and polarization variations would be visible in the integrated radiation of the system. The variations would depend on phase i.e. the aspect of the scatterers as seen from Earth and would also vary due to eclipses/occultations of light or scattering region. The main features of Shakhovskoi's observations, namely the sharp fluctuations near phase 0.4 and 0.9, were explained as due to irregular condensations inside the gaseous envelope becoming visible at these phases. Also an estimate of the mass in these condensations was made as follows. If one assumes the maximum polarization occurs when the average scattering angle is 90^{o} (and hence the scattered light is fully polarized) the ratio of fluxes of direct light (F_D) to scattered light (F_s) is, from observations:- $\sim$ 400 ($p = F_s/F_D$) F_s and F_D can be expressed as:

$$F_s \sim \alpha N_e \sigma \omega I$$
$$F_D \sim 4\pi R_*^2 I$$

where α = factor including the polarization scattering matrix, (cf. Van der Hulst 1957)

σ = electron scattering cross section

ω = dilution factor

and I = the star surface brightness (hottest)

then, N_e, the number of electrons scattering is just

$$N_e \sim \frac{4\pi R_*^2 P}{\alpha \sigma \omega}$$

with $\sigma = 0{\cdot}67.10^{-24}$ cm^2, $\alpha \sim 0{\cdot}42$ and $\omega \sim 0{\cdot}05$ (Struve 1941) and R_* determined from Boyarchuk (1959) and Abt et al (1962) of $\sim$ 16·6 $R_\odot$ then

$$N_e \sim 3.10^{48} \text{ electrons.}$$

For pure hydrogen $M_{cond} \sim N_e M_p$ where m_p is the mass of the proton. This gives $M_{cond} \sim 2{\cdot}5 \times 10^{29} M_\odot$. This was the first estimate of the amount of gaseous material scattering the light of the star to be made from polarimetric observations. This point will be reconsidered later (Chapter 5) in the light of recent theoretical developments. This stage may be regarded as the 'real' beginning of polarimetric observations of binary systems and only the start of polarimetric observations of β Lyrae itself.

A more detailed discussion of the results of Shakhovskoi, was given in Shakhovskoi (1965) together with observations of other binaries (dealt with in Section 1.3). In this paper he repeated the reduction of his earlier observations using an improved epoch i.e. JD 2437517·403 + $12^d{\cdot}93078E$ (Wood and Forbes 1963). This resulted in a phase shift of ∿ 0·08 relative to his previous observations. A new σ was calculated by means of (1.1) and was found to be smaller at ∿ 0.1%. This was entirely compatible with just observational error. A more detailed discussion of the feature of the polarization light curves was given. The sharp rise in the degree of polarization during primary minimum ($\Phi \sim 0{\cdot}0$) was explained as being due to the increase of the ratio of scattered light to direct light caused by the eclipse. The reduction in polarization at $\Phi \sim 0{\cdot}45$ was similarly explained as an eclipse of the densest point of the scattering region. A new envelope mass was derived under certain assumptions pertaining to the chemical composition of the envelope. Boyarchuk (1959) had assumed an overabundance of He in the atmosphere of the B9 star of $N_{He}/N_H \sim 0{\cdot}425$ compared to ∿ 0·17 for normal stars. Using this ratio a new mass of the envelope of $M_{env} \sim 1{\cdot}25\ 10^{17} M_\odot$ was obtained. Struve's (1958) determination from spectroscopic evidence, however, indicated an envelope mass ∿ 25 x higher than this, although Struve himself thought his estimate was on the high side.

In the same year as the above paper the first independent polarimetric observation of β Lyrae were published by Appenzeller (1965). These were made on the 14" refractor at Gottingen and the 24" rotatable telescope at Yerkes Observatory in 1963-64. Using Hiltner's polarimeter with 20 second integrations, measurements of β Lyrae's polarization were made in the V filter band (Johnson and Morgan 1951) centred on λ 5550 Å. The variability observed by

Shakhovskoi in the polarization was detected and is shown in Figure 1.3 as published by Appenzeller (1965). Three observations in the U filter (λ 3500 Å) were also taken with the polarization being smaller than in the V band at similar phases. The results are seen to be comparable to Shakhovskoi (1962) when the above phase shift is taken into account. A scattering polarization production mechanism (not named) was invoked to account for the observations. The main feature of the polarization curve was the sharp drop in polarization at secondary eclipse, $\Phi \sim 0{\cdot}5$. Also in that year Serkowski (1965) published his polarimetric observations of β Lyrae. He plotted Shakhovskoi's (1962) results, those of Appenzeller (1968) and his own together in a composite diagram (Figure 1.4). This shows that the Stokes parameters (Q,U) or (P_x, P_y) reach a maximum value of $\sim 0{\cdot}015$ magnitudes during primary eclipse ($\Phi \sim 0{\cdot}0$) with a less pronounced minimum at $\sim 0{\cdot}006$ mag. at secondary eclipse ($\Phi \sim 0{\cdot}5$). Secondary maxima in polarization were seen to occur at phases $\sim 0{\cdot}3$ and $0{\cdot}7$ with corresponding minima at $\sim 0{\cdot}15$ and $0{\cdot}85$. An interstellar polarization of $p \sim 0{\cdot}0045$ mag and $\theta \sim 174^{\circ}$ were found which together with the intrinsic variable component made up to observed polarization structure. An important fact seen in Figure 1.4 is that the basic structure of the polarization variations seemed to agree in all three independent sets of observations. This reinforced the belief that the polarization changes were in fact intrinsic to the star and not of an instrumental nature. Serkowski's instrument was that of Chojnacki and Serkowski (1965). Rucinski (1968) published similar results to the previous three reported. An investigation of the wavelength dependence of the polarization variations was initiated by Appenzeller and Hiltner (1967). Figure (1.5) shows the resulting intrinsic polarization curves in three colours U, B, and V. The change in characteristics of the polarization was found to be small although the amount of intrinsic polarization was largest in the blue (B), approximately 10% smaller in the visible (V) and $\sim$ half the size in the ultraviolet (U). Only during secondary eclipse were significant changes in position angle θ found. The interpretation of the results took a form similar to previous explanations in that scattering on gaseous material in the system was invoked. In this case however a disklike secondary and gas envelope were considered as the

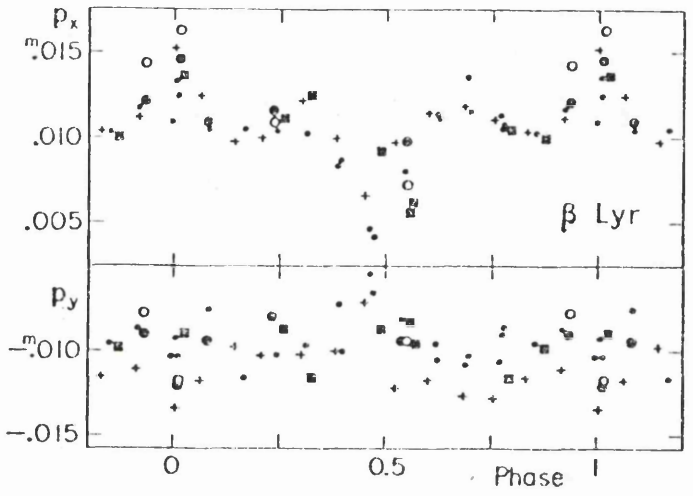

Figure 1.4 - Composite diagram of the variation of the Stokes parameters (Q,U) or (P_x, P_y) vs. phase for β Lyrae. The data of Shakhovskoi (1962) Appenzeller (1965) and Serkowski (1965) are shown.

Shakhovskoi - without filter - crosses
Appenzeller - V filter - small dots
Serkowski - without filter - squares
" - V band - filled circles
" - U band - open circles

(After Serkowski 1965)

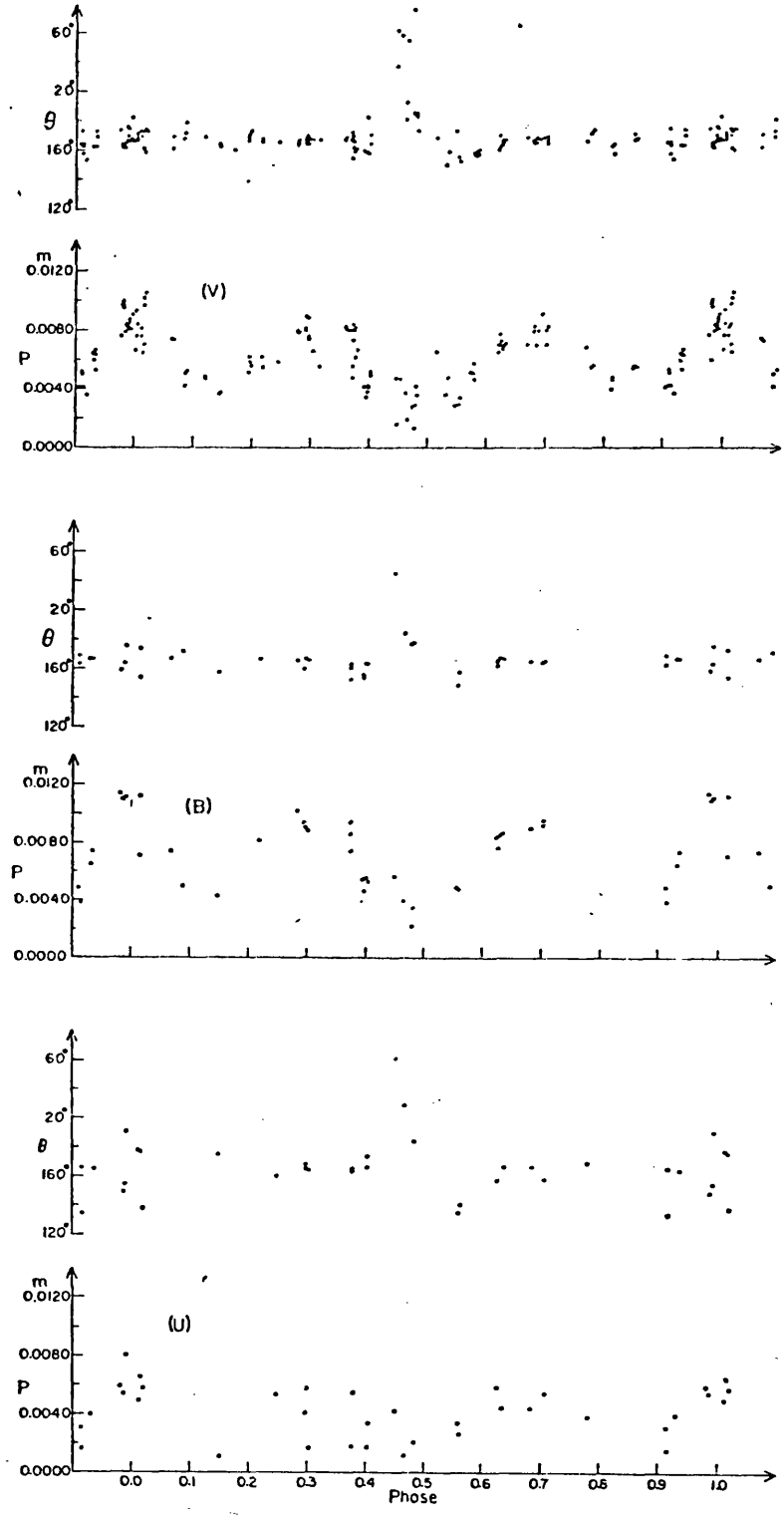

Figure 1.5 - The intrinsic polarization/position angle variations in three colours (U, B and V) of β Lyrae

(After Appenzeller and Hiltner 1967)

source of polarization. The smaller U band polarization was explained as due to higher absorption in the envelope at these wavelengths. The maximum polarization (at phases $\Phi \sim 0{\cdot}3$ and $0{\cdot}7$) was considered as due to an optimum 'average' scattering angle over the disk and envelope at these phases. Rucinski (1966) pointed out however that a more spherically condensed envelope could produce similar polarization structure if an orbital inclination of $\sim 75^{\circ}$ was present. The maximum polarization at $\Phi \sim 0{\cdot}0$ was again explained as due to the decrease in direct intensity due to the eclipse and hence an increase in the degrees of polarization. The absence of major changes of position angle θ outside eclipse was considered to rule out significant deviations from an orbital inclination of $i \sim 90^{\circ}$.

Coyne (1970 a,b) observed the multi-colour structure of the polarization curves. In Figure 1.6 his variation of the percentage polarization and intensity with wavelength are shown. The interpretation of this λ dependence (smaller at shorter wavelengths - maximum at $\frac{1}{\lambda} \sim 2\mu^{-1}$ i.e. 5000 Å) and the variability over orbital phase were in terms of a disk model similar to that proposed by Huang (1963) and Woolf (1965). This model involved a disk around the secondary component (cooler star) together with absorption producing the wavelength dependence. Additional material between the stars (gas stream) was also considered as a contributor to the observed polarization features.

In an attempt to obtain details concerning the nature of the circumstellar material in β Lyrae, McLean (1977) made observations of the Hα and Hβ emission lines using the dual narrow band wavelength scanning polarimeter of Clarke and McLean (1975). The intrinsic polarization was seen to be visible and variable at the Hβ emission peak (λ 4864 Å). He found that as with previous observations the maximum polarization occurred at primary minimum, a second maxima at $\Phi \sim 0{\cdot}3$ and $0{\cdot}7$ and the deepest polarization minimum occurred at secondary eclipse. McLean also showed that the polarization at Hα and Hβ was weaker than in the adjacent continuum. These observations bring us full circle back to Öhman's observations of 1934 who predicted similar effects. These were too small to observe satisfactorily until McLean (1975).

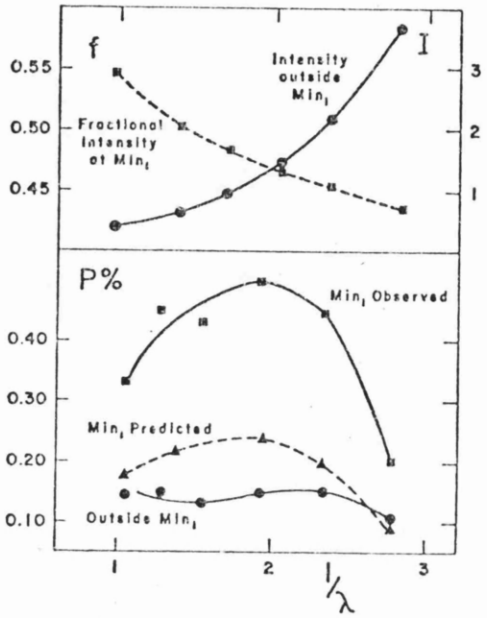

Figure 1.6 - Top - The intensity of β Lyrae outside primary eclipse (I) and the fractional intensity at primary eclipse (f) vs. inverse wavelength (μ^{-1}).

Bottom - The polarization at primary eclipse and outside primary eclipse vs $1/\lambda$ and the predicted variation out of primary eclipse when the effect of decrease of the non-polarized light is removed.

(After Coyne 1970a).

The detailed interpretation of the observations similar to those outlined above and a discussion of the theoretical models proposed to produce polarization variation intrinsic to binaries will be given in a later section (1.7). We now briefly consider the polarimetric observations published for other binaries during this period of time together with a short discussion of current observations (to 1980).

1.3 Observations of other binaries

A concerted effort was made to observe polarimetric variations from binaries after Chandrasekhar's (1946) theoretical predictions of intrinsic polarization from early type stars (i.e. those with hot electron scattering atmospheres). This polarization could however be observed in the integrated light of a star (i.e. over its disk) only if an asymmetry was present in the source causing the incomplete cancellation of the polarization effect from different areas of the visible surface of the star. Early type eclipsing variables were considered as possible candidates since the eclipse would introduce the necessary asymmetry and cause an overall intrinsic polarization (c.f. 1.7 for a discussion of this situation). In the same year, 1946, an observing program was initiated at Yerkes Observatory with the first preliminary report by Janssen (1946) involving the system U Sge. The results showed that polarization was present in the integrated light of the binary with the amount varying in both magnitude and position cycle with orbital phase. Hiltner (1947) undertook similar observations of early type binaries. He observed RY Per and obtained the variations indicated in Figure 1.7. He computed the polarization expected for a system similar to RY Per due to eclipse asymmetry (Figure 1.8) and noted that the observations were far from conclusive as regards the reality of variation of the intrinsic polarization for this system.

Shakhovskoi (1965) observed 17 eclipsing binaries for presence of intrinsic polarization and variation. Five systems V444 Cygni, β Lyr, RY Per, RY Sct and RZ Sct were found to exhibit variability. RY Per was then seen to vary by $\sim$ 1% in polarization at times of primary eclipse (Figure 1.9). The variations seen in AO Cas, AH Cep, CQ Cep, V380 Cygni, and CV Ser were found to fall within observational uncertainty. Hiltner and Mook (1967) also showed that the polarization of V444 Cygni was viable (Figure 1.10) and

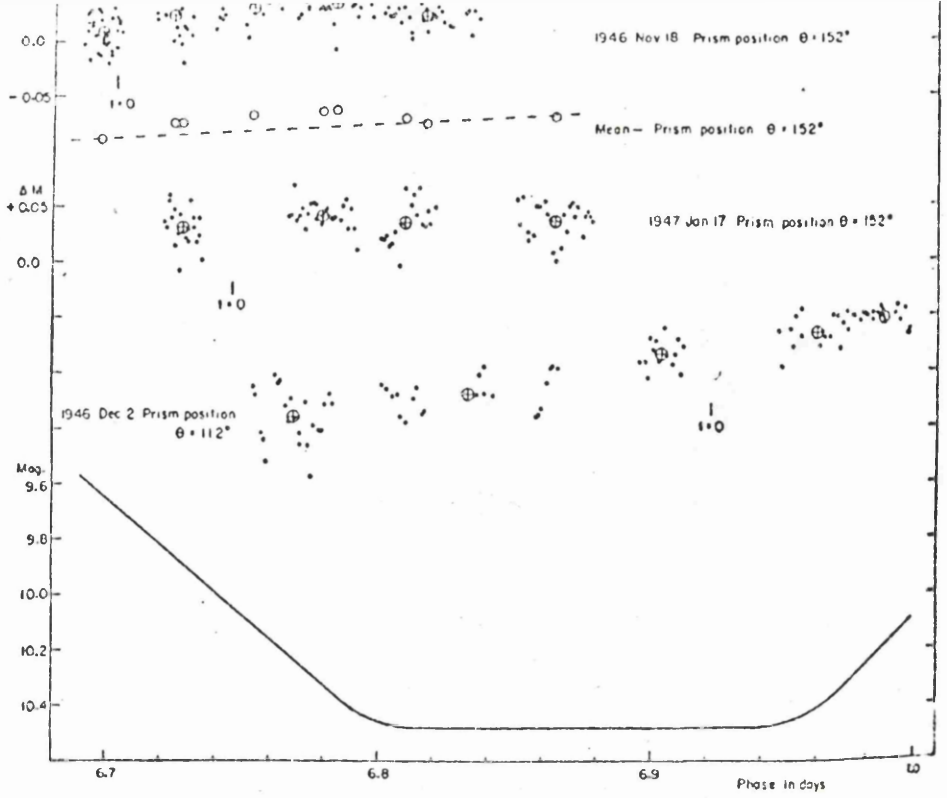

Figure 1.7 - Polarimetric observations of RY Per indicating the variability in amount of polarization as phase increases. The partial eclipse of RY Per is indicated at bottom.
(After Hiltner 1947).

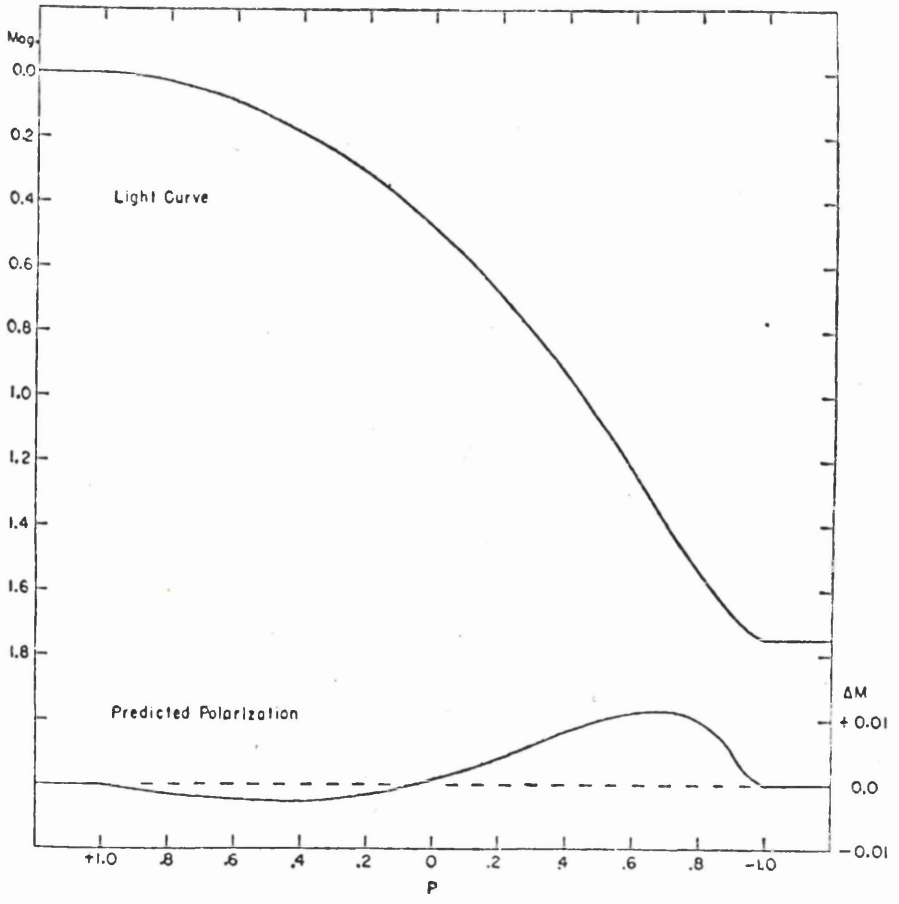

Figure 1.8 - Light curve and predicted polarization variations according to a model of electron scattering predicted by Chandrasekhar (1946) (After Hiltner 1947).

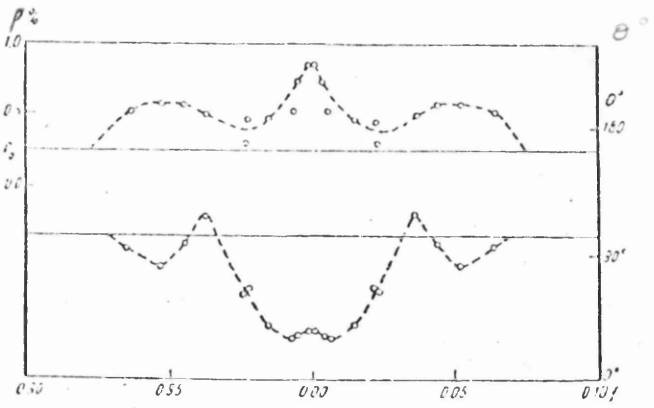

Figure 1.9 - Mean (binned) polarization and position angle variations for RY Per during eclipse observed by Shakhovskoi. The points (circles) are reflected about the 0.0 phase point with the horizontal line indicating the mean out-of-eclipse polarization curve. (After Shakhovskoi 1965).

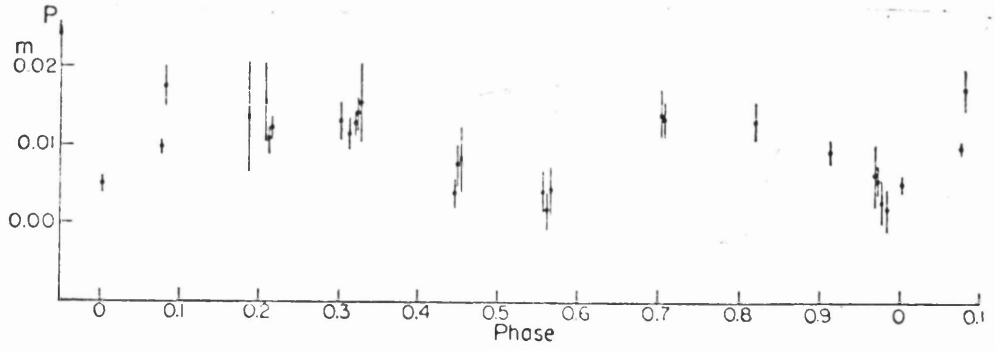

Figure 1.10 - Linear polarization of V444 Cygni vs. phase. This was the second binary (after β Lyrae) discovered to have variable polarization. The search for such systems was inspired by the predicted intrinsic nature of polarization of certain early type stars by Chandrasekhar (1946). (After Hiltner and Mook 1966).

associated it with an electron scattering mechanism (possibly the Chandresekhar effect) for this early, Wolf Rayet type binary.

In the following year Dibai and Shakhovskoi (1967) recorded significant variations of polarization during the eclipse phase of the system DQ Her (Nova Hercules 1934). This, they concluded was due to the increased contribution of the gaseous envelope to the total light of the system (i.e. radiation in the direct unpolarized star light) at times of eclipse and not the Chandrasekhar effect. Their maximum and minimum polarization levels for DQ Her were

Max: $Q = -0{\cdot}1\%$ $U = 0{\cdot}16\%$

Min: $Q = -0{\cdot}24\%$ $U = -.78\%$

In the period following, Serkowski (1970) undertook a survey of several early type eclipsing binaries, investigating primarily the wavelength dependence of the intrinsic polarization but also the temporal variation. The systems in which variations were found were TT Hya and V 453 Sco. TT Hya was seen to have the largest variations in the B filter ($\sim 0{\cdot}016$ mag. at times of primary eclipse). V453 Sco produced observations contrary to this however with smaller polarizations inside eclipse than outside. U Oph was observed by Coyne (1970) again in an attempt to establish the variations predicted by Chandresekhar. The largest changes were seen to occur near times of eclipse, supporting Chandresekhars interpretation. Additional variations outside eclipse were also present and interpreted as being caused by material in the process of transference between the components scattering the light of one or both stars.

A detailed six colour polarimetric and photometric study of W Ser was made by Kruszweski (1972). Again this is an eclipsing system with an extensive envelope and invisible secondary component (Sahade and Struve 1957). The polarization was found to be variable and intrinsic in origin (c.f. Figure 1.11). Highest polarization occurred at primary eclipse but other variations outside this phase were present. Other similar observations were made of ε Aur: Coyne (1972), CX Can: Whelan and Warden (1973), U Cep: Coyne (1974), GK Cep: Lester et al (1975), AM Her: Michalsky et al (1977) and AN Uma: Kreminski and Serkowski (1977) with, in most cases, the intrinsic nature of the variable polarization being established.

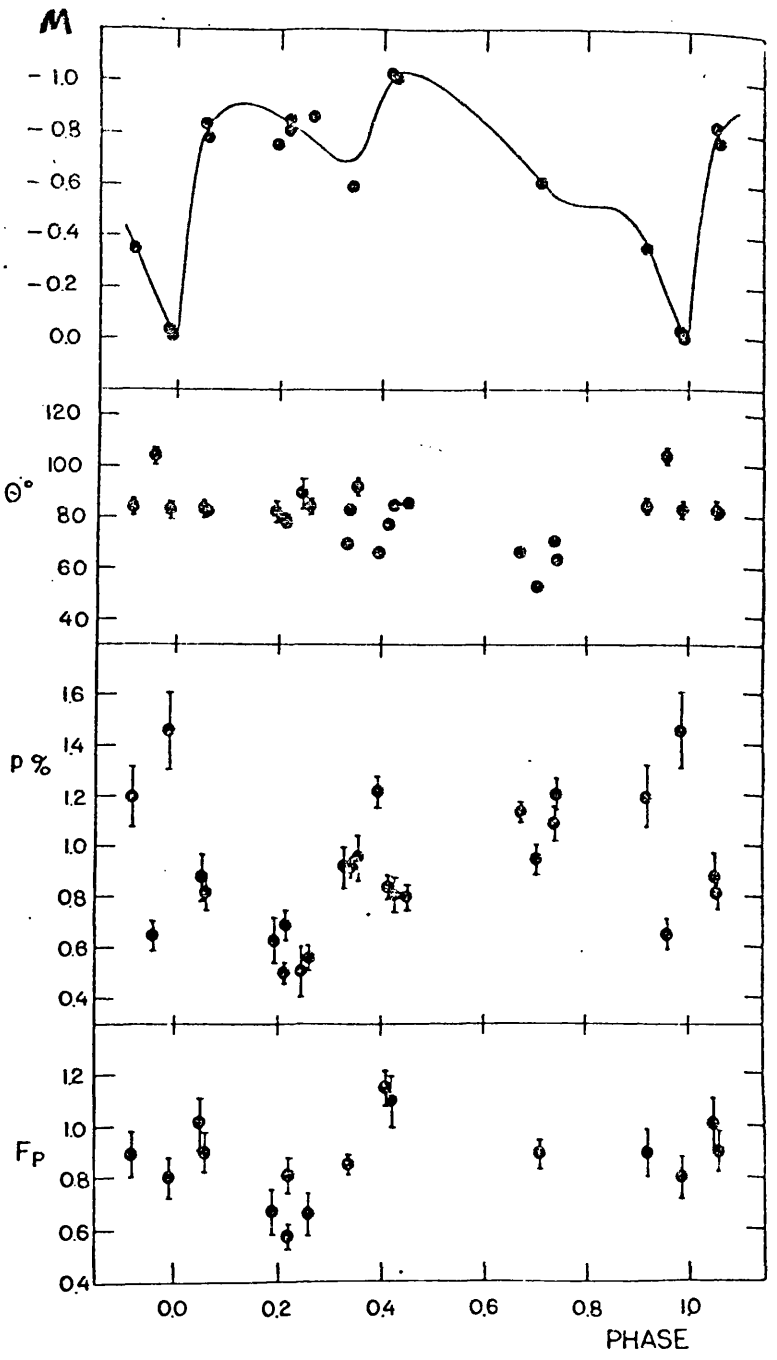

Figure 1.11 - Magnitude, position angle, degree of polarization and polarized flux variations with phase for the eclipsing binary W Ser (After Kruzewski 1972)

It was in the mid 70's that a group at Oregon University under the direction of J. C. Kemp began an extensive program of polarimetric observations of binary systems. Kemp and Rudy (1975) investigated the polarization of the White Dwarf binary BD + $16^{\circ}.516$ this time in an attempt to obtain evidence for a strongmagnetic field in the system. This was motivated by the discovery of a magnetic field in the eclipsing binary DQ Her by Swedlund et al (1974). A magnetic field would produce linearly polarized light (as well as circularly polarized) by interaction of the radiating atoms and the magnetic field. The magnetic field could cause both thermal and non-thermal emissions of polarized radiation. The thermal contribution would be caused by atomic or molecular processes such as bound-bound, bound-free and free-free transition occurring in the presence of a magnetic field. For example the effect of a magnetic field on a bound-bound transition would be to split the spectral lines into components of different polarization (Angel 1974). The non-thermal component would be the result of synchrotron radiation by relativistic electrons and would involve the spiralling of the electrons around the field lines. The electrons would then radiate pure linear polarized radiation in regions of uniform magnetic field. (cf. Jackson 1962). Under the assumption of a synchronous spin and orbit of the system the polarization would vary with the orbital period of the system (in this case $\sim$ 12.5 hrs). A polarization of $p \sim 0.15\%$ and $\theta \sim 50^{\circ}$ when averaged over the whole period was found and was concluded as probably being of interstellar in origin. Evidence for variability was marginal due to the short orbital period and comparatively long integration times necessary to obtain an observation (of the order of hrs.). Rudy and Kemp also looked for evidence of the Chandrasekhar effect at times of ingress and egress of the white dwarf eclipse but again the evidence was marginal in nature.

Other observational evidence for variability of the intrinsic polarization from binaries was presented by Pfeiffer and Koch (1973a,b, 1977) - RS CVn; Piirola (1977) - AW UMa, WU UMa, VW Cep and SW Lac; Pfeiffer (1979) - RS CVn; McLean (1980) - HD 50896; van Paradijs (1980) - Vela X-1 and HD 153919 and Piirola (1980) - HD 77581 and Vela X-1. The observations of McLean (1980) will be considered in

detail in Chapter 6 where we apply many of the techniques discussed in earlier chapters of this thesis in an attempt to obtain a clearer picture of the nature of that particular (and peculiar) system HD 50896.

Also worth mentioning at this stage is the method of establishing intrinsic polarization of Pfeiffer (1977). He undertook a survey of 20 spectroscopic or eclipsing binaries and attempted to establish the existence of intrinsic polarization by comparing the observed wavelength dependence with the interstellar wavelength dependence based on theory and on observations of unpolarized stars. Differences between these two behaviours indicated the existence of polarization intrinsic to the object observed, in this case the binaries. Once the intrinsic nature of the polarization had been established a more detailed (temporal) study could then be undertaken along the lines detailed above. He found 5 systems with clear differences between the interstellar λ dependence and assumed polarization λ dependence and 5 others whose polarization was suspected but not confirmed conclusively.

From this time however, to the present day much emphasis of observations has been on the occurrence of variable polarization, phase-locking to the orbital period of the binary, due to scattering in gaseous material in the system. The term phase-locking means that the polarization should vary periodically at some harmonic (or combination of harmonics) of the binary orbital frequency.

Two main lines of interest have grown. Firstly the detailed observation and modelling of polarization variations inside the <u>eclipse phase</u> of an eclipsing binary undertaken by Piirola at the University of Helsinki, and secondly the long term observations at <u>all phases</u> intending to establish phase locking of the polarimetric variations. The latter case is the one we are primarily concerned with in this thesis, the chief exponent of such observations being J.C. Kemp in Oregon. Piirola's observations and theoretical interpretation will nevertheless be considered in (1.6). We now summarize the observational work of Kemp and colleagues whose data forms the basis on which the analytic work of this thesis is tested.

1.5 Observations of Kemp et al.

The observations of Kemp et al are in many cases used in later chapters to test the models of such polarimetric variation developed and extended here. We shall deal with the observations made of Cygnus X-1 in a separate section (1.6) as this system is of special significance and will be frequently referred to throughout this thesis.

In the early 70's Pfeiffer and Koch (1973) reported the discovery of variable linear polarization of the system AO Cas. Rudy and Kemp (1976) undertook detailed observations of this system claiming that the polarimetric variations were phase locked to the binary period. Some 38 observations in the B filter were made spanning $\sim$ 20 orbital periods. The resulting Q,U variations with phase, Φ are shown in Figure (1.12a,b) together with the Q,U locus, namely the variations plotted in the Q,U plane. (Figure 1.12c). They found by a powerspectrum analysis that the observations were phase-locked with the strongest peak occurring in the power vs. frequency domain at a period of 1.76 days i.e. half the orbital period. This was termed the second harmonic of the binary period. The solid curves in Figure (1.12) indicate their hand-drawn smooth mean curves. The Q,U locus was used by Rudy and Kemp (1976) for modelling purposes and was seen to have certain predominant features. The sense of rotation along the curve was seen to be unambiguous and was interpreted as the orbital revolution direction on the sky. This circulation as pointed out by Rudy (1980) cannot be found by spectrophotometric methods. Also the degenerate nature of the conjunction points 0.0 and 0.5 phase (i.e. the same polarization at both) was noticed together with the different polarization values at the two quadratures ($\Phi \sim 0.25$ and 0.75). The interpretation of this behaviour is in terms of variable scattering angles in a revolving gaseous stream between the two stars as illustrated in Figure (1.12d). The reflection effect and the effect of tidal distortion of the components were ruled out as candidates for the production of significant amounts of the polarization variations due to the symmetry effect of these processes on the Q,U locus. (The polarization at $\Phi \sim 0.25$ and 0.75 would be the same in those cases). The process was assumed to involve an envelope (stream) in the orbital plane of the binary since it would

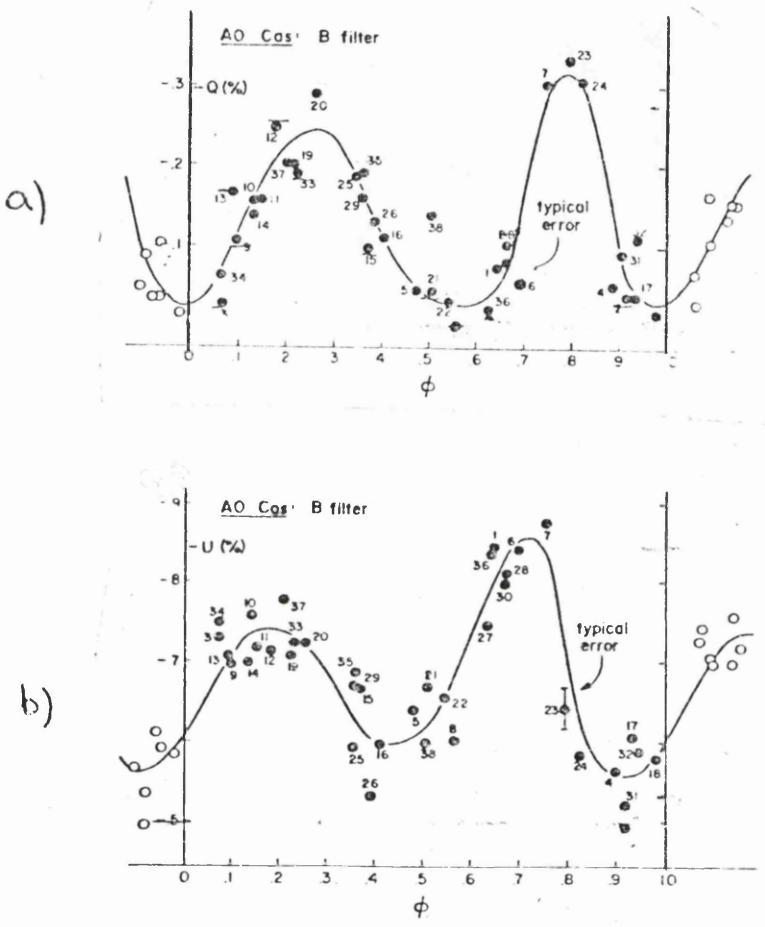

Figure 1.12 - (a),(b) B filter Stokes parameter (Q,U) variations for the binary AO Cas. The smooth curves are the handdrawn 'best fit' variations.

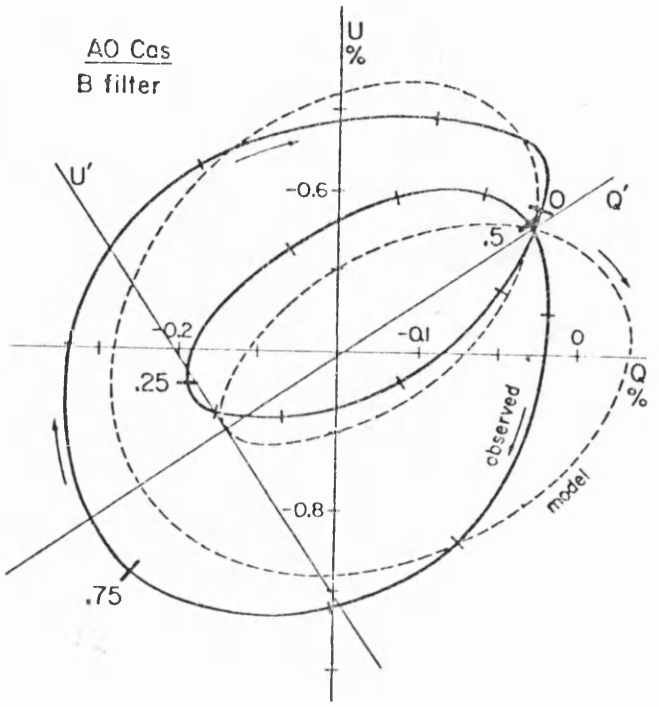

c)

Figure 1.12 (c) Smoothed 'best fit' Q,U locus of data in (a) and (b). Dotted line indicates the predicted Q,U locus due to the interpreted scattering model.

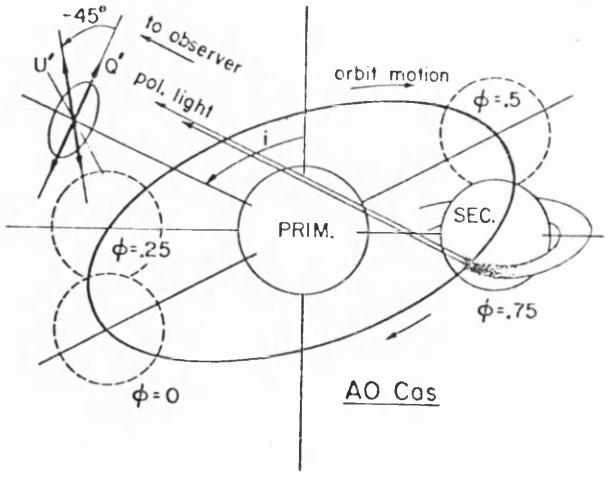

d)

Figure 1.12 (d) Schematic representation of the model used to explain the Q,U, variations of AO Cas. Light from both stars is scattered by a gas stream with the darker region indicating the effective centre of the scattering region.

otherwise produce different polarizations at phases 0.0 and 0.5. The model included as well as variation of the scattering angle, an 'empirical stream shadowing effect' (of part of the scattering region) taken as $S(\phi) = \cos^2(\pi(\phi - \phi_o))$ where ϕ_o is the orbital phase of maximum visibility of the stream (here taken as $\phi_o = 0.75$). The shadowing effect is thus used to produce variable occultation of the stream during the orbital period. The dashed line in the Q,U diagram (Figure 1.12c) is the resultant smoothed model fit. Rudy and Kemp (1976) find that the model needed a gas stream directed onto the secondary star with the point of impact on the advancing hemisphere of that star, with a stream mass of 3×10^{-10} $M_\odot$ (this is seen to be small compared to estimates mentioned earlier for β Lyr i.e. $\sim 10^{-8}$ $M_\odot$).

Rudy and Kemp next observed the system u Herculis. (Rudy and Kemp 1977). They again reported linear polarization variations synchronous with the orbital period with maximum power in a powerspectrum analysis of the data occurring at 1.025^d or half the orbital period (2nd harmonic component c.f. Figure 1.13a). Their observations spanned some 14 months and indicated a peak to peak amplitude of polarization variations of $\sim$ 0.06%. This was then the smallest variation discovered in the polarization of binary systems. The Q,U variations vs. orbital phase are shown in Figure 1.13 b,c, together with the Q,U locus (Figure 1.13d). The main features of this locus were, the doubly periodic figure (circlingthe origin twice per orbital period). The values of polarization at $\Phi \sim 0.0$ and 0.5 and 0.25 and 0.75 being approximately degenerate ($P(0.0) \sim P(0.5)$ and $P(0.25) \sim P(0.75)$) and that these points call out the extreme values of the QU locus. Four sources of polarization were considered as possible candidates for the production of the observed variations namely the Chandrasekhar effect, tidal distortion or non-sphericity effects, the reflection effect and scattering on gaseous circumstellar material. Rudy and Kemp (1977) indicated that the reflection effect would most likely account for the major features of the polarization locus (i.e. scattering and reflection of light from the hotter component in the atmosphere of the cooler star cf. Figure 1.13c). They calculated the reflection models predictions (that of Figure 1.13c) and obtain a Q,U locus as shown (dashed curve) in Figure 1.13c). The main features of this

Figure 1.13 (b) Model proposed to explain the observed polarimetric variations in u Her. Scattering of light from the primary star (1) occurs in the facing hemisphere of the secondary star (2). An inclination of $\sim 76^{\circ}$ is found when best fitting the data.

Figure 1.13 (c) The above model's predictions in the Q,U plane (dotted line) together with the 'best fit' harmonic curve through the data. The same general trend is observed in both.

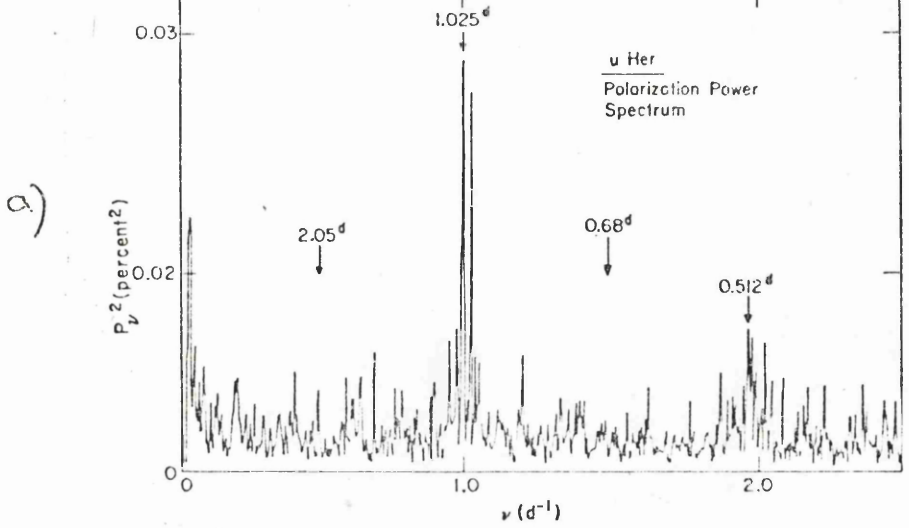

Figure 1.13 (a) Powerspectrum (power vs. frequency) of u Her data. The frequency with the highest power is seen at half the orbital period indicating dominant second harmonics

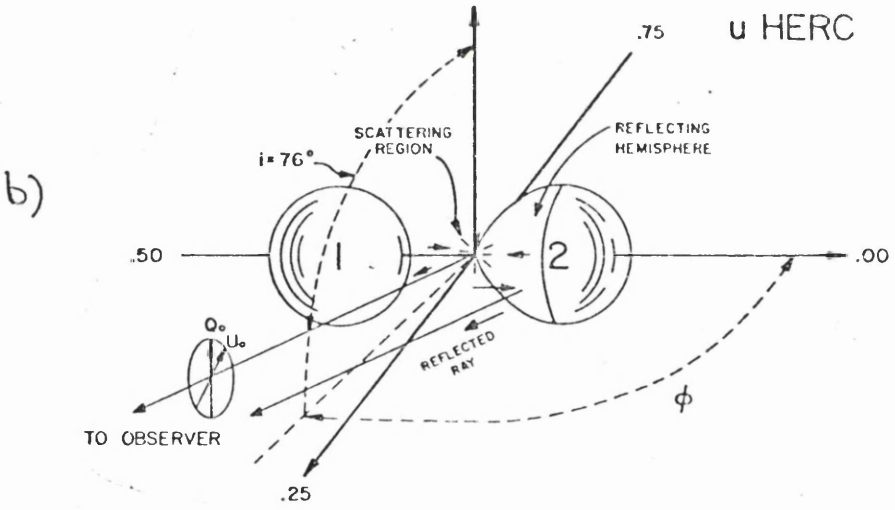

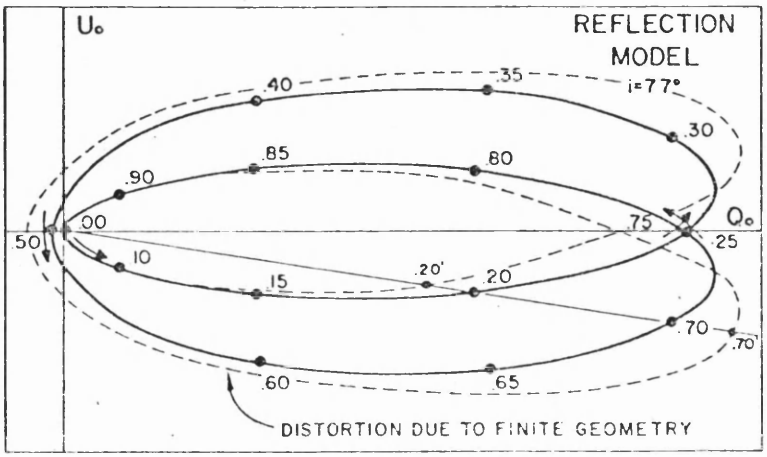

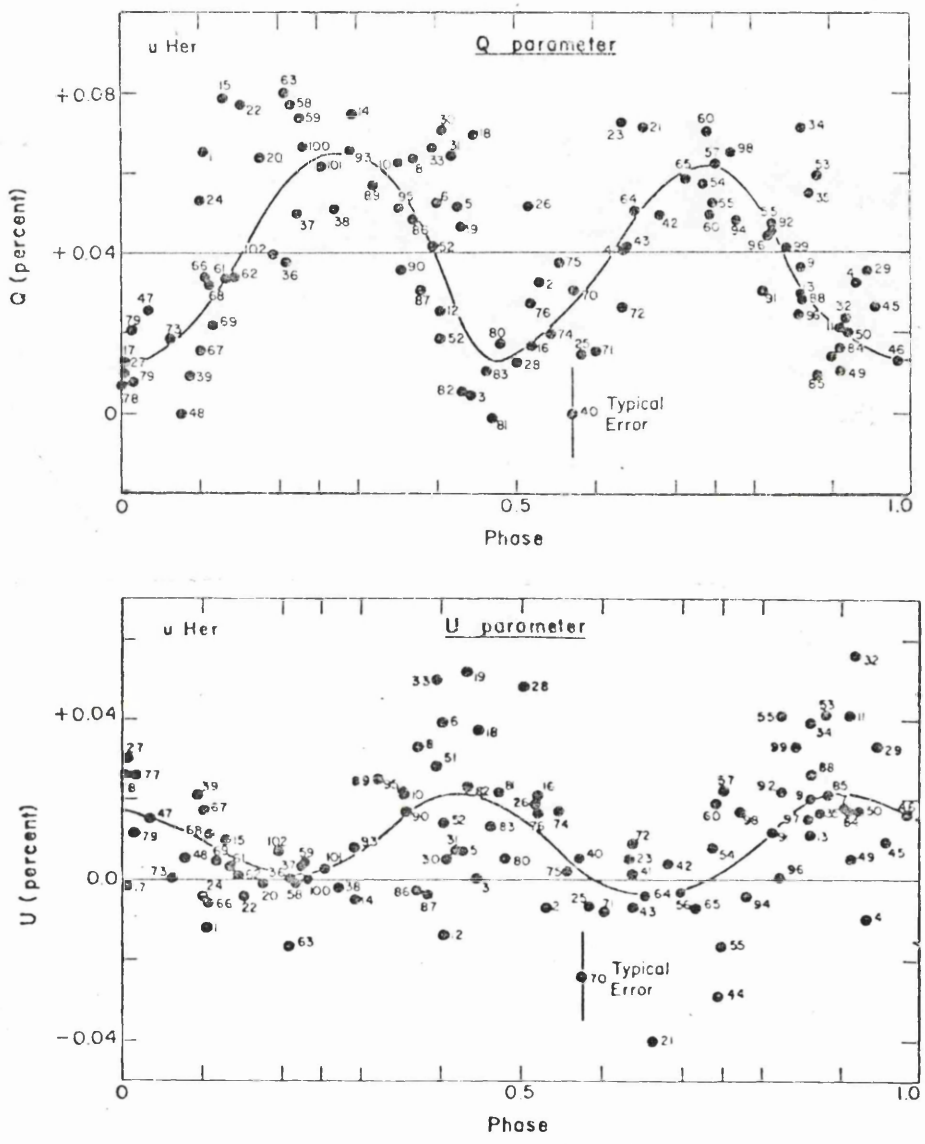

d)

Figure 1.13 (d) The data (Q, vs Φ and U vs. Φ) for u Her.
(After Rudy and Kemp 1977)

are seen to be similar to those observed. The form of the Q and U variations predicted by the model however are seen to be complicated:

$$Q(\phi) = \frac{\sin^2 2\pi(\phi - 0.5) - \cos^2 i \cos^2 2\pi(\phi - 0.5)}{1 + \sin^2 i \cos^2 2\pi(\phi - 0.5)} \left(\frac{\pi - \theta}{\pi}\right)$$

$$U(\phi) = \frac{\cos i \sin 4\pi(\phi - 0.5)}{1 + \sin^2 i \cos^2 2\pi(\phi - 0.5)} \left(\frac{\pi - \theta}{\pi}\right)$$

where θ is defined as $\cos^{-1}(-\sin i \cos \phi)$. ϕ is the orbital phase and i is the inclination of the system to the line of sight. The $i = 77^{\circ}$ best fit value of the inclination is comparable to Batten et al (1967) of $i = 75.9^{\circ}$. Their conclusion was that the reflection mechanism would give a satisfactory agreement between observation and model but may not account for all the observed variations. Gas streaming was thought to influence the observed Q,U locus to some extent.

The helium rich binary σ Ori E was the next system to be observed Kemp and Herman (1977). Over a period of 3 months they found variations in polarization of $\sim 0.15\%$. Figure 1.14 a,b,c shows their observations (Q and U vs Φ and Q,U locus). Two sets of observations are shown one being in the blue (B filter) with the other in the ultraviolet (U filter). The nature of the variations presented are seen to be different in each of the two columns, with the U filter observations producing a larger scatter of values at similar phases. The size of the variations are also larger in the U filter. Power spectrum analysis of the data (Figure 1.14d) indicates the evidence (albeit inconclusive) for phase locking at the 1.19^{d} (second harmonic) period. The variations were explained as being due to a combination of the reflection effect on a disk of material (reflection of the B stars light by the disk) and local polarization effects associated with the disk emission itself. This disk was proposed as having a size (diameter) greater than the diameter of the B star so therefore its edges would still be visible at times of total eclipse. This would produce polarization at times of eclipse (cf. Figure 1.14e) as observed in the data. The details of the model proposed were formulated not only from polarimetric evidence but also utilizing the spectroscopic line strength variations with phase of Groote and

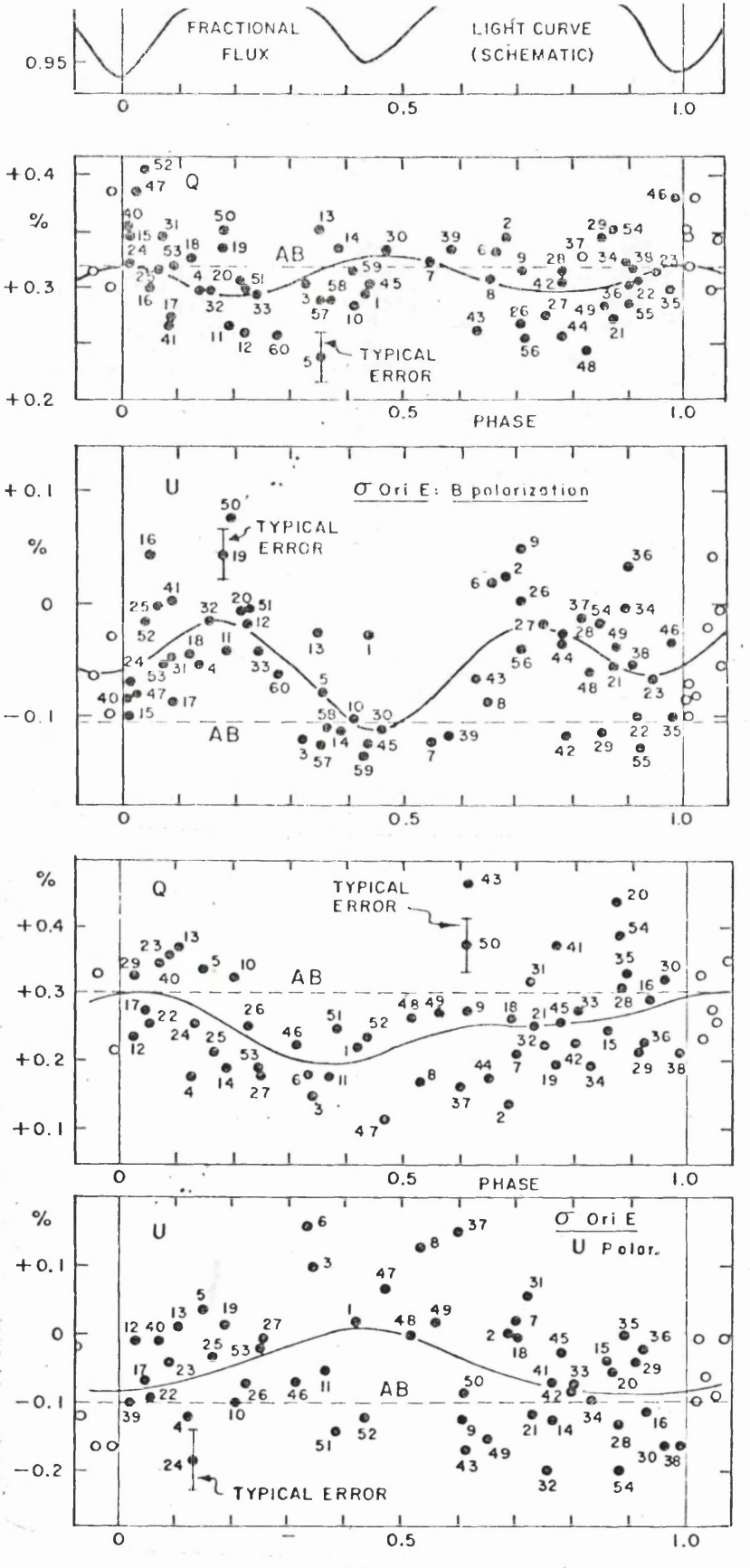

Figure 1.14 (a) Polarimetric observations of the eclipsing binary σ Ori E in both B and U filters together with a schematic light curve.

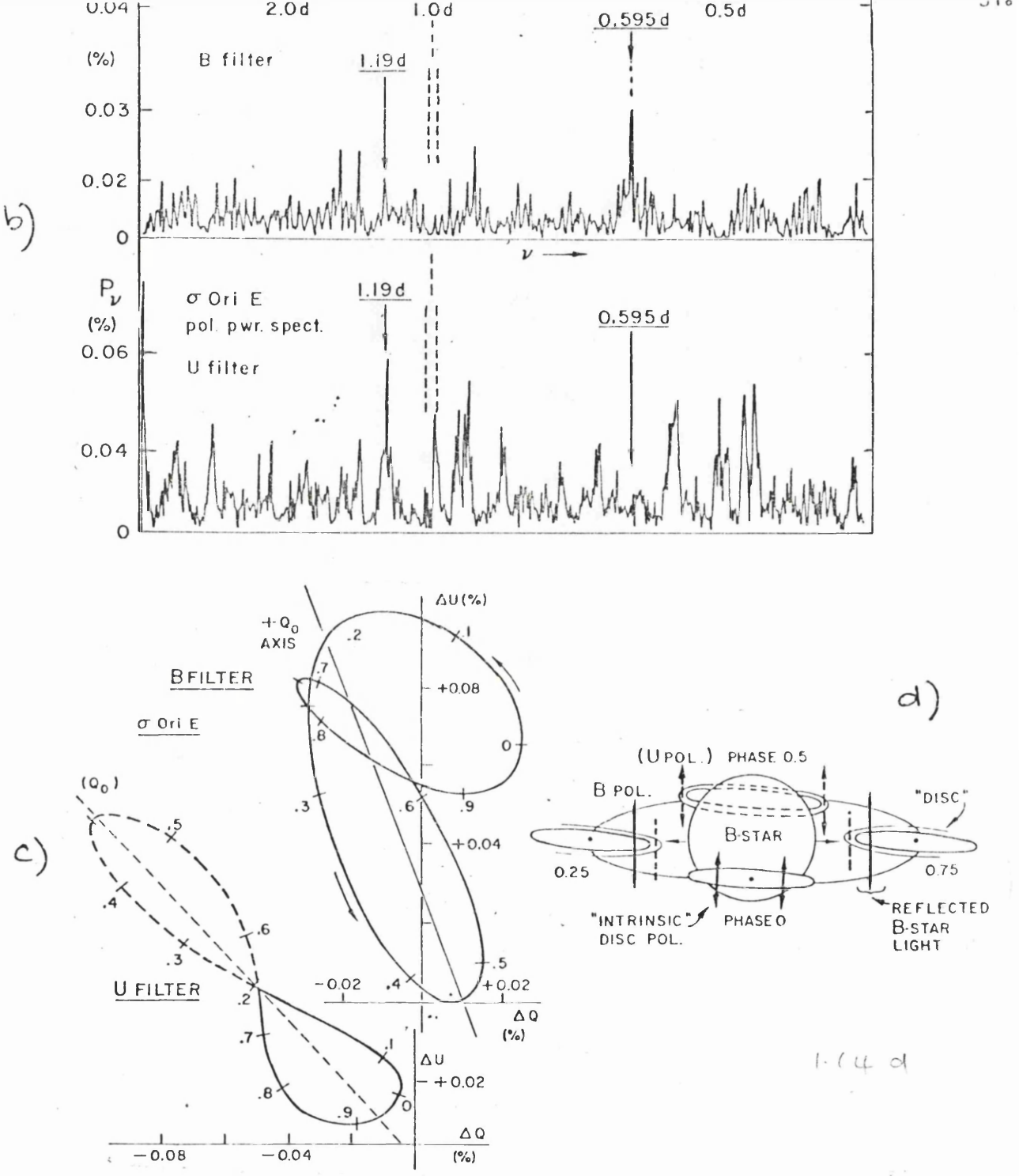

Figure 1.14 (b) Power spectrum of the data shown in 1.14 a indicating the different nature of the variations in B and U filter.

(c) Q,U loci for σ Ori E (B and U filter) again showing the difference between the two filters data.

(d) Model invoked for σ Ori E to explain the observations. Scattering of B star light occurs in the eclipsed accretion disk. (After Kemp and Herman 1977)

Hunger (1977). The difference between the U filter Q, U locus data and that in the B filter (evident in Figure 1.14c) was considered as possibly due to either intrinsic UV light emission (and scattering) from a disk hotspot, or by the opacity of the disk rising sharply in the UV implying the disk contribution to the total light being different in the UV. This was also the first paper to note the possibility of determining orbital inclinations from the shape of the Q,U variation (locus) but without detailed modelling of the variations. It was stated that a crude estimate of i could be obtained from the eccentricity of the second harmonic best fit component of the Q,U locus from the relation:

$$e = \frac{\sin^2 i}{(1 + \cos^2 i)} \qquad (1.2)$$

where e is the aforementioned eccentricity (Rudy 1977). Proof of this result will be presented later (Chapter 2). For σ Ori E an inclination of $i \sim 76^\circ$ was estimated with a formal error, based on the uncertainty in the second harmonic Fourier coefficients obtained from the data, of $\pm 8^\circ$.

A similar determination was made for the system HD 47129 (Plaskett's Star) by Rudy and Herman (1978). Linear polarization was first detected in this system by Shulov (1966) but was not seen to be variable until later observations by Hayes (1975) and Pfeiffer and Koch (1977). Polarization variations synchronous with the binary period were announced by Rudy and Herman (1978) who asserted the predominantly second harmonic behaviour was indicative of scattering from circumstellar material (c.f. Figure 1.15). The inclination obtained from the above expression (2) was $i \sim 71^\circ \pm 9^\circ$ for this binary. The erratic nature of the changes of polarization seen in Figure 1.15 were regarded as being caused by short term fluctuations in the nature of the scattering region. Comparison of the polarimetric variations with spectroscopic studies of HD 47129 by Struve et al (1958) indicated that possible scattering material was present between the two stars but its nature could be changeable over a variety of timescales.

A major contribution to polarimetric observations of binaries (over the whole orbital period) appeared in the same year as the HD47129 results. Rudy and Kemp (1978) presented observations of

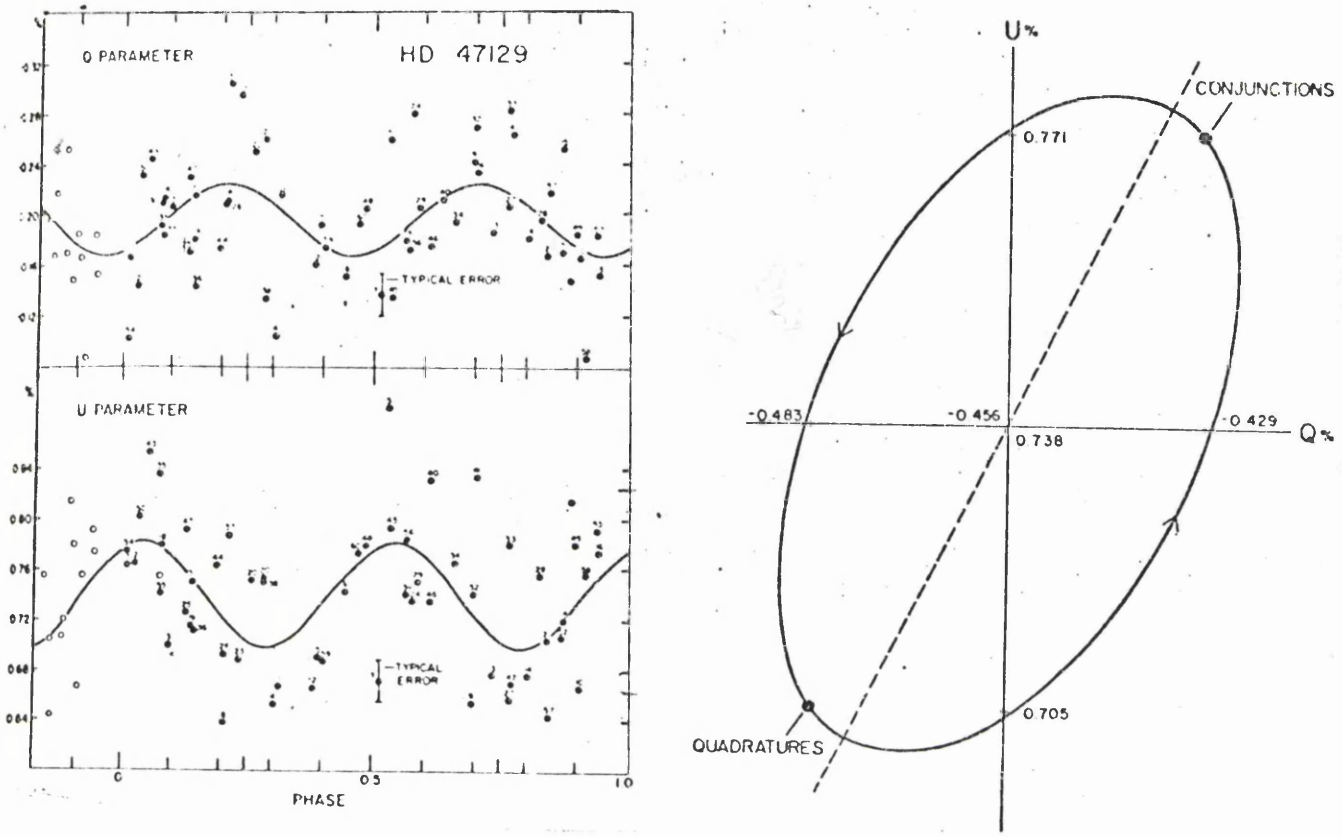

Figure 1.15 - HD 47129 polarimetric observations and best second harmonic curves. The second harmonic Q,U locus is also shown (After Rudy and Herman 1978).

β Per (Algol), U Sge and V444 Cygni together with an outline of a method of interpretation of the variations involving Thomson scattering in an arbitrary, optically thin, corotating circumstellar envelope. This analysis allowed for one - point light sources but assumed the source and scattering region symmetric about the orbital plane of the system. In the independent analysis by Brown, McLean and Emslie (1978) no symmetry requirements were imposed but only point light sources were included. These model analyses will be discussed in Chapter 2. The observations of the above three binaries and those of u Her and AO Cas were interpreted in Rudy and Kemp (1978) in terms of the model proposed. The observations of β Per, U Sge and V 444 Cygni are shown in Figure (1.16 a,b and c). The inclinations obtained from the model (i.e. Equation (2)) were seen to be close to previously determined values (photometrically etc.). Table I shows both values and the formal errors on the polarimetric determinations.

STAR	INC (OTHER)	INC (POLARIMETRY)	FORMAL ERROR
ALGOL	82^{o}	81^{o}	$\pm 4^{o}$
AO CAS	57^{o}	63^{o}	$\pm 9^{o}$
U HER	76^{o}	77^{o}	$\pm 5^{o}$
U SGE	90^{o}	87^{o}	$\pm 3^{o}$
V444 CYG	80^{o}	72^{o}	$\pm 6^{o}$

Table I - Polarimetric determination of inclination i together with previous estimates (photometric etc.). Also shown is the formal error on the former quantity.

These errors are 'formal' in the sense that they do not take into account the acceptability of the model itself (i.e. its fit to data), but are only a perturbation about the 'best fit'. It is this very point that first sparked out interest in the fit of the polarimetric binary model (of Brown et al and Rudy and Kemp) to observational data and resulted in the work presented in this thesis.

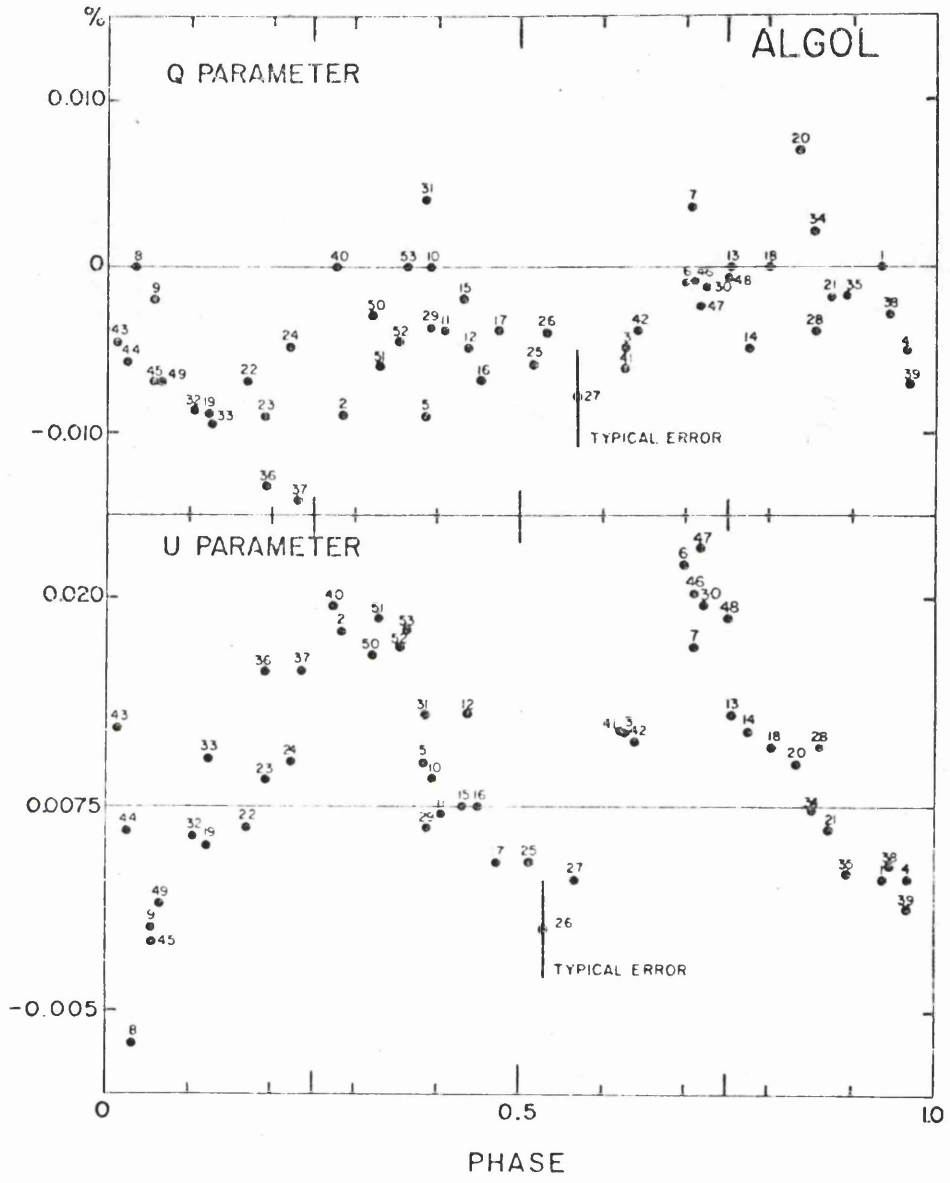

Figure 1.16 (a) Linear polarization variations observed in βPer (Algol). (After Rudy and Kemp 1978).

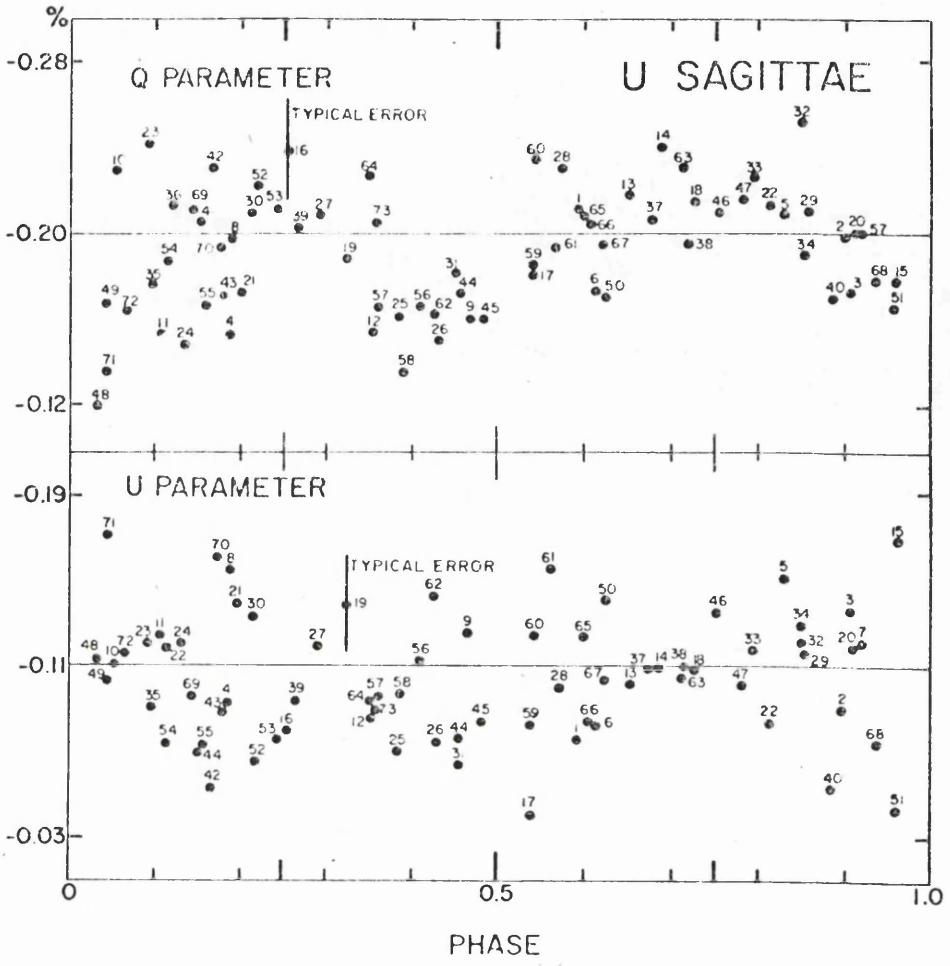

Figure 1.16 (b) Linear polarization variations observed in U Sge. (After Rudy and Kemp 1978)

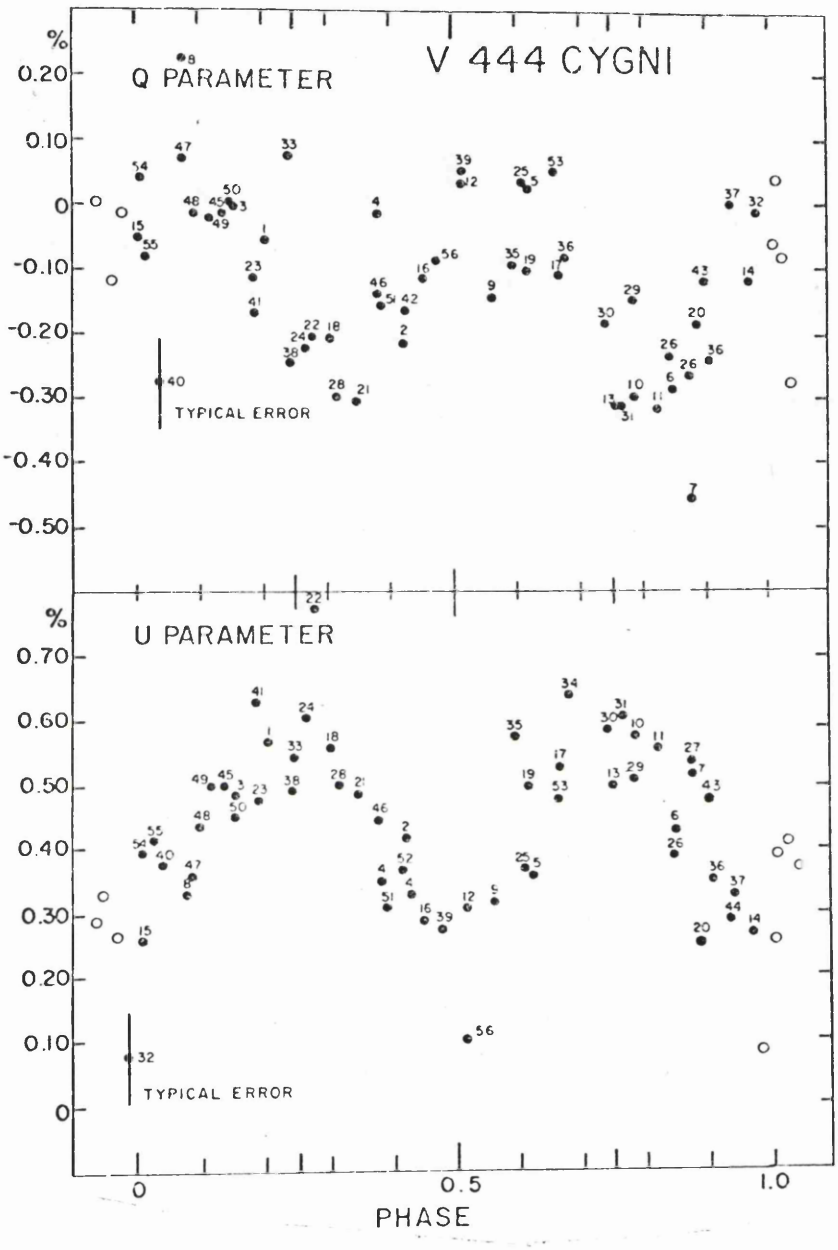

Figure 1.16 (c) Linear polarization variations observed in V 444 Cygni. (After Rudy and Kemp 1978)

1.6 Cygnus X-1

Photometric and spectroscopic data on Cygnus X-1 (see Appendix 1) indicates the presence of an orbital period of 5.6 days. The system is seen in the visible as an OB supergiant star with a faint (unobserved) compact companion and is referred to in the Henry Draper catalogue as HD 226868. Such a system would be a likely candidate to produce variable linear polarization due to

(a) Tidal distortion of the optical star by the compact object. (The short orbital period implies a close orbit).

(b) The X-ray nature of the system indicating the probable existence of mass transfer (accretion and accretion disk) and hence there would exist (hot) circumstellar material capable of Thomson scattering the primaries light.

Gehrels (1972) reported a large constant polarization of this system (interstellar) but did not search for intrinsic variability associated with the above mechanisms (or any other). The first reported discovery of variable linear polarization intrinsic to the system appeared in 1975. In that year Nolt et al (1975) published observations taken at Oregon University Observatory, in the V Filter. Due to the low flux of Cygnus X-1 ($m_V \sim 9.6$) observations were integrated for time intervals of 3 to 5 hours. 23 observations were presented showing variations in the linear polarization of $\sim 1\%$ (extreme max. to min of P). These are shown in Figure 1.17. The periodic (i.e. phase locked) nature of the variations was not established conclusively here since the observing run spanned only a small number (4) orbital periods: the curves in Figure (1.17a) indicate the least-squares 1st and 2nd harmonic regression (solid line) and the direct Fourier analysis curve (dashed line) for both Stokes parameters. Statistical tests were employed to support the 'reality' of the Q.U. pattern (e.g. the variance ratio test- Henmerle 1967), a statistical significance of 87% (Q) and 97% (U) being quoted. The interpretation of the observations was again referred to the Q,U locus (Figure 1.17b) with the polarization cross-over pointbeing close to phase 0.25 and 0.75 and the extreme values of polarization falling close to phases 0.0 and 0.5. Under the assumption that

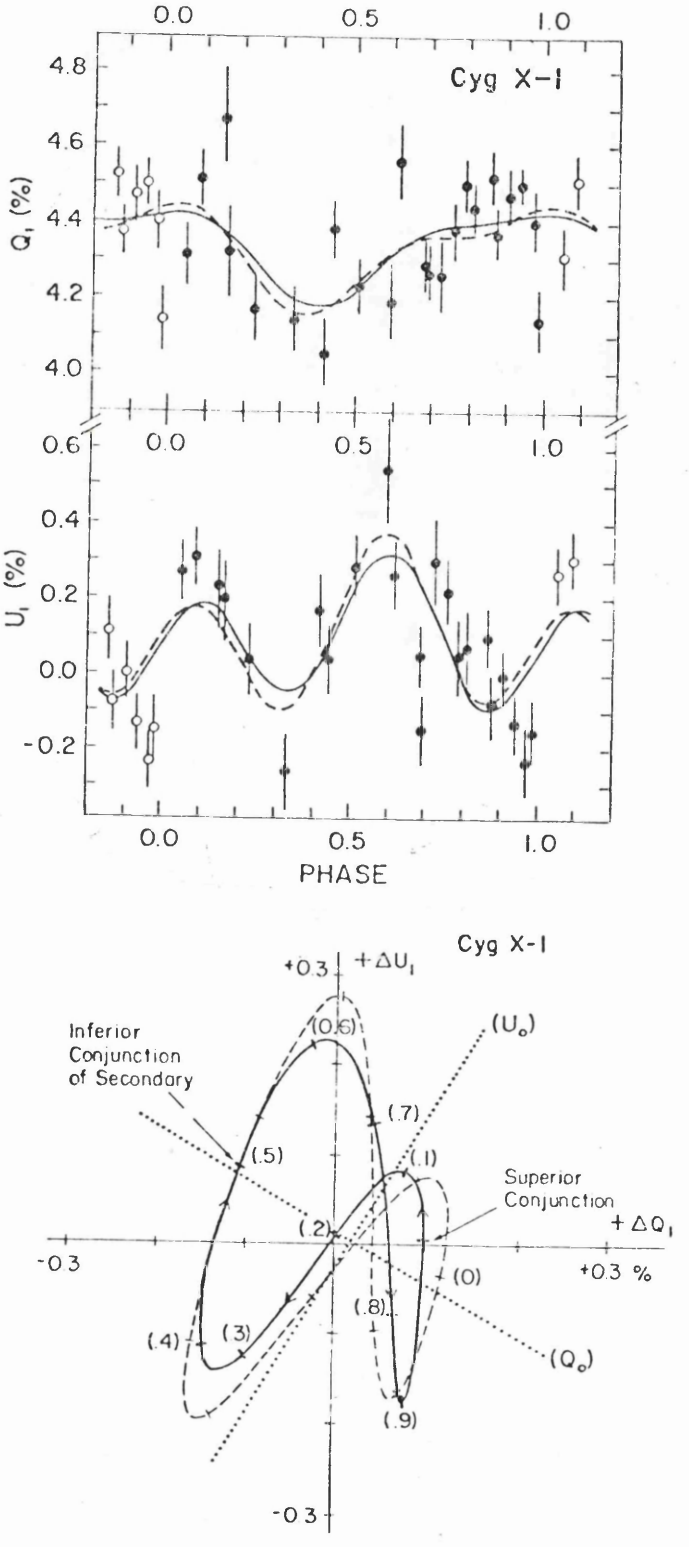

Figure 1.17 - The first published percentage polarization variations for Cygnus X-1

(a) the Q,U phase variations together with the least mean square regression (1st and 2nd harmonics) of data. (Solid line). The dashed line indicates the Fourier 'best fit' 1st and 2nd harmonic behaviour.

(b) the Q,U locus of both of the above 'best fits' for Cygnus X-1. Phases are marked at 0.1 intervals (After Nolt et al 1975)

asymmetric gas streams played no significant role in the polarization. The locus was concluded as being 'consistent with the geometry and phasing required by a binary model'. More detailed interpretation was left until further data had been collected. These appeared in 1976 (Kemp et al 1976). Some 110 nights observations were presented covering a period of time of 16 months and were referred to as 'an interim report on the long range observational studies of the variable linear polarization of Cygnus X-1'. A power spectrum technique aimed at establishing periodicities phase locked to the binary period was presented (c.f. Appendix 2). The variations were not found to be phase locked at the 1st harmonic of the binary period (i.e. 5.6 day period) but marginal evidence was claimed for a component phase-locked at half the orbital period (2.8 day - second harmonic).

Typical power spectrums produced are shown in Figure 1.18. Here the combined U,B and V filter data have been analysed from which the conclusion of marginal phase locking was made. The horizontal dashed line shows the power levels expected from measuring noise. This conclusion was justified by the apparent tendency for concentration of excess power around the 2.8 day period. To account for the lack of complete phase-locking Kemp et al (1976) proposed that a gas stream (producing the polarization) wandered about or changed its structure on timescales larger than the orbital period. This would produce phase, as well as amplitude, modulation of the observed polarization. The dips, or in the terminology of Kemp et al (1976) the antipeaks, occurring at 2.8 days (and possible 5.6 days) were thought to be due to periodic modulation of this sort and not random modulation (c.f. Middleton 1960).

In a letter to Nature (Kemp et al 1977) 225 nights observations were presented for Cygnus X-1, with a possible interpretation of very long period variability in terms of a third body in the system proposed. A 39.2 day period was detected by the power spectrum method of the above paper. This period was undetected in other observational data e.g. B photometry - Walker and Nolt (1977), X-Ray flux - Nolt and Walker (1977). An interpretation of this long period in terms of a 3rd body was also given by Milgrom and Shaham (1977). They considered the polarization varying at this period (7 x the orbital period) as due to Thomson scattering of optical photons by flared material at the

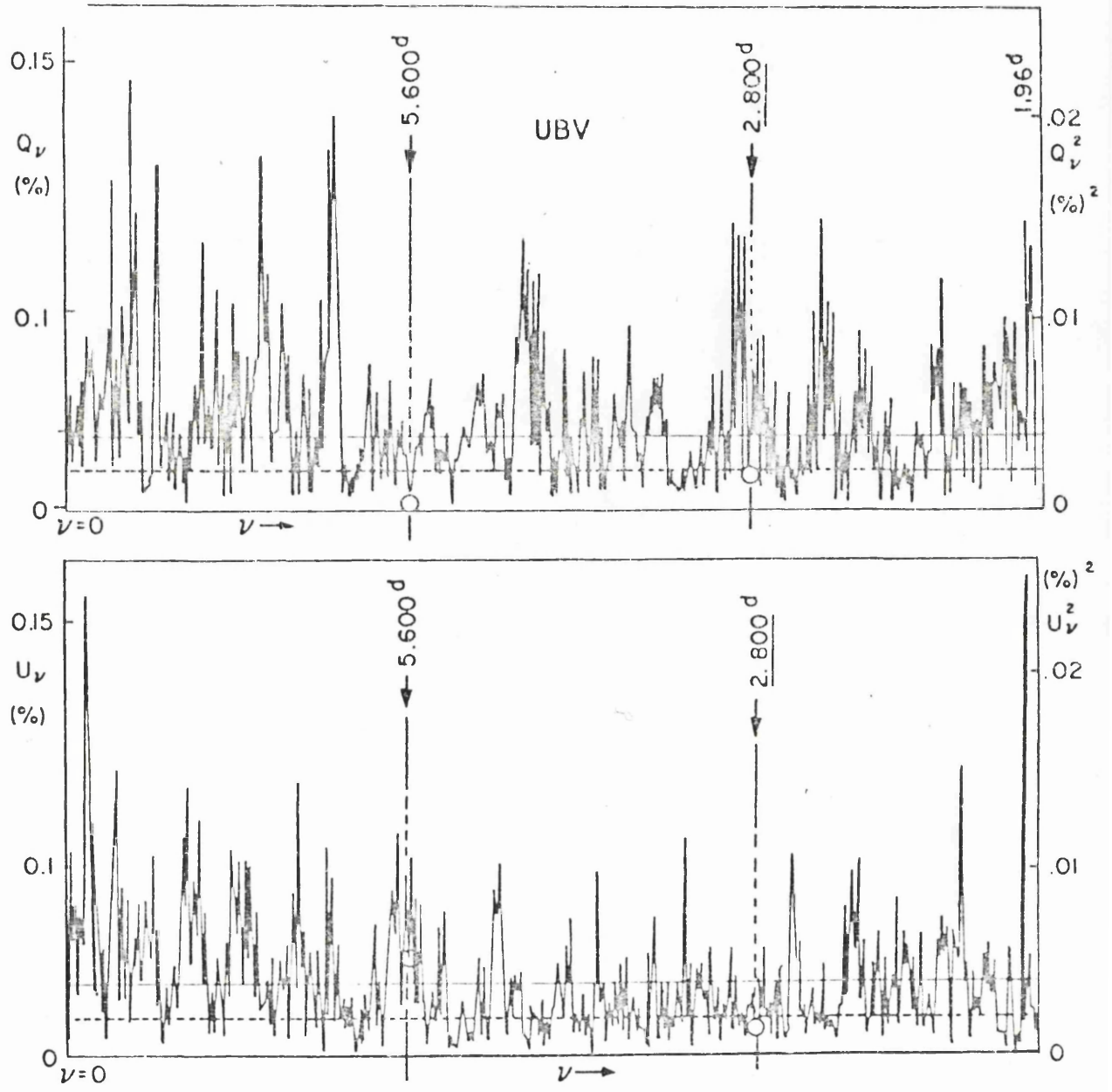

Figure 1.18 - Powerspectrum of combined (1974/75) U, B and V observations of Cygnus X-1. These indicate the apparent absence of 5.6 day and 2.8 day (1st and 2nd harmonics of the binary period) peaks. (After Kemp et al 1976).

outer parts of an accretion disk and the incoming flow of matter (Rees 1975). The third body was proposed as tidally distorting the optical star sufficient to cause structural variability of the outer regions of the accretion disk. An eccentric orbit 3rd body would hence produce a variable effect over its orbital period (39.2 days). This modulated rim structure to the accretion disk should also produce X-ray modulations at the same period. Longer period variations could also occur according to Milgrom and Shaham, due to effects such as precession of the nodes of the eccentric 3rd body orbit. The reality of this 39.2 day period was however questioned by Walker et al (1977) due to the absence of any other observation evidence at this period including such observations as (a) 399 nights B band photometry (1972-1976) (Walker and Quintanilla 1978), (b) X-ray light curves and (c) 215 radial velocity observations. The latter put limits on the radial velocity of a third body in the system of < 10 km s^{-1}. Data (a) and (b) were both searched for a 39 day period using two different techniques (Lafler and Kinman 1965 and Gray and Desicachary 1973) with negative results. Walker et al (1977) concluded that the 'reality' of this 39.2 day period seen only in the U band polarimetric data was thus doubtful.

Kemp et al (1978a) analysed the new V band data for this system (amounting to 180 nights) in terms of a model involving 1st and 2nd harmonics. The Q,U locus of the dominant second harmonic component is shown in Figure (1.19). This takes the form of an ellipse of eccentricity $e \sim 0.91$. This they quoted as giving an inclination for the system of $i \sim 77.8^{\circ}$ (from the above equation (2)). A formal error of $di \sim 6.7^{\circ}$ was also obtained. The change in the second harmonic component of the data occurring over the observing period was indicated in Figure 1.19. This was due to the addition of more data points to the analysis. The interpretation of the variations neglected however the 1st harmonic (and any other present) in the data. The main conclusions reached in this paper are that (a) the variations present are predominantly second harmonic in nature and (b) there is a wavelength dependence to the polarimetric variations. The U band variations were seen to be smaller than in the V band by at least a factor 2. The polarization variations are assumed to

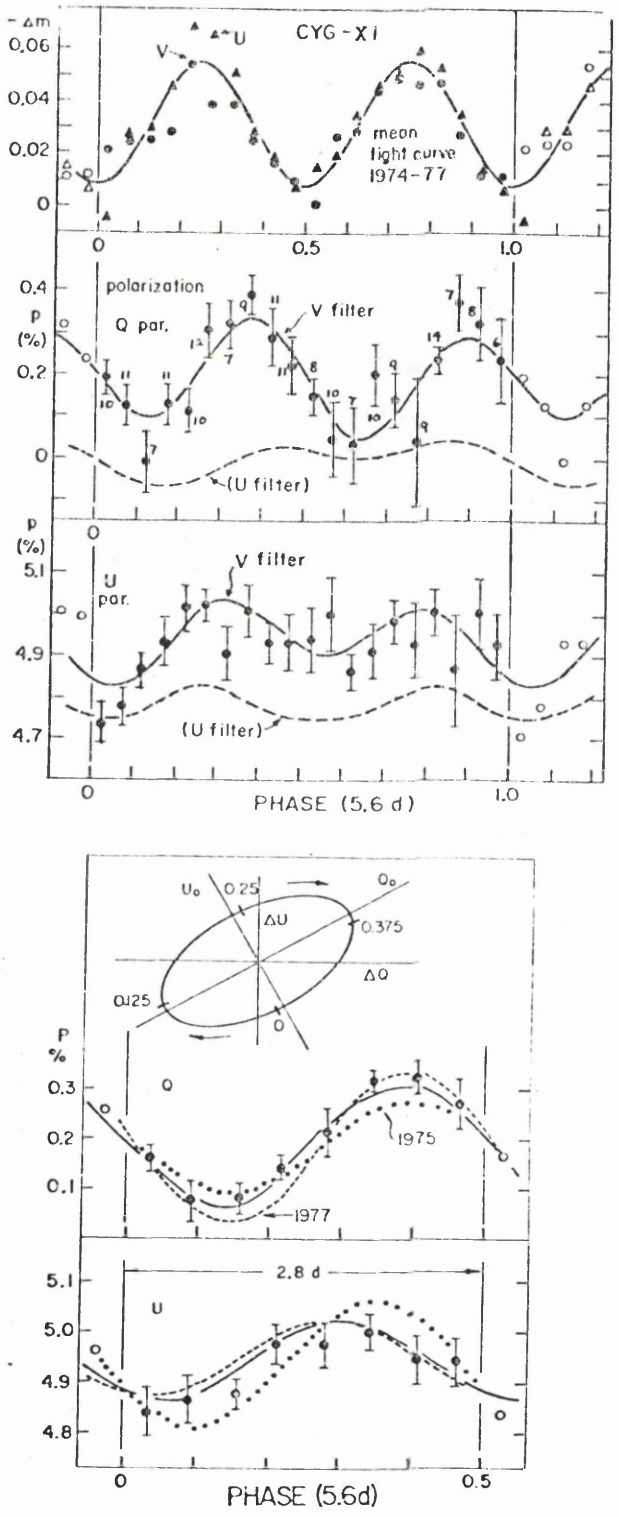

Figure 1.19 - Light curve and V band polarization (binned) variations for Cygnus X-1. The solid areas are the four parameter linear regression fit using 1st and 2nd harmonics with the dashed lines indicating the U band regression curves. The number of observations binned to obtain the mean points are shown above the data in the V filter P curves. Also shown is the U band Q,U variations folded into a 2.8 day period. The curves are the regressed 2.8 d sinusoids for differing data sets. The 2.8 day Q,U ellipse ($e \sim 0.91$) is also shown. (After Kemp et al. 1978)

be caused by simple reflection or scattering by a symmetric gas stream, hence the dominant nature of the second harmonic. The wavelength dependence of the variations was also seen to be contrary to those previously established (i.e. for β Lyrae the U band polarization was seen to be larger than in the V band). One possible explanation of this rests on the origin of the radiation lying in a cool ($T \lesssim 10^4 K$) object, with reduced UV emission. Infrared polarization observations by Belofsky et al (1978) have indicated the amplitude of variations at 2.2μ are comparable in size to those at 5500 Å i.e. in the V band (but not significantly greater). Since only 8 nights observations were taken, phase coverage was too incomplete for detailed analysis of the IR structure. Their results are consistent with the above ideas with the emission peaking at longer λ than the UV .

Further analysis of observations to establish a 39/78 day periodicity in Cygnus X-1 was published by Kemp et al (1978b). In this the existence of longer period variations in optical photometry, U band polarimetry, radial velocity curves and X-ray data was discussed. The V band polarimetric data of Kemp et al was seen to exhibit a 39 day periodicity with the X-ray data of Holt et al (1976) (2-6 keV) and U band photometry of Nolt and Kemp possibly containing a contribution from a 78 day period. Optical photometry in both B and V bands produced no long period variations. The radial velocity data (Abt et al 1977) permitted a third body of mass $\lesssim 1\ M_\odot$ (the variations in radial velocity were ~ 4 kms^{-1} at 78.4 days and 2.8 kms^{-1} at 39.2 days). Phase binned plots on a 78.4 day period of the V filter photometry, X-ray flux and V filter polarimetry are given in Figure (1.20) intending to lend support to the existence of this long period. Three possible explanations of periods so long compared to the orbital period were presented, related to variations caused by (a) a third star (Mazeh and Shaham 1977) (b) a precessing accretion disk (Katz 1977) and (c) a stellar pulsation (Wolff and Kondo 1978). Further discussion of the third body hypothesis was given by Kemp et al (1978b).

More data were added to the previous observations in Kemp et al (1979). The collective data set then numbered 348 observations spanning 3 years and a phase binned analysis in terms of a heavily eclipses 'hotspot' scattering region (heated by reflection) on an accretion disk was presented. The phase binned (5.6 d. period) mean points are shown

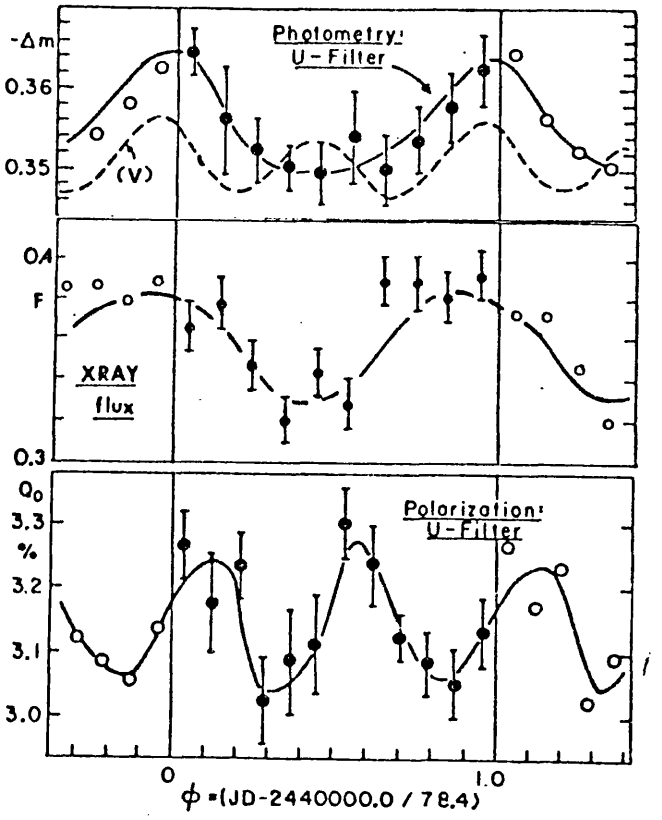

Figure 1.20 - Cygnus X-1 - U Band photometry, X-Ray flux and U band polarimetry folded (and binned) onto a 78.4 day period. This was done in an attempt to establish a long period variation in the system. A model involving a third body was proposed and variations at the assumed orbital period were thought to be observed in the U band polarimetry. (After Kemp et al 1978).

in Figure (1.21a) for the V band polarimetry (315 pts) observations. A composite mean light curve (U,B and V band) by Lester et al (1979). Kemp et al (1978a), Walker and Quintanilla (1978) and Lester et al (1976) was used in addition to the polarimetric data in modelling the binary. The Q,U locus is shown in Figure 1.21b with the solid curves indicating a 20 harmonic Fourier analysis of the data, arbitrarily smoothed by a displaced Gaussian function $\exp(-(n-1.5)^2/A)$ where n is the number of the harmonic (n=2, second harmonic). A, an arbitrary constant was given the value 7. Only harmonics above n=2 were smoothed by this method. The model prediction with an inclination $i \sim 65^\circ$ is also shown. This model, of geometry shown in Figure (1.21c) is based on the reflection mechanism mentioned previously where scattering takes place in a region situated on the inner face of the secondary body, in this case an accretion disk. Obscuration of the scattering region takes place by the secondary (disk) at certain phases (Φ - 0.4 to 0.5), the region being assumed never to be eclipsed by the primary component. The apparent slight asymmetry (i.e. the shoulder at phase 0.9) in the light curve would also be explained by such a model.

Details of this model were given in a further paper (Kemp (1980).

In this paper Kemp discusses the standard accretion disk model of Shakura and Sunyaev (1973), Novikov and Thorne (1973) and Pringle and Rees (1972) in an attempt to establish the physical size and detailed geometry of the accretion disk he proposed for Cygnus X-1. The detailed geometry of the accretion disk invoked is shown in Figure (1.21d). The main physical arguments presented stem from the fact that Kemp's accretion disk/scattering hot spot model, mentioned above, needs exceptionally thick outer regions of the disk to allow occultation of the scattering region (see Figure 1.21d). Apart from the standard disk models, mentioned above, Kemp includes radiative heating and heating by the primary to increase the thickness of the disk to a value consistent with the inner eclipse model.

The main consideration Kemp has seen to be to justify his polarimetric observations in terms of the thick accretion disk model. He states that the Hβ light curves of Guinan et al (1979) have not been quantitatively analysed (even though he uses them as evidence

Figure 1.21 (a) Q,U variations with phase in the V band for Cygnus X-1. Some 318 points have been folded and binned (40 bins) to obtain the mean points shown. The resulting error bars are due to binning and observational error.

(b) Q,U locus of the above data. The solid line is the smoothed data locus found by applying a displaced Gaussian smoothing function to $n > 2$ harmonics. The dotted line is the Q,U locus predicted by the model invoked.

(c) Schematic representation of the model for the variations seen in the V band polarimetry of Cygnus X-1. Scattering of light from the primary (hatched) occurs in an accretion disk (preferrentially in a hotspot region) with variable occultation of the hotspot occurring as the orbit progresses.
(After Kemp et al 1979)

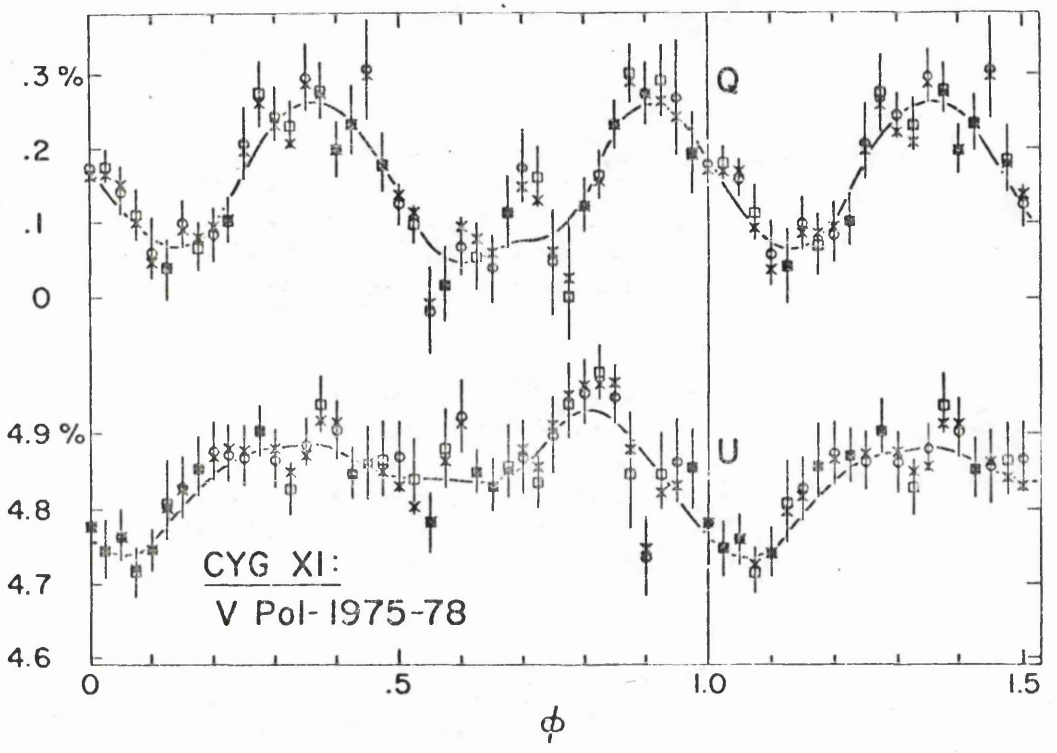
a)
.3 %
.2
.1
0
4.9 %
4.8
4.7
4.6
Q
U
CYG XI:
V Pol- 1975-78
0
.5
1.0
1.5
φ

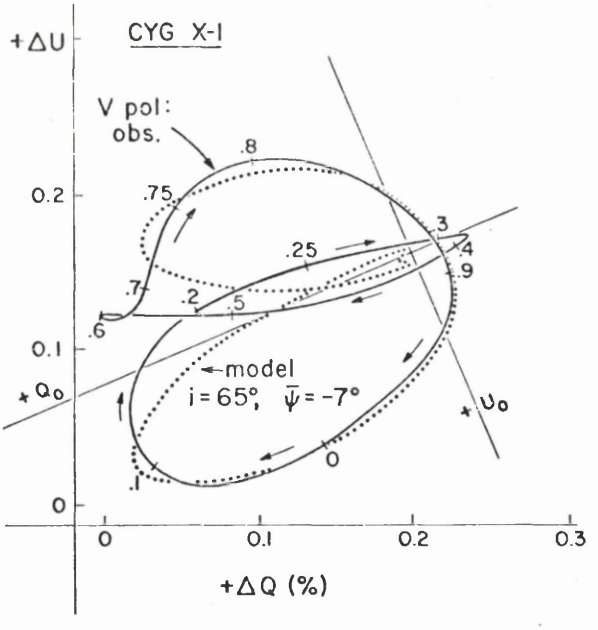
b)
CYG X-I
+ΔU
V pol:
obs.
model
i = 65°, ψ̄ = -7°
Q₀
U₀
+ΔQ (%)
0
0.1
0.2
0.3

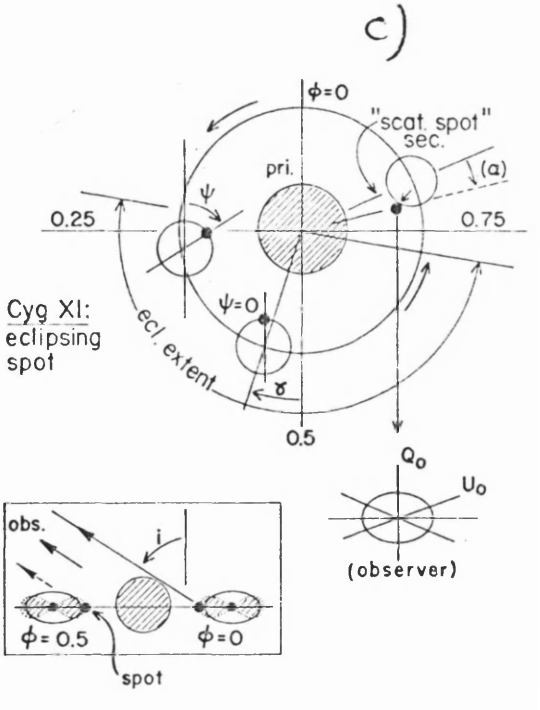
c)
φ=0
"scat. spot"
sec.
pri.
(a)
ψ
0.25
0.75
ψ=0
Cyg XI:
eclipsing
spot
ecl. extent
γ
0.5
Q₀
U₀
(observer)

obs.
i
φ = 0.5
φ=0
spot

for the inner eclipse phenomenon) but that they are 'probably also consistent with the indicated disk edge height'. The scattering region producing the observed polarimetric variations is sketched in Figure (1.21e). The claims that mass inflow takes place in a narrow gas stream from the primary and that at interior radii (a) the standard models of Shakura and Suryaev (1973) hold. In the outer regions other aspects (see above) come into play and there is surface evaporation and vertical streaming of material. A large ionized region is proposed as existing on the inner edge of the disk face, strongly heated by the primary: and is the source of the eclipsed polarized light observed by Kemp. Kemp also asserts that due to the absence of strong modulation of the X-ray flux (assumed to come from the central region of the disk i.e. the compact object secondary) as seen by Holt et al (1976) and, he claims, the necessity of the inner eclipse to produce the polarization variations and Balmer emission features observed (Kemp et al 1979, and Guinan et al 1979), an inclination in the range 55° to 60° is necessary. This model was invoked because Kemp assertsthat the canonical model does not fit the data. This is reconsidered in Chapter 2. It merely remains to be said that such complicated models should only be considered once simpler ideas have been found incapable of explaining the observations satisfactorily.

Still more data was presented in Kemp (1980) in a reply to a paper (Simmons, Aspin and Brown 1980) on the simple model for polarimetric variations of Brown, McLean and Emslie (1978). This data involving some 528 nights observations is shown in Figure (1.22). Further reference to this paper will be given in Chapter 2 where the work of Simmons, Aspin and Brown will be discussed.

Because of its intrinsic interest Cygnus X-1 has therefore been one of the most comprehensively observed binaries polarimetrically. In retrospect however, this circumstance may have been disadvantageous to the development and acceptance of polarimetric techniques and observations due to the particularly complicated nature of Cygnus X-1 data implied by many varying observations. This complexity may render its polarization variations too complex to interpret in terms of the simple phase locked models proposed. Our later results suggests that a similar effect on other binaries might have been more fruitful.

Figure 1.21 (d) Geometry of the Cyg X-1 system, scaled to the mean parameters adopted in the model discussion. The top view of the accretion disk in middle left indicates qualitative particle-orbit shapes based on Paczynski (1977). Lower sketch distinguishes between mechanical or density heights h, h'; and "optical" H, H'. The primed heights represent schematically the outer flaring due to primary illumination.
(After Kemp 1980).

Figure 1.21 (e) An attempt to picture qualitatively the disk shape, especially as relates to the mass flow and the feed-in point of the gas stream. The primary is to the right. A diffuse region, thought responsible for the "inner eclipse" effect in the polarization and Balmer-line emission, lies inside the disk facing the primary.
(After Kemp 1980).

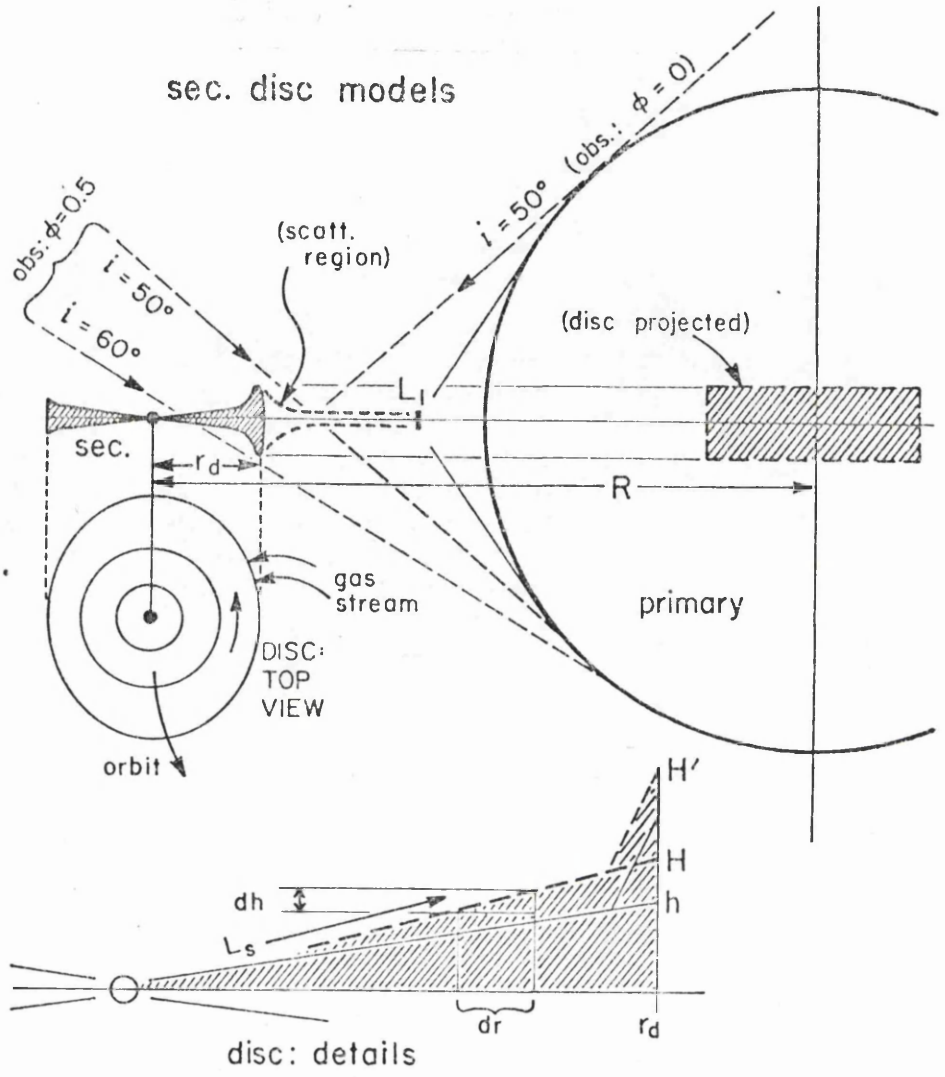
sec. disc models
obs: φ=0.5
i = 50°
i = 60°
(scatt. region)
i = 50° (obs.: φ = 0)
(disc projected)
L1
sec.
rd
R
gas stream
primary
DISC: TOP VIEW
orbit
H'
H
h
dh
Ls
dr
rd
disc: details

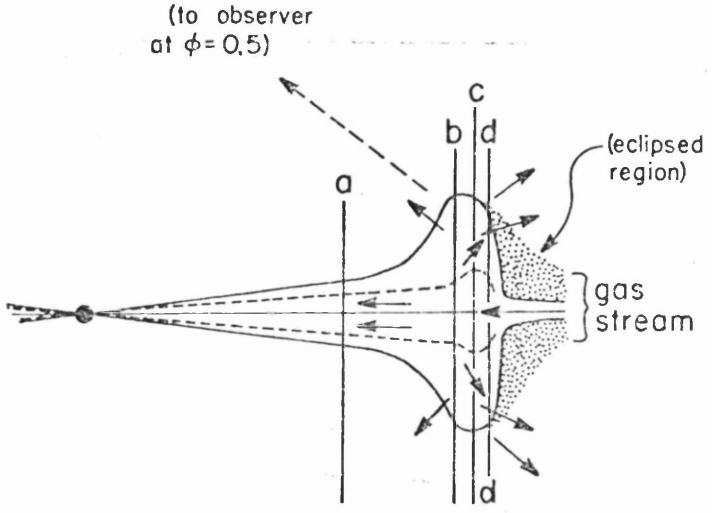
(to observer at φ = 0.5)
c
b
d
a
(eclipsed region)
gas stream
d

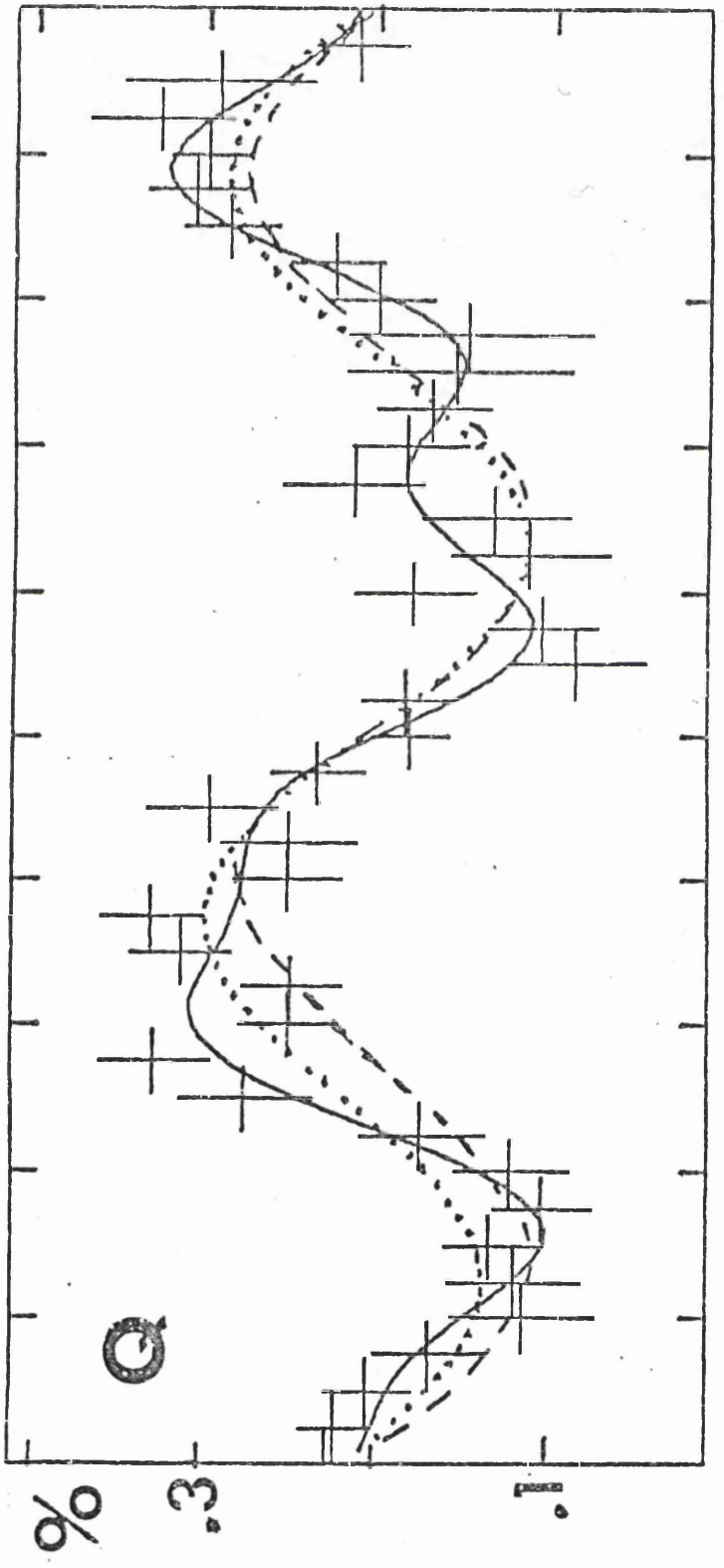

Figure 1.22 - V band Q(a) and U(b) variations of polarization for Cygnus X-1 with phase. The data involving 528 observations taken from 1975 to 1980 has been folded and binned on the 5.6 day orbital period. Error bars and curves indicating the 2nd harmonic (dashed line), 1st and 2nd harmonic (dotted line) and first 5 harmonic (solid line) 'best fits' are shown. (After Kemp 1980).

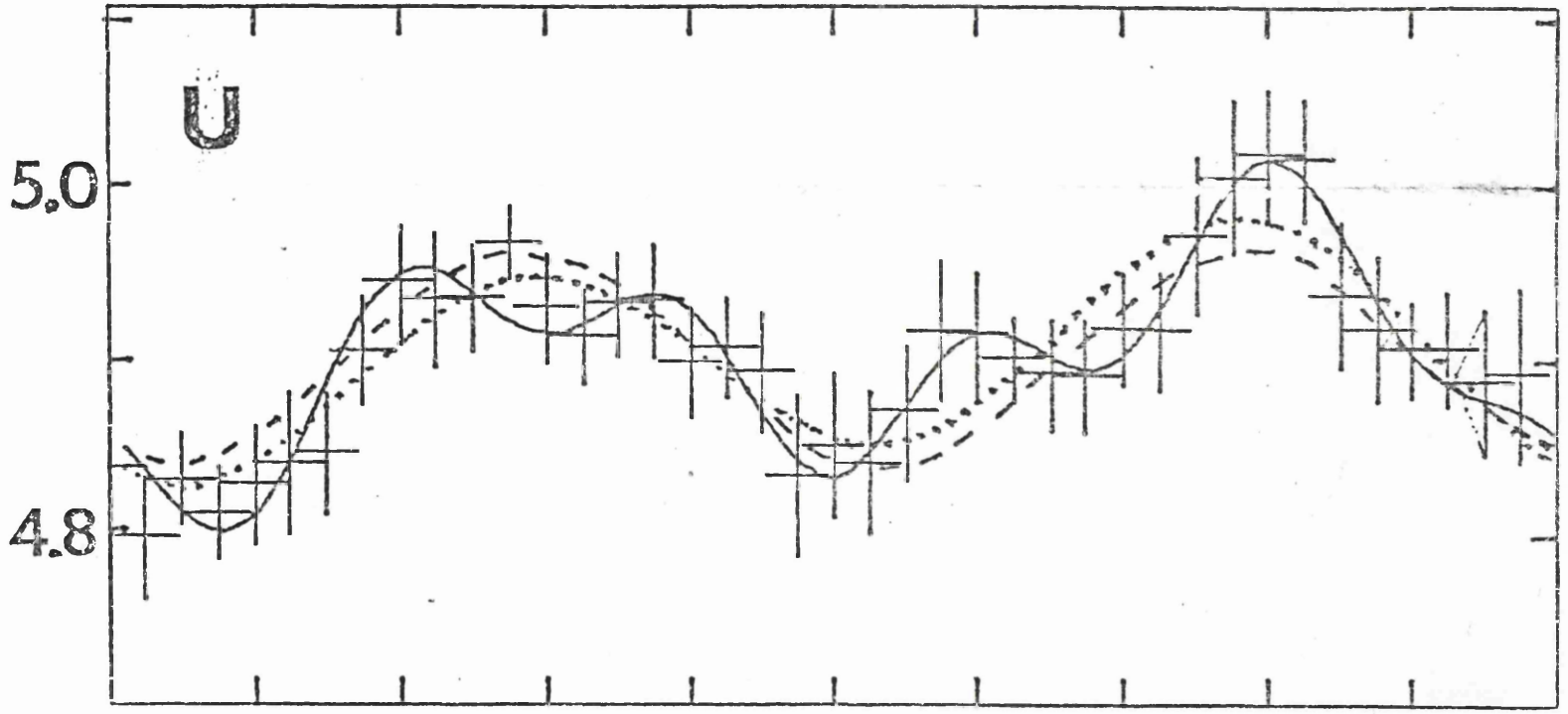

b)

Other independent polarimetric observations have also been made of Cygnus X-1. Dolan (1972, 1974, 1977) has observed Cygnus X-1 intermittently over many years. His data however fails to compare with the observational achievement of Kemp et al in their continued program.

We now consider the work on polarimetric observations of binaries inside the eclipse phase by Piirola, as an alternative way of proceeding with polarimetry of binaries.

1.7 Observations and interpretation of polarimetric binaries during eclipse.

While most of this thesis is concerned with binary diagnostics based on the variation in light scattered in rotating envelopes, we describe briefly here another important technique of analysis applicable to the effect of eclipses (cf. modelling of photometric light curves in and out of eclipse). This technique pioneered by Piirola at Helsinki involves observing the binary at times of eclipse and, with comparison to details of the light curve at similar phases, interpretation of the variations observed in terms of mass transference etc. The only system for where this has been comprehensively achieved is the semidetached binary U Cep(Piirola 1980).

Intrinsic polarimetric variations were first discovered for this system by Piirola (1975a). A large increase of polarization was observed during primary eclipse presumably due to reduction by the eclipse of the depolarized direct light of the primary, to the polarized fine scattered in an circumstellar envelope. This envelope was probably related to the spectroscopic and photometric outburst reported in 1974-75. (Batten et al 1979, Plavec 1974, Rhomb and Fix 1975). Qualitative interpretations (by the aforementioned authors) of this outburst were related to the sudden increase in size of the primary and the formation of a ring or disk around it. The polarimetric observations made on a 60 cm Ritchey Chretion telescope at Helsinki using a polarimeter designed by Piirola (1973, 1975a) were in the B filter. A total of 485 observations were made on 37 nights (cf. Piirola 1977, for details) covering some 20 primary eclipses. Figure (1.23a) shows a sample of the observations in terms of the degree

Figure 1.23 - (a) Example of the polarimetric observations of U Cep during eclipse by Piirola. Variations in polarization and position angle are clearly seen.

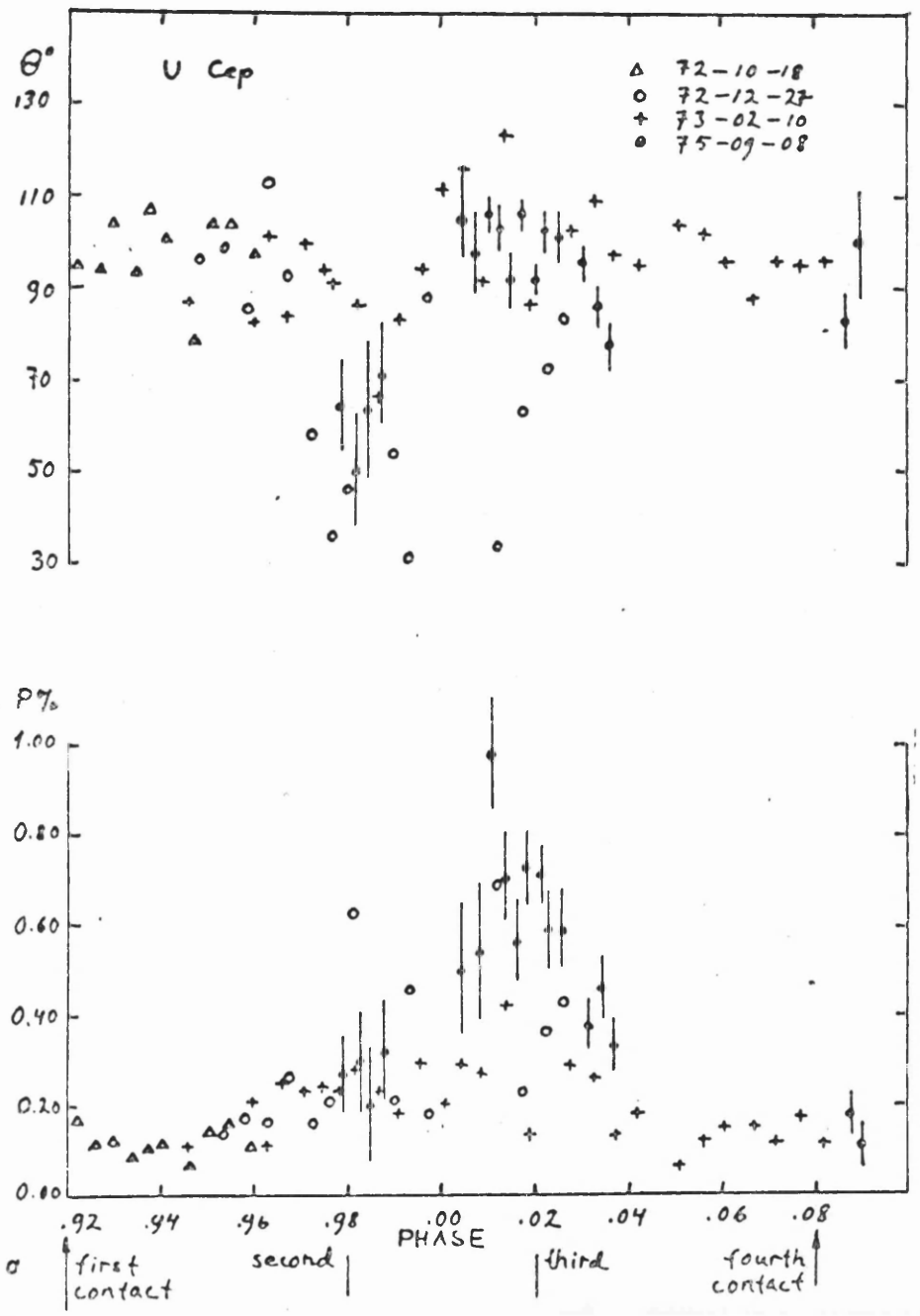
θ°
U Cep
72-10-18
72-12-27
73-02-10
75-09-08
130
110
90
70
50
30
P%
1.00
0.80
0.60
0.40
0.20
0.00
.92
.94
.96
.98
.00
.02
.04
.06
.08
PHASE
a
first contact
second
third
fourth contact

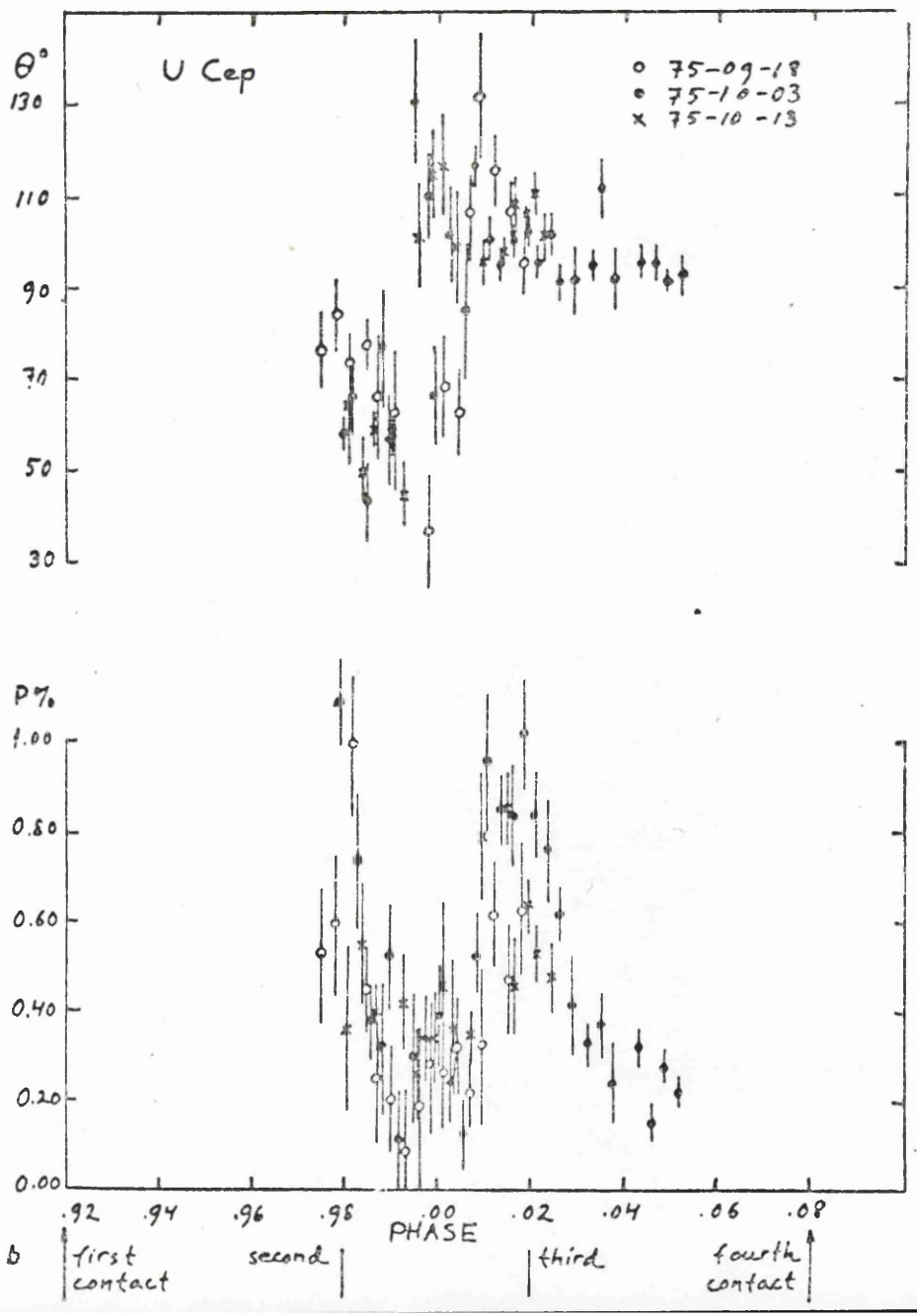
θ°
U Cep
75-09-18
75-10-03
75-10-13
130
110
90
70
50
30
P%
1.00
0.80
0.60
0.40
0.20
0.00
.92
.94
.96
.98
.00
.02
.04
.06
.08
PHASE
b
first contact
second
third
fourth contact

of polarization p and position angle θ here covering the period October 1972 to October 1975. The major features of these curves are: the increase in the degree of polarization near second contact of the eclipse (commencement of total eclipse), then the decrease towards mid eclipse with an increase again towards third contact (end of total eclipse). The overall structure of the polarization variations is seen to change over the observing period (i.e. the pattern of the polarization curves changed). The model used in qualitatively explaining the polarization variations is that of Hall and Walter (1974). This involves, at times of eclipse, a small primary totally eclipsed by the secondary with part of the circumstellar material visible at different times during the eclipse. Theoretical (Predergast and Taam 1979) and observational (Hall and Walter 1974 and Walter 1975) evidence for the nature and positioning of such material was also quoted by Piirola (1980). Much of the discussion in the paper by Piirola (1980) is of a qualitative nature involving explanations of the changes of polarization observed as the eclipse progresses. Mean curves covering the eclipse period ($\Phi \sim 0.9 \rightarrow 0.1$) are also shown in Figure (1.23b) and are in terms of the Stokes parameters Q and U (instead of p_X, p_Y). Large changes in the shape of the primary eclipse light curve were observed at times when changes in the polarization curve were seen. These photometric variations were also independently explained in terms of a circumstellar disk by Olson (1976). Model calculations involving such a geometry however do not explain all the photometric and polarimetric variations observed. (The assumptions of the model used include optical thinness of the disk and a hotspot on the primary). Intermediate partial optical thickness of the material and an increase in size of the primary by $\sim$ 15% $\rightarrow$ 20% during mass exchange periods was found to satisfactorily explain some of the features of the observed polarization variations (Piirola 1979b).

A spherical outer envelope of size $\sim 1.1\ R_B$ the radius of the primary and an equatorial disk of outer radius $1.7 \times R_B$ are used in theoretical calculations producing results that agree well with observations. An orbital inclination of $\sim 83^\circ$ is also needed to explain variations in the position angle of the polarization. Figure 1.23c shows the mean points (binned value of observations)

Figure 1.23 - (b) Mean curves (binned) for U Cep over all observing periods. Q,U (i.e. P_x, P_y) variations, degree of polarization and position angle changes are all shown.

1.23b

b)

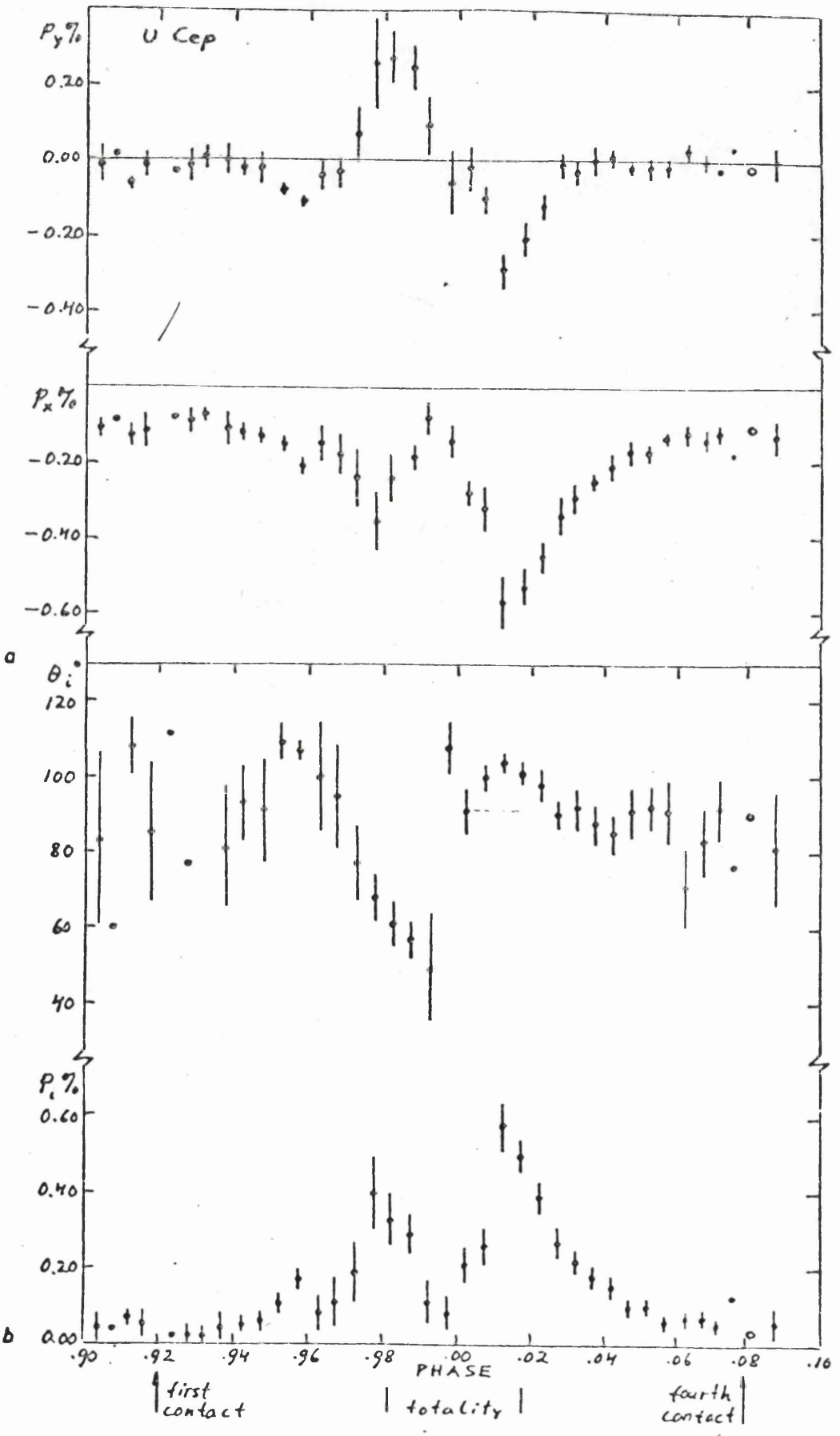
U Cep
P_y %
0.20
0.00
−0.20
−0.40
P_x %
−0.20
−0.40
−0.60
a
θ_i °
120
100
80
60
40
P_i %
0.60
0.40
0.20
b 0.00
.90
.92
.94
.96
.98
.00
.02
.04
.06
.08
.10
PHASE
first contact
totality
fourth contact

Figure 1.23 - (c) Binned Q,U variations and error bars with the fit of the model invoked by Piirola. The fit is seen to be a reasonable one. The model used involves scattering on gaseous material in the binary with variable eclipsing of the material occurring at various times of the phase interval 0.9 to 0.1. (After Piirola (1980) a,b).

23.c

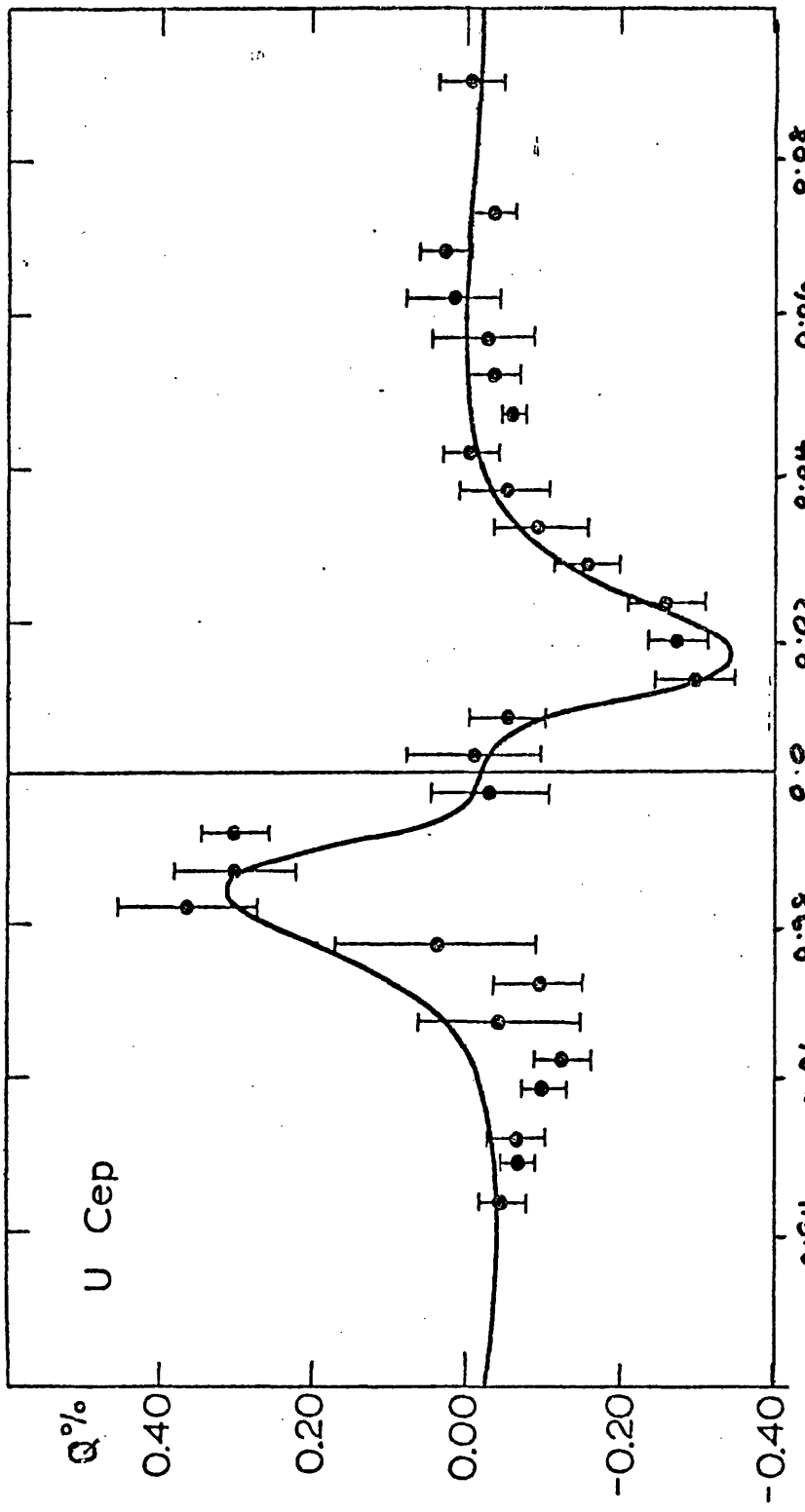

c)

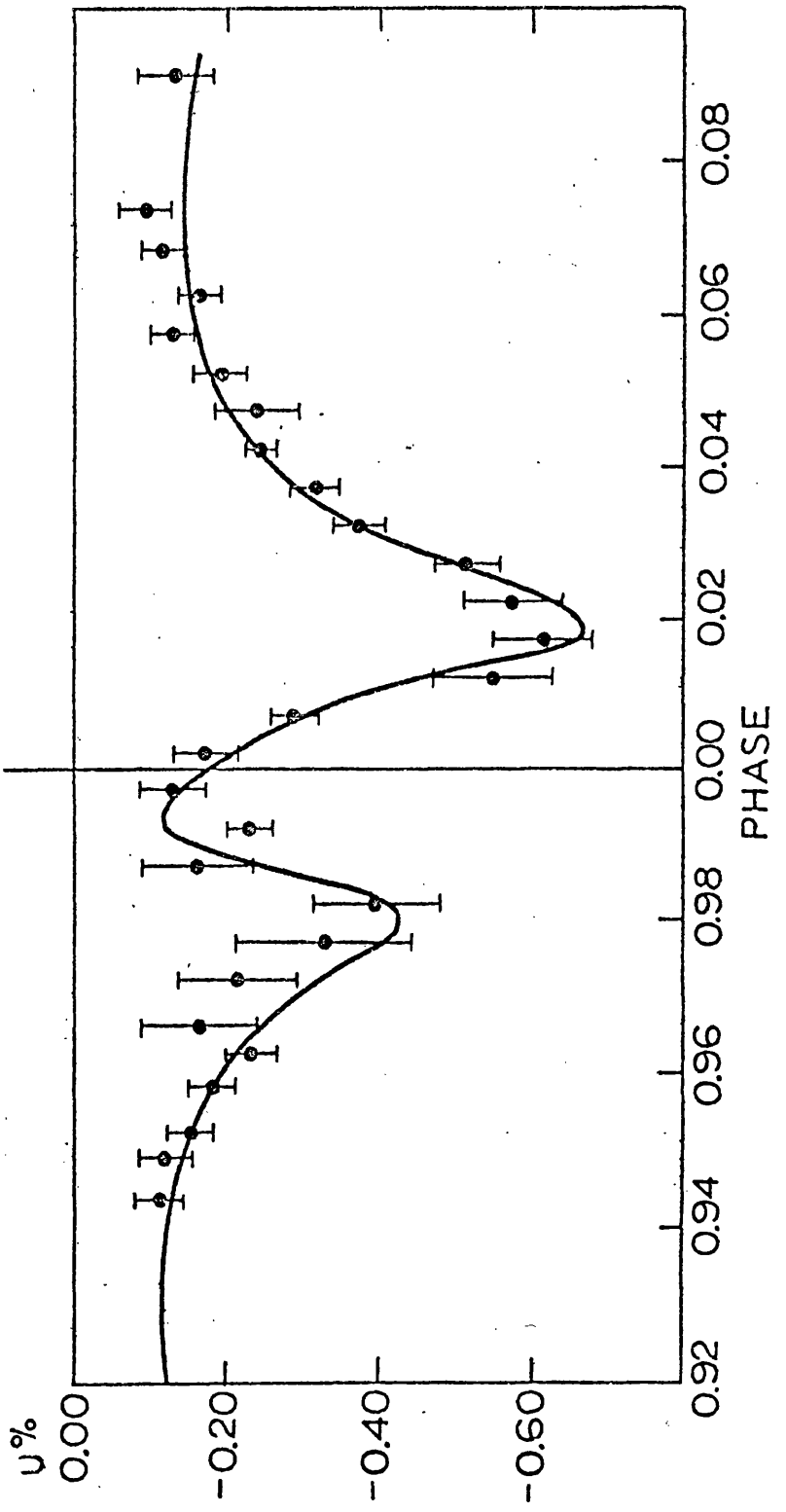

23 c

for the observing session September 1975 - October 1975 together with the above model's predictions. The agreement is seen to be reasonable.

Such modelling may not however be unique but nevertheless the technique of observing only during primary eclipse does seem to be informative and it appears that the values of derived parameters (such as i) are more sensitively determined by such eclipse data than in the non-eclipsing systems we consider.

1.7 Theoretical investigations of polarization production mechanisms

Various mechanism have been proposed over the last thirty-five years to explain the polarization (both constant and variable) observed in various astronomical objects. Some of these had been theoretically proposed prior to determining observational evidence of their existence whilst others have risen out of detailed observations of many sorts. The first mechanism we shall deal with here has been named the Chandrasekhar effect.

1.7.1 The Chandrasekhar Effect (Scattering in Stellar Atmospheres)

In the middle forties Chandrasekhar pioneered the way in calculating the transfer of energy in stellar atmospheres by radiation, i.e. radiative transfer). In paper X of a series (Chandrasekhar 1946) he calculated the transfer of radiation in an atmosphere governed by Thomson scattering on free electrons. He showed that the polarization of emergent radiation for the atmosphere depended on the law of darkening and differed by $\sim$ 25% from the edge to the centre of the disk. The degree of polarization of the emergent radiation was found to vary from 0% at the centre of the disk to $\sim$11% at the limb. The two states of polarization (polarized with the E vector in the meridian plane and perpendicular to that plane) were also found to vary differently with μ ($=\cos\theta$ where θ is the angle between the line of sight and the normal to the element on the disk considered). He also noted that under favourable conditions the polarization predicted may be observable in early type stars (i.e. those thought to have free electron envelopes).

These stellar types are in general rapid rotators and hence may not be spherically symmetric causing the polarization from different parts of the disk not to cancel and leaving a preferential plane of polarization. It was this paper that stimulated interest in the possibllity of detecting intrinsic polarization from stars. In particular eclipsing binaries containing early type components were observed with the hope that intrinsic polarization would be visible due to the asymmetry caused by the eclipse. The integrated light of spherical stars in eclipsing binaries (out of eclipse) would produce no polarization due to cancellation of the polarization from different parts of the stars surface. Eclipsing binaries were in fact close binaries in general, would however show polarization in eclipse as mentioned above, but also out of eclipse if significant tidal distortion of the components was present (again involving an asymmetry). Numerical calculations for actual atmospheres have been performed by Nagirner (1962) with a summary of the results by Shakhovskoi (1965). Atmospheres of O and B type stars based on models of Underhill (1957) were used with, for example, a maximum (local) degree of polarization (at the limb) of 2.1% for an O5 star and 3.3% for a B1.5 star being formed. According to Nagirner's calculations elipsoidality of the star less than $\sim \frac{1}{2}$ would not produce significant polarization anywhere on its disk. Shakhovskoi (1965) obtained a qualitative picture of the change in polarization during a partial eclipse of a spherical star using Nagirner's data. These are shown in Figure (1.24) with the numbers referring to degree of eclipse considered.

Buerger and Collins (1970) considered the polarization from a binary resulting from initially tidally distorted binary components. Two similar stars were assumed with a reflection/heating effect included for both components. Figure 1.25 shows their expected polarization variations with orbital phase when seen at various orbital inclinations. The maximum polarization expected in this case was found to be $\sim \frac{1}{2}\%$ at $i = 90^{\circ}$. This value decreased as the orbital inclinations became smaller. (Clearly as $i \to 0^{\circ}$ the amplitude of polarization P must go to zero while the θ variations would be uniform with phase, this situation being equivalent to simple rotation of the polarimeter).

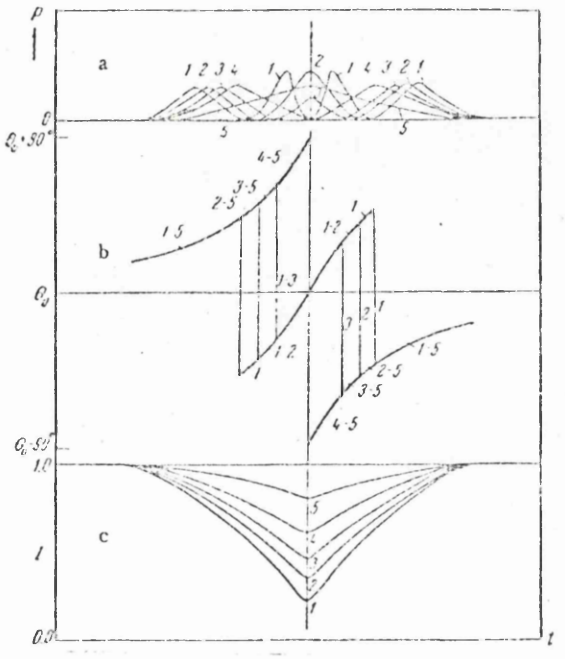

Figure 1.24 - Predicted changes of polarization and position angle together with light variations at times of a partial eclipse of a binary system. The intrinsic polarization variations are caused by a consideration of the eclipse and photospheric scattering (The Chandrasekhar effect). Numbers 1 to 4 indicate differing degrees of partial eclipse. The discontinuity at phase 0.0 is spurious. The jump of 180° in θ is in effect non-existent since $\theta = \theta + 180°$.
(After Shakhovskoi 1965)

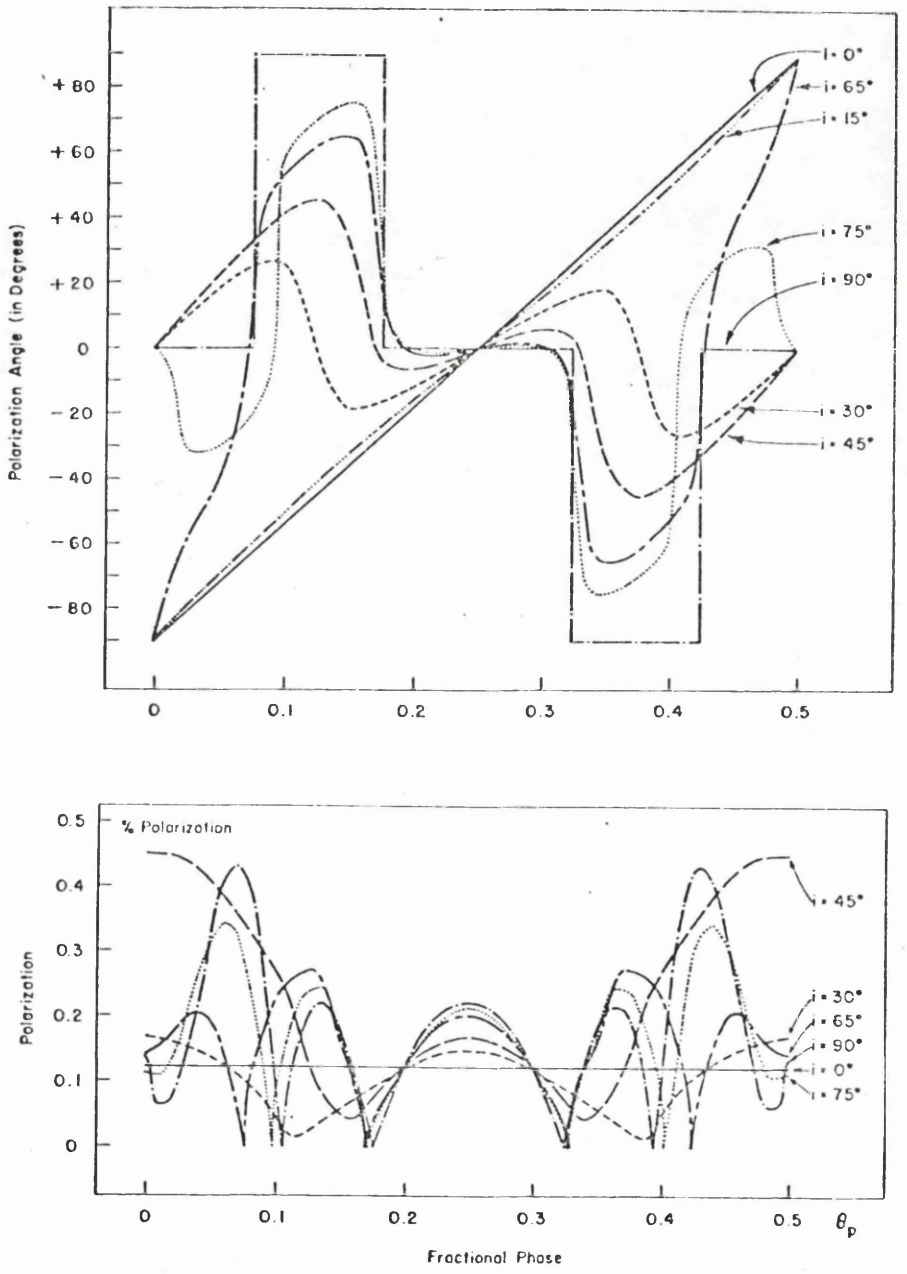

Figure 1.25 - Variations in polarization angle and degree of polarization with orbital phase and inclination predicted by a model involving a contact binary (of similar types) with polarization resulting from scattering in the atmosphere of the two stars.
(After Buerger and Collins 1970).

Cassinelli and Haisch (1974) also considered the resultant polarization of early type stars rotationally distorted and hence asymmetric. They, however, applied that results primarily to single stars (Be stars, Wolf-Rayet stars etc.). They considered both disk like envelopes and Roche type geometry and found polarizations as high as 6% for the disk and 2% for the latter Roche geometry. An interesting point to note in this paper is that they explained the polarization (wavelength variations) of HD50896 observed by Serkowski (1970) and Fellner and Serkowski (1972) in terms of their radiative transfer models. HD50896 has recently been proposed as being a Wolf-Rayet type binary system (Firmani et al 1979) and has been subject of detailed polarimetric observations by McLean (1980). Interpretation of these variations in terms of the models discussed in this thesis are presented in Chapter (8). These papers represent a sample of the work inspired by the Chandrasekhar effect. We shall now go on to consider the reflection effect.

1.7.2 The Reflection Effect

Dombrovskii (1960) showed how the scattering and radiation of light from a bright component on the atmosphere of a bright companion would result in a net polarization in the integrated light of binary system. The heated hemisphere introduces an asymmetry into the system and produces polarization variations as the aspect of the binary changes with the observations. The variations predicted are illustrated in Figure 1.26. In this figure we have re-evaluated, Dombrovskii's analytic expressions for the variations in degree polarization with phase at differing orbital inclinations. It is seen that the amplitude of P variations decrease as the inclination decrease and reach a constant level at $i \sim 0^{\circ}$. The plane of polarization will however then vary periodically with the varying positions of the stars (cf. above). This was acknowledged in Shakhovskoi (1965) as being a method of discovering binaries with low ($i \sim 0^{\circ}$) inclinations.

Collins and Buerger (1974) calculated the polarization resulting from illumination of a stellar atmosphere as an external point source. This can be considered in some cases analogous to a hot binary component illuminating the near side of a cool companion i.e.

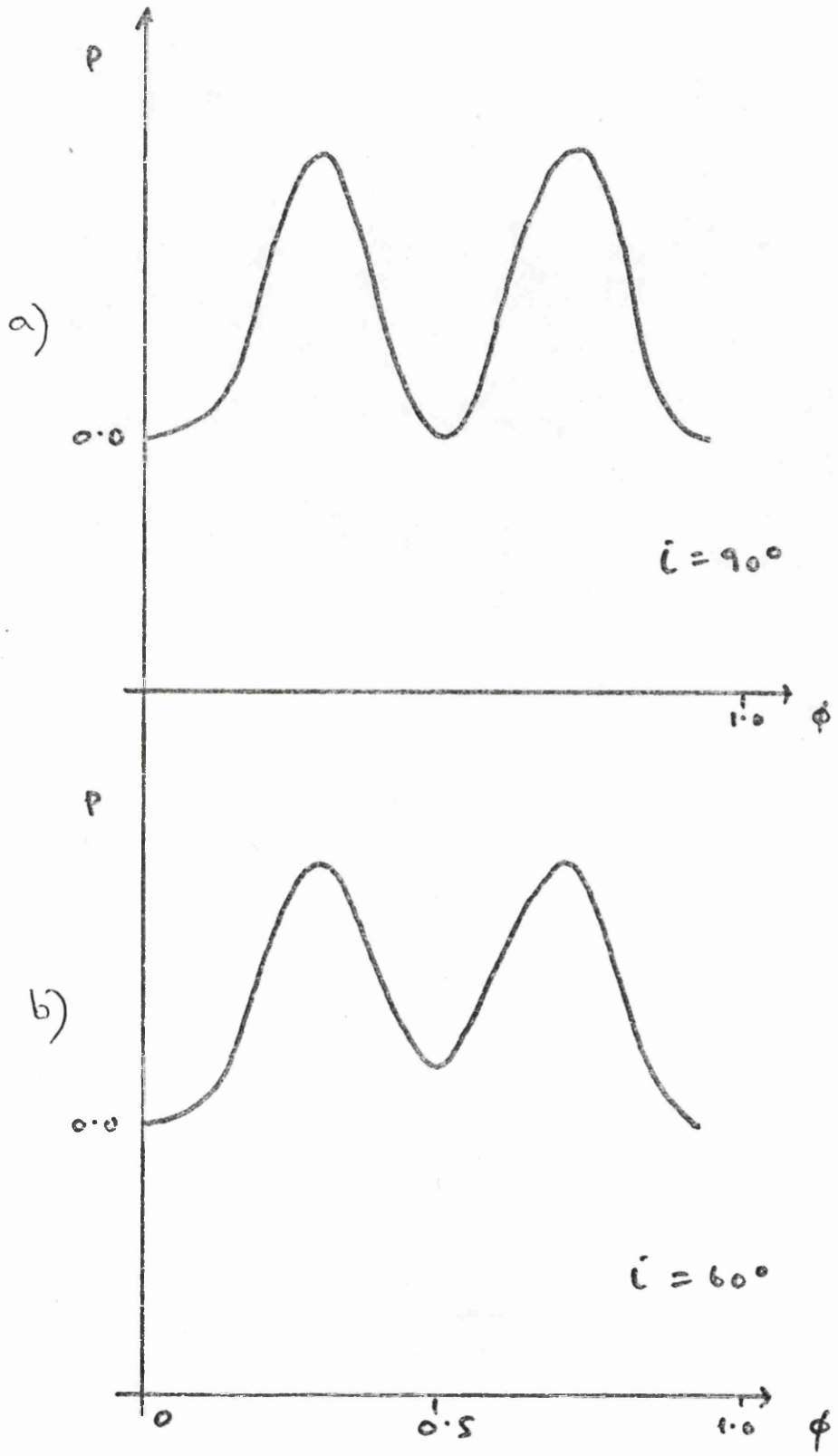

Figure 1.26 - Variation of degree of polarization of binary system with increasing phase due to the reflection effect predicted by Dombrovskii (1960). Curve (a) is for inclination i = 90°. (b) i = 60°; (c) i = 45° and (d) i = 0°.

26c

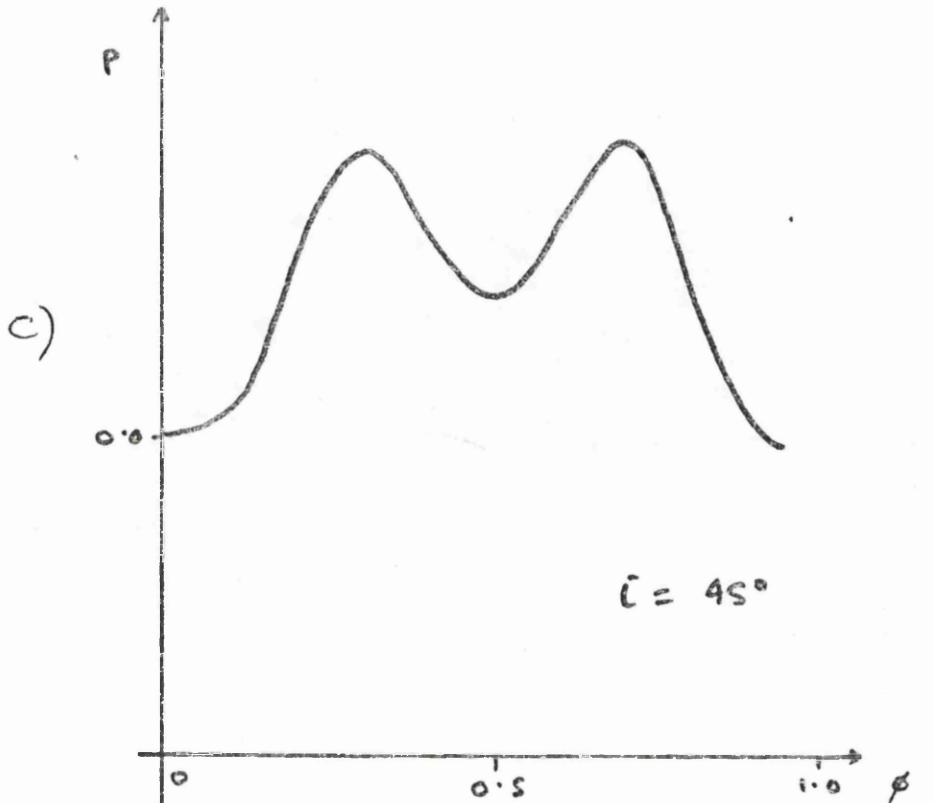

26d

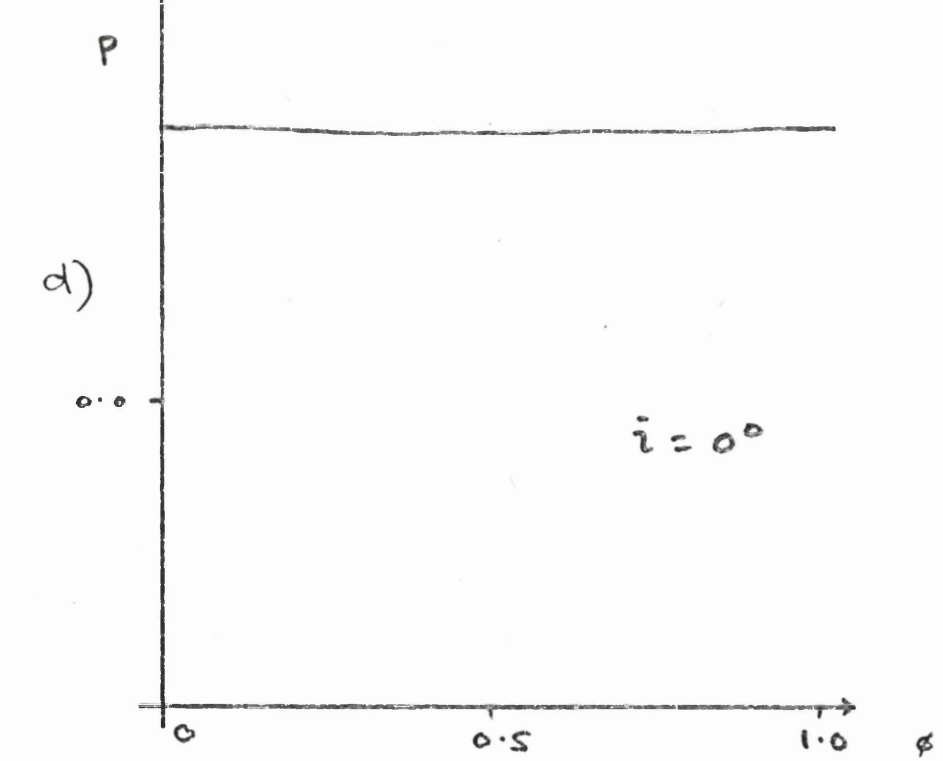

causing the so called 'reflection effect'. They calculated a limb polarization of $\sim$ 2% for a relatively cool star ($T_e \simeq 10000K$). Rudy and Kemp (1977) used this idea in interpreting the polarization variations observed in the system u Her. Two criteria must be met to obtain polarization effects sufficient for observation. These are that the hotter star must (1) produce sufficient UV light to ionize a significant portion of the cooler star's envelope hence creating free electrons for scattering of optical radiation, and (2) must produce sufficient visible light to compete with the photospheric radiation of the secondary. The polarization will thus be strongest at those wavelengths at which the hotter star produces significantly more radiation (to be scattered) than the cool star. This radiation will be strongly anisotropic due to the unidirectional nature of radiation (i.e. towards the cool star from the hot star). Rudy and Kemp produced a simple "skeletonized" model for such variations which is seen to reproduce the observed variation reasonably accurately. A schematic representation of the model was shown earlier in Figure (1.13b). Whether this model is unambiguous was not considered however. Later in this thesis an alternative model will be applied to uHer data in an attempt to investigate this question.

A theoretical study of ellipsoidality in close binaries was made by Gnedin et al (1976). In this paper refers specifically to X-ray binaries they also considered the question of the effect of a hotspot on the surface of the optical ellipsoidal component. The ellipsoidal nature of the optical star and the 'hotspot' were considered results of the closeness of an X-ray emitting compact companion. Tidal distortion would cause the ellipsoidality and X-ray heating in the optical star atmosphere (reflection of X-ray) would result in a hotspot. Their figures for the difference between the polarization curves with no hotspot and those with a significant hotspot are shown in Figure (1.27a). The curves are symmetrical over each half of the orbital phase and hence are only shown in phases 0° to 180° (i.e. $\Phi \sim 0.0$ to 0.5). Q,U loci for a similar hotspot + ellipsoidality combination are shown in Figure (1.27b) for inclinations $i = 0^\circ, 30^\circ, 60^\circ$ and 90°, and a mass ratio $q \sim 0.7$.

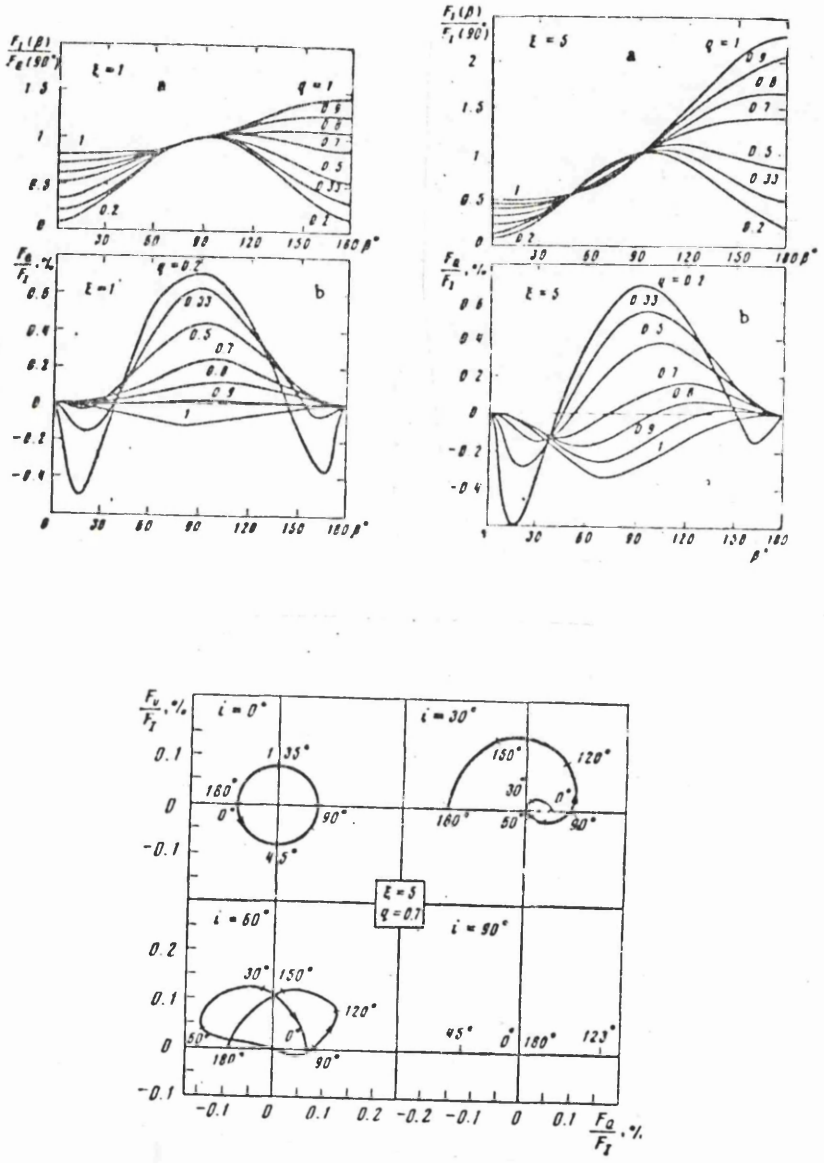

Figure 1.27 - The change in radiant flux and polarization when a hotspot is introduced into a model of a binary system involving an ellipsoidal component. The top diagram (ξ = 1) shows the polarization changes with phase for just an ellipsoidal star while at the bottom (ξ = 5) a hotspot on the surface of the ellipsoidal star is introduced. A range of mass ratios of q (0.2 to 1.0) are shown in each case. The compared Q,U loci are shown for the hotspot at inclinations i = 0°, 30°, 60° and 90° and q = 0.7.
(After Gnedin et al 1976).

These examples of the reflection effect and related phenomena producing polarization variations in the integrated light of binary systems show an alternative method of production of such changes. A third mechanism considered in the literature as a potential producer of linear polarimetric variations in binaries is one involving scattering on circumstellar gas in the form of envelopes, shells, disks or streams or infact a combination.

1.73 Scattering in Gaseous Circumstellar envelopes

This mechanism was first suggested as being a potential producer of polarized light variations in binaries by Shakhovskoi (1962) and Shulov (1962). A more detailed consideration was made by Shakhovskoi (1965). Here is an attempt to explain the observations of β Lyrae, in which he made a qualitative study of the effect causing the variation. Three basic factors were considered that would effect the size and position of the binary polarization. Those were a change in the ratio of envelope radiation to the total light of the system (variation of "luminosity" of the stars), an eclipse of part of the scattering region, causing a change in scattering geometry, and the presence of small concentrations whose scattering angle would vary as binary phase increase. For eclipsing binaries (those that Shakhovskoi was interested in) the first factor would probably dominate the variation, due to the large change in light at times of primary eclipse ($\Delta M \sim 2$ mag.) all proceeded to estimate the degree of polarization from such a binary under the assumption of Thomson scattering in an optically thin envelope with a thin ring geometry.

The Stokes parameters in this case for a given small element value of the ring can be expressed as

$$I = k(1 + \cos^2 \psi)$$
$$Q = k \sin^2 \psi \cos^2 \phi$$
$$U = k \sin^2 \psi \sin^2 \phi$$

where k is a constant ($k = \sigma_o n_e I_o dw$), σ_o scattering cross section, n_e the electron number per scattering volume and $I_o dw$ is the intensity of variation incident on that volume. ϕ is the position angle of the plane of scattering and ψ is the scattering angle. The degree of polarization $\bar{P} = \sqrt{\bar{Q}^2 + \bar{U}^2} / \bar{I}$ where the barred quantities refer to the

mean values of the Stokes parameters. Both ψ and ϕ are expressed in terms of the position of an element of the ring (designated α) and the orbital inclination i via the relations:

$$\cos \psi = - \cos \alpha \sin i$$
$$\cos (\phi - \phi_o) = \sin \alpha / \sin \psi$$

For $\phi_o = 0$ (zero point of position angle taken as normal to orbit).:

$$\bar{I} = \frac{k}{2} (2 + \sin^2 i)$$

$$\bar{Q} = \frac{k}{2} (\sin^2 i)$$

$$\bar{U} = 0$$

These equations are derived by substitution of the relations (2) into (1) and integrating over all α($0 \leq \psi < 2\pi$). $\bar{P}$ is therefore given by:

$$\bar{P} = \left(\frac{\sin^2 i}{2 + \sin^2 i} \right)$$

and depends only on the orbital inclination i. For $i \sim 90^o$ it is seen that $\bar{P} \sim \frac{1}{3}$. The plane of vibration of the polarization is that of the normal to the orbit. Variations in this polarization would occur at times of eclipse (i.e. the direct flux from the system decreases). At these times P will be related to $\bar{P}$ by the equation: $P = \bar{P} \frac{1}{\ell}$ where ℓ is the relative brightness of the system during eclipse. Shakhovskoi (1965) also noted that higher polarizations may occur for a different geometry(in particular the mentioned gas streams).

A arbitrary density distribution (scattering geometry) was considered theoretically by Brown, McLean and Emslie (1978). Two point sources of radiation were considered and general expressions for the Stokes parameters derived. The explicit dependence of these relations on inclination was established and a simple method of determing orbital inclinations from observed polarimetric variations was discussed. This paper forms the starting point of the work presented in this thesis and will be dealt with fully in Chapter 2. The basic assumption of this model should however be noted here,

namely (1) corotation of the scattering region and light source(s) (a stationary scattering geometry would therefore appear in the frame rotating with the system); (2) Thomson scattering in an optically thin arbitrary envelope (1st order scattering only); (3) no variable obscuration/eclipse effects of either light source or scattering region (variability only therefore due to changing aspect of binary). Various extensions to this work have been made in recent years. Rudy and Kemp (1978) investigated the effect of an extended light source (as opposed to point sources in Brown, McLean and Emslie 1978) under the addition assumption, however, of an orbital plane symmetric scattering envelope. Details of this will also be given in Chapter 2. Additional work on this problem was presented by Milgrom (1979) who considered the effect of an arbitrary radiation field and distribution of scattering and by Daniel (1978, 1980) who included multiple scattering by Monte Carlo methods but only for simple envelope geometries.

Daniel (1980a) presented this for envelopes illuminated by a single star at their centres (or an extension of previous work by Brown and McLean 1977) and was generalized to binary systems in Daniel (1980b), in particular the system Cygnus X-1 was investigated. An optically thick prolate ellipsoid (Roche lobe geometry) was assumed, and a comparison of the model predictions for both the photometric and polarimetric light curves and data (of Kemp) indicated reasonable agreement. Figure (1.28) shows the fit to Kemp's polarimetric data for a model involving an ellipsoid defined by E_1, E_2, optical depth $\tau \sim 2$ and $i \sim 73^{\circ}$.

This section has briefly outlined theoretical modelling undertaken regarding the polarization variations, observed in the integrated light from binary systems, by scattering of gaseous material present in a system. Before proceeding to the next Chapter it remains to note another proposed model for production of polarization variations in a binary system, in particular an X-ray binary containing a black hole component.

1.7.4 The Polarimetric (Gravitational Lens) signature of a Black Hole

Dolan (1977) presented a qualitative study of the polarimetric variations one may expect to observe due to the presence of a black

Figure 1.28 - Kemp et al (1979) observations (light curve and Q,U variations) of Cygnus X-1 with Daniel (1980) and best fit model curves. The model used includes multiple scattering in an optically thick ellipsoidal envelope. A phase shift of 0.05 relattive to the light curve fit is required in the polarimetry to obtain the 'best fit'.
(After Daniel 1980)

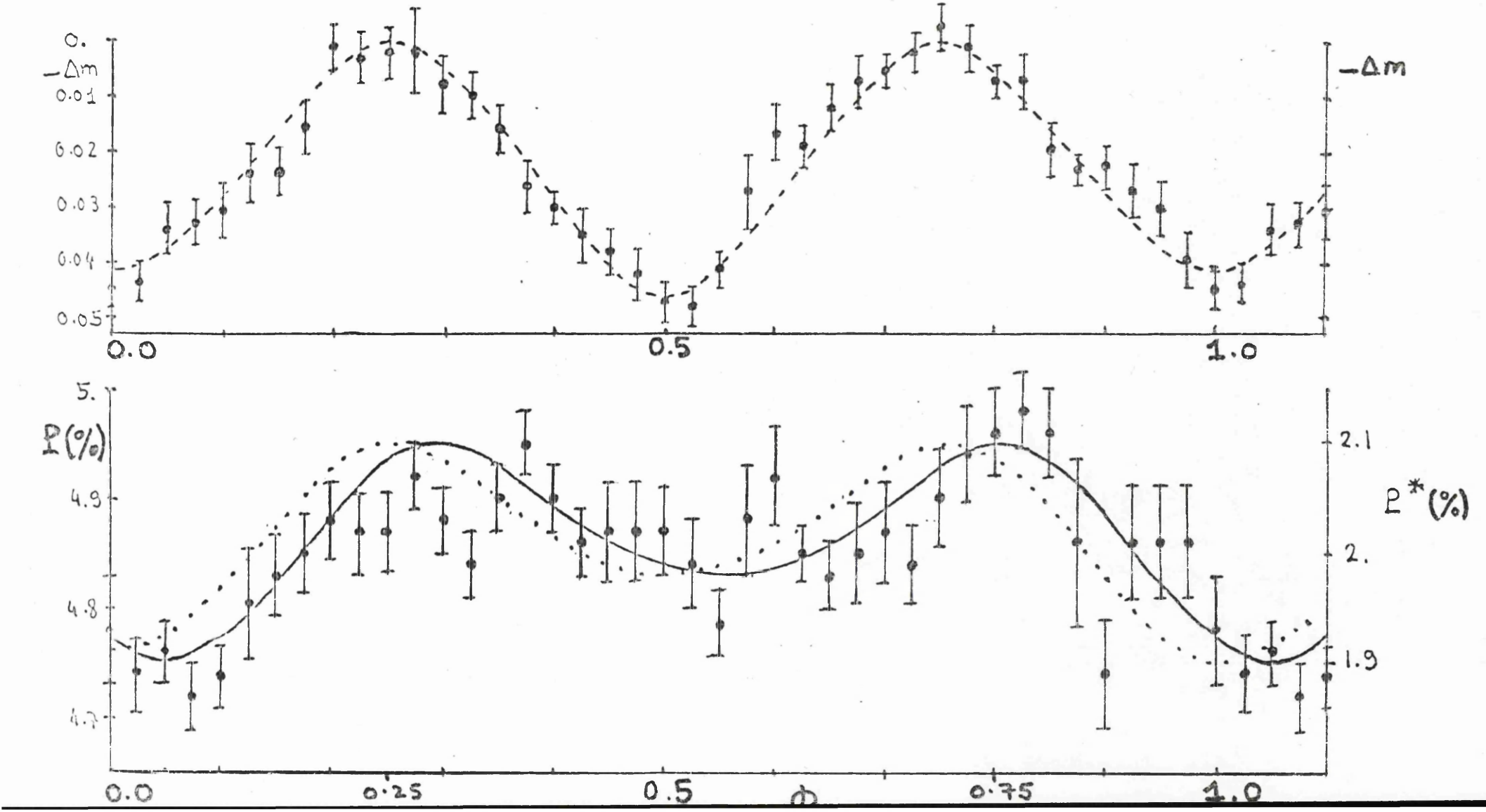
0.
−Δm
0.01
0.02
0.03
0.04
0.05
0.0
0.5
1.0
−Δm
5.
P(%)
4.9
4.8
4.7
2.1
2.
1.9
P*(%)
0.0
0.25
0.5
Φ
0.75
1.0

hole in a binary system. This was particularly of interestfor the system Cygnus X-1 which was the progenitor of such an object.

Dolan considers the polarization variations caused by an increase in luminosity of the system at times of eclipse of an optical star by a black hole, which is a result of a 'gravitational lens' effect caused by the black hole component. This increase in luminosity called the Einstein photometric effect was calculated by Link (1969) and Maeder (1973). Dolan, using Cygnus X-1 parameters obtained by Bolton (1975) calculated the total increase in partial luminosity for the primary during eclipse as $\sim 2 \times 10^{-5}$. Calculations of this effect indicated a maximum change in polarization of the order $\sim 0.1\%$ and should be independent of wavelength. The shape of the variations would depend on the nature of the transit/eclipse. Schematic representation of the results are shown in Figure(1.29) as presented by Dolan (1977). Changes in the position angle of the polarization would depend on the ratio of the magnitude of intrinsic polarization to the interstellar and the position in the orbit plane of the transit in relation to the plane of the interstellar component. If the change in polarization is small compared to the interstellar then a negligible change in position angle is expected.

1.8 Resumé of plan of thesis

In this thesis we intend to show the complicated nature of determining physical and orbital parameters of binaries from polarimetric observation. In particular the procedure for analysing such variations due to Brown, McLean and Emslie (1978) is extended to take proper account of data noise (Chapter 2). We follow this by a thorough testing of the procedure of determining binary parameters (in particular i) from noisy data by applying the canonical model (of Chapter 2) to simulated data (Chapter 3). This is followed by a statistical analysis of the bias of the polarimetric inclination estimator used in the canonical model (Chapter 4). Chapter 5 contains the application of the canonical model of Chapter 2 to the data of AO Cas, HD 47129, β Per (Algol), σ Ori E, μ Her, U Sge and V444 Cygni.

Relaxation of the canonical model assumption concerning a corotating scattering envelope is considered in Chapter 6 where, by means of introduction of an eccentric orbit scattering 'blob', we investigate the problems of distinguishing between the corotating and

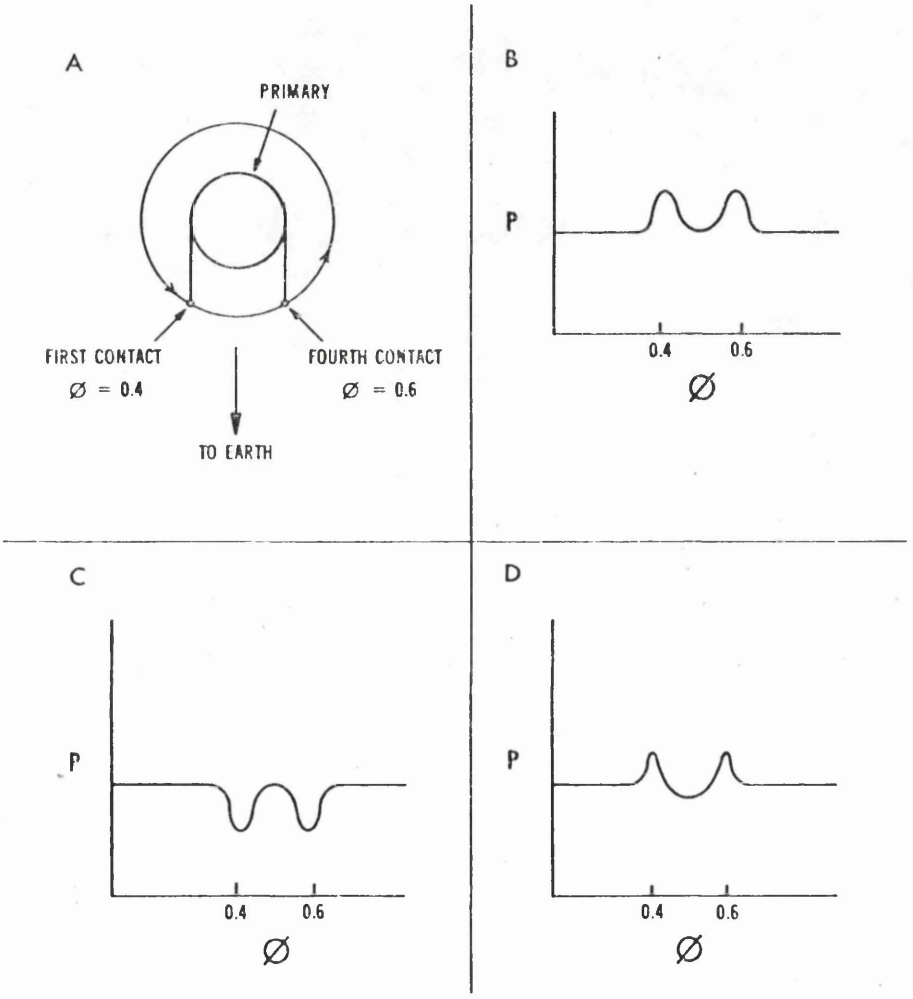

Figure 1.29 - Schematic representation of the variation in polarization predicted by the presence of a black hole in a binary system. As the black hole transits the visible component it acts on a gravitational lens increasing the luminosity of the system slightly Thus when used to normalize the interstellar polarization would produce a variable effect.

(a) - the orientation of the system at time of variability.

(b) - the characteristic black hole signature in polarization at time of central transit of the black hole. The plane of the system is taken as perpendicular to the interstellar polarization direction.

(c) the same as(b)but with the orbital plane parallel to the plane of interstellar polarization.

(d) the same as (b) but with a non-central transit.

(After Dolan 1977).

non-corotating cases Also in Chapter 6 we develop an optimization procedure for the eccentric model similar to that for the canonical model mentioned in Chapter 2.

Specific cases of a canonical model i.e. an accretion disk and accretion wake are considered analytically/numerically in Chapter 7.

Chapter 8 generalises the canonical model optimization procedure to enable data in raw form (i.e. at unequal phase points) to be analysed and the application of this technique to the large data set of Cygnus X-1 is dealt with in Chapter 9. A similar procedure is outlined in Chapter 10 for the Wolf Rayet binary HD50896 where we also consider both canonical model and eccentric model with the data of HD50896 supplied by McLean (1980). Our main conclusions are discussed in Chapter 11 where also the possibilities for further work are outlined.

We now proceed to Chapter 2 where a discussion of the basic model of Brown, McLean and Emslie (1978) is made and the optimization of the model to real data is considered, in particular in relation to the system Cygnus X-1.

CHAPTER 2. THE CANONICAL MODEL OF POLARIMETRIC BINARIES

2.1 Introduction

We have seen in the preceeding review that modelling of the observed polarimetric variations from certain binaries, in terms of scattering on circumstellar material, has generally taken the form of a detailed discussion of the positioning and nature of the scattering region. The existence of specific geometrical density distributions of gas e.g. gas streams, wakes or accretion disks have been involved in various papers (e.g. Kemp 1980). These models are seen to reproduce the smoothed polarimetric observations satisfactorily. However the uniqueness of these interpretations is questionable since the data are noisy and many of the models involve a considerable number of free parameters. It is thus more appropriate first to interpret the observed polarimetric variations in terms of a general simple 'canonical' model. This may be found either to be a good representation of the data, hence making more specific or detailed modelling unnecessary, or not to fit, in which case more detailed models would be required. Such a model was proposed by Brown, McLean and Emslie (1978) who derived general expressions for the linear polarization Stokes parameters from a totally arbitrary (optically thin) distribution of scatterers illuminated by two point sources of arbitrary brightness, in circular orbits about one another. This work extended their previous calculations on the polarization resulting from scattering in a circumstellar envelope centred on a single point light source (Brown and McLean 1977). The details of the binary model form the basis of the analysis in later chapters of this thesis. We therefore consider the early development of the so called 'canonical' model in detail.

2.2 Polarization by Thomson Scattering in Optically Thin Binary Envelopes

The existence of gaseous material in a close binary was predicted and its effects observed many years ago (cf. Chapter 1). In binaries this circumstellar material may well be of a non-spherically symmetric form on which optical radiation from the stars is polarized by scattering. In general this intrinsic polarization should vary with the binary period and be dependent on the scattering mechanism and the orientation of the system w.r.t. the observer. Brown, McLean and Emslie (1978)

undertook to express the Stokes parameters, describing the polarization, from a close binary with an arbitrary shaped envelope, under certain simplifying but, nevertheless, reasonable assumptions to define a 'canonical' model. The implicit assumptions of the model here described are that:

(a) the envelope should be optically thin;

(b) single Thomson (electron) scattering should be the polarizing mechanism ;

(c) no variable obscuration/occultation of the scattering region should take place nor should eclipses/occultations of the stars themselves occur in the data interval to be analysed;

(d) the circumstellar envelope should corotate with the stars i.e. the envelope density distribution would be time independent in the frame of reference rotating with the binary.

Assumption (a) and (b) have been seen to be approximately true for some systems. (Batten 1973). The validity of assumptions (c) and (d) however will depend on the type of systems observed. One deviation from corotation of the envelope would arise in the presence of an orbital eccentricity which can sometimes be detected by spectroscopic observations of the radial velocity curve. Other forms of non-corotation i.e. some changes occurring in the scattering distribution seen in the rotating coordinate system over the orbit, are less easily detected. Thus a typical system suitable for such analysis would be one spectroscopically detected shown to have a circular orbit with no significant light variations (eclipses) and close enough to allow the possibility of mass transference/loss so that hot material (i.e. free electrons) would be available for scattering purposes. Such binaries are not uncommon (c.f. Batten 1973,1975).

The Brown et al (1978) representation of the geometry of the model is illustrated in Figure (2.1). A point source O of unpolarized primary radiation with isotropic intensity I_o (J sterad^{-1}s^{-1}) is at the origin of a cartesian coordinate system (x,y,z). The Ox axis is towards the observer and the Oz axisis arbitrarily orientated in the plane of the sky. Light is scattered by free electrons illustrated as a (representative point P) through an angle ψ and in general is linearly polarized perpendicular to the local scattering place. This polarization

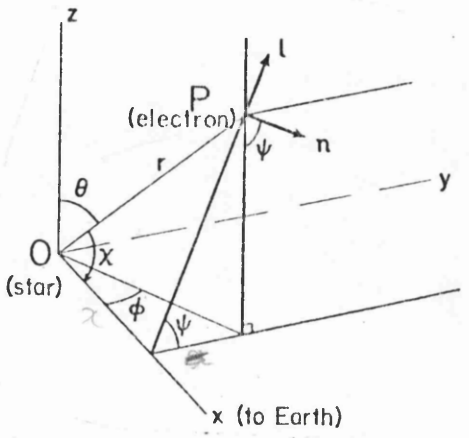

Figure 2.1 The scattering geometry. The axial system (x,y,z) is centred on the illuminated star (O) with Ox towards the observer. The plane through $P(r,\theta,\phi)$ perpendicular to OX is shown by heavy lines. It contains the unit vectors $\underline{n}$ and $\underline{\ell}$. Light incident on an electron P is scattered through an angle ψ and has partial linear polarization along $\underline{n}$. (After Brown et al 1978).

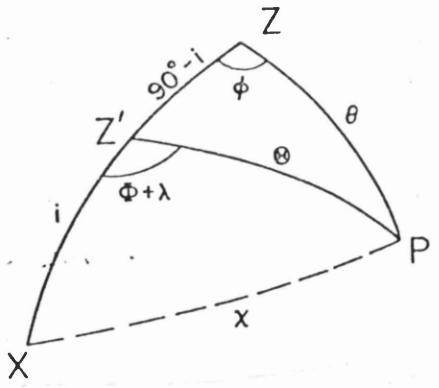

Figure 2.2 Spherical triangle for transformation from line of sight coordinates of Figure 2.1 to a system corotating with the binary pair O_1, O_2. For either star the z'axis is normal to the orbit. $P(R,\theta,\Phi)$ is a general point. Ox, Oz, Oz' are coplanar and λ is the longitude of the binary pair measured from the reference plane zz'x. (After Brown et al 1978).

is described by the intensity Stokes parameters $I_1(\underset{\sim}{r})$, $I_2(\underset{\sim}{r})$ and $I_3(\underset{\sim}{r})$ where xOz is the reference plane. The light scattered by the whole envelope towards the earth is given by the volume integrals:

$$\left.\begin{matrix} I_1 \\ I_2 \\ I_3 \end{matrix}\right\} = I_o \sigma_o \int_v \frac{n(\underset{\sim}{r})}{r^2} dv \left\{\begin{matrix} 1 + \cos^2 \psi \\ \sin^2 \psi \cos 2\Psi \\ \sin^2 \psi \sin 2\Psi \end{matrix}\right. \qquad (2.1)$$

where for Thomson scattering n(r) is the electron number density at P(r); r is the distance OP; $\sigma_o = 3\sigma_T/16\pi$ where σ_T is the Thomson scattering cross-section per electron and dv is the element volume. The angle ψ is between the reference plane and the unit normal (n) to the local scattering plane at $P(r,\theta,\phi)$ where r,θ and ϕ are spherical coordinates in a frame fixed relative to the observer. It is easily shown from Figure (2.1) that the simple trigonometrical relations:

$$\begin{aligned} \frac{x}{r} &= \sin\theta \cos\phi = \cos\psi \\ \frac{y}{r} &= \sin\theta \sin\phi = \sin\psi \cos\Psi \\ \frac{z}{r} &= \cos\theta = \sin\psi \sin\Psi \end{aligned} \qquad (2.2)$$

hold. Using these we eliminate ψ and Ψ from (2.1) giving an integration over r,θ,ϕ where $dV = r^2 \sin\theta \, dr \, d\theta \, d\phi$.
When the virtually undimmed direct light I_o has been added we have:

$$I = I_o + I_1 = I_o \left\{ 1 + \sigma_o \int_o^\infty \int_o^\pi \int_o^{2\pi} n(r,\theta,\phi)(1+\sin^2\theta \cos^2\phi) \sin\theta \, dr \, d\theta \, d\phi \right\}$$

$$I_2 = \left\{ I_o \sigma_o \int_o^\infty \int_o^\pi \int_o^{2\pi} n(r,\theta,\phi)(\sin^2\theta \sin^2\phi - \cos^2\theta) \sin\theta \, dr \, d\theta \, d\phi \right\} \qquad (2.3)$$

and $$I_3 = \left\{ I_o \sigma_o \int_o^\infty \int_o^\pi \int_o^{2\pi} n(r,\theta,\phi)(\sin 2\theta \sin\phi) \sin\theta \, dr \, d\theta \, d\phi \right\}$$

Generalization to two or more light sources is simple due to the linearity of the Stokes parameters i.e. in terms of normalized Stokes parameters,

$$(Q = I_2/I, \quad U = I_3/I) \qquad I = \sum_{j=1}^{N} I_j; \qquad Q = \sum_{j=1}^{N} f_j Q_j;$$

$$U = \sum_{j=1}^{N} f_j U_j \qquad (2.4)$$

for N sources. f_j is the fractional intensity contributed by the jth star. Integrations in (2.3) are all performed centred on the j^{th} source of light.

In terms of the degree of polarization P_r and position angle θ, we have $P_r = (Q^2 + U^2)^{\frac{1}{2}}$ and $\tan \theta = U/Q$. It should be noted also that the integrals (2.3) hold for all forms of Rayleigh scattering since the angular dependence is the same as for Thomson scattering (Van der Hulst 1957).

For a binary system with circumstellar matter of arbitrary density distribution the variability of the Stokes parameters can be expressed simply by a change of coordinate system to (x', y', z') fixed in the rotating binary frame with origin centred on the primary component O, and the z' axis perpendicular to the systems orbital plane. In this system an arbitrary point in the envelope has polar coordinates (R_1, θ_1, and Φ_1) with the second star O_2 located along the $\theta_1 = 90^o$, $\Phi_1 = 0^o$ line (for considerations of the light from the secondary the roles are reversed).

During the binaries orbital period the line of sight maintains a fixed angle of inclination i with the Oz' axis but rotates uniformly around it so that the observer is seen from each star in the direction $\theta_1 = \theta_2 = i$, $\Phi_1 = \Phi_2 = -\lambda$ where λ is the longitude of star 2 w.r.t. star 1. This is measured from an appropriate zero point. The obvious choice of reference plane is the rotation axis (normal to the orbit) projected onto the plane of the sky. We therefore take Oz, Ox and Oz' to be coplanar. A spherical triangle ZZ'P can be constructed in this reference system (see Figure 2.2) and we can obtain relations between the line of sight coordinates and the corotating frame of reference i.e. $(r, \theta, \phi) \rightarrow (R, \theta, \Phi)$. Substitution of these into (2.3) and (2.4) yield the expressions, in the corotating frame (the natural frame) for the

Stokes parameters I, Q and U. These were given as:

$$I = I_o \left[1 + \tau_o \{ 2(1+\gamma_o)+(1-3\gamma_o)\sin^2 i + \sin 2i(\gamma_1 \cos\lambda - \gamma_2 \sin\lambda) + \sin^2 i(\gamma_3 \cos 2\lambda - \gamma_4 \sin 2\lambda) \} \right]$$

$$Q = \tau_o \{(1-3\gamma_o) \sin^2 i + \sin 2i (\gamma_1 \cos\lambda - \gamma_2 \sin\lambda) - (1 + \cos^2 i) (\gamma_3 \cos 2\lambda - \gamma_4 \sin 2\lambda) \} \quad (2.5)$$

$$U = 2\tau_o \{\sin i(\gamma_1 \sin\lambda + \gamma_2 \cos\lambda) - \cos^2 i (\gamma_3 \sin 2\lambda + \gamma_4 \cos 2\lambda) \}$$

where

$$\tau_o = \frac{\sigma_o}{2} \sum_{j=1}^{2} f_j \iiint \{n\} \, dR_j \sin\theta_j \, d\theta_j \, d\Phi_j$$

$$\tau_o \gamma_o = \frac{\sigma_o}{2} \sum_{j=1}^{2} f_j \iiint \{n \cos^2\theta_j\} \, dR_j \sin\theta_j \, d\theta_j \, d\Phi_j$$

$$\tau_o \gamma_1 = \frac{\sigma_o}{2} \sum_{j=1}^{2} f_j \iiint \{n \sin 2\theta_j \cos\Phi_j\} \, dR_j \sin\theta_j \, d\theta_j \, d\Phi_j \quad (2.6)$$

$$\tau_o \gamma_2 = \frac{\sigma_o}{2} \sum_{j=1}^{2} f_j \iiint \{n \sin 2\theta_j \sin\Phi_j\} \, dR_j \sin\theta_j \, d\theta_j \, d\Phi_j$$

$$\tau_o \gamma_3 = \frac{\sigma_o}{2} \sum_{j=1}^{2} f_j \iiint \{n \sin^2\theta_j \cos 2\Phi_j\} \, dR_j \sin\theta_j \, d\theta_j \, d\Phi_j$$

$$\tau_o \gamma_4 = \frac{\sigma_o}{2} \sum_{j=1}^{2} f_j \iiint \{n \sin^2\theta_j \sin 2\Phi_j\} \, dR_j \sin\theta_j \, d\theta_j \, d\Phi_j$$

The integral limits are $(0,\infty)$, $(0, \pi)$, $(0, 2\pi)$ and $n = n(R_j, \theta_j, \Phi_j)$. These integrals (2.6) are a set of mean optical depths obtained by weighted integration over solid angle. For two sources of light they are averaged between the stars and again weighted according to the relative brightness. Equations (2.5) were also presented in an alternate form viz:

$$I = I_o \left[1 + \tau_o \{ 2(1+\gamma_o)+(1-3\gamma_o) \sin^2 i + G \sin 2i \cos(\lambda+\lambda_1) + H \sin^2 i \cos 2(\lambda+\lambda_2)\} \right] \quad (2.7a)$$

$$Q = \tau_o \{ (1-3\gamma_o)\sin^2 i + G \sin 2i \cos(\lambda+\lambda_1) - H(1+\cos^2 i)\cos 2(\lambda+\lambda_2) \}$$

$$U = 2\tau_o \{ G \sin i \sin(\lambda+\lambda_1) - H(\cos i \sin 2(\lambda+\lambda_2) \} \qquad (2.7b)$$

where

$$\tan\lambda_1 = \frac{\gamma_2}{\gamma_1} : \tan 2\lambda_2 = \frac{\gamma_4}{\gamma_3}$$

$$G = (\gamma_1^2 + \gamma_2^2)^{\frac{1}{2}} : H = (\gamma_3^2 + \gamma_4^2)^{\frac{1}{2}} \qquad (2.8)$$

This is a convenient representation since G and H are now amplitudes (with A = H/G defined as the relative amplitude) and $\Delta\lambda = \lambda_1 - \lambda_2$ being a phase difference between the 1st and 2nd harmonic contributions.

It was pointed out by Brown et al that even though determination of the integrals (2.6) from observations would give more insight into the envelope distribution in a binary than for a single star, the function n itself is still unknown since infinitely many geometry functions can have the same 5 moments $\tau_o\gamma_o - \tau_o\gamma_4$. However it is useful to use this idea with observations when attempting to determine the general form of the envelope and other parameters associated with the binary. They interpreted the weighted optical depths as follows. The first integral, for τ_o is seen to be an effective Thomson scattering optical depth integrated over all directions with γ_o being an inverse measure of the effective degree of flattening of the envelope towards the orbital plane of the binary. Thus the factor $(1 - 3\gamma_o)$ decreases from 1 for a plane envelope to -2 for a prolate envelope passing through 0 for a spherically symmetric distribution. γ_1 and γ_2 are seen to be measures of the effective degree of asymmetry about the orbital plane of the system since symmetry of the envelope causes cancellation of the θ dependence. Separately γ_1 and γ_2 were seen to measure the above asymmetry along the line joining the two stars, and in the perpendicular direction respectively.

The integrals γ_3 and γ_4 measure the effective concentration of material towards the orbital plane (because of the $\sin^3\theta$) with γ_3 and γ_4 separately measuring that concentration near $\Phi \sim \pi/4$ or $3\pi/4$ and

$\Phi \sim 0$ or $\pi/2$ respectively. From physical considerations it was generally assumed that $H >> G$ in most cases indicating that the material in the binary would tend to be concentrated near and symmetric about the orbital plane of the system.

The general picture therefore for this model is one of second harmonic (2λ) variations in polarization caused by a symmetric or orbital plane concentrated distribution of material with first harmonics (λ) variations added when an asymmetry about the orbital plane is introduced into the scattering region. The amount of polarization and the ratio of Q to U depends also on the inclination of the binary w.r.t. the observer In this paper Brown et al also showed how the weighted integrals were related to the coefficients of terms up to 2nd harmonics in a Fourier representation of $n(R,\theta,\Phi)$. They found that the relations,

$$\begin{aligned}
\gamma_o &= \tfrac{1}{2}\,(1 - \bar{A}_{10}\,/2\bar{A}_{00}\,) \\
\gamma_1 &= \bar{C}_{11}/4\,\bar{A}_{00} \\
\gamma_2 &= \bar{D}_{11}/4\,\bar{A}_{00} \\
\gamma_3 &= \tfrac{1}{4}\,(\bar{A}_{02}/\bar{A}_{00} + \bar{A}_{12}/\,2\bar{A}_{00}\,) \\
\gamma_4 &= \tfrac{1}{4}\,(\bar{B}_{02}/\bar{A}_{00} + \bar{B}_{12}/\,2\bar{A}_{00}\,)
\end{aligned} \qquad (2.9)$$

held where $\bar{A}_{k\ell}$ indicated the average over the sources of $A_{k\ell}$. $A_{k\ell}$ were defined by the equation:

$$\begin{aligned}
\tau_j\ (\theta\,,\Phi) = \sum_{k=0}^{\infty}\sum_{\ell=0}^{\infty}\ (-1)^{k+\ell}\Big[& A_{k\ell}\cos 2k\theta\ \cos \ell\Phi \\
& + B_{k\ell}\cos 2k\theta \sin \ell\Phi + C_{k\ell}\sin 2k\theta \cos \ell\Phi \\
& + D_{k\ell}\sin 2k\theta \sin \ell\Phi\ \Big]\,.
\end{aligned}$$

Similar meanings were given to $\bar{B}_{k\ell}$, $\bar{C}_{k\ell}$ and $\bar{D}_{k\ell}$. $A_{k\ell}$ etc. are therefore the Fourier coefficients of the expansion of the optical depth $\tau_j\,(\theta,\Phi) = \int_o^{\infty} n(R_j,\theta_j,\Phi_j)\sigma_o.\ \sin\theta_j\ dR_j$ in terms of Fourier harmonics. Of particular note is the fact that the polarization variations depend only on the Fourier terms in the expansion of $\tau_j(\theta,\Phi)$ up to 2nd harmonics.

Discussion of the model assumptions was also presented and the effect on the polarization of the assumptions being invalid was considered.

In most cases the γ's would become λ-dependent when breakdown of the assumptions (such as non-corotation, occultation or absorption effects) occurred. Also it was thought that in some cases the presence of higher harmonic structure would occur eg. if the orbit of the stars was eccentric. This point is considered in Chapter 6. Brown et al (1978) computed various Q,U loci for different inclinations, i, relative amplitudes, A,and phase differences $\Delta\lambda$. These are shown in Figure (2.3). Here we see loci for i = 30°, 60°, 80° and 90°, A = 0.5, 1.0 and 5.0 and $\Delta\lambda = 0$, $\pi/8$ and $\pi/4$.

They then go on to investigate the determination of binary parameters from observed polarization variations. Two approaches are considered, firstly that of predicting an extensive sequence of Q,U loci i.e. as parametric plot of $Q(\lambda)$, $U(\lambda)$ (as functions of binary phase) for a wide range of primary parameters (i.e. the density distribution integrals and the orbital inclinations) for comparison with data, secondly investigating, what model-independent parameters can be inferred unambiguously from data by formal inversion of (2.7). This contrasts with testing one specific ad hoc model (eg. Rudy and Kemp 1976) which, as mentioned earlier, gives no indication of the uniqueness of the interpretation.

Though presenting problems of uniqueness, the first of these approaches illustrates the properties of the canonical model particularly clearly and is easily compared with most polarimetric data which is published in the form of a Q,U locus. The shape of the locus (swept out during the orbital period) was seen to be unaffected by translation or rotation of the coordinate frame in which they were measured and was considered particularly interesting since any interstellar polarization would have no effect. (Indeed at least one component of the interstellar polarization can be measured in the model). Special simple cases of the loci of Figure (2.3) were also discussed by Brown et al (1978). These involved the case of envelope symmetry about the orbital plane ($\gamma_1 = \gamma_2 = 0$ i.e. A = ∞). Only second harmonic variations would then be present, with the parametric equations of the locus traced out per orbit being that of an ellipse:

Figure 2.3a Matrices of Stokes parameter loci swept out during the binary period for a useful range of factors A, $\Delta\lambda$ when the orbital inclinations is fixed at $i = 90^{\circ}$ (lower) and $i = 80^{\circ}$ (upper). Fiduciary marks along the locus indicate the phase at intervals of $\pi/2$. The shape of the loci are in this case Lissajous Figures. N.B. the last row are drawn to half scale w.r.t. the first two rows since the size increases with increasing A. (After Brown et al 1978).

Figure 2.3b As Figure 2.3a but with $i = 60^{\circ}$ (lower) and $i = 30^{\circ}$ (upper). (After Brown et al 1978).

General Envelopes: i = 80°

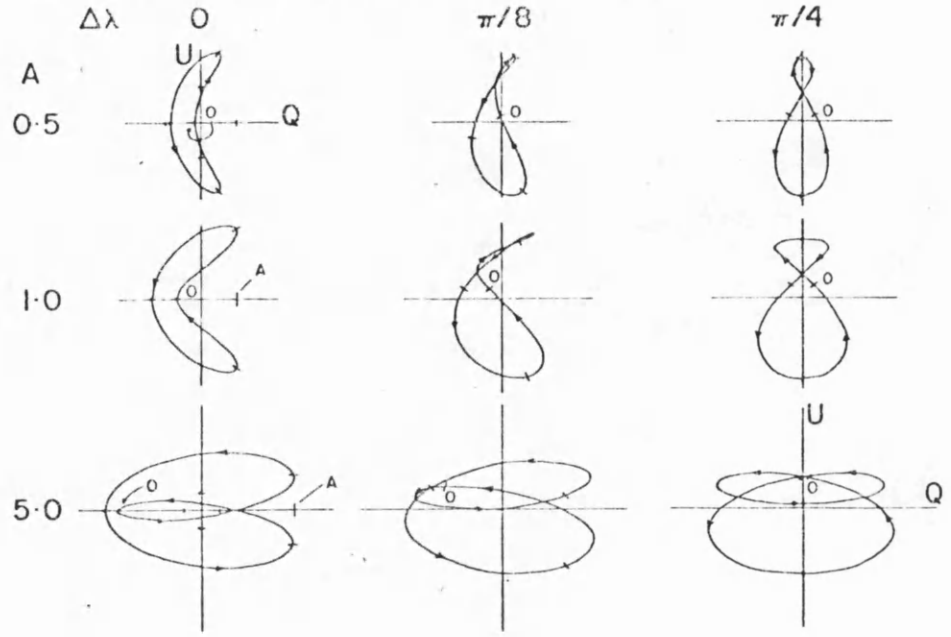

General Envelopes: i = 90°

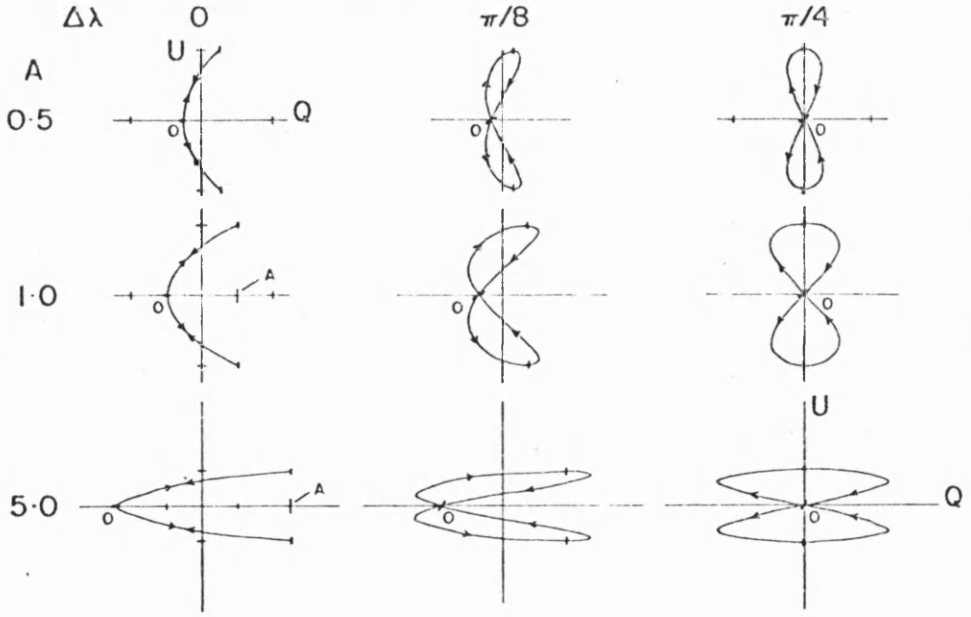

General Envelopes: i = 30°

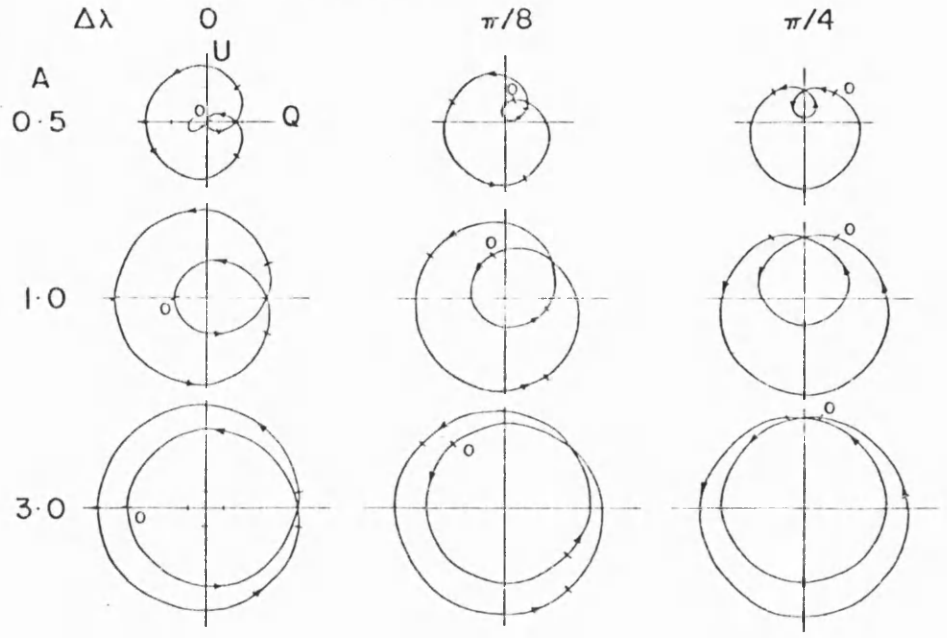

General Envelopes: i = 60°

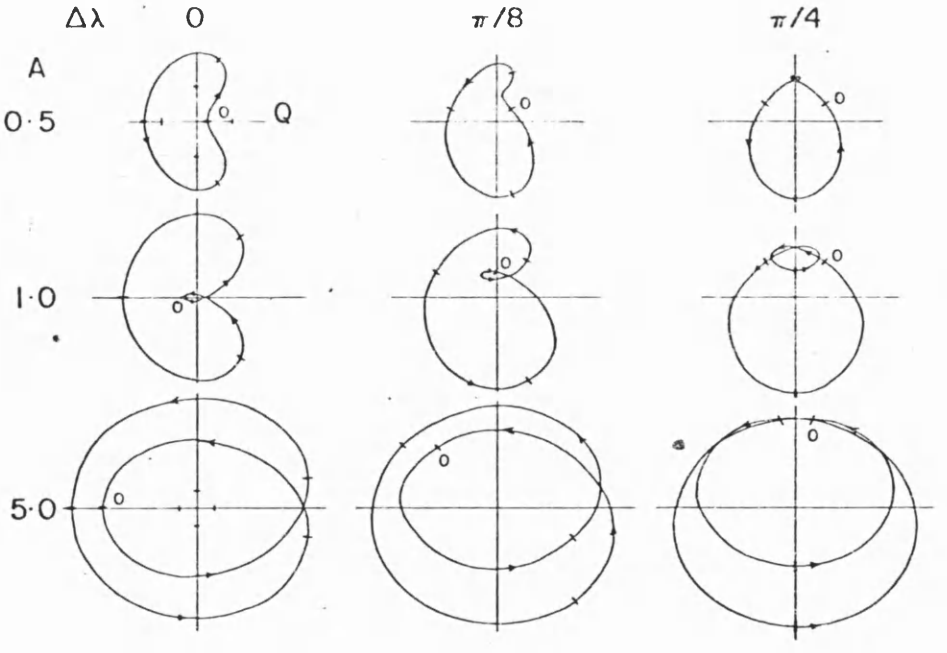

$$\frac{\left[Q - \tau_o (1 - 3\gamma_o) \sin^2 i\right]^2}{\left[\tau_o H(1+\cos^2 i)\right]^2} + \frac{U^2}{\left[2\tau_o H \cos i\right]^2} = 1 \qquad (2.10)$$

The (Q,U) ellipse would have eccentricity e:

$$e = \sin^2 i / (2 - \sin^2 i) \qquad (2.11)$$

from which we see that at $i = 0^o$ the ellipse becomes a circle ($e = 0$), and for $i = 90^o$ a straight line ($e = 1$). - these cases are clear from the basic properties of Thomson scattering.

Figure (2.4) shows the main details of the ellipse when the envelope is symmetric. The ellipse is executed twice per orbit since second harmonics ($\cos 2\lambda$, $\sin 2\lambda$) are involved (basically because the scattering function is the same for scattering angle ψ as for $\pi - \psi$). Also quoted as a case of special interest was the loci for non-symmetric envelopes when $i = 90^o$, giving a Lissajous Figure of frequency ratio 2:1. These loci would in general be compared to observed Q,U loci for an approximate idea of the nature of the binary parameters involved.

Formal inversion of the equations(2.7) is necessary for anything more than this. Two techniques of formal inversion were described in Brown et al (1978), one a purely geometric method (based on manipulation of the Q,U data), and the other an analytic method in terms of Fourier harmonic coefficients. The geometrical method of inversion includes the properties of the harmonic representation of $Q(\lambda)$ and $U(\lambda)$. We take:

$$Q(\lambda) = p_o + p_1 \cos \lambda + q_1 \sin \lambda + p_2 \cos 2\lambda + q_2 \sin 2\lambda$$

and

$$U(\lambda) = u_o + u_1 \cos \lambda + v_1 \cos \lambda + u_2 \cos 2\lambda + v_2 \sin 2\lambda$$

as the model predictions of variable polarization. We see that the cosine and sine functions are identical but negative at phases λ and $(\lambda + \pi)$. However at these phases twice the angle i.e. 2λ and $2(\lambda + \pi)$ are identical and positive since $2\lambda = 2\lambda + 2\pi$. Therefore addition of $Q(\lambda)$ and $Q(\lambda + \pi)$ eliminates the λ term (1st harmonic). Subtraction of $Q(\lambda)$ and $Q(\lambda + \pi)$ however eliminates the 2λ terms (2nd harmonics) and similarly for U. For data with just first and second harmonics separation of the harmonics can therefore be achieved by forming from

Figure 2.4 Relationship of the properties of all envelopes, with material concentrated in or symmetrical about the orbital plane of the binary, to the eccentricity, size and orientation of the resulting elliptical Q,U locus (executed twice per orbit).
(After Brown et al 1978).

Figure 2.5 (a) We show the observed polarization variations in the blue spectral region with phase for the close binary system AO Cas as published by Rudy and Kemp (1976) relative to the standard coordinate system (Q',U'). Also shown is an independent estimate of the interstellar polarization for AO Cas.
(b) and (c) the (Q'_+, U'_+) locus is formed by taking $\frac{1}{2}(Q'(\lambda) + Q'(\lambda + \pi))$ and similarly for U'. The (Q'_-,U'_-) locus is found by taking $\frac{1}{2}(Q'_-(\lambda) - Q'(\lambda + \pi))$ and similarly for U'. (b) the (Q_+U_+) locus is seen to approximate to an ellipse swept out twice per binary orbit while the (Q_-U_-) locus is more a complicated figure.
(After Brown et al 1978).

Envelopes Symmetric About Orbital Plane:

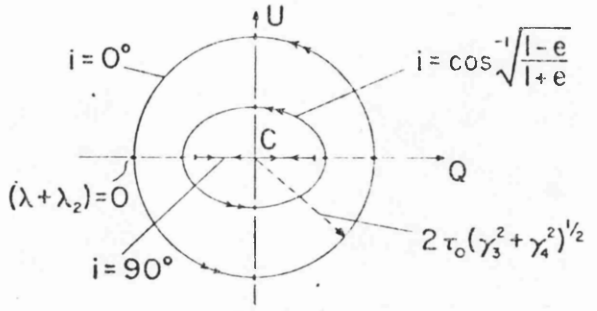

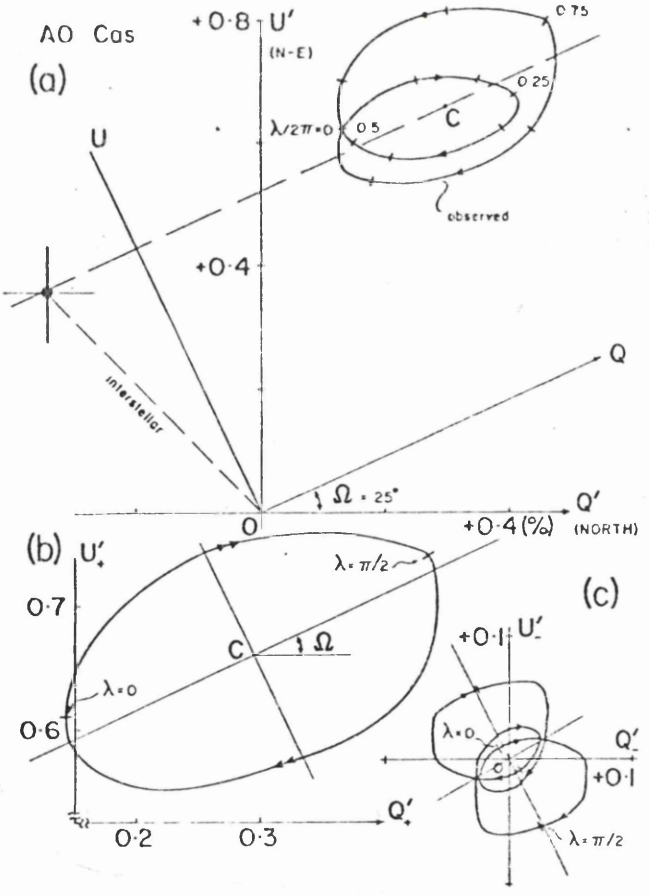

the $Q(\lambda)$ and $U(\lambda)$ data new subsidiary data sets:

$$\begin{aligned} Q_+(\lambda) &= \tfrac{1}{2}\,(Q(\lambda) + Q(\lambda + \pi)) \\ Q-(\lambda) &= \tfrac{1}{2}\,(Q(\lambda) - Q(\lambda + \pi)) \\ U+(\lambda) &= \tfrac{1}{2}\,(Q(\lambda) + U(\lambda + \pi)) \\ U-(\lambda) &= \tfrac{1}{2}\,(U(\lambda) - U(\lambda + \pi)) \end{aligned} \qquad (2.12)$$

So that we eliminate 1st harmonics in (Q+ , U+) and 2nd harmonics in (Q −, U−) from the data. The (Q+, U+) locus would then be an ellipse of eccentricity $e = \sin^2 i/(2 - \sin^2 i)$ swept out twice per orbital period. The orientation angle of the system, Ω with respect to the observers reference axis is also found directly (see Figure 2.5) from the orientation of the Q+, U+ figure. The (Q−, U−) locus would when formed involve 1st harmonics only from data conforming to the canonical model seen to be an ellipse centred on the origin. The ratio the semimajor to semiminor axis of this ellipse would give the moment integrals $\tau_o \gamma_1$, $\tau_o \gamma_2$ and its eccentricity $e = \sin i$. Two determinants of i (one from the 2nd harmonics and one from the 1st harmonic locus) were therefore obtained thus providing a self-consistency check.

The Fourier coefficient method was an analytic way of obtaining the same results. This involved expressing the observed data as a Fourier series viz:

$$\begin{aligned} Q'(\lambda) &= p'_o + p'_1 \cos\lambda + q'_1 \sin\lambda + p'_2 \cos 2\lambda + q'_2 \sin 2\lambda \\ U'(\lambda) &= u'_o + u'_1 \cos\lambda + v'_1 \sin\lambda + u'_2 \cos 2\lambda + v'_2 \sin 2\lambda \end{aligned} \qquad (2.13)$$

where the primed quantities are in the observers frame of reference. Comparison of these with the theoretical series obtained in (2.7)after rotation through an angle Ω to the observers frame((2.7) being expressed in the natural frame of the system) they obtained for the inclination i,

$$\left(\frac{1 - \cos i}{1 + \cos i}\right)^2 = \frac{(u'_1 + q'_1)^2 + (v'_1 - p'_1)^2}{(v'_1 + p'_1)^2 + (u'_1 - q'_1)^2} \qquad (2.14)$$

and

$$\left(\frac{1 - \cos i}{1 + \cos i}\right)^4 = \frac{(u'_2 + q'_2)^2 + (v'_2 - p'_2)^2}{(p'_2 + v'_2)^2 + (u'_2 - q'_2)^2}$$

and for the rotation angle Ω ,

$$\Omega = \tfrac{1}{2}\left[\tan^{-1}\left|\frac{u_1' + q_1'}{v_1' - p_1'}\right| - \tan^{-1}\left|\frac{u_1' - q_1'}{v_1' + p_1'}\right|\right]$$

and

$$\Omega = \tfrac{1}{2}\left[\tan^{-1}\left|\frac{u_2' + q_2'}{v_2' - p_2'}\right| - \tan^{-1}\left|\frac{u_2' - q_2'}{v_2' + p_2'}\right|\right]$$

As can be seen from the form of the equations the first and second harmonics give relations for i and Ω independent of each other. This meant that two determinations of both parameters (i and Ω) were possible from any set of data under consideration. The correspondence of the two results would then indicate something of the goodness of fit of the model. i.e. if i (or Ω) from both 1st and 2nd harmonics were different the model may well be suspect. Application of these ideas was made in Brown et al (1978) to data published by Rudy and Kemp (1976) for AO Cas; Kemp and Herman (1977) for σ Ori E and Nolt et al (1976) for Cygnus X-1. The geometric inversion of the AO Cas data is shown in Figure (2.5). The Q,U locus is seen to be a double looped figure with phases 0.0 and 0.5 corresponding to approximately the same polarization. The secondary data sets (Q+, U+) and (Q-, U-) are also shown. The (Q+, U+) figure is seen to approximate reasonably well to an ellipse with the (Q-,U-) locus being considerably more complicated than the predicted 1st harmonic ellipse behaviour mentioned above.

Brown et al proceed in analysing this data set with the second harmonic (Q+, U+) locus giving an inclination of $i = 71^{\circ}$. The (Q-,U-) locus was considered unable to give results by the above technique because of its complicated nature.

Data for σ Ori E by Kemp and Herman (1977) was also analysed with the resulting (Q,U) loci of smoothed observations and theoretical predictions being shown in Figure (2.6). An inclination of $i = 76^{\circ}$ was formed for this system from the (Q+, U+) curve with the (Q-, U-) 1st harmonic curve being too distorted, possibly because of the low level of polarization detected (< 0.1%), to enable suitable parameter determination.

The Cygnus X-1 data (shown in Figure 2.7) by Nolt et al produced on i from the (Q-,U-) locus of $i = 30^{\circ}$. The (Q+, U+) locus however gave contradictory results with $i = 80^{\circ}$. The possibility of the 'figure of eight' locus being spurious was noted and was eventually

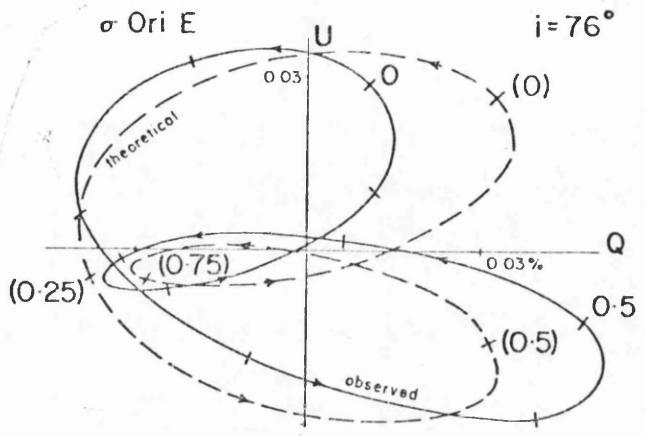

Figure 2.6 The solid curve shows the smoothed weak variation of the intrinsic Stokes parameters (Q,U) with phase for the binary σ Ori E (in blue light) from observations by Kemp and Herman (1977). A theoretical locus (dashed curve with phase in brackets) based on the canonical model of Brown et al (1978) is shown superimposed. The orbit inclination is i = 76° by this simple method. (After Brown et al 1978).

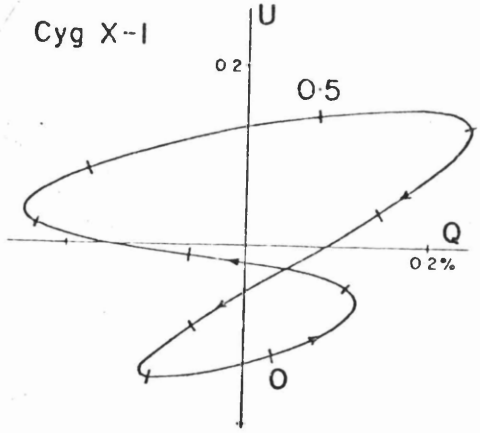

Figure 2.7 Shown here is the shape of the variations of the Stokes parameters over the 5.6^d period of the peculiar Xray binary Cygnus X-1 as reported by Nolt et al (1975).
(After Brown et al 1978).

confirmed by Kemp et al (1978) who, with more data produced a 2nd harmonic dominant Q,U locus with lower 1st harmonics.

In this way, Brown et al (1978) started the modelling of linear polarization variations in terms of the 'canonical'model. Other contributions to these ideas were made by Rudy and Kemp (1978) and Milgrom (1978,1979).

In a paper presenting observations of β Per (Algol), USge and V444 Cygni, Rudy and Kemp (1978) independently detailed a simple model close to that outlined above. They regarded the model as primarily one for obtaining orbital inclinations from phase-locked polarimetric variations (i.e. variations periodic with the binary period). Their model however had the additional assumption that the envelope should be confined to the orbital plane of the binary; within an Appendix a more general treatment of orbital plane symmetry of the envelope being considered. They similarly found that the second harmonic behaviour of the predicted polarization enabled an estimate of the systems orbital inclination to be made by using the equation $e = \sin^2 i/(1+\cos^2 i)$ where e, as we have seen, is the eccentricity of the 2nd harmonic polarization ellipse. On the other hand Rudy and Kemp included the effect of non-point light sources in their calculations. By considering a geometry as in Figure (2.8) they calculate the Stokes parameters when arbitrarily shaped sources and scattering clouds displaying mirror symmetry about the orbital plane are present in the system. They first consider, two scatterers and two light sources. Due to the linearity of the Stokes parameters they stated that the total polarization for this configuration was given by:

$$\begin{aligned} Q_{k,j} &= Q_{11} + Q_{12} + Q_{21} + Q_{22} \\ U_{k,j} &= U_{11} + U_{12} + U_{21} + U_{22} \end{aligned} \qquad (2.16)$$

which includes all contributions of light from sources 1 and 2 scattered on particles 1 and 2. Q_{11}, U_{11} etc. are defined as

$$\begin{aligned} Q_{ab} &= \frac{R_{ab}}{I_o}(1 - \cos^2 \theta_{ab}) \cos 2 \theta_{ab} \\ U_{ab} &= \frac{R_{ab}}{I_o}(1 - \cos^2 \theta_{ab}) \sin 2 \theta_{ab} \end{aligned} \qquad (2.17)$$

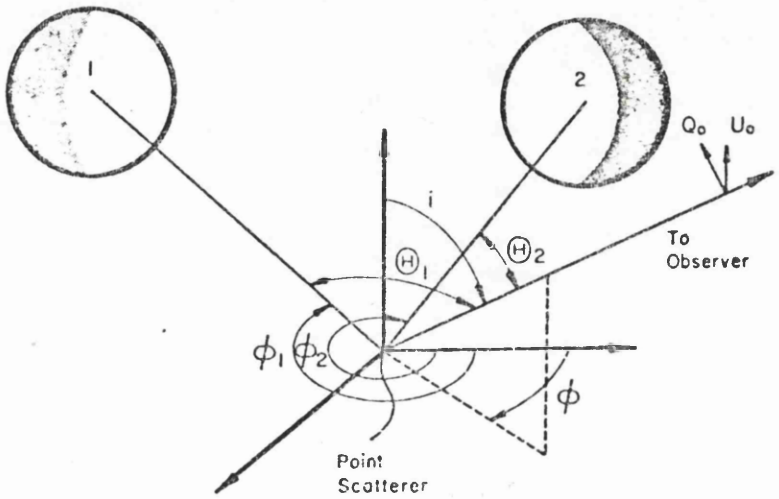

Figure 2.8 A schematic representation of a point scatterer in the orbital plane of a binary system. The position of the scatterer is fixed relative to the two stars (1 and 2) with the coordinate system fixed at the scatterer. Light from both stars contributes to the polarization from the whole system. (after Rudy and Kemp 1978)

where θ_{ab} in the scattering function $(1 - \cos^2 \theta_{ab})$ is the scattering angle and may be found from

$$\cos \theta_{ab} = \frac{r_{ab} \cdot r_o}{|r_{ab}|} \qquad (2.18)$$

The angle θ is that between the polarization and the direction of Q_o (i.e. the rotation angle between the natural and laboratory frame of reference) R_{ab} is the intensity dependence and can incorporate an inverse square law, limb and gravity darkening. Mirror symmetry of the envelope restricts $R_{11} = R_{22}$ and $R_{12} = R_{21}$. The Q_{kj} and U_{kj} contributions were when considered and simplified of the form:

$$Q_{kj} = \frac{1}{I_o}(R_{11} \cos^2 \alpha + R_{12} \cos^2 \beta)\{\sin^2 i - (1 + \cos^2 i) \cos 4\pi (\phi - \phi_{kj})\}$$

$$U_{ab} = \frac{1}{I_o}(R_{11} \cos^2 \alpha + R_{12} \cos^2 \beta)\{2\cos i \sin 4\pi (\phi - \phi_{kj})\} \qquad (2.19)$$

where ϕ_{kj} is the azimuthal coordinate of both sources as measured from the designated scatterer. By letting $(R_{11} \cos^2 \alpha + R_{12} \cos^2 \beta) = T_{kj}$ The total Stokes parameters are just the functions Q_{kj} U_{kj} summed overall sources/scatterers i.e.

$$Q_o = \sum_{k,j} Q_{kj} = \sum_{k,j} \frac{T_{k,j}}{I_o}\left[\sin^2 i - (1+\cos^2 i)\cos 4\pi(\phi - \phi_{kj})\right]$$

$$U_o = \sum_{k,j} U_{kj} = \sum_{k,j} \frac{T_{k,j}}{I_o}\left[2 \cos i \sin 4\pi (\phi - \phi_{kj})\right] \qquad (2.20)$$

We shall return to the application of the above results to the observations presented in a later section when comparing them to our results.

Milgrom (1978) criticized the canonical analysis of the system Cygnus X-1 by both Kemp et al (1978) and Brown et al (1978). Those results involved application of the above model to U and V band data and an inferred inclination of $i = 76^o \pm 8^o$ was quoted. Milgrom claimed that the observations of Cygnus X-1 did not infact imply a value of 76^o for i and that such a simple model could not reproduce the data without addition of more details. He followed by claiming that variable

obscuration of the scattering region occurred and invalidated the canonical model, in particular rendering the inferred inclination non-unique. He demonstrated the effect of occultation by considering an analytic representation of a ring of material in a binary system with variable obscuration present. The contribution continues with discussion of this variable obscuration effects.

In the following year Milgrom (1979) followed up this earlier paper with one considering the linear polarization produced by single Rayleigh scattering in a system made up of arbitrary distributions of scatterers, absorbers and radiation field. This was a somewhat more general formalisation of rotating systems (eg. binaries) than that of Rudy and Kemp (1978). Milgrom's inclusion of the possibility of phase dependent absorption/obscuration relaxed one of the implicit assumptions of the canonical model and he showed that in general, with this effect included, the canonical model relates between the eccentricity of the 1st and 2nd harmonic ellipses and inclination no longer held. Milgrom considered the Stokes parameters (Q,U) as given by the relations:

$$\begin{pmatrix} Q(i,\phi_o) \\ U(i,\phi_o) \end{pmatrix} = R \int d^3r \, d\Omega \begin{pmatrix} (q(i,\theta,\phi-\phi_o) \\ (u(i,\theta,\phi-\phi_o) \end{pmatrix} n(\bar{r}) I(\bar{r},\Omega) V(\bar{r},i,\phi_o) \qquad (2.21)$$

where the integral is over the volume dr^3 of the envelope and solid angle $d\Omega$ ($= r^2 \sin\theta \, dr \, d\theta \, d\phi$) covering the surface of the light source $n(\bar{r})$ is the number density of scatterers, $q(i,\theta,\phi-\phi_o)$ and $u(i,\theta,\phi-\phi_o)$ are related to the Rayleigh scattering functions. $I(\bar{r},\Omega)$ is the intensity of the primary radiation field in direction $\Omega = (\theta,\phi)$ and $V(\bar{r}, i,\phi_o)$ is a visibility function $= e^{-\tau_a(\bar{r},i,\phi_o)}$ (τ_a is the optical depth for absorption from $\bar{r}$ to ∞ along the line of sight). The visibility function is therefore a probability that a photon which scatters at $\bar{r}$ into the line of sight will reach the observer. He expressed the scattering contribution functions q and u in terms of spherical harmonics and obtained expressions for the 1st and 2nd harmonic contributions to the Stokes parameters (Q,U)

$$\begin{pmatrix} Q_\ell \\ U_\ell \end{pmatrix} = R \begin{pmatrix} R_e \\ I_m \end{pmatrix} \sum_{k=0}^{2} \begin{pmatrix} f_k^q(i) \\ f_k^u(i) \end{pmatrix} \left[\lambda_{k,k+1}(i) \, e^{j\ell\phi_o} + {}_{k,k-1}(i) \, e^{-j\ell\phi_o} \right] \qquad (2.22)$$

where $f_k^q(i)$, $f_k^u(i)$ are inclination dependent coefficients in the functions q and u viz:

$$q(i,\theta,\phi - \phi_o) = - R_e \left[\sqrt{3} \sin^2 i \, Y_2^o (\theta,\phi - \phi_o) + \sin i \cos i \, Y_2^1 (\theta,\phi - \phi_o) + 0.5 (\cos^2 i + 1) \, Y_2^2 (\theta,\phi - \phi_o) \right] \quad (2.23)$$

$$u(i,\theta,\phi - \phi_o) = - I_m \left[\sin i \, Y_2^1 (\theta,\phi - \phi_o) + \cos i \, Y_2^2 (\theta,\phi - \phi_o) \right] \quad (2.24)$$

($Y_1^m (\theta,\phi - \phi_o)$ are spherical harmonics of order e)
$\lambda_{k,k+1}(i)$ and $\lambda_{k,k-1}(i)$ are said to contain all the information about the system required to determine the polarization and are defined as

$$\lambda_{k,m}(i) = \int d^3 r \;\; a_k(\bar{r}) \; v_m (\bar{r},i) \quad (2.25)$$

where $a_k(\bar{r})$ and $v(\bar{r},i)$ are the angular transform of the intensity and visibility function. From these results Milgrom considered certain special cases of binary systems (eg. $i \sim 0^o$, mirror symmetric of scatterers around orbital plane) and proceeded to indicate the application of the results to specific radiation fields and density distributions (eg. non-isotropic radiation field and disc geometry).

It is from this point in time that the work related in this thesis originated.

2.3 Additional Diagnostic Use of the (Q+ U+), (Q-,U-) Data Sets.

Following on from the analysis of Brown et al (1978), it is possible to obtain more information about the variations of parameters predicted by the canonical model when good data is available, than the simple determination of inclination from the (Q+ U+), (Q- U-) data loci as mentioned above. If the subsidiary (Q+ U+) (Q- U-) loci are not exactly as predicted by the canonical model (i.e. not ellipses of 2nd and 1st harmonics of the binary phase, respectively) then investigation may be made in to the differences between the observed and predicted loci giving the variation of canonical model parameters

(γ_1, γ_2, γ_3, γ_4 and λ_1 and λ_2) with phase. In the canonical model the above quantities are all constant over orbital phase. Forming the (Q+ U+), (Q- U-) loci as in equation (2.12) gives us the figures in the laboratory frame of reference with the rotation angle Ω given by the orientation of the major axes of the (Q+ U+) locus w.r.t. the Q+ axis (cf. Figure 2.5). If we rotate the (Q,U) data by this angle and hence obtain them in the 'natural' frame of reference of the binary (defined earlier) we can reform the (Q+ U+) and (Q- U-) loci which will now also be in the natural frame. We can then compare the observations and model predictions (also in the natural frame) in the way outlined below.

From the analysis of Brown et al (1978) we know that the subsidiary Stokes parameter data set (Q- U-) is given by:

$$Q_-(\lambda) = (\gamma_1^2 + \gamma_2^2)^{\frac{1}{2}} \cos(\lambda + \lambda_1) \sin 2i$$
$$\text{and} \quad U_-(\lambda) = (\gamma_1^2 + \gamma_2^2)^{\frac{1}{2}} \sin(\lambda + \lambda_1) \sin 2i \qquad (2.26)$$

If the γ's and λ's are constant over much of the locus (phase) but vary during part of it then we can find the constant γ and λ values from the best fit ellipses to the unmodulated data and then calculate the modulating factors for the rest of the orbit (cf. rectification of photometric light curves - e.g. Russell and Merrill 1977). We therefore obtain two sets of (Q-, U-) data the first being the observations and the second the model predictions estimated from the unmodulated observations, i.e.:

$$Q_-^{o,m} = (\gamma_1^{o,m^2} + \gamma_2^{o,m^2})^{\frac{1}{2}} \cos(\lambda + \lambda_1^{o,m}) \sin 2i$$
$$\text{and} \quad U_-^{o,m} = (\gamma_1^{o,m^2} + \gamma_2^{o,m^2})^{\frac{1}{2}} \sin(\lambda + \lambda_1^{o,m}) \sin 2i \qquad (2.27)$$

where the superscripts o and m refer to the observed and model values of the equations.

The idea is clearer with reference to Figures (2.9) below

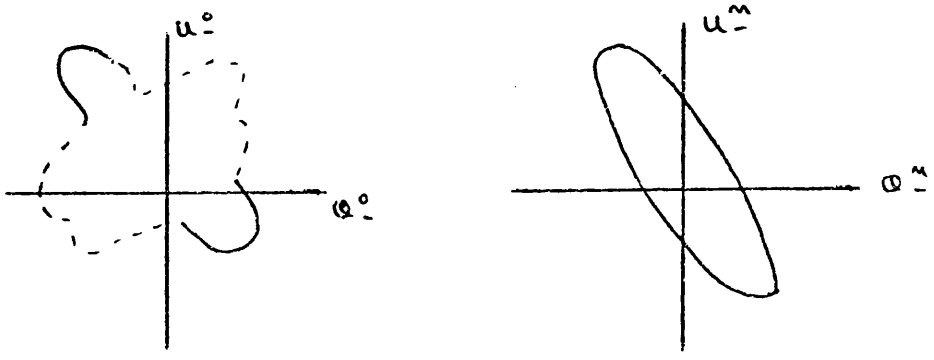

Figure 2.9 (Q_-,U_-) observed and model values

The observations have canonical model behaviour over part of the orbital cycle (solid line) but depart from this at certain phases (dashed line). The 'best fit' canonical model structure is shown in the left diagram and is the underlying elliptical structure. γ_1^o , γ_2^o there refer to the observations ($\underline{Q}^o$, $\underline{U}^o$) (left diagram) and γ_1^m , γ_2^m are from the model (right diagram).

The values of γ_1^o γ_2^o will be phase dependent (i.e. $\gamma_1^o(\lambda)$) since the locus is not as predictable by the canonical model while the values of γ_1^m , γ_2^m will be constant, due to the simple ellipse behaviour.

From the model we have that;

$$\frac{\underline{Q}^{m,o}}{\underline{U}^{m,o}} = 2 \tan (\lambda + \lambda_1^{m,o}) \frac{\sin i}{\sin 2i} = \tan (\lambda + \lambda_1^{m,o}) \sec i \qquad (2.28)$$

and therefore

$$\lambda_1^{m,o} = \tan^{-1} \left(\frac{\underline{U}^{m,o}}{\underline{Q}^{m,o}} \cos i \right) - \lambda \qquad (2.29)$$

The variation of λ_1 with longitude (λ) from the observations (^{o}) is therefore

$$\lambda_1^o(\lambda) = \tan^{-1} \left(\frac{\underline{U}^o}{\underline{Q}^o} \cos i \right) - \lambda \qquad (2.30)$$

where i the inclination is determined from the model by the relation between the eccentricity of the (Q- U-) ellipse and the indication given above.

Now, we know that

$$\frac{(\gamma o^2 + \gamma o^2)}{(\gamma^{m2} + \gamma^{m2})} = \left[\frac{\underline{Q}^o \cos (\lambda + \lambda_1^m)}{\underline{Q}^m \cos (\lambda + \lambda_1^o)} \right]^2 = B^2 \qquad (2.31)$$

or

from (a) and that

$$\left[\frac{\underline{U}^o \sin (\lambda + \lambda_1^m)}{U^m \sin (\lambda + \lambda_1^o)} \right]^2 = C^2$$

$$\frac{\gamma_2^{m,o}}{\gamma_2^{m,o}} = \tan \lambda_1^{m,o} \qquad (2.32)$$

we want the variation of γ_1^o with respect to γ_1^m and similarly for $\gamma_2^{m,o}$, and therefore from (b) dividing through by $\gamma_1^{m,2}$

$$\frac{\gamma_1^{0\,2}}{\gamma_1^{m\,2}} + \frac{\gamma_2^{0\,2}}{\gamma^{m\,2}} = B^2\left(1 + \frac{\gamma_2^{m\,2}}{\gamma^{m\,2}}\right) \qquad (2.33)$$

and hence substituting for γ_2^0 in terms of γ_1^0 and γ_1^0 :

$$\frac{\gamma_1^{02}}{\gamma_{1m}^2} + \frac{\gamma_1^0 \tan \lambda_1^o}{\gamma_{1m}^2} = B^2(1 + \tan \lambda_m^2)$$

$$= B^2 \sec^2 \lambda_m$$

$$\therefore \quad \frac{\gamma_1^0}{\gamma_1^m} = \frac{B \cos \gamma_1^0}{\cos \lambda_1^m} \quad \text{or } C\frac{\cos \gamma_1^0}{\cos \lambda_1^m} \qquad (2.34)$$

similarly for γ_2 we obtain:

$$\frac{\gamma_2^0}{\gamma_2^m} = \frac{B \sin \lambda_p^0}{\sin \lambda_1^m} \quad \text{or } \frac{C \sin \lambda_p^0}{m\, \lambda_1^m} \qquad (2.35)$$

Equations (2.31, (2.34) and (2.35) therefore give the variation of λ_1^0 γ_1^0 and γ_2^0 with the binary longitude.

Similar manipulation for λ_2^0, γ_3^0 and γ_4^0 give:

$$\lambda_2^0 \ (= \lambda) = \tan^{-1} \left\{ \frac{U_+^m}{Q_+^m} (\cos^2 i + 1) \right\} - \lambda \qquad (2.36)$$

and $$\frac{\gamma_3^0}{\gamma_3^m} = \frac{D \cos \lambda_2^0}{\cos \lambda_2^m} = \frac{C \sin \lambda_2^0}{\sin \lambda_2^m} \qquad (2.37$$

$$\frac{\gamma_4^m}{\gamma_4^m} = \frac{D \sin \lambda_2^0}{\sin \lambda_2^m} = \frac{E \cos \lambda_2^0}{\cos \lambda_2^m} \qquad (2.38)$$

where $$D = \left\{ \frac{Q_+^0 \cos 2(\lambda + \lambda_2^m)}{Q_+^m \cos 2(\lambda + \lambda_2^0)} \right\} \qquad (2.39)$$

and $$E = \frac{U_+^0}{U_+^m} \frac{\sin 2(\lambda + \lambda_2^m)}{\sin 2(\lambda + \lambda_2^0)}$$

We therefore obtain relations for the variations of these parameters with orbital phase by this simple manipulation. We can then relate the

changes in values to physical changes in the system (i.e. variation in position of the centroid of the scattering regions etc.) good data with small errors would however be necessary to obtain conclusive results. This is not the case with current data, making use of the above technique unsuitable at present.

2.4 The Optimization of Canonical Model Parameter with Polarimetric Observations.

The canonical model of Brown, McLean and Emslie (1978) in principle enabled the determination of certain binary system parameters, including the orbital inclination, from observations of its intrinsic polarization variations, under certain assumptions regarding the general nature of the binary. A problem in this direct approach is that the observations are by no means perfect and have associated with them an uncertainty which we here term σ_{dat}. This quantity has been estimated previously, (Rudy and Kemp 1978) by repeated observation of the Stokes parameters over a short period of time ($\sim$ 1 hr) and treating the resultant spread in values statistically. This treatment, which was not specified in detail in the above paper, presumably take the form :

$$\sigma_{dat}^2 = \frac{1}{(n-1)} \sum_{j=0}^{n-1} (x_j - \bar{x})^2 \qquad (2.40)$$

where σ_{dat} is a simple standard derivation of the N observations x_j from their mean $\bar{x}$. This error on each observations would, if significant, tend to make inclinations (or any other parameter) imprecise and create associated uncertainty in it. Traditional techniques of calculating an error in a specific parameter (estimated by a least squares analysis of observations) hence concentrated on the so-called formal error analysis. This approach was used by Rudy and Kemp (1978) and produce satisfactorily small uncertainties in the inclination (e.g. $\pm 7^{\circ}$ - see Table I below) when applying the canonical model. Details of the formal error technique are given in Wolberg (1972). Formal derivation of the error on least squares parameter is given in Chapter 4 where we investigate the statistical bias of the inclination estimator. In brief the method is one of establishing the error on parameters found by least squares fitting to

observations when the acceptability of the model is not in question. In the case of 2nd harnomic variation in polarization only, if the derivation of the model predictions for the true values of model parameter is small then by expanding the inclination estimate around the true values in terms of a Taylor series we can obtain an estimation of the error in the optimum parameter by the relation:

$$\sigma^2_{f.\ell.e} = \left[\left(\frac{\partial h}{\partial \hat{p}}\right) \sigma^2_{\hat{p}} + \left(\frac{\partial h}{\partial \hat{q}}\right) \sigma^2_{\hat{q}} + \left(\frac{\partial h}{\partial \hat{u}}\right)\sigma^2_{\hat{u}} + \left(\frac{\partial h}{\partial \hat{v}}\right) \sigma^2_{\hat{v}}\right]$$

where $h = h(\hat{p}, \hat{q}, \hat{u}, \hat{v})$ is the inclination estimator relation, ($\hat{p}$, $\hat{q}$, $\hat{u}$ and $\hat{v}$) are the optimum values of the Fourier harmonic coefficients of the expansion of the data (i.e. $\hat{Q} = \hat{p} \cos 2\lambda + \hat{q} \sin 2\lambda$ and $\hat{U} = \hat{u} \cos 2\lambda + \hat{v} \sin 2\lambda$) and $\sigma^2_{\hat{p}}$ etc. are the variance of these parameters.

The assumption of this technique is that derivations of the predicted value from the true values are small and that errors in the observed parameters p, q, u, v are uncorrelated. In the case of Rudy and Kemp (1978), the resulting expression for the error σ in the predicted eccentricity of the second harmonic ellipse in terms of Fourier coefficients obtained from the data is:

$$\sigma = \left[\left(\frac{\partial e}{\partial p_2} \sigma^2_{p_2}\right)^2 + \left(\frac{\partial e}{\partial q_2} \sigma^2_{q_2}\right)^2 + \left(\frac{\partial e}{\partial u_2} \sigma^2_{u_2}\right)^2 + \left(\frac{\partial e}{\partial v_2} \sigma^2_{v_2}\right)^2\right]^{\frac{1}{2}} \quad (2.41)$$

where the derivatives are evaluated at the calculated values of p_2, q_2, u_2 and v_2 . The factor e is the eccentricity of the 2nd harmonic ellipse and the best fit model parameters, and is given by the relation:

$$e^2 = \frac{2\left[(p_2^2 + q_2^2 - u_2^2 - v_2^2)^2 + 4(p_2u_2 + q_2v_2)^2\right]^{\frac{1}{2}}}{p_2^2 + q_2^2 + u_2^2 + v_2^2 + \left[(p_2^2 + q_2^2 + u_2^2 + v_2^2)^2 + 4(p_2u_2 + q_2v_2)^2\right]^{\frac{1}{2}}}$$

(Rudy and Kemp 1978). The error in the inclination could then be calculated from the error in e since it is from the value of e that i is calculated.

Rudy and Kemp (1978) applied this idea to observations of 5 binaries and obtained inclinations similar to those estimated by other methods.

The formal errors were seen to be small. Table I gives the results of Rudy and Kemp (1978).

TABLE I

Star	i_{other}	i_{pol}	F.E.
κ Her	76°	77°	$\pm 5^{\circ}$
U Sge	90°	87°	$\pm 3^{\circ}$
Algol	82°	81°	$\pm 4^{\circ}$
V444 Cyg.	$\sim 80^{\circ}$	72°	$\pm 6^{\circ}$
AO Cas	$\sim 57^{\circ}$	63°	$\pm 9^{\circ}$

At first sight these results appeared to agree well with other determinations for those systems, with a small error associated to them. Unfortunately on inspection of the folded data plotted vs. phase (before binning), this good agreement seemed contrary to its implications with the observations being widely spread at similar phases and the relatively (to the amplitude of variations) high errors on the data. (cf. Figure 1.16 abc - USge, V444 Cyg and Algol data). Since the formal error took no account of errors in modelling it seemed appropriate to undertake a thorough statistical analysis of the application of the canonical model to noisy data. This would give answers to the questions of whether the model is an acceptable fit to the data and what error bounds can be set for the model parameters, in particular the inclination consistent with the goodness of fit of the model. In a paper entitled 'A Critique of the Polarimetric Evidence on the Nature of Cygnus X-1', Simmons, Aspin and Brown (1980) carried out the necessary analysis and applied it to the observations (by Kemp) of Cygnus X-1. We shall now consider the details of the statistical analysis and fitting procedure.

The predictions of the canonical model is that the Stokes parameters Q and U should vary with binary longitude λ(= 2π x phase ϕ) according to the theoretical form:

$$Q(\lambda) = p_o + p_1 \cos\lambda + p_2 \cos 2\lambda + q_1 \sin\lambda + q_2 \sin 2\lambda$$
$$U(\lambda) = u_o + u_1 \cos\lambda + u_2 \cos 2\lambda + v_1 \sin\lambda + u_2 \sin 2\lambda \qquad (2.43)$$

where the 10 coefficients depend on products of certain simple functions of inclination i and certain weighted integrals over the electron density distribution (cf. § 2.1). In the framework of the model we require constraints on the 1st and 2nd harmonic coefficients so that they correspond to the same i and θ (the orientation angle of system or sky) viz:

$$\frac{p_1}{v_1} = -\frac{q_1}{u_1} = \cos i$$
$$\frac{p_2}{v_2} = -\frac{q_2}{u_2} = \frac{(1 + \cos^2 i)}{2 \cos i} \qquad (2.44)$$

The observations of the Stokes parameters are herein referred to as (Q', U') and are in the laboratory frame of reference. They are related to the similar qualities in the natural frame of reference (Q,U) by the relations:

$$Q' = Q \cos\theta + U \sin\theta$$
$$U' = -Q \sin\theta + U \cos\theta \qquad (2.45)$$

Correspondingly the harmonic coefficients (p', p', etc.) are in the laboratory frame and the unprimed coefficients (p_1, p_2 etc.) are in the natural frame of reference. The data $Q'(\lambda)$, $U'(\lambda)$ are not continuous functions of phase but are, by phase binning of the folded observations (folded onto the orbital period of the binary), at uniformly spaced intervals of phase. The total phase ($\phi = 0.0 \rightarrow 1.0$) is therefore divided into N uniformly spaced bins, r = 0, N - 1 for which the theoretical predictions becomes:

$$Q_{t,r} = p_o + p_1 \cos r\left(\frac{2\pi}{N}\right) + p_2 \cos 2r\left(\frac{2\pi}{N}\right) + q_1 \sin r\left(\frac{2\pi}{N}\right) + q_2 \sin 2r\left(\frac{2\pi}{N}\right)$$
$$U_{t,r} = u_o + u_1 \cos r\left(\frac{2\pi}{N}\right) + u_2 \cos 2r\left(\frac{2\pi}{N}\right) + v_1 \sin r\left(\frac{2\pi}{N}\right) + v_2 \sin 2r\left(\frac{2\pi}{N}\right) \qquad (2.46)$$

with similar expressions for $Q'_{t,r}$, $U'_{t,r}$ (rotated as in Equation 2.45) in terms of the primed coefficients. The problem, then is to examine the compatibility of the set of N pairs of predicted $Q'_{t,r}$, $U'_{t,r}$ values subject to the constraints with a set of N pairs of binned observations $Q'_{ob,r}$, $U'_{ob,r}$. The goodness of fit can be measured by the statistic

$$\chi^2_{2N} = \sum_{r=0}^{N-1}\left[\left(\frac{Q'_{ob,r} - Q'_{t,r}}{\sigma_r}\right)^2 + \left(\frac{U'_{ob,r} - U'_{t,r}}{\hat{\sigma}_r}\right)^2\right] \quad (2.47)$$

where σ_r and $\hat{\sigma}_r$ are the standard deviations in the nth binned means $Q'_{ob,r}$ and $U'_{ob,r}$ respectively, the errors being assumed normally distributed. Then χ^2_{2N} will be distributed according to the chi squared distribution for 2N degrees of freedom.

The canonical model involves 12 parameters, $(i,\theta, \{p\}_{10})$ where $\{p\}_{10}$ denotes the set of 10 harmonic coefficients in (2.16) of which 8 are independent after the four constraints (2.34) are applied. The most general treatment of the problem would be to find the domain of all the parameters in 12-dimensional space which satisfies the constraints and give an acceptable χ^2_{2N}. We would then take the acceptable range of one parameter as a measure of the accuracy with which we can infer it from the data. It would then be possible to reject a model if no acceptable χ^2 was found for any domain of parameters (or if accpetable χ^2 values are found only for parameter ranges which are unacceptable on the grounds of theory or of independent data). Clearly with so many parameters (12) such a general search is computationally intractable. However since we are most interested in the parameter i by focussing attention on it and using certain simplifying features of the data we have found an analytic procedure whereby the acceptability of the canonical model can be tested (in terms of χ^2) and a confidence interval assigned to it. It may however help to clarify the following procedure and the nature of the error limits quoted in latter sections to briefly explain the meaning of a confidence interval in the situation encountered with the canonical model and observations.

The ideal situation when measuring a physical quantity is when we know that the quantity in question behaves in a certain way. In

measuring it we could then assign a confidence interval to our result so that, for example, we could say that our spread of results have a 90% probability of containing the true value. When the model or law governing the physical parameter variations, is not in question we can say that we have formed an absolute confidence interval. (in the above example a 90% absolute confidence interval). In practice, however, especially in many astrophysical situations we do not know the nature of the changes observed so therefore we do not know whether the model we use, within whose framework we relate the quantity measured, is acceptable or reasonable. When this is the case we can only use the classical notion of confidence intervals in a 'formal' way i.e. we assume the model is correct so proceed from there. In this context the phrase 'formal confidence interval' or 'formal' error has been used by e.g. Rudy and Kemp (1978) and Bahcall (1977) who note that their errors do not take into account modelling errors. This formal approach can be misleading. To explain this further we consider the example of a binary showing periodic Q,U variations and a model predicting constant polarization $(\bar{Q},\bar{U})$. Then neither random or real fluctuations in the observed Q,U will greatly affect their mean values (in a long run of data) since $\sigma_{\bar{Q}}^2 = \sigma_Q^2/N$ for N observations of Q each with precision σ_Q. Thus $\bar{Q},\bar{U}$ can have arbitrarily small formal errors despite the fact that the model concerned is wildly at variance with the observations. (Figure 2.9), a fact that would however be revealed in a large χ^2 value of the model 'fit' to the data. What we need in this situation is for a simultaneous answer to the questions: of whether the model fits the data and what is the confidence interval for a given parameter described by the model. This is achieved by asking for what range of values of the chosen parameter are the models predictions compati ble with the data in terms of the χ^2test? Such a range of parameters we term the relative confidence interval (relative in the sense of a confidence interval relative to the model).

As in any statistical test we must, however, decide in advance what we will consider to be an acceptable value of χ^2_{2n} i.e. we must choose a % significance level at which to reject the model. We here have chosen this level as 10% significance (this is a somewhat arbitrary choice) and we say that the corresponding range of i is in the 90% relative confidence interval (R.C.I.). Therefore all values of i

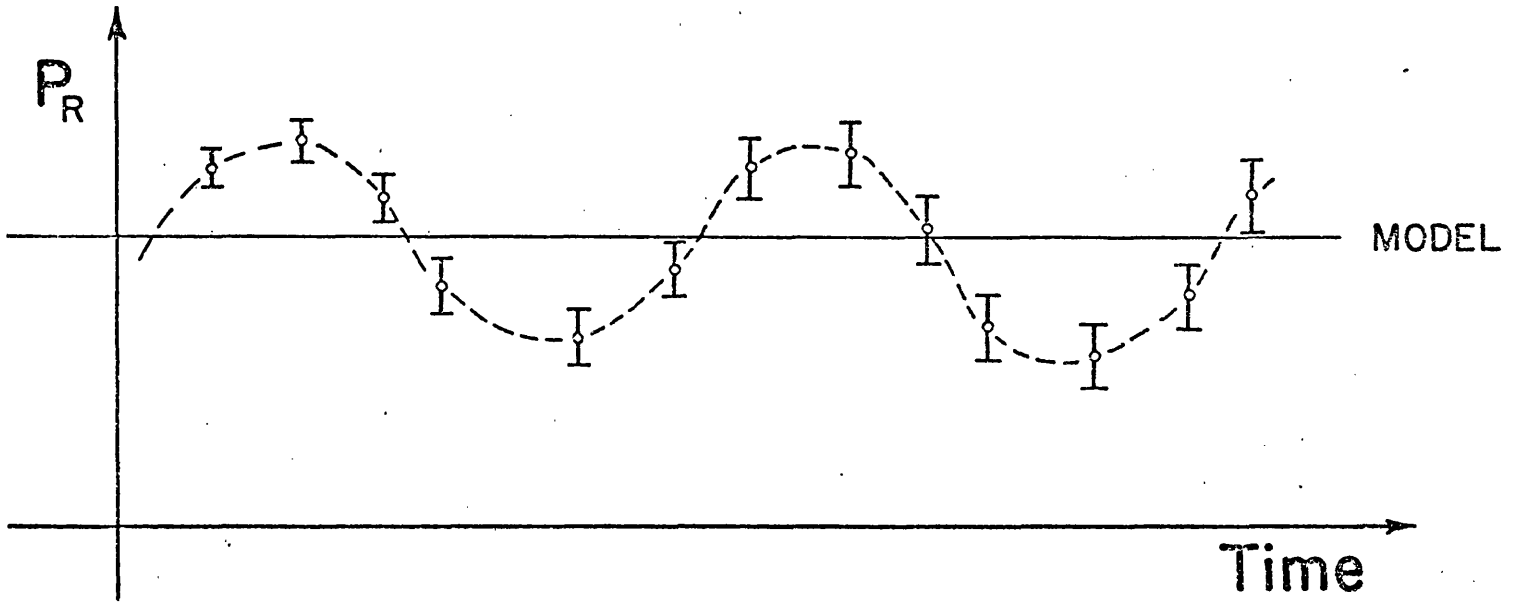

Figure 2.9

Schematic diagram showing 'real' variability in polarization. A model which predicts constant polarization displays a small formal error yet would have an unacceptable chi-squared.

for which χ^2_{2N} is less than $\chi^2_{10\%,2N}$ are in the 90% R.C.I. and produce acceptable fits to the observations. The details of the fitting procedure are as follows. The canonical model predicts the Stokes parameters in the natural frame given by (2.28). For a given inclination i the coefficients satisfy the constraints (2.29).

We define $Q_{t,r} = Q_t\,(r.\,\frac{2\pi}{N})$ where r = 0, 1, ...N-1 (similarly for $U_{t,r}$) with, as stated previously, the primed and unprimed quantities corresponding to laboratory and natural frame values respectively, the transformation:

$$\begin{pmatrix} X \\ Y \end{pmatrix}' = \begin{pmatrix} \cos\theta & \sin\theta \\ -\sin\theta & \cos\theta \end{pmatrix} \begin{pmatrix} X \\ Y \end{pmatrix} \qquad (2.48)$$

holds for

$$\begin{pmatrix} Q_t \\ U_t \end{pmatrix} \begin{pmatrix} Q_{ob} \\ U_{ob} \end{pmatrix} \begin{pmatrix} q_j \\ v_j \end{pmatrix} \begin{pmatrix} p_j \\ u_j \end{pmatrix}_{j=0,2.}$$

This follows from the rotational properties of the Stokes parameters. The measure of the goodness of fit of model to data (necessarily in the lab frame) is

$$F'(p') = \sigma^2\,\chi^2 = \sum_{r=0}^{N-1} (Q'_{ob,r} - Q'_{t,r})^2 + (U'_{ob,r} - U'_{t,r})^2 \qquad (2.49)$$

where with only slight loss of generality we have assumed $\sigma_r = \delta_r = \sigma$ (which is close to the actual case). This makes χ^2_{2N} rotationally invariant resulting in considerable simplification and allows analytic treatment in terms of least squares.

We wish to minimize Equation (2.49) subject to the primed constraints:

$$\frac{(p'_1 \cos\theta - u'_1 \sin\theta)}{(q'_1 \sin\theta + v'_1 \cos\theta)} = -\frac{(q'_1 \cos\theta - v'_1 \sin\theta)}{(p'_1 \sin\theta + u'_1 \cos\theta)} = \cos i$$

and (2.50)

$$\frac{(p'_2 \cos\theta - u'_2 \sin\theta)}{(q'_2 \sin\theta + v'_2 \cos\theta)} - \frac{(q'_2 \cos\theta - v'_2 \sin\theta)}{(p'_2 \sin\theta + u'_2 \cos\theta)} = \frac{1 + \cos^2 i}{2 \cos i}$$

(a) for any fixed value of inclination w.r.t. the variables p' and θ and (b) with respect to i, p' and θ (N.B. θ enters through constraints (2.50) We use the method of Lagrange multipliers to do this. We know that:

$$F'(p') = F(p,\theta);\quad p = p(p',\theta) \qquad (2.51)$$

and therefore if $\{p', \theta_o, i_o\}$ is optimal for F' subject to the proved constraints (2.50) then $\{p = p(p',\theta_o), \theta_o, i_o\}$ will be optimal for F subject to the unproved constraints (2.44). Thus the problem reduces to minimizing the function $F(p,\theta)$ with respect to p and θ_o and in case (b) of above with respect to i also. Writing the constraints (2.44) as $g_1 = 0$, $g_2 = 0$, $g_3 = 0$ and $g_4 = 0$ with:

$$\begin{aligned} g_1(p_1,v_1,c) &= p_1 - v_1 c \\ g_2(q_1,u_1,c) &= q_1 + u_1 c \\ g_3(p_2,u_2,c) &= p_2 c - \left(\frac{1+c^2}{2}\right) v_2 \qquad (2.52) \\ \text{and} \quad g_4(q_2,u_2,c) &= q_2 c + \left(\frac{1+c^2}{2}\right) u_2 \end{aligned}$$

where $c = \cos i$

We obtain 12 additional Lagrange equations

$$\frac{\partial F}{\partial \{p\}} + \sum_{\ell=1}^{4} \lambda_\ell \frac{\partial g_\ell}{\partial \{p\}} = 0 \qquad (2.53)$$

$$\frac{\partial F}{\partial c} + \sum_{\ell=1}^{4} \lambda_\ell \frac{\partial g_\ell}{\partial c} = 0 \qquad (2.54)$$

and

$$\frac{\partial F}{\partial \theta} + \sum_{\ell=1}^{4} \lambda_\ell \frac{\partial g_\ell}{\partial \theta} = 0 \qquad (2.55)$$

where p are the 10 Fourier coefficients (p_o, u_o, p_1, q_1, u_1, v_1, p_2, q_2, u_2, v_2) and λ_ℓ are the undetermined Lagrange multipliers. We need therefore to evaluate the partial derivatives $\frac{\partial F}{\partial p}$, $\frac{\partial F}{\partial c}$ and $\frac{\partial F}{\partial \theta}$ (but since F does not involve c $\frac{\partial F}{\partial c} = 0$).

Consider $\frac{\partial F}{\partial p_k}$:

$$\frac{\partial F}{\partial p_k} = - \sum_{r=0}^{n-1} (Q_{ob,r} - Q_{t,r}) \frac{\partial Q_{t,r}}{\partial p_k} \qquad (2.56)$$

Now we know:

$$Q_{b,r} = \sum_{j=0}^{2} p_j \cos r_j \beta + q_j \sin r_j \beta \qquad (2.57)$$

where $\beta = 2\pi/N$

and hence

$$\frac{\partial Q_{t,r}}{\partial p_k} = \cos r k \beta. \qquad (2.58)$$

Substituting in (2.46) and using the orthogonality relations:

$$\sum_{r=0}^{N-1} \cos r m \beta \cos r n \beta = \begin{cases} 0 & m \neq n \\ N/2 & m=n;\ n \neq 0, N \\ N & m=n=0,N \end{cases} \qquad (2.59)$$

and similarly for $\sum_{r=0}^{N-1} \sin r m \beta \sin r n \beta$

gives:

$$\frac{\partial F}{\partial p_o} = -2N (\bar{p}_1 - p_o)$$

$$\frac{\partial F}{\partial p_1} = -N (\bar{p} - p_1) \qquad (2.60)$$

$$\frac{\partial F}{\partial p_2} = -N (\bar{p}_2 - p_2)$$

where $\bar{p}_o = \frac{1}{N} \sum_{r=0}^{N-1} Q_{ob,r}$; $\bar{p}_k = \frac{2}{N} \sum_{r=0}^{N-1} Q_{ob,r} \cos r k \beta$ (2.61)

Similar treatment of $\frac{\partial F}{\partial q_k}$, $\frac{\partial F}{\partial u_k}$, $\frac{\partial F}{\partial v_k}$ $k = 0,1,2$

yields expressions with:

$$\begin{matrix} \bar{q}_k \\ \bar{v}_k \end{matrix} = \frac{2}{N} \sum_{r=0}^{N-1} \begin{matrix} Q_{ob,r} \\ U_{ob,r} \end{matrix} \sin r k \beta \qquad (2.62)$$

and $\bar{u}_o = \frac{1}{N} \sum_{r=0}^{N-1} U_{ob,r}$; $\bar{u}_k = \frac{2}{N} \Sigma U_{ob,r} \cos rk\beta$ $k = 1,2$

$\frac{\partial F}{\partial \theta}$ is similarly evaluated. $\frac{\partial U_{ob,r}}{\partial \theta} = Q_{ob,r}$ and

$\frac{\partial Q_{ob,r}}{\partial \theta} = -U_{ob,r}$ and the orthogonality relations (2.59) yield:

$$\begin{aligned} \frac{\partial F}{\partial \theta} = {} & 2N(p_o\bar{u}_o - u_o\bar{p}_o) + N(p_1\bar{u}_1 - u_1\bar{p}_1) \\ & + N(q_1\bar{v}_1 - v_1\bar{q}_1) + N(p_2\bar{u}_2 - u_2\bar{p}_2) \\ & + N(q_2\bar{v}_2 - v_2\bar{q}_2) \end{aligned} \qquad (2.63)$$

The Lagrange equations take the form:

$$\left.\begin{aligned} -2N (\bar{p}_o - p_o) = 0 \\ -2N (\bar{u}_o - u_o) = 0 \end{aligned}\right\} \quad \text{i.e. } p_o = \bar{p}_o \text{ and } u_o = \bar{u}_o \qquad (2.64)$$

and

$$
\begin{aligned}
&\text{(i)} && -N(\bar{p}_1 - p_1) + \lambda_1 && = 0 \\
&\text{(ii)} && -N(\bar{q}_1 - q_1) + \lambda_2 && = 0 \\
&\text{(iii)} && -N(\bar{u}_1 - u_1) + \lambda_{2c} && = 0 \\
&\text{(iv)} && -N(\bar{v}_1 - v_1) - \lambda_1 c && = 0 \\
&\text{(v)} && -N(\bar{p}_2 - p_2) + \lambda_3 c && = 0 \qquad (2.65) \\
&\text{(vi)} && -N(\bar{q}_2 - q_2) + \lambda_4 c && = 0 \\
&\text{(vii)} && -N(\bar{u}_2 - u_2) + \lambda_4 (1+c^2)/2 && = 0 \\
&\text{(viii)} && -N(\bar{v}_2 - v_2) - \lambda_3 (1+c^2)/2 && = 0
\end{aligned}
$$

Optimization w.r.t. by (2.55) gives:

$$\text{(ix)}\ (p_1\bar{u}_1 - u_1\bar{p}_1) + (p_2\bar{u}_2 - u_2\bar{p}_2) + (q_1\bar{v}_1 - u_1\bar{q}_1) + (q_2\bar{v}_2 - u_2\bar{q}_2) = 0$$

and correspondingly w.r.t.c :

$$\text{(x)}\ -\lambda_1 v_1 + \lambda_2 u_1 + \lambda_3 (p_2 - cu_2) + \lambda_4 (q_2 + cu_2) = 0$$

Using the constraints (2.44) and (2.65) (i), (ii), (iii), and (iv) we obtain:

$$p_1 = \frac{c^2}{1+c^2}\left(\bar{p}_1 + \frac{\bar{v}_1}{c}\right), \quad q_1 = \frac{c^2}{1+c^2}\left(\bar{q}_1 - \frac{\bar{u}_1}{c}\right) \qquad (2.66)$$

$$u_1 = -\frac{q_1}{c} \quad \text{and} \quad v_1 = \frac{p_1}{c}$$

Similarly (2.44) and (2.65) (v), (vi), (vii), and (viii) gives

$$p_2 = \frac{\alpha^2}{1+\alpha^2}\left(\bar{p}_2 + \frac{\bar{v}_2}{\alpha}\right), \quad q_2 = \frac{\alpha^2}{1+\alpha^2}\left(\bar{q}_2 - \frac{\bar{u}_2}{\alpha}\right) \qquad (2.67)$$

$$u_2 = -\frac{q_2}{\alpha} \quad \text{and} \quad v_2 = \frac{p_2}{\alpha}$$

where $\alpha = (1 + c^2/2c)$.

Equation (2.65) (ix) upon substitution of these values yields after slight manipulation:

$$\frac{c^2-1}{c^2+1}\left(\bar{p}_1\bar{u}_1 + \bar{q}_1\bar{v}_1\right) + \frac{\alpha^2-1}{\alpha^2+1}\left(\bar{p}_2\bar{u}_2 + \bar{q}_2\bar{v}_2\right) \qquad (2.68$$

This in case (a) for given inclination determines the optimal value of θ. This value of θ together with (2.66) and (2.67) alternatives

all the harmonic coefficients $\{p\}$.

Using the rotational transforms:

$$p_1 = \bar{p}'_1 \cos\theta - \bar{u}'_1 \sin\theta : \quad q_1 = \bar{q}'_1 \cos\theta - \bar{v}'_1 \sin\theta \qquad (2.69)$$

etc. we can write (2.68) on the form:

$$\tan 2\theta = \frac{\Gamma B'_1 - B'_2}{A'_2 - \Gamma A'_1} \qquad (2.70)$$

where $$\Gamma = \frac{1 + 6c + c^4}{1 - c^4}$$

and: $$A'_k = \bar{p}'^2_k + \bar{q}'^2_k - \bar{u}'^2_k - \bar{v}'^2_k$$

and $$B'_k = 2(\bar{u}'_k \bar{p}'_k + \bar{v}'_k \bar{q}'_k)$$

The functions A'_k and B'_k can be found directly from observations in the laboratory (primed) frame and consequently θ_{opt} is determined directly.

The set of chosen i, θ_{opt} and $\{p\}_{opt}$ (from (2.66), (2.67)) can then be used to form χ^2_{2N} and we call the χ^2_{2N} value at the optimum parameter values (for each inclination). inf χ^2_{2N}.

In case (b) where we need to optimize w.r.t. inclination (in the form of c) also we use (2.65) (X) to obtain by substituting from the $\lambda'_\ell s$

$$(\bar{p}_1 - p_1)p_1 + (\bar{q}_1 - q_1)q_1 - \frac{1-c^2}{1+c^2}(p_2(\bar{p}_2 - p_2) + q_2(\bar{q}_2 - q_2)) = 0 \qquad (2.71)$$

or by eliminating p_1, q_1, p_2, q_2 throughout by the equations (2.66) and (2.67) we obtain:

$$\frac{c^2}{1+c^2}\left[A_1 + \frac{1-c^2}{c} I_1\right] - \frac{1-c^2}{1+c^2}\left[\frac{\alpha^2}{1+\alpha^2}\left(A_2 + \frac{1-\alpha^2}{\alpha} I_2\right)\right] = 0 \qquad (2.72)$$

where A_k and I_k are defined as

$$A_k = \bar{p}_k^2 + \bar{q}_k^2 - \bar{u}_k^2 - \bar{v}_k^2$$

and $$I_k = \bar{p}_k \bar{v}_k - \bar{q}_k \bar{u}_k \qquad (2.73)$$

Introducing $B_k = 2(u_k p_k + v_k q_k)$ it is simple to show that:

$$\begin{aligned} I_k &= I'_k \\ A_k &= A'_k \cos 2\theta - B'_k \sin 2\theta \qquad (2.74) \\ \text{and} \qquad B_k &= A'_k \sin 2\theta + B'_k \cos 2\theta \qquad k = 1,2 \end{aligned}$$

where A'_k , B'_k and I'_k are determined completely from observations (i.e. in the laboratory frame).

A complete solution therefore is given in
case (a) by (2.66), (2.67), (2.68) and in
case (b) by (2.66), (2.67), (2.68) and (2.72).

A special case occurs when we stipulate beforehand that we have a orbital plane symmetric density distribution and then (2.68) and (2.72) reduce to:

$$\begin{aligned} &\bar{p}_2\bar{u}_2 + \bar{q}_2\bar{u}_2 = 0 \\ \text{and} \qquad &A_2 + \frac{1-\alpha^2}{\alpha} I_2 = 0 \qquad (2.75) \end{aligned}$$

Equation (2.66) becomes redundant since all 1st harmonics are zero. (2.67) remains unchanged.

A slight complication to the problem of determining the minimum χ^2_{2N} by this procedure is that the method does in fact pick out any turning point, inf χ^2_{2N} and not only the global minimum. In case (a) (for fixed i) we see that from (2.78) four solutions for θ exist viz:

$$\begin{aligned} \theta_n &= \Omega + n\pi/2 \qquad n = 0,\ldots,3 \\ \text{with} \qquad \Omega &= \tfrac{1}{2} \tan^{-1} \left(\frac{\Gamma B'_1 - B'_1}{A'_2 - \Gamma A'_1} \right) \qquad (2.78) \end{aligned}$$

Two distinct solutions occur i.e. one from the pair for (θ_o, θ_2) and one from the other pair of solutions of (2.78) namely (θ_1, θ_3). Therefore θ_o and θ_1 will represent two solutions. It happens, however, that only one branch represents a minimum χ^2_{2N}. Figure (2.10) shows the resulting variation of $\sigma^2 \text{inf}\ \chi^2_{2N}$ with chosen inclination in schematic form. Actual simultaneous solution for θ_{opt}, i_{opt} must be attempted but we see analytically that if (c_o, θ_o) represents a solution ($c_o = \cos\ i_o$) then (c_o, $\theta_o + \pi$) ($-c_o$, $\theta_o + \pi/2$) and ($-c_o$, $\theta_o + 3\pi/2$) are also solutions. Thus if the turning point in inf χ^2_{2N} occurs at i_{opt} then another will occur at $\pi - i_{opt}$ on the second branch but only

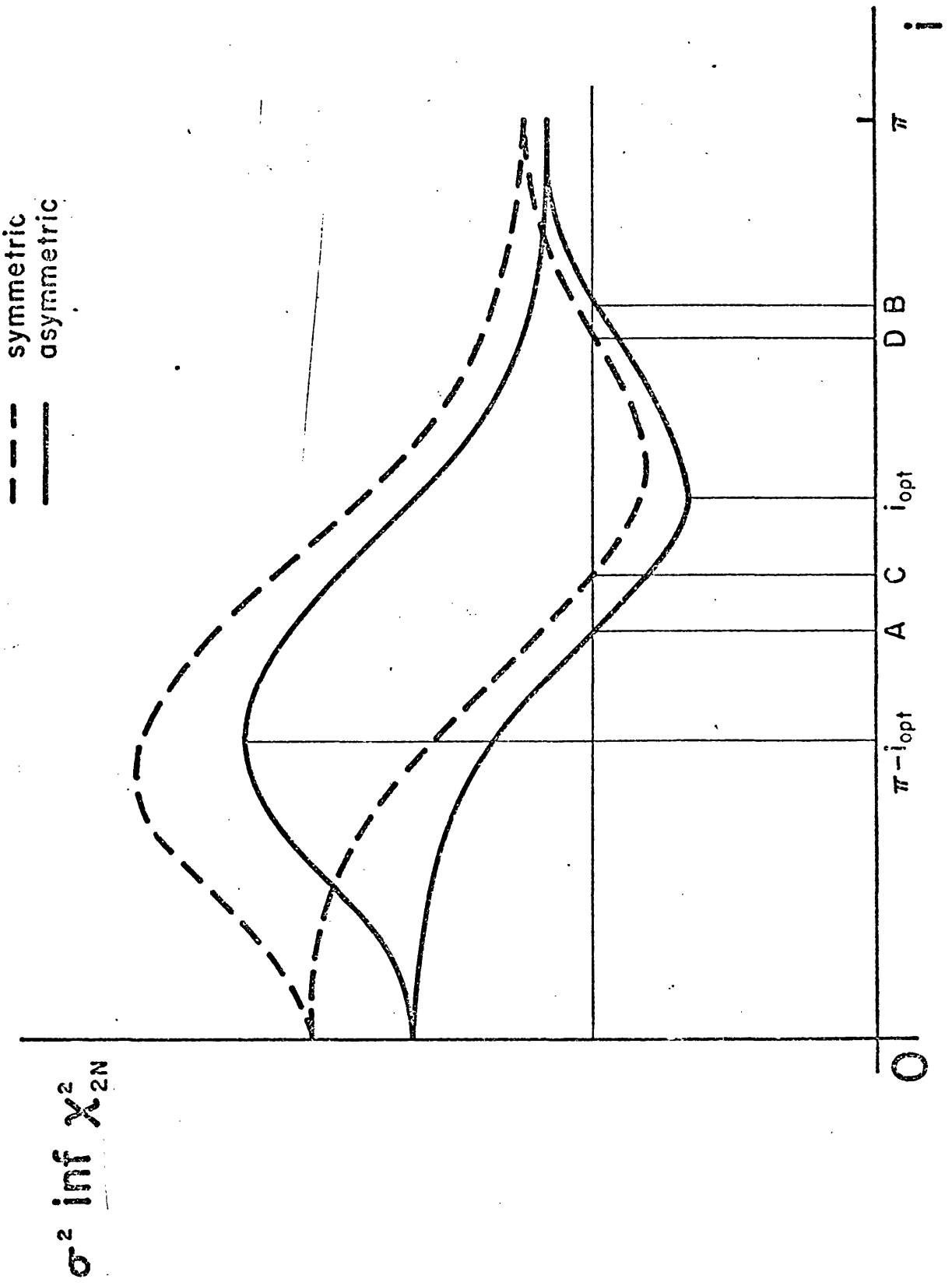

Figure 2.11

Representation of inf χ^2_{2N} as a function of inclination, i in schematic form. The four curves show the cases that could arise when determining i_{opt} and associated confidence intervals. The R.C.I. 's are indicated for the values of χ^2_{2N} at x% significance.

one will represent a minimum value. In Figure (2.11) both curves for the general canonical model involving 1st and 2nd harmonic variations, and the symmetric canonical model involving just 2nd harmonic variations in polarization are shown. The symmetric model having two less independent parameters should, for all values of i, produce inf χ^2_{2N} $(i)_{sym} \geq$ inf χ^2_{2N} $(i)_{asymm.}$ The corresponding x% relative confidence interval in i for the restricted case should also be smaller. This is indicated in Figure (2.11).

We may anticipate several possible cases which may arise in the variation of inf χ^2_{2N} with i. These are shown in Figure (2.12). In the case of curve 1 the model is acceptable but over a wide range (i_A, i_B) of inclination about i_{opt} at x% significance. Thus $[i_A, i_B]$ is the (100-x)% relative confidence interval on i and the model cannot be rejected when i is in this region. Case 2 shows the model acceptable and the R.C.I. of $[i_c, i_p]$ being narrow and therefore i_{opt} is well defined. For cases 3 and 4 the model is unacceptable and must be rejected at x% significance as being a bad fit to the data. In case 4 however the variation of inf χ^2_{2N} with i is sharp and in this case a Formal error analysis would produce a small error on i_{opt} even though through our analysis the model would be shown to be unacceptable. A crucial point however is the fact that the acceptability of the model and confidence interval will depend severely on the standard deviation on the observations (here binned observations) since a factor $1/\sigma^2$ occurs in the analysis. Thus slight improvement in the σ level could mean a large improvement in the model fit and substantial reduction of the R.C.I. In the extreme case the model could be shown to be unacceptable by the reduction in σ . Therefore we have shown that it is possible to obtain the optimum, constrained 'best fit' canonical model parameters from a set of observations and hence test the acceptability of the model, and from a model dependent error (called the R.C.I.) on the 'best fit' parameters by means of a χ^2 analysis. We have concentrated on the parameter i, the binary inclination since it is this parameter that had been controversially determined (as far as the error estimate was concerned) earlier (Rudy and Kemp 1978). Similar analysis could be undertaken to obtain R.C.I.'s for other binary parameters but will not be considered here.

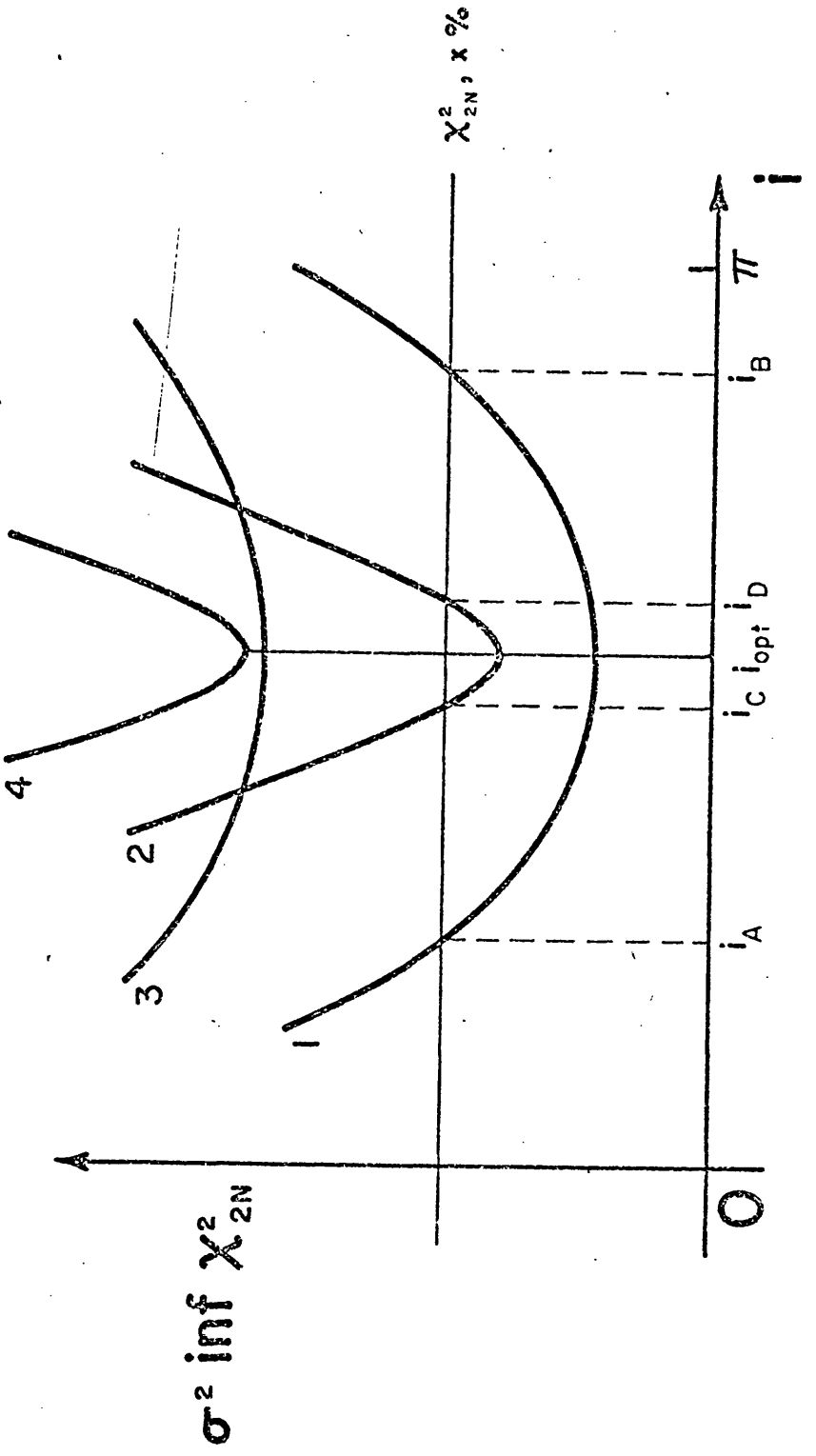

Figure 2.12 Representation of $\inf\chi^2_{2N}$ as function of inclination, i, in schematic form. The four curves show the cases that could arise when determining i_{opt} and associated confidence intervals. The "relative confidence intervals" are indicated for the value of χ^2_{2N}, x% (the horizontal line) corresponding to x% significance level.

To obtain a solution to the Equation (2.72), (2.76) that would give i_{opt} and θ_{opt} without choosing i (i.e. as in case b) we must resort to the Newton-Raphson numerical method of approximating the solution of two non-linear simultaneous equations (cf. Pollard 1979) since (2.57), (2.61) cannot be solved simply. This technique involves an iterative procedure that should converge to the correct values (correct within the tolerance set previously). We form the relations:

$$\frac{\partial f_1}{\partial \theta}(\theta_n, c_n)\, h_n + \frac{\partial f_1}{\partial c}(\theta_n, c_n) k_n \simeq - f_1(\theta_n, c_n)$$

and (2.77)

$$\frac{\partial f_2}{\partial \theta}(\theta_n, c_n)\, h_n + \frac{\partial f_2}{\partial c}(\theta_n, c_n) k_n \quad - f_2(\theta_n, c_n)$$

where

$$f_1(\theta, c) = \tan\theta - \frac{\Gamma B_1' - B_2'}{A_2' - \Gamma A_1'} = 0 \qquad (2.78)$$

where $c = \cos i$ and $\Gamma = \left(\frac{1 + 6c^2 + c^4}{1-c^4}\right)$

and

$$f_2(\theta, c) = \left(\frac{c}{1+c^2}\right)^2 \left[(A_1' \cos\theta - B_1' \sin\theta) + \left(\frac{1-c^2}{c}\right) I_1'\right] - \left(\frac{\alpha}{1+\alpha^2}\right)^2 \left[(A_2' \cos\theta - B_2' \sin\theta) + \left(\frac{1-\alpha^2}{\alpha}\right) I_2'\right] \qquad (2.79)$$

h_n and k_n are the adjustments to the initial estimation of c and θ (found by trial and error) so that:

$$c_{n+1} = c_n + h_n$$

and (2.80)

$$\theta_{n+1} = \theta_n + k_n$$

The partial derivatives are evaluated at the values (i_n, θ_n). We solve (2.77) for h_n and k_n and test whether their values are less than the stated tolerance. Differentiation of the functions f_1 and f_2 give:

$$\frac{\partial f_1}{\partial c} = - \left[\frac{B_1'}{(A_2' - \Gamma A_1')} + A_1 \frac{\Gamma B_1' - B_2'}{A_2' - \Gamma A_1'}\right] \frac{\partial \Gamma}{\partial c} \qquad (2.80)$$

where

$$\frac{\partial \Gamma}{\partial c} = 4c \frac{(3c^4 + 2c^2 + 3)}{(1-c^4)^2}$$

$$\frac{\partial f_2}{\partial c} = \left[2c \frac{(1-c^2)}{(1+c^2)^3} (A_1' \cos\theta - B_1' \sin\theta) + \frac{(1-6c^2+c^4)}{(1+c^2)^3} I_1' \right] - \left[2\alpha \frac{(1-\alpha^2)}{(1+\alpha^2)^3} (A_2' \cos\theta - B_2' \sin\theta) + \frac{(1-6\alpha^2+\alpha^4)}{(1+\alpha^2)^3} I_2' \right] \frac{\partial \alpha}{\partial c} \quad (2.82)$$

where $$\frac{\partial \alpha}{\partial c} = -\frac{(1-c^2)^2}{2c^2}$$

$$\frac{\partial f_1}{\partial \theta} = \sec^2\theta \quad (2.83)$$

and $$\frac{\partial f_2}{\partial \theta} = \frac{c^2}{(1+c^2)^2} (-A_1' \sin\theta - B_1' \cos\theta) - \frac{\alpha^2}{(1+\alpha^2)^2} (-A_2' \sin\theta - B_2' \cos\theta) \quad (2.84)$$

This method of finding i_{opt} and θ_{opt} was not in fact utilized in the analysis of real data since we usually considered case (a) of given i to obtain the variation of other model parameters over the whole range of i. Alternatively this method can be used for a straightforward fitting to obtain these optimum parameters. The stability of the method of solution is not considered here but the fact that the equation to be solved are highly non-linear may indicate that the solution may be intractable.

We now proceed to apply this technique to data of Cygnus X-1 in an attempt to test the relevance of the canonical model to the observations of Kemp et al (1979).

2.5 Application of the Optimization Analysis to Cygnus X-1 data.

Before we present the results of the application to Cygnus X-1 it is convenient to attempt to discuss the canonical model assumptions in relation to this system.

Numerous spectrophotometric studies have been made of Cygnus X-1 (Bolton 197 , 1975, Guinan and Hutching 1974 ab) which give a low eccentricity for the orbit of the stars. In fact Bolton (1975) quotes e = 0.06 as an upper limit from his spectroscopic studies. Since the bulk of scattering material is likely to belong to the accretion disk

and associated gas stream it is likely that the scatterers will be corotating with the binary. This approximately satisfies the corotation assumption above. The lack of strong eclipse behaviour (Walker and Quintanilla 1978, Holt et al 1976) indicates that no occultation effects effect the light source and reduce the possibility of variable obscuration of the scattering region. This latter possibility has been considered likely by Milgrom (1978). However if the majority of scattered light comes from the accretion disk then variable occultation of it could also produce a strong variable modulation of the systems Xray flux. This is not observed. The possibility of a large optical depth violating an assumption of the model is also seen to be unlikely. We can estimate the Thomson scattering optical depth τ_s by the formulae $\tau_3 \simeq \sigma_T \bar{n}_e L$ where $\bar{n}_e$ is the mean electron density along the path of scattered photon. Even with $L \simeq D$, the stellar separation $\simeq 3.10^{12}$ cm we would require $\bar{n}_e \simeq 10^{12}$ cm^{-3} over this enormous region to make $\tau_s \sim 1$. Values of $\bar{n}_e \sim 10^{11}$ cm^{-3} and $L \lesssim 10^{12}$ cm are more typical (Novikov and Thorne 1972) so that $\tau_s \lesssim 10^{-1}$. The single scattering assumption is then not entirely satisfactory for this τ_s, which is better treated by a Monte Carlo multiple scattering method (Daniel 1980a). The results of this treatment seem to differ only in the inferred extent of the envelope rather than in the geometric effectsof i. There therefore seems to be no strong a priori case for rejecting the assumption of the model. Further testing of these will be apparent from the χ^2 test when applying the model to the data.

The formidable task involved in establishing and quantifying phase locked polarization variations for Cygnus X-1 (in terms of Q,U loci) has been undertaken over the past 5 years by J.C. Kemp and colleagues at the Pine Mountain Observatory, Oregon. Numerous publications have indicated the updating and subsequent improvement in definition of the Q,U figures (Nolt et al 1975, Kemp et al 1976, 1978, 1979, Kemp 1980) for Cygnus X-1 and it has been established beyond doubt that the broad band linear polarization variations observed are real and at least partly locked to the binary orbital period of 5.6 days. The exact qualitative nature of these variations is, however, less clear. Kemp and collaborators have generally analysed their polarimetric data by best fitting a truncated Fourier series (in binary phase) by an

unconventional technique after folding the raw data on the photometrically established ephemeris and grouping into phase bins. In the first such analysis Nolt et al (1975) the data in the U band over a 45 day period were presented as describable by 1st and 2nd harmonic variations in Q and U, the corresponding smoothed locus being shown in Figure (2.13a). Analysis of this smoothed locus by Brown et al (1978) in terms of the canonical model (neglecting noise) led to the contradictory i values from 1st and 2nd harmonics mentioned above.

Subsequently Kemp et al (1976) using 113 nights data taken over 16 months, refuted the reality of these results, while Kemp et al (1978) asserted time phase locked variations were found in the B band and that folded Q,U variations based on 170 nights (over 3 years) were well fitted by 2nd harmonics only. This led to the double ellipse locus in the Q,U plane of Figure (2.13b) with a corresponding inclination of $i = 76^{\circ}$ and a formal linear error analysis led to an uncertainty of $\pm 6^{\circ}$. More recently still Kemp et al (1979) published a Q,U analysis based on 315 nights observations in the V band asserting real evidence for variation at phase harmonics other than 2nd (and particularly at the 1st harmonic). Using a 20 harmonic Fourier fit to the folded and binned data, with subsequent exponential damping of harmonics higher than 2nd, they published the Q,U locus of Figure 2.13c. The unsmoothed (Q,U) locus is shown for reference in Figure (2.14a).

The difference between Figure 2.13 a and b may be attributed to some wavelength dependent absorption effects, though Thomson scattering itself is wavelength independent. However the difference between (2.13b) and (2.13c) (both V band) might either indicate that Cygnus X-1 is not stable in its polarimetric behaviour (e.g. due to evolution effects in the envelope) or be due to random errors in the data. In Figure 2.13c we have superposed a typical error box for a set of binned data points (taken from Kemp et al 1979). This suggests that the latter interpretation may be correct. Kemp et al (1979) have, however, not discussed the question of errors in their smoothed damped data locus but have argued that the double looped form is incompatible with the canonical model, thereby invoking a model involving eclipsing of a small localized scattering region by a large accretion disk. In doing so they appear to consider also second harmonic symmetric canonical models and do not discuss the possibility that the double looped

c.f. 2.7

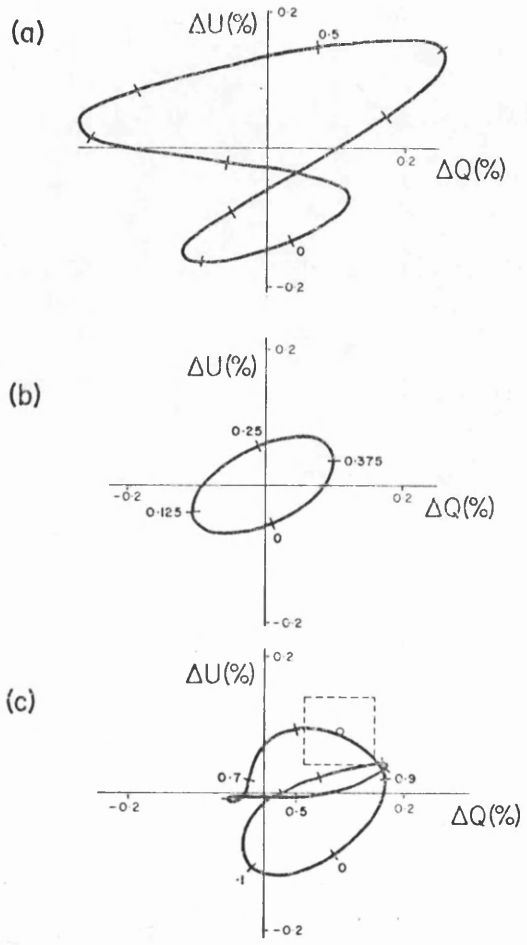

Figure 2.13 Three different Q,U loci (one in U-band, two in V-band) published for Cygnus X-1 (period $5^{d}.600$)

(a) obtained over a 45 day period (23 nights' observations) by Nolt et al (1975) in the U-filter. Consists of smoothed first and second harmonic Fourier 'best fit'.

(b) V-band locus Kemp et al (1978) using 170 nights over a period of 3 years. Resulting $2^{d}.8$ sinusoid 'best fit' gave a double ellipse with eccentricity e = 0.91.

(c) latest locus, in V band also, with data taken on 350 nights up to Nov.78 by Kemp et al (1979). Includes twenty harmonic Fourier fit of phase binned points with arbitrary exponential damping of harmonics higher than second. 1σ error box for binned data point is indicated.

Origins in all cases are arbitrarily translated with loci being only approximate but with correct orientation in all cases.

form arises from 1st harmonics in Q,U due to envelope assymmetry about the systems orbital plane. In fact the possibility of obtaining a double looped Q,U locus broadly similar to Figure (2.13c) from the canonical model can be seen from Figure (2.5) of Chapter 1 where Brown et al (1978) have used the canonical model to fit σ Ori E polarimetric data. Nevertheless if one accepts the smoothed and damped locus in Figure (2.13c) at face value (i.e. without errors) and analyse it in terms of the canonical model according to the procedure described in Brown et al (1978) one obtains initially contradictory values of i from 1st and 2nd harmonics. The separated geometric Q,U loci, namely (Q-, U-) and (Q+, U+) of Brown et al (1978) constructed as outlined in that paper and above are shown in Figure (2.14)b,c,d and e. Both the 20 harmonic (Q-,U-) and (Q+,U+) unsmoothed loci (Figure 2.14 b and c) and the corresponding smoothed versions (Figure 2.14 d and e) are given. As can be seen, the 1st harmonic curves (Q-,U-) are approximately elliptical in shape (especially the smoothed locus) with the 2nd harmonic (Q+,U+) locus being more complicated. The inclusion of 20 harmonics in these cases (and in the smoothed case especially damped n > 2 harmonics) have tended to deform the purely 1st harmonic and 2nd harmonic ellipses of the (Q+, U+) (Q-, U-) diagrams. In fact the curves shown contain contributions from all odd harmonics, including 1st - (Q-,U-) and all even harmonics including 2nd, (Q+, U+). The damping reduces the effect of the n > 2 harmonics severely. In the case of the (Q+,U+) loci an approximate ellipse could be constructed as in Figure 2.15 with the extrema values lying at approximately phases 0.0 and 0.5. The eccentricities of the ellipses (the Q-,U- curve and the constructed Q+,U+ ellipse) are in fact $e_- = 0.794$ and $e_+ = 0.871$ which indicate by the method of Brown et al (1978) inclinations of $i_- = 53^\circ$ and $i_+ = 75^\circ$ and are contradictory. This might lead one to believe that Kemp et al (1979) are right in rejecting the canonical model. However, in the presence of data noise, there is only one correct procedure for testing the acceptability of the model and that is to follow the method outlined above. We now therefore address ourselves to this problem.

The complete run of V band data that we analyse represents a total of 62 binary periods and has been provided by Kemp. The data points were represented according to their phase by folding on the 5.600 day photometric ephemeris and, to remove irregular phase spacings,

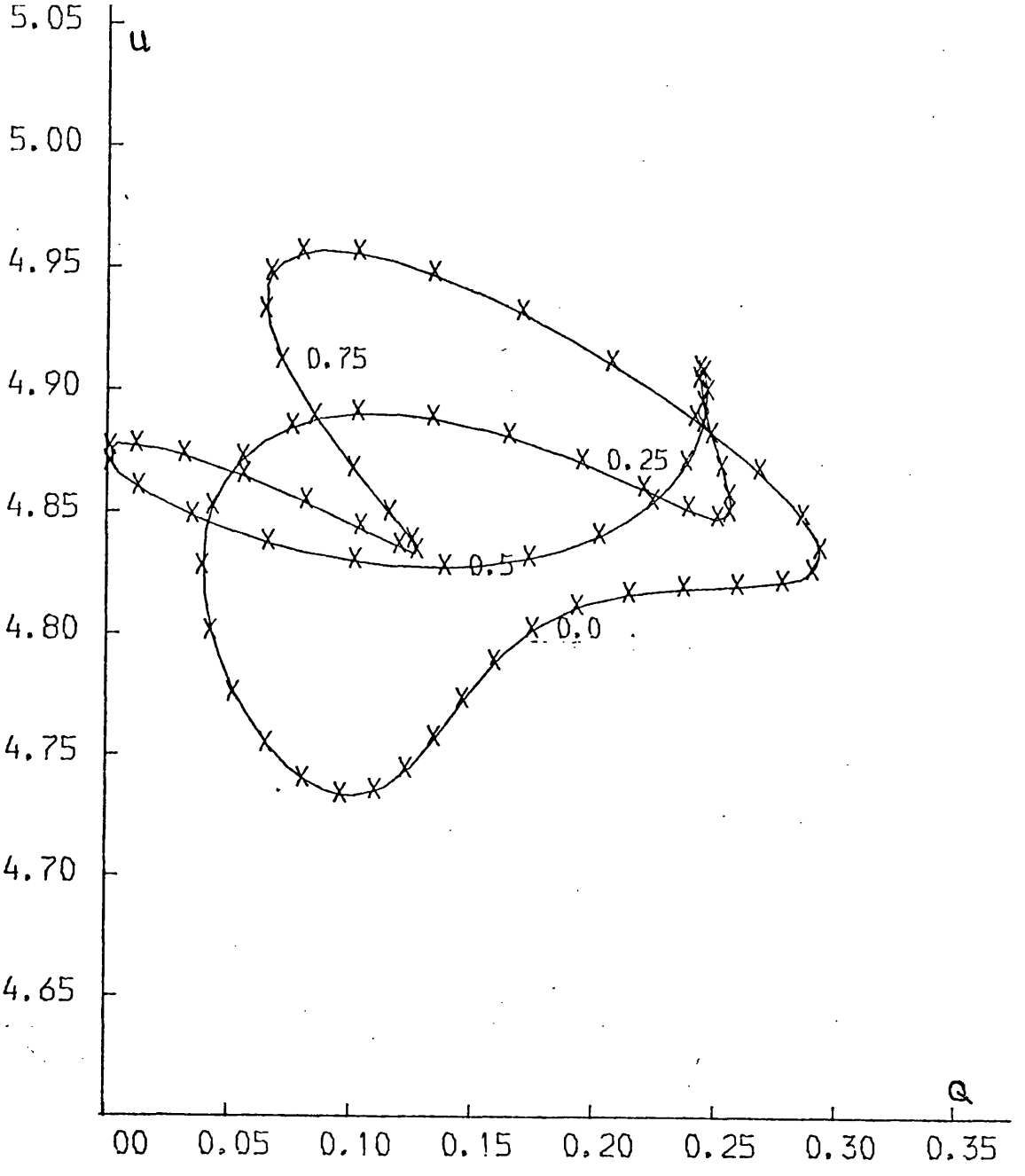

Figure 2.14a Q,U locus for Cygnu X-1 formed with 20 harmonics fitted to the data of Kemp et al (1979). The orbital phases are given at 0.25 intervals.

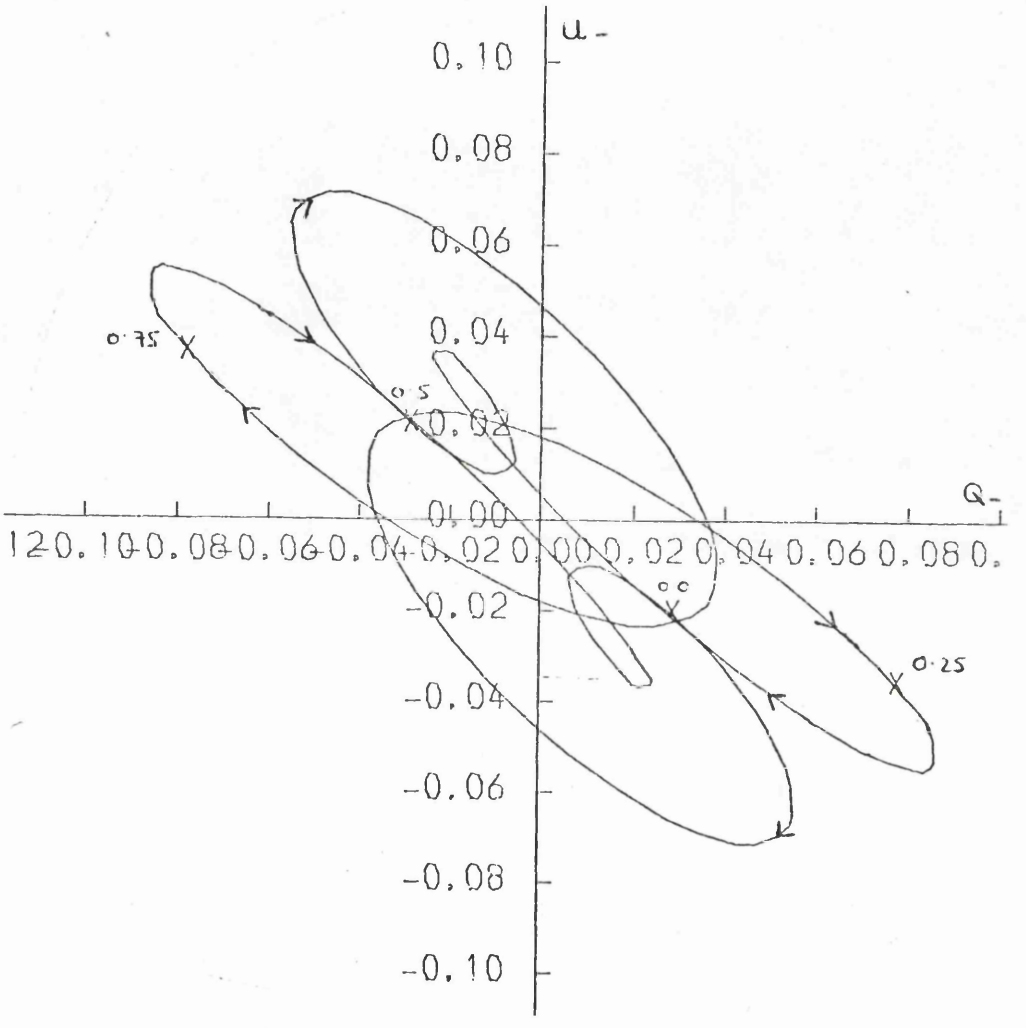

Figure 2.14b The (Q-,U-) locus (formed as in Brown et al 1978) for the 20 harmonic 'data' set of Figure (2.13a). Orbital phases are given at 0.25 intervals.

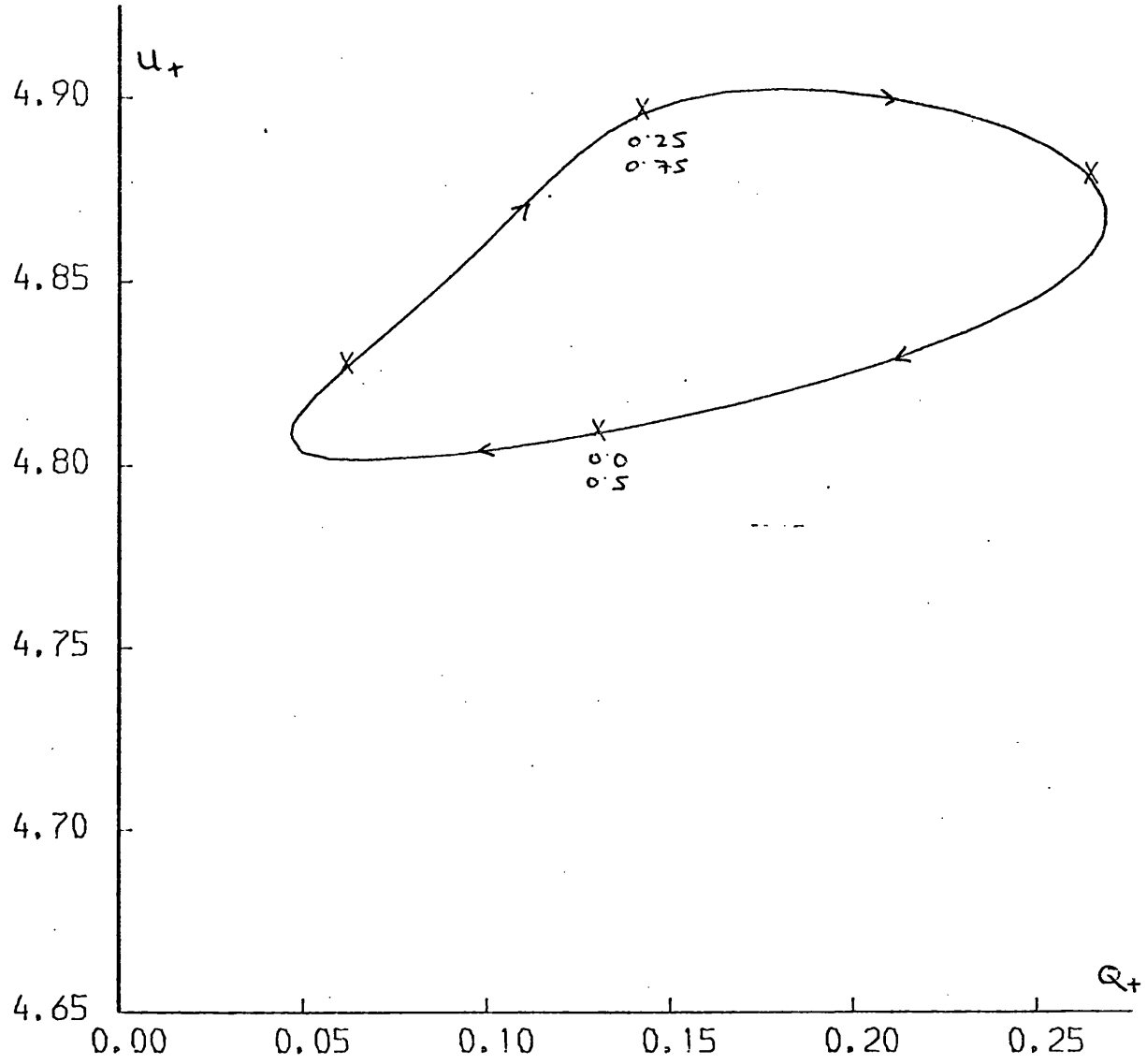

Figure 2.14c The (Q+,U+) ocus of the data set of Figure (2.13a). Orbital phases are given at 0.75 intervals. The locus is swept out twice per orbital period.

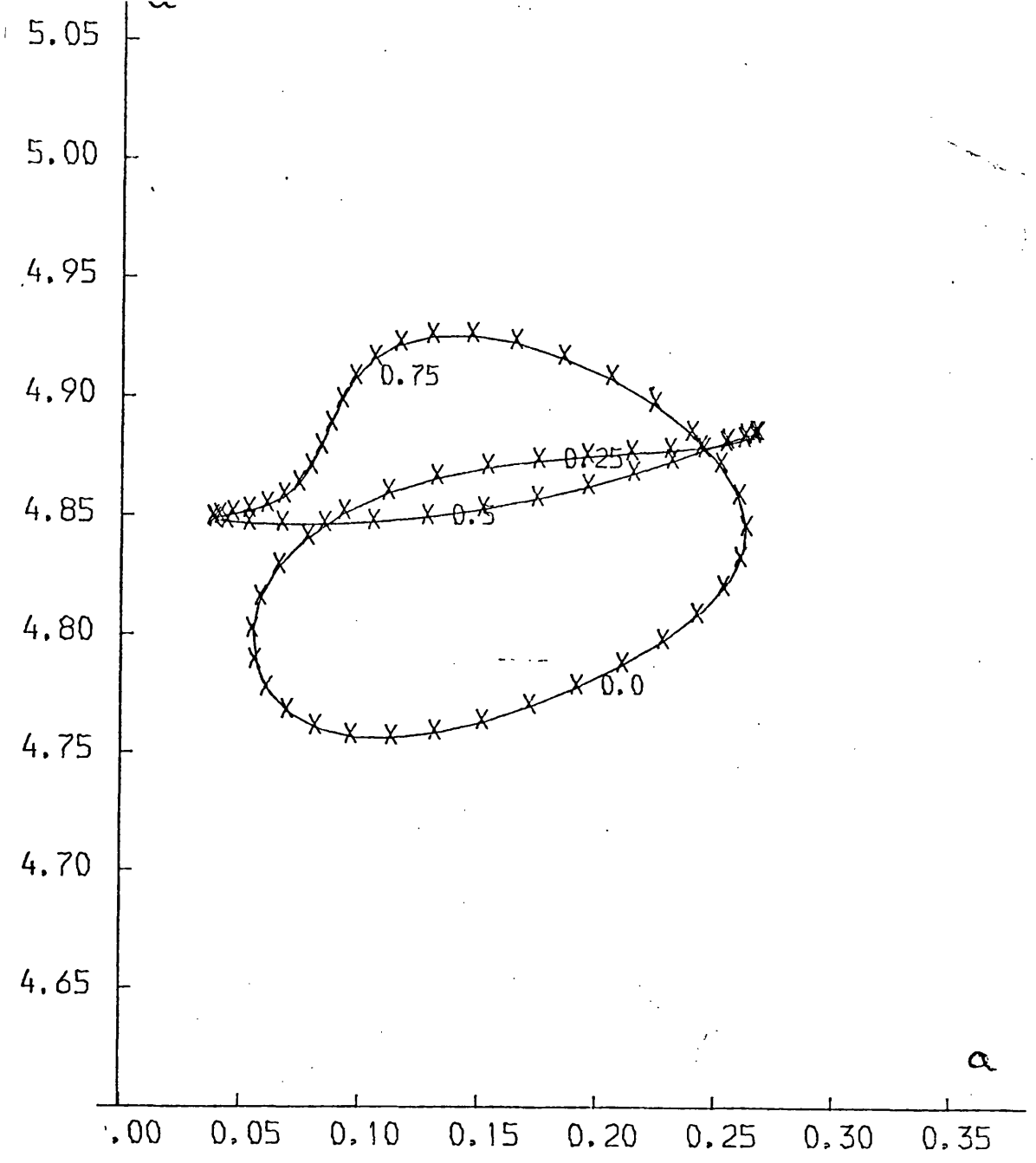

Figure 2.14d Q,U locus for Cygnus X-1 as Figure (2.13a) but with harmonics greater than second smoothed by a displaced Gaussian function: $\exp(-(n-1.5)^2/A)$ with n equal to the number of the harmonic (n=2, second harmonics) A = 7.0.

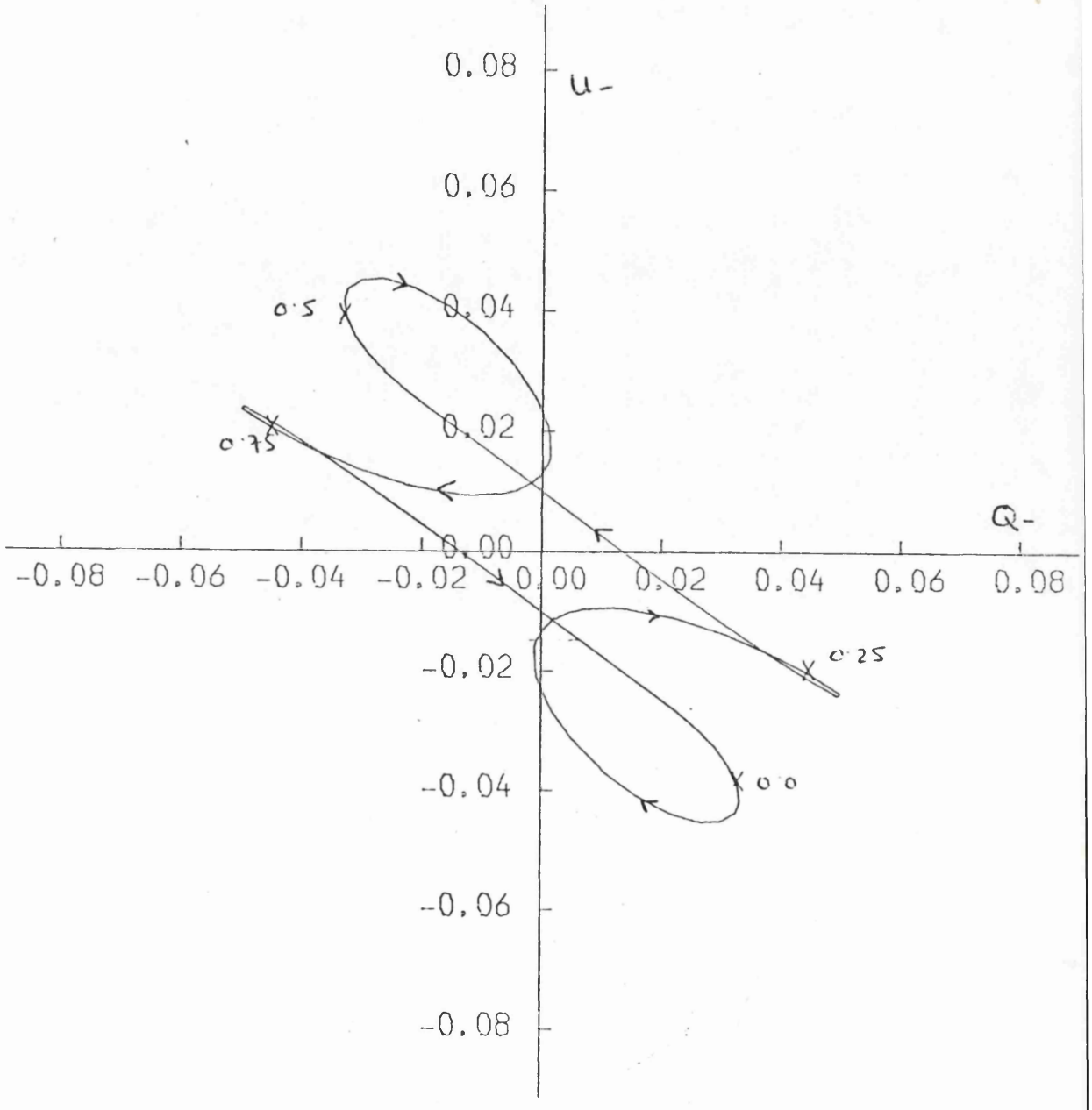

Figure 2.14 e As Figure (2.13b) but with the smoothing factor reducting odd harmonic contributions greater than second (i.e. 3rd, 5th etc.)

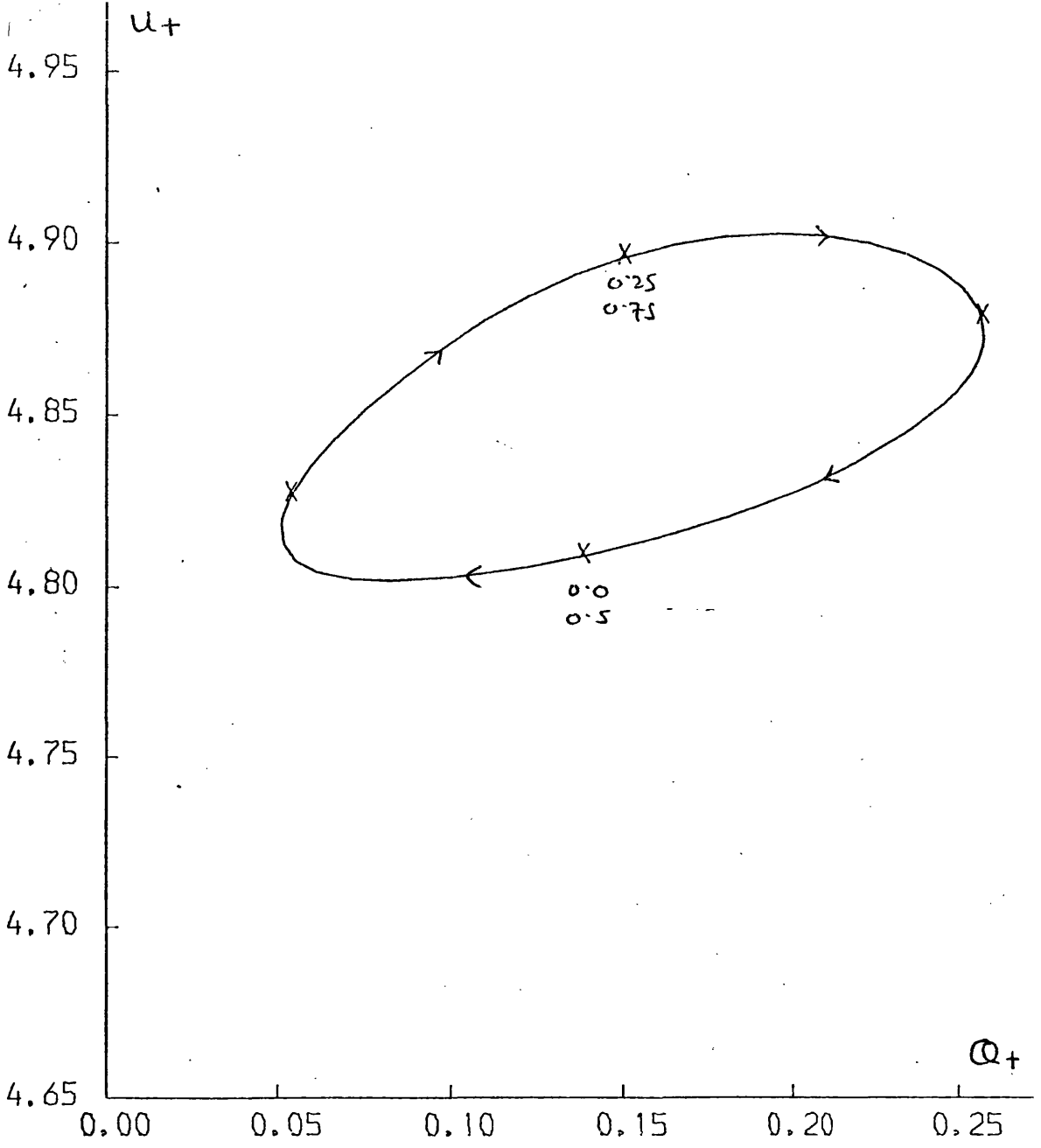

Figure 2.14f As Figure (2.13c) but with the smoothing factor reducing even harmonic contributions greater than second. (i.e. 4th, 6th etc.). Using the relation $e = \sin^2 i \ (2 - \sin^2 i)$ with $e = 0.871$ we obtain one inclination $i = 75^{\circ}$.

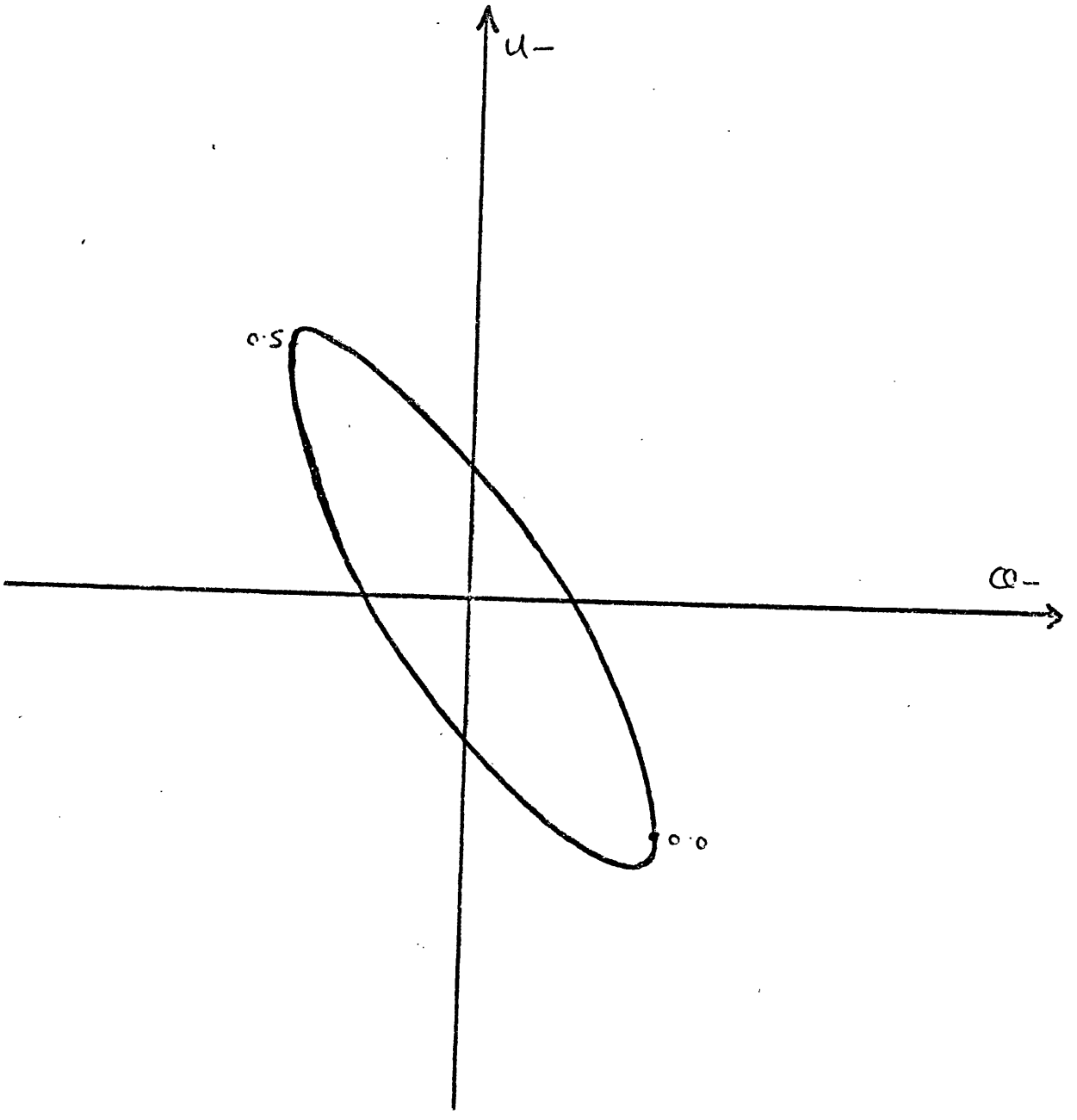

Figure 2.15 Ellipse constructed from Figure (2.13f) in order to give estimate of orbital inclination following Brown et al (1978) by the relation e = sin i. We find e = 0.794 giving one inclination of i = 53°.

were placed in two non-independent sets of 20 phase bins of width $\Delta\phi = 0.05$ one commencing at $\phi = 0.0$ and the other at $\phi = 0.05$. $Q'_{ob,r}$ and $U'_{ob,r}$ are thus calculated from the means of the bins at corresponding phases and the variance estimated from the dispersion in each bin. In Figure (2.16) we show the binned data points $Q'_{ob,r}$, $U'_{ob,r}$ plotted against phase together with a typical binned error bar σ. Superposed are the best fit curves for the canonical model (solid line) and for the symmetric canonical model (dashed line) determined as described above. In Figure (2.17 ab) we show the Q,U results in the form of a locus in the Q,U plane:

(a) data points joined sequentially to give the semi-raw form, which is evidently very noisy; and

(b) the best fit for the canonical model (solid line) and the symmetric canonical model (dashed line).

Superposed on each figure is an error bar to indicate the data noise. We note also that visual comparison of models and data is best made on Figure (2.16) rather than on the Q,U locus of Figure (2.17a) since apparent similarities of locus <u>shape</u> may mask large separations of corresponding <u>phase</u>.

In Figure (2.18) we show the variation of inf $\chi^2_{2N}(i)$ with i, computed as discussed above (case (a)) for both the canonical and symmetric canonical models, based on the approximation $\sigma^2 = \frac{1}{2N} \sum_{0}^{N-1} (\sigma_l^2 + \delta_r^2)$ which yields $\sigma = 0.051\%$. Superposed on the figure are the $\sigma^2\chi^2_{2N}$ lines corresponding to 90% and 75% confidence i.e. 10% and 25% significance. Directly from Figure (2.18) we can then read the optimum fit, i_{opt} and relative confidence interval about it for Cygnus X-1 inclination, based on the noisy polarimetric data, viz:

<u>canonical model</u>:

$i_{opt} = 102^\circ$ ($|i| = 78^\circ$)

$85^\circ \lesssim i \lesssim 150^\circ$ ($30^\circ \lesssim |i| \lesssim 85^\circ$) at 10% sig.

$87^\circ \lesssim i \lesssim 127^\circ$ ($53^\circ \lesssim |i| \lesssim 87^\circ$) at 25% sig.

<u>symmetric canonical model</u>:

$i_{opt} = 101^\circ$ ($|i| = 79^\circ$)

$90^\circ \lesssim i \lesssim 125^\circ$ ($55^\circ \lesssim |i| \lesssim 90^\circ$) at 10% sig.

$95^\circ \lesssim i \lesssim 110^p$ ($70^\circ \lesssim |i| \lesssim 85^\circ$) at 25% sig.

where we have written $|i|$ to denote the magnitude of i in the range

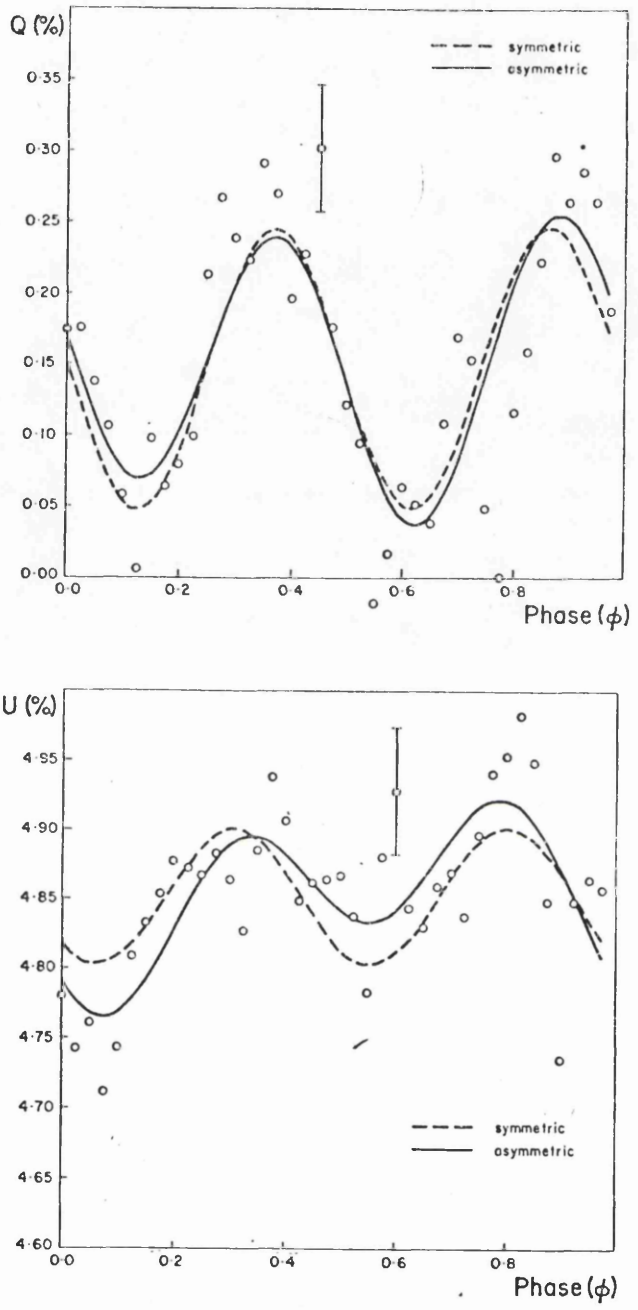

Figure 2.16 Q and U binned data points of Kemp et al (1979) plotted against phase ϕ. The binned points have equal phase separation and the 'typical 1σ error' given by Kemp is shown. Superposed are our calculated χ^2 best fit symmetric and asymmetric canonical model curves.

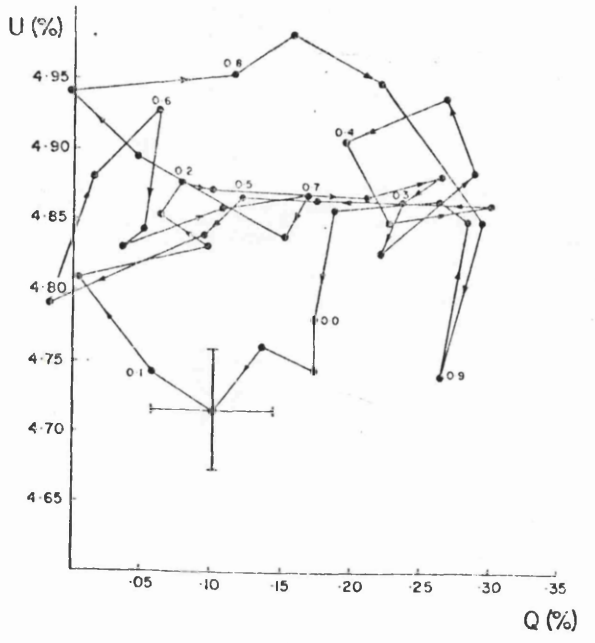

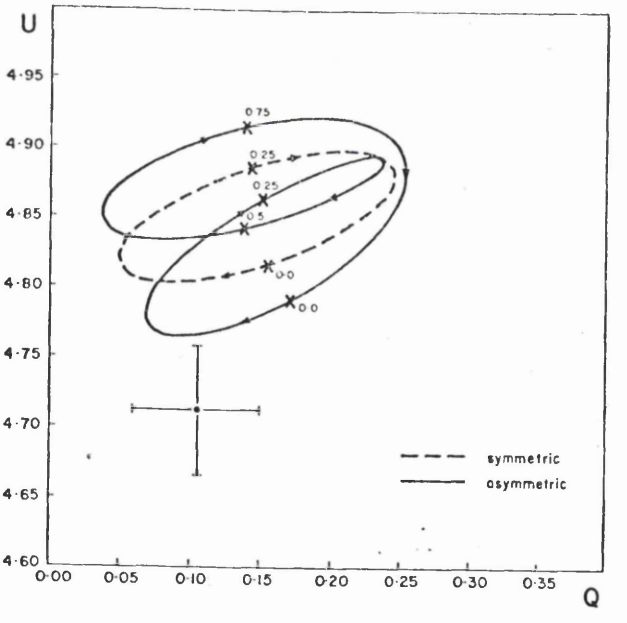

Figure 2.[illegible] (a) Data in Figure 5 presented in the form of a locus in the Q,U plane. We have joined the points sequentially and indicated the 1σ error box.

(b) Plot, in same plane as above, of our best fit fit symmetric and asymmetric canonical model loci ($i_{opt} = 101^{\circ}$, $i_{opt} = 102^{\circ}$ respectively).

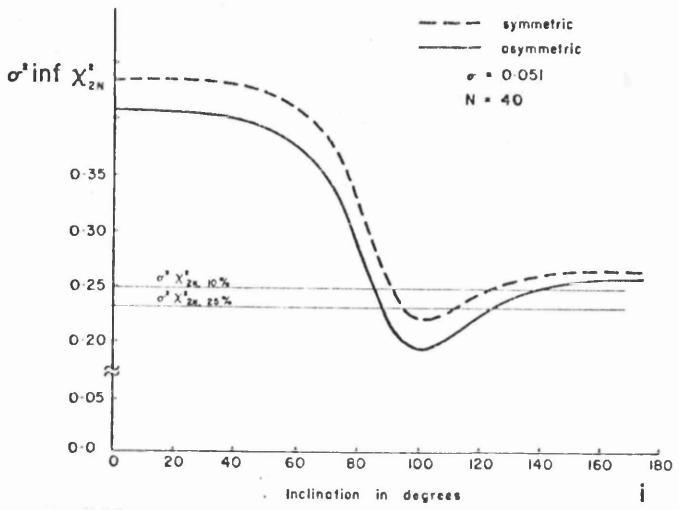

Figure 2.18 Calculated $\sigma^2 \inf \chi^2_{2N}$ ($N = 40$) plotted as function of inclination i for symmetric and asymmetric canonical models. Irrelevant upper branches of $\sigma^2 \inf \chi^2_{2N}$ curves are suppressed.

$[0^\circ, 90^\circ]$. This is the range usually quoted (since spectrophotometric methods do not yield the quadrant of the inclination). Examination of these figures shows that for both the canonical and symmetric canonical model the value of $|\, i_{opt}\,|$ is close to that obtained from simple empirical fitting to the smoothed data. (Brown et al 1978; Rudy and Kemp 1978; Kemp et al 1978). However the R.C.I. in i are much larger than the formal errors on i obtained by previous authors. Specifically we note that with $i_{opt} = 102^\circ$ the canonical model yields a χ^2_{2N} fit to the data which is acceptable at 70% significance but a canonical model with any i in the range 85° to 150° is acceptable at the 10% significance level. The breadth of the R.C.I. indicates however, that this i_{opt} has little physical meaning.

Thus it is not possible to make a statistically sound inference (cf. Milgrom 1978; Kemp et al 1979) that the polarimetric analysis in terms of the canonical model is in conflict with the spectroplotometric $i \simeq 30^\circ$. On the other hand, of course, the relative confidence interval on the polarimetric i is so large that the data cannot confirm the spectrophotometric i either. In order to test the consistency of the two i values properly it will be necessary to improve polarimetric accuracy σ sufficiently to substantially reduce the R.C.I. on i. In a later Chapter (3) we establish criteria for the measured data accuracy and also apply our analysis to polarimetric data of other binaries (Chapter 5).

As far as a symmetric canonical model is concerned, the significance of fit to the Cygnus X-1 data is lower, as anticipated, but at $i_{opt} = 101^\circ$ the model is still acceptable at 35% significance while at the 1% level all values in the range $[90^\circ, 125^\circ]$ render the symmetric canonical model consistent with the data. We also have χ^2 tested the hypothesis that Cygnus X-1 has constant polarization and found that it can be rejected at the 10^{-6}% significance level. This confirms the basic discovery of Kemp et al (1976) that Cygnus X-1 is a polarimetric variable.

The symmetric and asymmetric canonical models are thus in agreement for a wide range of inclinations with Kemp's polarimetric data (Kemp et al 1979). The errors on the data do not statistically require that we invoke mechanisms updating the canonical model (nor of course are the polarimetric data errors small enough to exclude such mechanisms either). All such requirements (e.g. Kemp 1979 observation hypothesis c.f. Chapter 1)

here the undesirable effect of introducing further free ad hoc parameters into the model. In addition to the several parameters required to describe the occulting geometry, Kemp's (1979) model implicitly depends on future parameters specifying the empirical damping factors applied to the higher harmonics (Kemp et al 1979).

We have not, for computational reasons, found the relative confidence intervals for the other model parameters since we are most interested in the inclination i. The values of the optimal fit harmonic coefficients (expressed in %) are however,

$$\begin{aligned} p_1 &= +\ 0.0051 & p_2 &= -\ 0.0052 \\ q_1 &= -\ 0.0052 & q_2 &= -\ 0.1065 \\ u_1 &= -\ 0.0274 & u_2 &= -\ 0.0392 \\ v_1 &= -\ 0.0268 & v_2 &= +\ 0.0019 \end{aligned}$$

where we omit the constant terms p_o, u_o since these are inextricably tied up with the interstellar component. We can investigate the physical significance of these coefficients by re-expressing them in the form (c.f. Brown et al 1978):

$$\begin{aligned} p_1 &= \tau_A \sin 2i \cos \lambda_A \ ; & p_2 &= -\tau_s (1+\cos^2 i) \cos 2\lambda_s \\ q_1 &= -\tau_A \sin 2i \sin \lambda_A \ ; & q_2 &= \tau_s (1+\cos^2 i) \sin 2\lambda_s \\ u_1 &= 2\tau_A \sin i \sin \lambda_A \ ; & u_2 &= -2\tau_s \cos i \sin 2\lambda_s \\ v_1 &= 2\tau_A \sin i \cos \lambda_A \ ; & v_2 &= -2\tau_s \cos i \cos 2\lambda_s \end{aligned} \qquad (2.85)$$

where τ_s and τ_A are measures of the mean scattering optical depths of the envelope material lying respectively symmetrically and asymmetrically about the orbital plane (equivalent to $\tau_o(\gamma_3' + \gamma_4)^2$ and $\tau_o(\gamma_1^2 + \gamma_2^2)$ of Brown et al 1978). λ_s and λ_A measure the longitude in the binary frame of the centroid of these two envelope components (equivalent to λ_2, λ_1 of Brown et al 1978).

Solution of these equations (2.85) with the above optimum values of the coefficients give:

$$\begin{aligned} \tau_A &= 1.95\ 10^{-4} \quad ; & \lambda_A &= 226^o \\ \tau_s &= 1.03\ 10^{-3} \quad ; & \lambda_s &= 136^o \end{aligned}$$

(N.B. the smallness of these optical depths indicates the self consistency of the single scattering hypothesis though not necessarily proving it cf. Daniel 1980b). From the range of numerical results we

obtained it seems that τ_s is comparatively well determined since it is rather insensitive to the value of i chosen and depend only on the root mean square of four second harmonic coefficients. Though a given τ_s could be reproduced by numerous plausible envelope models its physical significance can be seen in terms of the simple envelope model of a single localized scatterer containing N electrons and located at a distance ≃ binary separation D($\sim 3.10^7$ km). Assuming all the scattered light originates in a point primary, for this model $\tau_s = 3N\sigma_T/32D^2$ where σ_T is the Thomson cross section ($= 0.665\ 10^{-24}$ cm^{-2}) Then the above value of τ_s implies $N \simeq 2.10^{48}$ electrons or a total mass of $m \sim 3.10^{24}$ gms. This mass will be an underestimate since the finite size of the actual envelope and light source and multiple scattering will reduce the polarization for a given mass $M \simeq 3.10^{24}$ gms. is comparable to the mass transfer per orbital cycle required to power the Xray source (e.g. Oda 1977). This lends support to the accretion model concept and indicates that the material we are observing contributes substantially to accretion. The value of the asymmetric optical depth τ_A is less well defined since the first harmonics are small and improve the model fit to the delta only slightly. The nominal value quoted above, however, suggests that the degree of asymmetry of the envelope about the orbital plane is small ($\tau_A/\tau_s = 20\%$) but non-zero.

The angles λ_A, λ_S are also less well determined than τ_S since they depend on the ratio of harmonic coefficients. In particular little faith can be put in τ_A. The above $\tau_s = -44^o$ is broadly consistent with accretion models involving either a trailing gas stream (Oda 1977) or trailing accretion wake (Jackson 1975).

In conclusion it is clear that polarimetric analysis is potentially a very powerful diagnostic for close binaries but that acquisition of data with sufficiently low noise to be definitive in modelling is no trivial task. The possibilities concerning acquiring this improvement will be discussed in Chapter 3. Recent work however (McLean 1980) has shownthat such results can be obtained by using larger telescopes and shorter integration times.

In a reply to the paper of Simmons, Aspin and Brown (1980), the details of which have been presented above, Kemp (1980) criticized the analysis of his data in terms of the canonical model. He asserted that he did not find the Q,U curves (vs. phase ϕ) to conform to the

canonical model which due to the implicit assumptions does not allow obscuration or shadowing effect. He also claimed that non-canonical model structure suggested by an F-test on harmonics such as 3rd, 4th and 5th was present with a probability (as a group) of 0.85. He rejects our conclusions based on the asymmetric canonical model and criticizes what he considers to be our failure to recognize the cumulative aspect of the data in that errors would be reduced by binning due to the random noise structure of the Cygnus X-1 data.

In reply to this, a note added in proof to the Simmons, Aspin and Brown (1980) paper pointed out the fact that some of the data Kemp (1980) considers was taken after our paper was written. We use this new data set consisting some 528 nightly averages, with the canonical model. We found that the 90% confidence interval in i using the asymmetric model became $[\,48^\circ,\ 80^\circ\,]$ with $i_{opt} = 71^\circ$, and for the symmetric case $[\,62^\circ,\ 78^\circ\,]$ with $i_{opt} = 70^\circ$. The slight reduction of the binned data error (from 0.051% to 0.034%) is the crucial factor here in reducing the R.C.I. on i. The asymmetric canonical model is still acceptable at 10% significance, whilst the symmetric case is only acceptable at 5% sig. Thus even with Kemp's new data there is no strong case for rejecting the canonical model (or any other). Kemp attributed our conclusion in part to our alleged use of the data error σ_{dat} rather than the binned data error σ_{bin}, despite our explicit emphasis of this very point. Furthermore, contrary to his suggestion that we used σ_{dat} instead of σ_{bin} we would obviously have found the model less rather than more acceptable.

The fact that σ_{bin} exceeds σ is of the same order of magnitude as σ_{dat} is indeed essential to the non-trivial problem involved here and arises because of the intrinsic variation (both long and short term) of Cygnus X-1. These variations are reflected by the fact that the mean (short term) values of Q,U are not functions of binary phase, only but also change from one cycle to the next. This fact we explicitly discussed, contrary to Kemp's statements. Accepting nevertheless, the assumption that a phase locked model does represent some underlying facet of the data, we estimated parameter confidence intervals (e.g. on i) from this model. In doing this we gave σ_{bin} the variance occurring in Q,U within a single bin,

the value provided by Kemp in this previous paper. If the assumption of phase-locking is not realistic over many orbital periods, a possible alternative would be to take data over very short runs on large telescopes during quiescent periods (if any) between large intrinsic fluctuations. Which of these approaches, if either will work depends entirely on the statistical and physical character of Cygnus X-1 variations, which are largely unknown.

Our inclusion of 1st harmonics (by admitting the possibility of envelope asymmetry about the orbital plane) in the model does not, as Kemp asserts, 'single them out' or gives special significance to them. When they are not present in the data the constraints involving 1st harmonics become redundant. One consequence of increasing the number of five parameters in the model is, however to increase the number of acceptable solutions. Such many parameter models will, however only be testable on the basis of yet more detailed observations and analysis.

CHAPTER 3 - THE POLARIMETRIC ACCURACY REQUIRED FOR THE DETERMINATION OF BINARY INCLINATIONS

3.1 Introduction

In Chapter 2 we outlined the development of a procedure to obtain an optimum fit canonical model to noisy polarimetric data. This gave values of 'best fit' parameters (both physical and orbital parameters) predicted by the canonical model. Applying this to the data of Cygnus X-1 (Kemp et al 1979) we showed that the usually quoted 'formal error' gave an underestimate of the true uncertainty in the value of orbital inclination i in particular, when large noise was present on the observations. The new error on i we term the 'Relative Confidence Interval' (RCI) which took into account the acceptability of the model fit to the data (a point the formal error implicitly assumes), by means of a χ^2 test of 'goodness of fit' (c.f. Simmons et al 1980). The large RCI encountered for Cygnus X-1 ($30^{\circ} \leqslant |i| \leqslant 85^{\circ}$) at the 10% significance level indicated that the observational error (the error on the folded, binned observations) on the bin mean values was too great to establish inclinations by this technique unambiguously.

It is too this problem i.e. what size of error on the observations would give a satisfactory determination of inclination (amongst other parameters), that we address ourselves in this Chapter. We study here the statistical accuracy necessary in 'real' observations to test if the simple canonical model is valid at all and if it is not applicable to the data, what observational accuracy is required to determine i to say $\pm 5^{\circ}$. Also considered is the question of what inferences can be drawn regarding the real system when the canonical model is rejected on statistical grounds.

The basis of this chapter was published in Monthly Notices of the Royal Astronomical Society by Aspin, Simmons and Brown (1981).

The procedure we follow is to simulate noisy, polarimetric data of real systems by generating (from hypothetical canonical systems) 'observed' values of the Stokes parameters Q_{ob}, U_{ob} at each phase point. This is done by giving Q_{ob}, U_{ob} a gaussian distribution about the theoretically predicted values at each phase, with a prescribed standard deviation. This simulated data is then used to

redetermine the canonical physical parameters through the optimizing technique described in Chapter 2 (and Simmons et al 1980). Confidence intervals for inclinations and optimum values for the model parameters are found simultaneously using the χ^2 testing procedure. We again (as in Chapter 2) take the 90% confidence interval for inclination as the range of i values for which the data are acceptable at 10% significance according to the χ^2 criterion.

We investigate the dependence of the confidence intervals for i on (i) the true inclination i_o, (ii) the data noise σ and (iii) the intrinsic geometry and polarimetric amplitude of the generated model data. For that geometry and any given inclination we determine a value of the standard deviation σ_{nec}, which gives the minimum data accuracy necessary to determine inclinations to $\pm 5^o$.

3.2 Generation of Noisy Data and Fitting of the Canonical Model

The canonical model of Brown et al (1978) predicts that the normalised Stokes parameters of light from a pair of point stellar sources, Thomson scattered in a corotating binary envelope are given as functions of binary longitude λ(= 2π x orbital phase) by Equation (2.5). These values (Q,U) are in the natural frame of reference defined by the binary itself. We observe the Stokes parameters (Q_{ob}, U_{ob}) defined by the rotation given in Equation (2.45).

In practice the rotation angle is found to be immaterial when establishing confidence intervals at i. The expressions for Q_{ob}, U_{ob} therefore depend on 4 moment integrals (γ's), θ and i that is 6 independent parameters.

Using the expressions (2.5) and (2.45) we generate noisy data Q_{ob} , U_{ob} values about the canonical system predictions at N equally spaced phase points specifically for various values if i, σ . To some extent we also investigate the effect on the confidence intervals of changing the geometry (the γ's) and θ. These however do not have any significant effect on the R.C.I. on i for specific i and σ . The two representative intrinsic geometries we consider in order to define a generating model for the simulated data are defined by:

$$\begin{aligned} G_s &: \tau_o = 0.1 \quad \gamma_3 = 1 \quad \gamma_2 = \gamma_4 = \gamma_1 = 0 \\ G_A &: \tau_o = 0.1 \quad \gamma_1 = \gamma_3 = 1, \ \gamma_2 = \gamma_4 = 0. \end{aligned} \tag{3.1}$$

From equations (3.1) it can be seen that G_s corresponds to a distribution of scatterers completely symmetric about the systems orbital plane (and hence only 2nd harmonic variations in polarization are present). An asymmetry is introduced into the scatterers in G_A which introduces 1st harmonic variations of polarization.

In practice actual 'observed' values of the Stokes parameters at N equally spaced phase points are calculated by binning the raw observations as adopted by observers of polarimetric binaries (Kemp et al 1976 and Kemp, private communication). The error value σ taken here is therefore equivalent to that obtained for the binned data points. Our estimate of the confidence intervals have mostly been found for a bin number N = 40 with some calculated for a reduced number (N = 20). From the analysis of the final error, however, we could expect the breadth of the R.C.I. for i to be approximately proportioned to $1/\sqrt{N}$ if discretization error due to binning were the only source of scatter in each bin. The error on each bin (or in fact the mean bin error over all the bins) would increase by a factor $\sqrt{40/20}$ i.e. $\sqrt{2}$, if we reduced the number of bins from 40 to 20, due to the additional spread of observations in the larger bin.

The generation of the noise on the Q,U values predicted by the canonical model is achieved by using a standard library program on the ICL 2976 computer of the University of Glasgow. The library (NAG) routine is one that picks a (pseudo) random number from a normal distribution whose mean and standard deviation are specified by the user. We therefore randomly displace the predicted (theoretical) values of Q,U so that the simulated observations (Q_{obs}, U_{obs}) lie distributed normally about them. The value of the standard deviation of the normal distribution is a free parameter in the procedure and is given a range of values for each inclination i. Noisy data for each given scattering region geometry, G, with input parameter (3.1) i and θ is then fitted with the canonical model as in Chapter 2, to yield the optimum values of the parameters. These should, depending on the noise level chosen, accord more or less with the input values. In fitting the data whether generated by a symmetric G_s or asymmetric G_A model) we investigate the fit of both the general canonical model with an asymmetrically distributed model geometry M_A and the symmetric canonical model M_s with envelope symmetry about the orbital

plane. Thus we have four combinations of intrinsic (generating) geometries G and fitting model M, i.e. G_S, M_S ; G_S M_A; G_A, M_S and G_A, M_A.

We now follow the optimizing procedure outlined in Chapter 2 (for Cygnus X-1) where we minimize the χ^2 statistic subject to the model constraints and obtain the optimum values of τ_o, γ's θ_1 and i and the 90% confidence interval on i. One point of interest to note, before proceeding is that we expect the confidence interval for the asymmetric model fit (M_A) to be broader than that associated with the symmetric model fit (M_S) since the former has more free parameters. Also the optimum fit of the former model should be slightly better in all cases since it admits 1st harmonic variations. When 1st harmonics are not present in the generating model we note that the two fitting models should tend to agree (i.e. G_S, M_S and G_A, M_A should produce similar results). In fitting M_S to G_A data it is expected that for small enough values of σ no acceptable χ^2 can be found for <u>any</u> value of i, i.e. the model is unacceptable, due of course to the effect of the 1st harmonics in the data. As noted in Chapter 2 Kemp (1980a) asserted that this was already true for Cygnus X-1 data a conclusion we refuted in Chapter 2 and Simmons <u>et al</u> (1980), by showing that a M_S model was not ruled out by the data at 90% confidence while a M_A model with 1st harmonic variations gave a wide region of acceptable i values .

We obtained results on fitting the canonical model for 5 different sets of noisy data (each having five different σ) for each of 5 true inclinations i_o as follows. For each i_o and σ and G,M combination we average the confidence intervals obtained over 10 such random realizations of noisy data in an attempt to obtain the <u>average</u> behaviour of the fitting procedure and hence smoothing out any statistical irregularities.

3.3 <u>Results of Model testing procedure</u>

Our results are most conveniently represented in graphical form (Figure 3.1). Here we plot the upper, i_+ and lower i_-, 90% confidence limits as a function of data standard deviation σ , for different input inclinations i_o. We show this, for conservations of intrinsic

Figure 3.1 a - e

Graphical representation of the Relative Confidence Interval for 5 true inclinations (i_o) at 10% significance and illustrate the rapidly increasing accuracy necessary for inclination determinatiion as i_o increases. The amplitude of variation, A, is also given to enable direct comparison with observations. The same intrinsic geometry G_s is taken to generate data throughout, and fitted with M_s.

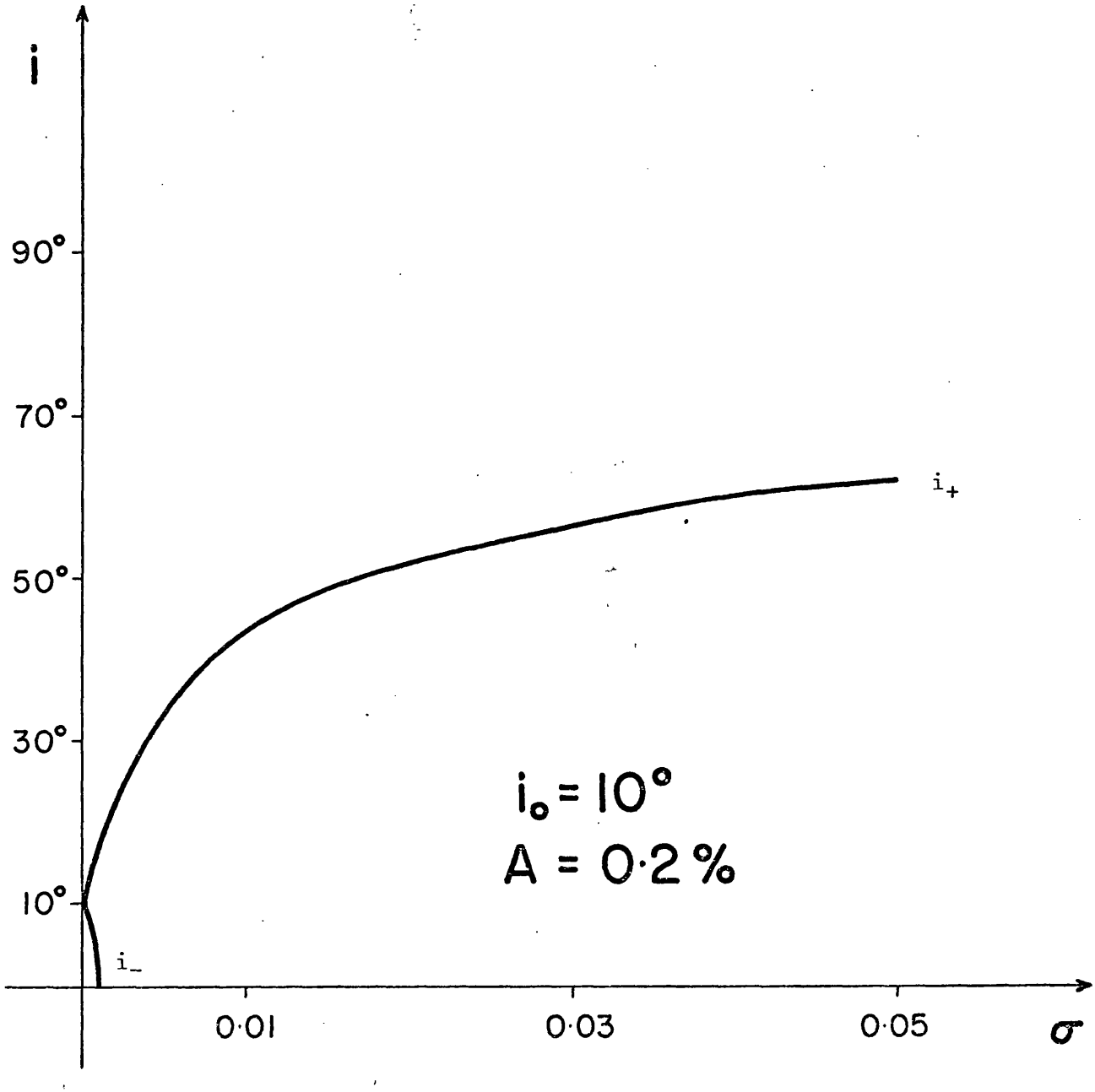

Figure 3.1a

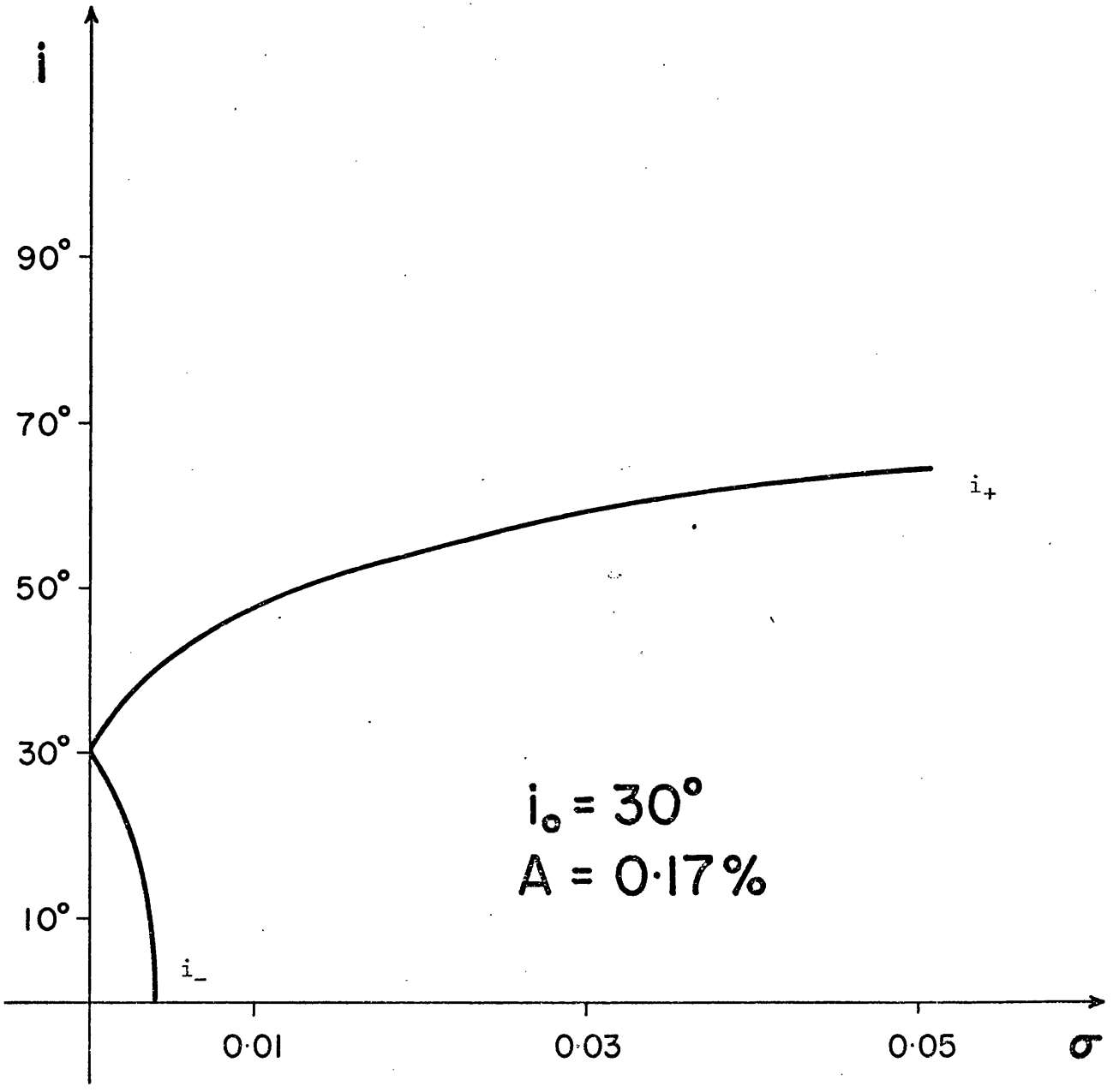

Figure 3.1b

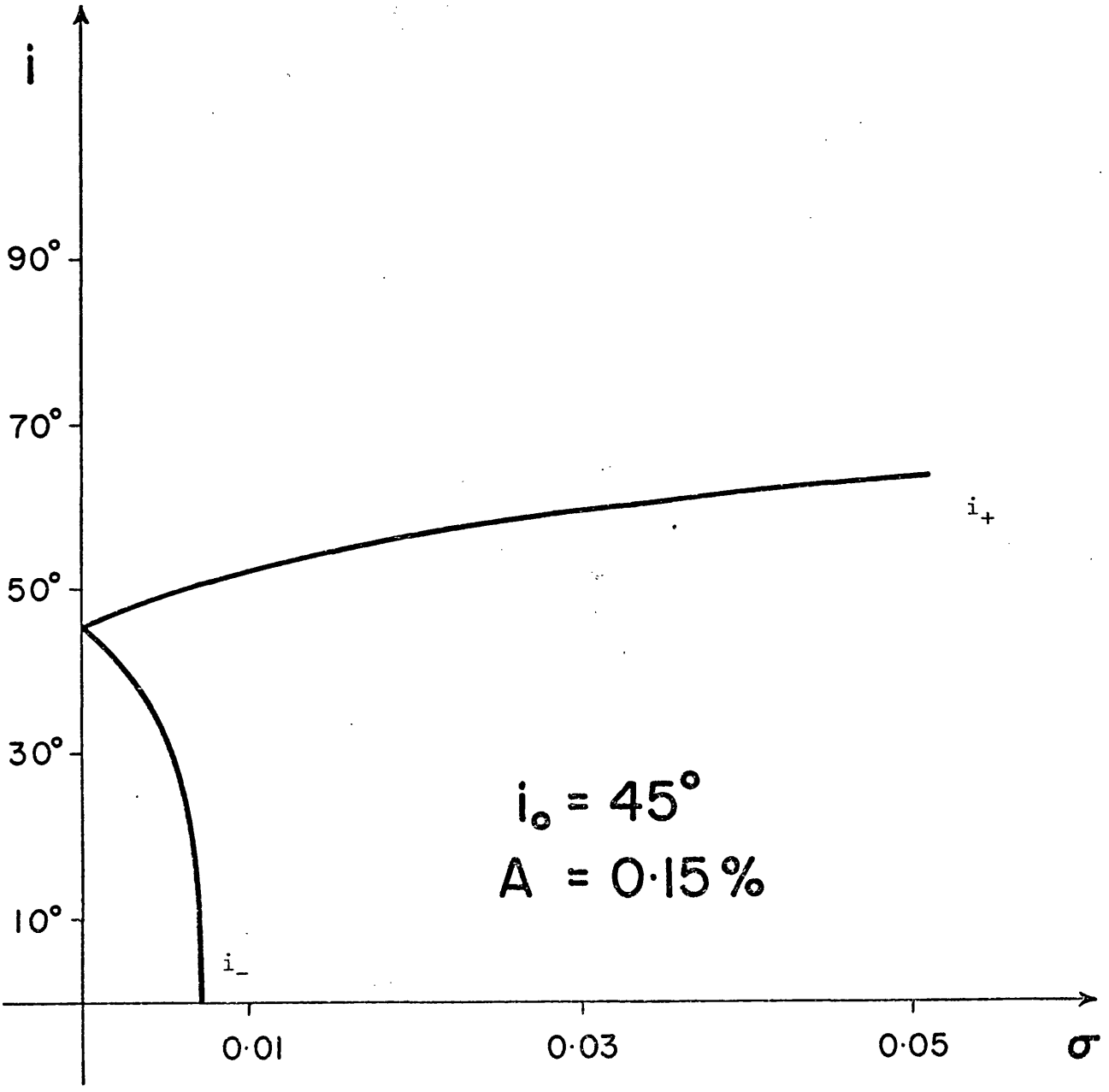

Figure 3.1c

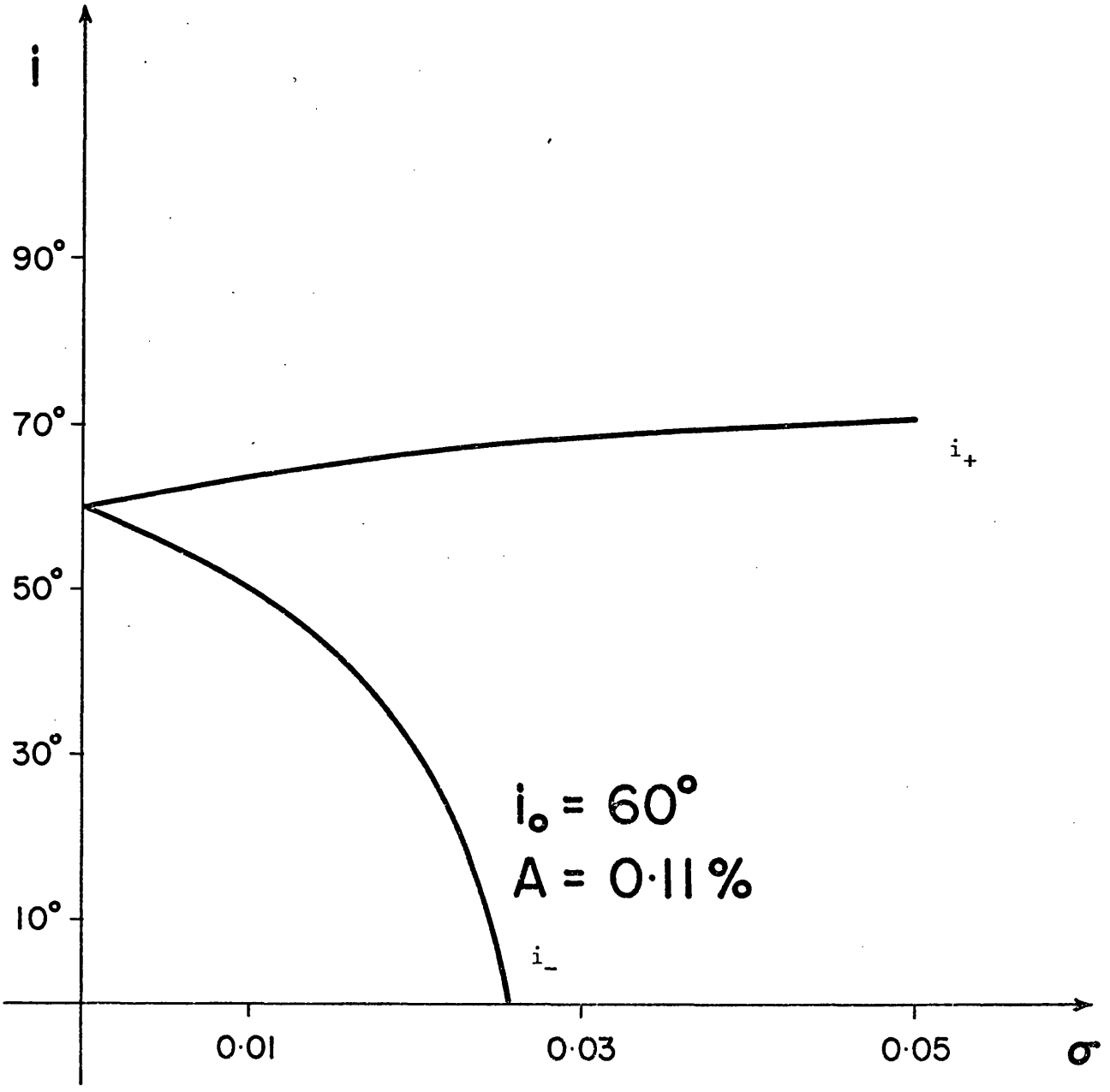

Figure 3.1d

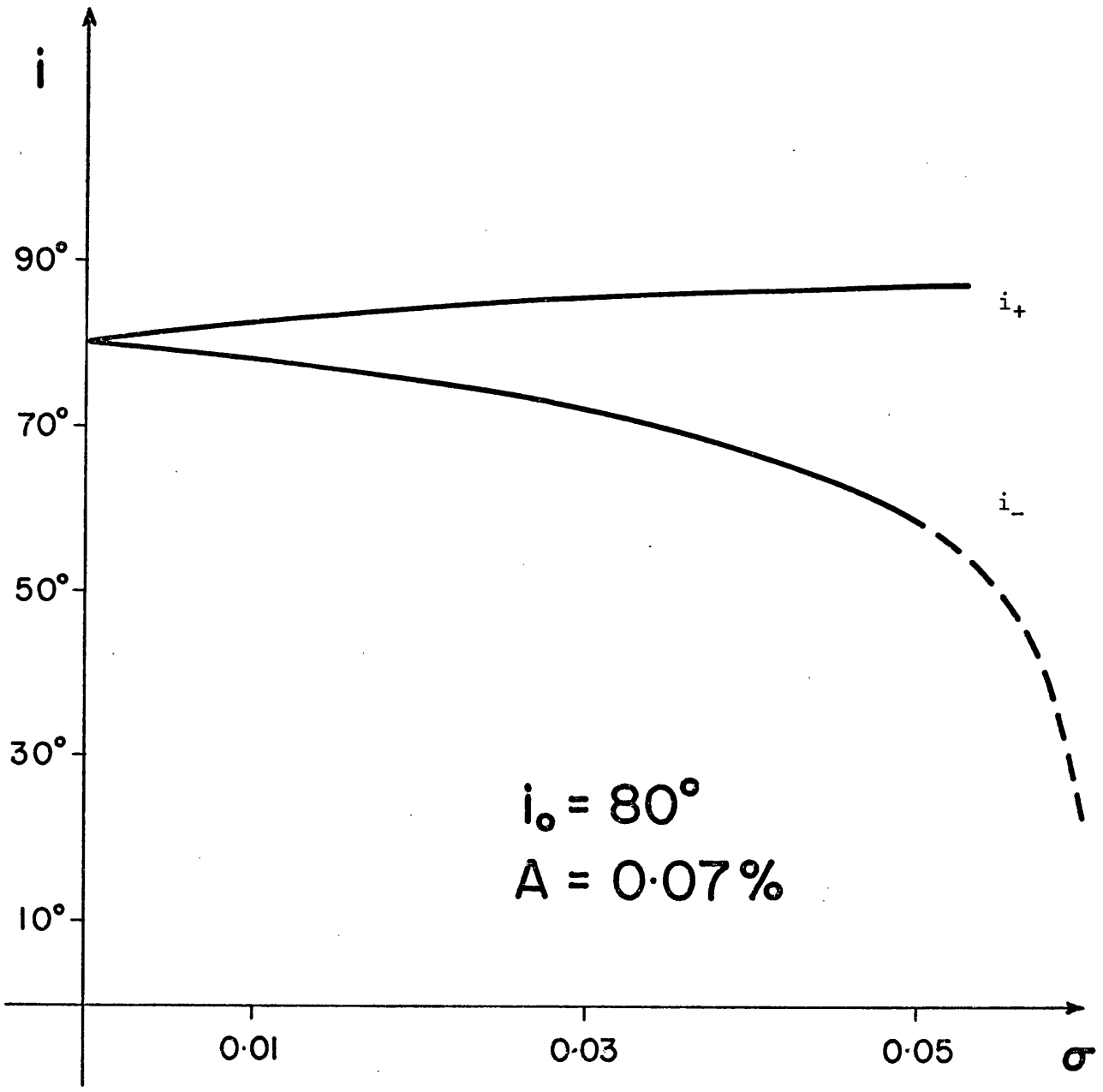

Figure 3.1e

geometry and fitting model G_s, M_s (Figure 3.1), since as mentioned above the G_s, M_A results will be similar to those of G_s, M_s. The G_A, M_s results were found to produce no acceptable fit, as anticipated, for small values of the noise level. At higher noise (larger σ) all inclinations became compatible with the data, according to the χ^2 test. This meant that the size of the error on the observations outweighed the presence of 1st harmonics in the data making the χ^2 values of all i-values less than the test level of $\chi^2_{2N,10\%}$. The results for G_A, M_A were found to be similar in nature to those of G_s, M_s at similar amplitudes of variations. We only therefore deal with G_s, M_s.

In the Figures (3.1) the width of 90^o confidence interval is just $i_+ - i_-$ at each noise level.

It is clear from Figure (3.1) that at any given σ the confidence interval for inclinations rapidly broadens as the input inclination i_o decreases to zero. Consequently the error on the data has to be very much smaller at lower inclinations than at higher ones to determine i. with any reasonable accuracy. Our calculations show that this important result (i.e. that a greater accuracy of observation is necessary to determine lower inclinations) was approximately independent of the intrinsic geometry considered (i.e. for similar amplitude models, from which the observations were calculated, the results of model fitting were of the same order). For G_s, M_A the confidence intervals were found to be slightly broader reflecting the fact that M_A contains 2 more free parameters than M_s, though the essential features of Figure (3.1) remained unchanged. Table I gives the values of A/σ, the signal to noise ratio for each true inclination i_o, above which the lower limit of the 90% confidence interval goes to $i = 0^o$ for the geometry/model combination G_s, M_s (the values are approximately the same for G_s/M_A and G_A/M_A).

Table I

i_o	A/σ
10^o	190
30^o	45
45^o	22
60^o	4.3
80^o	1.2

The corresponding value of A/σ for Cygnus X-1 data (Kemp et al 1979) was found to be ~ 1.96 meaning that only if the true inclination of the system was $\gtrsim 70^{\circ}$ and the canonical model was in fact predicting the correct polarimetric behaviour of Cygnus X-1, would we get a 90% confidence interval whose lower limit would not be $i = 0^{\circ}$. This as we saw in the preceding Chapter (2) was in fact the case. The optimum inclination obtained was $|i_{opt}| \sim 78^{\circ}$ with a 90% confidence interval for a m_A fit of $[\,30^{\circ}, 85^{\circ}\,]$. In graphical form the above results (Table I) are given in Figure (3.2).

By the method outlined above, i.e. generation of simulated data for particular intrinsic geometries and best fitting with both canonical models, it is possible also to obtain for any given i_o a value of $\sigma = \sigma_{nec}$ at which the inclination determination has a confidence interval of $\sim \pm 5^{\circ}$. To get an idea of the relevance of this however a relative measure of the data error $R = \sigma_{nec}/A$ is taken (i.e. σ_{nec} relative to the amplitude of variations in the phase binned data) since any value of σ would have a different significance depending on the size of the polarimetric variations (e.g. small or large noise signal ratio) We here define the amplitude of variations that we use as:

$$A = \frac{|Q_{max} - Q_{min}| + |U_{max} - U_{min}|}{4} \qquad (3.2)$$

which is the average size of variations of the phase binned data in both Stokes parameters. Q_{max}, Q_{min} and U_{max}, U_{min} are therefore the maximum and minimum values not of the data points, but of the best fit curves through these points over the binary phase . Table II presents the values of σ_{nec}, A and the quantity $\log(\sigma_{nec}/A)$ for G_s , M_s; G_s,M_A and G_A,M_A and each i_o chosen with this definition of amplitude the quantity $\sigma_{nec}(i)/A(i)$ is almost independent of the precise geometry of the system. It is also convenient to plot $\log(\sigma_{nec}/A)$ against i_o for the cases above as in Figure (3.3). This representation indicates an approximately linear relation between the logarithm of the function σ_{nec}/A and i_o with smaller values of σ_{nec}/A being necessary at lower i_o (i.e. for constant A, smaller σ_{nec} or constant σ_{nec}, larger A).

Using the values of σ_{nec} and A from Figure (3.3) and Table II (and the value of N) it is possible to estimate empirically the accuracy

INC	A(%) (G_s)	SIGMA(%) (G_s/M_s)	LOG(SIGMA/A) (G_s/M_s)
10^o	.2	.0006	-2.5
30^o	.17	.002	-1.9
45^o	.15	.006	-1.4
60^o	.11	.012	-.96
80^o	.07	.03	-.37

INC	A(%) (G_s)	SIGMA(%) (G_s/M_a)	LOG(SIGMA/A) (G_s/M_a)
10^o	.2	.0005	-2.6
30^o	.17	.0015	-2.05
45^o	.15	.004	-1.57
60^o	.11	.009	-1.09
80^o	.07	.025	-.45

TABLE 2.

INC	A(%) (G_a)	SIGMA(%) (G_a/M_a)	LOG(SIGMA/A) (G_a/M_a)
10^o	.22	.0015	-2.2
30^o	.23	.007	-1.5
45^o	.23	.009	-1.4
60^o	.2	.013	-1.2
80^o	.16	.03	-.75

TABLE 2.

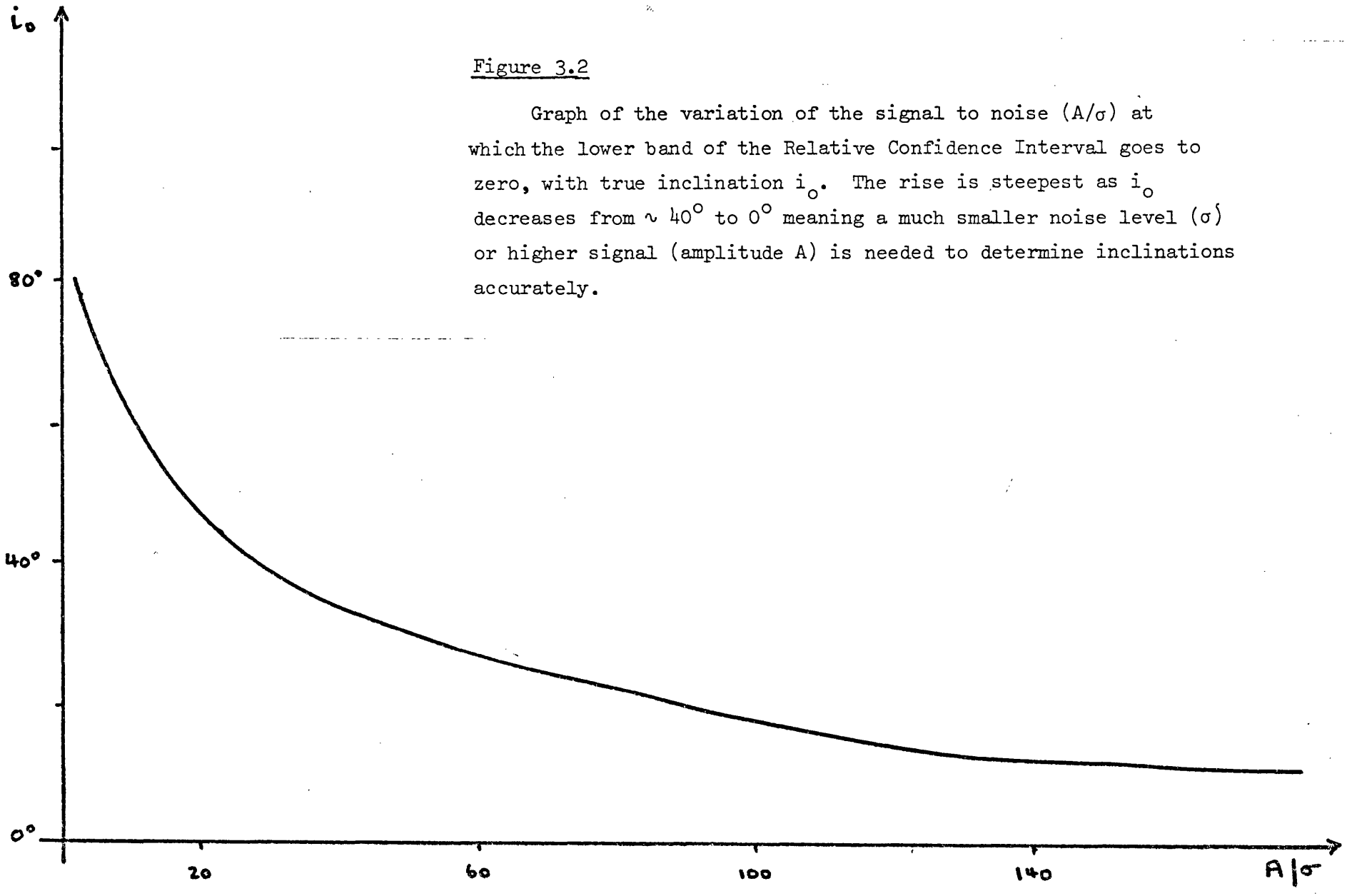

Figure 3.2

Graph of the variation of the signal to noise (A/σ) at which the lower band of the Relative Confidence Interval goes to zero, with true inclination i_o. The rise is steepest as i_o decreases from $\sim 40^\circ$ to 0° meaning a much smaller noise level (σ) or higher signal (amplitude A) is needed to determine inclinations accurately.

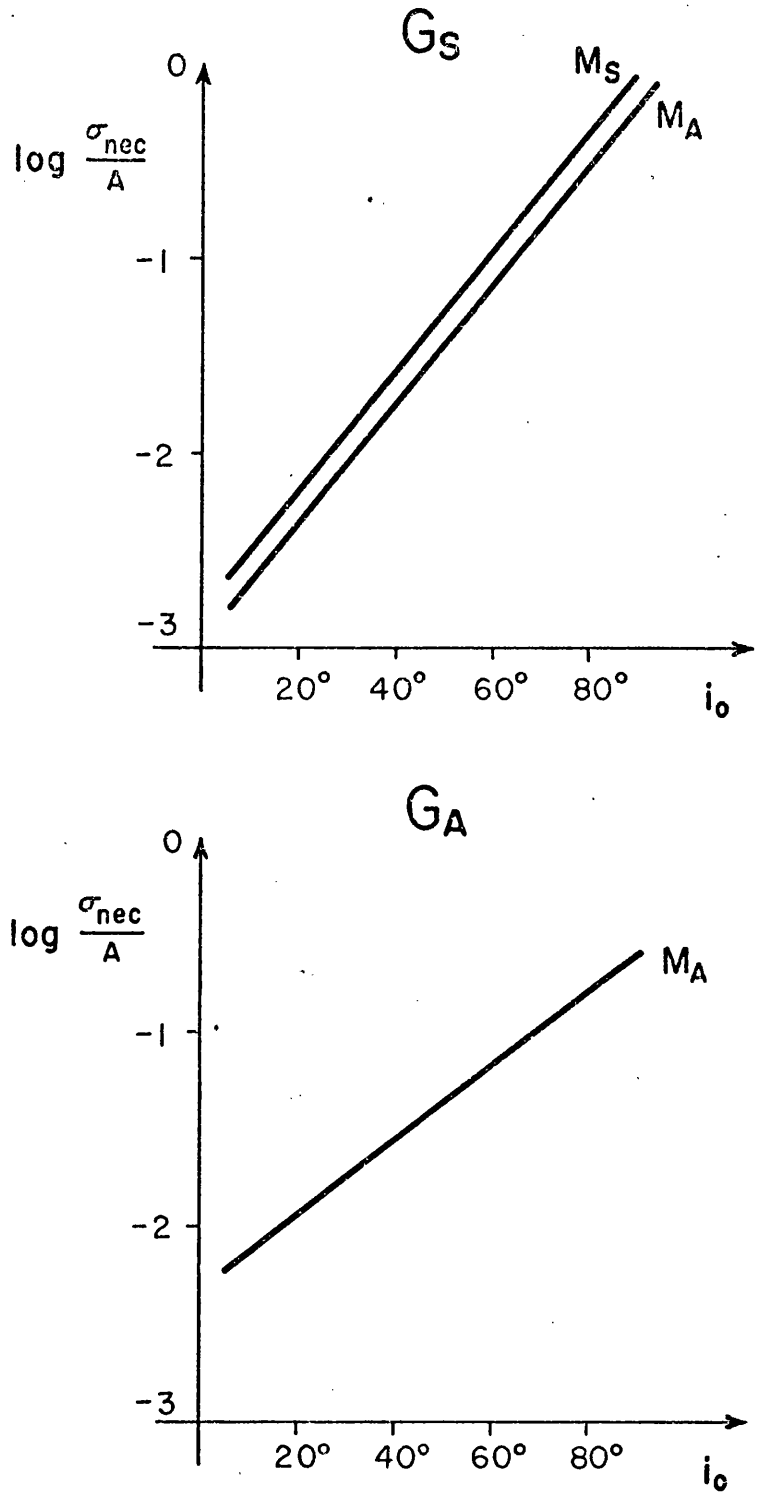

Figure 3.3 Plot of log (σ_{nec}/A) vs i_o for three cases of noisy data and model fitting (i.e. G_s/M_s, G_S/M_A and G_A/M_A). The behaviour is approximately linear in all cases.

σ_o required of observations for determination of i in any particular binary. This can be done using the approximate relation:

$$\frac{\sigma_o}{A_o \sqrt{N_o}} = \frac{\sigma_{nec}(i)}{A(i) \sqrt{N}}$$

where the suffix o refers to the observationally determined quantities. This approximate relation makes use of the known fact of the data noise namely that changing the amplitude of variations A alters the effect of a certain σ. Changing the number of bins N has a similar effect with a $1/\sqrt{N}$ dependence (cf above). For a given observational error σ_o and amplitude A_o, (and N_o) all obtained from observations, we obtain a lower bound to values of i that can usefully be determined. To illustrate this let us consider the polarimetric binary data for U Sagittae (Rudy and Kemp 1978). If we take the quoted 'typical error' on the observations on the standard deviation σ_o we can estimate the left hand side of (3.3). With A_o = 0.025% and N_o = 20 (the number of bins) then with σ_o = 0.027% we find that

$$\frac{\sigma_o \sqrt{N}}{A_o \sqrt{N_o}} = 1.3 \qquad (3.3)$$

where N = 40 and is the number of bins used in the simulated data testing of the model outlined above. Using the values of σ_{nec}, A from Table II we find this value to be considerably larger than σ_{nec}/A for any i_o (the highest σ_{nec}/A (in G_A, M_A) is for $i_o = 80^o$ with $\sigma_{nec}/A \sim 0.18$). Hence it would not be possible to determine i with any degree of accuracy (i.e. any inclination $0 \leq |i| \leq 90^o$ would fit the data). However the error used is not the correct value since it is necessary to phase bin the folded data before analyses, thus changing the error. Phase binning (N_o = 20) yields $\sigma_o \simeq$ .0015% thus making the discrepancy slightly smaller. This slight decrease in the noise when going from raw data to binned observations is probably a result of only partial (or incomplete) phase l cking, an assumption implicit in the canonical model. To be able to determine the inclination $i > 80^o$ for USge to the $\pm 5^o$ level (with a symmetric canonical model) in this

case would mean that $\sigma_{o,nec}$ would have to be $\simeq$ 0.0076% or 0.33 σ_o(unbinned) and 0.51 σ_o (binned). This value decreases as the inclination to be determined decreases. At $i = 10^o$ $\sigma_{o,nec} = 5.3 \times 10^{-5}$% i.e. 0.02 σ_o (unbinned) or 0.0269% σ_o(binned) would be necessary. More recent observations McLean (1980) have aimed at improving significantly the observational accuracy and if we consider the data before phase binning, the value of σ_o would be appreciably smaller and approaching σ_{nec} for inclinations $i_o > 60^o$. This improvement in data makes accurate model testing and determination of inclinations (and other parameters) feasible in the near future. Comparing this estimate of the R.C.I. on USge with the formal linear error quoted by Rudy and Kemp (1978) i.e. $i = 87^o \pm 3^o$ we see that the formal analyses gives a gross underestimate of the true error when the fit of the canonical model is taken into account. Direct fitting of the observations of Kemp et al will be presented in Chapter 5 and essentially confirm this idea that the data error is too large to obtain accurate values of model parameters.

The discrepancy between the formal linear error and the real confidence interval on i (our R.C.I.) are therefore seen to grow rapidly with increasing σ and at the observational accuracy of Rudy and Kemp (1978) (when binning the observations) the R.C.I. and f.l. e. bear no resemblance to each other. The problems of the behaviour of the optimum inclination when a large confidence interval is present on that i was also investigated numerically, the results of which inspired the analytic work of Chapter 4 where this is investigated more thoroughly. It was found that as the data noise increased, the optimum value of inclination found from 'best fitting' the simulated data, tended to be greater than the actual value i_o. This is illustrated in Figure (3.4) where we have taken the G_A, M_A i_+, i_- confidence interval curve for $i_o = 10^o$ and 60^o and superimposed the trend of the optimum inclination value (dotted line). For the case of $i_o = 10^o$ the variance of i_{opt} from the true value i_o is increasing significantly towards higher σ levels. At $i_o = 60^o$ this increasing trend is not as apparent but is still, nevertheless, visible. These results indicated a bias in the polarimetric estimator used to obtain i towards higher inclinations when substantial noise was present in the data. Thus the

Figure 3.4 a,b

The upper and lower confidence interval bands (solid line) and trend of the optimum inclination (dashed line) for the geometry model combination G_A/M_A and the inclinations $i_o = 10^o$ (3.4a) and 60^o (3.4b). The bias in the optimum inclination is seen to be strongest at lower inclinations.

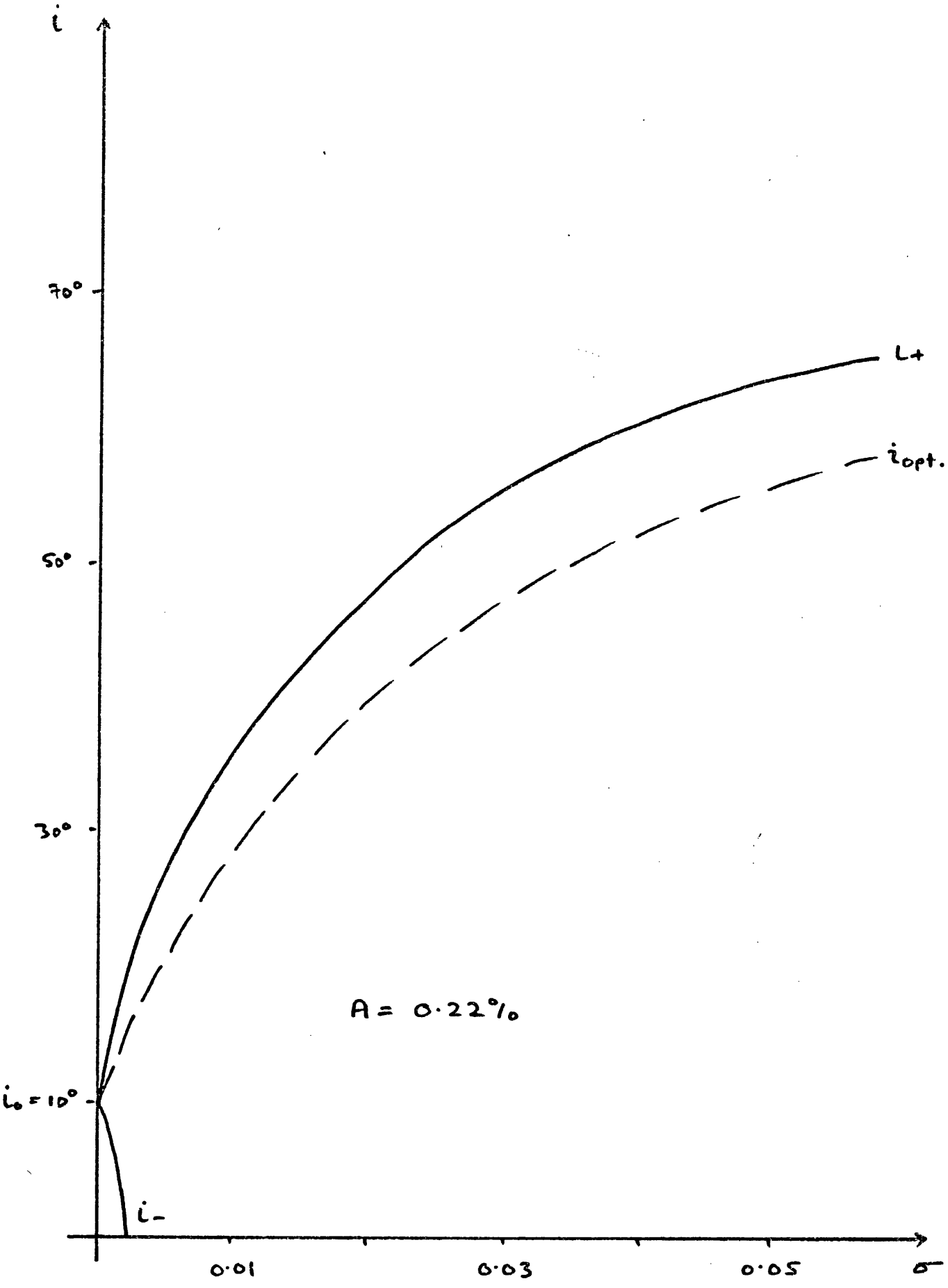

Figure 3.4a

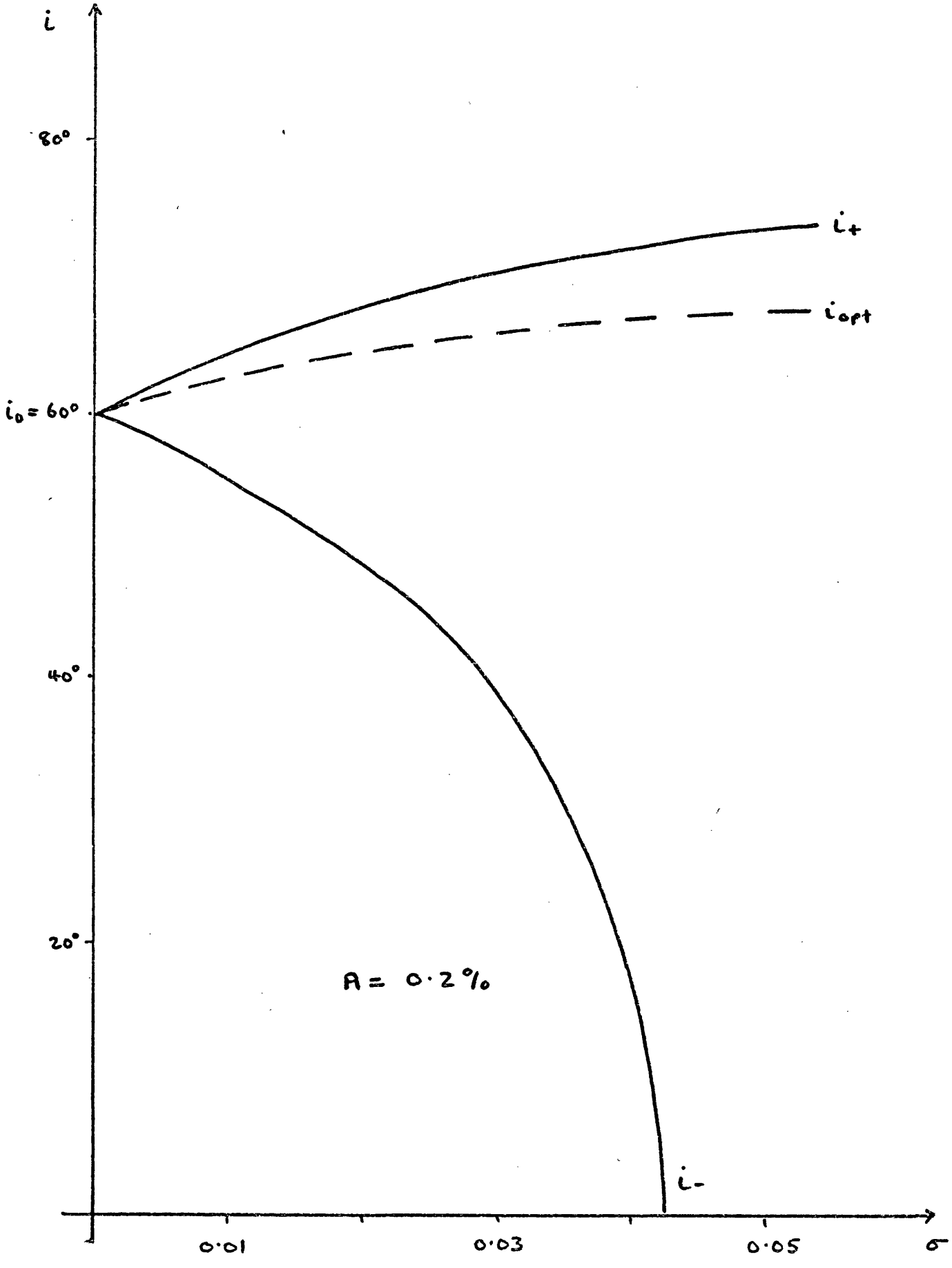

Figure 3.4b

apparent accord of photometrically and polarimetrically determined i values and may be an artefact of the selection of high inclination binaries to observe (e.g. USge is, like many of the others observed by Kemp eclipsing) and the bias of the polarimetric estimator for inclination towards high values. We shall return to this problem in the next Chapter (4).

We have also investigated the effect of changing the number of phase points N. Reducing N from 40 to 20 has the general effect predicted above i.e. the relative Confidence Interval is broader by $\sqrt{2}$ at small values and by $\sim$ 2 at larger interval values due to the effect of the broader bin on the data (bin) error and its effect on the Confidence Interval.

3.4 Discussion of the problems of inclination alternatives

The results presented above indicate that very small values of data error (on the binned observations) are needed to obtain a reasonably accurate determination of binary inclinations from polarimetry. Reducing the value of the data error is however non-trivial. It is known that non-phase-locked physical fluctuations of the binary system (short term random, changes in the scattering region for example) can give rise to errors (i.e. deviations of data points from a phase locked curve) that are considerably larger than those of measurement alone. In principle, if the canonical model is a fair description of the average behaviour of the system (i.e. if variations about phase locking are random), both types of errors can be considerably reduced by averaging the Q and U observed on different orbital cycles but in the same phase interval (bin) and is achieved by folding the data on the binary period. It should be possible therefore when many cycles are taken for the error on each phase bin to be made very small. The difficulty arising from this approach is that systematic evolution (or coherent variation) of the scattering region would produce anomalous results (i.e. the scattering contribution may be different at similar phases but at later orbital cycles). Crucial to this question then, is the time period over which such envelope evolution effects are significant. If too many cycles are taken together, then the assumption of phase locking breakdown due to long term evolution of the envelope.

If too few cycles are taken then (i) binning might no longer be practical for a manageable number of phase points or (ii) short term random physical fluctuations might be too large to be reduced by averaging. Hence phase binning and folding would tend to make the canonical model acceptable, but for an extremely wide range of parameters determination would thus be inaccurate and inconclusive. In this situation a combination of techniques might be necessary to make any progress. Stability of the scattering region geometry could be tested by sequential analysis of the Q,U data, that is by taking the data of cycles 1 - A, A/2 - 3A/2 etc. separately where A could be 5 or 10 depending on the coverage of the cycles. One would expect to find the same inclinations for each block of data considered unless the canonical model was not valid or at least was not valid over such a number of cycles. In this case a smaller number of cycles would have to be analysed. When the number of cycles does not permit the binning technique or the long term stability of the system is in doubt, a non-equal phase interval analysis would be necessary. If sequential analysis indicated that envelope evolution was not significant during the complete set of cycles, then the usual binning techniques could be used, thus averaging out the random fluctuations. When (and if) a consistent i value and 'mean envelope' model have been found in this way some insight should be possible into the evolutionary behaviour of the envelope by study of the residuals between the unbinned Q,U values and the predicted mean model value (cf. Chapter 2).

Both these techniques are considered in later Chapters (8 and 9) with the application of them to data for several binaries including, Cygnus X-1. The results presented here should be approximately valid for unequal phase interval analyses (Chapter 8) providing the intervals between successive observations are not too unequal. Then other effects might enter into the problem of accurately determining inclinations from polarimetry.

In conclusion we note that the main points pertaining to the determination of binary inclinations by polarimetric modelling are that

(a) the accuracy of the determination of binary inclination is strongly dependent on the value of the true inclination present. At low inclinations extremely small, values of data error σ are needed for any sort of accuracy in i.

(b) The Relative Confidence Interval on an optimum inclination is seen to broaden drastically (more drastically the lower the inclination) when as the noise on the data increases from zero.

(c) The current accuracy levels (Rudy and Kemp 1978) are significantly larger than the necessary predicted accuracies even to determine inclinations $> 60^{\circ}$. An accuracy of observation attained by McLean (1980) is however close to the required level and therefore further observations may provide suitably low noise levels for unambiguous model testing and parameter determination, provided the scatter due to binning (i.e. non phase locking) is not too great.

CHAPTER 4 - STATISTICAL INVESTIGATION OF THE BIAS OF THE POLARIMETRIC INCLINATION ESTIMATOR

It became apparent when numerical testing of the optimization procedure for canonical model and observations, that when significant noise was present on the data the value of the inclination inferred from the predictions of the model tended to be greater than the true value. This discrepancy increased (especially at low inclinations) when the noise level increased (cf. Figures 3.4 a,b). We therefore further investigated this effect by undertaking a statistical study of the least squares estimator (ℓ,s,e) for the inclination obtained from the canonical model, in particular for the case of 2nd harmonic data (data varying at the 2nd harmonic of the binary period). The underlying bias observed when testing the canonical model (Chapter 3) was obscured by the fact that most of the observations, to date (pre-1980), were of binaries whose inclination was known to be high by the presence of eclipses in the photometric light curves (β Per, u Her, σ Ori E, USge, V444 Cygni) and indeed it was their high inclinations which permitted their identification as binaries. The polarimetric inclinations obtained using the least squares procedure were found to be in reasonable agreement with the photometrically determined values hence casting no suspicion on the polarimetric inclination estimator.

We investigate here the bias of the polarimetric method previously used by workers in the field by establishing the true frequency distribution (the distribution of inferred i values at a certain true inclination and h^{noise} level) of the ℓ.s.e. of the inclination. This distribution will depend on the true (input) parameter of the model, and on the error distribution of the data. For simplicity, and without much loss of generality we take this data error distribution to be normal (Gaussian) with the variance at each data point the same. Two methods of establishing this distribution are apparent. The first is the analytic formation of the distribution, which because of the number of free parameters in the model, would be considerably advantageous. Alternatively we can use the computer to construct the frequency distribution which is simpler but can be both expensive on computer time, considering the number of samples

needed, and so can really only be used for a small number of assigned input parameters. Unfortunately, the analytic treatment is only practical for a small number of special cases and we use it here when (a) the noise levels become arbitrarily large and (b) when the true inclination of the binary is zero. These two cases are nevertheless instructive as to the nature of the distribution function. We derive the corresponding frequency distributions in closed analytic form. The cases where the true inclination and noise level are arbitrary we treat only for one intrinsic geometry of the scattering region (and one rotation angle θ) using a computer random sample method.

Although we do in fact establish the frequency distribution for the ℓ.s.e. of the inclination, a good deal about the frequency distribution can be learnt from the behaviour of its central measure and dispersion. It is very simple to calculate approximately the mean and variance of the ℓ.s.e. from the random sampling of the computer method, and hence demonstrate directly the dependence of the mean on the signal to noise ratio, and the bias of the inclination estimator. We shall also derive an expression for the mean value or expectation value of the ℓ.s.e. of the inclination using a standard (Taylor's expansion) technique. This demonstrates the approximate functional dependence of the bias on the noise level for low values of noise.

The formal error analysis used by previous authors (e.g. Rudy and Kemp 1978) depends on the errors on the data being extremely small. When this is not the case both the bias of the estimator and the correlation effects between the model parameters become important. In addition to the variance on the ℓ.s.e. of inclination, we also calculate the formal linear error for the case of computer sampling We give a brief discussion of this formal error and a derivation of the expressions used to calculate it for the present case.

4.2 The Least Squares Estimator of Inclinations and its Bias

Under the simplifying assumptions of an orbital plane symmetric scattering envelope the canonical model of Brown et al (1978) predicts the variation of the Stokes parameters with orbital phase (ϕ) as:

$$Q(\lambda) = p_c + p_2 \cos 2\lambda + q_2 \sin 2\lambda$$
$$U(\lambda) = u_c + u_2 \cos 2\lambda + v_2 \sin 2\lambda \qquad (4.1)$$

where $\lambda = 2\pi\phi$ and p_c, u_c are the constant polarization levels containing contributions from the interstellar polarization and polarization of circumstellar origin. The coefficients p_2, q_2, u_2, v_2 are related to the geometry and optical thickness of the scattering region by relations outlined in Chapter 2 and in particular satisfy the non-linear constraints:

$$\frac{p_2 \cos 2\theta - u_2 \sin 2\theta}{q_2 \sin 2\theta + v_2 \cos 2\theta} = \frac{1 + \cos^2 i}{2 \cos i} = \frac{-q_2 \cos 2\theta - v_2 \sin 2\theta}{p_2 \sin 2\theta + u_2 \cos 2\theta} \qquad (4.2)$$

where i is the binary inclination and θ is the orientation of the polarimeter to the plane defined by the rotation axis of the binary and the line of sight.

All the coefficients (p_c, u_c, p_2, q_2, u_2, v_2) i and θ are unknown a priori and have to be inferred from the polarimetric data. Here we denote the estimators of these parameters (i.e. the relation whereby the values are inferred from the data) by a circumflex (i.e. $\hat{p}_2$, $\hat{q}_2$, $\hat{i}$ etc.). The problem is then of simultaneous point estimation establishing a simultaneous confidence region for these parameters. This was the approach outlined in Chapter 2 and Simmons, Aspin and Brown (1980). To establish a unique confidence interval for any one parameter, i say, from 'real' observations is not usually possible since the distribution of the corresponding estimator i will be dependent (in most cases) on the true value of the remaining free parameters as well as the true value of i (i_o). Under certain circumstances approximate procedures for establishing confidence intervals can be justified, although as we demonstrate below can lead to erroneous results.

The least squares fitting procedure used by Rudy and Kemp (1978), Rudy (1979) and implicitly by Brown et al (1978) yield an estimator for the cosine of the inclination given by Equation (10) of Brown et al (1978).

$$\hat{\cos i} = \frac{1 - f^{\frac{1}{4}}}{1 + f^{\frac{1}{4}}} = h(\hat{p}_2, \hat{q}_2, \hat{u}_2, \hat{v}_2) \qquad (4.3)$$

where $$f \equiv \frac{(\hat{p}_2 - \hat{v}_2)^2 + (\hat{q}_2 + \hat{u}_2)^2}{(\hat{p}_2 + \hat{v}_2)^2 + (\hat{q}_2 - \hat{u}_2)^2} \qquad (4.4)$$

and
$$\begin{pmatrix} p_2 \\ u_2 \end{pmatrix} \equiv \frac{2}{N} \sum_{r=0}^{N-1} \begin{pmatrix} Q_{ob,r} \\ U_{ob,r} \end{pmatrix} \cos \frac{4\pi r}{N}$$
$$\begin{pmatrix} q_2 \\ v_2 \end{pmatrix} \equiv \frac{2}{N} \sum_{r=0}^{N-1} \begin{pmatrix} Q_{ob,r} \\ U_{ob,r} \end{pmatrix} \sin \frac{4\pi r}{N} \qquad (4.5)$$

where $(Q_{ob,r}, U_{ob,r})$ are the binned observations at phase point r, and N is the number of binned observations. (Simmons et al 1980). The binned observations are formed by folding the actual observations onto the binary period (determined usually by spectrophotometry) and then averaging the values falling in each phase bin. We assume for convenience that $Q_{ob,r}$ and $U_{ob,r}$ are all independent and normally distributed with the same variance σ^2. Hence $\hat{p}_2$, $\hat{q}_2$, $\hat{u}_2$ and $\hat{v}_2$ are the ℓ.s.e's of the Fourier coefficients of Equation (4.1).

We can simply estimate the variance on these parameters due to the corresponding variance on the data σ . If we have a data set $x_1, x_2, \ldots x_n$ and we form the quantity

$$z = a_1x_1 + a_2x_2 + \ldots . a_nx_n$$

where the coefficients a's can take any value then if the error on each x_j is σ , the error on z will be $\hat{\sigma}^2 = \sum_j (a_j)^2\sigma_j^2$ In our case $(z = \hat{p}_2, \hat{q}_2, \hat{u}_2 \text{ or } \hat{v}_2)$ $x_j = Q_{ob,j}$ (or $U_{ob,j}$) and $a_j = \frac{z}{N} \cos \frac{4\pi j}{N}$. The variance $\tilde{\sigma}_c^2$ therefore is

$$\tilde{\sigma}_c^2 = \sum_{j=0}^{N-1} (\frac{2}{N} \cos (\frac{4\pi j}{N}))^2\sigma^2 = (\frac{2}{N})^2\sigma^2 \sum_{j=0}^{N-1} (\cos (\frac{4\pi j}{N}))^2$$

and

$$\tilde{\sigma}_c^2 = (\frac{2}{N})^2\sigma^2 \text{ or } \tilde{\sigma}_c^2 = (\frac{2}{N})\sigma$$

since $$\sum_{j=0}^{N-1} \cos (\frac{4\pi j}{N}) = 1.$$

These parameters if independently and normally distributed have the same variance $\tilde{\sigma}_c^2 = \frac{2}{N}\sigma^2$. The precise form of $\hat{\theta}$ and $\hat{p}_o$, $\hat{u}_o$ do not interest us here and can be found in Chapter 2.

The frequency distribution for both $\hat{\cos i}$ and for $\hat{i}$ defined by $\cos^{-1}(\hat{\cos i})$ can be easily found from that of f but because the distribution of f takes a much simpler form we shall deal with it rather than those of $\hat{i}$ or $\hat{\cos i}$. The form of these distributions will depend on the true values of all the parameters that occur in the model and on the value of σ^2.

The analytic form of the distribution of f can now be found in certain special cases. We write:

$$z_1 = \frac{(\hat{p}_2 - \hat{v}_2)}{\sqrt{2}\,\sigma} \quad , \quad z_2 = \frac{(\hat{q}_2 + \hat{u}_2)}{\sqrt{2}\,\sigma} \quad , \quad z_3 = \frac{(\hat{p}_2 + \hat{v}_2)}{\sqrt{2}\,\sigma} \tag{4.6}$$

and $z_4 = \dfrac{(\hat{q}_2 - \hat{u}_2)}{\sqrt{2}\,\sigma}$.

Since $\hat{p}_2$, $\hat{q}_1$, $\hat{u}_2$ and $\hat{v}_2$ are all normally distributed and independent with the same variance $\hat{\epsilon}_c^2 = \frac{2}{N}\sigma^2$, z_1, z_2, z_3 and z_4 will be similarly distributed but with variance 1 and mean μ_1, μ_2, μ_3 and μ_4 given by:

$$\frac{(p_o - v_o)}{\sqrt{2}\,\sigma} \quad , \quad \frac{(q_1 + u_o)}{\sqrt{2}\,\sigma} \quad , \quad \frac{(p_o + v_o)}{\sqrt{2}\,\sigma} \quad \text{and} \quad \frac{(q_o - u_o)}{\sqrt{2}\,\sigma} \tag{4.7}$$

The first special case we consider is one with the assumption of arbitrarily large noise levels (i.e. $\sigma \to \infty$). z_1, z_2, z_3 and z_4 will have standard normal distributions and thus $(z_1^2 + z_2^2)$ and $(z_3^2 + z_4^2)$ will both have central chi-squared distributions with 2 degrees of freedom. f, defined by $f = (z_1^2 + z_2^2)/(z_3^2 + z_4^2)$ will consequently have the corresponding F distribution i.e.

$$F_\infty(f) = \frac{1}{(1 + f)^2} \tag{4.8}$$

Furthermore the expectation value of the cosi estimator

$$\langle \hat{\cos i} \rangle = \left\langle \left(\frac{1 - f^{\frac{1}{4}}}{1 + f^{\frac{1}{4}}} \right) \right\rangle = \int_o^\infty \frac{1}{(1 + f)^2} \left(\frac{1 - f^{\frac{1}{4}}}{1 + f^{\frac{1}{4}}} \right) df = 0 \tag{4.9a}$$

This enables us to find the probability of inferring a value of inclination between any two specified values. Denoting the inclination reduced to the first quadrant by $|\hat{i}|$ it follows from (4.4) that

$$\text{Prob}\{\alpha \leq |\hat{i}| \leq 90^\circ\} = \frac{1 - f(\alpha)}{1 + f(\alpha)} \qquad (4.9b)$$

where $$f(\alpha) = \left(\frac{1 - \cos\alpha}{1 + \cos\alpha}\right)^4 \qquad (4.9c)$$

Evidently the probability of inferring a high inclination from data that in effect is white noise is extremely high. For example by substituting $\alpha = 60^\circ$ and 75° we have

$$\text{Prob}\{60^\circ \leq |\hat{i}| \leq 90^\circ\} = 81/82 \simeq .98$$

$$\text{Prob}\{75^\circ \leq |\hat{i}| \leq 90^\circ\} = 0.79.$$

In the other case mentioned earlier (i.e. $i_o = 0^\circ$) we have $p_o = v_o$ and $q_o = -u_o$. Writing $w = z_1 + z_2$ and $y = z_3 + z_4$ we see that w will have a central χ^2 distribution (the mean of w is zero) and y a non-central χ^2 distribution (a non-zero mean y) given by:

$$W(w) = \frac{e^{-w/2}}{2}, \quad Y(y) = e^{-\gamma} \sum_j \frac{i\, y^j\, e^{-y/2}}{(j!)^2\, 2^{j+1}} \qquad (4.10)$$

where $\gamma = \frac{1}{2}(u_3^2 + u_4^2)^2 = \dfrac{(p_o^2 + q_o^2)}{\sigma^2}$ (cf. Abramowitz and Stegun 1972)

the distribution of $f = w/y$ will now be given by

$$F(f) = \int_o^\infty W(yf)\, Y(y)\, y\, dy$$

$$= e^{-\gamma} \sum_j \frac{j}{(j!)^2\, 2^{j+2}} \int_o^\infty y^{j+1}\, e^{-y(f+1)/2}\, dy \qquad (4.11)$$

The integral can be reduced to the form of a gamma function and hence:

$$F(f) = \frac{e^{-\gamma}}{(f+1)^2} \sum_j \left(\frac{\gamma}{f+1}\right)^j \frac{(j+1)}{j!} = \frac{e^{-\gamma}}{(f+1)^2} \frac{d}{d\xi}(\xi\, e^{\xi}) \qquad (4.12)$$

where $\xi = \frac{\gamma}{(f+1)}$. The cumulative distribution $\mathcal{F}$ (the distribution of f less than are specified upper limit) for f now takes the form:

$$\mathcal{F}(f) = \int_0^f F(f')\, df' = 1 - \frac{e^{-\frac{f}{f+1}}}{f+1} \qquad (4.13)$$

when the true inclination i_o is zero therefore, the frequency distribution is given by equation (4.12). An important factor is the measure of the signal to noise ratio given by:

$$\gamma = \frac{N}{2} \left(\frac{A}{\sigma}\right)^2 \qquad (4.14)$$

where A is the amplitude of variations of the polarization defined as $A = \frac{(p_2^2 + q_2^2)^{1/2} + (q_2^2 + v_2^2)^{1/2}}{2}$; N is again the number of data points. It follows from (12) that the cumulative probability: i.e.

$$\text{Prob}\{0 \leq f \leq f_o\} = 1 - \frac{e^{-\gamma f_o/f_o+1}}{f_o + 1} \qquad (4.15)$$

As $\gamma \to 0$ (i.e. $\sigma \to \infty$) this result necessarily agrees with Equation (4.9).

In Table I we use (4.15) to calculate the probability of inferring an inclination less than any given value α, for different values of γ and α. The dependence on the intrinsic geometry enters only through the amplitude factor in γ. We again observe that the bias of the estimator $\hat{i}$ particularly at high noise levels (small γ) is significant. For example we see that at $\gamma = 60$ there is only $\sim$ 50% probability of obtaining an inclination less than 60^o and a 10% probability of $\hat{i}$ being $< 50^o$. At $\gamma = 20$ the 50% probability level is at $\sim 67^o$ (i.e. 50% probability that $\hat{i} < 67^o$) and a 5% probability that $\hat{i} < 50^o$ making this lower range of i values extremely improbable at this γ for $i_o = 0^o$. We notice that for Cygnus X-1 data (Kemp et al 1979) $\gamma = 80$.

We can also obtain an approximate expression for the expectation value of $\cos\hat{i}$ ($<\cos\hat{i}>$) for arbitrary i_o. From (4.3) and (4.4) we can expand $h(\hat{p}_2, \hat{q}_2, \hat{u}_2, \hat{v}_2)$ around the values p_o, q_o, u_o, v_o (the true values) using a Taylor expansion. At low noise this should be

ALPHA→ / GAMMA	10°	20°	30°	40°	50°	60°	65°	70°	75°	80°
20	.000	.000	.001	.001	.046	.226	.426	.683	.896	.985
40	.000	.000	.001	.013	.087	.394	.662	.894	.998	1.00
60	.000	.000	.002	.019	.127	.525	.800	.964	.999	1.00
80	.000	.000	.002	.025	.165	.628	.882	.988	1.00	1.00
100	.000	.000	.003	.021	.202	.701	.931	.996	1.00	1.00
180	.000	.000	.005	.054	.332	.890	.992	1.00	1.00	1.00

TABLE I

True inclination $i_o = 0^\circ$. This Table gives the Prob$\{|\hat{i}| < \alpha\}$ with $\gamma = \left(\frac{A}{\sigma}\right)^2 \frac{N}{2}$. Cygnus X-1 phase binned data corresponds to a = 80. Data published by Rudy and Kemp (1978) yields smaller values (than 80) for seven other binaries.

valid since $\hat{p}_2$, $\hat{q}_2$, $\hat{u}_2$, $\hat{v}_2$ are unbiased. Thus:

$$h(\hat{q}_2, \hat{q}_2, \hat{u}_2, \hat{v}_2) = h(p_o, q_o, u_o, v_o) + \frac{\partial h}{\partial \hat{p}} (\hat{p}_o - p_o)$$
$$+ \frac{\partial h}{\partial \hat{q}} (\hat{q}_2 - q_o) + \frac{\partial h}{\partial \hat{u}} (\hat{u}_2 - u_o) + \frac{\partial h}{\partial \hat{v}} (\hat{v}_2 - v_o)$$
$$+ \frac{1}{2!} \frac{\partial^2 h}{\partial \hat{p}^2} (\hat{p}_2 - p_o)^2 + 2 \frac{\partial^2 h}{\partial \hat{p}\, \partial \hat{q}} (\hat{p}_2 - p_o)(\hat{q}_2 - q_o)$$
$$+ \ldots\ldots + \frac{\partial^2 h}{\partial \hat{q}^2} (\hat{q}_2 - q_o)^2 + \ldots\ldots \qquad (4.16)$$

Taking the mean of both sides and noting that $h(p_o, q_o, u_o, v_o) = \cos i_o$ we have since $\hat{p}$, $\hat{q}$, $\hat{u}$, $\hat{v}$ are all independent (and hence when we take the mean all the $(\hat{p} - p_o)$ $(\hat{q} - q_o)$ are zero).

$$< \hat{\cos i} > = \cos i_o + \frac{1}{2!} \left\{ \frac{\partial^2 h}{\partial \hat{p}^2} + \frac{\partial^2 h}{\partial \hat{q}^2} + \frac{\partial^2 h}{\partial \hat{u}^2} + \frac{\partial^2 h}{\partial \hat{v}^2} \right\} \left[\frac{\sigma}{\Gamma} \right]^2$$
$$+ \frac{1}{4!} \left\{ \frac{\partial^4 h}{\partial \hat{p}^4} + \ldots\ldots \right\} \left[\frac{\sigma}{\Gamma} \right]^4 \qquad (4.17)$$

Evaluation of the second order derivatives and substitution into the above equation (4.17) yields (with $i_o = 0$):

$$< \hat{\cos i} > = \cos i_o - \frac{\cos i_o}{2} \frac{(1 + 6 \cos^2 i_o + \cos^4 i_o)}{\sin^6 i_o} \left[\frac{\sigma}{\Gamma} \right]^2$$
$$+ \left[\frac{\sigma}{\Gamma} \right]^4 \qquad (4.18)$$

where $$\Gamma = \frac{(1 + 2 \cos i_o)}{2} (p_o^2 + q_o^2)^{\frac{1}{2}}$$

which gives us the expectation value of $\hat{\cos i}$ as a function of the inclination i_o, the true parameters p_o, q_o and σ.

As pointed out earlier, the general case of the distribution function for arbitrary inclination and noise can only be treated numerically. An approximate frequency distribution for f can be found using the fact that $\hat{p}_2$, $\hat{q}_2$, $\hat{y}_2$, $\hat{v}_2$ are independently and normally distributed with variance $\frac{2}{N} \sigma^2$ and using Equation (4.4) we can construct a histogram by randomly coupling $\hat{\cos i}$ from these normal

populations. This we have done for different values of true inclination i_o and σ^2 taking a typical intrinsic geometry corresponding to a scattering optical depth τ_o of $\sim$ 0.1 and typical density moments (in the notation of Brown et al (1978) see Chapter 2) $\gamma_3 = \gamma_4 = 1$. ($\theta = 0^o$). We take a sample of 200 $\hat{i}$ for f at each i_o (15^o, 45^o, 75^o) and γ (20, 80, 320, 1280). Figure (4.1) shows the resulting histograms for $\hat{i}$. These were formed using the ICL 2976 computer of the University of Glasgow utilizing standard (NAG) library routines (G05DDF) to produce pseudo-random numbers from a normal distribution with mean and standard deviation specified by the user. The coefficients p_o, q_o, u_o, v_o (for each i_o) were randomly perturbed using these numbers and the function f defining the inferred inclination via Equation (4.3) from Equation (4.4) was determined. The inclination range 0^o to 180^o was divided into 10^o bins and the sample of 200 determinations placed into the appropriate bin. One can easily see the general trend for the mode of the distribution at say $i_o = 15^o$. As γ decreases from 1280 to 20 the mode shifts from $\sim 45^o$ to 65^o and is significantly different from the input $i_o = 15^o$. The difference between the true inclination i_o and the model of the crude distribution here formed decreases as i_o increase until at $i_o = 75^o$, for example, all inferred values fell with the 70^o -80^o bin at $\gamma = 1280$ with the mode still being centred on 75^o at $\gamma = 20$. Further discussions of this and the previous special cases will be given in the Section (4.4).

In statistical terminology an estimator is said to be biased if its expectation value is not equal to the true value of the parameter it estimates. In our case for inclinations this is when:

$$< \cos \hat{i} > \neq \cos i_o \quad .$$

In the case of $\sigma \to \infty$ we have seen that $(\cos \hat{i}) = 0$ corresponding to an inferred inclination of 90^o. At low noise levels we have the expectation value approximately given by Equation (4.18). Thus the bias is approximately quadratic in σ/Γ (Γ defined by (4.18) the noise to signal ratio, at low noise levels.). For typical accuracy of polarimetric data obtained by Kemp et al (1979) for Cygnus X-1 ($\gamma \sim 80$) we can see this bias is significant e.g. when $i_o = 40^o$ $< \cos \hat{i} >$ = 0.44 corresponding to an inferred $i = 64^o$. Results for specific

FIGURES 4.2 a,b,c

These sho a histogram representation of the frequencies of inferred values of inclination for different values of the signal to noise ratio variable γ. All the histograms were based on 200 random (computer generated) samples conforming to the same intrinsic scattering geometry and position angle ($\theta = 0^{\circ}$). High values of γ correspond to low noise levels. In all cases the mode shifts towards 90° with increasing noise and towards the true inclination (indicated by the dash on the x axis) as the noise decreases.

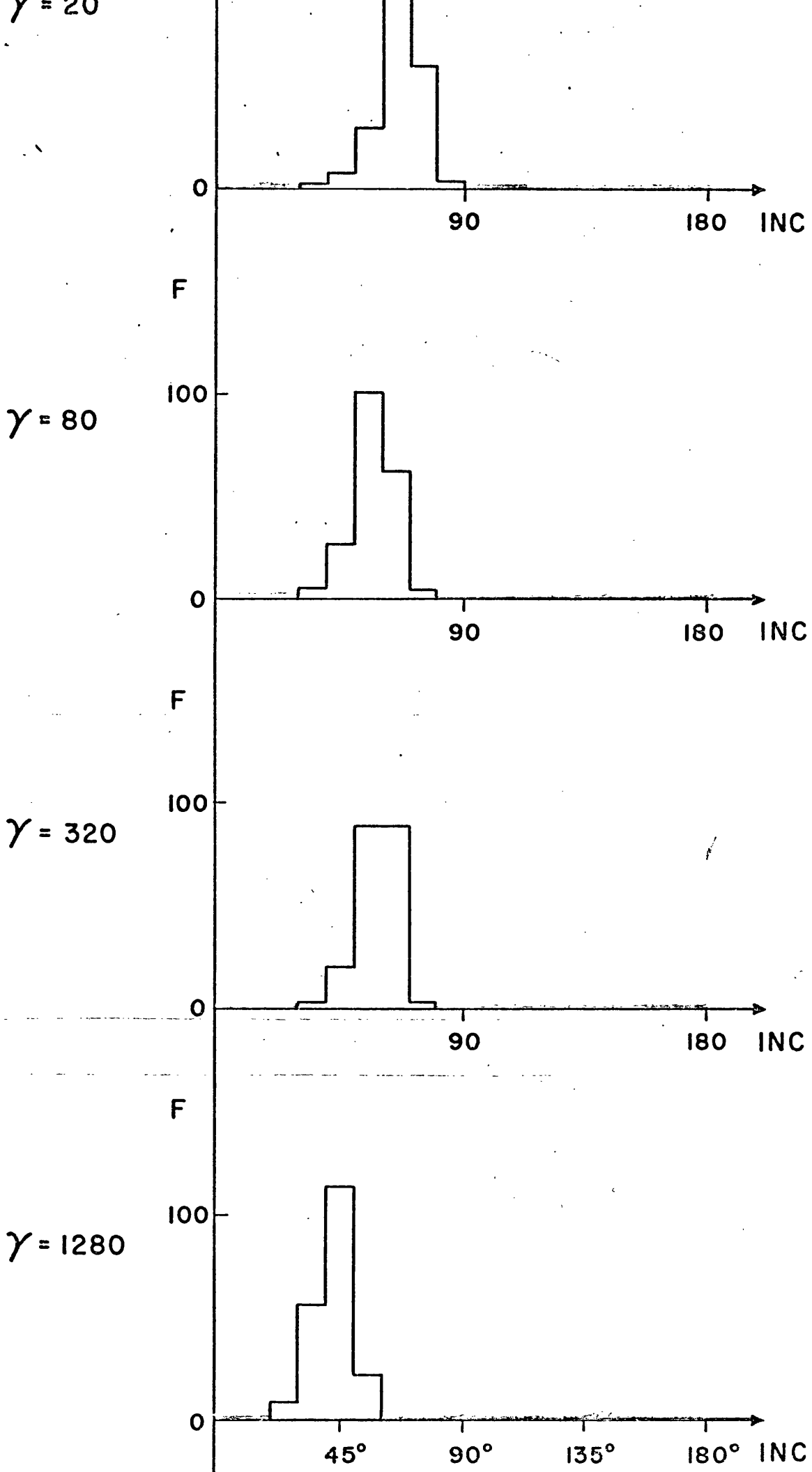
γ = 20
0
90
180 INC
F
γ = 80
100
0
90
180 INC
F
γ = 320
100
0
90
180 INC
F
γ = 1280
100
0
45°
90°
135°
180° INC

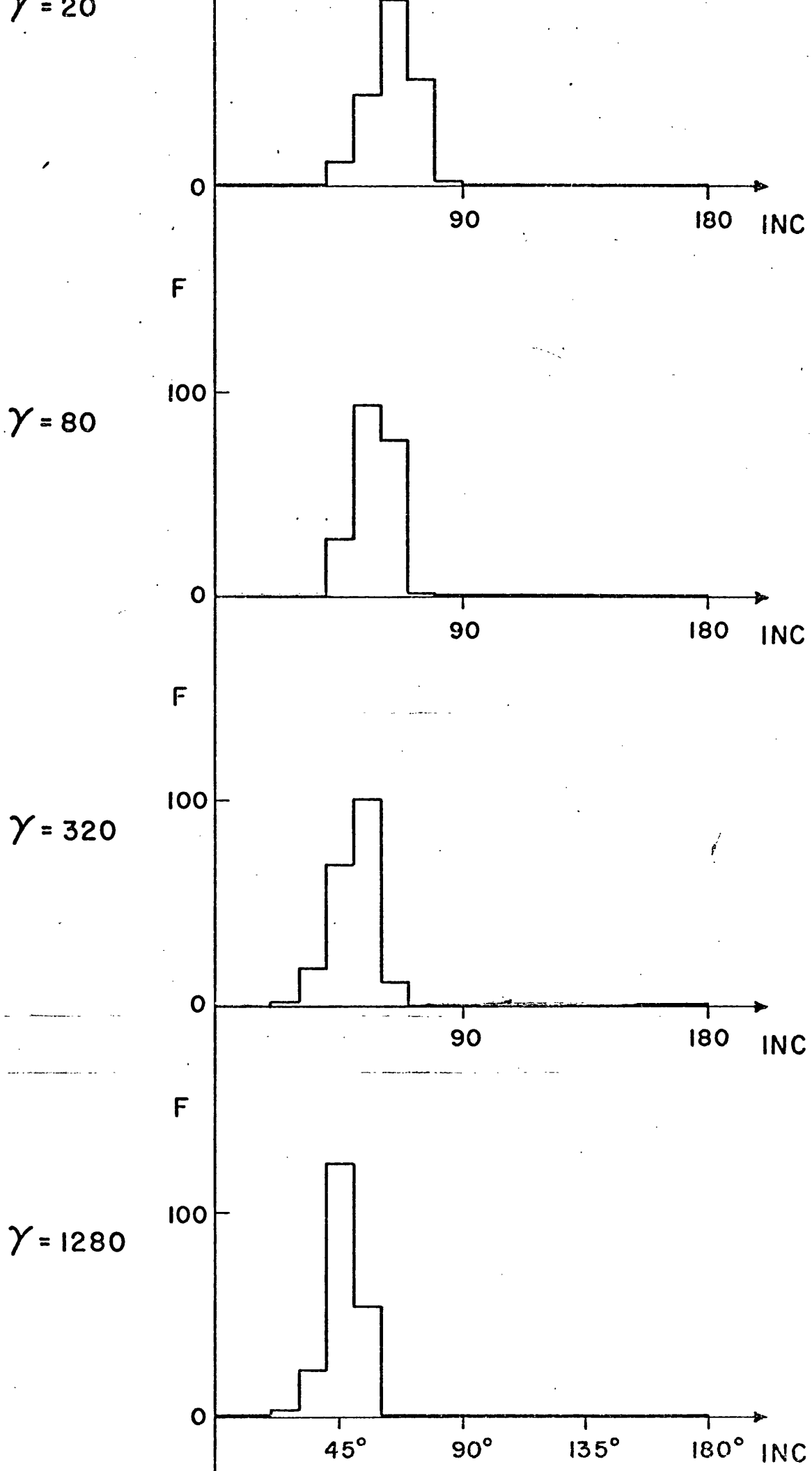
γ = 20
0
90
180
INC
F
γ = 80
100
0
90
180
INC
F
γ = 320
100
0
90
180
INC
F
γ = 1280
100
0
45°
90°
135°
180°
INC

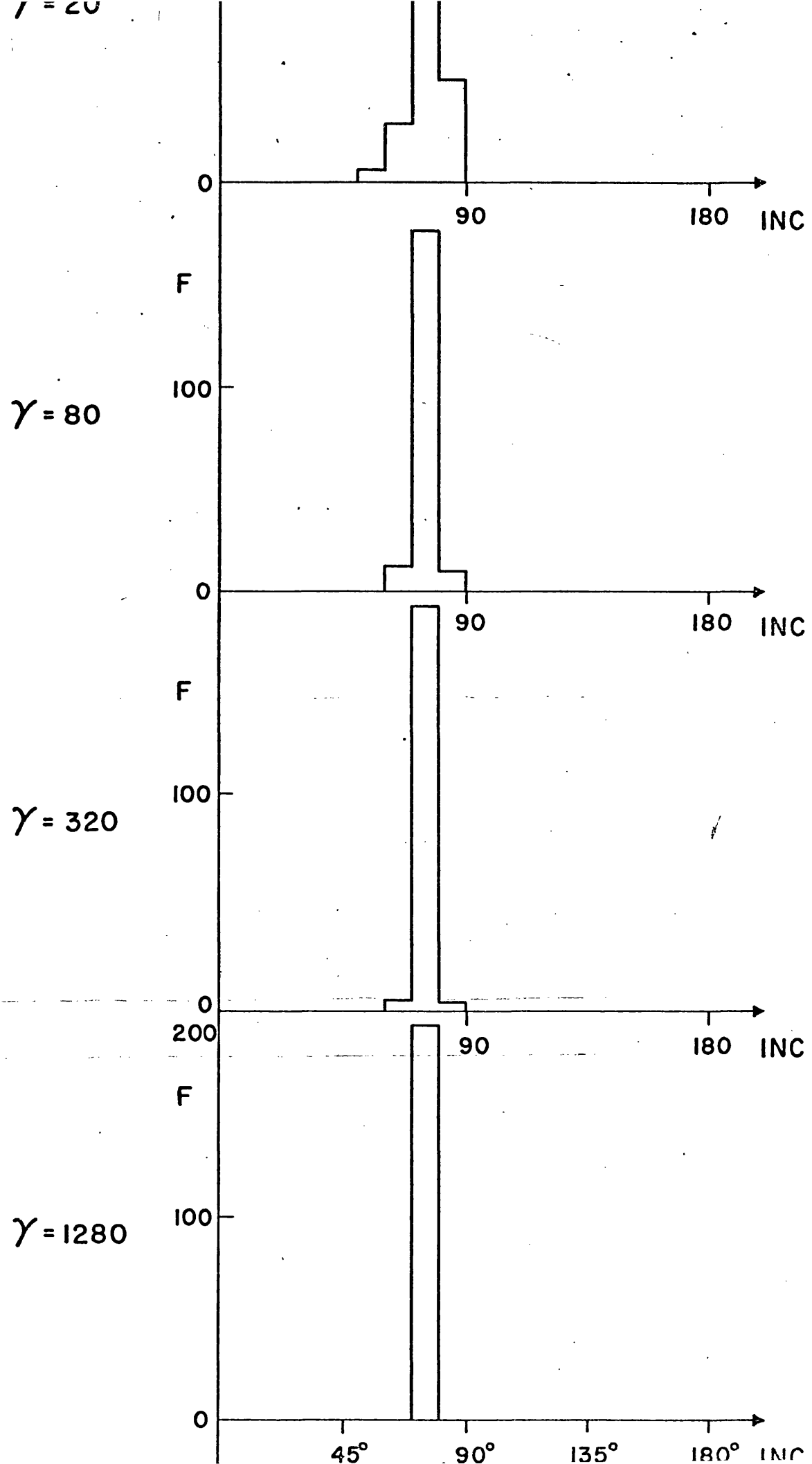
γ = 20
0
90
180
INC
F
γ = 80
100
0
90
180
INC
F
γ = 320
100
0
90
180
INC
200
F
γ = 1280
100
0
45°
90°
135°
180°
INC

i_o and γ's are given in Table II together with the standard derivative on the inferred i.

Figure (4.2) shows the mean inferred inclination ($i = \cos^{-1}(\cos \hat{i})$) against noise to signal (σ/A) for the intrinsic geometry considered above (dotted line). We should not expect the essential features to change with a change in scattering geometry (i.e. different i_o, γ_3, γ_4). Also shown is the standard deviation of $\hat{i}$ for each value of i_o and σ/A. Even at low noise levels the estimator $\hat{i}$ is seriously biased towards high inclinations when the true inclination i_o is low. This standard deviation on $\hat{i}$ is also found to be larger than the formal linear error, the main details of which are now related.

4.3 Formal linear error analysis

Previous authors have used the formal linear error to indicate a confidence interval for the true value of the inclination. This procedure is based on the assumption that the large number limit approximation is valid (an infinitely large sample will give the true value of the parameter) and that cos i is both an unbiased estimator and normally distributed. The formal linear error used is given by Wolberg (1967). From the expansion of the inclination estimator $h(\hat{p}_2, \hat{q}_2, \hat{u}_2, \hat{v}_2)$ around the true values p_o, q_o, u_o, v_o using the Taylor expansion above (Equation 4.16) we take the formal linear error as:

$$\sigma^2_{f.\ell.e} = \left(\frac{\partial h}{\partial Q_i} \right)^2_{opt} \sigma^2_{Q_i} \qquad (4.19)$$

where Q_i are the data value (cf. the error on $\hat{p}_2$, $\hat{q}_2$, $\hat{u}_2$, $\hat{v}_2$ above). The derivative is evaluated at the optimum value. In our case this may be reduced to

$$\sigma^2_{f.\ell.e} = \left(\frac{\partial h}{\partial \hat{p}_2} \right)^2 + \left(\frac{\partial h}{\partial \hat{q}_2} \right)^2 + \left(\frac{\partial h}{\partial \hat{u}_2} \right)^2 + \left(\frac{\partial h}{\partial \hat{v}_2} \right)^2 \frac{2\sigma^2}{N} \qquad (4.20)$$

Using expression (4.3) and after some manipulation one obtains

$$\sigma^2_{f.\ell.e} = \left(\frac{1}{\alpha} + \frac{1}{\beta} \right) \left(\frac{\alpha}{\beta} \right)^{\frac{1}{2}} \left[1 + \frac{1}{(\alpha/\beta)^{1_4}} \right]^4 \frac{\sigma^2_o}{N} \qquad (4.21)$$

X	GAMMA	INPUT INCLINATION		
		0^o	30^o	75^o
0.1	2000	$41^o.0^{+4}_{-5}$	$43^o.0^{+4}_{-4}$	$75^o.0^{+0.7}_{-0.5}$
0.2	500	$46^o.0^{+6}_{-6}$	$48^o.0^{+6}_{-5}$	$75^o.0^{+1.2}_{-1.1}$
0.3	222	$52^o.0^{+8}_{-8}$	$53^o.0^{+6}_{-6}$	$75^o.0^{+1.6}_{-1.3}$
0.4	125	$54^o.0^{+8}_{-8}$	$57^o.0^{+6}_{-6}$	$75^o.0^{+3.3}_{-3.2}$
0.5	80	$57^o.0^{+7}_{-7}$	$59^o.0^{+7}_{-6}$	$75^o.0^{+3.6}_{-3.6}$
0.8	31	$58^o.0^{+7}_{-7}$	$62^o.0^{+8}_{-8}$	$75^o.5^{+5.0}_{-5.0}$
1.0	20	$66^o.0^{+7}_{-7}$	$67^o.0^{+7}_{-7}$	$76^o.0^{+6.0}_{-6.0}$

X = SIGMA(DATA)/A ; A = AMPLITUDE OF VARIATION

TABLE II

This Table shows the expected value of the inferred inclination and deviation of the expected value against true inclination i_o and noise to signal ratio. Corresponding values of Υ are given in column 2. The formal linear error evaluated by assuming $\cos \hat{i}$ to be normally distributed was smaller by a factor 2 when $i_o = 75^o$, by approx. 10% at $i_o = 30^o$ and the same at $i_o = 0^o$ for the range of noise to signal considered. The values shown here were calculated by computer random sampling techinques.

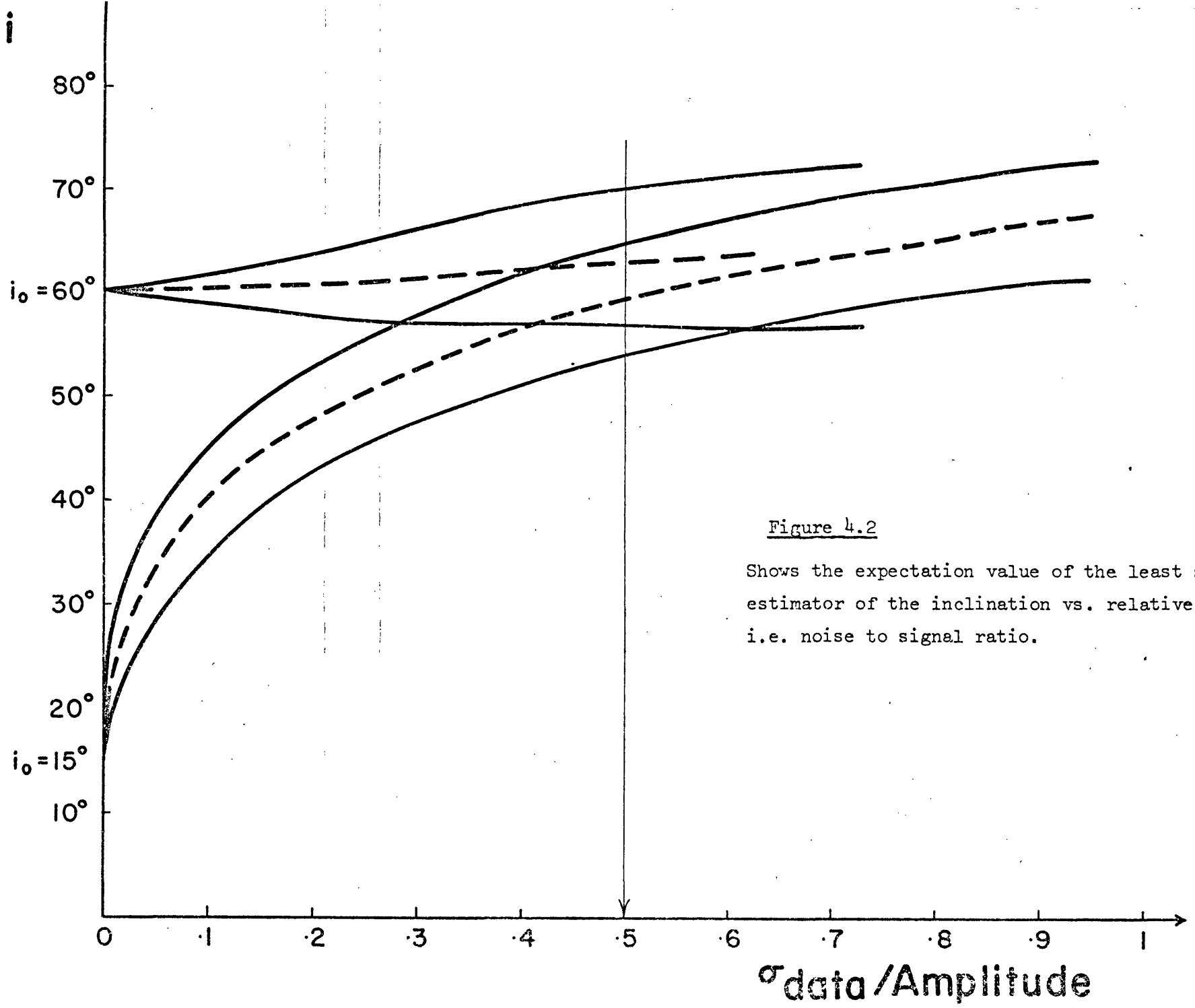

Figure 4.2

Shows the expectation value of the least squares estimator of the inclination vs. relative data error i.e. noise to signal ratio.

where $\alpha = (\hat{p}_2 - \hat{v}_2)^2 + (\hat{q}_2 - \hat{u}_2)^2$ and $\beta = (\hat{p}_2 + \hat{v}_2)^2 + (\hat{q}_2 - \hat{u}_2)^2$

Numerical evaluation of this shows that for a particular case the formal linear error is consistently smaller than the standard deviation in $\hat{\cos i}$ particularly at high inclinations (by a factor ~ 2) for the range of γ's considered (cf. Table II).

In the limit of $\sigma \to 0$ the estimator $\hat{i}$ does become unbiased no matter what the true inclination i_o. If the canonical model is still in agreement with the polarimetric data this formal error would give meaningful results regarding the measure of the accuracy of the determination. However at any other σ level, we would expect the confidence interval derived from the formal analysis to be narrower than the relative confidence interval of Chapter 2. This discrepancy is not serious at low data noise and because of the bias of the ℓ.s.e when i_o is low this more conservative approach is justified.

4.4 Discussion of the Bias effect.

If at the level of accuracy of polarimetric measurement the canonical model is consistent with the polarimetric data, then because of the bias of the ℓ.s.e. of inclination towards higher inclinations the method of inclination determination used by previous authors will tend to give inclinations that are considerably higher than their true values.

The quantitative results are given in the Tables I and II and Figure 4.1 and 4.2. The signal/noise ratio achieved for polarimetric data (considered in the context of the canonical model) corresponds to γ values ranging from 80 for Cygnus X-1 (Kemp long data run) to extremely poor values of around 10 for shorter data runs (eg. USge). (This latter figure may partly be a result of phase binning an insufficient number of points). At these levels of accuracy any inferences drawn from the polarimetric data about the inclination must be extremely dubious if a least squares procedure has been used. Taking the most optimistic value of γ, $\gamma = 80$, a true inclination, i_o, of 15° will yield, on average an inferred inclination of approximately 59°, $i_o = 30^\circ$ to an inferred value of 57°, and $i_o = 45^\circ$ to an inferred value of 58°. In all these cases the true inclination

actually lies well outside the 1σ error limits (and indeed the formal linear error). For $i_o = 60^o$ the inferred inclination corresponds fairly well yielding $62^o \pm 4^o$, and for true inclinations greater than 60^o the ℓ.s.e. corresponds closely to the true value, and the bias is negligible.

Thus we see that even at relatively low levels of noise a true low inclination would be interpreted in all likelihood as considerably higher, and conversely, if a high inclination is inferred, it is probable that the true inclination is low. Only if it is known from other sources (eg. eclipsing) that the true inclination is above a certain value could useful statements be made when this method is adopted. Thus an upper limit on the inclination could be effectively determined. This corresponds closely to the findings of Chapter 3 and Aspin et al 1980, where we established confidence intervals using the method of χ^2 testing. For example when $i_o = 60^o$, and at signal/noise ratio corresponding to $\gamma = 80$ we found any inclination between 0^o and 75^o compatible with the data (at 10% significance). Even if the inadequacies of the modelling are ignored, and the limit of the best observational accuracy presently achievable is taken (cf. Aspin et al 1980) and with 40 phase points the arrived at value of γ is approximately 2000. At $i_o = 0$, $< \hat{i} > = 40^o$; $i_o = 30^o$, $< \hat{i} > 38^o$; $i_o = 45^o$, $< \hat{i} > = 46^o$ for this value of γ, showing that at even this accuracy the bias of the method is important for true inclinations below 45^o.

The inclinations obtained by Rudy and Kemp (1977, 1978) and Kemp and Herman (1977), Rudy (1977) for the seven binary systems Algol, AO Cas, HD 47129, σ Ori E, u Her, U Sge, and V444 Cygni using this polarimetric method were all in fact high. Further more the signal/noise ratios indicated by the value of γ for the phase binned data best fitted by the canonical model were poor (cf. Chapter 5 and Aspin 1980). Table III gives the photometrically determined inclination, the polarimetrically determined value, and the signal to noise ratio γ. For illustration of the problem we also give in the table the expectation value of the inferred (ℓ.s.e) inclination from polarimetric modelling at the corresponding value of γ when the true inclination is taken to be zero. Although the choice of $i_o = 0$ was entirely arbitrary, it could be justifiably argued that the

STAR	INC PHOT.	INC POL.	GAMMA	LSE(INC0=0°)
ALGOL	82°	80°	67°	$57^{\circ}\pm7^{\circ}$
AO CAS	57°	67°	35°	$63^{\circ}\pm8^{\circ}$
HD47129	--	74°	32°	$64^{\circ}\pm9^{\circ}$
ORI E(B)	--	76°	26°	$65^{\circ}\pm10^{\circ}$
ORI E(U)	--	76°	10°	$75^{\circ}\pm12^{\circ}$
U HER	76°	77°	29°	$65^{\circ}\pm10^{\circ}$
U SGE	90°	87°	5°	$79^{\circ}\pm12^{\circ}$
V444 CYG	80°	76°	17°	$67^{\circ}\pm10^{\circ}$

TABLE III

Comparison of the polarimetrically determined inclinations (Rudy and Kemp and our own) with photometric values where known. The signal/noise ratio for the polarimetric data is shown also. The mean least squares estimator for inclination at corresponding values of signal to noise are shown when the true inclination is assumed zero.

agreement of the polarimetric inclinations of these authors on the one hand with the photometrically determined values is only slightly better than would be obtained with the ℓ.s.e. corresponding to $i_o = 0$. In other words the apparent agreement between the two methods for obtaining inclination could well be fortuitous.

It is quite unlikely, at the current levels of accuracy, for the ℓ.s.e. to yield a low inclination, irrespective of the true inclination. However, selection effects that pick out for observation mainly those binaries with high inclinations largely preclude this possible disagreement between photometry and polarimetric least square determinations. One exception to this rule is Cygnus X-1. For Cygnus X-1 photometry has given consistently lower inclinations than those derived from a least squares analysis of polarimetric data using the canonical model. Polarimetry has yielded values around 80° (Kemp et al 1979, Brown et al 1978), whilst light curve analysis has produced values between 30° and 45° (Hutchings, 1974a,b, Guinan et al 1979). Since ellipsoidal variations have been used to explain the light curve, even photometric determinations should be treated with caution: also by invoking a somewhat ad hoc occulting model specifically for Cygnus X-1, Kemp (1979) has brought the inclination from polarimetry down to approximately 60°). This discrepancy for Cyg X-1 reinforces the argument above, as well as the conclusions of Chapter 2 and Simmons et al (1980).

CHAPTER 5 - REAPPRAISAL OF THE POLARIMETRIC DATA FOR 7 BINARIES

5.1 Introduction

In Chapter 2 we developed a technique to obtain the optimum 'best fit' model parameter values from the canonical model of polarimetric binaries when applied to observations. Numerical testing of the optimization procedure and a statistical investigation of the bias of the polarimetric inclination estimator was undertaken in Chapter 3 and 4 respectively to establish the limitations of the canonical model in the presence of data noise.

The canonical model optimizing procedure was applied to the data of Cygnus X-1 (of Kemp et al 1979) in Chapter 2 where we found that a large range of inclinations would make the canonical model statistically acceptable at 10% significance and hence produce a $\chi^2 < \chi^2_{2N,10\%}$. Data for other systems is also available and here we apply the canonical model optimizing procedure to them. The systems that have been comprehensively observed polarimetrically (i.e. over many orbital periods) are Algol (β Per), AO Cas, HD 47129 (V band data), σOri E (in the U filter and B filter) and, μ Her, USge V444 Cygni (also in the V band) (cf. Chapter 1 Section 1.4 for references). We note that most of the observations of these systems were taken before the canonical model was developed (i.e. pre-1978) and are therefore of systems not necessarily best suited to description by the model (i.e. some are eclipsing systems and some may have eccentric orbits) nor were the data themselves acquired in convenient format (eg. uniform spacing). Quantitative polarimetric modelling of these systems was undertaken when those observations were published (c.f. Chapter 1). The analysis was applied to timing of extrema and zero points of (Q,U) and interpreted in terms of gas streams (Ao Cas), accretion disks (σ Ori E) and extended envelopes. These models, have the feature in common with that proposed for Cygnus X-1 (Kemp et al 1979, Kemp 1980) in that they contain many free parameters which are adjusted to produce satisfactory agreement. As in the case of Cyg X-1, however, such complexities are unjustified by the data until simpler (eg. canonical model) ideas have been shown to be irreconcilable with the observations. We therefore apply the canonical

model optimizing procedure to the data for these systems in this Chapter to assess the need or otherwise for more detailed models.

We have also seen in Chapter 2 how for Cygnus X-1 the formal error of Kemp et al (1979) of $\pm 7^{\circ}$ on the optimum inclination $i \sim 78^{\circ}$ was much smaller than the 90% Relative Confidence interval established through the optimizing procedure. It is also of interest to compare these two qualities for the 7 systems mentioned above and in particular to see whether the real error (relative confidence interval) on i is any nearer the usually quoted formal error (cf. Chapter 4) for any of these systems than for Cyg X-1.

Of crucial importance to the question of whether the canonical model is a valid representation of the data is the size of the errors assigned to the observations. The canonical model optimization procedure has included the assumption that the data points are at equally spaced phase intervals and that the error on each of these points is equal. This situation is achieved by folding the raw observations on to the binary period (established by other spectrophotometric methods) and phase binning the resulting data set. Phase binning, as we have seen, in Chapter 2 entails combining into one value, the raw observations within a certain range of phases (i.e. all the observations within, say the phase interval 0.1 to 0.15 are combined (averaged) to give a bin observation value at phase 0.125). A problem arises however when attempting to establish the error on each binned observational value when not only the observational error on each point but significant dispersion of observations is present within the bin. We shall establish a procedure to calculate this in Section 5.2. In Section (5.3) we apply the canonical model to the binned observations and present the resulting 'best fit' model parameters and confidence intervals for the 7 systems. In that section we also estimate the accuracy of binned observations necessary to obtain orbital inclinations to $\sim \pm 5^{\circ}$ for these systems using the procedure outlined in Chapter 3.

It is of course not the only aim of polarimetry to obtain an accurate inclination value. It is possible to estimate from polarimetric 'best fit' model parameters such quantities as the mean optical depth of scattering material and from this estimate (for an assumed size scale)

the number of scatterers (i.e. electrons in Thomson scattering). Thus, when say a gas stream is thought to be present in the system the scatterer number density and mass transfer rate between the stars can be assessed. We consider this aspect of the 'best fit' model parameters for the binary AO Cas (thought to have a gas stream - Abyankhar 1957) and show that polarimetry can give an independent check on the values of these parameters established by other methods (Section 5.4).

In the light of the results obtained we obtain further possible improvements in observational and analytic techniques to enable more complete diagnostics of binary systems (Section 5.5). We now proceed to discuss the problems of binning polarimetric observations under the assumptions implicit to the canonical model.

5.2 Phase Binning and its Implications

An implicit assumption of the canonical model is one of corotation of the scattering region and light source and subsequent phase locking of the observations. This means that in the frame rotating with the binary the scattering envelope is stationary and hence at each longitude λ the polarization (ie. Q,U) should be equal to that at longitude $(\lambda + 2\pi)$. If this assumption were exactly true then phase binning N observations in one bin would reduce the raw data error σ_{dat} to a bin error $\sim \sigma_{dat}/\sqrt{N}$. If phase locking does not strictly hold due to variations in the scattering region geometry and distribution, but varies only randomly about locking then binning would average them out in the long term. If variations about phase locking are large, however, and particularly if they are non-random, binning produces a bin error larger than σ_{dat}. In any event this technique would give a reasonable representation of some average behaviour of the system. To investigate the phase locking nature of the polarimetric variations Kemp and colleagues undertook a power spectrum analysis (cf. Chapter 1) of many of their sets of observations. That is they calculated the Fourier amplitude over frequency for their data. Then if phase locking is present Fourier peaks should appear in the power versus frequency slot at some harmonic frequency of the binary orbital frequency (i.e. if the binary period is 5.6 days as in Cygnus X-1

then power peaks may occur, when the variations are phase locked at frequencies 5.6 d, 2.8 d, 1.87 d, 1.4 d etc. giving 1st, 2nd, 3rd or 4th harmonics respectively). Kemp et al (1978) applied this technique to Cygnus X-1 with the resulting power spectrum being shown in Figure (1.18) and to their α Her data as shown in Figure (1.13a). Comparison of these two spectra (power versus frequency) shows the differing nature of the variations in the two systems. The Cygnus X-1 power spectra indicates the absence of strong peaks at harmonics of binary period whereas that of α Her observations shows clearly the peak at 1.025 days (i.e. the second harmonic of the binary period). This indicates that the phase-locking assumption is much better for the α Her data than for Cygnus X-1).

Observations, therefore, that are found in this way to be phase locked should, when folded onto the binary period, give (Q,U) values approximately equal to similar phases. A schematic representation of this is given in Figure (5.1) a raw observational error, here termed σ_{dat} is calculated at the time of observations, by repeated sampling of the Q,U values over a short period of time with the resulting spread being treated statistically (cf. Chapter 1). Rudy and Kemp (1978) in observing Algol, U Sge and V444 Cygni sampled (Q,U) eight times in a period of $\sim$ 1 hr to estimate σ_{dat} as the standard deviation of the sample which is of course the correct procedure to obtain a value of a quantity subject to short term statistical fluctuations with a normal distribution. The estimate of the bin error in this case (Figure 5.1a) is relatively simple. If we have a sample of m observations used to establish one polarisation (Q,U) value (m = 8 Rudy and Kemp 1978) and have l (Q,U) values in each bin (n=5 for Figure 5.1a) then if the dispersion of (Q,U) values in the bin is less than the observational error (as in Figure 5.1a) then all m × n (= M) samples of (Q,U) can be considered from one parent population hence the population mean of each (Q,U) value should be unique with the sample mean and estimate of the bin error $\hat{\sigma}_{bin}$ being:

$$Q_{bin} = \frac{1}{n} \sum_{i=0}^{n} q_i \quad ; \quad U_{bin} = \frac{1}{n} \sum_{i=0}^{n} u_i \qquad (5.1)$$

and

$$\hat{\sigma}^2_{bin,j} = \frac{1}{(m-1)} \left(\hat{\sigma}^2_{dat,j} + \hat{\sigma}^2_{disp,j} \right) \qquad (5.2)$$

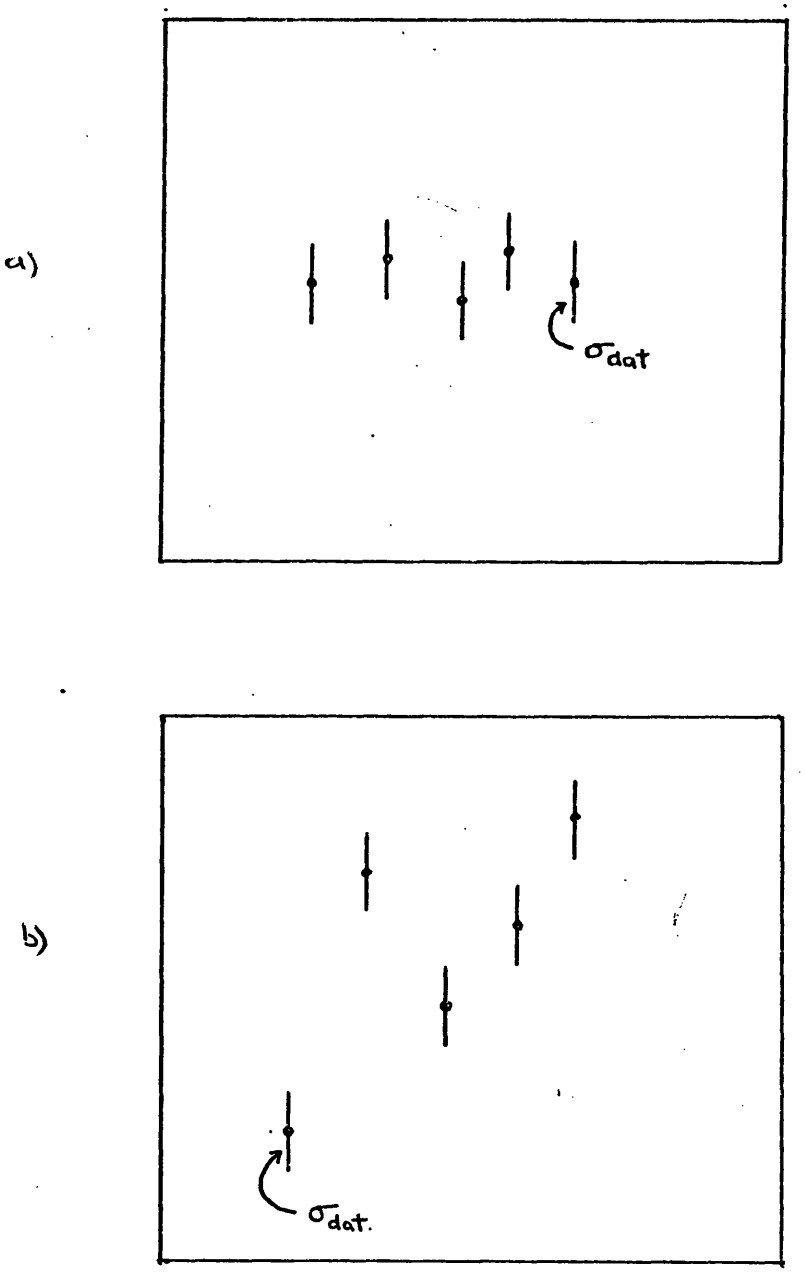

FIGURE 5.1

Schematic representation of the two cases of observations within a phase bin.

where (q_l, u_i) are the samples of (Q,U) making up each observation (Q,U), (Q_{bin}, U_{bin}) are the bin mean values of (Q,U), $\hat{\sigma}_{disp,j}$ is the estimator for the standard deviation of the observations (Q,U) within the jth bin and $\hat{\sigma}_{bin,j}$ is the estimator of the jth bin standard deviation.

Explicitly:

$$\hat{\sigma}^2_{dat,j} = \frac{1}{2M} \sum_{k=0}^{n-1} \sum_{i=0}^{m-1} (q_{i,k} - Q_{dat,j})^2 + (u_{i,k} - U_{dat,k})^2 \qquad (5.3)$$

and $$\hat{\sigma}^2_{disp} = \frac{1}{2n} \sum_{k=0}^{n-1} (Q_{dat,k} - Q_{bin})^2 + (U_{dat,k} - Q_{bin,k})^2 \qquad (5.4).$$

This gives us a value of σ_{bin} <u>for each bin</u> (N= 40 or so usually). The bin error we use in the analysis is therefore the mean of all these i.e.:

$$\hat{\sigma}^2_{bin} = \frac{1}{N} \sum_{j=0}^{N-1} \hat{\sigma}^2_{bin,j} \qquad (5.5)$$

If however phase locking is incomplete or partial (or even absent) then the situation can schematically be represented by Figure (5.2b). In this case each of the n (Q,U) values cannot be considered as from the same parent population and will have different population means and standard deviations. Any choice of $\hat{\sigma}_{bin}$ in this situation is to some extent arbitrary. Our choice of

$$\hat{\sigma}^2_{bin} = \frac{1}{n} (\hat{\sigma}^2_{dat} + \hat{\sigma}^2_{disp}) \qquad (5.6)$$

An alternative method of estimating σ_{bin} would be to calculate the quantity:

$$\chi^2_{x\%} = \frac{\sum_{i=0}^{n-1} (Q_i - Q_{bin,j})^2}{\hat{\sigma}^2_{bin}} \qquad (5.7)$$

for each bin (and for U) and by chosing the significance x% at which to evaluate χ^2, obtain an estimate of $\hat{\sigma}^2_{bin}$ by inverting (5.7) (i.e. chose x = 50% then

$$\hat{\sigma}^2_{bin} = \sum_{i=0}^{n-1} (Q_i - Q_{bin,j})^2 / (\chi^2_{50\%})).$$

This is again an arbitrary choice in that x can be taken as any value.

However Equations (5.6) has the desired properties that

(i) if $\hat{\sigma}_{dat} \to 0$ $\quad \hat{\sigma}_{bin}^2 \to \hat{\sigma}_{disp}^2/n$

(ii) as $m \to \infty$ (constant $\hat{\sigma}_{dat}^2$) $\quad \hat{\sigma}_{bin}^2 \to \hat{\sigma}_{disp}^2/n$

(iii) $\hat{\sigma}_{bin}^2 > \hat{\sigma}_{disp}^2/n$.

If σ_{bin} is large, which is likely when the situation of Figure (5.1b) is encountered, this will be reflected in wide confidence intervals for the model parameters. In effect we are using the various in a bin as a measure of the effective data error in parameter estimation in recognition of the fact that the model used does not fit the data within the raw data error σ_{dat}.

We noted in Chapter 2 that the value if inf χ^2 obtained for each inclination is severely dependent on σ_{bin} (i.e. dependent on $\hat{\sigma}_{bin}^2$) and therefore a slight change in $\hat{\sigma}_{bin}$ could mean a large change in inf χ^2 and the size of the confidence interval. Other estimates of $\hat{\sigma}_{bin}$ in the latter case above would give different confidence limits.

5.3 Application of the Canonical Model

After folding the observations (obtained over many orbital periods) onto the binary period it is seen that $\hat{\sigma}_{disp}$ is significantly larger than $\hat{\sigma}_{dat}$. We therefore take (5.6) as the estimate of $\hat{\sigma}_{bin}$. This implies that phase locking is weak and may in fact be an invalid assumption.

For three of the data sets $\hat{\sigma}_{bin} > \hat{\sigma}_{dat}$ (AO Cas, HD47129 and U Her; cf. Table I for numerical values). For the other five sets of data (eight in total because of the two sets for σ Ori E) $\hat{\sigma}_{bin} \sim \hat{\sigma}_{dat}$ meaning that the decrease in error due to the total number of (Q,U) values binned together is offset by the increase due to a large $\hat{\sigma}_{disp}$. Applying the canonical model (cf. Chapter 2) involving 1st and 2nd harmonic variations of polarization we find that at 10% significance:

(a) i_{opt} is close to previous determinations (both spectrophotometric and polarimetric) for all eight data sets (see Table II).

(b) for AO Cas, HD 47129, σ Ori E (both sets) u Her, USge and V444 Cygni the Relative Confidence Interval on the optimum inclination determination is much larger than the previously quoted Formal error (cf. Table II).

STAR	SIGMA % DAT	SIGMA % BIN
ALGOL	.0028	.00187
AO CAS	.024	.0365
HD47129	.016	.0323
σ ORI E(B)	.015	.017
σ ORI E(U)	.037	.034
U HER	.011	.085
U SGE	.023	.0152
V444 CYG	.063	.054

TABLE I.

STAR	INC (OTHER)	INC (ASPIN)	R.C.I.
ALGOL	$80^{\circ} \pm 7^{\circ}$	79°	$[-^{\circ}----^{\circ}]$
AO CAS	$67^{\circ} \pm 15^{\circ}$	61°	$[0^{\circ}, 88^{\circ}]$
HD47129	$74^{\circ} \pm 15^{\circ}$	69°	$[0^{\circ}, 180^{\circ}]$
σ ORI E(B)	$76^{\circ} \pm 14^{\circ}$	70°	$[-^{\circ}----^{\circ}]$
σ ORI E(U)	$76^{\circ} \pm 14^{\circ}$	82°	$[0^{\circ}, 180^{\circ}]$
U HER	$77^{\circ} \pm 8^{\circ}$	76°	$[0^{\circ}, 94^{\circ}]$
U SGE	$87^{\circ} \pm 5^{\circ}$	88°	$[0^{\circ}, 180^{\circ}]$
V444 CYG	$76^{\circ} \pm 10^{\circ}$	75°	$[0^{\circ}, 109^{\circ}]$

TABLE II

(c) For HD47129, σ Ori E (U filter) and U Sge all inclinations in the range $[0^\circ, 180^\circ]$ would produce acceptable χ^2 values with the canonical model.

(d) For AO Cas, U Her and V444 Cygni the 90% Relative Confidence Intervals were $[0^\circ, 88^\circ]$, $[0^\circ, 94^\circ]$ and $[0^\circ, 109^\circ]$ respectively.

(e) Algol and σ Ori E (B filter) data were seen to produce no acceptable fit for any inclination (i.e. $\inf \chi^2_{2N}(i) > \chi^2_{10\%,2N}$ for all i). This means that even at these high noise levels the data exhibits variations not representable by the canonical model. Any reduction in $\hat{\sigma}_{bin}$ would only result in a larger deviation between $\inf \chi^2(i_{opt})$ and $\chi^2_{10\%,2N}$.

(f) For all systems when the symmetric canonical model (2nd harmonics only) was used the same general results were found. The Confidence intervals were slightly smaller for AO Cas, U Her and V444 Cygni due to the reduction in the number of free parameters in the model fit. No change from the $[0^\circ, 180^\circ]$ confidence intervals for HD47129, σ Ori E (U filter) and U Sge were found. The optimum inclinations for the symmetric canonical model were close to those found in the asymmetric case. Table II gives the numerical results obtained in model fitting and Figures (5·2) through (5·9) show the resulting best fit 1st and 2nd harmonic (Q,U) versus phase curves and (Q,U) loci for all eight data sets (seven binaries).

Also shown are, in Figure (5·10) an example of the 2nd harmonic best fit curves for AO Cas and in Figure (5·11) the $\inf \chi^2$ variations with inclinations for the systems Algol, HD 47129 σ Ori E (B and U) and U Sge. Figures(5·12) show the best fit curves on the other minimum χ^2 of the other branch of the $\inf \chi^2$ vs. inclination curve. The optimizing procedure picks the minimum χ^2 value on both branches. The branches correspond to $\theta = \theta$ and $\theta = \theta + \pi/2$ (cf. Chapter 2). The minimum on the second branch is usually at $i = 0^\circ$.

The form of the results indicate that for the systems other than Algol at σ Ori E (B Filter) the bin error estimate $\hat{\sigma}_{bin}$ is too large to allow satisfactory model testing or determination of inclinations (and other parameters).

It is possible to obtain an estimate of the value of σ_{bin} required to obtain an optimum inclination to an accuracy of $\sim \pm 5^\circ$

FIGURES 5.2 to 5.9

In the following diagrams we show the data (Q and U) and 'best fit' general canonical model curves (i.e. 1st. and 2nd. harmonics) for the seven binaries re-analized in this chapter. We include the Q vs. ϕ, U vs. ϕ and the Q,U loci for all the systems.

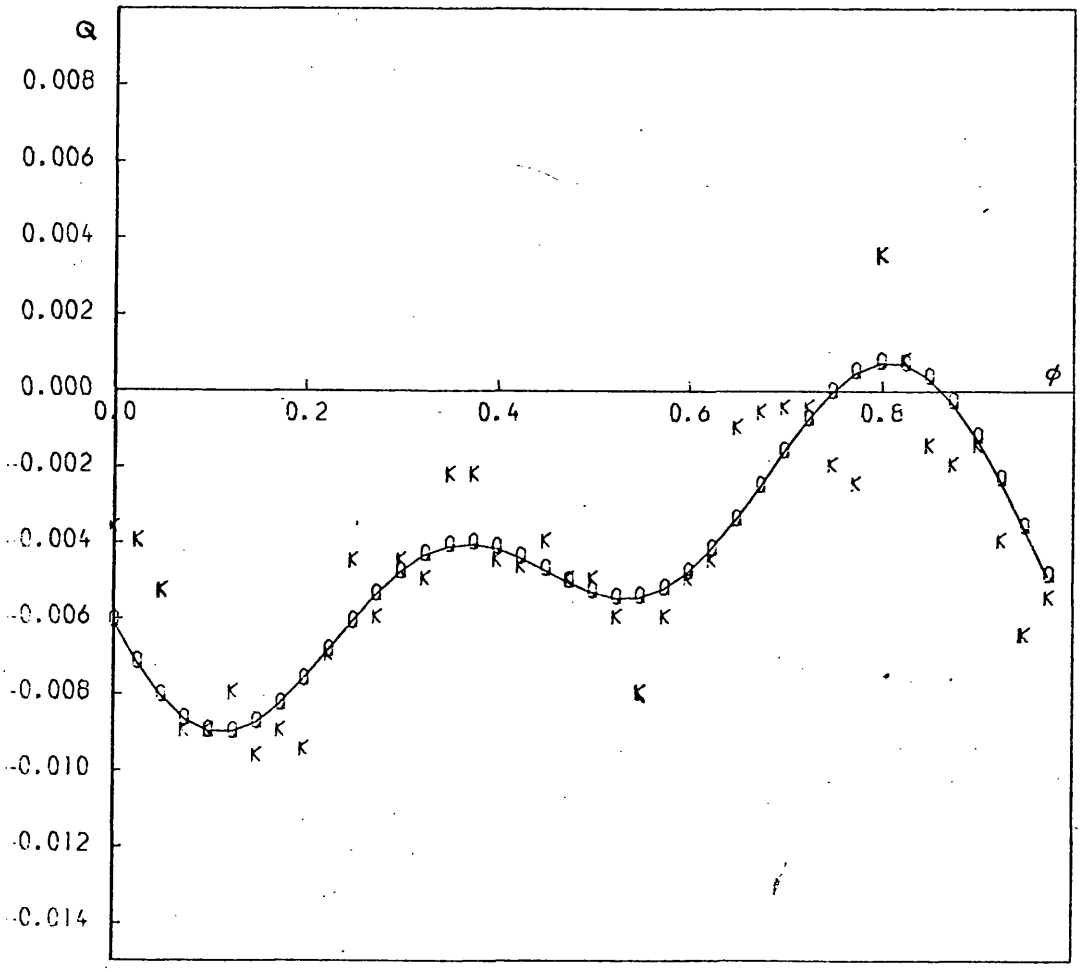

FIGURE 5.2a

Q vs. phase for Algol (data and best fit curves, 1st. and 2nd. harmonics, are shown).

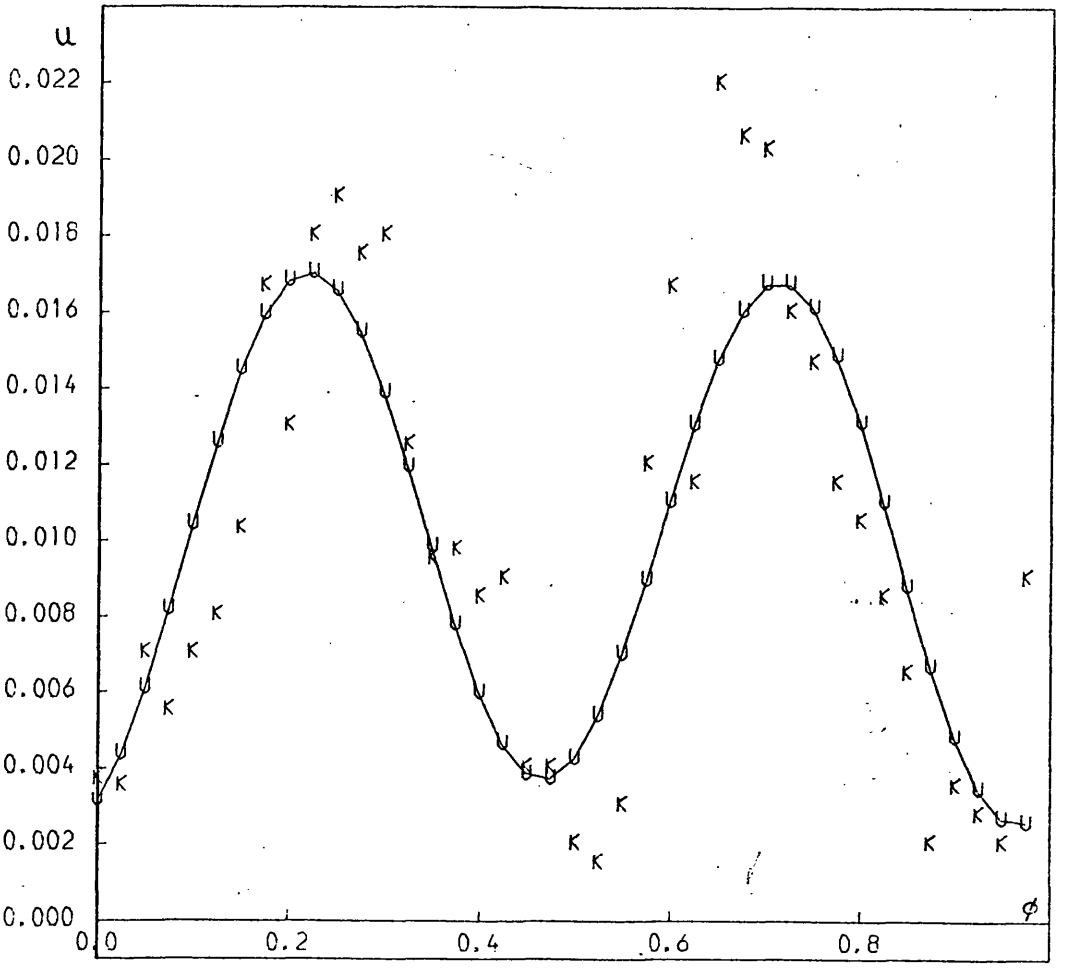

FIGURE 5.2b

U vs. phase for Algol (data and best fit curves 1st. and 2nd. harmonics, are shown).

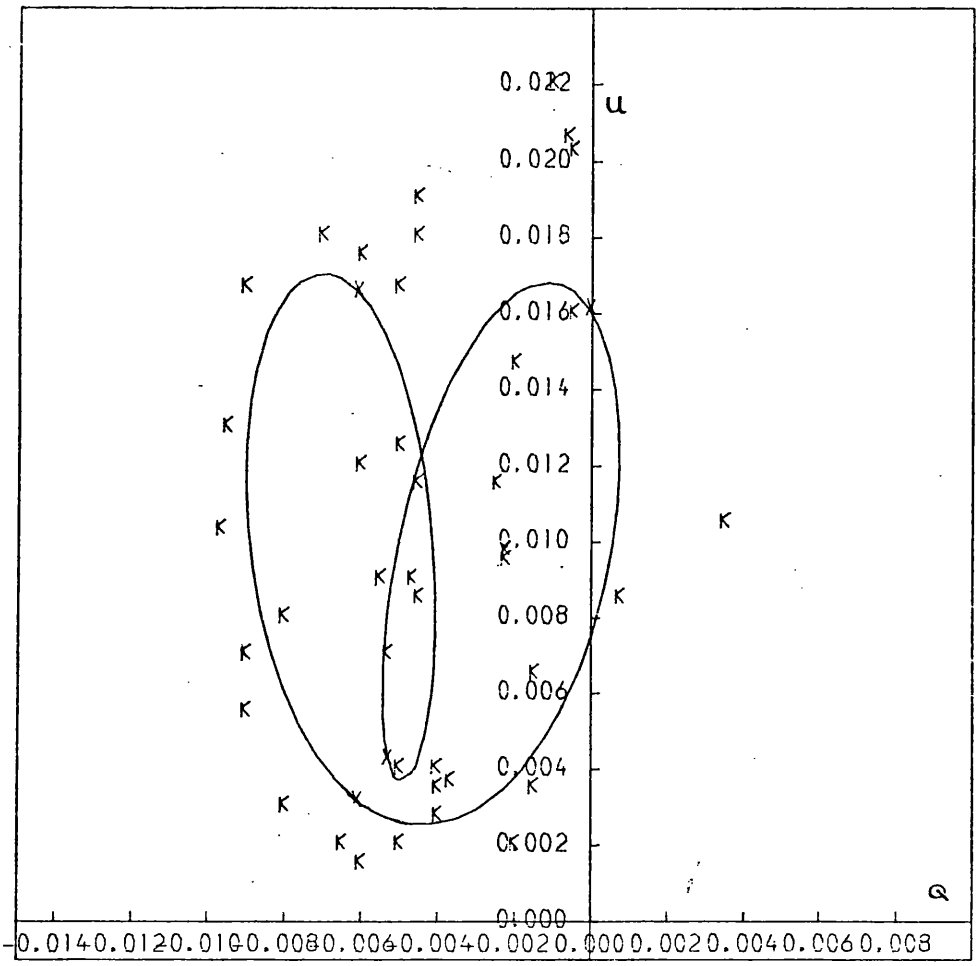

FIGURE 5.2c

Q,U locus for Algol. (data + best fit)

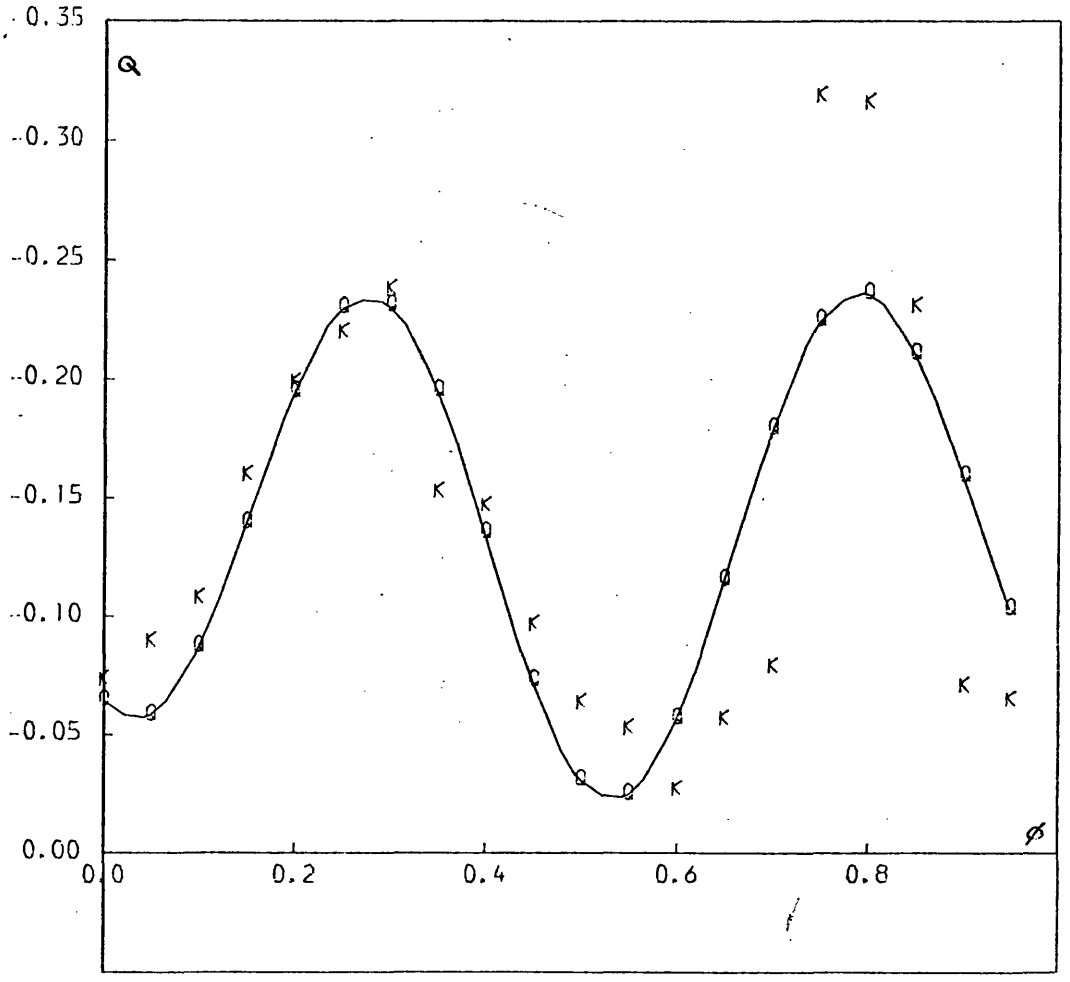

FIGURE 5.3a

Q vs. phase for AO Cas. (data + best fit)

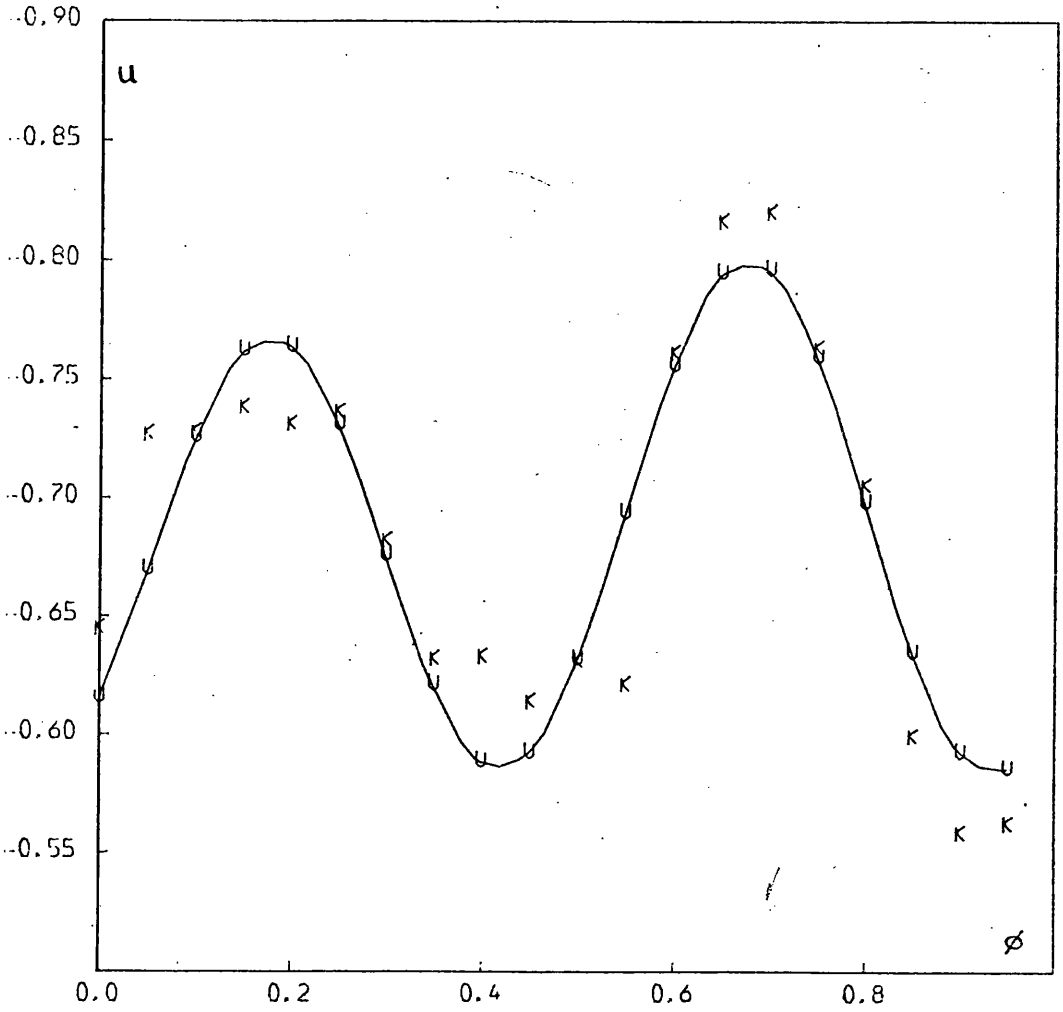

FIGURE 5.3b

U vs. phase for AO Cas. (data + best fit)

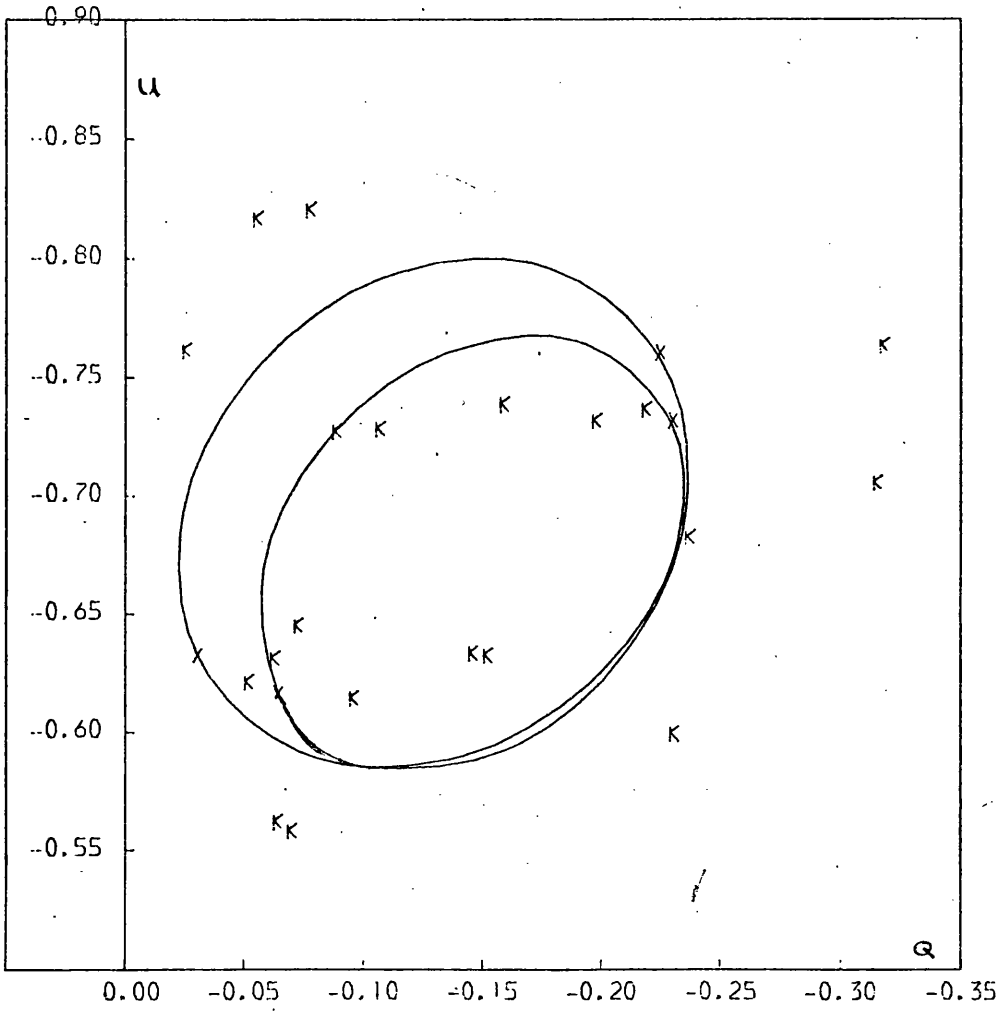

FIGURE 5.3c

Q,U locus for AO CAS. (data + best fit).

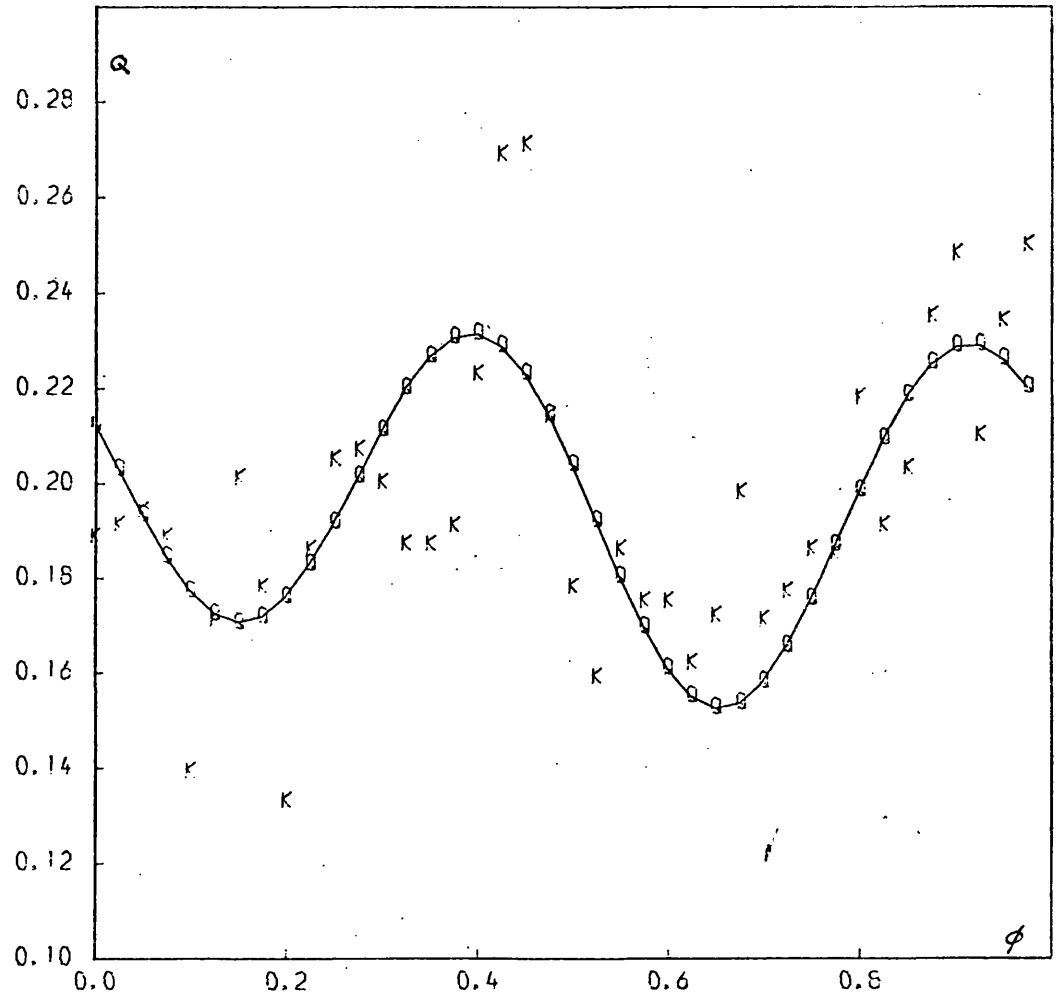

FIGURE 5.4a

Q vs. phase for HD 47129. (data + best fit)

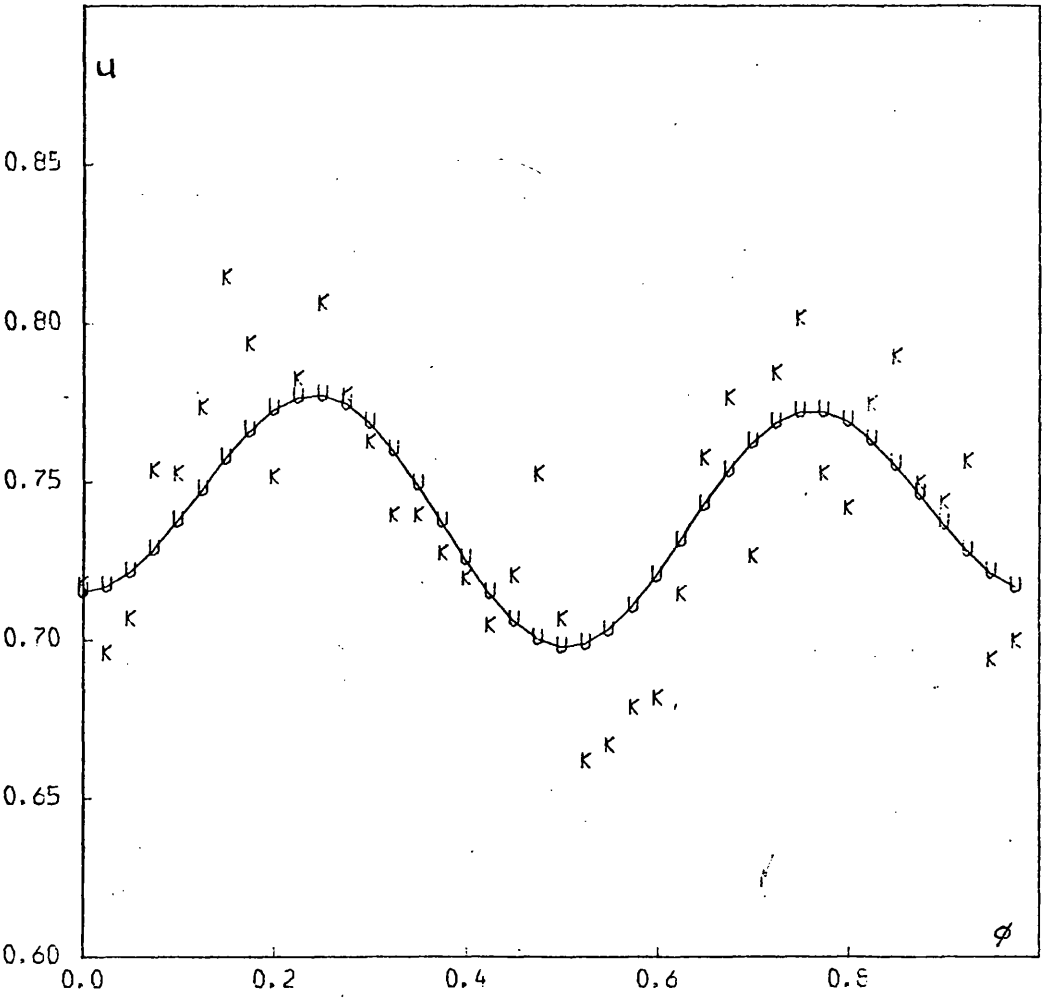

FIGURE 5.4b

U vs. phase for HD47129. (data + best fit)

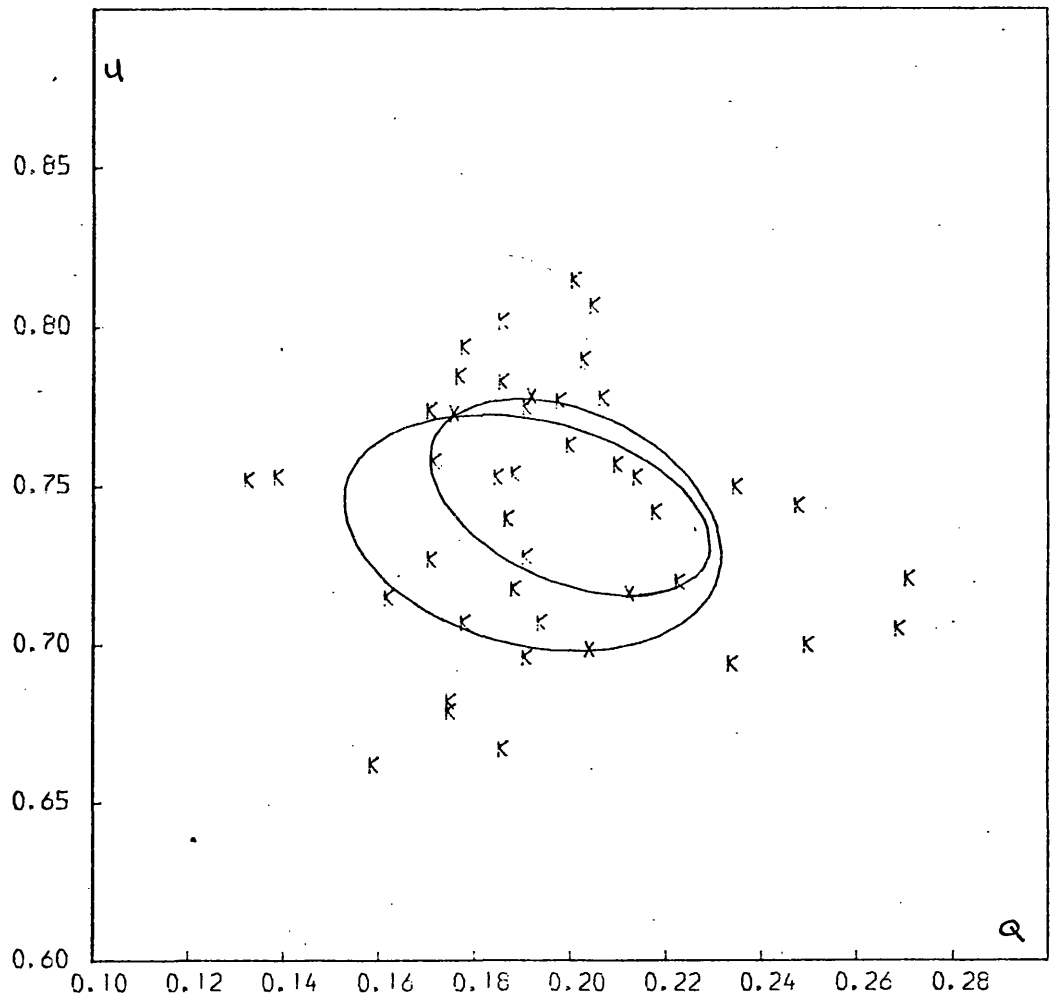

FIGURE 5.4c

Q,U locus for HD47129. (data + best fit)

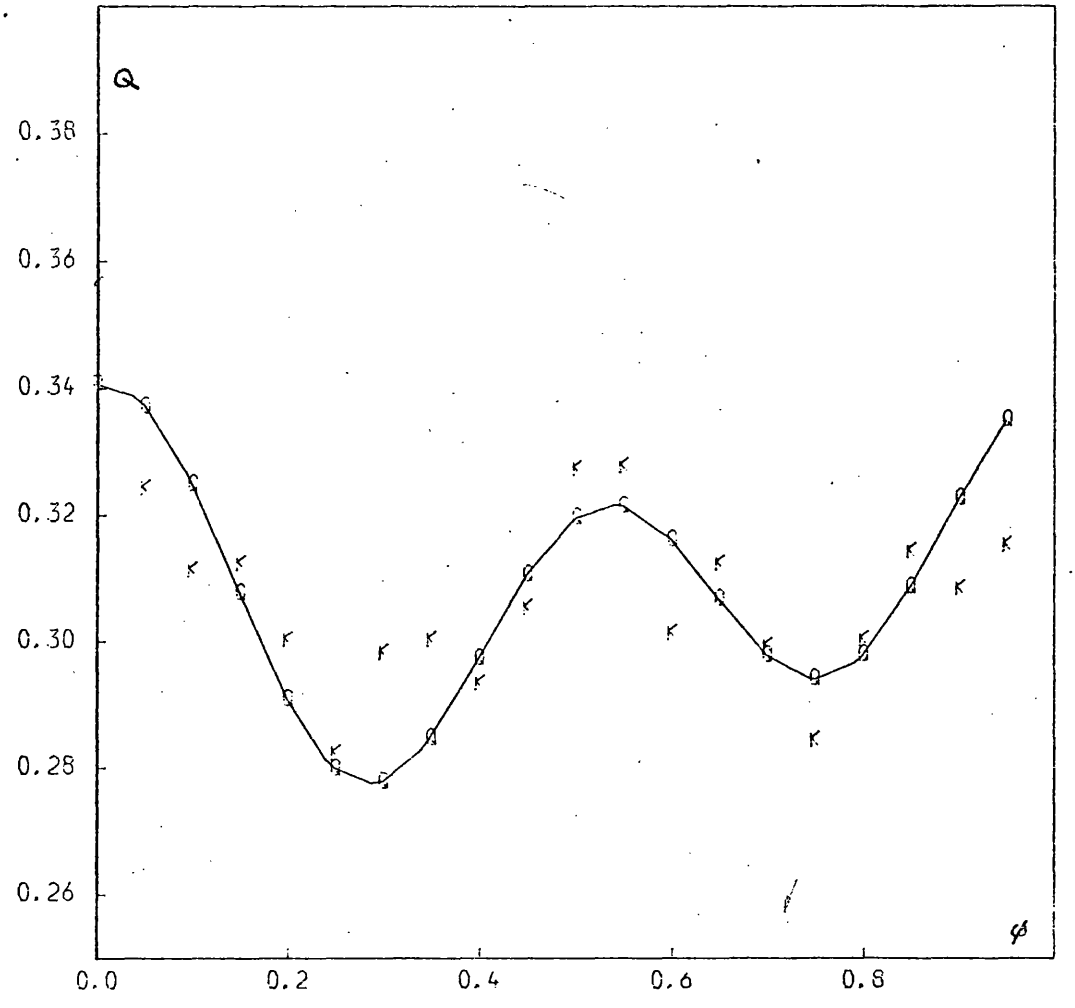

FIGURE 5.5a

Q vs. phase for σ-Ori E (B filter). (data + best fit)

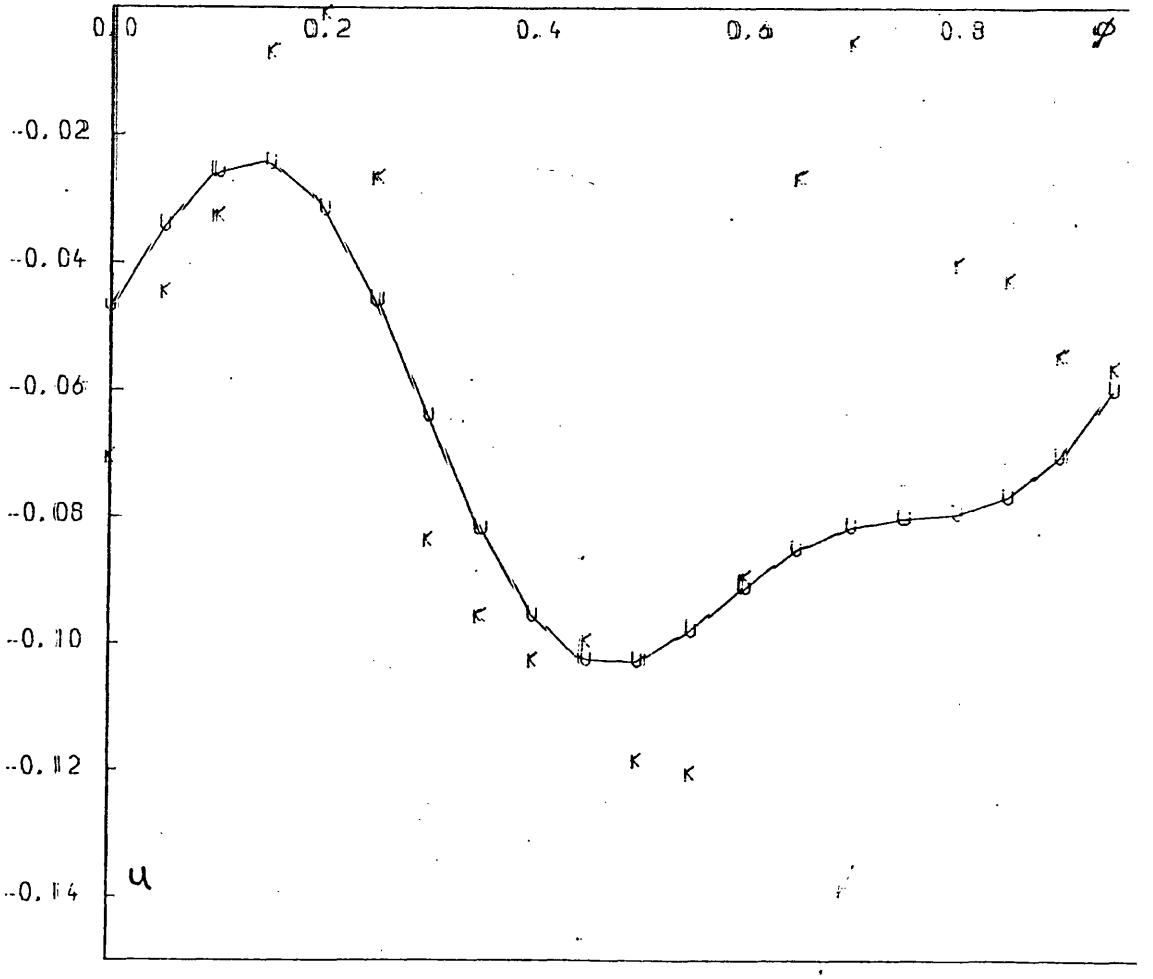

FIGURE 5.5b

U vs. phase for σOri E (B filter). (data + best fit)

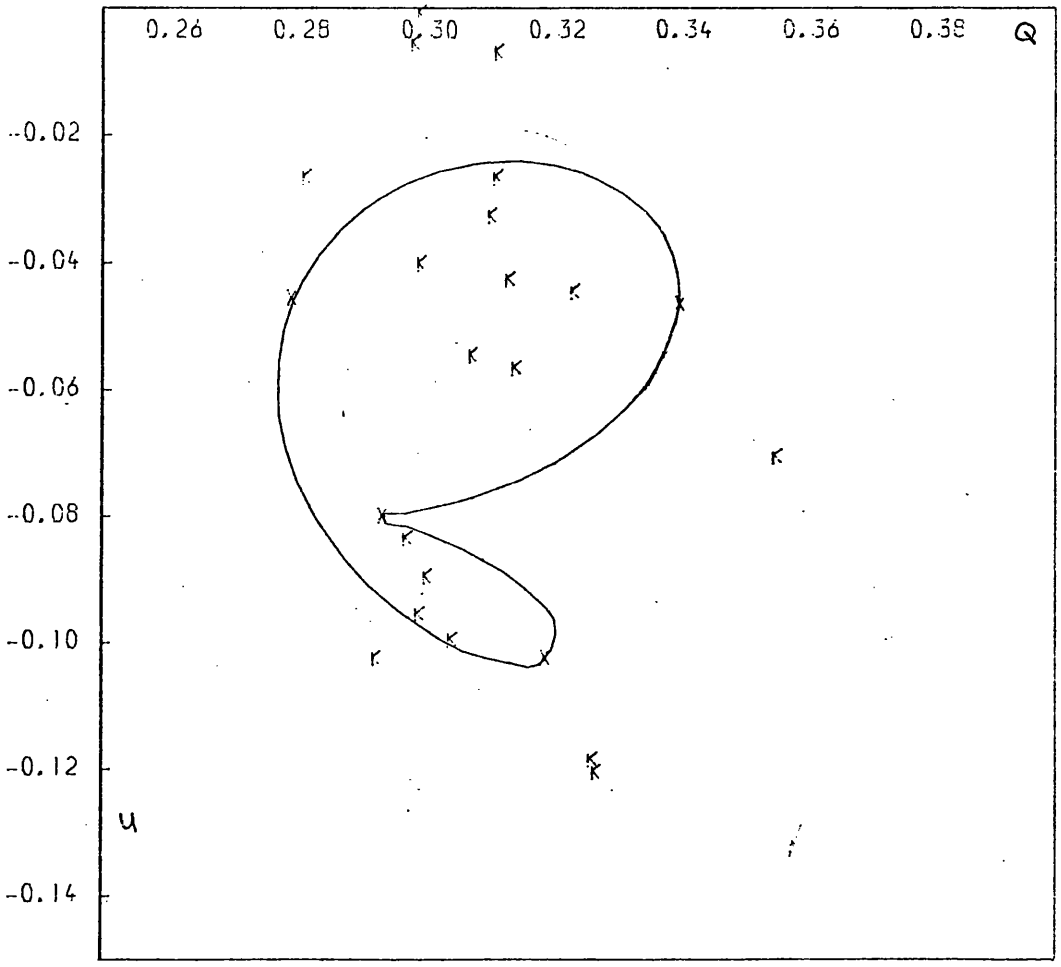

FIGURE 5.5c

Q,U locus for σ Ori E (B filter). (data + best fit)

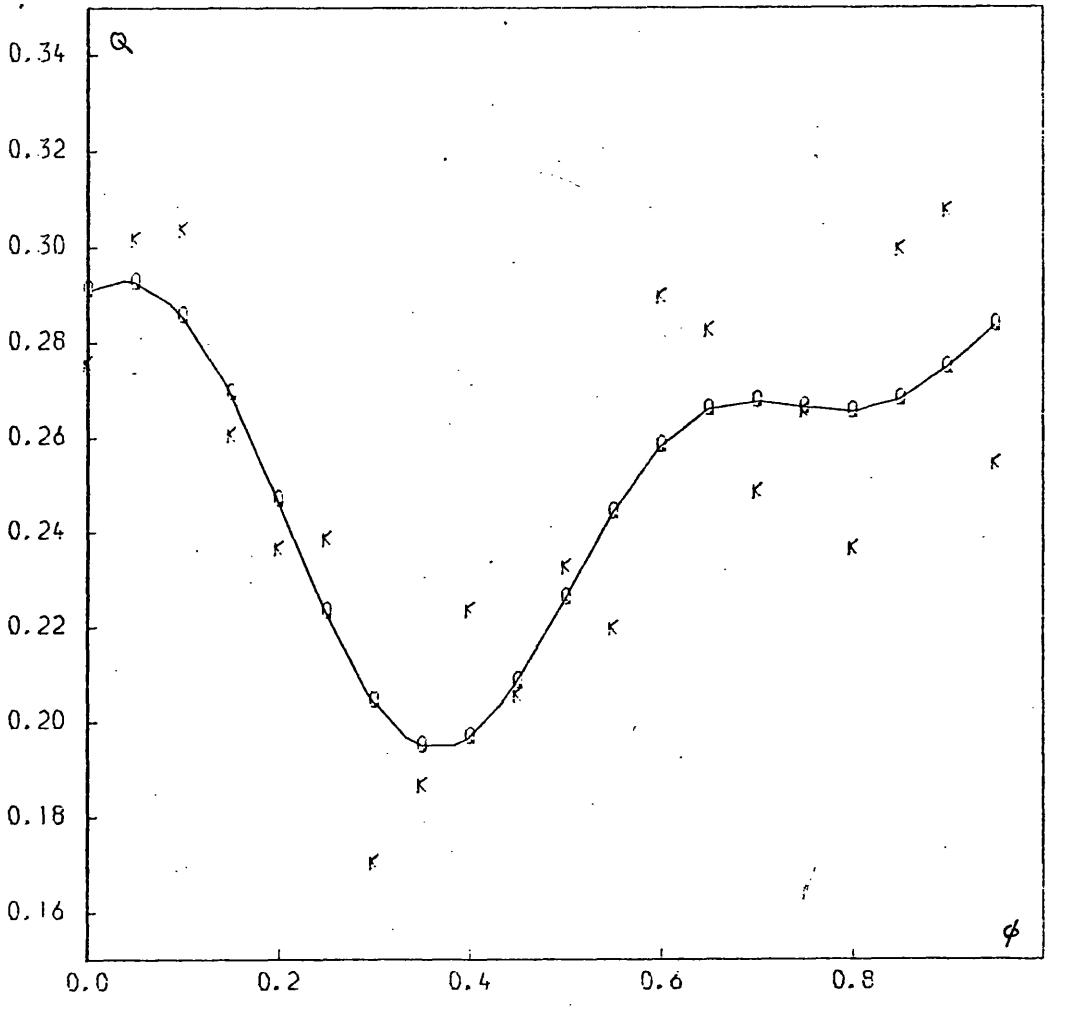

FIGURE 5.6 a

Q vs. phase for Ori E (U filter). (data + best fit)

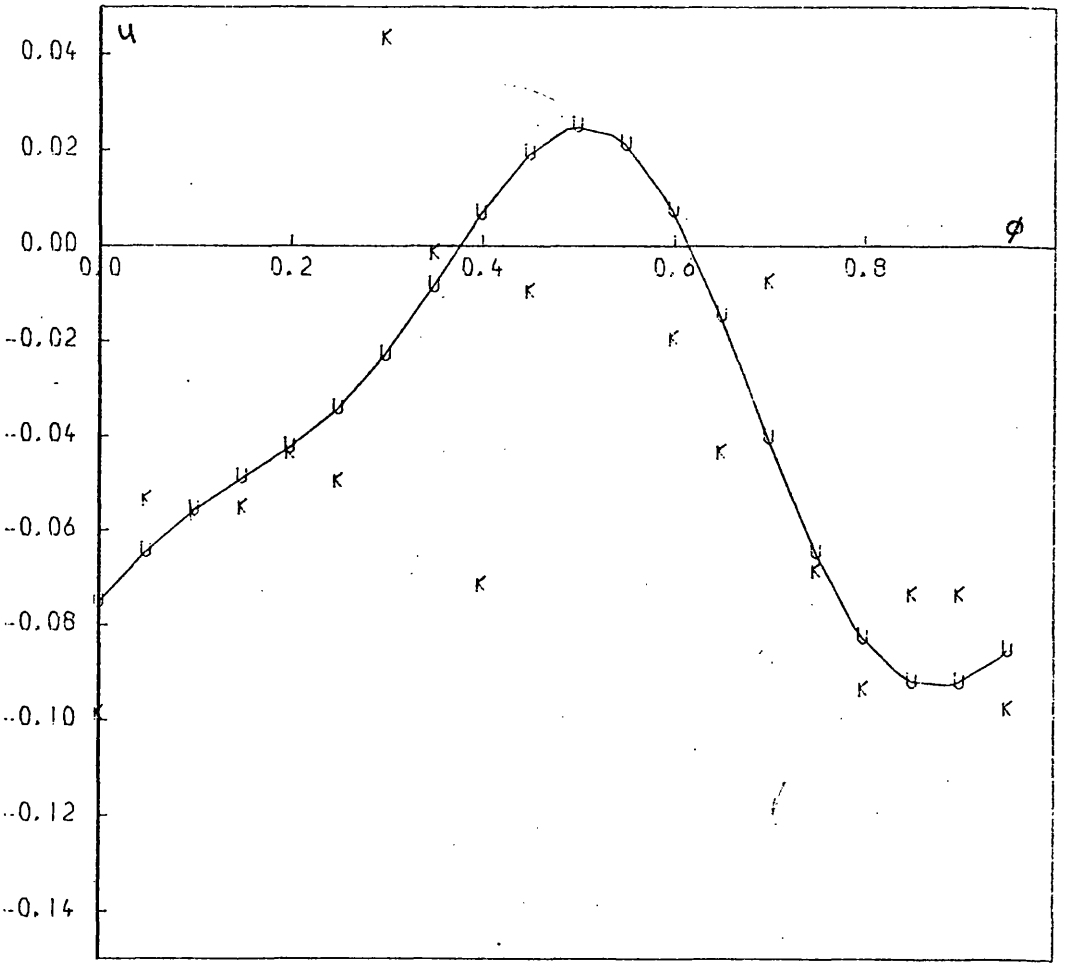

FIGURE 5.6b

U vs. phase for σ-Ori E (U filter). (data + best fit)

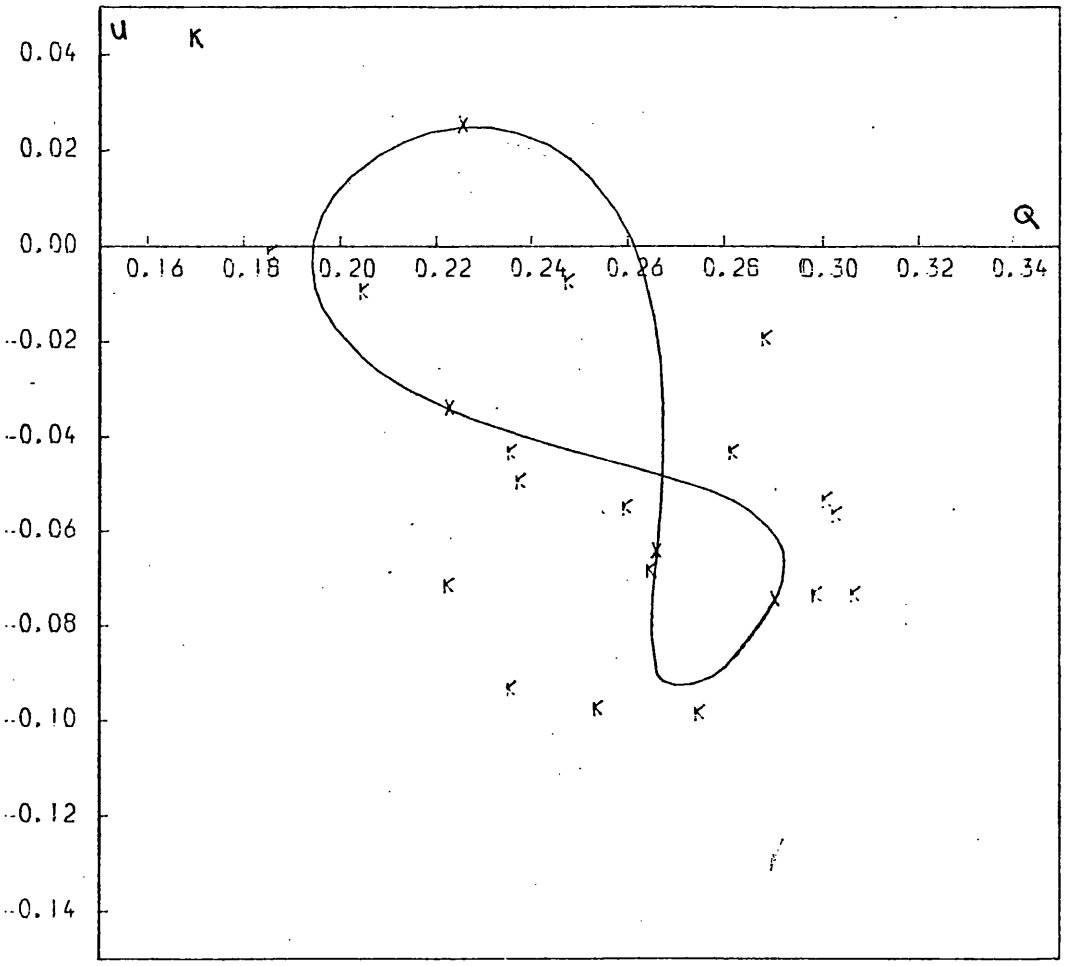

FIGURE 5.6c

Q,U locus for σ Ori E (U filter). (data + best fit).

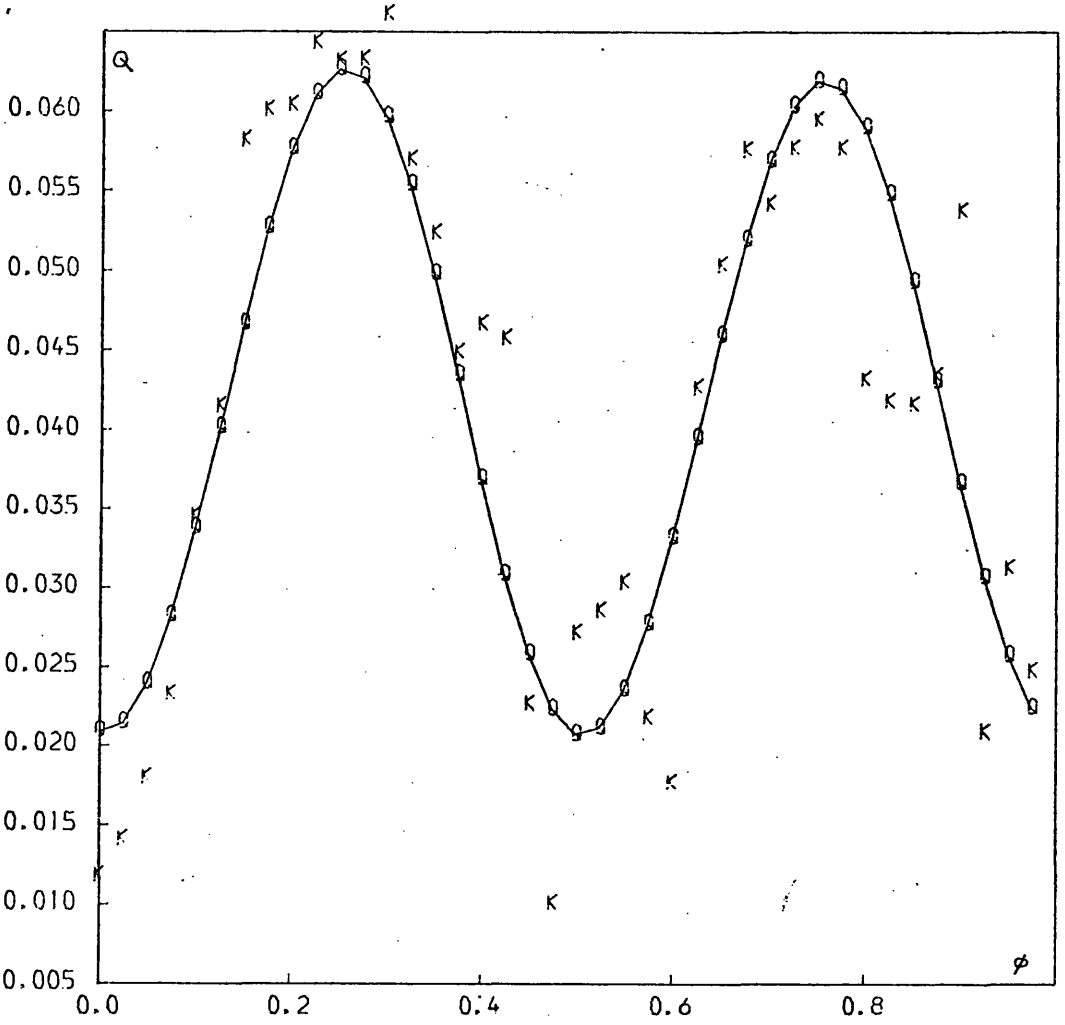

FIGURE 5.7a

Q vs. phase for u Her. (data + best fit)

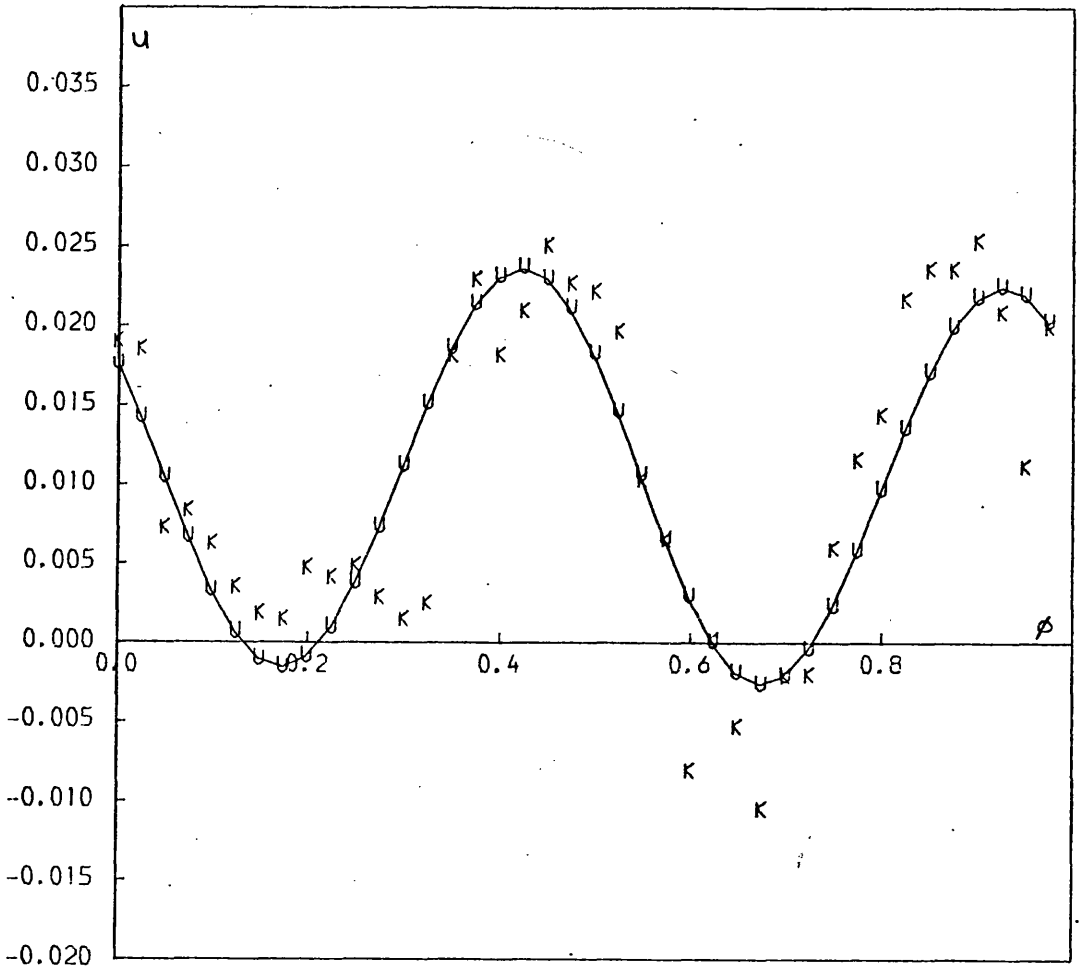

FIGURE 5.7b

U vs. phase for u Her. (data + best fit)

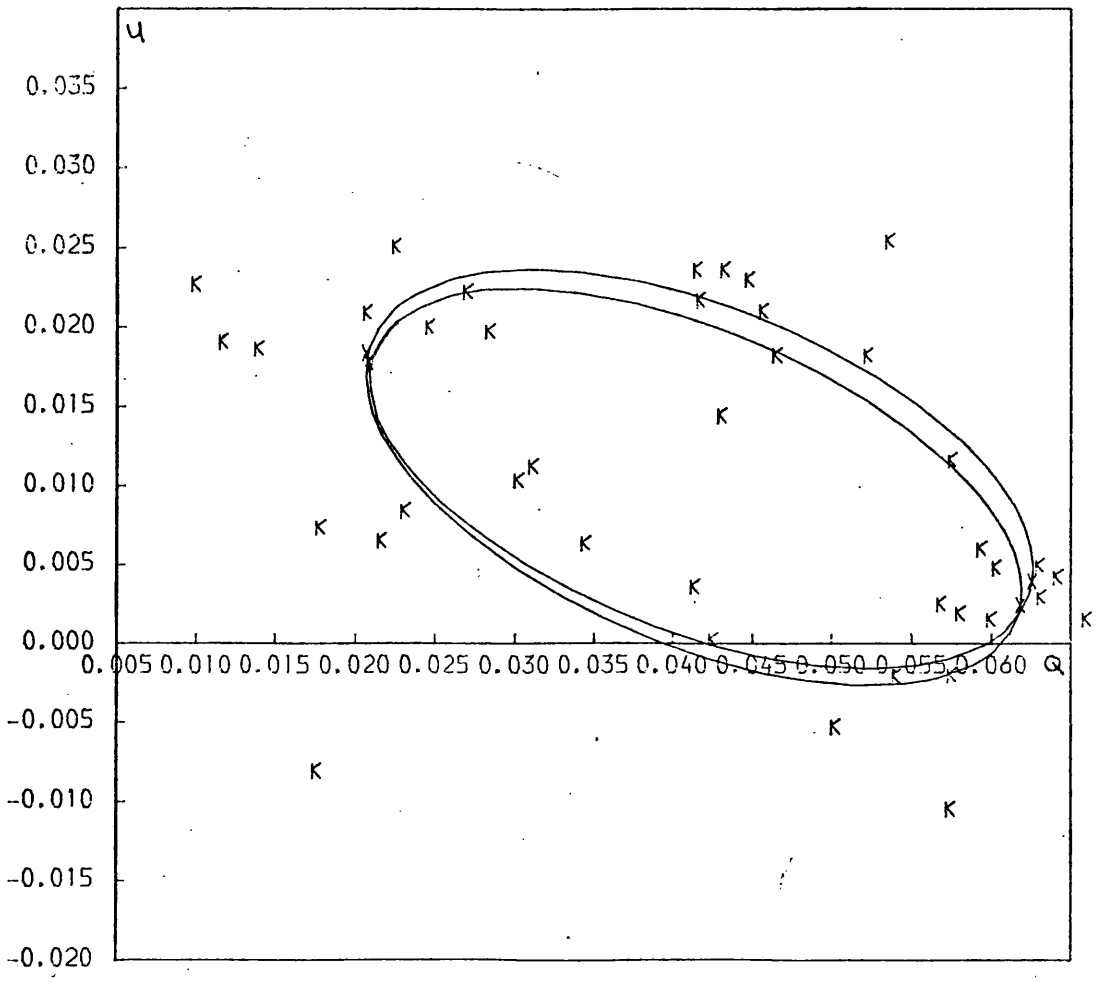

FIGURE 5.7c

Q,U locus for u Her. (data + best fit)

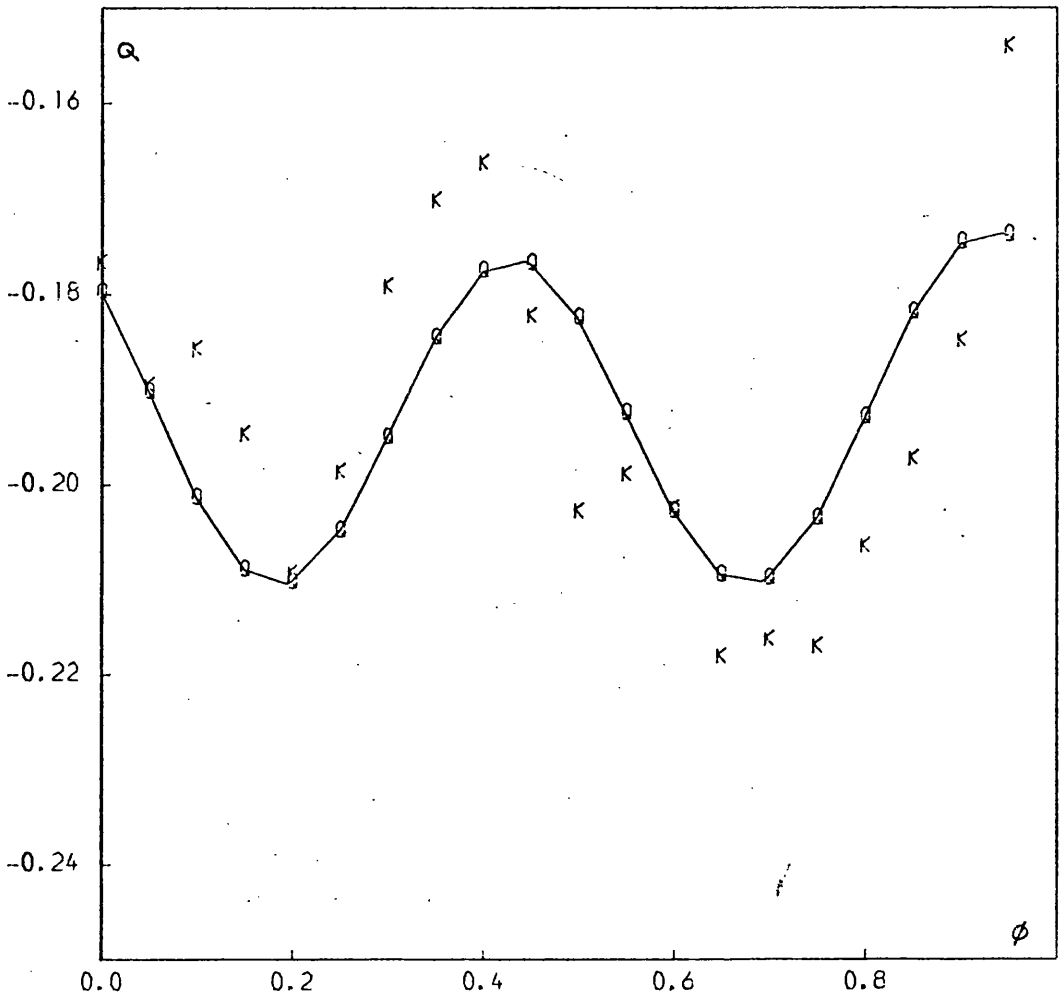

FIGURE 5.8a

Q vs. phase for U Sge. (data + best fit)

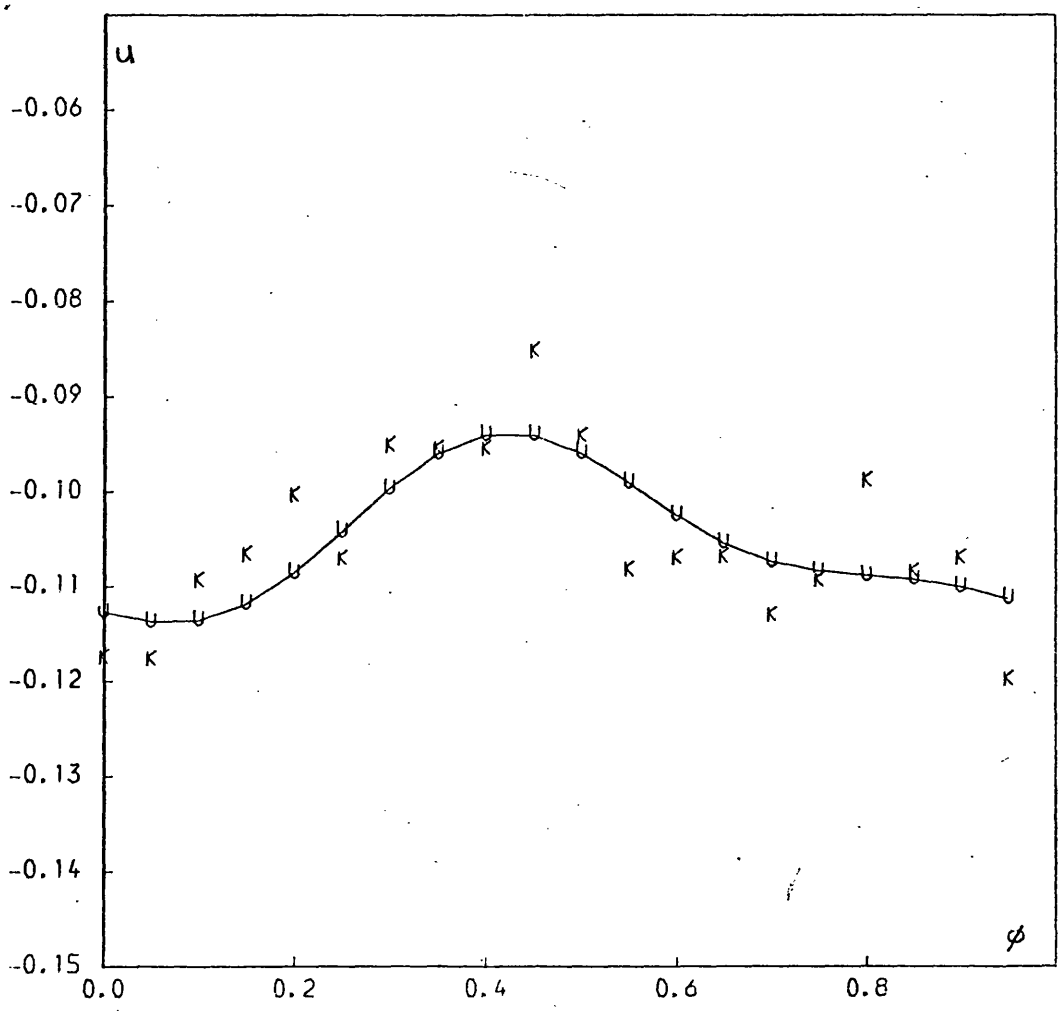

FIGURE 5.8b

U vs. phase for U Sge. (data + best fit)

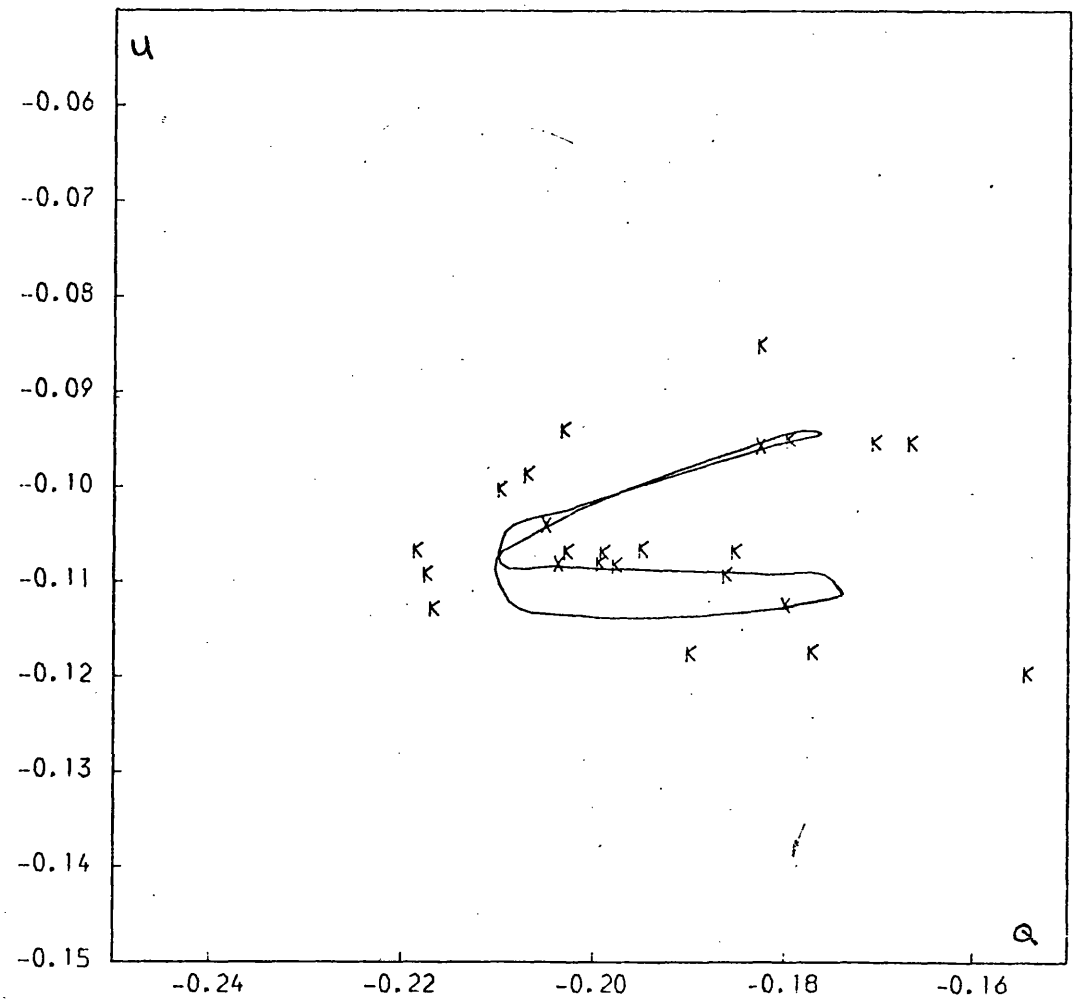

FIGURE 5.8c

Q,U locus for U Sge. (data + best fit)

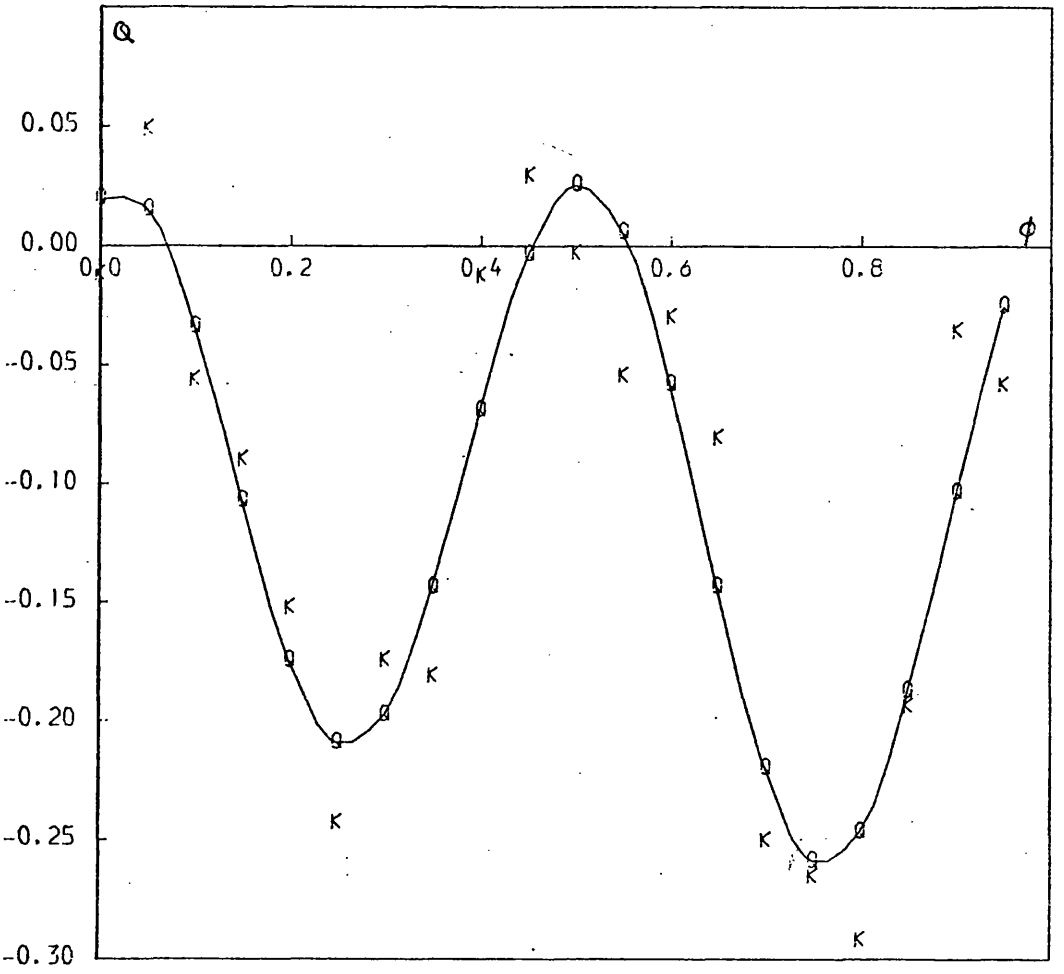

FIGURE 5.8a

Q vs. phase for V444 Cygni. (data + best fit)

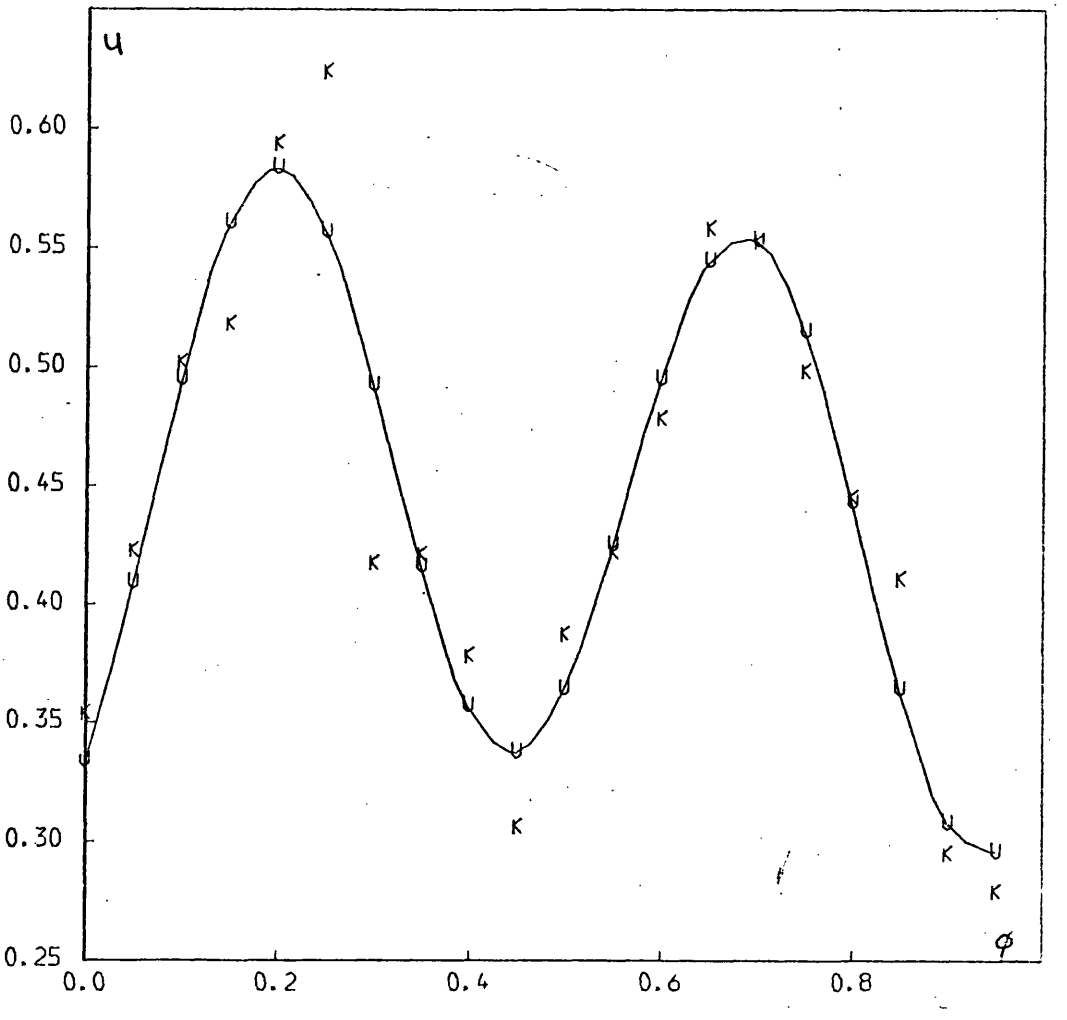

FIGURE 5.9b

U vs. phase for V444 Cygni. (data + best fit)

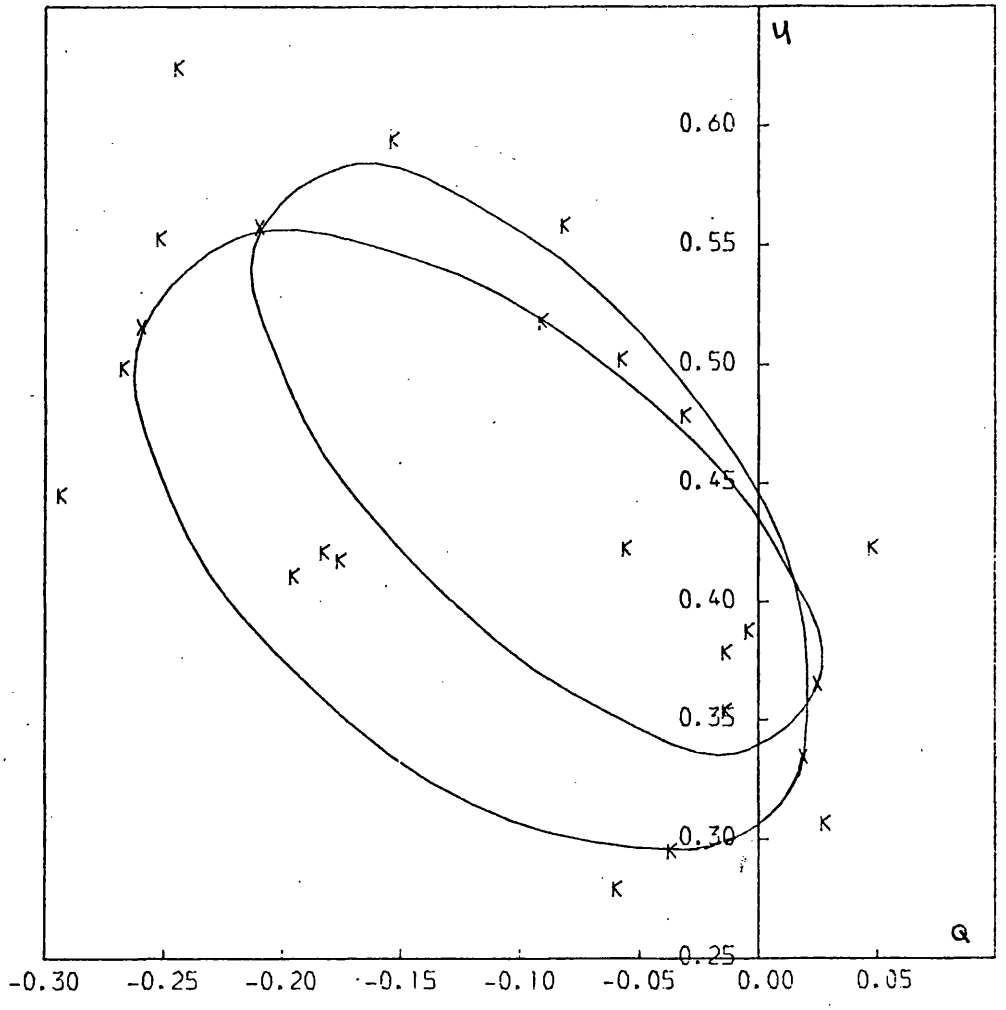

FIGURE 5.9c

Q,U locus for V444 Cygni. (data + best fit)

FIGURE 5.10 a,b and c

These diagrams show the Q vs. ϕ, U vs. ϕ and Q,U locus in both data and symmetric canonical model (i.e. 2nd. harmonics only) for the system AO Cas as an example of the fits encountered.

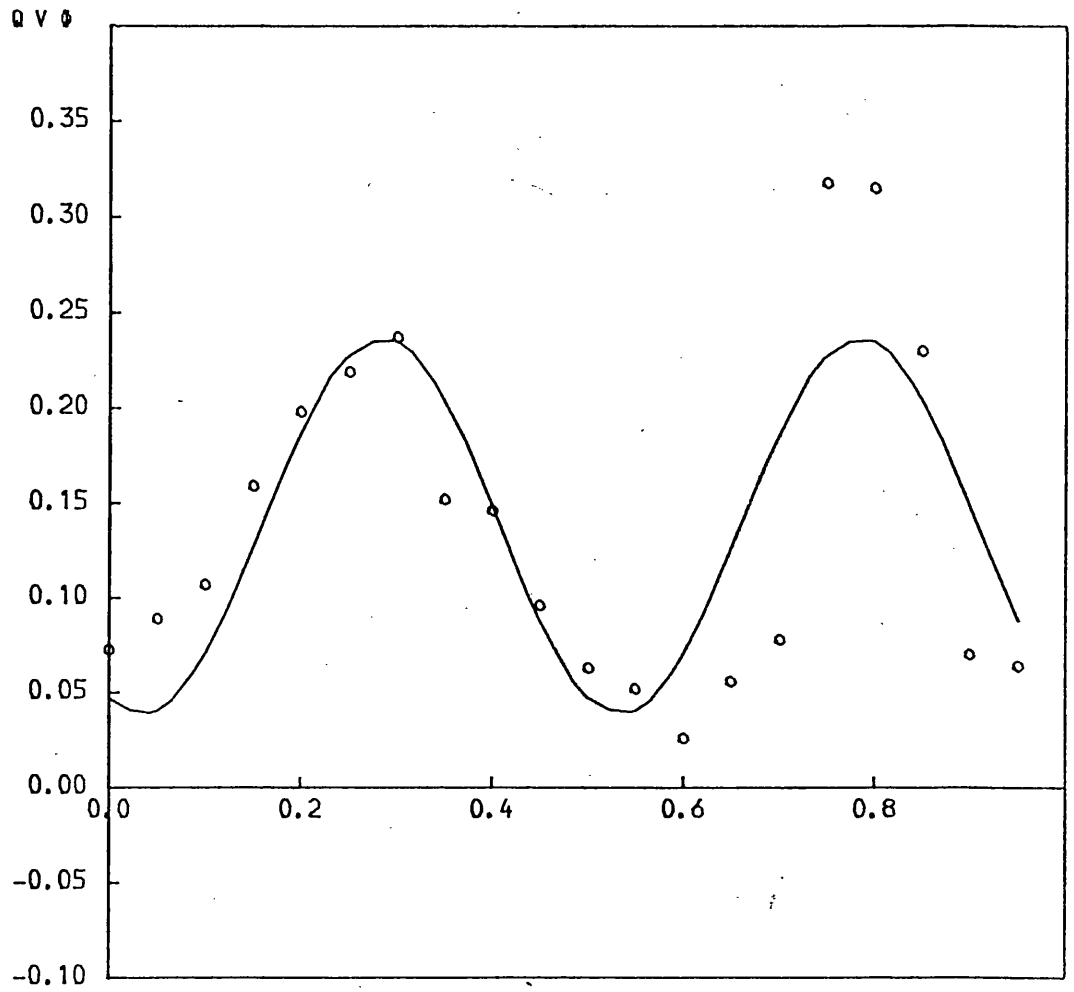

FIGURE 5.10a

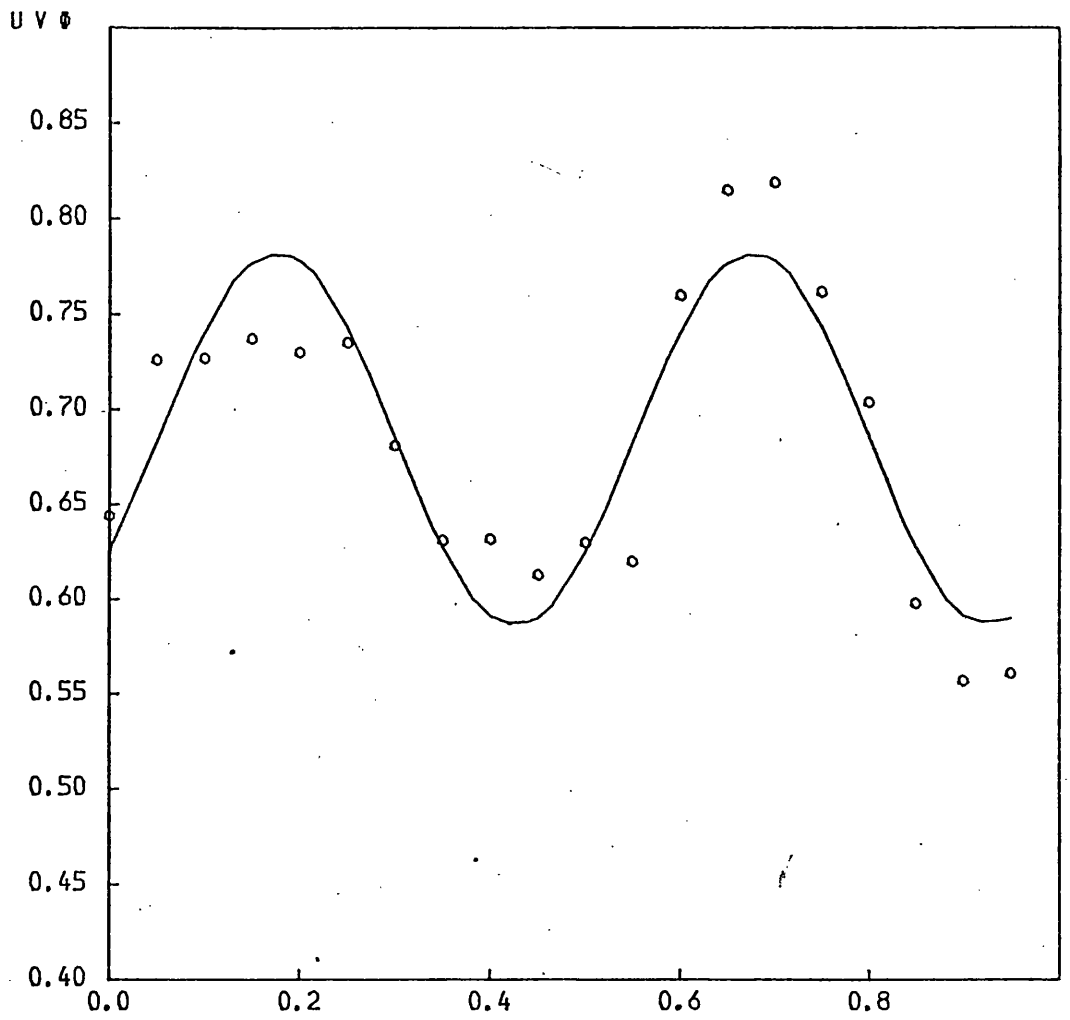

FIGURE 5.10b

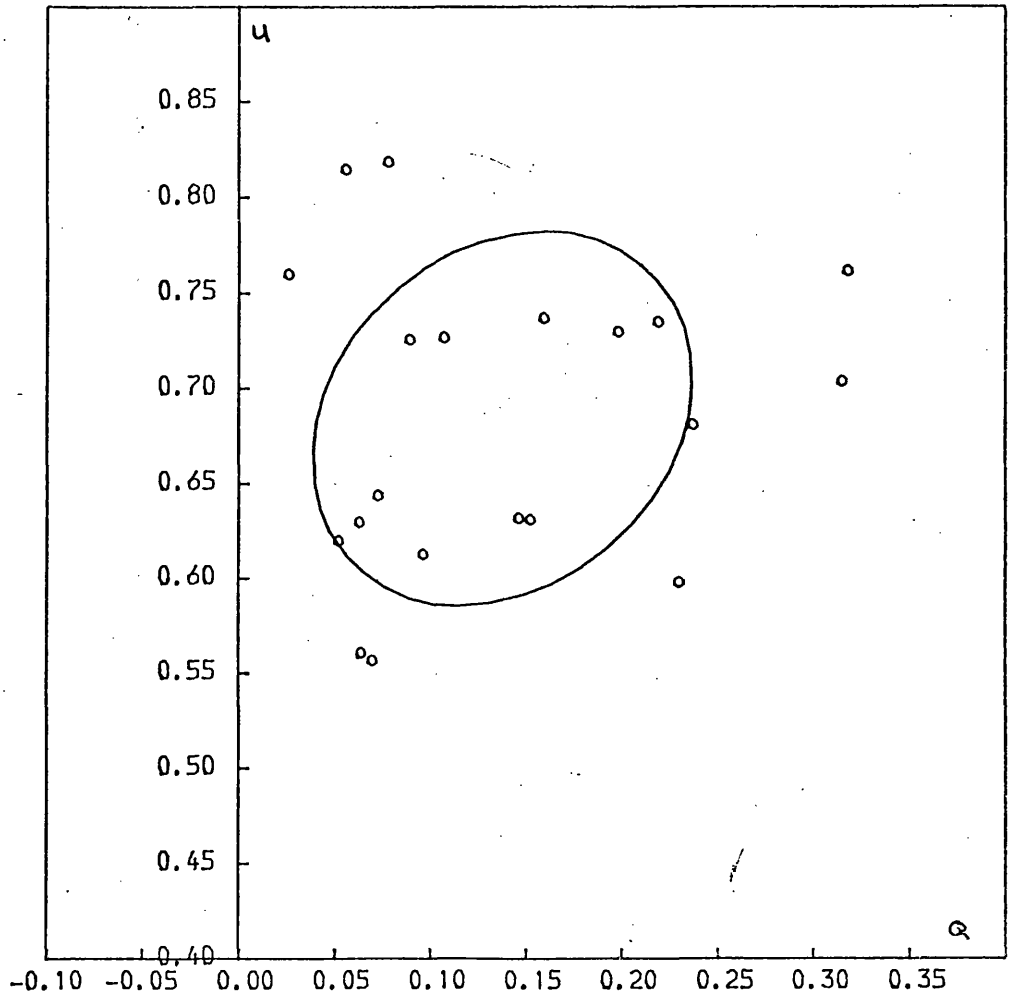
U
0.85
0.80
0.75
0.70
0.65
0.60
0.55
0.50
0.45
0.40
-0.10
-0.05
0.00
0.05
0.10
0.15
0.20
0.25
0.30
0.35
Q

FIGURE 5.10c

FIGURE 5.11 a,b,c,d,e

Shown here are the $\sigma^2\gamma^2$ vs. inclination,i curves for the binaries Algol(a),HD47129(b),σOri E(B filter)(c), σOri E(U filter)(d) and U Sge(e). Two branches are shown since two possible values of the rotation angle θ occur for each inclination value. Only one value of θ gives a minimum value of $\sigma^2\gamma^2$ however.

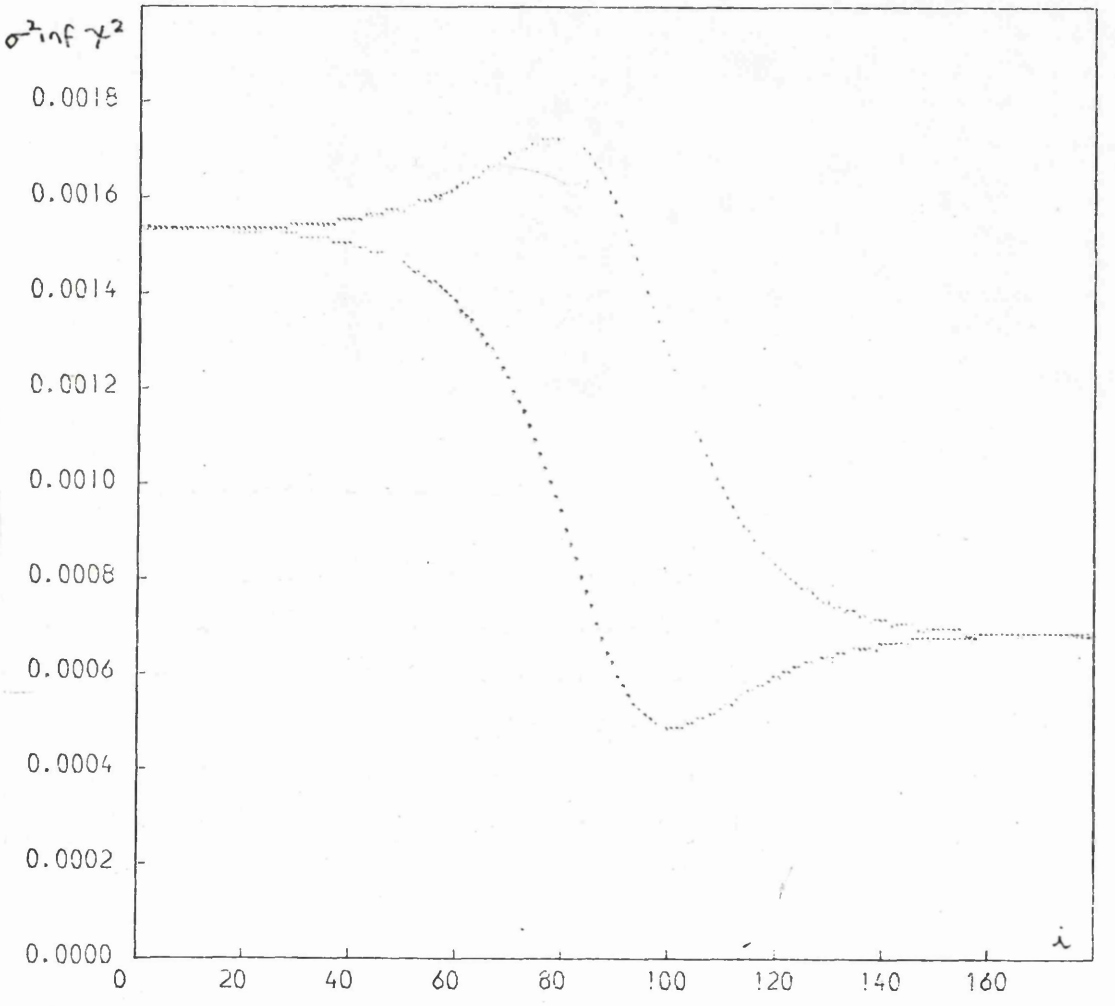
$\sigma^2_{inf}\ \chi^2$
0.0018
0.0016
0.0014
0.0012
0.0010
0.0008
0.0006
0.0004
0.0002
0.0000
0
20
40
60
80
100
120
140
160
i

FIGURE 5.11a

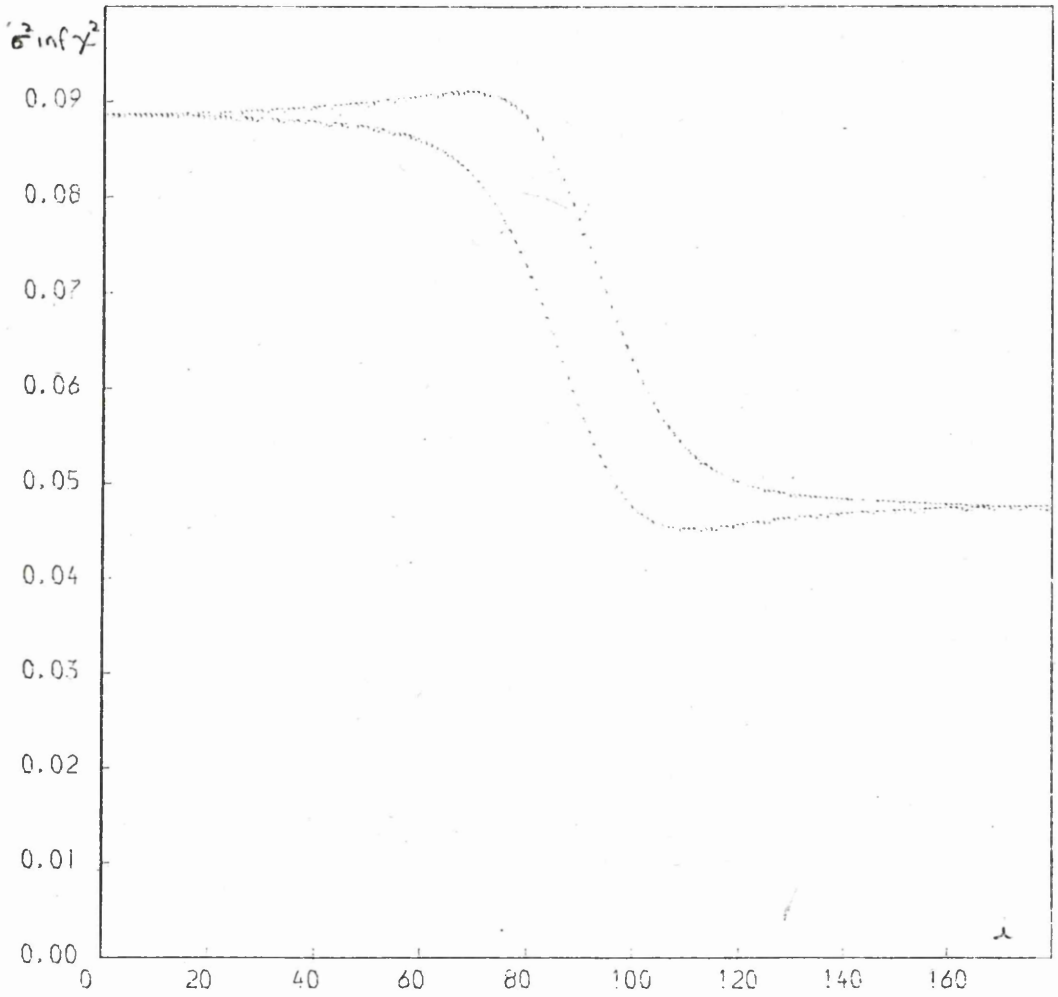
$\sigma^2 \ln \chi^2$
0.09
0.08
0.07
0.06
0.05
0.04
0.03
0.02
0.01
0.00
0
20
40
60
80
100
120
140
160
λ

FIGURE 5.11b

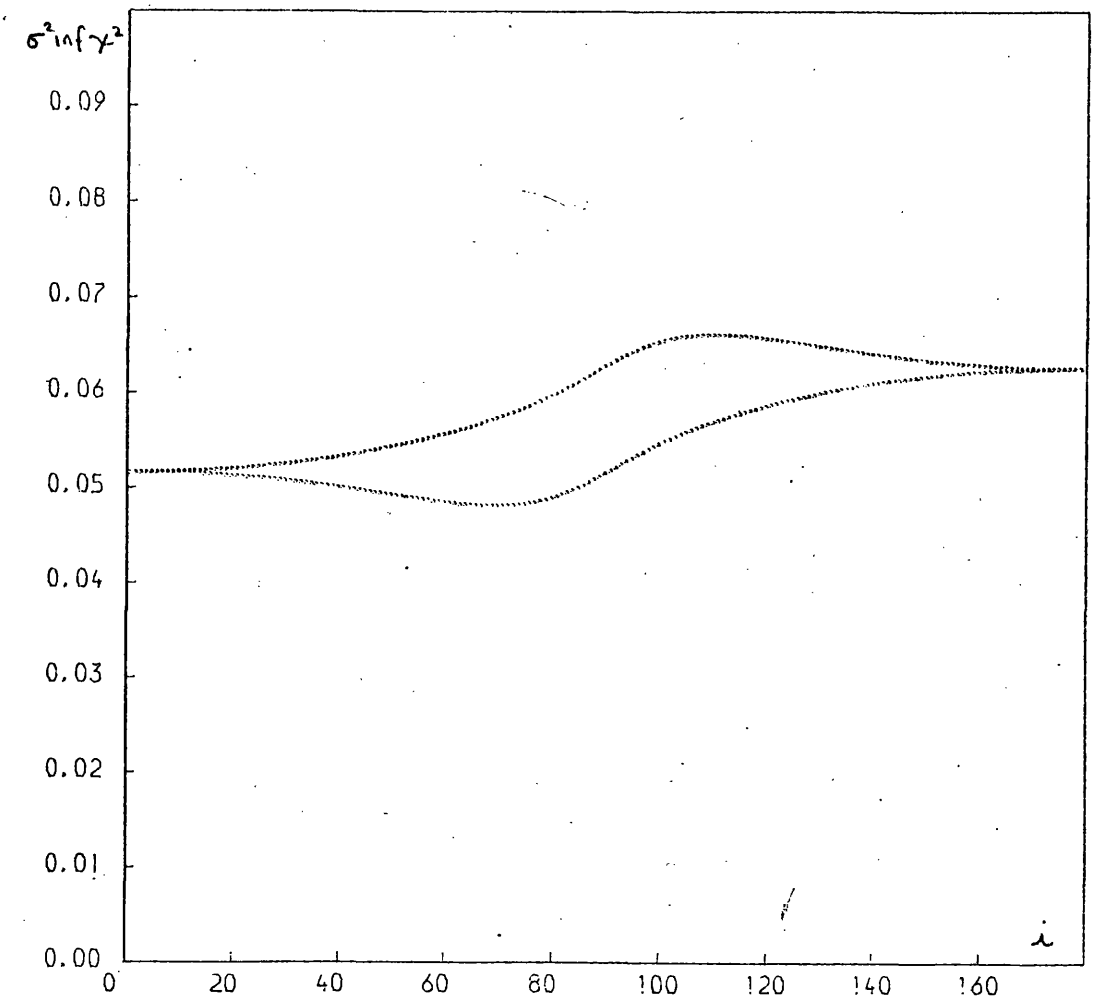
$\sigma^2 \inf \chi^2$
0.09
0.08
0.07
0.06
0.05
0.04
0.03
0.02
0.01
0.00
0
20
40
60
80
100
120
140
160
i

FIGURE 5.11c

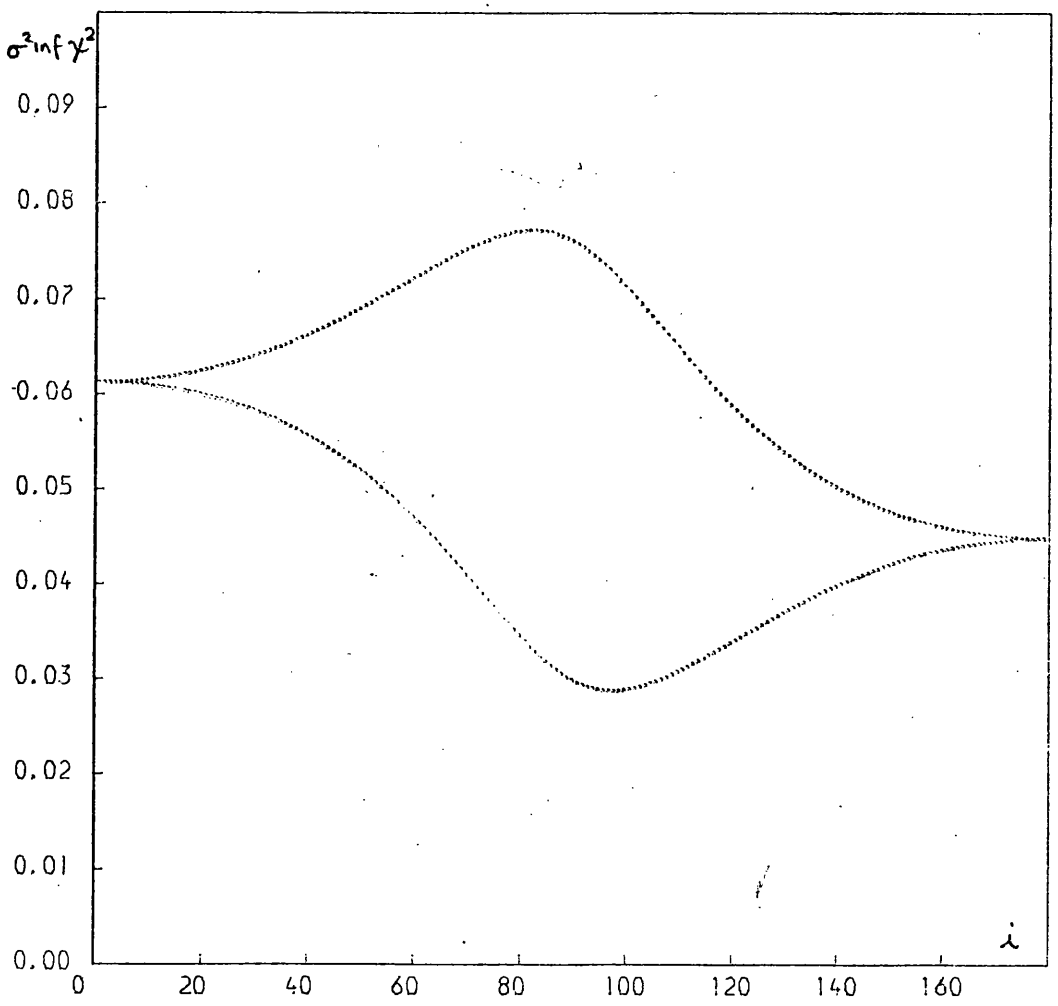
$\sigma^2 inf\, \chi^2$
0.09
0.08
0.07
0.06
0.05
0.04
0.03
0.02
0.01
0.00
0
20
40
60
80
100
120
140
160
i

FIGURE 5.11d

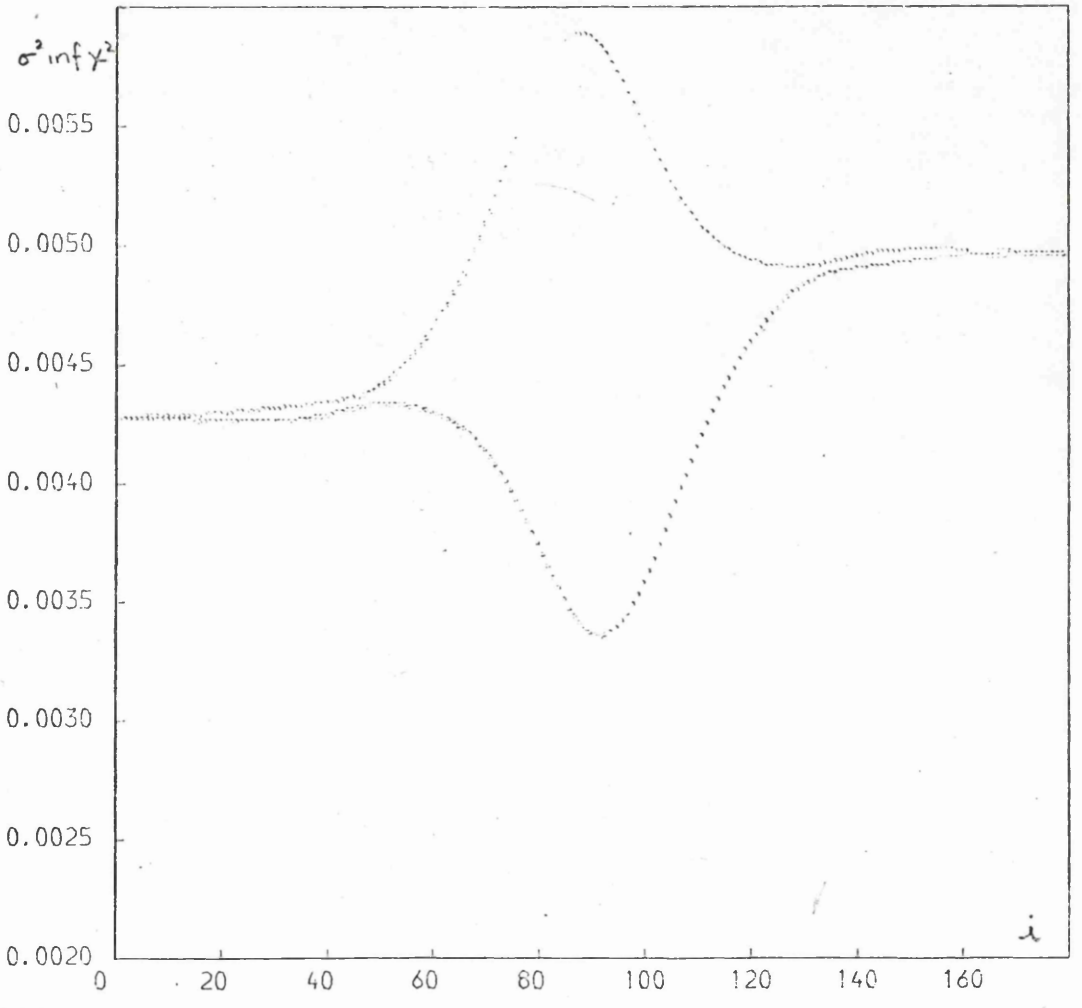
$\sigma^2 \inf \chi^2$
0.0055
0.0050
0.0045
0.0040
0.0035
0.0030
0.0025
0.0020
0
20
40
60
80
100
120
140
160
i

FIGURE 5.11e

FIGURE 5.12 a,b and c

The following three diagrams show the 'best fit' i.e. smallest $\sigma^2\gamma^2$ value, curves on the second branch of the $\sigma^2\gamma^2$ vs. i figure for ALGOL as an example of the fit encountered. The second branch usually gives a minimum $\sigma^2\gamma^2$ value at inclination $i = 0^\circ$.

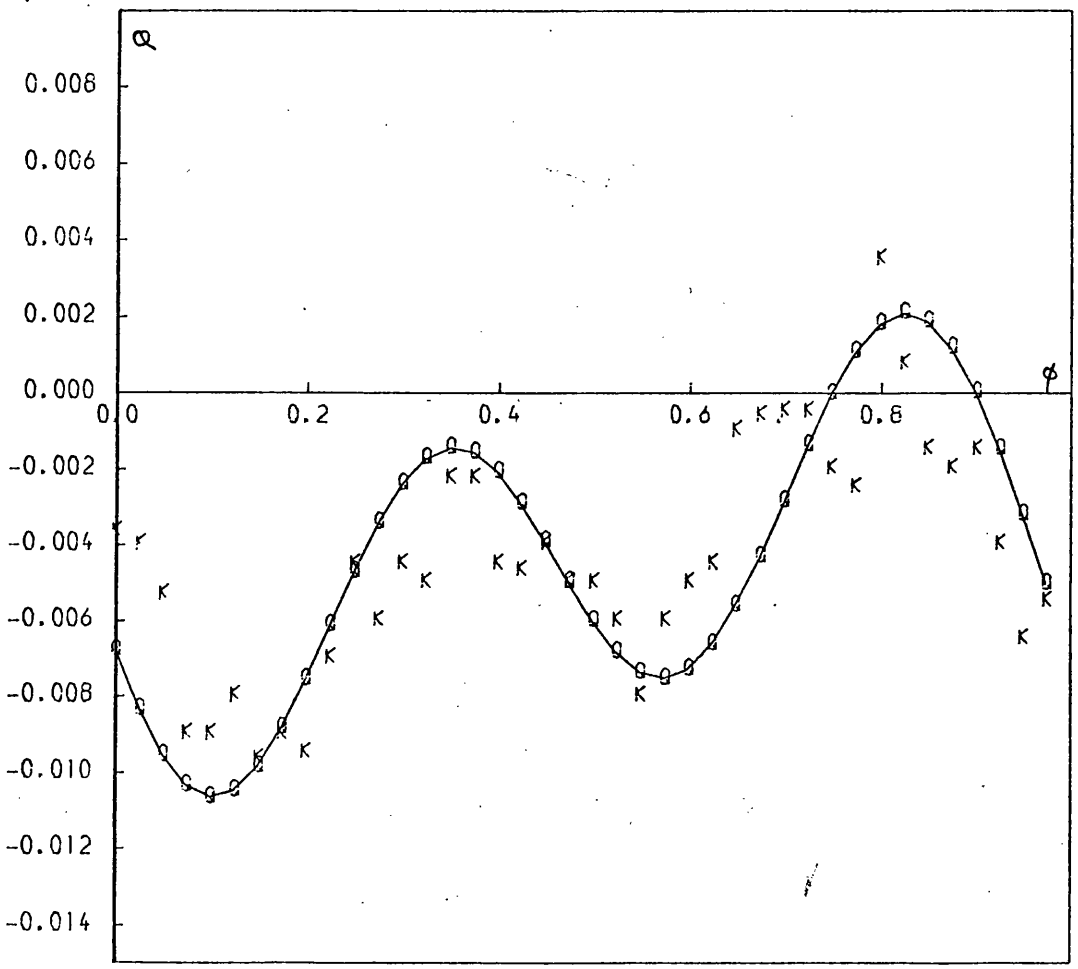
q
0.008
0.006
0.004
0.002
0.000
-0.002
-0.004
-0.006
-0.008
-0.010
-0.012
-0.014
0.0
0.2
0.4
0.6
0.8
φ

FIGURE 5.12a

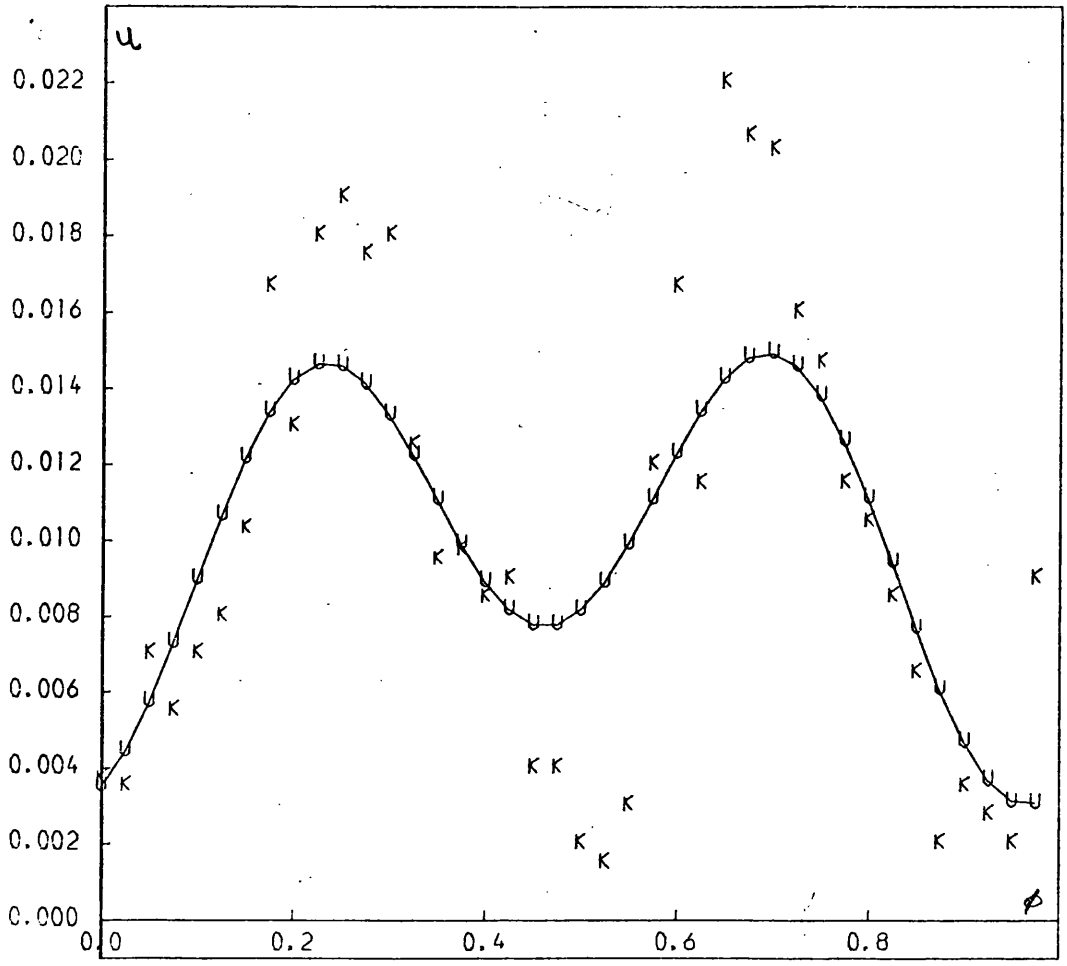
u
0.022
0.020
0.018
0.016
0.014
0.012
0.010
0.008
0.006
0.004
0.002
0.000
0.0
0.2
0.4
0.6
0.8
ϕ

FIGURE 5.12b

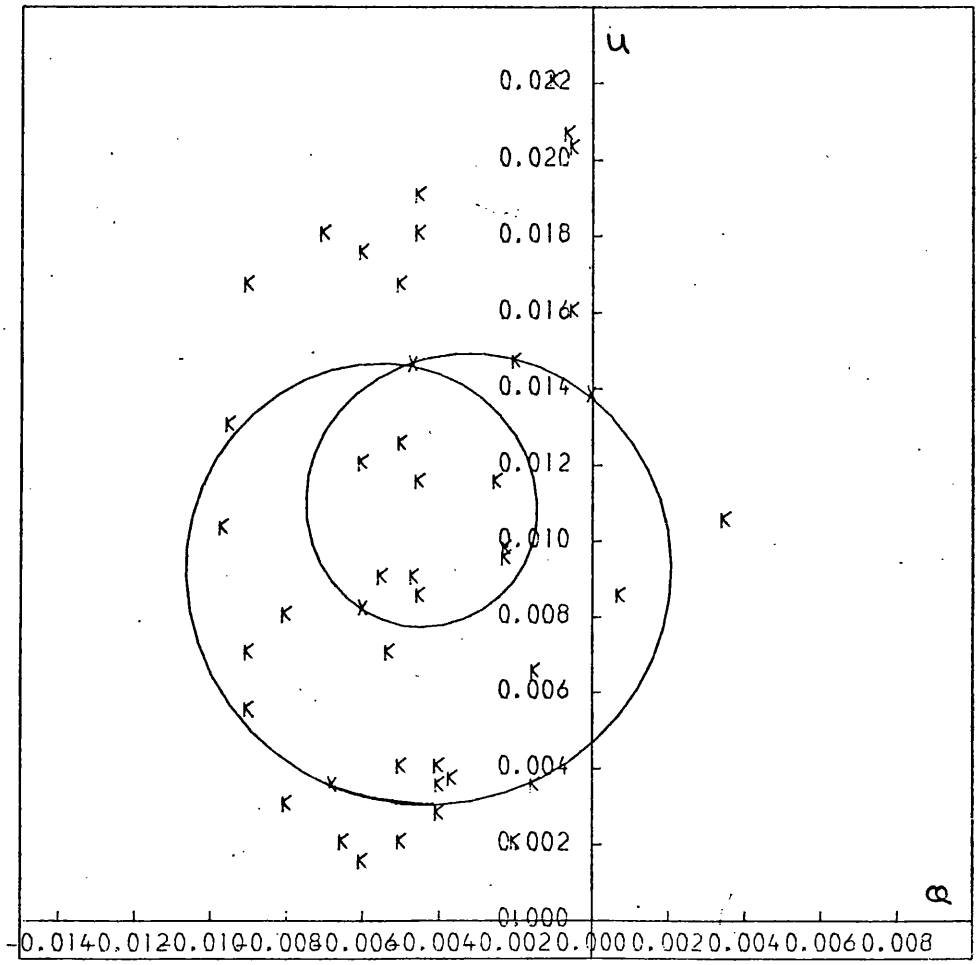
u
0.022
0.020
0.018
0.016
0.014
0.012
0.010
0.008
0.006
0.004
0.002
0.000
-0.014 -0.012 -0.010 -0.008 -0.006 -0.004 -0.002 0.000 0.002 0.004 0.006 0.008
v

FIGURE 5.12c

for these systems. In Chapter 3 (cf. Aspin et al 1981) we showed by numerically testing of the canonical model fitting procedure, how an estimate of this necessary accuracy could be made. The results depend on the amplitude of polarimetric variations, A, and the number of bins used in the observational reduction and on the true i_o. By comparing the actual observed values of A_o, N_o and σ_o with values A_e, N_e, σ_e used in the numerical calculations we can obtain the σ_{bin} necessary to obtain i to the required accuracy. We use the relation:

$$\sigma_{nec} = \sigma_o \frac{A}{A_o} \sqrt{\frac{N}{N_o}} \qquad (5\cdot8)$$

The values of A, N and σ_{nec} (for $i > 60^o$) are shown in Table III together with an improvement factor $I = \hat{\sigma}_{bin} / \sigma_{nec}$. We see that σ_{nec} is substantially smaller than σ_{bin} for all the systems and that I ranges from 4 (Algol) to 13 (U Sge). This means that, under the assumption that the data is of a form representable by the canonical model, $\hat{\sigma}_{bin}$ has to be 4 to 13 times smaller than present values (shown in Table I) to obtain accurate inclinations, if the true inclination is greater than 60^o. For inclinations $i > 10^o$ say σ_o decreases by a factor 8·7 and hence all σ_{nec} will be 8·7 times smaller to determine any inclinations greater than 10^o.

5·4 The Determination of the Physical Parameters of the scattering region - AO Cassiopeiae.

We now consider ways of determining values of certain physical parameters associated with the scattering region, from polarimetric 'best fit' model values (i.e. i, and $\underset{\sim}{p}$). We take the system AO Cas as an example of what can be determined from canonical model parameters observed in the previous section. We saw that on optimum inclinations of $i_{opt} = 61^o$ was obtained with a confidence interval of $| 0^o, 88^o |$. Even though the confidence interval on i is large, some of the other parameters - in particular the mean optical depth and hence the envelope mass - can be comparitively well determined. The model predicts that the optical depth of material distributed symmetrically about the orbital plane of the binary, τ_{sym}, is given by the relation:

STAR	A BIN	N BIN	SIGMA (INC>60°)	I
ALGOL	.0077	40	.0005	3.7
AO CAS	.138	20	.0064	5.7
HD47129	.071	40	.0046	7.1
σ ORI E(B)	.061	20	.0028	6.1
σ ORI E(U)	.077	20	.0035	9.7
U HER	.023	40	.0015	5.7
U SGE	.025	20	.0012	12.7
V444 CYG	.157	20	.0072	7.5

TABLE III

$$\tau_{sym} = (p_2^2 + q_2^2)^{\frac{1}{2}} / (1 + \cos^2 i)$$
$$= (u_2^2 + v_2^2)^{\frac{1}{2}} / (2 \cos i) \qquad (5\cdot9)$$

where (p_2, q_2, u_2, v_2) are the 'best fit' Fourier second harmonic coefficients of Q,U (i.e. coefficients of the cos 2λ, sin 2λ terms in the harmonic representation of (Q,U). i is the optimum inclination of the model fitting procedure. We note from (5·9) that even a 0^o - 180^o RCI on i introduces only a factor of 2 uncertainty in τ_{sym}. Also the optical depth of material asymmetric about the orbital plane can be estimated in:

$$\tau_{sym} = (p_1^2 + q_1^2)^{\frac{1}{2}} / (\sin 2i)$$
$$= (u_1^2 + v_1^2)^{\frac{1}{2}} / (\sin i) \qquad (5\cdot10)$$

At $i = 0^o$ all asymmetry about the orbital plane disappears from the data since the orbit is in the plane of the sky and hence (5·10) becomes meaningless sin $i \to 0$ and $u_1^2 + v_1^2 = 0$. In the case of AO Cas the best fit 1st harmonic coefficients (p_1, q_1, u_1, v_1) are small and in fact the 1st harmonic amplitude is < 10% of the dominant 2nd harmonic amplitude. We therefore consider the symmetric optical depth from now on as adequate for AO Cas. Physically, also AO Cas is thought to contain a gas stream (Batten 1973) which should be approximately symmetric about the orbital plane making considering of the asymmetric optical depths unnecessary. This model with zero asymmetry is also consistent with the high noise level of data (as seen by larger confidence interval on i).

At i_{opt} therefore:

$$p_2 = -0\cdot1058\%$$
$$q_2 = 0\cdot0303\% \qquad (5\cdot11)$$

giving a $\tau_{sym} = 8\cdot8.10^{-4}$ (converted from %). Taking the orbital period as P = 3·52 days (Wood 1947) and the masses M_1 and M_2 of the two giant O stars of 18 $M_\odot$ and 22 $M_\odot$ respectively (Hutchings and Hill 1971) the semimajor axis of the orbit, a (the stellar separation) is found by use of Keplers 3rd law namely:

$$p^2 = \frac{4\pi^2 a^3}{G(m_1 + m_2)} \qquad (5\cdot12)$$

This quantity, a, turns out to be $\sim$ 0.15 A.U. or 33 $R_\odot$. If we assume the gas stream has a 'typical length' of a/2 (i.e. surface to surface) and a typical dimension of $\sim R_1$ the radius of the primary star, which from Hutchings and Hill (1971) is estimated as $R_1 \sim 11\ R_\odot$ then by inverting the relation

$$\tau = \frac{3}{32}\ \sigma_T\ \frac{N}{R^2} \qquad (5.13)$$

where σ_T is the Thomson scattering cross-section, N is the number of scatterers and R is the typical path length of a photon. This relation is derived from the definition of optical depth i.e.

$$\tau = \int_o^L \sigma_T\ \frac{n}{R^3}\ d\ell\ .$$

We take $\sigma_T = 0{\cdot}665\ 10^{-26}\ cm^2$; $R = R_1$ the radius of the primary, and $\tau = \tau_{sym} = 8{\cdot}8\ 10^{-4}$. This gives an $N = 2{\cdot}4\ 10^{47}$ electrons. To find the electron density in the scattering region we divide this figure by the volume of the envelope (gas stream). We take the volume:

$$V = \frac{a}{2}\ \times \pi\ (\frac{R_1}{2})^2 \qquad (5.14)$$

i.e. a cylinder between the stars of radius $R_1/2$ and length $\frac{a}{2}$. This gives an electron density in this region of $n_e = 4{\cdot}5\ 10^{12}\ cm^{-3}$.

We can also estimate the timescale of mass transfer between the two stars and hence the mass transfer rate $\dot{M}$. Following Paczyński (1968) we take the time for material to transfer from one star to the other as the dynamical timescale (i.e. the free fall time between the stars). This timescale is derived as follows. We equate the kinetic energy of a particle of mass m to the potential energy due to the fall out the secondary body, i.e.

$$\tfrac{1}{2}\ mv^2 = +\frac{GMm}{r} \qquad (5.15)$$

where G is the gravitational constant and m is the mass of the secondary. This can be written

$$(\frac{dr}{dt})^2\ r = +\ 2\ Gm \qquad (5.16)$$

or

$$\frac{dr}{dt}\, r^{\frac{1}{2}} = (2\,Gm)^{\frac{1}{2}} \qquad (5.17)$$

and

$$dr\, r^{\frac{1}{2}} = (2\,Gm)^{\frac{1}{2}}\, dt \qquad (5.18)$$

integrating we obtain:

$$\frac{2}{3}\, r^{3}{}_{2} = (2\,Gm)^{\frac{1}{2}}\, t + c \qquad (5.19)$$

when $t = 0, r = a$ the separation of the stars therefore

$$\frac{2}{3}\, r^{3}{}_{2} = (2\,Gm)^{\frac{1}{2}}\, t + \frac{2}{3}\,(a)^{3}{}_{2} \qquad (5.20)$$

we want the time when r, the distinct from the secondary is zero hence

$$t = \frac{2}{3}\,\frac{(a^{3}{}_{2})}{(2\,Gm)^{\frac{1}{2}}} \qquad (5.21)$$

$$= \frac{2}{3}\,\left(\frac{a^{3}}{Gm}\right)^{\frac{1}{2}}\,\frac{1}{\sqrt{2}} \qquad (5.22)$$

and by Keplers 3rd Law: $2\pi\,\left(\frac{a^{3}}{Gm}\right)^{\frac{1}{2}} = P$, the binary period. Therefore:

$$t = \frac{\sqrt{2}}{3}\,\frac{P}{2\pi} \qquad (5.23)$$

and therefore the dynamical timescale t is defined as

$$t = \frac{P}{3\sqrt{2}} = 7.5 \times 10^{-2} \times P. \qquad (5.24)$$

For AO Cas, P = 3·52 days and therefore t = 6·3 hours. Thus $m = N\, m_p/t = 2.73\ 10^{-7}\ m_\odot/yr.$ where m_p is the mass of the proton.

We therefore have calculated approximate values of N, n_e and M which are:

$$N = 2.4\ 10^{47} \text{ electrons}$$
$$n_e = 4.5\ 10^{12}\ cm^{-3} \qquad (5.25)$$
and $$M = 2.73\ 10^{-7}\ M_\odot\ yr^{-1}.$$

for AO Cas, from polarimetric 'best fit' quantities. We can compare these to estimates of these parameters for other systems namely:

$n_e \sim 10^{10}$ cm^{-3} (TT Hya - Peters 1980)

$n_e \sim 10^{11}$ cm^{-3} (β Lyrae - Dadaev 1954)

$n_e \sim 10^{11}$ cm^{-3} (WZ Sge - Gobatskii 1967)

$n_e \sim 10^{12}$ cm^{-3} (RZ Sct - Hansen and McNamara 1959)

Also we have

$\dot{M} \gtrsim 10^{-7}\ M_\odot\ yr^{-1}$ (β Per - Söderhjelm 1980)

$\dot{M} \sim 10^{-6}\ M_\odot\ yr^{-1}$ (U Cep - Olsen 1980)

$\dot{M} \sim 2{\cdot}5 \times 10^{-8}\ M_\odot\ yr^{-1}$ (TT Hya - Peters 1980)

which are seen to be in the same general region as our estimates of n_e and $\dot{M}$. Thomas (1977) also indicates that $\dot{M} \sim 10^{-7}\ M_\odot\ yr^{-1}$ is a reasonable estimate for close binaries. Traditional methods of estimating n_e have relied on the accuracy of the Inglis-Teller method (Inglis and Teller 1939). This involves the relation:

$$\log n_e = 23{\cdot}26 - 7{\cdot}5 \log n \qquad (5.26)$$

where n is the quantum number of the last Balmer line visible in the binary spectra. This formula relates the charge density in an extended atmosphere/envelope to the quantum (no. of the last visible Balmer line: the series being terminated by the overwhelming effect of Stark Broadening on the lines. (cf. Lang (1974)). If we take our polarimetric estimate of n_e and invert (5.26) we see that n = 26. This value is significantly less than that obtained from Kraft's (1958) spectroscopic observations of U Cr B on which Batten (1973) quotes $n \sim 53$. Also Struve et al (1957) quote a visible Balmer line to $n \sim 24$ indicating an n_e of $\sim 8 \times 10^{12}$ cm^{-3}. (Batten 1973). Therefore we predict that n = 26 Balmer series line should be visible in the spectra of AO Cas (with Hα, n = 1 then; n = 26 is = 3664·7Å with the Balmer limit, n = ∞ being λ_∞ = 3646·0 Å) if one assumes one value of n_e reasonable.

The values of N, n_e and M are however affected by factors assumed in the model (including the geometry) tending to change the observed polarization from the polarization from the total number of scatterers

present in the binary. For example a real system has extended light sources and not point sources as in the canonical model. This will tend to change the amount of polarization observed (decrease it) according to Milgram (1979) and cause an underestimate of N. Similarly, not all the electrons will be contributing to the observed polarization (eg. if absorption occurs on the envelope is near spherical) and hence N will be a lower limit only. Nevertheless it remains that polarimetry, in the presence of good data (i.e. small errors) can give a useful estimate of the above 3 parameters.

We also investigate the dependence of these on inclination, (i.e. we look at the best fit model parameters at each inclination ($i = 0^o$ to 180^o) and calculate N, n_e and $\dot{M}$). The results of this are shown in Table IV. As i increases from $i = 0^o$, the values of τ_{sym}, n_e and $\dot{M}$ increase to a maximum at $i \sim 105^o$ (the exact maximum was unknown since we increase i in steps of 15^o) and then decrease again to a level high than in the $i = 0^o$. The electron density varies between $2.7\ 10^{10} < n_e < 5.9\ 10^{12}$ cm^{-3} with the mass transfer rate varying between $1.6.10^{-9}\ M_\odot\ yr^{-1} < \dot{M} < 3.6.10^{-7}\ M_\odot\ yr^{-1}$. Our optimum n_e and $\dot{M}$ values are seen to be near the upper limit of these ranges. The values assumed for M_1, M_2 and R_1 are also only estimates and hence the inferred n_e and $\dot{M}$ will only be approximate. Nevertheless the values obtained are of the correct order of magnitude when compared with previous determinations which also assume values of quantities in the same way as we assume M_1, M_2 and R_1. 4 combinations of techniques may well lead to a consistent estimate of these parameters i.e. Polarimetric determination as above; Inglis-Teller spectroscopic analysis; Hβ emission observations (U Cr B-Struve et al (1957); light curve effects (AD Her - Korsch and Walter 1969); Stream dynamics (WZ Sge - Gorbatskii 1967) or curve of growth analysis (HD 47129 - Abyankhar 1959).

5.5 Discussion and Conclusions

It is clear that with the present size of σ_{dat} and σ_{disp} found for the 7 binaries considered here any estimate of orbital inclinations will be unreliable. McLean (1980) has provided observations with much smaller σ_{dat} comparing favourably with σ_{nec}, for the system HD 50896.

INC	P2	Q2	TAU ($.10^{-5}$)	N ($.10^{+46}$)	n_e ($.10^{+10}$)	$\dot{M}$ ($.10^{-9}$)
.0	-.01067	+.00042	5.339	1.430	27.301	16.605
15.0	-.01069	+.00062	5.539	1.483	28.326	17.228
30.0	-.01116	+.00130	6.420	1.719	32.830	19.967
45.0	-.01370	+.00253	9.287	2.487	47.493	28.886
60.0	-.02305	+.00542	18.942	5.074	96.865	58.915
75.0	-.05218	+.01313	50.428	13.508	257.868	156.839
90.0	-.10567	+.02683	109.022	29.204	557.492	339.076
105.0	-.11857	+.03140	114.956	30.793	587.835	357.531
120.0	-.10575	+.03031	88.006	23.574	450.024	273.712
135.0	-.09652	+.03127	67.639	18.118	345.876	210.367
150.0	-.09270	+.03445	56.511	15.137	288.971	175.757
165.0	-.09059	+.03833	50.887	13.631	260.212	158.266
180.0	-.08974	+.04020	49.166	13.170	251.413	152.914

System = AO CAS

Orbital Period	=	3.5	Days
Mass 1	=	18	M(Sun)
Mass 2	=	22	M(Sun)
Primary Radius	=	11	R(Sun)
Envelope Volume	=	5.239 .10+ 35	cm-3
Timescale of Xfer	=	.2625	Days

TAU = Optical Depth of Scatterers (Symmetric)
N = Number of Scatterers (Electrons)
n_e = Electron Density (cm-3)
$\dot{M}$ = Mass Transfer Rate (M(Suns)/yr.)

TABLE IV

This means that model testing and parameter determination should improve to a satisfactory level with new data (cf. Chapter 10). In order to reduce σ even further it is necessary to treat the data in an unbinned (raw) form and to restrict observations to few enough orbital cycles for rotational effects to dominate systematic changes in the envelope. Then the error used in the χ^2 analysis will be σ_{dat} which, with large enough telescopes and may be small enough to allow suitable analysis. Such a technique is presented in Chapter 8 where we generalize the optimization procedure of Chapter 2 to unequal phase interval observations.

The correlation between i_{opt} obtained here and other values from polarimetry, photometry and spectroscopy of these systems should be treated with caution. The bias of the inclination estimator discussed in Chapter 4 has tended to push up the optimum inclination value due to the presence of data noise and hence the correlation between our values of i and other determinations is illusory. The inclinations of the eclipsing binaries β Per, σ Ori E, u Her, U Sge and V444 Cygni are however high (due to the presence of the eclipse) but how high is not certain. Our estimates are consistent with this eclipse behaviour but are, as mentioned above biased. The large confidence intervals obtained were also expected from the numerical testing of the canonical model in Chapter 3.

We have shown that it is possible to obtain estimates of the number of scatters N, the electron density n_e and the mass transfer rate $\dot{M}$ for polarimetric binary systems (the parameter n_e can be found for systems that are assumed to have a specific envelope geometry. $\dot{M}$ is calculated for binaries with a gas stream). We have presented the procedure for determination of these parameters for the system AO Cas as an example of the method used. Due to the high uncertainty in the optimum inclination of AO Cas ($i_{opt} = 61^\circ$ with a R.C.I. of $[0^\circ, 88^\circ]$) the values of N, n_e and $\dot{M}$ can only be assumed approximate. No more can be said about them, than that they seem reasonable value when compared to other (non-polarimetric) determinations. More accurate data is needed before definitive parameter determinations can be attempted.

We now proceed to Chapter 6 where we present analysis relaxing the assumption of corotation of the scattering region and light source implicit in the canonical model, by inclusion of a scattering region in an eccentric orbit.

CHAPTER 6 THE EFFECT OF ORBITAL ECCENTRICITY ON THE CANONICAL MODEL PREDICTIONS

6.1 Introduction

When applying the optimization technique of Chapter 2 to real observations to obtain the 'best fit' canonical model parameters, we have seen that the results are inconclusive in that in most cases wide confidence intervals on the optimum inclination were obtained (cf. Chapter 5). In some cases (HD 47129, σ Ori E, U Filter, U Sge) the R.C.I. was from 0° to 180° meaning at the significance level considered (10%) all inclinations in that range would produce an acceptable fit to the data. For β Per (Algol) and σ Ori E (B filter) data however, no acceptable fit was found meaning that processes not consistent with the canonical model behaviour were probably present in the data. The assumptions of the canonical model may thus be inapplicable for some systems (even in binned data form). Many binary systems have been found to exhibit photometric and/or spectroscopic behaviour indicating the presence of an eccentric orbit of the binary (Batten 1973, 1975). Such behaviour for eclipsing binaries take the form of non-symmetric light curves, with unequal interval between successive minimum (i.e. primary to secondary eclipse time $\neq$ secondary to primary eclipse) and distorted radial velocity curves respectively. Examples of these are shown in Figure (6.1). Non eclipsing systems would still exhibit a distorted radial velocity curve indicating an eccentricity e, of the relative orbit. Cygnus X-1 itself has been found to show spectroscopic variations consistent with an eccentricity of $e \sim 0.06$ (Bolton 1975).

The processes of mass transfer thought to be occurring in such binaries do however effect the radial velocity curves substantially and it may be the case that, in the case of Cygnus X-1 for example, the $e \sim 0.06$ is caused by the effects of such variable mass exchange rate and not by eccentricity. Nevertheless it is clear that many binaries will have non-circular orbits, so hence invalidating the canonical model. With the increase in polarimetric accuracy expected in the near future (cf. McLean 1980) such non-canonical model structure of the observations could mean that the model would have to be rejected in many cases.

FIGURE 6.1a

Shows the effect of orbital eccentricity on the light curve of an eclipsing binary system. The timing of the primary and secondary minimum of the light curves are shifted by amounts depending on the longitude of the periastron of the orbit , ω.

FIGURE 6.1b

Shows the effect of a similar eccentricity on the radial velocity curves derived from the positioning of the spectral lines in the systems spectrum . For $e = 0.0$ the radial velocity curve is sinusoidal ; it is ditorted as e increases and as ω changes.

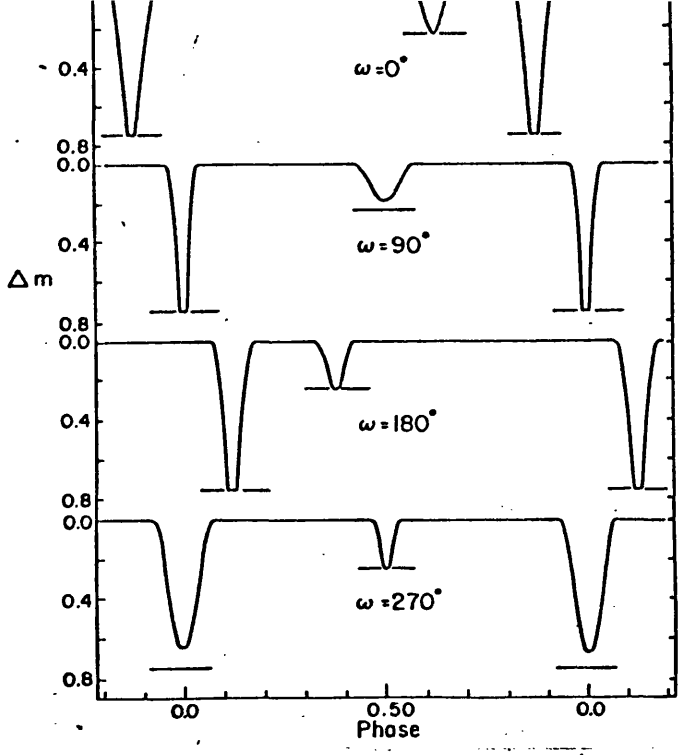
0.4
ω=0°
0.8
0.0
0.4
ω=90°
Δm
0.8
0.0
0.4
ω=180°
0.8
0.0
0.4
ω=270°
0.8
0.0
0.50
0.0
Phase

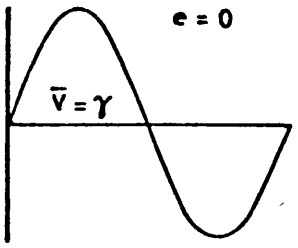
e = 0
v̄ = γ

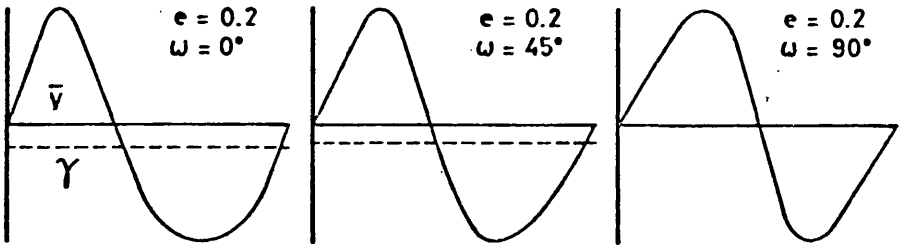
e = 0.2
ω = 0°
v̄
γ
e = 0.2
ω = 45°
e = 0.2
ω = 90°

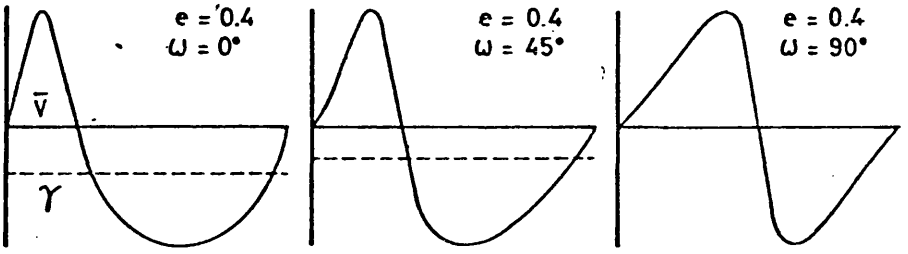
e = 0.4
ω = 0°
v̄
γ
e = 0.4
ω = 45°
e = 0.4
ω = 90°

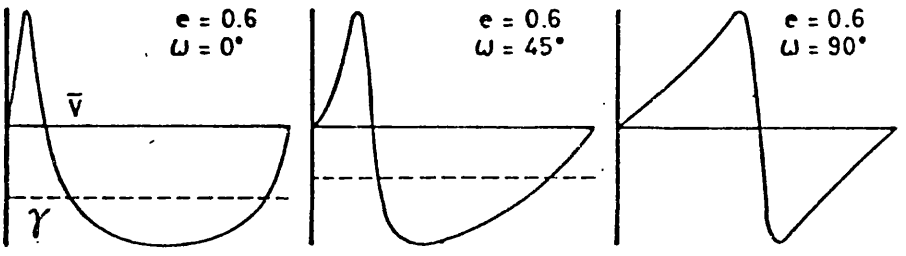
e = 0.6
ω = 0°
v̄
γ
e = 0.6
ω = 45°
e = 0.6
ω = 90°

It is therefore appropriate to investigate theoretically the effect of such an eccentric orbit on the canonical model predictions and hence extend the model to include such effects. In the present preliminary analysis we restrict ourselves to cases where the scattering envelope is symmetric about the orbital plane of the binary hence, in canonical model terms we would only observe 2nd harmonic variations in the polarization. From a purely qualitative study of introducing an $e \neq 0.0$ we see that the scattering envelope geometry would no longer be static in the corotating frame and would introduce a physical λ (longitude) dependence of the weighted optical depths τ_3 and τ_3 where $\tau_3 = \tau_o\gamma_3$ and $\tau_4 = \tau_o\gamma_4$ in the notation of Brown et al (1978) and of Chapter 2, that is the canonical model predicts λ- independent τ_3, τ_4's via the relations.

$$\begin{aligned} Q &= -(1 + \cos^2 i)(\tau_3 \cos 2\lambda - \tau_4 \sin 2\lambda) \\ U &= -2 \cos i (\tau_3 \sin 2\lambda + \tau_4 \cos 2\lambda) \end{aligned} \qquad (6.1)$$

with constant τ's whereas when $e \neq 0.0$; $(\tau_3, \tau_4) \Rightarrow (\tau_3(\lambda), \tau_4(\lambda))$. Consequently the double elliptical (Q,U) locus predicted for the $e = 0.0$ case (Q,U eccentricity $E = \sin^2 i/(1 + \cos^2 i)$) will no longer be so simple if $e \neq 0$ for several reasons. In addition to physical changes in the τ's, a geometric λ-dependence of τ_3, τ_4 will arise due to the variation of the separation of the light source and scattering region. Non-uniform variation of λ with time t will also occur due to the non-uniform sweeping of the radius vector from light source to scattering region in the orbit. This time variation will introduce extra harmonics into the (Q,U) variations. Clearly in general these three factors will have a rather complicated effect on the time variation of (Q,U) which would have to be found to be a computational method incorporating a model of the physics governing the envelope distribution. The complexity will be particularly great when both stars contribute in the scattered light. To illustrate the terms some of these effects may take, we restrict ourselves here to a simple case, but on which is nevertheless realistic in a number of interesting binaries. We consider an idealized system in which light from the primary is scattered on a localized 'envelope' near the secondary star. Hence

only one light source and one localized scattering region which we called the scattering 'blob' is included. In the notation of Brown et al (1978) the one light source will give $f_1 = 1$, $f_2 = 0$ (cf. Chapter 2).

This description may approximate well to certain X-ray binary systems where the light of a luminous primary (OB supergiant or Wolf-Rayet star) is polarized by scattering off an accretion disk or wake associated with an optically faint (compact) companion (cf. polarimetric model proposed for Cygnus X-1 Kemp et al 1979, Kemp 1980). It is also appropriate to semi-detached binaries with weak gas streams between a cool giant star and a bright (possibly Be-type) companion. We proceed now to investigate the purely geometric effect of introducing a non-zero eccentricity (§ 6.2) taking the scattering blob to be unchanged physically throughout the orbit. Later (§ 8) we discuss the effect of such physical variations on the observed (Q,U) locus. We also analytically optimize the model, here referred to as the 'eccentric model', to 'real' observations in §6.3 following a similar procedure to that outlined in Chapter 2 for the canonical model and discuss possible binary systems where the effect of $e \neq 0.0$ may be observable. In §6.5 we apply the model to Cygnus X-1 data of (Kemp et al 1979) in an attempt to improve the fit and reduce the confidence intervals on the optimum inclination predicted by the asymmetric canonical model.

6.2 Geometric effect of Eccentric orbits on (Q,U)

We consider a secondary object in an orbit about the primary star with semi major axis a and eccentricity e. The instantaneous longitude of the secondary measured about the orbital axis from the plane containing the axes and the earth, is λ and periastron occurs at $\lambda = \lambda_p$. Figure (6.2) illustrates this arrangement. The primary is fixed at one focus of the relative orbit (i.e. the orbit of the secondary relative to the primary star) of the relative orbit. Around the secondary is an optically thin Thomson-scattering region of extent small composed to a which we idealize as a point scatterer containing N electrons. We note here that Brown et al (1978) indicated that many cases of non-point scatterers (i.e. extended density distributions) can be replaced (or are equivalent to) a point

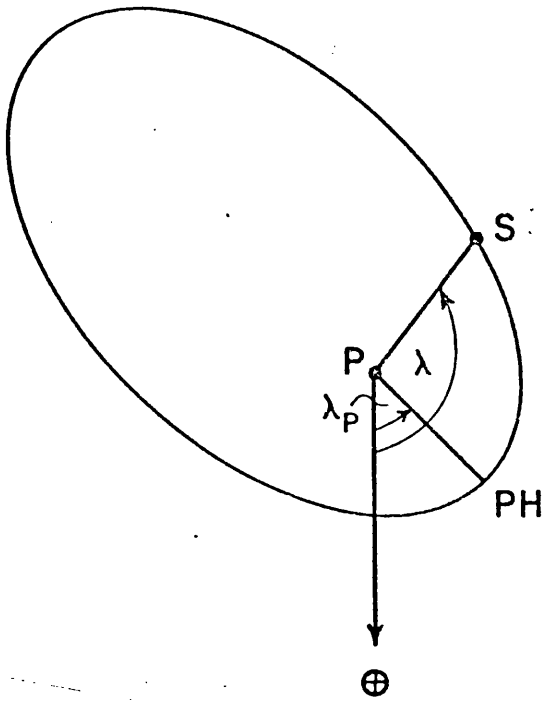

FIGURE 6.2

This diagram shows the geometrical set-up of the eccentric orbit calculations. P is the point light source, S is the scattering region and PH is the periastron of the orbit. The earth direction is indicated by the ⊕ sign.

scatterer with a certain number of scatterers and position relative to the binary. Then the density distribution function about the primary in spherical polars with the X-axis passing through the secondary is simply:

$$n(R_1, \theta_1 \Phi_1) = \frac{N}{R_1^2} \delta(R_1 - R(\lambda)) \delta(\Phi_1) \delta(\theta_1 - \frac{\pi}{2}) \qquad (6.2)$$

where δ is the Dirac-delta function and $R(\lambda)$ is the stellar separation at longitude λ . This we substitute into the equations defining the weighted optical depths τ_3, τ_4 namely,

$$\begin{Bmatrix} \tau_3 \\ \tau_4 \end{Bmatrix} = \frac{3}{32\pi} \sigma_T \sum_{j=1}^{2} f_j \int_{R_{j=0}}^{\infty} \int_{\theta_{j=0}}^{\pi} \int_{\phi_{j=0}}^{2\pi} n(R_j, \theta_j, \Phi_j) \sin^3 \theta_j$$

$$\begin{Bmatrix} \cos 2\Phi_j \\ \sin 2\Phi_j \end{Bmatrix} dR_j \, d\theta_j \, d\Phi_j \, . \qquad (6.3)$$

and due to the nature of (6.2) we obtain:

$$\tau_3 = \tau_* \left[\frac{a}{R(\lambda)}\right]^2 \quad ; \quad \tau_4 = 0 \qquad (6.4)$$

where $\tau_* = 3 \sigma_T N / 32\pi a^2$.

We know from two body orbit theory that the variation of R, the distance between the two bodies, with longitude λ is given by,

$$R(\lambda) = \frac{a(1-e^2)}{1 + e \cos(\lambda - \lambda_p)} \qquad (6.5)$$

where λ_p is the longitude of the periastron of the orbit. The function $a(1-e^2)$ is the semi-latus rectum of the orbit and the angle $(\lambda - \lambda_p)$ is the true anomaly of the secondary body. This is the angular displacement of the secondary, measured about the focus (i.e. primary position) from 0 at the periastron of the orbit (angle - $\hat{PHPS}$) (cf. Roy 1978). If we substitute (6.5) into (6.4) and hence into (6.1) after some manipulation, the exact results:

$$Q(\lambda) = -\tau_* \frac{(1+\cos^2 i)}{(1-e^2)^2} \left[\frac{e^2}{4} \cos 2\lambda_p + e \cos(\lambda + \lambda_p) \right.$$

$$+ (1 + \frac{e^2}{2}) \cos 2\lambda + 3e \cos(3\lambda - \lambda_p)$$

$$\left. + \frac{e^2}{4} \cos 2(2\lambda - \lambda_p) \right] \qquad (6.6)$$

$$U(\lambda) = -\frac{2\tau_* \cos i}{(1-e^2)^2} \left[\frac{e^2}{4} \sin 2\lambda_p + e \sin(\lambda + \lambda_p) \right.$$

$$+ (1 + \frac{e^2}{2}) \sin 2\lambda + 3e \sin(3\lambda - \lambda_p)$$

$$\left. + \frac{e^2}{4} \sin 2(2\lambda - \lambda_p) \right] \qquad (6.7)$$

Equations (6.6) and (6.7) show immediately that the effect of non-zero e is to introduce extra harmonics into the <u>phase</u> (λ) variations of (Q,U). These are seen to be first, third and fourth where previously (e = 0) only second harmonics were present. A constant polarization level of order e^2 is introduced together with first and third harmonics of order e. The second harmonics are modified by an e^2 term with the fourth harmonics of order e^2 also. Since all these harmonics arise from the basic (e = 0) second harmonics the Q harmonic variations are all proportional to $(1 + \cos^2 i)$. Likewise the U harmonic variations all have an inclination dependence of cos i. This i dependence is quite different from that of the first and second harmonic in the general (asymmetric) canonical model where the first harmonics have different inclination terms than the second harmonics. This fact can be used as an additional diagnostic test to distinguish $e \neq 0$ from envelope assymetry and we shall see later (§ 6.3) their effect.
If we put e = 0.0 in Equations (6.6) and (6.7) we see that the (Q,U) variations reduce to the symmetric canonical form of

$$\begin{aligned} Q(\lambda) &= -\tau_* (1 + \cos^2 i) \mid \cos 2\lambda \mid \\ U(\lambda) &= -2\tau_* \cos e \mid \sin 2\lambda \mid \end{aligned} \qquad (6.8)$$

with $\tau_4 = 0$ $\tau_o \gamma_4 = 0$. (cf. Brown <u>et al</u> 1978). This reduction to one less free parameter ($\tau_4 = 0$) relative to the symmetric canonical model occurs because we have restricted the azimuth of the scatterer to be

that of the secondary star hence fixing $\lambda_2 = 0$ in the notation of Brown et al (1978).

Physically the presence of a large eccentricity in a close binary is not expected. Tidal effects between the two stars tend over relatively short periods of time to circularize or decrease the eccentricity of the orbit (Zahn 1975, Lecar et al 1976). The additional zero and fourth harmonic terms in the Q,U variations are of order e^2 so if e is reasonably small these harmonics will give a negligible contribution to the resultant Q,U locus and are dropped in further analysis (but not in the diagrams 6.3). These equations can be seen by deriving the locus described during one orbit in the (Q,U) plane by eliminating λ from the parametric equations (6.6) and (6.7) or by straight forward computation of Q,U for different λ. We have computed these loci (an example is given in Figure 6.3) where the constant terms in (6.6) and (6.7) are dropped for a range of input parameters { e, i, λ_p }. In Appendix 3 we present the sets of diagrams for the parameter ranges $0{\cdot}0 \leq e \leq 0{\cdot}55$ (in steps of $0{\cdot}05$) and $i = 75°, 135°$ with $\lambda_p = 0°, 75°$. Also shown are the secondary data sets (Q_+, U_+) and (Q_-, U_-) loci of Brown et al (1978) which separate out odd and even harmonics respectively by forming $Q_+(\lambda) = \frac{1}{2}(Q(\lambda) + Q(\lambda + \pi))$, $Q_-(\lambda) = \frac{1}{2}(Q(\lambda) - Q(\lambda + \pi))$ and similarly for the U Stokes parameter. An example of these loci is given in Figure (6·4) overleaf. By looking at the progression of increase e for the same i and λ_p one can see the change in the structure of the loci due to the increasing e and e^2 contributions.

In Figure (6·3) (the Q,U loci) we have plotted the quantity $Q(1 - e^2)^2 (-\tau_*(1 + \cos^2 i)$ versus $U(1 - e^2)^2/(-2\tau_* \cos i)$. (i.e. Since neither τ_* nor i appear inside the square brackets of (6.6) and (6·7) we have scaled Q and U accordingly). The effect of the $(1-e^2)$ terms is one of changing the binary size scale (i.e. periastron distance). The parameters used for calculating Figure (6·3) and (6·4) are therefore $i = 70°$, $\lambda_p = 0°$, $60°$, $120°$, $180°$ and e = 0·0, 0·1, 0·2, 0·3. As can be seen from the set of figures in Appendix 3 the effect of increasing i from $0°$ (where at e = 0 the locus is a circle) is to flatten the true loci in the U direction by a factor $2 \cos e/(1 + \cos^2 i)$ relative to the circle (i = 0 case). It is also immediately clear from

FIGURES 6.3

Shown are the Q',U' loci (plotted as described in the text) for different values of the eccentricity,e, the longitude of periastron,λ_p and inclination,i as predicted by the eccentric model.

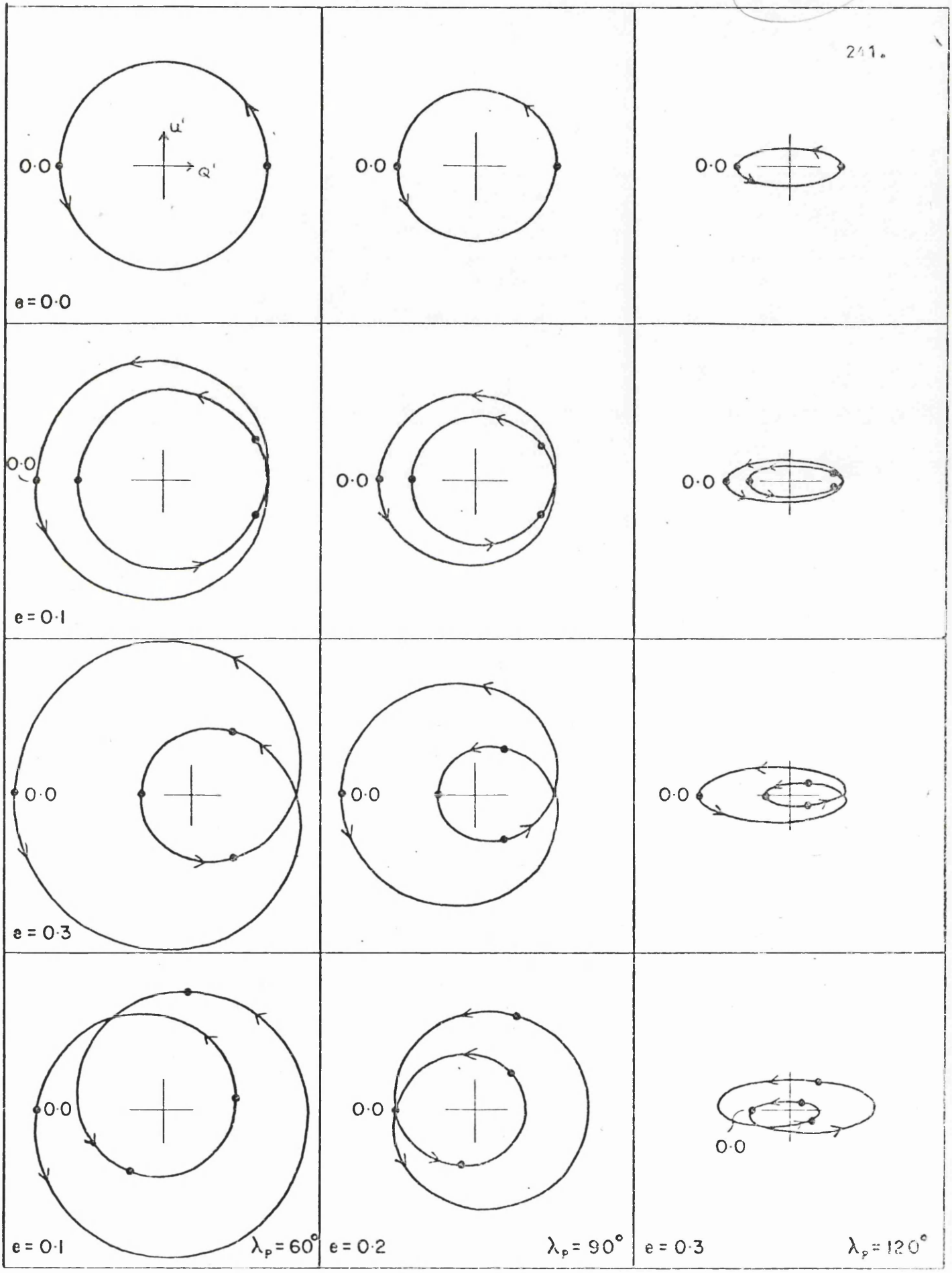
i = 10
i = 45
i = 80
Q'
P'
0·0
e = 0·0
e = 0·1
e = 0·3
e = 0·1
λp = 60°
e = 0·2
λp = 90°
e = 0·3
λp = 120°

e = 0.1/0.15

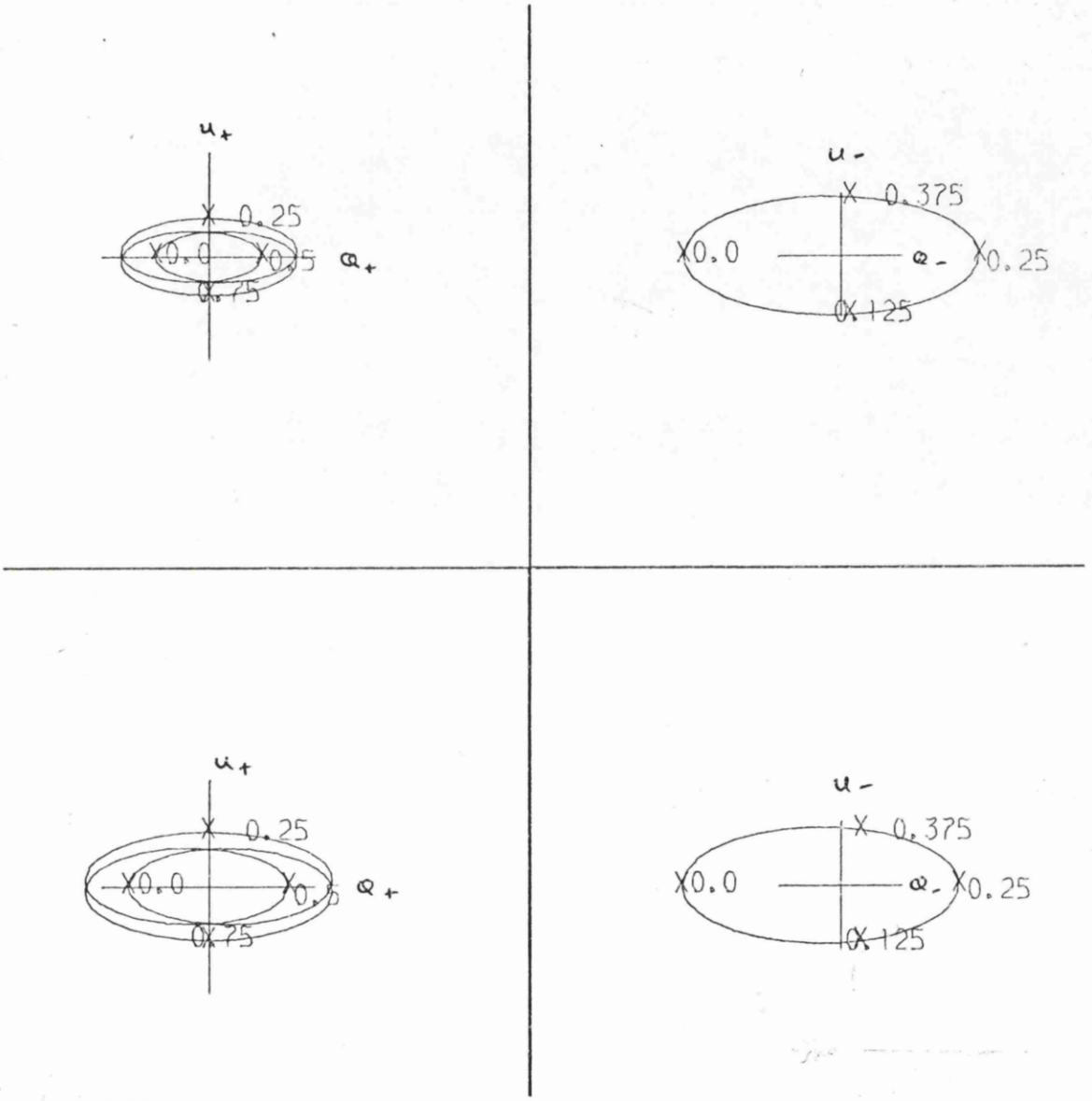

FIGURE 6.4

Examples of the Q_+, U_+ and Q_-, U_- loci produced from the eccentric orbit model predictions. The two top diagrams have parameters e = 0.1, i = 78^o and λ_p = 0^o. The bottom two diagrams have e = 0.15, λ_p = 0^o and i = 78^o.

Equations (6·6) amd (6·7) (or the physics of the situation) that the effect of values of $i > 90^\circ$ simply leads to reflection of the $(180^\circ - i)$ locus in the Q axis (since the Q inclination factor does not change $(1 + \cos^2 i)$ and the U factor cos i goes to - cos i).

The general form of the loci in Figure (6·3) and Appendix 3 is that of a double looped figure, one loop being always contained within the other. Remembering that we are dealing here only with an envelope symmetric about the orbital plane, it is at once clear that by comparison with Figures (2·3) of Chapter 2 (also Figures 3 to 7 of Brown et al 1978) a case of non-zero eccentricity (with a symmetric envelope) might be misinterpreted from its (Q,U) locus as a corotating (e = 0·0) asymmetric envelope which can result in double looped loci resembling Figures (6·3). The general form of the (Q_+, U_+), (Q_-, U_-) loci is that of a complicated (double looped) figure (for $e \neq 0{\cdot}0$) involving odd harmonics (1st and 3rd) and an elliptical shape (distorted at higher e) including even harmonics (2nd and 4th). Specifically then, inspection of the relevant equations in the two cases (e = 0 corotating and $e \neq 0$ non-corotating) shows that an eccentricity of say $e \sim 0{\cdot}2$ could be misinterpreted (on qualitative grounds or quantitatively in the presence of data noise) as an envelope asymmetry about the orbital plane of about 20% since either of these interpretations introduces first harmonics in $Q(\lambda)$, $U(\lambda)$ with amplitude about 0·2 of the dominant second harmonic amplitude. Nevertheless, the forms of locus possible from the eccentricity of the orbit are not identical to those for the asymmetric corotating e = 0, case, specifically in the containment of one (Q,U) loop within the other, and the presence of a third harmonic component in the $e \neq 0$ case.

Variation of λ_p the periastron longitude merely rotate the loop intersection point around the locus. In order to examine adequately the possible diagnostics of the eccentricity of the orbit, however, we must consider its predictions (6·6)and (6·7) in terms of Fourier coefficients rather than the morphology of the (Q,U) Figures (6·3). In doing so it is more appropriate to express the equations as a Fourier series in time rather than phase λ since it is the former in which observational data will usually be expressed (certainly in the cases where the binary phases are known e has been assumed to be zero). Kepler's law tells us that when an orbit of a body about another is eccentric the area swept out by the radius vector (between the two stars)

has to be equal in equal time intervals. Due to the variation of this radius vector via equation (6·5) this means that the orbiting bodies' velocity must vary at different stages of the orbit. This means that in equal time intervals (equal phases when e = 0) different intervals of orbital phase will pass over the whole orbit and therefore the actual time of equal phase intervals will not be equal (e.g. the time passage during the phase interval 0·1 to 0·2 will not equal the 'real' time passage during phase 0·3 to 0·4).

Here we measure time t in angular units $\Lambda = \frac{2\pi t}{T}$ (where T is the orbital period) and $\Lambda = 0$ when $\lambda = 0$. We denote by Λ_p the 'time' of periastron passage ($\lambda = \lambda_p$). Then λ and Λ are interrelated through the 'two body problem' relations involving the eccentric anomaly, E and Kepler's equation viz:

$$\tan\left(\frac{v_s}{2}\right) = \left(\frac{1+e}{1-e}\right)^{\frac{1}{2}} \tan\frac{E}{2} \qquad (6\cdot9)$$

where v_s is the true anomaly of the secondary (scattering blob) and

$$E - e \sin E = M \qquad (6\cdot10)$$

where M is the mean anomaly of the scatterer.

Solution of (6·9) and (6·10) for $\lambda(\Lambda)$ and substitution in (6·6) and (6·7) would yield the desired $Q(\Lambda)$, $U(\Lambda)$ form but in general, due to the nature of Kepler's equation, this must be done numerically. Since, however, only cases of rather small e are of practical interest (on physical grounds) we consider here only the solution to order e, which is analytic. We must express τ_3 and τ_4 (equal to $\sigma_o N \cos^2 \Phi_s / 2R_s^2$ and $\sigma_o N \sin 2\Phi_s / 2R_s^2$ respectively) in terms of time, hence R_s the distance between the primary and secondary and Φ_s, the longitude of the secondary, must be known as function of <u>time</u>. Now Φ_s is measured in a frame rotating uniformly with angular velocity = $2\pi/T$. At time of zero phase this frame has its x axis pointing towards the observer with the origin centred on the primary star. We measure time by $\Lambda = 2\pi t/T$ and let $\Lambda_p = 2\, t_p/T$ where t_p is the time of periastron passage of the scatterer. It should be noted that this is not the same as the time that the x-axis (from which Φ_s is measured) lies along the line joining the primary and periastron since the x axis rotates at a uniform rate while the scatter does not consequently $\Lambda_p \neq \lambda_p$ except when e = 0. This means a correction

to λ_p which however is not time dependent and will only effect the phasing of the loci and not its shape. Clearly from Figure (6·5),

$$\Phi_s = \lambda_p + v_s - \Lambda \qquad (6\cdot11)$$

Thus by the standard treatment of eccentric orbits we know that v_s is related to E by equation (6·9) and this E is related to the mean anomaly M by equation (6·10) (Kepler's equation). M is defined as the angle rotated about the axis with the same centre as the ellipse (orbit) by a point moving with constant angular speed, of the same period i.e.:

$$M = \frac{2\pi}{T}\ (t - t_p) = \Lambda - \Lambda_p \ . \qquad (6\cdot12)$$

Hence we know $\lambda(\Lambda)$ and $\lambda_p(\Lambda_p)$ since

$$E - e \sin E = \Lambda - \Lambda_p \qquad (6\cdot13)$$

and we know E from (6·13) and hence v_s from (6·9). To find Λ_p we consider v_s at $\Lambda - 0\cdot0$ ($\equiv\lambda = 0$). In this case from Figure (6·5) we see that

$$v_s(0) = 2\pi - \lambda_p \qquad (6\cdot14)$$

and hence $E(0) = 2 \tan^{-1} \left(\left(\frac{1-e}{1+e}\right)^{\frac{1}{2}} \tan \frac{v_s}{2}\right)$ (6·15)

using Kepler's equation with $\Lambda = 0$ gives

$$\Lambda_p = -(E(0) - e \sin E(0)) \qquad (6\cdot16)$$

and hence Λ_p for any chosen λ_p. Also from Figure (6·5) we see that, in general, $v_s = (\lambda - \lambda_p)$ hence we now solve (6·9) for E (knowing the timings Λ and Λ_p) and insert into (6·9) for $\lambda(\Lambda)$ (since we know $\lambda_p(\Lambda_p)$). We are, as stated above, only interested in the solution to small e and so we only perform the remaining analysis to order e (i.e. neglect terms of e^2 and higher).

Kepler's equation (6·10) in general needs to be solved numerically using an iterative procedure (Newton-Raphson for example). However for terms of order e and above we may approximate the solution to (6·10) as follows. For small e, we can consider as a first approximation

$$E - e \sin E = \lambda - \lambda_p \rightarrow E \simeq \lambda - \lambda_p \qquad (6\cdot17)$$

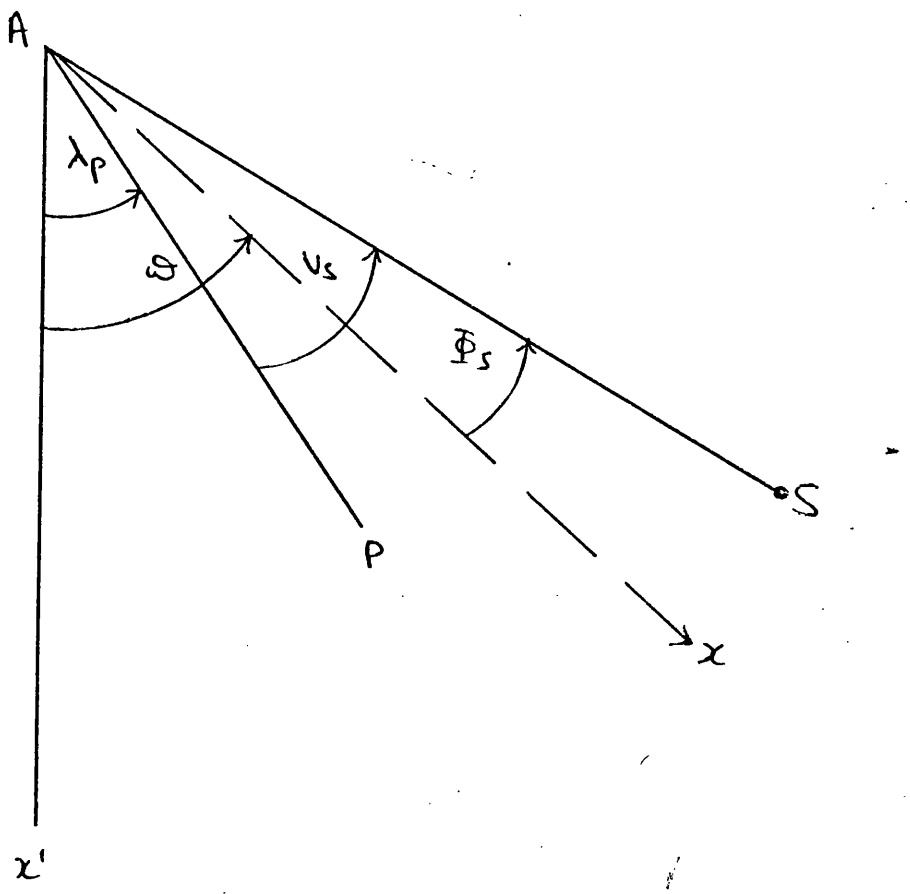

FIGURE 6.5

Diagram showing the angles used to calculate $\lambda_p(\Lambda_p)$. A is the point light source, S is the scattering region position. λ_p is the longitude of the periastron of the orbit, Λ_p is the time of periastron passage. v_s is the true anomaly.

and hence:

$$E = (\lambda - \lambda_p) + e \sin (\lambda - \lambda_p) \qquad (6\cdot18)$$

Therefore we substitute (6·18) into 6·9) and take only terms of e and above (i.e. e^2 etc. negligible).

Insertion of the resulting equation into (6·6) and (6·7) and expanding to the same order yields the following for the Fourier time series expansion of Q,U (constant terms being ignored):

$$\begin{aligned} Q(\Lambda) &= \tau_* (1 + \cos^2 i) \sum_{j=1}^{3} (p_j \cos j\Lambda + q_j \sin j\Lambda) \\ U(\Lambda) &= 2\tau_* \cos i \sum_{j=1}^{3} (u_j \cos j\Lambda + v_j \sin j\Lambda) \end{aligned} \qquad (6\cdot19)$$

where

$$\begin{aligned} p_1 &= e \cos \Lambda_p & u_1 &= e \sin \Lambda_p \\ q_1 &= -e \sin \Lambda_p & v_1 &= e \cos \Lambda_p \\ p_2 &= -1 & u_2 &= -4 e \sin \Lambda_p \\ q_2 &= 4e \sin \Lambda_p & v_2 &= -1 \\ p_3 &= -3 e \cos \Lambda_p & u_3 &= 3 e \sin \Lambda_p \\ q_3 &= -3 e \sin \Lambda_p & v_3 &= -3 e \cos \Lambda_p \end{aligned} \qquad (6\cdot20)$$

In practice it is actually only necessary to insert the solution to order e of (6·9) and (6·10) into the second harmonic terms of (6·6) and (6·7) since the other harmonics are already of order e. In these terms it is thus sufficient to set $\lambda = \Lambda$.

Therefore a complete solution to the problem is obtained under the assumption of small e (e^2 and higher negligible). We can now compare these relations with the asymmetric (corotating) canonical model predictions to establish the problems and solutions of diagnostic in the two cases.

6·3 Applications to Diagnostics of Eccentric Orbits

In the case of exact data from which the coefficients $\{ p_j, q_j, u_j, v_j \}$ $j = 1,2,3$ can be found, equations (6·19) and (6·20) represent an overdetermination of the system's parameters, namely e, Λ_p, i and τ_*. Their solution would thus yield a number of consistency checks (similar

in nature to the case of 1st and 2nd harmonics of Brown et al (1978) (related in Chapter 2) on the eccentric orbit model using the equations:

$$\left(\frac{p_1^2 + q_1^2}{u_1^2 + v_1^2}\right)^{\frac{1}{2}} = \left(\frac{p_3^2 + q_3^2}{u_3^2 + v_3^2}\right)^{\frac{1}{2}} = \left(\frac{1 + \cos^2 i}{2 \cos i}\right)$$

$$-\frac{q_1}{p_1} = \frac{q_3}{p_3} = \frac{u_1}{v_1} = -\frac{u_3}{v_3} = \tan \lambda_p \qquad (6.21)$$

and

$$\frac{(p_1^2 + q_1^2)^{\frac{1}{2}}}{-p_2} = \frac{(p_3^2 + q_3^2)^{\frac{1}{2}}}{-3p_2} = \frac{(u_1^2 + v_1^2)^{\frac{1}{2}}}{-v_2} = \frac{(u_3^2 + v_3^2)^{\frac{1}{2}}}{-3v_2} = e$$

while τ_* can then be found from any one of the 12 Fourier coefficients in (6.19). In practice however the presence of noise in the data usually means that the parameters cannot be solved for in this way (cf. Simmons et al 1980 and Chapter 2). Rather one must utilize the relationships between the Fourier coefficients expressed in (6.21) as constraints in obtaining an optimized fit to noisy data in terms of a unique set of best fit model parameters (here i, τ_*, θ , e, λ_p) and their associated confidence intervals. This we have done for the canonical model (cf. Chapter 2) and shall consider this model's optimization in Section (6.4).

Nevertheless consideration of the analytic solution (6.21) is informative in terms of eccentric orbits diagnostics in the limit of zero noise. In particular we may compare the coefficients (6.19) predicted by the eccentric model analysis with those for a general (asymmetric corotating) canonical model. These relations, of Brown et al (1978), take the form,

$$\begin{aligned}
p_1 &= \tau_1 \sin 2i & u_1 &= 2\tau_2 \sin i \\
q_1 &= -\tau_2 \sin 2i & v_1 &= 2\tau_1 \sin i \\
p_2 &= -\tau_3 (1 + \cos^2 i) & u_2 &= 2\tau_4 \cos i \\
q_2 &= \tau_4 (1 + \cos^2 i) & v_2 &= -2\tau_3 \cos i \\
p_3 &= 0 & u_3 &= 0 \\
q_3 &= 0 & v_3 &= 0
\end{aligned} \qquad (6.22)$$

which have solutions:

$$\frac{(p_2^2 + q_2^2)^{\frac{1}{2}}}{(u_2^2 + v_2^2)^{\frac{1}{2}}} = \frac{(1 + \cos^2 i)}{2 \cos i} \qquad (6.23)$$

$$\frac{(p_1^2 + q_1^2)^{\frac{1}{2}}}{(u_1^2 + v_1^2)^{\frac{1}{2}}} = \cos i \qquad (6.24)$$

$$-\frac{p_1}{q_1} = \frac{v_1}{u_1} = \frac{\tau_1}{\tau_2}$$

$$-\frac{p_2}{q_2} = \frac{v_2}{u_2} = \frac{\tau_3}{\tau_4} \qquad (6.25)$$

$$\frac{(u_2^2 + v_2^2)^{\frac{1}{2}}}{2} \quad \frac{(u_1^2 + v_1^2)^{\frac{1}{2}}}{(p_2^2 + q_2^2)^{\frac{1}{2}}} = (\tau_3^2 + \tau_4^2)^{\frac{1}{2}} \qquad (6.26)$$

$$\frac{(u_1^2 + v_1^2)^{\frac{1}{2}}}{2 (u_1^2 + v_1^2 - p_1^2 - q_1^2)^{\frac{1}{2}}} = (\tau_1^2 + \tau_2^2)^{\frac{1}{2}} \qquad (6.27)$$

Comparison of (6.19) with (6.23) - (6.27) shows that sufficiently good polarimetric data would in fact let us distinguish unambiguously between an interpretation in terms of an eccentric orbit and one involving a corotating asymmetric envelope. Similar relations for the first harmonics in the two cases (eccentric and canonical models) predict different inclination relations (i.e. $(1 + \cos^2 i)/(\cos i)$ and $\cos i$ respectively). The third harmonics, present in the eccentric model are in fact all zero as predicted by the canonical model. Of course we recognise that higher harmonics such as third (and obscure) can be interpreted in a corotating model by involving further hypotheses such as variable occultation (cf. Milgrom 1978; Kemp et al 1979 also Chapter 1). Even if the data are only used to determine the first two harmonics coefficients, such discrimination may still be possible. For example suppose we assume we were dealing

with a corotating asymmetric envelope and wanted to derive i from a two harmonic fit to Q,U data. Then by (6.23) and (6.24) we obtain two independent i values, following Brown et al (1978), which should agree to within their error estimates, if the hypothesis is to be consistent with the data. Alternatively we may consider the eccentric model of the type described here. Comparison of (6.19) and (6.23), (6.24) shows that the second harmonics give similar results whereas, the first harmonics as mentioned above, include different inclination relations and hence we obtain different inclination values. In fact if the system were actually a corotating one of inclination, say i_o and we tried to derive an inclination i_e from the first harmonics on the basis of an eccentric orbit hypothesis we would obtain:

$$\frac{2 \cos i_e}{1 + \cos^2 i_e} = \frac{(u_1^2 + v_1^2)^{\frac{1}{2}}}{(p_1^2 + q_1^2)^{\frac{1}{2}}} = \frac{1}{\cos i_o} \qquad (6.28)$$

which on inspection has no real solution for i_e, for any i_o. Thus the constraints here permit distinction between the models.

Again one might try to derive an estimate of the ratio of the mean optical depths of material asymmetric and symmetric about the orbital plane on the assumption of a corotating model when in reality the system is an eccentric orbit case. This would be described by the $(\tau_1^2 + \tau_2^2)^{\frac{1}{2}} / (\tau_3^2 + \tau_4^2)^{\frac{1}{2}}$ (i.e. G/H in the rotation of Brown et al 1978) which is given in terms of the Fourier coefficients by (6.26) and (6.27). If, however, these coefficients in fact arise from an eccentric orbit case of inclination i_e then inserting expressions (6.20) into (6.21) and (6.22) shows that one would find

$$\frac{(\tau_1^2 + \tau_2^2)^{\frac{1}{2}}}{(\tau_3^2 + \tau_4^2)^{\frac{1}{2}}} = - e^2 \left[\frac{1 + \cos^2 i_e}{1 + \cos^2 i_e}\right] \qquad (6.29)$$

which has no solutions for i_e for real τ values. This would again show that an incorrect model was being used.

6.5 Optimization of eccentric model and observed data.

It is of course necessary when considering the compatibility of a model with observational data to consider some acceptability parameter that gives a measure of the 'goodness of fit'. This procedure was followed for the general canonical model in Chapter 2 where we obtained expressions for the optimum model parameters using observations. Here, as in Chapter 2, we take the statistic χ^2 as the measure of the acceptability of the model fit, and we follow the analysis outlined in that Chapter for the eccentric model by minimizing the function

$$F(p,\theta, e, \lambda_p, i) = \sigma^2\chi^2 = \sum_{r=1}^{N-1} (Q'_{ob,r} - Q'_{t,r})^2 + (U'_{ob,r} - U'_{t,r})^2 \qquad (6.30)$$

subject to a set of constraints linking the Fourier harmonic coefficients of the model defined in (6.20). The constraints here are linear in the harmonic coefficients and for the eccentric orbit model take the form:

$$\frac{p_1}{v_1} = \frac{p_2}{v_2} = \frac{p_3}{v_3} = \frac{-q_1}{u_1} = \frac{-q_2}{u_2} = \frac{-q_3}{u_3} \quad \frac{1 + \cos^2 i}{2 \cos i} = \qquad (6.31)$$

$$\frac{u_1}{v_1} = \frac{-u_3}{v_3} = \tan \Lambda_p = t \qquad (6.32)$$

$$\frac{p_1}{p_2}(1 + t^2)^{\frac{1}{2}} = \frac{p_3}{3p_2}(1+t^2)^{\frac{1}{2}} = \frac{p_1}{p_2}^T \frac{p_3}{3p_2}^T = - e \qquad (6.33)$$

where $T = (1 + \tan^2 \Lambda_p)^{\frac{1}{2}}$ (i.e. $T = \sec \Lambda_p$).

and $$4q_1 = -q_2 \, . \qquad (6.34)$$

These are readily obtainable from the harmonic coefficients (6.20) and are in the natural frame of the binary (defined in Chapter 2). Unlike the canonical model which has only one (2nd) harmonic for the symmetric distribution of scatterers we now have three (1st, 2nd and 3rd) harmonics meaning 6 independent coefficients. This fact, and the

nature of the constraints, breaks the rotational symmetry encountered with the canonical model (cf. Simmons et al 1980) thus making the solution more complicated. However the procedure is still similar to that in the above mentioned paper (and Chapter 2). We form the Lagrange equations:

$$\frac{\partial F}{\partial p} + \sum_{k=1}^{11} \lambda_k \frac{\partial g_k}{\partial p} = 0 \qquad (6.35)$$

where p refers to the set of 12 harmonic coefficients { p_1, q_1, u_1 v_1, p_2, ... etc}. This gives us eleven relations involving the three harmonics instead of four relations for the two harmonics of the asymmetric canonical model. The above equations (6.35) represent optimization of the function $F(p,\theta, e, i, \lambda_p)$ and the relations (6.31) → (6.34) when written in the form:

$$\begin{aligned}
g_1(p_1, v_1, \alpha) &= p_1 - v_1\alpha = 0 \\
g_2(q_1, u_1, \alpha) &= q_1 + u_1\alpha = 0 \\
g_3(p_2, v_2, \alpha) &= p_2 - v_2\alpha = 0 \\
g_4(q_2, u_2, \alpha) &= q_2 + u_2\alpha = 0 \\
g_5(p_3, v_3, \alpha) &= p_3 - v_3\alpha = 0 \\
g_6(q_3, u_3, \alpha) &= q_3 + u_3\alpha = 0 \\
g_7(v_1, u_1, t) &= v_1 t - u_1 = 0 \\
g_8(u_3, u_3, t) &= u_3 t + u_3 = 0 \\
g_9(p_1,p_2,e_1,T) &= p_1 T + p_2 e = 0 \\
g_{10}(p_3,p_2,e,T) &= p_3 T + p_2 e = 0 \\
g_{11}(q_1,q_2) &= 4q_1 + q_2 = 0
\end{aligned} \qquad (6.36)$$

with respect to the harmonic coefficients themselves. Other Lagrange equations necessary for a complete optimized solution are:

$$\frac{\partial F}{\partial \alpha} + \sum_{k=1}^{11} \lambda_k \frac{\partial g_k}{\partial \alpha} = 0 \qquad \text{(a)}$$

$$\frac{\partial F}{\partial e} + \sum_{k=1}^{11} \lambda_k \frac{\partial g_k}{\partial e} = 0 \qquad \text{(b)}$$

$$\frac{\partial F}{\partial \theta} + \sum_{k=1}^{11} \lambda_k \frac{\partial g_k}{\partial \theta} = 0 \qquad \text{(c)} \qquad (6.37)$$

$$\frac{\partial F}{\partial t} + \sum_{k=1}^{11} \lambda_k \frac{\partial g_k}{\partial t} = 0 \qquad \text{(d)}$$

The λ_k's in (6.35) and (6.37) are the 11 undetermined Lagrange multipliers. These four equations (6.37) are optimizations with respect to α(the inclination function), e, the eccentricity of the orbit, θ, the rotation angle between laboratory and natural frames of reference and t the longitude of periastron function ($t = \tan \Lambda_p$) respectively.

On forming the 12 Lagrange equations (6.35) we obtain a set of linear relations between the 12 harmonic coefficients (p) and the 11 unknown Lagrange multipliers viz:

$$
\begin{array}{lllllllllll}
-N(\bar{p}_1 - p_1) & +\lambda_1 & & & & & +T\lambda_9 & & & & = 0 \\
-N(\bar{q}_1 - q_1) & & +\lambda_2 & & & & & & & +4\lambda_{11} & = 0 \\
-N(\bar{u}_1 - u_1) & & +\alpha\lambda_2 & & & -\lambda_7 & & & & & = 0 \\
-N(\bar{v}_1 - v_1) & -\alpha & & & & -t\lambda_7 & & & & & = 0 \\
-N(\bar{p}_2 - p_2) & & & +\lambda_3 & & & +e\lambda_9 & +3e\lambda_{10} & & & = 0 \\
-N(\bar{q}_2 - q_2) & & & & +\lambda_4 & & & & & +\lambda_{11} & = 0 \\
-N(\bar{u}_2 - u_2) & & & & +\alpha\lambda_4 & & & & & & = 0 \\
-N(\bar{v}_2 - v_2) & & & -\alpha\lambda_3 & & & & & & & = 0 \\
-N(\bar{p}_3 - p_3) & & & & & +\lambda_5 & & +T\lambda_{10} & & & = 0 \\
-N(\bar{q}_3 - q_3) & & & & & & +\lambda_6 & & & & = 0 \\
-N(\bar{u}_3 - u_3) & & & & & & +\alpha\lambda_6 & & +\lambda_8 & & = 0 \\
-N(v_3 - v_3) & & & & & +\alpha\lambda_5 & & & +t\lambda_8 & & = 0
\end{array}
\qquad (6.38)
$$

where $\bar{p}_1$, p_2 etc. are in the natural frame and are related to the observations (transformed from laboratory frame to natural frame by Equation ( ) by:

$$
\begin{aligned}
\bar{p}_k &= \frac{2}{N} \sum_{r=0}^{n-1} Q_{ob,r} \cos r k \beta, \qquad k = 1,2,3 \\
\bar{q}_k &= \frac{2}{N} \sum_{r=0}^{n-1} Q_{ob,r} \sin r k \beta, \qquad k = 1,2,3 \\
\bar{u}_k &= \frac{2}{N} \sum_{r=0}^{n-1} U_{ob,r} \cos r k \beta, \qquad k = 1,2,3 \\
\bar{v}_k &= \frac{2}{N} \sum_{r=0}^{n-1} U_{ob,r} \cos r k \beta, \qquad k = 1,2,3
\end{aligned}
\qquad (6.39)
$$

where $\beta = 2\pi/N$.

It is now possible to eliminate the 11 unknown Lagrange multipliers from eleven of the equations in (6.38) leaving the optimum equation giving when used with the constants themselves the best fit harmonic coefficients.

The λ_k's are needed when determining the optimum parameters i, e, θ, λ_p via the Lagrange equations (6.37). We have for those unknown multipliers:

$$\lambda_1 = N\Big[(\bar{q}_1-q_1)t-(\bar{u}_1-u_1)\frac{t}{\alpha} -(\bar{v}_1-v_1)\frac{1}{\alpha} -(\bar{q}_2-q_2)\ t +(\bar{u}_2-u_2)\frac{4t}{\alpha} \Big]$$

$$\lambda_2 = N\Big[(\bar{q}_1-q_1) -(\bar{q}_2-q_2) +(\bar{u}_2-u_2)\frac{4}{\sigma} \Big]$$

$$\lambda_3 = N\Big[(\bar{v}_2-v_2)\frac{1}{\alpha} \Big]$$

$$\lambda_4 = N\Big[(\bar{u}_2-u_2)\frac{1}{\alpha} \Big]$$

$$\lambda_5 = N\Big[(\bar{q}_3-q_3)t +(\bar{u}_3-u_3)\frac{t}{\alpha} -(\bar{v}_3-v_3)\frac{1}{\alpha} \Big]$$

$$\lambda_6 = N\Big[(\bar{q}_3-q_3)\Big]$$

$$\lambda_7 = N\Big[-(\bar{q}_1-q_1)\alpha+(\bar{u}_1-u_1)+(\bar{q}_2-q_2)4\alpha-(\bar{u}_2-u_2)4 \Big]$$

$$\lambda_8 = N\Big[-(\bar{q}_3-q_3)\alpha+(\bar{u}_3-u_3) \Big]$$

$$\lambda_9 = N\Big[(\bar{p}_1-p_1)\frac{1}{T} - \frac{\lambda_1}{T} \Big]$$

$$\lambda_{10} = N\Big[(\bar{p}_3-p_3)\frac{1}{T} + (\bar{q}_3-q_3)\frac{t}{T} - (\bar{u}_3-u_3)\frac{t}{\alpha T} + (\bar{v}_3-v_3)\frac{1}{\alpha T} \Big]$$

$$\lambda_{11} = N\Big[(\bar{q}_2-q_2) - (\bar{u}_2-u_2)\frac{1}{\alpha} \Big]$$

Substitution of these multipliers (λ_k's) into (6.38) gives us the optimum equation defining the harmonic coefficients viz:

$$\begin{aligned} &(\bar{p}_1-p_1)\frac{e}{T} -(\bar{q}_1-q_1)\frac{et}{T} +(\bar{u}_1-u_1)\frac{et}{\alpha T} + (\bar{v}_1-v_1)\frac{e}{\alpha T} \\ &- (\bar{p}_2-p_2) + (\bar{q}_2-q_2)\frac{4et}{T} -(\bar{u}_2-u_2)\frac{4et}{\alpha T} -(\bar{v}_2-v_2)\frac{1}{\alpha} \\ &+ (\bar{p}_3-p_3)\frac{3e}{T} + (\bar{q}_3-q_3)\frac{3et}{T} -(\bar{u}_3-u_3)\frac{3et}{\alpha T} + (\bar{v}_3-v_3)\frac{3e}{\alpha T} = 0 \end{aligned} \qquad (6.41)$$

This can also be written as:

$$\sum_{j=1}^{3} (\bar{p}_j-p_j)p_j + (\bar{q}_j-q_j)q_j +(\bar{u}_j-u_j)u_j + (\bar{v}_j-v_j)v_j = 0 \qquad (6.42)$$

when eliminating e,α, t and T from (6.41) by using the constraints (6.31)→(6.34) i.e.

$$\begin{aligned}
p_1 &= -\frac{e}{T}p_2 & p_2 &= p_2 & p_3 &= -\frac{3e}{T}p_2 \\
q_1 &= +\frac{et}{T}p_2 & q_2 &= -\frac{4et}{T}p_2 & q_3 &= -\frac{3et}{T}p_2 \\
u_1 &= -\frac{et}{\alpha T}p_2 & u_2 &= +\frac{4et}{\alpha T}p_2 & u_3 &= +\frac{3et}{\alpha T}p_2 \\
v_1 &= -\frac{e}{\alpha T}p_2 & v_2 &= \frac{p_2}{\alpha} & v_3 &= -\frac{3e}{\alpha T}p_2
\end{aligned} \qquad (6.43)$$

These equations give us harmonic coefficient values in the natural frame (in terms of the barred quantities) but are directly related to the observation determined barred values (proved quantities):

$$\begin{aligned}
\bar{p}_k &= \bar{p}'_k \cos\theta - \bar{u}'_k \sin\theta \\
\bar{q}_k &= \bar{q}'_k \cos\theta - \bar{v}'_k \sin\theta \\
\bar{u}_k &= \bar{p}'_k \sin\theta + \bar{u}'_k \cos\theta \\
\bar{v}_k &= \bar{q}'_k \sin\theta + \bar{v}'_k \cos\theta
\end{aligned} \qquad (6.44)$$

We therefore need the optimum rotation angle, θ, between the two frames of reference. Optimization with respect to θ, by using equation (6.37c), gives:

$$\sum_{j=1}^{3} (p_j u_j - u_j p_j) + (q_j u_j - v_j q_j) = 0 \qquad (6.45)$$

which is similar to the optimum θ equation obtained in the canonical ($e = 0$) model case with addition of third harmonic terms.
On substituting from the constraints (i.e. using (6.43)) we obtain an expression for θ viz:

$$\tan\theta = -A/B$$

where

$$\begin{aligned}
A = {} & et(\bar{p}'_1 + \bar{u}_1\alpha) + e(\bar{q}'_1 - \bar{u}'_1\alpha) - 4et(\bar{p}'_2 + \bar{u}'_2\alpha) \\
& -T(\bar{q}_2 - \bar{u}_2\alpha) - 3et(\bar{p}'_3 - \bar{u}'_3\alpha) + 3e(\bar{q}'_3 - \bar{u}'_3\alpha)
\end{aligned} \qquad (6.46)$$

and

$$B = -e(\bar{p}_1'\alpha + \bar{v}_1') + et(\bar{q}_1'\alpha - \bar{u}_1') + T(\bar{p}_2'\alpha + \bar{v}_2') \\ -4et(\bar{q}_2'\alpha - \bar{u}_2') - 3e(\bar{p}_3'\alpha - \bar{u}_3') - 3et(\bar{q}_3'\alpha - \bar{u}_3') \tag{6.46}$$

This (Equation 6.46) together with (6.42), (6.43) and (6.44) form a complete set by which we determine θ, and the harmonic coefficients for the case of given α, e, λ_p. By this we mean that if we chose α , e and λ_p we can solve the problem completely. To obtain the optimum values of α, e and λ_p we need to form the Lagrange equations (6.37a),b),d) and substitute for the unknown multipliers (λ's)

Optimization w.r.t. gives:

$$-v_1\lambda_1 + u_1\lambda_2 - u_2\lambda_3 + u_2\lambda_4 - u_3\lambda_5 + u_3\lambda_6 = 0 \tag{6.47}$$

which on substituting from (6.40) after some manipulation gives:

$$\sum_{j=1}^{3} (\bar{u}_j - u_j)u_j + (\bar{v}_j - v_j)\, v_j = 0 \tag{6.48}$$

Optimization w.r.t. e gives:

$$\lambda_9 + 3\lambda_{10} = 0 \tag{6.49}$$

On substituting again gives:

$$\sum_{j=1}^{3} (\bar{p}_j - p_j)p_j + (\bar{q}_j - q_j)q_j + (\bar{u}_j - u_j)u_j + (\bar{v}_j - v_j)v_j \\ - (p_2 - p_2)p_2 - (v_2 - v_2)v_2 = 0 \tag{6.50}$$

Similarly for t we obtain:

$$-v_1\lambda_7 + v_3\lambda_8 + p_1 \frac{\partial T}{\partial t} \lambda_9 + p_3 \frac{\partial T}{\partial t} \lambda_{10} = 0 \tag{6.51}$$

where $T = (1 + t^2)^{1/2}$ and $\frac{\partial T}{\partial t} = \frac{t}{T}$

which gives the optimum equation:

$$\frac{\sum_{j=1}^{3} (\bar{q}_j - q_j)q_j + (\bar{u}_j - u_j)u_j}{\sum_{\substack{j=1 \\ j\neq 2}}^{3} (\bar{p}_j - p_j)p_j + (\bar{v}_j - v_j)v_j} = 0 \tag{6.52}$$

Equations (6.42), (6.43), (6.44), (6.46), (6.48), (6.50) and (6.52) from a complete set whereby all the optimum values of the model parameters can be found directly.

Two methods of obtaining the best fit parameters and optimum coefficients are possible. Firstly one may chose i(i, e,α), e and λ_p and run over a 3-D grid of these parameters picking out the minimum value of $\chi^2$and obtaining confidence intervals on all three parameters simultaneously. Alternatively we may use the optimum equations for all the parameters giving us i_{opt}, e_{opt}, $\lambda_{p\ opt}$ and p_{opt} together with the χ^2_{opt} value. It is the former method that we use to obtain best fit parameters to Cygnus X-1 data in Section (6.5).

The model was thoroughly tested using simulated data. This data was formed by using the constraints (6.31) - (6.34) for specific scatterer parameters and the optimization program was used to regain the input parameters successfully. Since the model is an extension of the symmetric canonical model (with more free parameters however) we expect that the presence of data noise will effect the confidence intervals and optimum values in a similar manner to that described in Chapter 3.

It should be noted here that an alternative approach to the problem of optimization of model (eccentric) and data is apparent. We want to minimize the function

$$F = \sum_{j=1}^{N} (Q_{ob,r} - Q_{t,r})^2 + (U_{ob,r} - U_{t,r})^2 \qquad (6.53)$$

with respect to the constraints (6.31) - (6.34). We know from these constraints that the relations (6.43) hold between the 1st, 2nd and 3rd harmonic coefficients and p_2 (for example. It is therefore possible to directly substitute these relations into the equation minimizing F subject to p_2 i.e.

$$\frac{\partial F}{\partial p_2} = 0 = \sum_{j=1}^{N} \left[2(Q_{ob,r} - Q_{t,r}) \frac{\partial Q_{t,r}}{\partial p_2} + 2(U_{ob,r} - U_{t,r}) \frac{\partial U_{t,r}}{\partial p_2} \right] \qquad (6.54)$$

Now $Q_{t,r} = \sum_{j=1}^{3} p_j \cos r j \beta + q_j \sin r j \beta$

and $U_{t,r} = \sum_{j=1}^{3} u_j \cos r j \beta + v_j \sin r j \beta$

where $\beta = 2\pi/N$.

We substitute directly for p_1, q_1, u_1, v_1 etc.in terms of p_2 and from the derivatives $\frac{\partial Q_{t,r}}{\partial p_2}$ and $\frac{\partial Q_{t,r}}{\partial p_2}$ i.e.

$$Q_{t,r} = p_2 \left(-\frac{e}{T} \cos r\beta + \cos 2r\beta - \frac{3e}{T} \cos 3r\beta \right.$$

$$\left. + \frac{et}{T} \sin r\beta - \frac{4et}{T} \sin 2r\beta - \frac{3et}{T} \sin 3r\beta \right) = xp_2 \qquad (6.55)$$

and $\frac{\partial Q_{t,r}}{\partial p_2} = x$

similarly for $U_{t,r}$. Substituting this into (6.54) and using the orthogonality relations:

$$\sum_{j=1}^{N} \cos m\lambda \cos n\lambda = 0 \qquad m \neq n$$

$$= N/2 \qquad m = n \quad \text{but } n \neq o,N$$

$$= N \qquad m = n = 0 \qquad (6.56)$$

and $\sum_{j=1}^{N} \sin m\lambda \cos n\lambda = 0$ etc.

we obtain the barred quantities (6.44) and hence after some manipulation:

$$p_2 = -\left[(\bar{p}_1'\alpha + \bar{v}_1')e + (\bar{p}_2'\alpha + \bar{v}_2')T - (\bar{p}_3'\alpha + \bar{v}_3')\, 3e \right.$$

$$\left. - (\bar{q}_1'\alpha - \bar{u}_1')\, et + (\bar{q}_2'\alpha - \bar{u}_2')\, 4et + (\bar{q}_3'\alpha - \bar{u}_3')\, 3et \right] \Big/ \frac{(1+\alpha^2)}{\alpha} T \qquad (6.57)$$

which with the constraints (6.31) → (6.34) gives us the optimum harmonic coefficients.

We now proceed to apply the model optimization to Cygnus X-1 data of Kemp et al (1979) in an attempt to reduce (or otherwise) the confidence intervals on the optimum inclination value found from the canonical model (corotating e = 0 case).

6.5 Cygnus X-1 - Application of the Eccentric Model.

The nature of the orbit of this peculiar X-ray binary system has been subject to numerous discussions, the most comprehensive of which was by Bolton (1975) and Bachall (1975). Like many binaries, this system shows frequent deviations from its mean periodic spectroscopic and photometric behaviour (Hutchings 1978) so that it takes long periods of time to reduce the noise in the data (if one assumes this is of a random nature). The value of eccentricity of the orbit of Cygnus X-1 is like taking other parameters subject to controversy. Bolton (1975) found an $e \sim 0.06$ and $\lambda_p \sim 330^\circ$ from detailed spectroscopic observations. Since only the primary star is visible the elements of the orbit are derived from its spectroscopic behaviour but possible complications are numerous and not fully understood. The primary star is probably tidally distorted (cf. photometric light curve variations - Lester et al (1973), Lester et al (1976), Petrov (1976), Walker and Quintinella (1977), Hilditch and Hill (1974) and Gunan et al 1978) and is losing mass by any or all of Roche lobe overflow, stellar wind and evaporation by X-ray heating. Optical line and continuum features may arise in the accreting material (disk, stream or wake) and to some extent should contribute to the velocity field and distort the orbital velocity behaviour of the spectral lines. This would make precise diagnosis of an eccentric orbit complicated.

Several attempts at modelling such effects have been made (Wilson and Sofia 1976, van Paradijs, Takens and Zwuderwijk 1978, Hutchings 1977). A contribution of several distorting effects however would make the possibility of applying the relevant corrections remote. Hutchings (1978) calculated a weighted mean light curve of several authors (mentioned above) and obtained an eccentricity $e \sim 0.04$ and $\lambda_p \sim 330^\circ$ assuming an orbital inclination of $i \sim 60^\circ$. Unequal maxima in the light curves indicate the possible presence of an eccentric orbit while in spectroscopy the deviation of the radial velocity curve from a sine-like form indicates the same.

These problems only accentuate the necessity for independent confirmation (or not) of these estimates. We attempt this by applying

the eccentric model herein described and run over a 3-dimensional grid of the model parameters e, λ_p and i. Due to the earlier small e approximation we only consider e values within the range $0 \lesssim 0 \lesssim 0.3$ with steps of $\Delta_e \sim 0.005$. The longitude of periastron, λ_p is given the range 0, 300^o in steps of $\Delta\lambda_p \sim 10^o$. The inclination i run over the range 0^o to 180^o in steps of $\Delta i \sim 1^o$. Two results of interest indicate that:

(a) At the Bolton (1975) e = 0.06 and $\lambda_p = 330^o$ the optimum inclination was $i_{opt} = 61^o$ with a χ^2 best fit $\sim$ 27 5 (with $\sigma_{bin} = 0.0341\%$). This means that at 10% significance the eccentric model (with 80 degrees of freedom) is unacceptable. This was also true at 25% significance. (75% confidence).

(b) An optimum eccentricity (one with the lowest χ^2 value) of $e_{opt} = 0.14$ and $\lambda_{o,opt} = 140^o$ at $i_{opt} = 53^o$ was found but the χ^2 level of 259 was again unacceptable at both 10% and 25% significance. The $\chi^2_{10\%,80}$ level was in fact $\sim$ 96.6 and the 25% level was 88.1, meaning that the optimum fit is wildly at variance with the data. The minimum in χ^2 was seen to be shallow with a large number of possible e and λ_p combinations producing χ^2 values around the 260 level but all have to be rejected.

6.6 Discussion of the model and conclusions

The simple model presented here for polarimetric variations from a binary system with an eccentric orbit predicts the addition of 1st and 3rd harmonics to the dominant 2nd harmonics of the e = 0 symmetric canonical model. This should enable an unambiguous interpretation of observational data provided that the errors in the data are of a satisfactory level. It is possible to obtain optimum values of the eccentricity, longitude of perihelion and inclinations by application of this model using equations (6.42), (6.43), (6.44), (6.46), (6.48), (6.50) and (6.52) for a complete solution. Two methods of use of the optimizing technique described by (a) running over a 3-D grid of parameters e, λ_p and i and (b) obtaining the optimum values of the parameters e_{opt}, $_{p,opt}$, i_{opt}, p_{opt} are available

The results of the application of this model to Cygnus X-1 data indicate that the behaviour and nature of the scattering region is not

The results of the application of this model to Cygnus X-1 data indicate that the behaviour and nature of the scattering region is not of the simple form considered in the eccentric model and produces polarization variations that are not consistent with the model. It remains to be seen whether the eccentric model will improve the fit of the general canonical model for any other data set.

Finally we emphasize that in the present analysis we have neglected any physical effects of orbital eccentricity on the scattering region. Little work has been done on the effect of eccentricity on accretion processes and rates in close binaries, partly on the grounds that eccentricities in such systems are small. However, high e values and their effect on mass transfer have been invoked in interpreting some systems (Haynes et al 1980) and it is in any case not clear that even a very small eccentricity cannot have an important effect on the transfer of mass (Bailey 1971, 1972). On the other hand the typical mass of an accretion disk is much greater than the mass transfer per orbital period, suggesting that even large modulations of the latter (due to eccentricity) cannot affect the scattered light from the disk significantly unless only a small part of the disk or only the matter in transit between the stars contributes much to the polarised scattered light (c.f. Kemp 1980). This topic is being investigated at the moment. Should the physical effects of eccentricity on the scattering region prove important some of our present conclusions may have to be revised.

We conclude this Chapter with a brief survey of spectroscopic binaries indicating possible candidates to test the eccentric models polarimetric predictions (i.e. those systems with significant orbital eccentricity).

6.7 Candidate polarimetric Binaries for testing of the Eccentric Model

A survey of the Dominion Astrophysical Observatory spectroscopic binary catalogue (Batten 1975) was undertaken in an attempt to find suitable binaries for observation and subsequent modelling in terms of the eccentric orbit model. Some 737 spectroscopic binaries were included in the catalogue (excluding the extended sections) with orbital periods (P) ranging from fractions of days (VV Puppis:P $\sim 0.07^{d}$)

A suitable candidate system was defined for our purposes as one which had an orbital period between 1 and 20 days with apparent magnitude brighter than ∿ 8th mag. These two conditions are imposed because orbital periods shorter than 1 day create problems when integrating or observating for any length of time i.e. significant variations may well occur within one integration period to invalidate the results. Orbital periods greater than about 20 days mean that the stars in the system would have a reasonable separation and hence the mass transfer/loss may not be of a sufficient level to ~~attain~~ create observable polarization effects. Also restrictions on possible observing time would mean that only a fraction of the period would be covered at any one time making analysis complicated, if evolution effects in the scattering region and modulated accretion were present in the system.

Further, stars fainter than ∿ 8th magnitude would require substantial integration periods to obtain accurate polarization measurements (since in general variable polarization in binaries has an amplitude < .5%). Table I lists the 49 possible binaries with elements in this range.

Many of the systems shown above are southern hemisphere objects. Those systems in the northern hemisphere most suitable for study are:

	R.A. hr	R.A. mm	Dec	Ref.
δ^2 UMaj	13	19.9	55° 27'	Fehrenbach & Prevet (1901)
HD 131041	14	46.3	49° 07'	Harper (1922)
HD 169981	18	22.1	29° 46'	Young (1919)
HD 185912	19	36.4	54° 44'	Harper (1919)
HD 224355	23	54.2	6° 19'	Beardsley (1965)
HD 2421	0	22.9	43° 51'	Udick (1912)
γ And B	01	57.8	41° 51'	Maestone (1960)
HD 18778	02	56.2	81° 05'	Abt (1961)
57 Ori	05	49.1	19° 44'	Pearce (1932)
α^2 Gem	07	28.2	32° 06'	Vinter & Hansen (1940)
HD 107325	12	15.3	27° 11'	Fehrenbach (1948)

Interesting southern hemisphere objects include

ζ^2 Cen	13	49.3	-46° 48'	Popper (1942)
β Cap	20	15.4	-15° 06'	Sanford (1939)

STAR	PERIOD	SP.TYPE	ECC	APP.MAG.
HD2421	3.956	A2	.152	5.09
U CEP	2.493	B8	.15	7.0
HD3264	13.504	A0	.507	7.42
HD8634	5.429	F4	.378	6.00
γAND B	2.67	2B9.5	.292	5.08
HD17581	8.25	A1	.227	6.38
HD18778	11.665	AM	.29	5.95
19τ⁵ERI	6.223	B8N	.2	4.28
RW TAU	2.769	A0+G	.293	8.0
HD25799	10.67	B3V	.2	6.87
μERI	7.33	B5IV	.39	4.02
57 ORI	7.827	B3K+B5	.25	5.86
2 MON	9.355	A5	.208	5.02
HD56310	2.770	B3	.21	6.79
α²GEM	9.213	A2	.499	1.99
HD65041	2.826	B3	.30	7.04
ε HYA C	9.905	F5	.62	7.5
HD88512	3.242	A3	.07	6.63
ε VEL	10.210	2F3.5	.56	3.84
HD100018	7.399	F2	.38	6.99
HD107325	0.491	K0	.30	5.47
24 CAM	7.337	F0	.21	6.72
UY VIR	1.995	A7V	.3	8.0
ζ²CEN	7.650	B3	.35	4.26
ζ²UMA	20.539	A2V	.54	2.27
1 CEN	9.945	F5	.25	4.23
ζ CEN	8.024	B2	.5	2.54
HD131041	12.822	F5	.39	5.6
βSCO	6.828	B0.5	.28	2.63
HD144426	8.855	A2	.38	6.11
0 HER	4.951	A0	.51	5.76
HD152270	8.82	WC6	.24	6.61
HD152830	11.848	F2	.31	6.09
HD158013	8.216	A2	.33	6.55
40 DRA	10.522	F5	.31	6.05
HD169981	9.612	A2	.47	5.83
HD174369	13.081	A2N	.39	6.53
DI HER	10.550	B5+B4	.37	8.0
HD181470	10.393	A0	.52	6.16
HD188164	7.638	A2V+A	.53	6.38
HD191201	8.334	2O9.5	.26	7.12
βCAP	8.678	B8	.36	3.08
αOCT	9.073	F4III	.39	5.14
14 PEG	5.305	A0	.53	4.98
HD214240	10.911	B2.5	.25	6.25
HD218407	3.337	B3	.27	6.06
HD218440	7.251	B3K	.38	6.26
HD224355	12.155	2F5	.28	5.62
28 ω PSC	2.158	F4IV	.35	4.01

TABLE I.

both are relatively bright objects ($m_v \sim 2.54$ and 3.08 respectively) with satisfactory periods ($p \sim 0.5$ and 0.36 respectively). It remains to be seen whether any of these binaries display intrinsic variable linear polarization at all.

CHAPTER 7 ACCRETION DISK AND WAKE MODELS

7·1 Introduction

The existence of accretion disks around secondary components in both 'normal' type and 'compact' type binary systems has been proposed many times in the last decade as explaining observed variations (both optical and X-ray, photometric, spectroscopic and polarimetric). Gas leaving the 'primary' star due to Roche lobe overflow, or a strong stellar wind, was thought to have too large an angular momentum to accrete directly onto the secondary. A ring or disk of material is thought to form enabling viscous dissipation of this angular momentum (Prendergast and Burbidge (1968), Rees 1972). Such disks would provide suitable scattering regions for light and hence, due to the orbital motion of the binary and hence the varying scattering angles, cause variability in the linear polarization of the integrated light of the system. A comprehensive discussion of the accretion processes involving disks was given by Aspin (1978).

Accretion wakes were also invoked in explanations of features in X-ray observations as being likely candidates for observation/occultation of the X-ray flux. Davidson and Ostriker (1973) and Pringle (1973) proposed models of the X-ray binary Cen X-3 involving an accretion wake while Jackson (1975) incorporated this idea in his interpretation of the dips in the light curve of the same system. An accretion wake can be the result of accreting by a compact object from a strong stellar wind. Gas streaming passed the compact object secondary (e.g. neutron star) forms a shock wave as in Figure (7·1). Gas is then accreted from behind the neutron star in a density enhanced tail called an accretion wake. Jackson (1975) considers the problems of calculating the accretion flow for a system similar to Cen X-3 and claims that the model used (cf. Figure 7·1) does not demand implausible values for any parameter of the calculation. The case therefore of calculating analytically and numerically the polarization variations expected from an accretion phenomena such as disks and wakes is backed strongly by previous theoretical models and observations. In this Chapter we consider this problem of polarimetric model parameters for disk and wake type envelopes. The exact geometric arrangement of the gaseous material is seen, from previous work, to indicate orbital plane symmetry of the disk/wake (Jackson 1975, Davidson and Ostriker (1973). Certain models

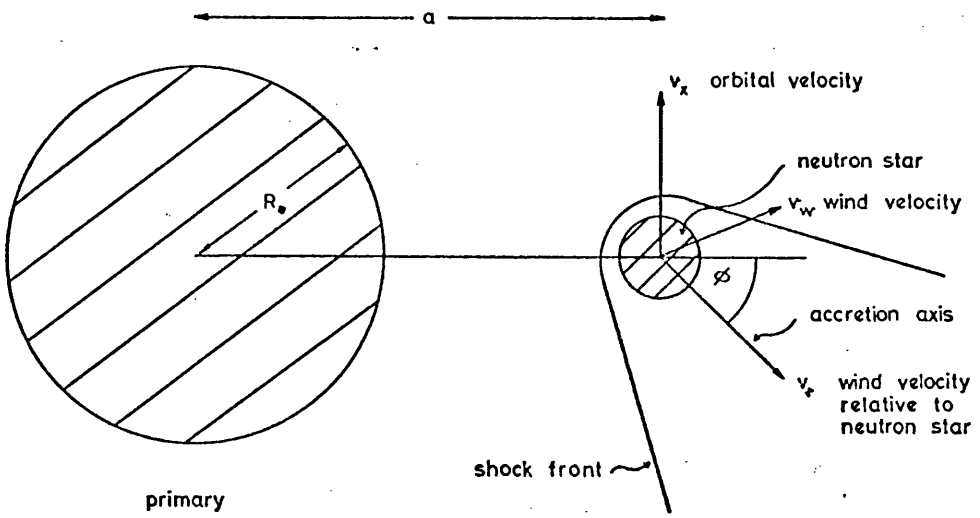

FIGURE 7.1

Schematic representation of the accretion of gas by a neutron star from a primary 'normal' type star via. an accretion wake formed behind the shock front.

of Her X-1 have postulated a twisted, precessing accretion disk but are related only to that particular system and do not concern us here (cf. Katz 1973, Roberts 1979, Pettersen 1975). We therefore make the simplifying assumption that the disk/wake is symmetric about and near to the orbital plane of the system and hence will only contribute second harmonic structure to the polarization (i.e. periodic at half the binary period).

7·2 Analytic form of the Q,U variations

From the analysis of Brown et al (1978) we have, under the above assumption that the Stokes parameters are given by

$$Q(\lambda) = -\tau_o \left| (1 + \cos^2 i)(\gamma_3 \cos 2\lambda - \gamma_4 \sin 2\lambda) \right|$$
$$U(\lambda) = -2\tau_o \left| \cos i(\gamma_3 \sin 2\lambda + \gamma_4 \cos 2\lambda) \right| \qquad (7\cdot1)$$

where

$$\tau_o \gamma_3 = \iiint n \sin^2\theta \cos 2\Phi \, dr \sin\theta \, d\theta \, d\Phi$$
$$\text{and } \tau_o \gamma_4 = \iiint n \sin^2\theta \sin 2\Phi \, dr \sin\theta \, d\theta \, d\Phi \qquad (7\cdot2)$$

for one light source with the constant term being dropped. The integral limits are $(0,\infty)$, $(0,\pi)$, $(0, 2\pi)$ and $n = n(R,\theta,\Phi)$. These integrals are a set of mean optical depths obtained by weighting integration over solid angle (cf. Chapter 2). Now we set up the geometry as in Figure (7·2) where the plane of the page is the orbital plane of the binary. S1 is the light source (point source approximation of primary star), S2 is the compact secondary (neutron star, black hole) and the circle (D) in (7·2a) is the accretion disk. Wake geometry can be similarly considered (Figure 7·2b) by considering the wake as a sector of a disk (ω). An element of the envelope is specified in the two coordinate system (R,Θ,Φ) centred on the light source and (r,θ,ϕ) centred on the compact secondary (i.e. centre of the disk) by (R,Φ) or (r,ϕ) since the disk can be considered to be planar (i.e. in the plane of the orbit) and hence

$$\Theta = \frac{\pi}{2} \quad ; \quad \theta = \frac{\pi}{2} \qquad (7\cdot3)$$

and hence $$n \, dR \, d\Theta \, d\Phi \rightarrow \alpha(R,\Phi) dR \, d\Phi \qquad (7\cdot4)$$

where $\alpha(R,\Phi)$ is the accretion disk/wake surface density distribution in the coordinates centred on the primary star.

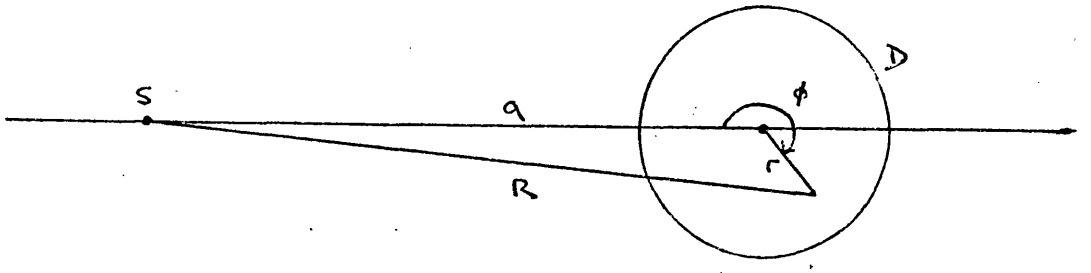

FIGURE 7.2a

Schematic representation of the geometry of the accretion disk calculation.

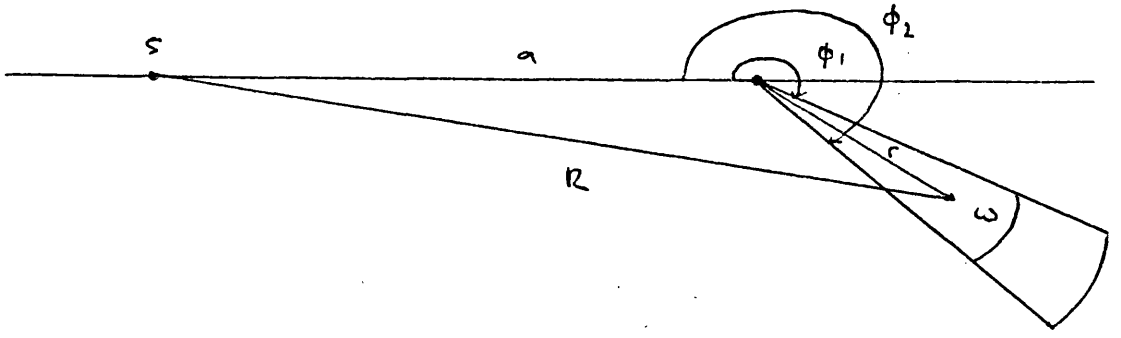

FIGURE 7.2b

Schematic representation of the geometry of the accretion wake calculation.

In both diagrams S is the point light source, a is the semi-major axis of the orbit (circular)

We transform the coordinates $(R, \Phi) \rightarrow (r, \phi)$ since α is expressed in coordinates centred on the secondary star and hence on integration will also be centred on that star. We therefore need the Jacobian of the coordinate transformation. This is defined as

$$J(R,\Phi/r,\phi) = \partial(R,\Phi)/\partial(r,\phi) = \left.\frac{\partial R}{\partial r}\right|_{\phi}\left.\frac{\partial \Phi}{\partial \phi}\right|_{r} - \left.\frac{\partial R}{\partial \phi}\right|_{r}\left.\frac{\partial \Phi}{\partial r}\right|_{\phi} \qquad (7\cdot5)$$

(cf. Margenau and Murphy 1956).

The Jacobian for the transformation, in fact is a simple function i.e.

$$J(R,\Phi/r,\phi) = r/R \qquad (7\cdot6)$$

therefore

$$\frac{dR}{R}\, d\Phi = \frac{r}{R^2}\, dr\, d\phi \qquad (7\cdot7)$$

and

$$R^2 = r^2 + a^2 - 2ar\cos\phi \qquad (7\cdot8)$$

from Figure (7·2) where a is the semimajor axis of the orbit (i.e. the separation of the stars). We therefore need to evaluate the functions:

$$\tau_o = \frac{\sigma_o}{2}\int_o^r \int_{\phi_1}^{\phi_2} \alpha(r)\,\frac{r}{R}\, dr\, d\phi \qquad a)$$

$$\tau_o \gamma_3 = \frac{\sigma_o}{2}\int_o^r \int_{\phi_1}^{\phi_2} \alpha(r) r\, dr\, d\phi \cos\frac{2\Phi}{R} \qquad b) \qquad (7\cdot9)$$

$$\tau_o \gamma_4 = \frac{\sigma_o}{2}\int_o^r \int_{\phi_1}^{\phi_2} \alpha(r) r\, dr\, d\phi \sin\frac{2\Phi}{R} \qquad c)$$

where σ_o is related to the scattering cross-section and the limits (ϕ_1, ϕ_2) define the disk ($\phi_1 = 0^o$, $\phi_2 = 180^o$) or wake ($\phi_1 = 290^o$, $\phi_2 = 320^o$ for example), and hence substitute their values into Equation (7·1).

We therefore integrate out the ϕ dependence first and (retrospectively) have to numerically integrate the r dependence due to the complexity of the resulting function.

We first consider Equation (7·9a)

$$\tau_o = \frac{\sigma_o}{2} \int_o^r \int_\phi^{\phi_2} \frac{\alpha(r)\, r\, dr\, d\phi}{(a^2 + r^2 - 2ar\cos\phi)} \qquad (7\cdot10)$$

Let $X = \dfrac{a^2 + r^2}{2ar}$ and $m^2 = \dfrac{X-1}{X+1}$

$$\therefore \quad \tau_o = \frac{\sigma_o}{4a} \int_o^r \alpha(r) \int_{\phi_1}^{\phi_2} \frac{d\phi}{(X - \cos\phi)}\, dr \qquad (7\cdot11)$$

Now using the half angle theorem:

$$u = \tan\phi/2 \; ; \quad \cos\phi = \frac{1-u^2}{1+u^2} \; ; \quad d\phi = \frac{2du}{(1+u^2)} \qquad (7\cdot12)$$

we obtain

$$\tau_o = \frac{\sigma_o}{2a} \int_o^r \frac{\alpha(r)}{(1+X)} \int_{\phi_1}^{\phi_2} \frac{du\ dr}{(m^2 + u^2)} \qquad \text{a)}$$

$$= \frac{\sigma_o}{2a} \int_o^r \frac{\alpha(r)}{(1+X)} \frac{1}{m} \tan^{-1}\left(\frac{u}{m}\right) \Big|_{\phi_1}^{\phi_2} dr \qquad \text{b)} \qquad (7\cdot13)$$

Now for $\tau_o \gamma_3$ we have Equation (7·9b).
From Figure (7·2) we see that:

$$\frac{\sin\Phi}{r} = \frac{\sin(2\pi - \phi)}{R} \qquad (7\cdot14)$$

$$\therefore \quad \sin\Phi = \frac{-r}{R}\sin\phi$$

and since we want to express the cos 2Φ term in (7·9b) in terms of (r, ϕ) we have:

$$\cos 2\Phi = 1 - 2\sin^2\Phi = \frac{R^2 - 2r^2\sin^2\phi}{R^2} \qquad (7\cdot15)$$

and therefore it follows that

$$\cos 2\Phi = (a^2 - 2ar\cos\phi + r^2\cos 2\phi)\,/\,R^2 \qquad (7\cdot16)$$

after trivial manipulation.

Therefore we can split (7·9b) into three parts A, B and C where

$$\tau_o \gamma_3 = \tau_o \gamma_3\,(A) + \tau_o \gamma_3\,(B) + \tau_o \gamma_3\,(C)$$

and

$$\tau_o \gamma_3(A) = \frac{\sigma_o}{2} a^2 \int_o^r \int_{\phi_1}^{\phi_2} \frac{\alpha(r) r}{(a^2 + r^2 - 2ar\cos\phi)^2}\, dr\, d\phi \qquad (7\cdot17)$$

$$\tau_o \gamma_3(B) = -\frac{\sigma_o}{2} \int_o^r 2a \int_{\phi_1}^{\phi_2} \frac{\alpha(r) \cos\phi \, r \, dr \, d\phi}{(a^2 + r^2 - 2ar\cos\phi)^2} \quad (7.18)$$

$$\tau_o \gamma_3(C) = +\frac{\sigma_o}{2} \int_o^r \int_{\phi_1}^{\phi_2} \frac{\alpha(r) \, r^2 \cos 2\phi \, dr \, d\phi}{(a^2 + r^2 - 2ar\cos\phi)} \quad (7.19)$$

Considering Equation (7.17) we have, with a similar substitution as in (7.11)

$$\tau_o \gamma_3(A) = \frac{\sigma_o}{4} \int_o^r \frac{\alpha(r)}{r} \int_{\phi_1}^{\phi_2} \frac{(1+u^2)}{(m^2 + u^2)^2} \frac{1}{(1+X)^2} du \, dr \quad (7.20)$$

which is

$$= \frac{\sigma_o}{4} \int_o^r \frac{\alpha(r)}{(1+X^2)r} dr \left[\int_{\phi_1}^{\phi_2} \frac{du}{(m^2 + u^2)^2} + \int_{\phi_1}^{\phi_2} \frac{u^2 \, du}{(m^2+ u^2)^2} \right] \quad (7.21)$$

using the standard separation technique (cf. 2·173 - Gradshteyn and Ryzhik (1963) we find:

$$\int_{\phi_1}^{\phi_2} \frac{du}{(m^2 + u^2)^2} = \left[\frac{u}{2m^2(m^2+ u^2)} + \frac{1}{2m^3} \tan^{-1}\left(\frac{u}{m}\right) \right] \quad (7.22)$$

and using 2.17 of

$$\int_{\phi_1}^{\phi_2} \frac{u^2 \, du}{(m^2+ u^2)^2} = \left[\frac{u}{2(m^2- u^2)} + \frac{1}{2m} \tan^{-1}\left(\frac{u}{m}\right) \right] \quad (7.23)$$

the total solution becomes:

$$\tau_o\gamma_3(A) = \frac{\sigma_o}{8} \int_o^r \frac{\alpha(r)}{(X+1)\, r} \left\{ \frac{1}{m^2} \left(\tan^{-1}\left(\frac{u}{m}\right)(1+m^2) + \frac{u}{(m^2+ u^2)} \right) \frac{(1-m^2)}{m} \right\} dr \quad (7.24)$$

where $X = \frac{a^2+ r^2}{2ar}$ and $m = \frac{X-1}{X+1}$.

Similarly for Equation (7.18) after substitution by half angles:

$$\cos\phi = \frac{1-u^2}{1+u^2} \qquad d\phi = \frac{2du}{(1+u^2)} \; ; \quad X = \frac{a^2+r^2}{2ar} \; ; \quad m = \frac{X-1}{X+1}$$

we have:

$$\tau_o\gamma_3 = -\frac{\sigma_o}{2a} \int_o^r \frac{\alpha(r)}{(X+1)^2 r} \left[\int_{\phi_1}^{\phi_2} \frac{(1-u^2)\,du}{(m^2+u^2)^2} \right] dr \qquad (7.25)$$

which yields;

$$\tau_o\gamma_3 = -\frac{\sigma_o}{4a} \int_o^r \frac{\alpha(r)}{(X+1)^2 r^2 m} \left[\frac{(1-m^2)}{m^2} \tan^{-1}\left(\frac{u}{m}\right) + \frac{(1+m^2)u}{m(m^2+u^2)} \right] \qquad (7.26)$$

Equation (7.19) for $\tau_o\gamma_3$ (C) is more complex due to the cos 2 dependence but simplifying by expansion and substitution i.e.:

$\cos 2\phi = \cos^2\phi - \sin^2\phi$ and using the half angle theorem we obtain

$$\cos 2\phi = \frac{u^4 - 6u^2 + 1}{(1+u^2)^2}$$

$\therefore$ (7.19c) becomes:

$$\tau_o\gamma_3(C) = \frac{\sigma_o}{2a} \int_o^r \frac{\alpha(r)}{(1+X)^2} \int_{\phi_1}^{\phi_2} \frac{(u^4 - 6u^2 + 1)}{(m^2+u^2)(1+u^2)}\, du\, dr \qquad (7.27)$$

we now use partial fractions to simplify this expression viz:

$$\frac{u^4 - 6u^2 + 1}{(m^2+u^2)^2(1+u^2)} = \frac{Au + B}{(m^2+u^2)^2} + \frac{Cu + D}{(m^2+u^2)} + \frac{Eu + F}{(1+u^2)} \qquad (7.28)$$

Solving for the coefficients A, B, C, D, E, and F we obtain $A=C=E=0$;
$B = (1 + 6m^2 + m^4)/(1 - m^2)^2$ $D = (m^4 - 2m^2 - 7)/(1 - m^2)$ and $F = 8/(1-m^2)^2$.

This gives us, for the integration:

$$\int_{\phi_1}^{\phi_2} \left\{ \frac{(m^4+6m^2-1)}{(m^2-1)^2(m^2+u^2)^2} + \frac{(m^4-2m^2-7)}{(m^2-1)^2(m^2+u^2)} + \frac{8}{(m^2-1)^2(1+u^2)} \right\} du \qquad (7.29)$$

which when integrated out gives:

$$\tau_o\gamma_3(C) = \frac{\sigma_o}{8a^2}\int_o^r \frac{\alpha(r)}{(1+X)^2}\left\{\frac{(m^4+6m^2-1)u}{m^2(m^2+u^2)} - \tan^{-1}\left(\frac{u}{m}\right)\left[\frac{(m^4+6m^2-1)}{m^3} + \frac{(2m^4-4m^2-14)}{m}\right] - 16\tan^{-1}(u)\right\} dr \qquad (7.30)$$

$$\therefore \quad \tau_o\gamma_3 = \tau_o\gamma_3(A) + \tau_o\gamma_3(B) + \tau_o\gamma_3(C)$$

Considering Equation (7.9c) we see that we need to express $\sin 2\phi$ in terms of (r,ϕ). This by similar manipulation as in the case of $\cos 2\Phi$ gives

$$\sin 2\Phi = (2ar\sin\phi - r^2\sin 2\phi) \qquad (7.31)$$

and (7.9c) therefore can be divided into two parts

$$\tau_o\gamma_4(A) = \sigma_o a \int_o^r \int_{\phi_1}^{\phi_2} \frac{\alpha(r)\, r^2 \sin\phi \, dr d\phi}{(a^2 + r^2 - 2ar\cos\phi)^2} \qquad (7.32)$$

and

$$\tau_o\gamma_4(B) = \frac{\sigma_o}{2} \int_o^r \int_{\phi_1}^{\phi_2} \frac{r^2 \sin 2\phi \, dr \, d\phi}{(a^2+r^2-2ar\cos\phi)^2} \qquad (7.33)$$

Considering (7.32) we have after substitution in terms of half angles:

$$\tau_o\gamma_4(A) = \frac{\sigma_o}{a} \int_o^r \frac{\alpha(r)}{(X+1)^2}\int_{\phi_1}^{\phi_2}\left[\frac{u\,du}{(m^2+u^2)^2}dr\right] \qquad (7.34)$$

Using Equation (2.175) of Gradshteyn and Ryzhik (1963) we obtain:

$$\tau_o\gamma_4(A) = -\frac{\sigma_o}{2a}\int_o^r \frac{\alpha(r)}{(X+1)^2}\,\frac{1}{(m^2+u^2)}\int_{\phi_1}^{\phi_2} dr \qquad (7.35)$$

$\tau_o\gamma_4(B)$ after similar manipulation gives

$$\frac{\sigma_o}{a^2}\int_o^r \frac{\alpha(r)}{(X+1)^2}\int_{\phi_1}^{\phi_2}\frac{u(1-u^2)}{(1+u^2)(m^2+u^2)^2}\,du\,dr \qquad (7.36)$$

Using the partial fraction technique we obtain:

$$\tau_o\gamma_4(B) = \frac{2\sigma_o}{a^2}\int_o^r \frac{\alpha(r)}{(X+1)^2(m^2-1)^2}\left[\frac{(m^2+1)(m^2-1)}{4(m^2+u^2)} + \log\left(\frac{1+u^2}{m^2+u^2}\right)\right]_{\phi_1}^{\phi_2} dr \qquad (7.37)$$

Therefore the three integrals are:

$$\tau_o = \frac{\sigma_o}{2a}\int_o^r \frac{\alpha(r)}{(1+X)m}\tan^{-1}\left(\frac{u}{m}\right)\Bigg|_{\phi_1}^{\phi_2} dr \qquad (7.38)$$

$$\tau_o\gamma_3 = \frac{\sigma_o}{8}\int_o^r \frac{\alpha(r)}{(1+X)^2mr}\left\{\frac{1}{m^2}\tan^{-1}\left(\frac{u}{m}\right)(1+m^2) + \frac{u(1-m^2)}{m(m^2+u^2)}\right\}\Bigg|_{\phi_1}^{\phi_2} dr$$

$$- \frac{\sigma_o}{4a}\int_o^r \frac{\alpha(r)}{(X+1)^2r^2m}\left\{\frac{(1-m^2)}{m^2}\tan^{-1}\left(\frac{u}{m}\right) + \frac{u(1+m^2)}{m(m^2+u^2)}\right\}\Bigg|_{\phi_1}^{\phi_2} dr$$

$$+ \frac{\sigma_o}{8a^2}\int_o^r \frac{\alpha(r)}{(X+1)^2}\left\{\frac{u}{m}\frac{(m^4+6m^2-1)}{(m^2+u^2)} - \tan^{-1}\left(\frac{u}{m}\right)\frac{(m^4+6m^2+1)}{m^3}\right.$$

$$\left. - \tan^{-1}\left(\frac{u}{m}\right)\frac{(2m^4-4m^2-14)}{m}\,dr\right.$$

$$\left. - 16\tan^{-1}(u)\right\} dr \qquad (7.39)$$

$$\tau_o\gamma_4 = \frac{\sigma_o}{a}\int_o^r \frac{\alpha(r)}{(X+1)^2}\frac{1}{m^2+u^2}\Bigg|_{\phi_1}^{\phi_2} dr$$

$$+ \frac{2\sigma_o}{a}\int_o^r \frac{\alpha(r)}{(X+1)^2(m^2-1)^2}\left\{\frac{(m^2+1)(m^2-1)}{4(u^2+m^2)} + \log\left[\frac{1+u^2}{m^2+u^2}\right]\right\} dr \qquad (7.40)$$

These Equations (7.38, 7.39, 7.40) combined with Equation (7.1) give $Q(\lambda)$ and $U(\lambda)$ for the accretion disk/wake model geometry.

In reality the (Q,U) locus will never be more than an ellipse since only second harmonics are involved

7.3 Discussion and comments on the numerical integration

To specify disk or wake it is necessary to change the limits of the ϕ integration. For a disk $\phi_1 = 0^\circ$ and $\phi_2 = 180^\circ$. Since the geometry is symmetrical about the line of centres of the stars, integration is only necessary over half the disk with the result being multiplied by a factor 2.

For an accretion wake it is necessary to specify the angular extent of the wake by ϕ_1, ϕ_2 as in Figure (7.2b) where $\phi_1 \sim 290^\circ$ and $\phi_2 = 320^\circ$. A consideration of different (ϕ_1, ϕ_2) will give a wake in any position relative to the line joining the star.

To proceed further with the integration requires the use of a computer to numerically integrate the equations (7.38),(7.39 and (7.40). A program for this was developed for both a PET microcomputer and the 2976 Glasgow University computer system involving the use of a Simpsons rule integration. The number of integration steps necessary to produce values of τ_o, $\tau_o\gamma_3$, $\tau_o\gamma_4$ accurate to three decimal places was of the order 200. Due to the simple elliptical nature of the (Q,U) loci for all wake/disk dimensions we do not give any numerical results (i.e. values of τ_o, $\tau_o\gamma_3$ and $\tau_o\gamma_4$) for disk sizes specified by ξ and η in Figure (7.1a) or accretion wakes defined by ϕ_1, ϕ_2 and ξ, η .

Typical radial dimensions considered numerically for both disk/wakes were approximately 0.1a to 0.6a (a = binary separation)

It is also possible to specify the radial density distribution of material in the disk or wake by the factor $\alpha(r)$. Numerically results are not given due to the same reason as above. A typical $\alpha(r) \sim 1$ and $\sim r^{-3/2}$ (for disks/wakes respectively) radial density distribution were considered since these are the forms of the density decrease along the disks/wakes estimated by Jackson (1975) for Cen X-3. It is however possible to incorporate any other function $\alpha(r)$ in the calculations.

One final point to note is that a narrow wake with constant $\alpha(r)$ (i.e. independent of r and with $\phi_1 = 0$ and $\phi_2 = 10^\circ$ say with the results they multiplied by (2) would approximate to a gas stream between the two components. A combination of gas geometries can also be treated by simple summation of the Stokes parameters after calculation.

CHAPTER 8: GENERALIZATION OF THE CANONICAL MODEL OPTIMIZATION PROCEDURE FOR DATA AT UNEQUAL PHASE INTERVALS

8•1 Introduction

In Chapter 2 we developed a technique of minimizing the statistic χ^2 , with respect to a set of model parameters that satisfied a number of constraints imposed by the canonical model to establish confidence regions for these parameters. Throughout, it was implicitly assumed that polarimetric observations were at equal phase intervals. To this end raw observations were phase binned. The method of optimization was thus simplified. Furthermore since observations tended to be published in this manner (cf. Rudy and Kemp 1976 for example) the above analysis was appropriate. However the process of phase binning the observations tended to increase, or at least not decrease, the error on the (Q,U) value as would be expected when variations of (Q,U) within a bin were due to random variations only.

In Chapter 5 we applied the optimization procedure to data for 7 binaries and found that due to the large σ on the phase bins a model fit (in the case of 6 of the data sets available) was found for a wide range of orbital inclinations. In two cases however the model had to be rejected as being incompatible with the variations present in the data. This fact was however probably due to non-random variations being present in the folded data (taken over many orbital periods). When binning took place the error on each mean (Q,U) value would then be large. The lack of phase locking of observations would also cause a large spread in the values of Q,U values in the bins and hence a large σ value.

Problems are also encountered when the system observed is a priori known not to be of a kind representable by the canonical model. This may occur if eclipses or occultations manifest themselves in the light curve or radial velocity curves of the binary. The polarimetric observations of these systems may well result in canonical model structure over only part of the orbital period but not during the eclipse/occultation phases. Binning would then reduce the error at the canonical structure phases but increase it dramatically during the eclipse phases. Thus the average σ over all bins would still be significantly larger than necessary

to obtain a good model fit. An alternative procedure in analysing this type of data would be to just look at data at those phase out-of-eclipse and not data that is known to be of a nature violating one or more of the canonical model assumptions.

In this chapter we develop an analysis that allows the treatment of these more general cases for which data are at unequal phase intervals. The case where eclipsing occurs would be one particular case of this. Investigation of the long term nature of the polarization structure could also be investigated by analysing sequences of data taken over shorter time intervals (maybe only a few orbital periods) and thus avoiding the often inefficient averaging over many tens of periods. Therefore three ways of analysing data would be open to us i.e.

(a) new observations at unequal phase intervals,
(b) analysis of out-of-eclipse data only, and
(c) a sequential analysis of long sets of observations (i.e. Cygnus X-1 data consisting of 528 points spanning some 5 years of observations, Kemp 1980).

We shall return to the application of these techniques to previously analysed data presently available is of systems that exhibit eclipses (e.g. Algol) and have been taken over long time intervals (many orbital periods). We now proceed to the analytic minimization of χ^2 w.r.t. the canonical model constraints for data taken at unequal phase intervals.

8.2 Unequal phase interval analyses

We wish to minimize the statistic

$$\sigma^2 \chi^2 = F(p,i,\theta) = \sum_{r=0}^{N-1} (Q_{ob,r} - Q_{t,r})^2 + (U_{ob,r} - U_{t,r})^2 \qquad (8\cdot1)$$

where p is the set of harmonic coefficients defining $(Q_{t,r}, U_{t,r})$. $(Q_{ob,r}, U_{ob,r})$ and $(Q_{t,r}, U_{t,r})$ are the observations and theoretical values of the Stokes parameters at phase point r in the natural frame of reference. (The interval between successive r need not be equal in phase). We do this subject to the constraints (again in the natural frame) imposed by the model i.e.

$$g_1 = p_1 - c\, v_1 = 0$$
$$g_2 = q_1 + c\, u_1 = 0$$
$$g_3 = p_2 - \alpha v_2 = 0$$
$$g_4 = q_2 - \alpha u_2 = 0$$

$$c = \cos i$$
$$\alpha = \frac{1 + c^2}{2c} \qquad (8.2)$$

We again (as in Chapter 2) follow the Lagrange technique of undetermined multipliers forming the equations:

$$\frac{\partial F}{\partial p} + \sum_{k=1}^{4} \lambda_k \frac{\partial g_k}{\partial p} = 0 \qquad \text{(a)}$$
$$\frac{\partial F}{\partial \theta} + \sum_{k=1}^{4} \lambda_k \frac{\partial g_k}{\partial p} = 0 \qquad \text{(b)} \qquad (8.3)$$

where F is given by (8.1) and the g_k's by (8.2) forming (8.3a) and eliminating the λ_k's we obtain a set of 6 equations:

$$\frac{\partial F}{\partial p_o} = \frac{\partial F}{\partial u_o} = 0$$
$$\frac{\partial F}{\partial p_1} + \frac{1}{c}\frac{\partial F}{\partial v_1} = 0 \quad ; \quad \frac{\partial F}{\partial q_1} - \frac{1}{c}\frac{\partial F}{\partial u_1} = 0 \qquad (8.4)$$
$$\frac{\partial F}{\partial p_2} + \frac{1}{\alpha}\frac{\partial F}{\partial u_2} = 0 \quad ; \quad \frac{\partial F}{\partial q_2} - \frac{1}{\alpha}\frac{\partial F}{\partial u_2} = 0$$

We form the derivatives of F with respect to the harmonic coefficients p_o, u_o, p_1,... etc and obtain from Equation (8.4):

$$p_o + C_1 p_1 + C_2 p_2 + S_1 q_1 + S_2 q_2 = \bar{p}_o$$
$$u_o + C_1 u_1 + C_2 u_2 + S_1 v_1 + S_2 v_2 = \bar{u}_o \qquad (8.5)$$

$$2\left(p_o C_1 + \frac{u_o}{c} S_1\right) + \left((1 + C_2) + \left(\frac{1 - C_2}{c^2}\right)\right) p_1$$
$$+ \left((C_1 + C_3) + \left(\frac{c_1 - C_3}{c\alpha}\right)\right) p_2 + \left(S_1 - \frac{S_2}{c^2}\right) q_1 \qquad (8.6)$$
$$+ \left((S_1 + S_3) - \left(\frac{S_3 - S_1}{c\alpha}\right)\right) q_2 = \left(\bar{p}_1 + \frac{\bar{v}_1}{c}\right).$$

$$2(p_o S_1 - \frac{u_o}{c} C_1) + (S_1 - \frac{S_2}{c}) p_1$$

$$+ ((S_3 - S_1) - (\frac{S_1 + S_3}{c\alpha})) p_2 + ((1 - C_2) + (\frac{1 + C_2}{c^2})) q_1$$

$$+ ((C_1 - C_3) + (\frac{C_1 + C_3}{c\alpha})) q_2 = (\bar{q}_1 - \frac{\bar{u}_1}{c}) \qquad (8.7)$$

$$2(p_o C_2 + \frac{u_o}{\alpha} C_2) + ((C_1 + C_3) + (\frac{C_1 - C_3}{c\alpha})) p_1$$

$$+ ((1 + C_4) + (\frac{1 - C_4}{\alpha^2})) p_2 + ((S_3 - S_1) - (\frac{S_1 - S_3}{c\alpha})) q_2$$

$$+ (S_4 - \frac{S_4}{\alpha^2}) q_2 = (p_2 + \frac{v_2}{\alpha}) \qquad (8.8)$$

$$2(p_o S_o - \frac{u_o}{\alpha} C_2) + ((S_1 + S_3) + (\frac{S_1 - S_3}{c\alpha})) p_1$$

$$+ (S_4 - \frac{S_4}{\alpha^2}) p_2 + ((C_1 - C_3) + (\frac{C_1 + C_3}{c\alpha})) q_1$$

$$+ ((1 - C_4) + (\frac{1 + C_4}{\alpha^2})) q_2 = (\bar{q}_2 - \frac{\bar{u}_2}{\alpha}) \qquad (8.9)$$

where
$$C_k = \frac{1}{N} \sum_{r=0}^{N-1} \cos k \lambda_r$$
$$S_k = \frac{1}{N} \sum_{r=0}^{N-1} \sin k \lambda_r \qquad (8.10)$$

(λ = longitude of observations = $2\pi \times$ phase)

and
$$\bar{p}_k = \frac{2}{N} \sum_{r=0}^{N-1} Q_{ob,r} \cos r k \beta$$
$$\bar{q}_k = \frac{2}{N} \sum_{r=0}^{N-1} Q_{ob,r} \sin r k \beta \qquad \beta = \frac{2\pi}{N}$$
$$\bar{u}_k = \frac{2}{N} \sum_{r=0}^{N-1} U_{ob,r} \cos r k \beta \qquad k = 1,2 \qquad (8.11)$$
$$\bar{v}_k = \frac{2}{N} \sum_{r=0}^{N-1} U_{ob,r} \sin r k \beta$$

$$\text{also} \quad \bar{p}_o = \frac{1}{N} \sum_{r=0}^{N-1} Q_{ob,r} \; ; \quad y_o = \frac{1}{N} \sum_{r=0}^{N-1} U_{ob,r} \tag{8.12}$$

$(Q_{ob,r}, U_{ob,r})$ are in the natural frame of the binary.

For equally spaced data $C_k = 0$ for $k \neq 0$ and $S_k = 0$ for all k, and Equations (8.5) to (8.10) reduce to those encountered in Chapter 2.

Differentiating F with respect to Q gives:

$$2(\bar{u}_o p_o - u_o \bar{p}_o) + p_1(\bar{u}_1 - \frac{\bar{q}_1}{c}) + q_1(\bar{v}_1 + \frac{\bar{p}_1}{c})$$
$$+ p_2 (\bar{u}_2 - \frac{\bar{q}_2}{\alpha}) + q_2(\bar{v}_2 + \frac{\bar{p}_2}{\alpha}) = 0 \tag{8.13}$$

It is possible to simplify equations (8.5) to (8.10) and equation (8.13) by writing then in matrix form i.e.

see overleaf

Let (8.14) have the form:

$$A \, \underline{P} = \underline{\bar{P}} \tag{8.16}$$

where $\underline{\bar{P}}$ is a vector whose components involve only the barred quantities (i.e. 'data' in the natural frame).

To solve for $\underline{P}$, $\underline{\bar{P}}$ has to be evaluated from both the observed data (laboratory frame) and the unknown angle θ, the rotation angle between the natural and laboratory frame.

Specifically

$$\underline{\bar{P}} = k \, C \tag{8.17}$$

where
$$k = \begin{pmatrix} \bar{p}'_o & -\bar{u}'_o & \\ \bar{u}'_o & \bar{p}'_o & \\ \bar{p}_1 + \frac{\bar{v}_1}{c} & -\bar{u}'_1 + \frac{\bar{q}'_1}{c} & \\ \bar{p}'_2 + \frac{\bar{v}'_2}{c} & -\bar{u}'_2 + \frac{\bar{q}'_2}{c} & \end{pmatrix} \tag{8.18}$$

and
$$C = \begin{pmatrix} \cos\theta \\ \sin\theta \end{pmatrix} \tag{8.19}$$

where

$$A \begin{pmatrix} p_o \\ u_p \\ p_1 \\ q_1 \\ p_2 \\ q_2 \end{pmatrix} = \begin{pmatrix} \bar{p}_o \\ \bar{u}_o \\ \bar{p}_1 + \frac{\bar{v}_1}{c} \\ \bar{q}_1 - \frac{\bar{u}_1}{c} \\ \bar{p}_2 + \frac{\bar{v}_2}{\alpha} \\ \bar{q}_2 - \frac{\bar{u}_2}{\alpha} \end{pmatrix} \tag{8.14}$$

$$\begin{pmatrix}
1 & 0 & C_1 & S_1 & C_2 & S_2 \\
0 & 1 & S_1/c & -C_1/c & S_3/\alpha & -C_2/\alpha \\
2C_1 & \frac{2S_1}{c} & (1+C_2)+(\frac{1-C_2}{c^2}) & S_2(1-\frac{1}{c^2}) & (C_1+C_3)+(\frac{C_1-C_3}{c\alpha}) & (S_1+S_3)-(\frac{S_3-S_1}{c\alpha}) \\
2S_1 & \frac{-2C_1}{c} & S_2(1-\frac{1}{c^2}) & (1-C_2)+(\frac{1+C_2}{c^2}) & (S_3-S_1)+(\frac{S_1+S_3}{c\alpha}) & (C_1-C_3)+(\frac{C_1+C_3}{c\alpha}) \\
2C_2 & \frac{2S_2}{\alpha} & (C_1+C_3)+(\frac{C_1-C_3}{c\alpha}) & (S_3-S_1)-(\frac{S_1-S_3}{c\alpha}) & (1+C_4)+(\frac{1-C_4}{\alpha^2}) & S_4(1-\frac{1}{\alpha^2}) \\
2S_2 & \frac{-2C_2}{\alpha} & (S_1+S_3)-(\frac{S_3-S_1}{c\alpha}) & (C_1+C_3)+(\frac{C_1+C_3}{\alpha c}) & S_4(1-\frac{1}{\alpha^2}) & (1-C_4)+(\frac{1+C_4}{\alpha^2})
\end{pmatrix} = A \tag{8.15}$$

The barred quantities are measured in the laboratory frame. Therefore (8.14) becomes:

$$A\,\underline{P} = k\,C \qquad (8.20)$$

and

$$\underline{P} = (A^{-1}\,k)\,C$$

since we want to find $\underline{P}$.

Determination of θ is achieved as follows:

We see that

$$C^T B\,\underline{P} = 0 \qquad (8.21)$$

where $C^T = (\cos\theta \;\; \sin\theta)$

and

$$B = \begin{pmatrix} 2\bar{u}'_o & -2\bar{p}'_o & \bar{u}'_1 - \bar{q}'_1/c & \bar{v}'_1 + \bar{p}'_1/c & \bar{u}'_2 - \bar{q}_2/\alpha & \bar{v}'_2 + \bar{p}'_2/\alpha \\ 2\bar{p}'_o & 2\bar{u}'_o & \bar{p}'_1 + \bar{v}'_1/c & \bar{q}'_1 + \bar{u}'_1/c & \bar{p}'_2 + \bar{v}'_2/\alpha & \bar{q}'_2 - \bar{u}'_2/\alpha \end{pmatrix} \qquad (8.22)$$

which is (8.13) defined in terms of the observed quantities $\bar{p}'_k$, $\bar{q}'_k$, $\bar{u}'_k$, and $\bar{v}'_k$. θ can be obtained from equations (8.21) and (8.20) i.e.

$$C^T B\,(A^{-1}\,k)\,C = 0 \qquad (8.23)$$

i.e.

$$C^T X\,C = 0$$

where

$$X = B\,A^{-1}\,k = \begin{pmatrix} X_{11} & X_{12} \\ X_{21} & X_{22} \end{pmatrix} \qquad (8.24)$$

contains entirely known quantities.

We therefore obtain a quadratic for θ viz:

$$x_{11}\cos^2\theta + (x_{12} + x_{21})\cos\theta\sin\theta + x_{22}\sin^2\theta = 0 \qquad (8.25)$$

or

$$x_{11} + (x_{12} + x_{21})\,t + x_{22}\,t^2 = 0 \qquad (8.26)$$

where $t = \tan\theta$.

From (8.26) we obtain θ and hence using (8.20) (we know A, A^{-1}, k,C) we can find $\underline{P}$ and $\underline{P}'$. The Fourier coefficients in the natural and laboratory frame of reference respectively. From these we can find the optimum 'best fit' model parameters for any given inclination i

and a complete solution.

Two values of Q will be found on solving the quadratic but only one will give a minimum value of χ^2.

We now relate the procedure we adopt to measure the acceptability of model and observations.

8.3 Model testing and the Relative Confidence Interval

The optimum parameter set to observational data is found, as in Chapter 2, by running over a grid of inclination i where $0^o \leq i \leq 180^o$. The optimum inclination is the one giving the minimum χ^2 value and hence by the above procedure the optimum value of the other parameters are found. It is at this point necessary to estimate the uncertainty in this i_{opt} value by considering the χ^2 test as the acceptability criterion and constraint on allowable i values. Hence derive a Relative Confidence Interval (cf. Chapter 2). To obtain a value for χ^2 from (8.1) we need to divide F by the quantity σ^2. This strong dependence on σ is unfortunate since only small changes in it will mean large changes in the value of χ^2 and hence in the size of the Relative Confidence Interval on i_{opt}. Since we are primarily interested in the range of acceptable (i.e. consistent with the data in terms of the χ^2 test) i values (and other model parameters) we find the confidence interval and by using an estimate of $\sigma = \hat{\sigma}$ obtained from the residuals between model and data values of (Q,U). We do this also since we want to define an error on our i_{opt} estimate regardless of the acceptability of the optimum model fit to the data details and only with respect to some average behaviour (cf. later). We define:

$$\hat{\sigma}^2 = F/(2N - p) \qquad (8.27)$$

and we term $\hat{\sigma}$ as unbiased estimate of σ since it does not depend on the observational error σ_{dat}. This is fact means that we are giving χ^2 <u>median</u> value i.e.:

$$\chi^2 = (2N - p) \qquad (8.28)$$

with it having a significance level of 50%. We find the Confidence Interval by (a) choosing a significance level (10% say) and (b) finding the range of i values for which:

$$\frac{F(i)}{(2N-p)} < \chi^2_{10\%,2N} \qquad (8.29)$$

This range we call the Relative Confidence Interval (R.C.I.). If the variation of F(i) one i is small then the R.C.I. will be broad. The converse is also true in that a sharp minimum in F(i) would give a narrow R.C.I.

The problem of estimating the acceptability of a model fit to data is not trivial. We have on the observations, an error here termed σ_{dat} and it may at first sight seem reasonable to use this together with the F value obtained at i_{opt} to give a value of $\chi^2_{(i_{opt})}$. This procedure can however lead to a wrong rejection of the model. As an example of this consider the problem of applying Ohm's law to a section of wire. Ohm's law can be considered the fitting model and 'observations' (i.e. current A at different voltages V) are obtained. This would, under ideal circumstances, give a linear relation between V and I (gradient = Resistance, R) with the observations lying on the best fit line. If however the temperature stability of the line is uncertain the 'observations' may be spread about the best fit model. The observations may well have small errors on them but denote significantly from the model (Figure 8.Ø a,b) indicates these two cases

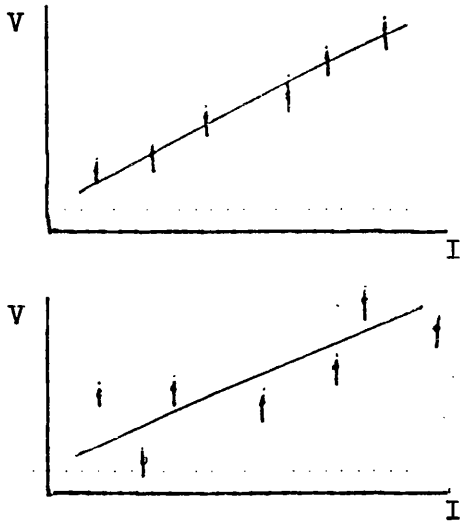

(Figure 8.Ø a,b)

Using σ_{dat} to calculate the model acceptability in the former case would give a good (high) significance to the 'best fit'. In the second case however σ_{dat} would give a bad(low) significance to the fit

and the model would be rejected as an unaccceptable fit to the observations which situations we are dealing with here is uncertain. Hence only 'acceptability of the model fit' calculated using σ_{dat} should be treated with constraint with more weight being given to the R.C.I. calculated as outlined above.

If both model acceptability and R.C.I. are good (i.e. high significance to model fit and narrow R.C.I.) then a reliable i_{opt} can be anticipated. Narrow R.C.I. and low significance model fits (at i_{opt}) do not rule out the possibility of a reliable i_{opt}. On the other hand broad R.C.I. and low significance i_{opt} fit would not indicate a good determination of i_{opt} and associated model parameters.

The advantages of this technique over the binned analysis of Chapter 2 is that since data can now be at unequal intervals of phase we can analyse small incomplete sections of data and obtain values of i and the other free parameters of the model. This means that only part of the phase need be covered observationally and hence the observing time is reduced with those sections of phase that are not covered being unimportant.

The model has been thoroughly tested using simulated data as with the model of Chapter 2, with the input parameters being required exactly (when the noise on the data was zero). Part of the phase coverage here in some cases removed and the resulting incomplete data set analysed. This also gave exact results. The minimum phase coverage necessary to obtain accurate results from the model fitting is not well defined. We estimate that phase coverage amounting to at least $\sim$ 0.4 would be necessary if noise was present on the data to obtain sensible results. The model is expected to behave in a manner similar to the binned canonical model of Chapter 2 when noise is present on the data (cf. Chapter 3).

We now attempt to re-analyse the data of the seven binaries first considered in Chapter 5 to illustrate the technique available using this analysis (i.e. out-of-eclipse analyses, sequential analysis).

8.4 Reanalysis of the data for 7 binaries

The data analysed in Chapter 5 dates back to the period 1975 to 1978 and were not taken with analysis in terms of the canonical model

in mind. Hence some of the systems include one or more of the canonical model assumptions (i.e. some are eclipsing binaries and possibly include obscuration of the scattering regions). This data may be utilized however by an out-of-eclipse analysis as considered above. (Section 8.4.2). Also the data was taken over long periods of time (many orbital periods) and a sequential analysis may also be attempted (Section 8.4.3). Firstly however we fit all the data available with the unequal phase interval analysis canonical model to confirm the results of Chapter 5 in that the spread of observations within a small phase interval is too great to enable satisfactory parameter determination. In Chapter 5 this meant that the calculated issue of σ_{bin} was large and hence a wide range of inclinations were statistically acceptable.

8.4.1 All Available data

The data we shall analyse for the 7 binaries β Per (Algol, AO Cas, HD47129, σ Ori E (B and U Filter data sets), U Sge, u Her and V444 Cygni were taken over periods of time shown in Table I. It is seen that the observations spanned a large number of orbital periods, from 16.6 (HD47129) to 209.2 (u Her). The average number of observations per orbital period was small ranging from 3.61 (HD47129 with orbital period = 14.39 days) to 0.49 (u Her with orbital period = 2.05 days). If phase locking of observations is present this is a suitable procedure. However if phase locking is absent or partial the (Q,U) values in subsequent orbital cycles would be unrelated to previous values at similar phases and hence this long time interval. A particular case of the breakdown of phase locking would be a systematic long term evolution of the scattering region which would produce a considerable spread in (Q,U) values in any given bin over long time intervals.

The (Q,U) values at the start of the observing run may be unrelated to those obtained at the end of the period of observations due to the changes that had occurred in the geometry and distribution of the scattering material. On inspection of the data plotted versus phase ϕ (Figures 1.10, 1.11) it is seen that this indeed may be the case since many phases occur in some of the data sets where (Q,U) are in fact multivalued. It may be possible to define a short term phase locked structure to the data (over a small number of orbital periods) and

STAR	NO. PTS. (N)	JD(DAYS) RANGE	P(DAYS)	T (O.P)	N/T
ALGOL	51	92.8	2.867	32.4	1.57
AO CAS	38	69.9	3.52	19.9	1.91
HD47129	60	238.7	14.39	16.6	3.61
U HER	102	428.8	2.05	209.2	0.49
σ ORI E	60	68.95	1.19	57.9	1.03
σ ORI E	54	64.85	1.19	54.5	0.99
U SGE	73	164.8	3.38	48.8	1.5
V444 CYG	56	94.0	4.21	22.3	2.51

P = ORBITAL PERIOD
T = NUMBER OF PERIODS COVERING OBSERVATIONS

TABLE I.

the data could then be analysed sequentially to yield an improved parameter determination occurring. We attempt this in Section (8.4.3). However we fit the 8 data sets with the general canonical model with the resulting best fits and optimum inclinations being given in Table II and Figures (8.1) to (8.8) inclusive. The values of σ_{dat} and $\hat{\sigma}$ are also given showing in Table II; the increase from σ_{dat} to $\hat{\sigma}$ in all cases due to the poor fit of the model. In all cases the model has to be rejected at 0.1% significance (in some case at levels as low as 0.001% sig.) as being a bad representation of the structure present in the polarization data. Using $\hat{\sigma}$ we calculated the R.C.I.'s to be broad at 0°, 90° in most cases (i.e. any inclination would produce an acceptable fit (on the basis of $\hat{\sigma}$) with the canonical model).

8.4.2 Analysis of out-of-eclipse data.

The eclipse region of 6 of the binaries under analysis was found from published light curves i.e. Algol - Guinan et al (1978); AO Cas - Wood (1948); u Her - Soderhjelm (1978); σ Ori E - Hesser et al (1977); U Sge - Struve (1949) and V444 Cyg - Cherepashchuk (1975); HD47129 was found to exhibit no eclipse behaviour (Abycnkhar and Spinrad 1958). The evidence for eclipses in AO Cas was reanalysed by Hutchings and Hill (1972) who claim that the eclipse is grazing only. We still consider this as an eclipsing binary for the present analysis.

The eclipse regions, given in Table III were taken out of the complete sets and the remaining data reanalysed (see Table III). The only system to show a significant reduction in the 40% confidence interval was AO Cas where the R.C.I. became $[\,10^{\circ}, 84^{\circ}\,]$. The significance of the model fit was still however small (<.001%) meaning that the model has still to be regarded as a bad fit to the observations even outside eclipse. U Sge did show, however an increased model significance (compared to the complete raw data set) of $\sim$ 5%. The ratio of σ to σ_{dat} (i.e. X) also increased for all systems compared to in the complete data sets. No significant improvement was found when using this reduced data set.

8.4.3 Sequential Analysis

We have seen that the data for the 7 binaries cover a large number of orbital periods (Table I). It may be possible that the multivalued

TABLE II

STAR	SIGMA (%) DAT	SIGMA (%) HAT	X	IOPT(UES)	IOPT(BIN)	RCI 10%
ALGOL	.0028	.0041	1.46	78°	79°	0°,90°
AO CAS	.024	.057	2.38	69°	61°	0°,85°
HD47129	.016	.049	3.06	72°	69°	0°,90°
U HER	.011	.016	1.46	74°	76°	0°,90°
σ ORI E(B)	.015	.039	2.6	77°	70°	0°,90°
σ ORI E(U)	.037	.076	2.05	85°	82°	0°,90°
U SGE	.023	.029	1.26	85°	88°	0°,90°
V444 CYG	.063	.094	1.5	76°	75°	0°,90°

X = SIGMA(HAT)/SIGMA(DAT)
ACCEPTABILITY OF MODEL < .1% IN ALL CASES

FIGURES 8.1 to 8.8.

In these figures we show the best fit canonical model (solid line) produced by the unequal phase interval analysis of chapter 8. Seven binaries are reanalyzed. Both the general (1st and 2nd harmonics) model and the symmetric (2nd harmonics only) model are shown.

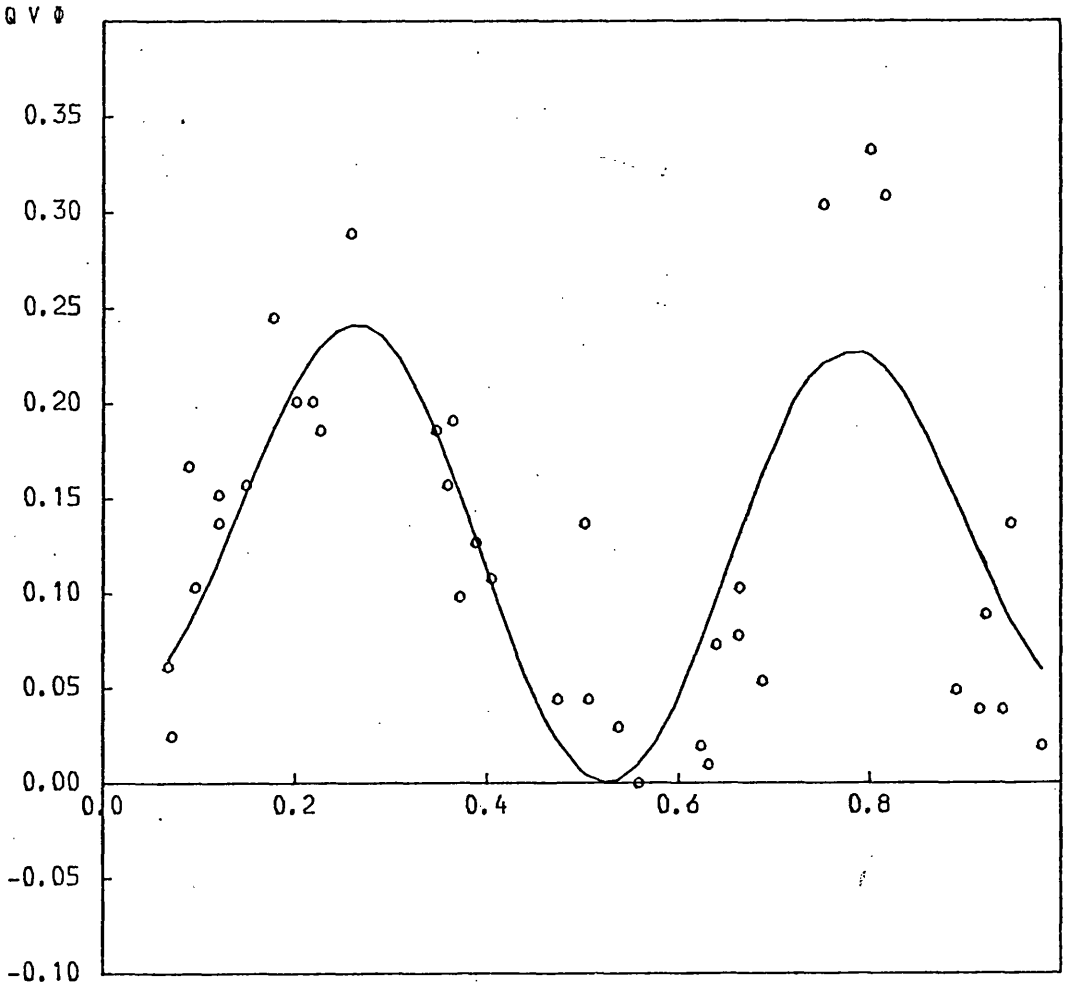

FIGURE 8.1 a

Plot of raw data and best fit canonical model (1 and 2 harmonics) for the system AO Cas.

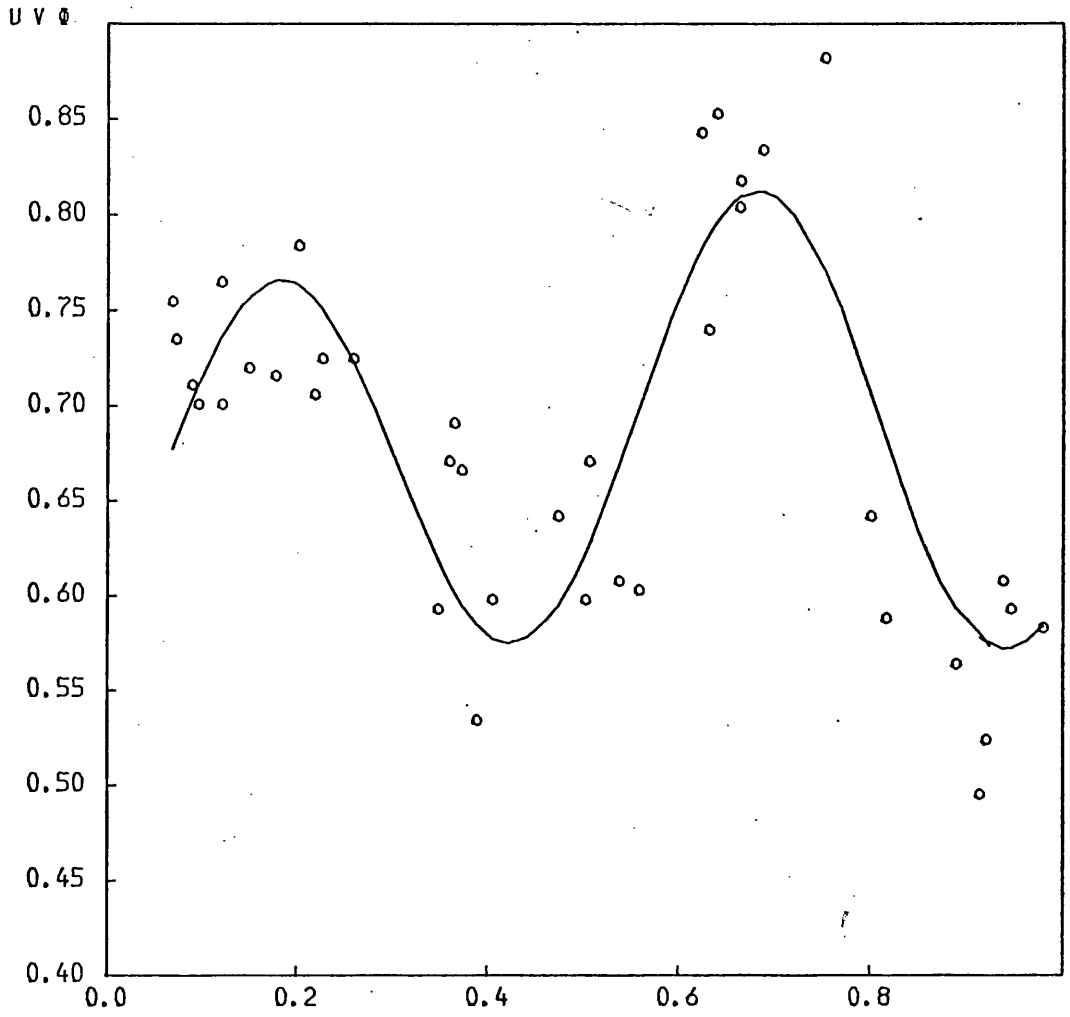

FIGURE 8.1b

see 8.1a

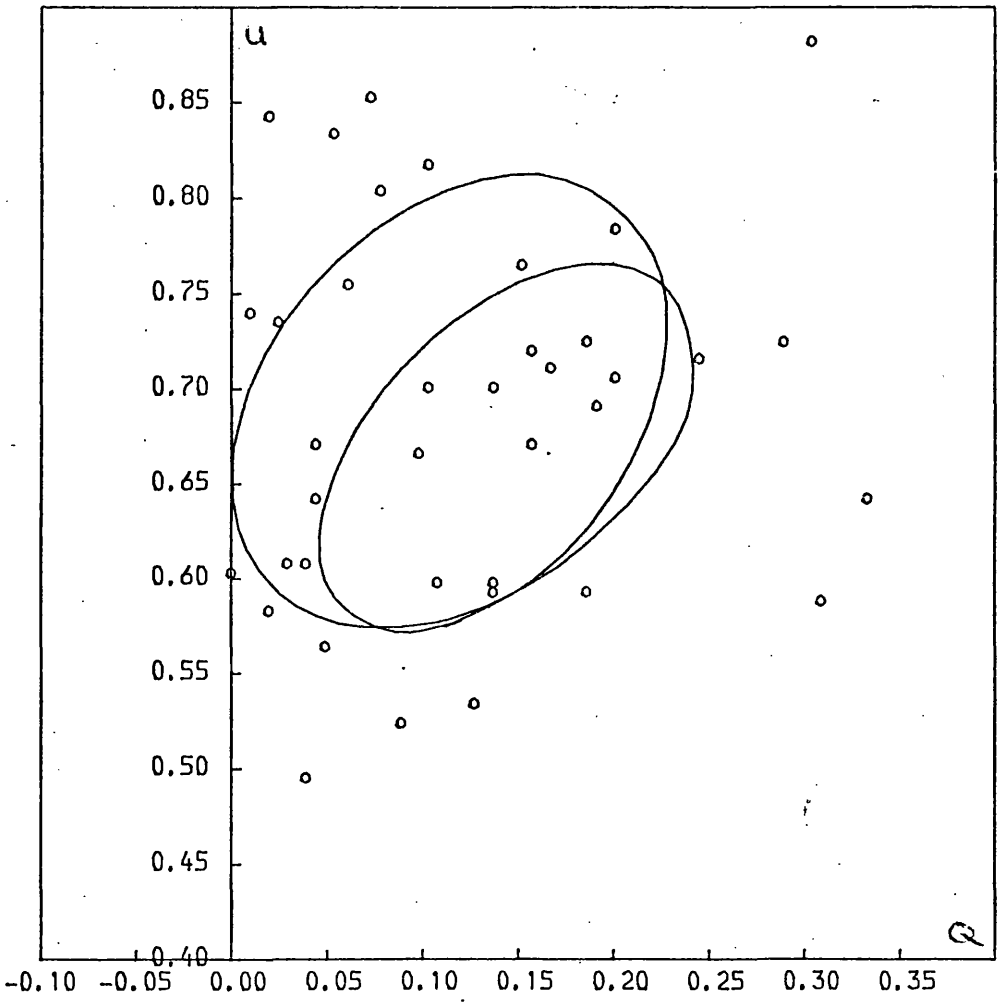

FIGURE 8.1c

see Firure 8.1a

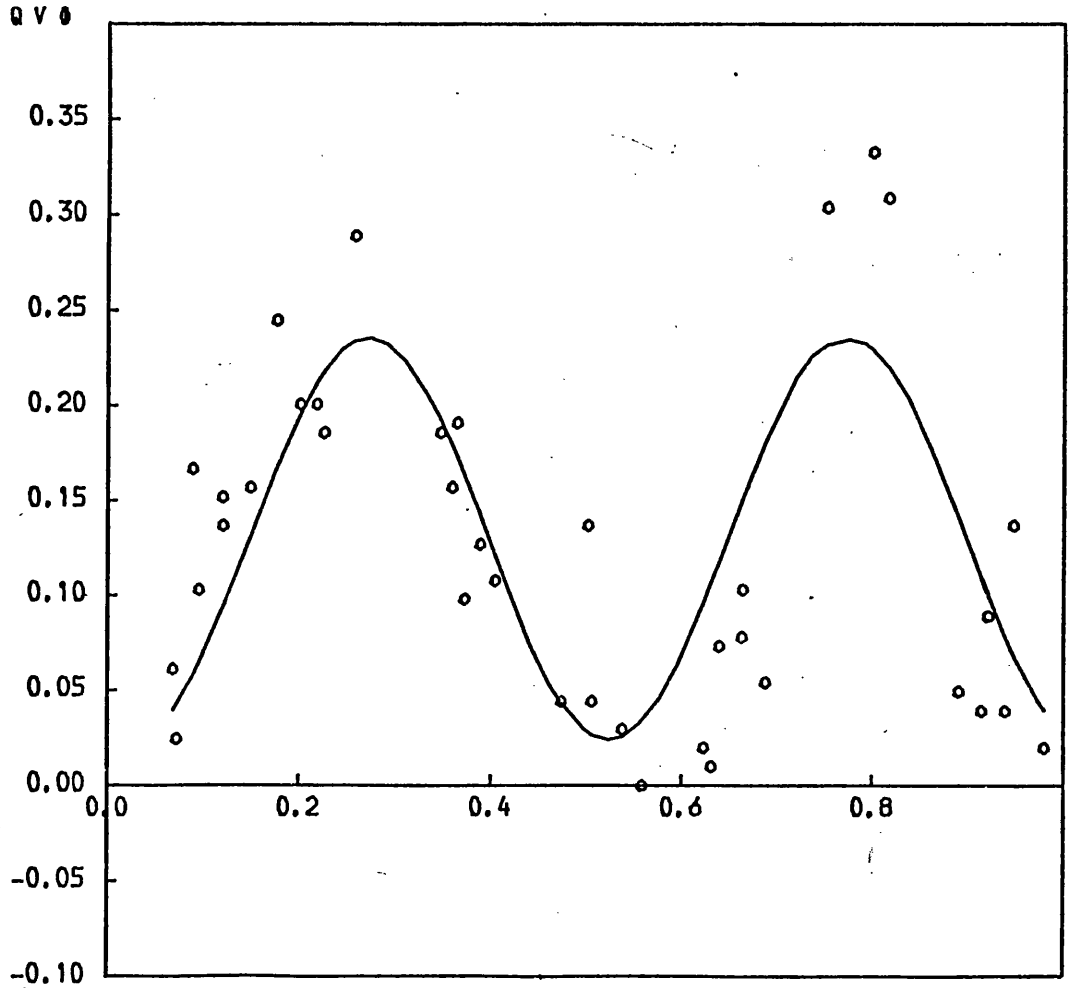

FIGURE 8.1d

Plot of raw data and best fit canonical model (2 harmonics only) for AO Cas.

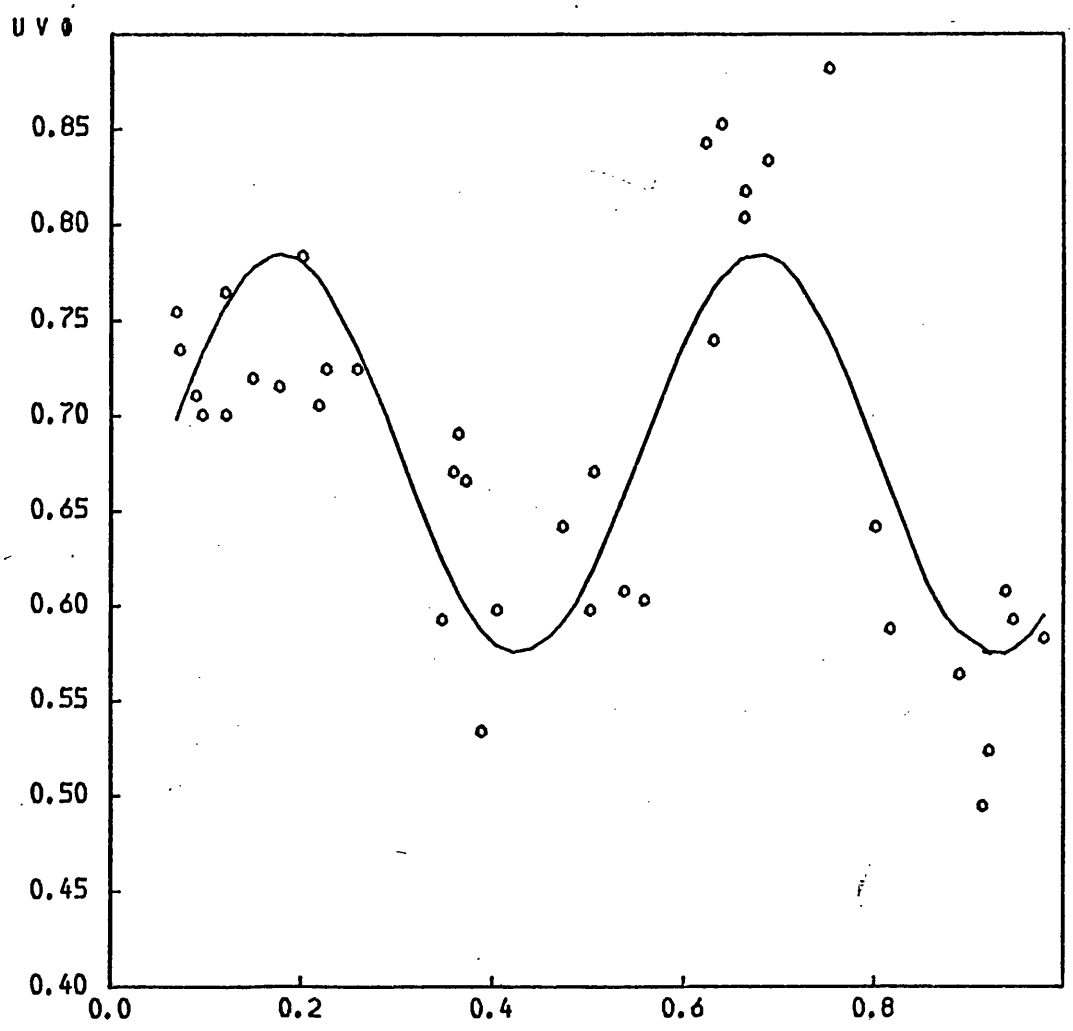

FIGURE 8.1e

see 8.1d

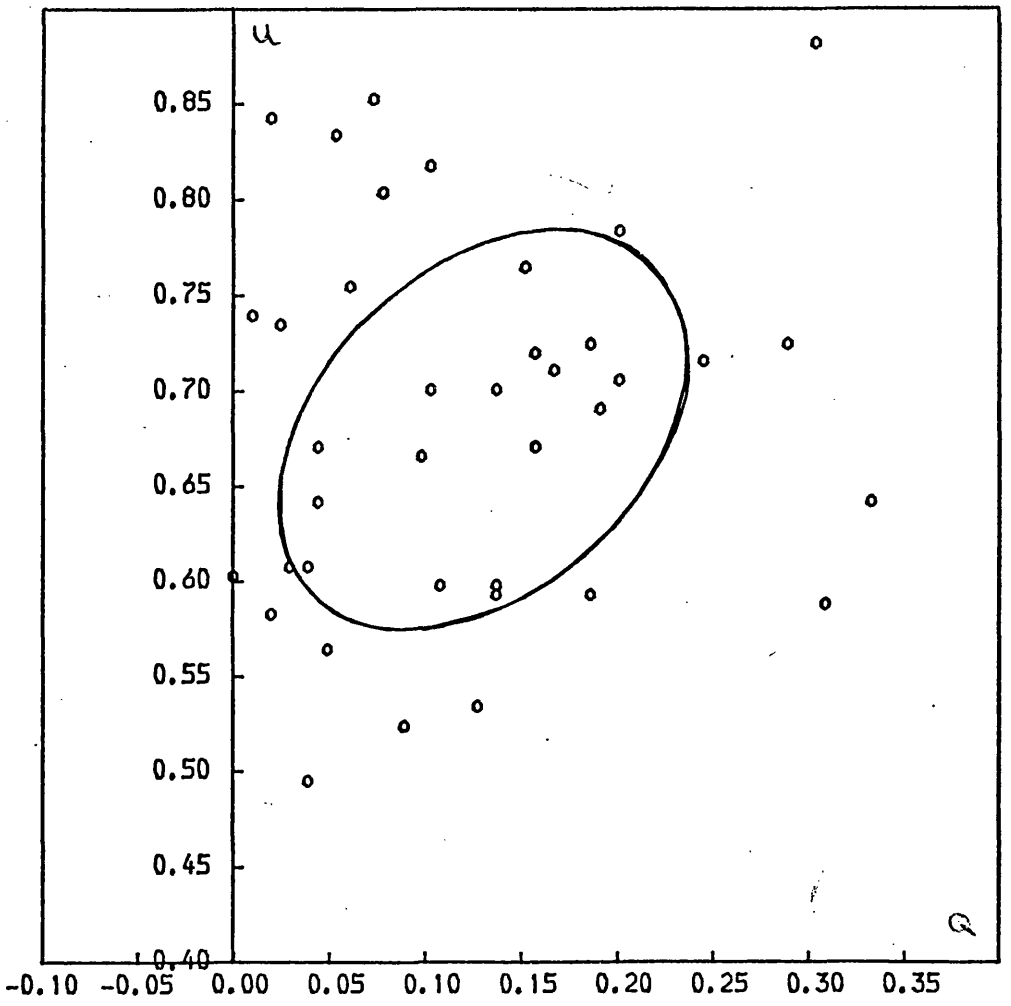

FIGURE 8.1f

see 8.1d

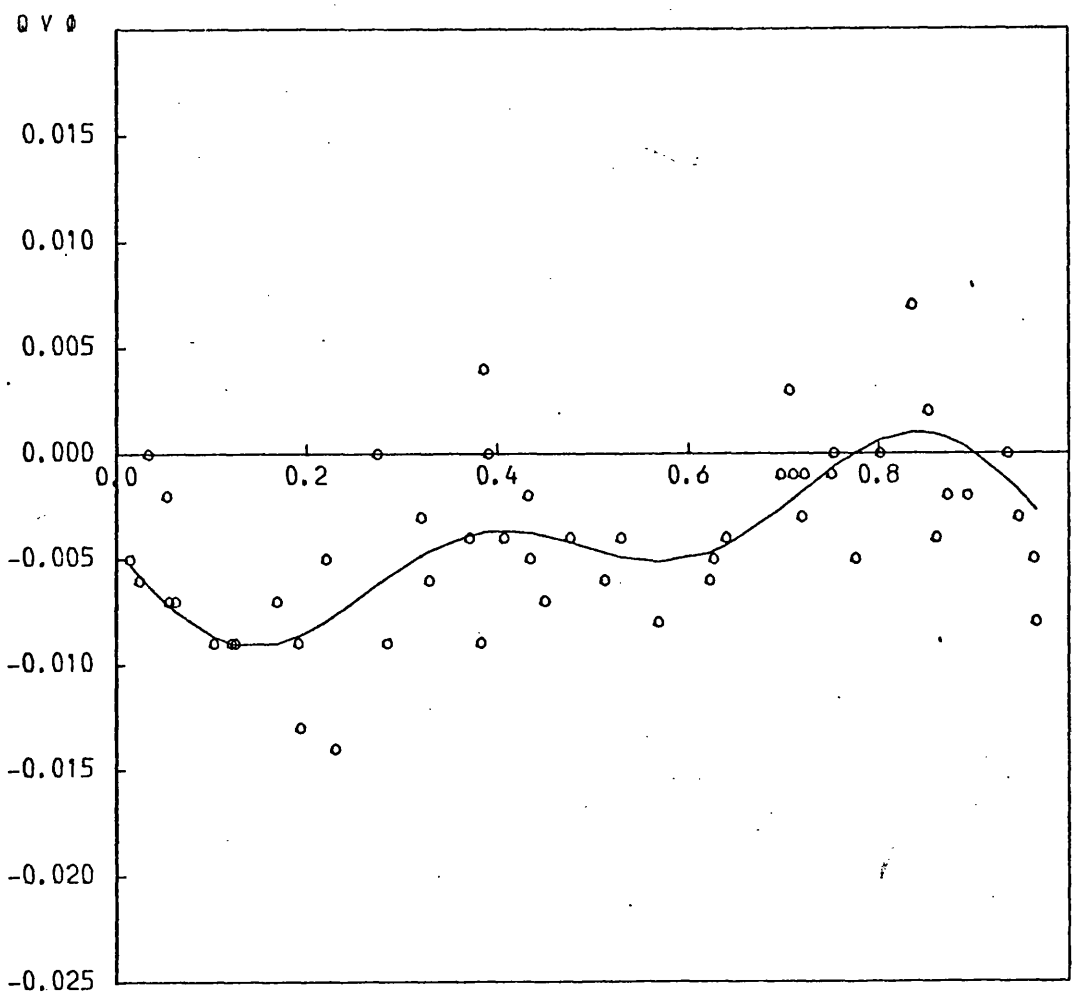

FIGURE 8.2a

Plot of raw data and best fit canonical model (1 and 2 harmonics) for the system Per (algol).

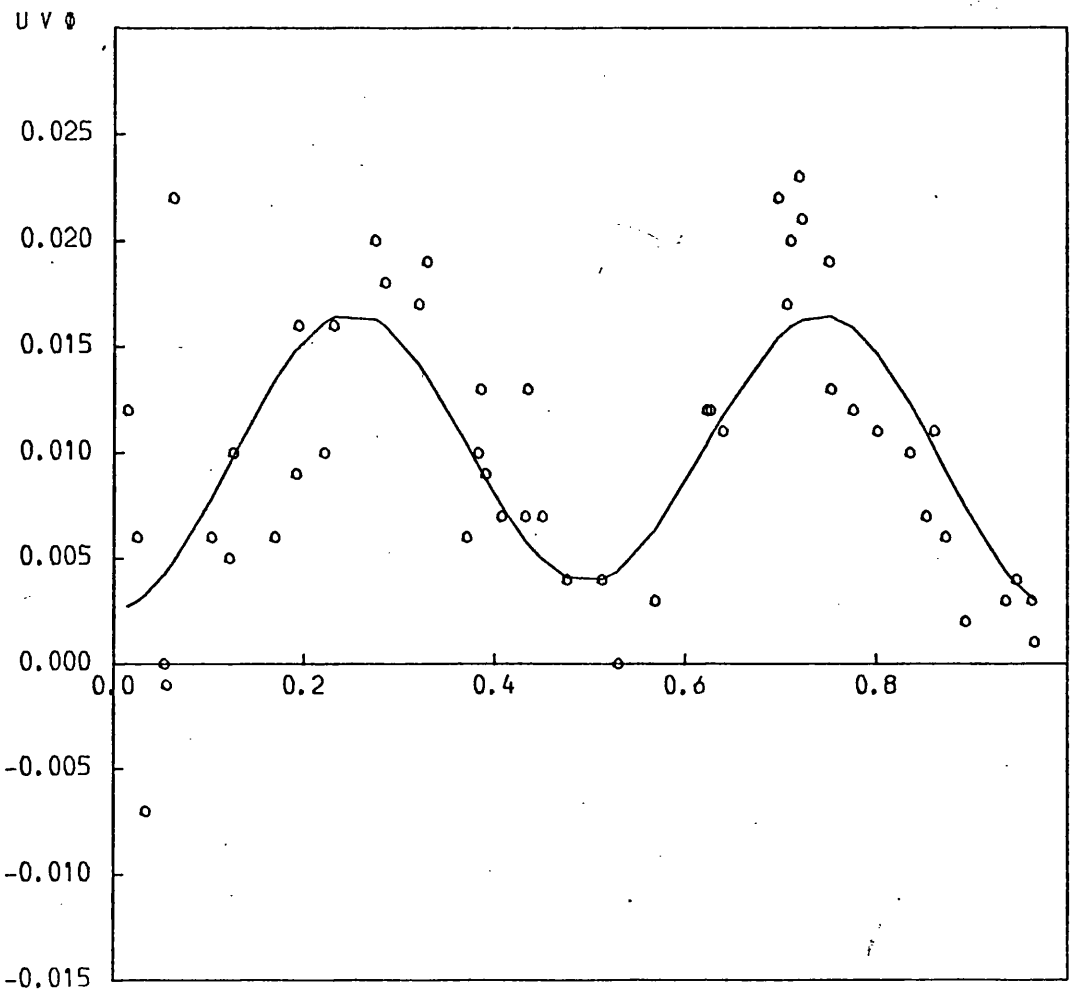

FIGURE 8.2b

see 8.2a

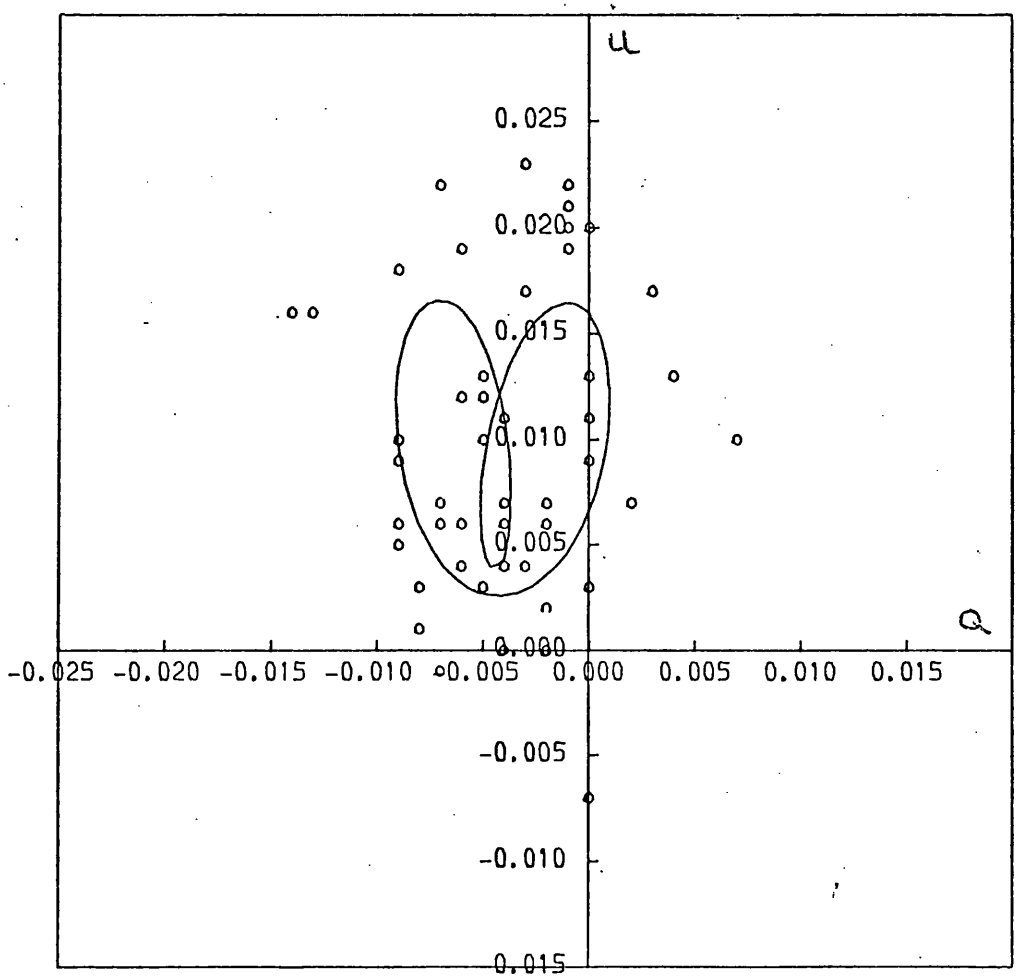

FIGURE 8.2c

see 8.2a

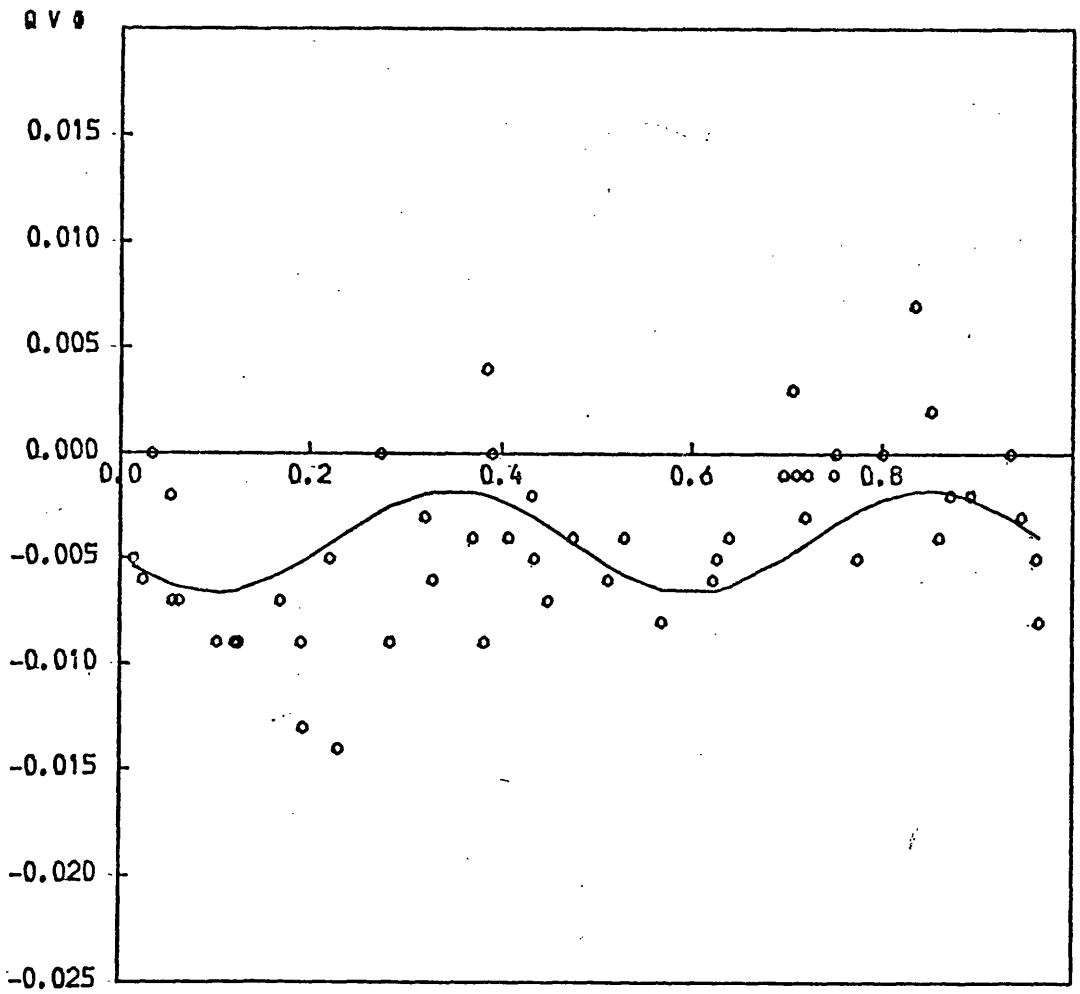

FIGURE 8.2d

Plot of raw data and best fit canonical model (2 harmonic only) for Algol.

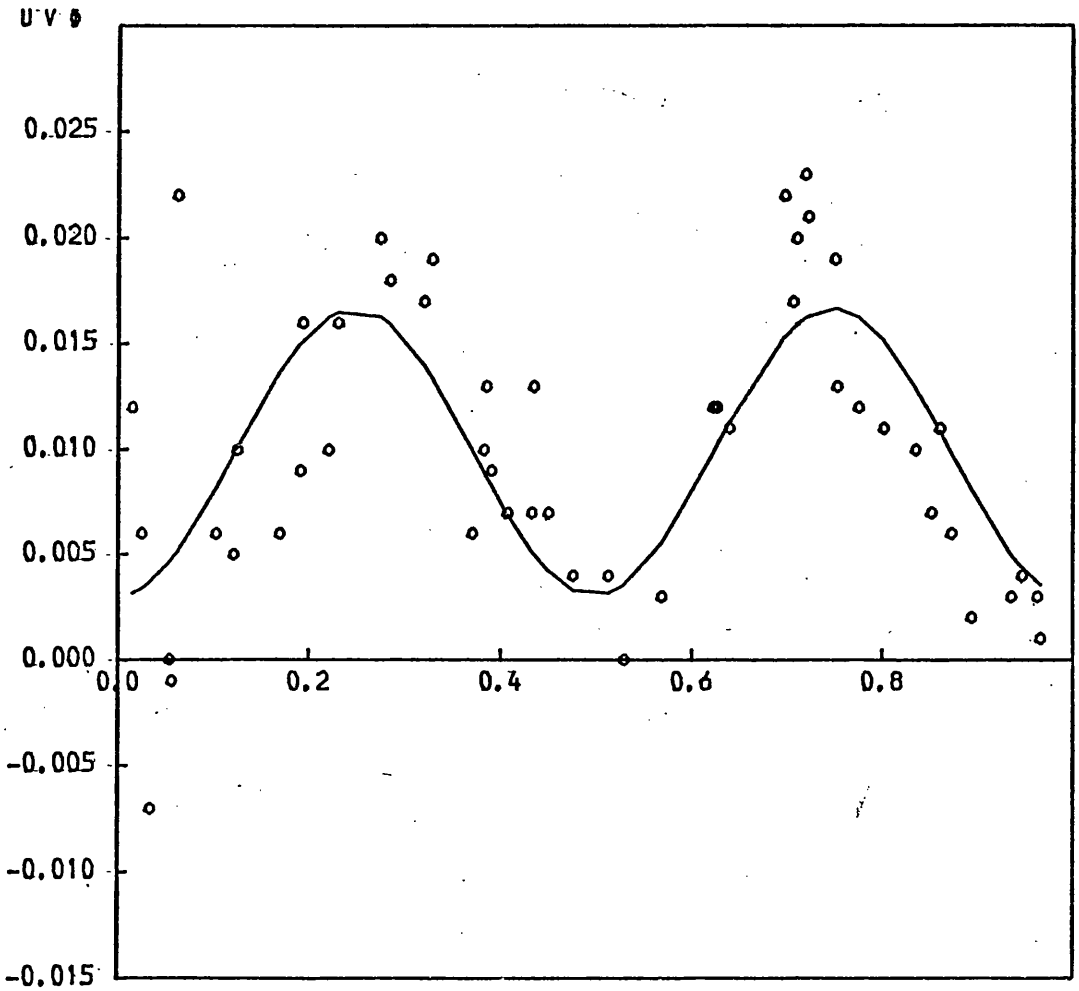

FIGURE 8.2e

see 8.2d

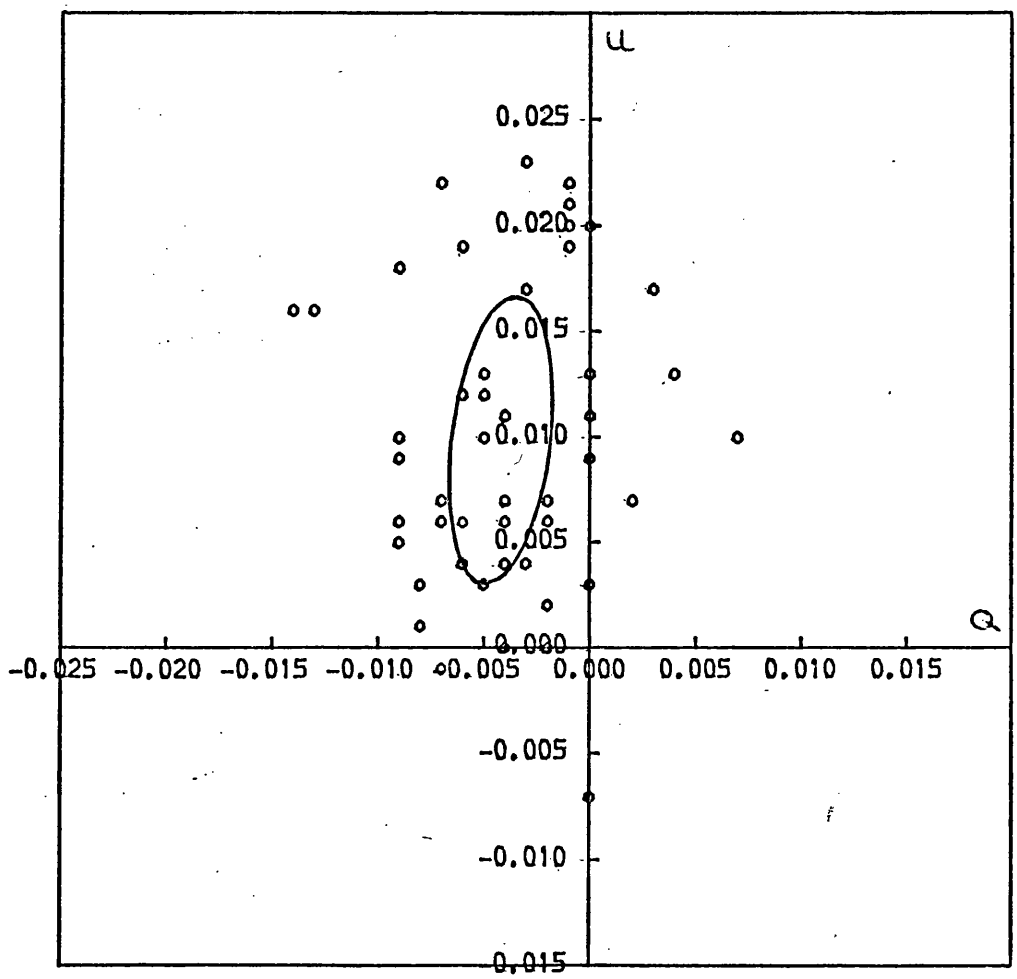

FIGURE 8.2f

see 8.2d

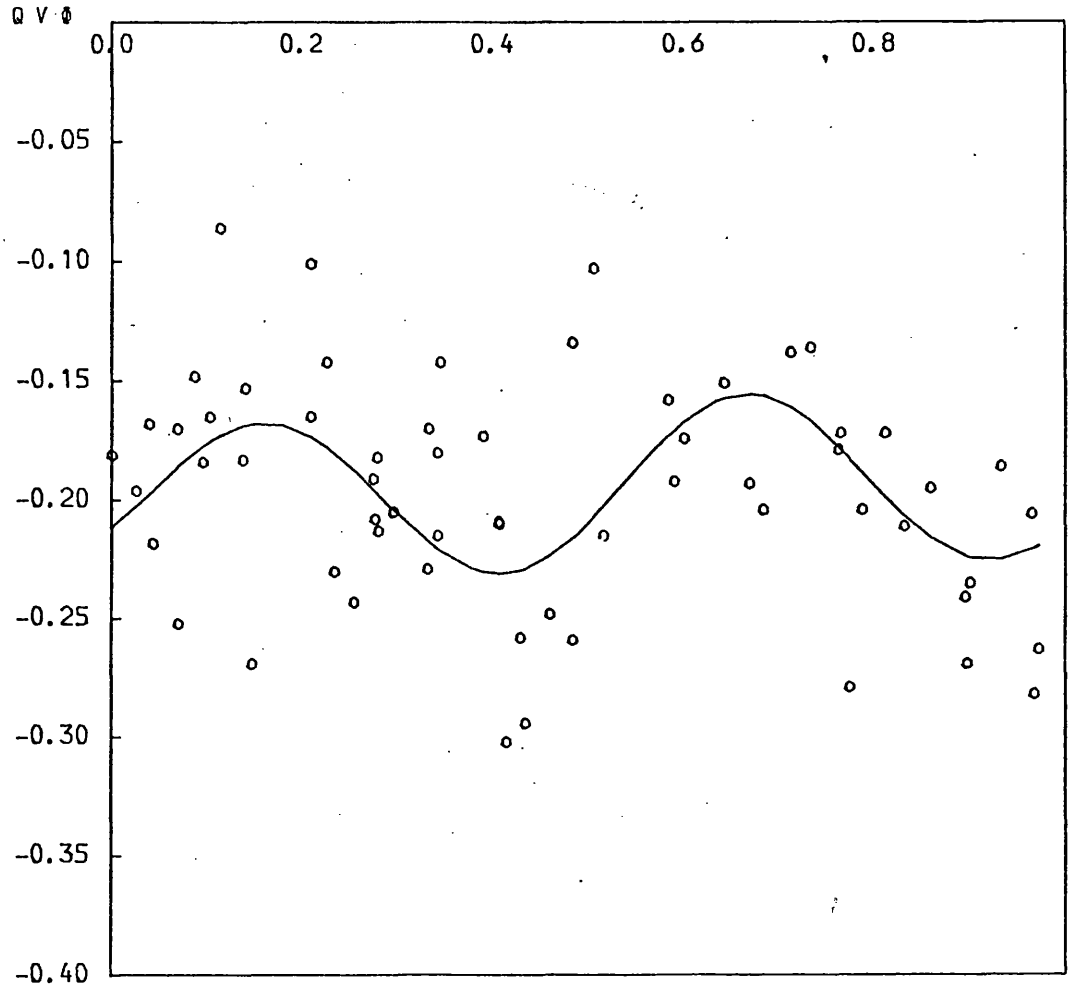

FIGURE 8.3a

Plot of raw data and best fit canonical model (1 and 2 harmonics) for the system HD47129.

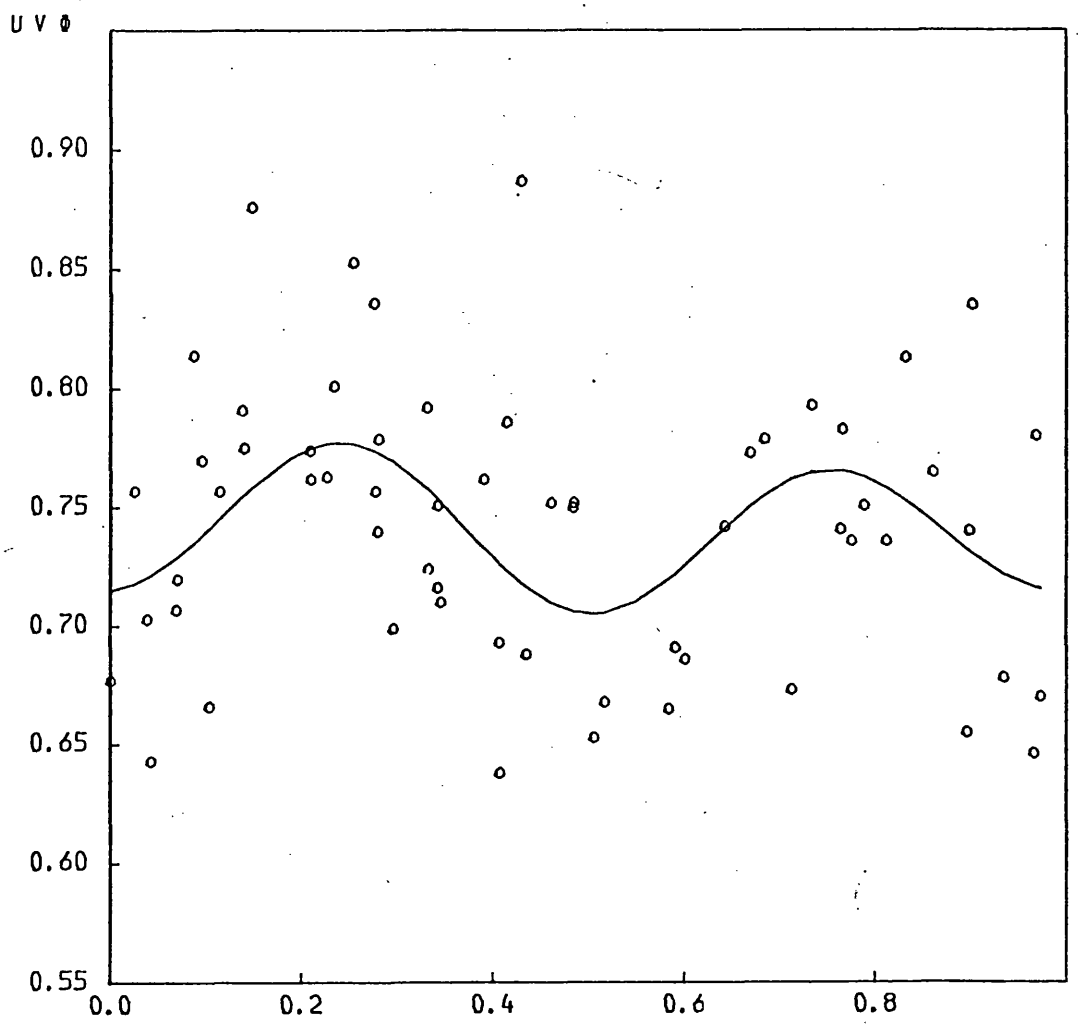

FIGURE 8.3b

see 8.3a

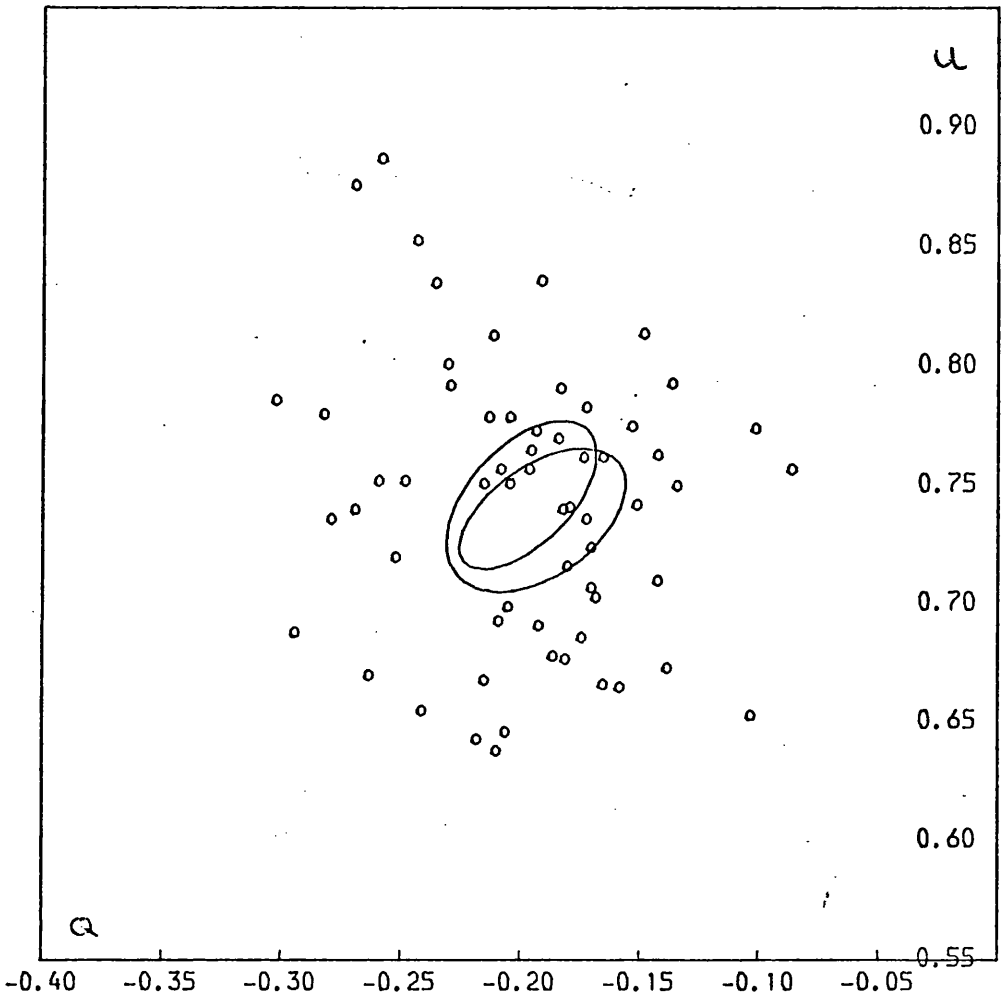

FIGURE 8.3c

see 8.3a

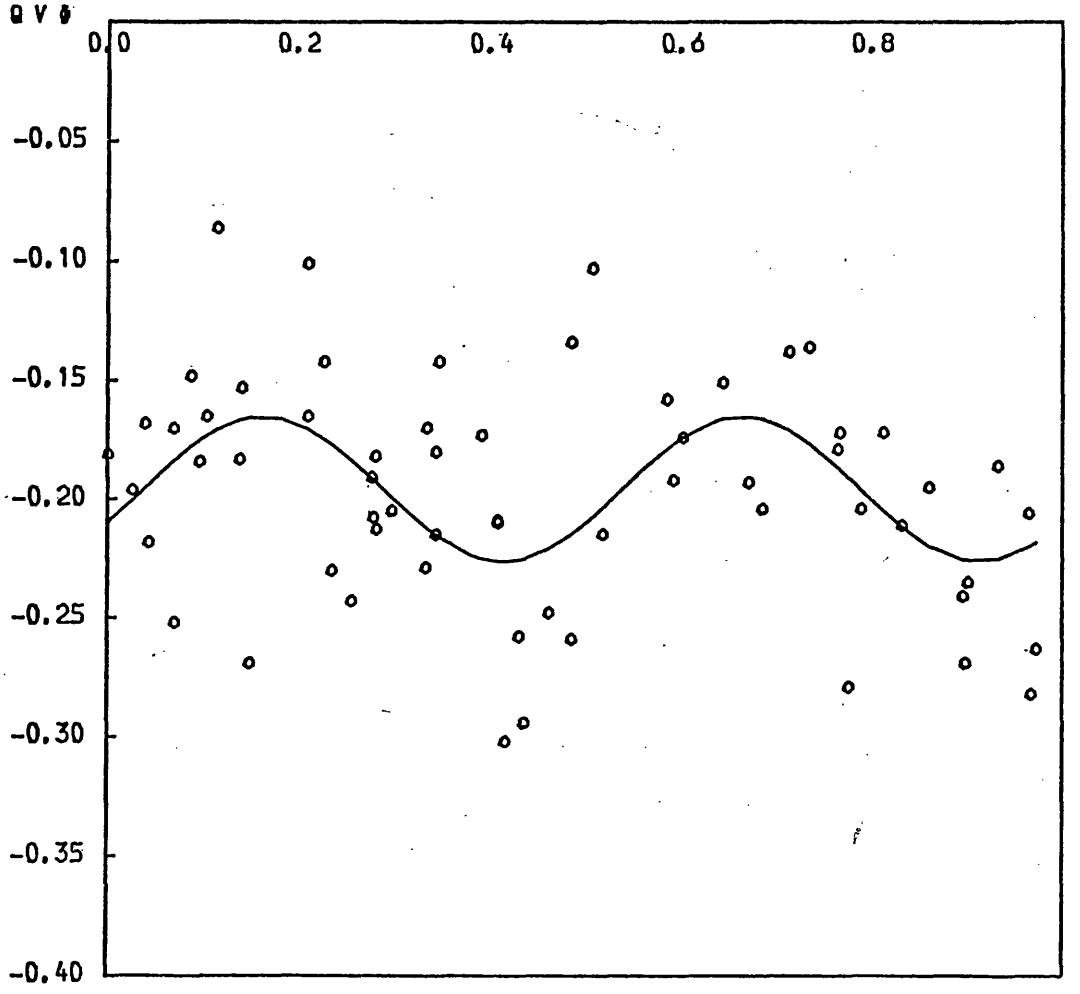

FIGURE 8.3d

Plot of raw data and best fit canonical model (2 harmonics only) for the syseem HD47129.

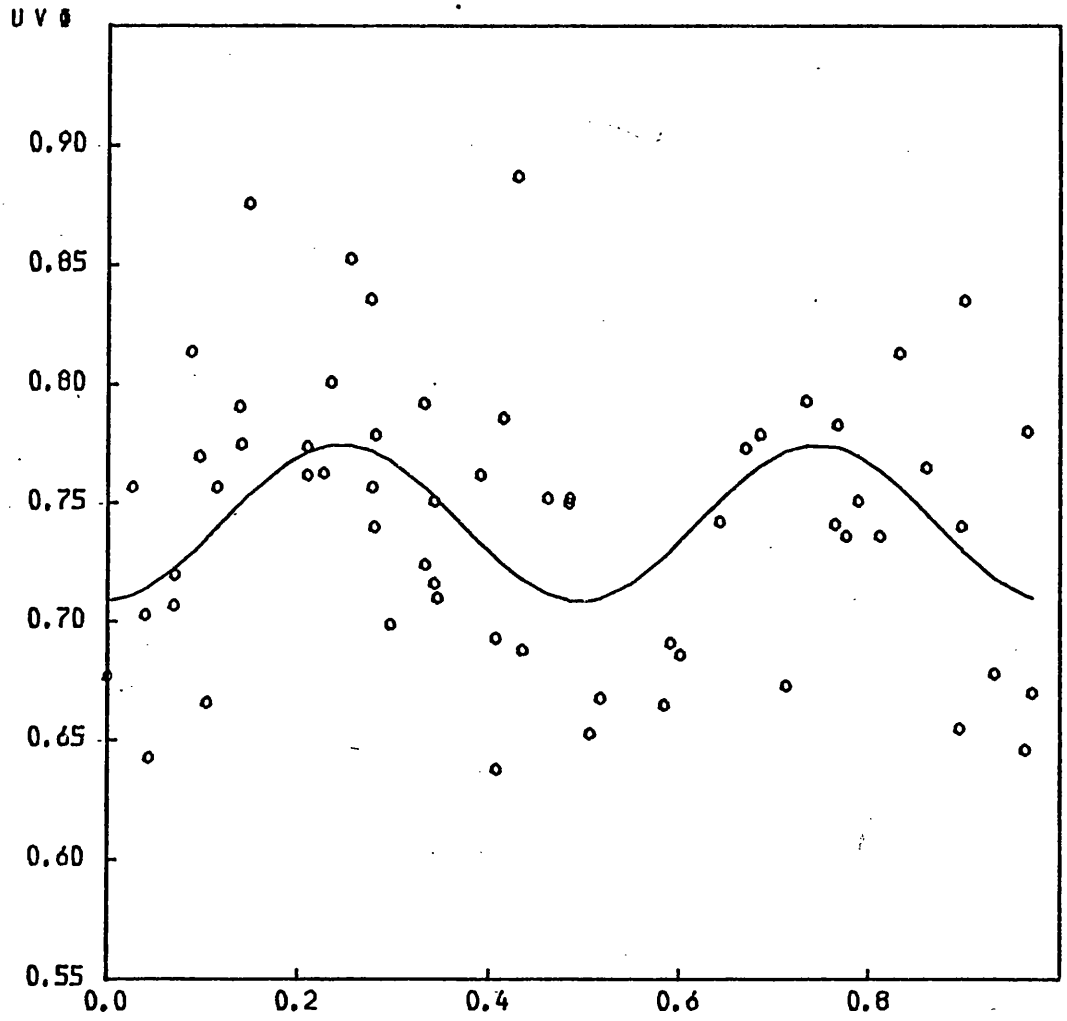

FIGURE 8.3e

see8.3d

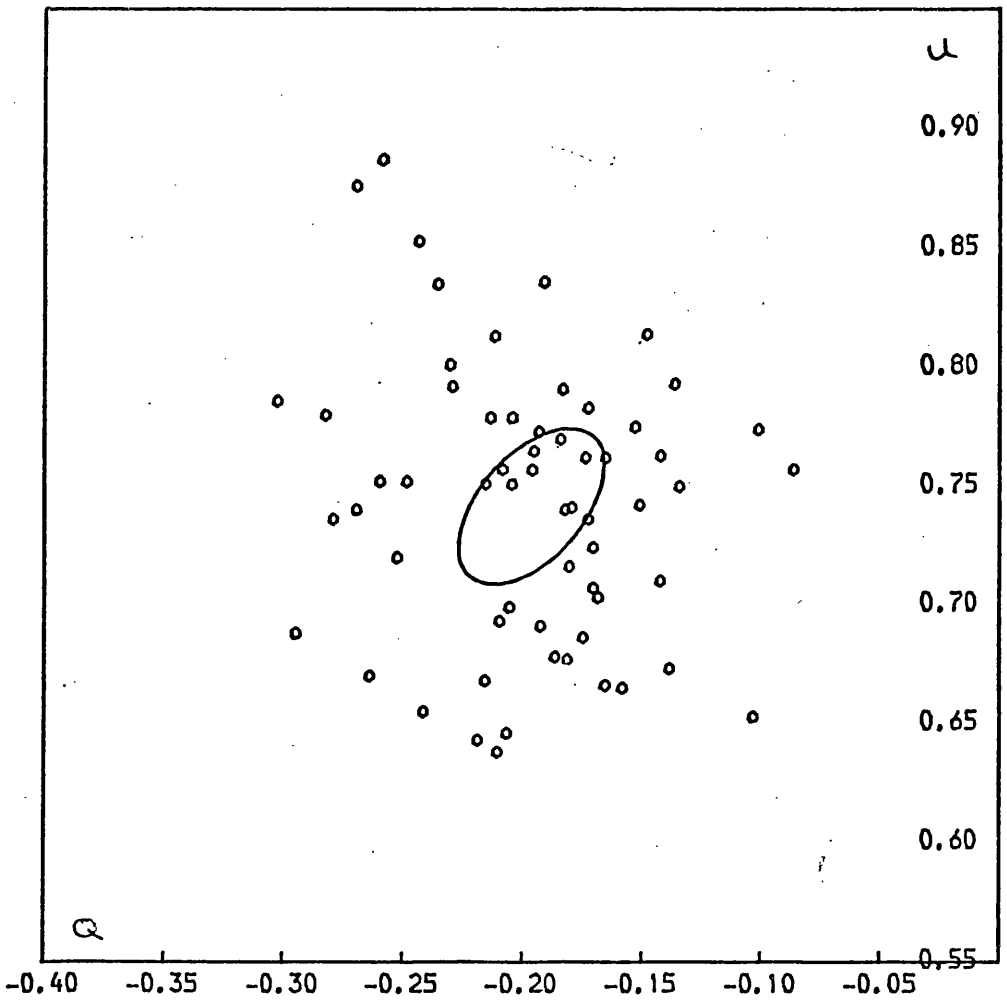

FIGURE 8.3f

see 8.3d

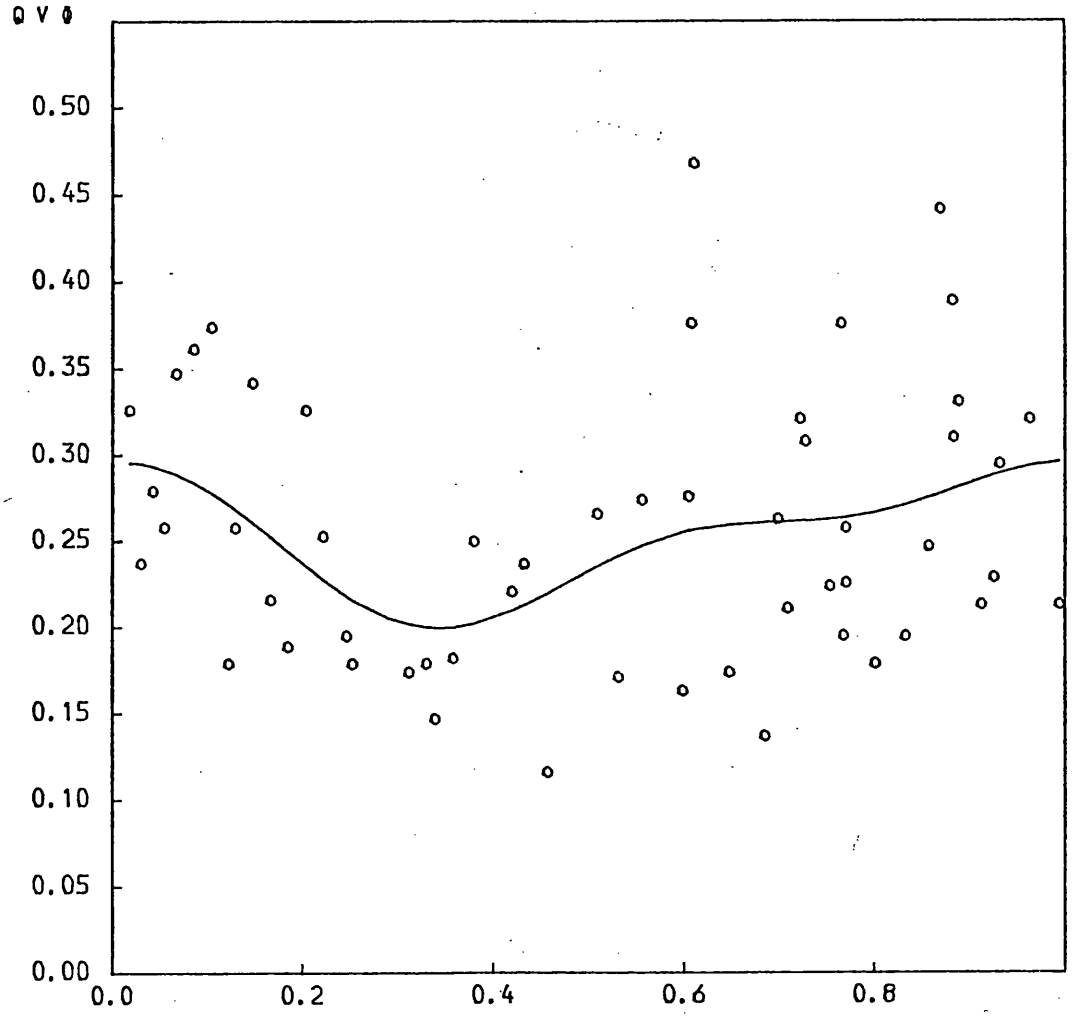

FIGURE 8.4a

Plot of raw data and best fit canonical model (1 and 2 harmonics) for the system Ori E (in the B filter).

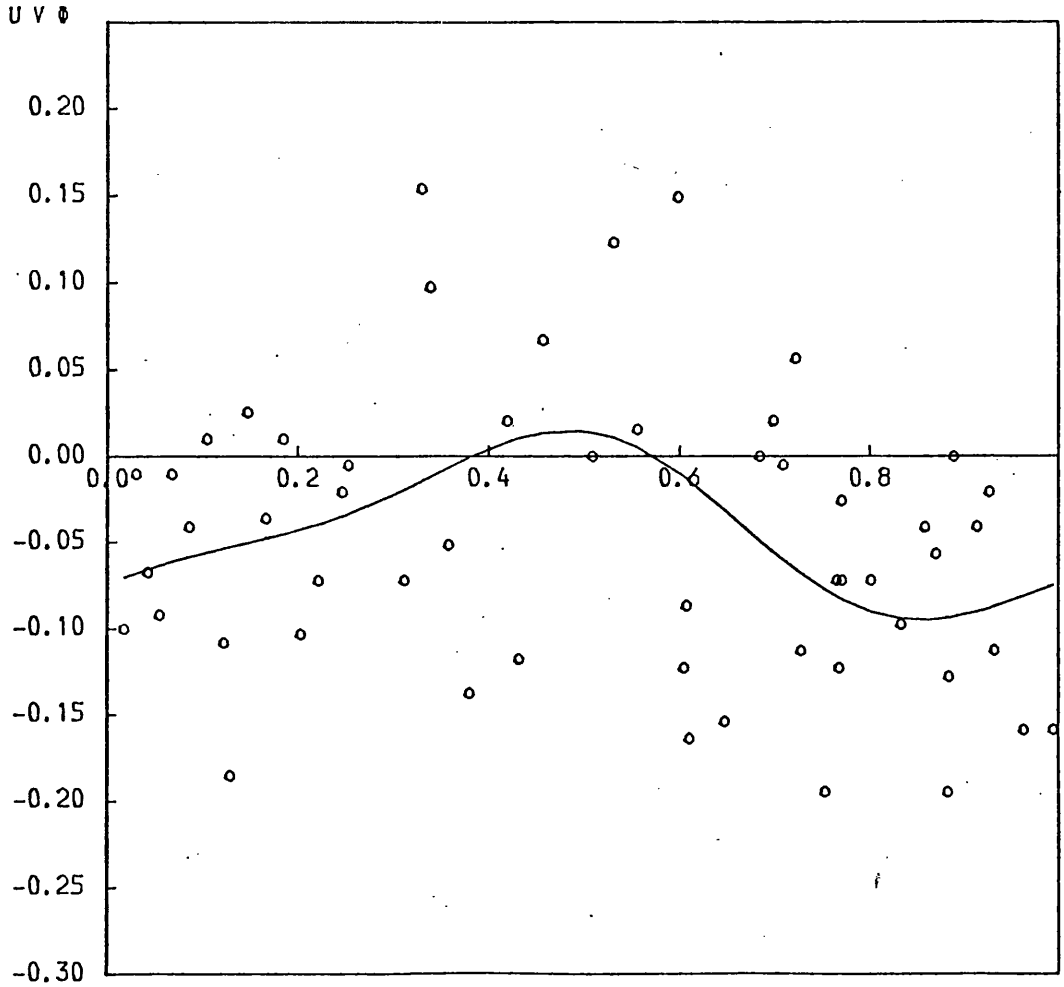

FIGURE 8.4b

see 8.4a

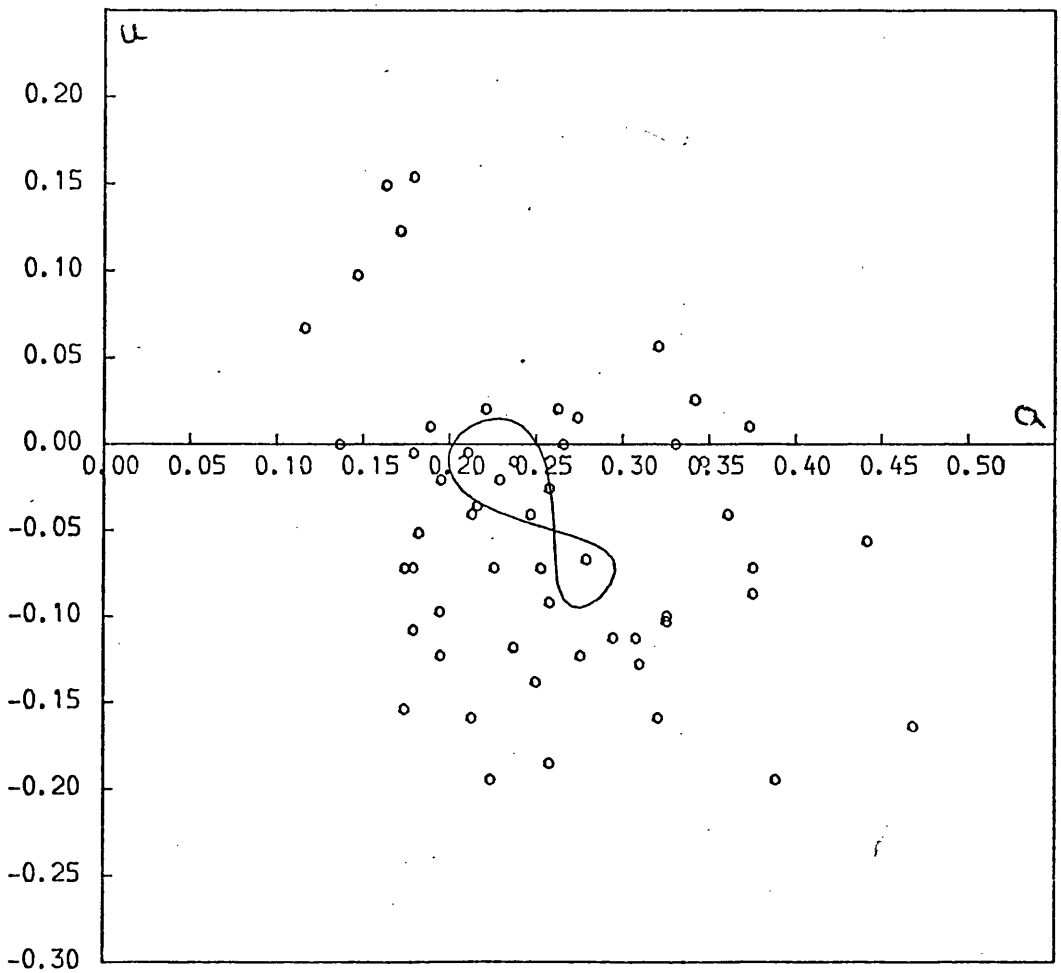

FIGURE 8.4c

see 8.4a

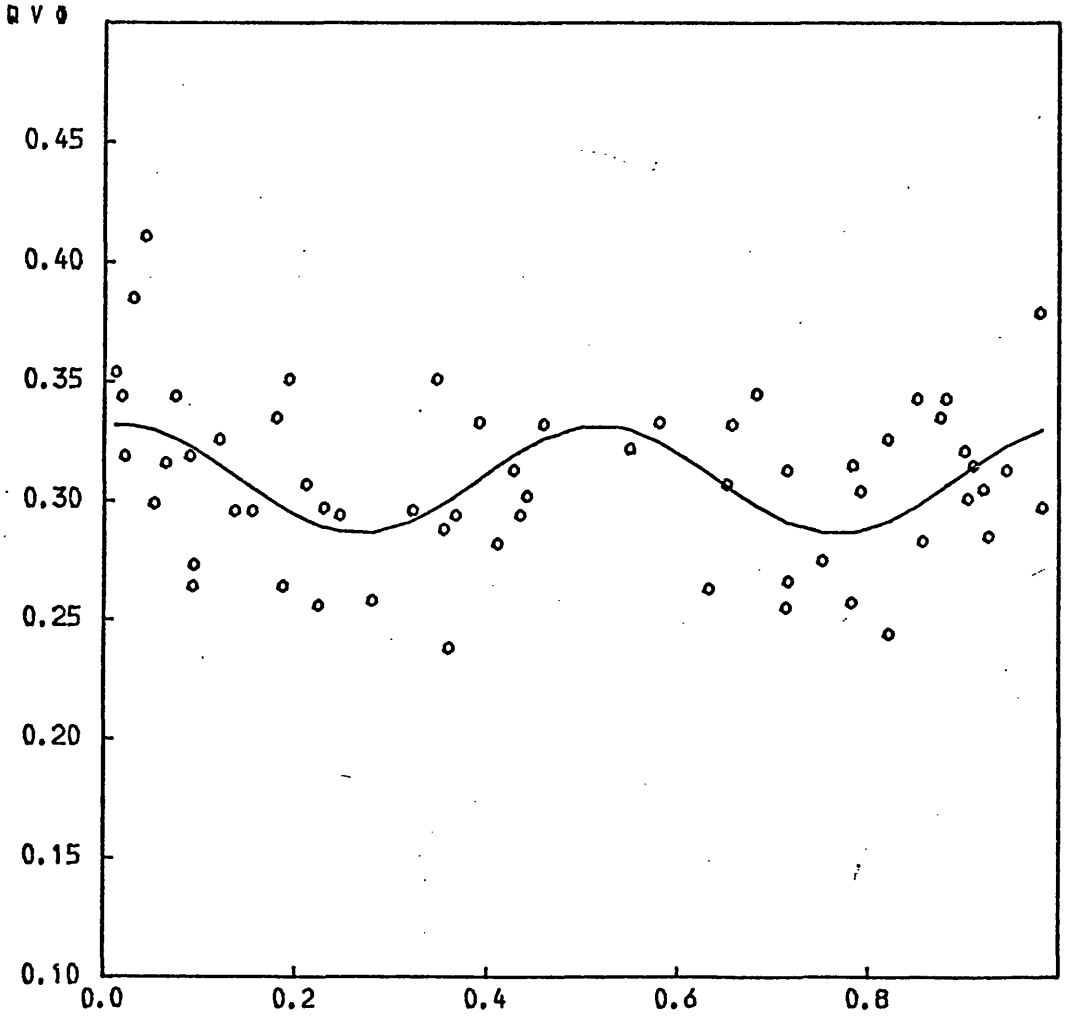

FIGURE 8.4d

Plot of raw data and best fit canonical model (2 harmonics only) for the system Ori E (in the B filter).

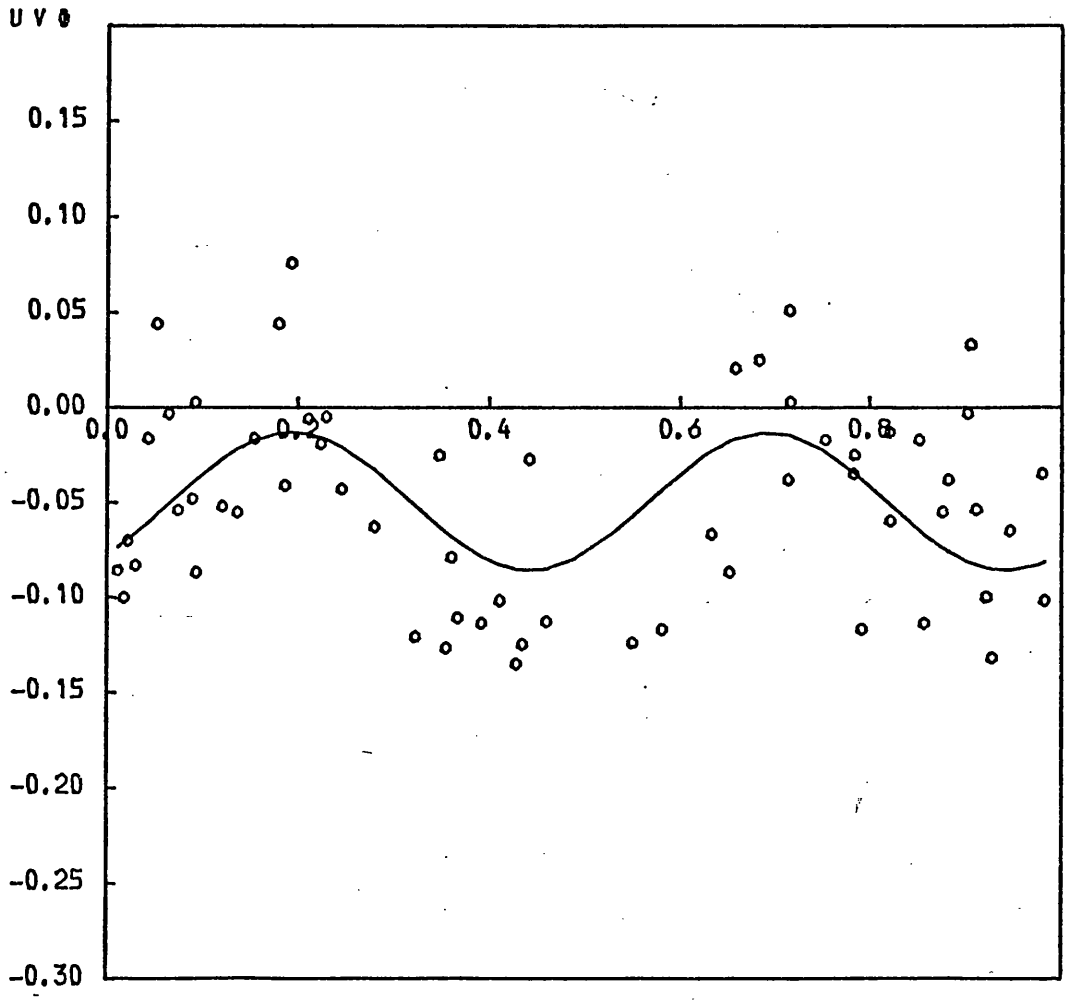

Figure 8.4e

see 8.4d

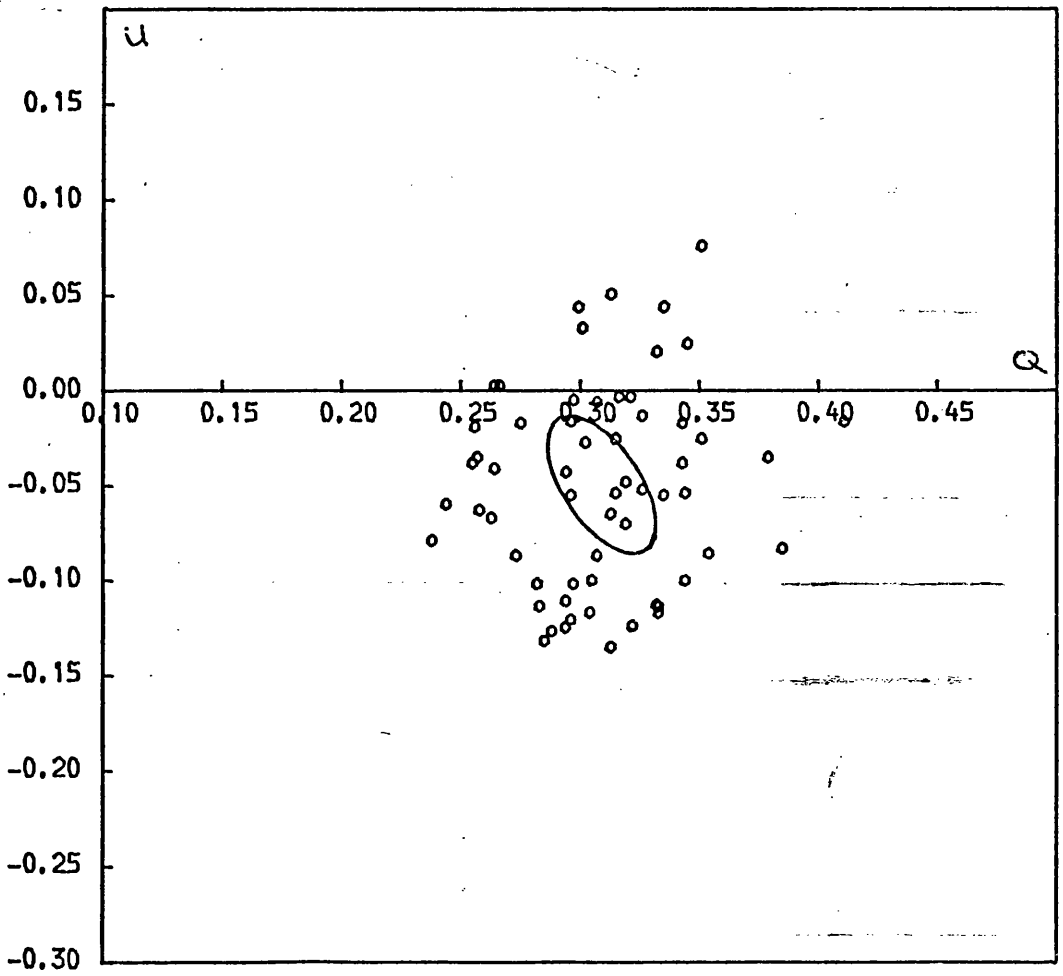

FIGURE 8.4f

see 8.4d

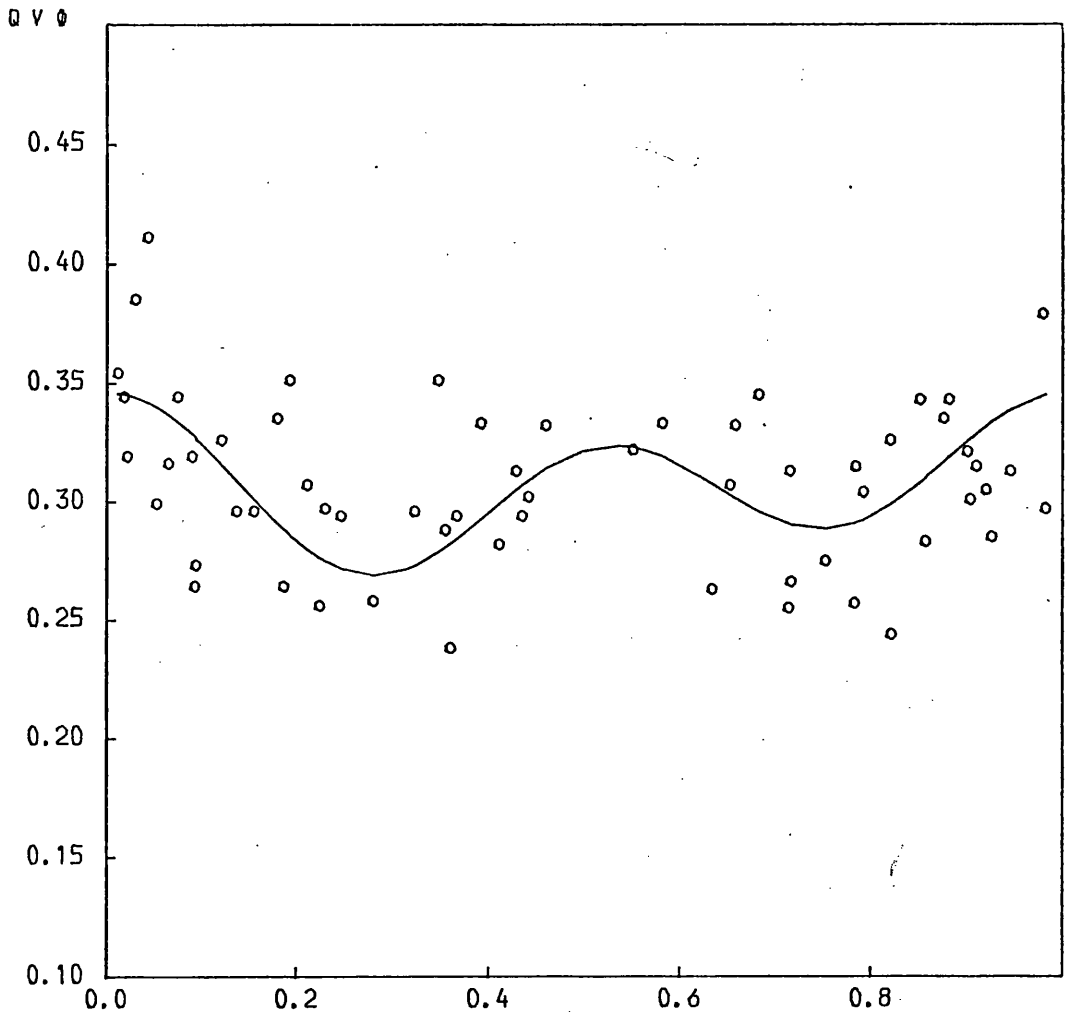

FIGURE 8.5a

Plot of raw data and best fit canonical model (1 and 2 harmonics) fot the system Ori E (in the U filter).

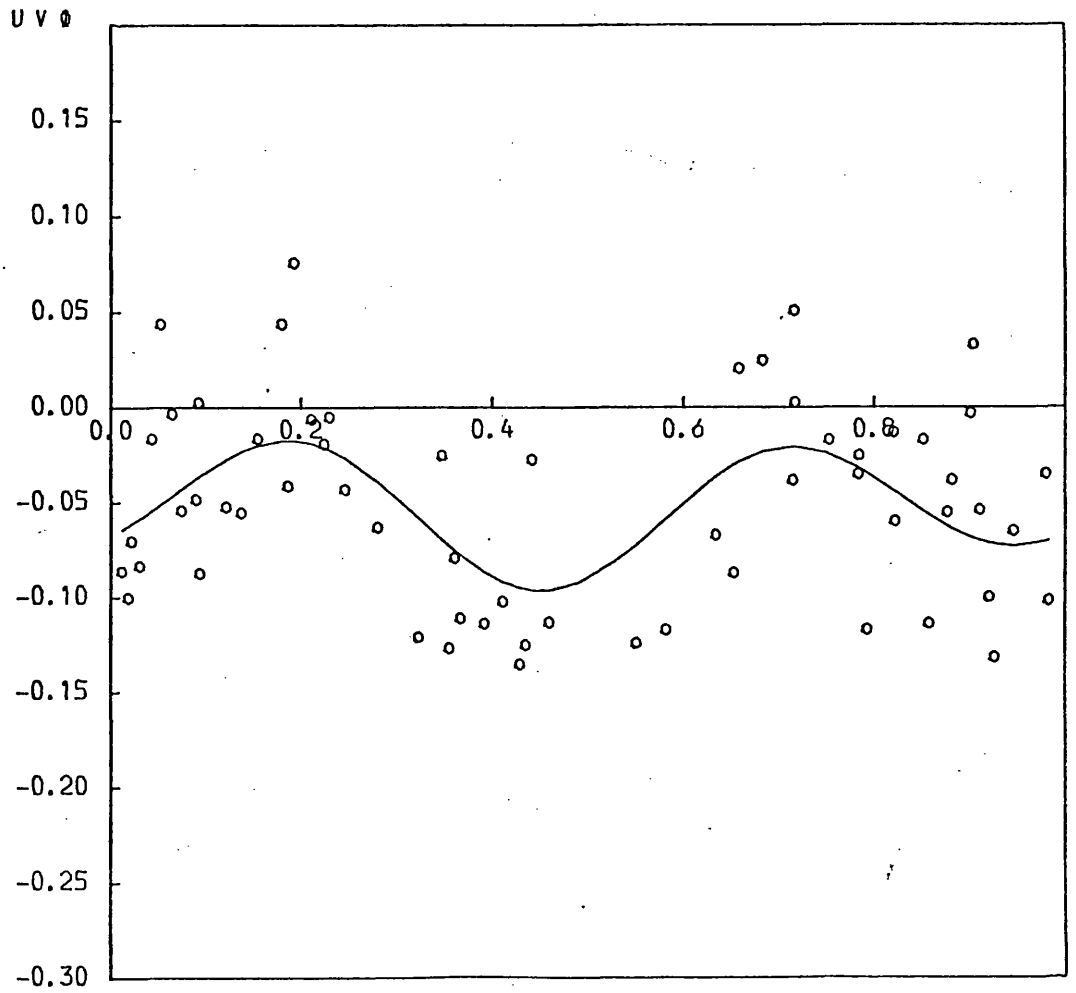

FIGURE 8.5b

see 8.5a

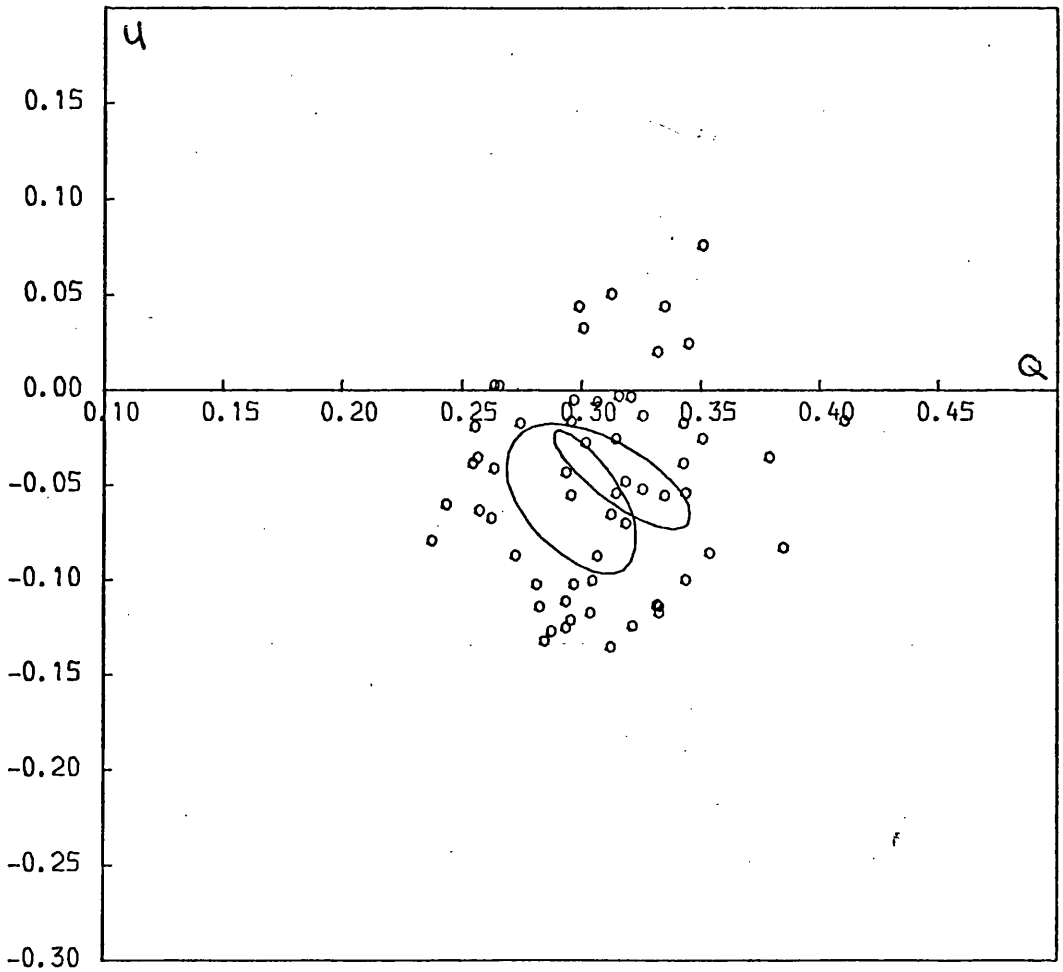

FIGURE 8.5c

see 8.5a

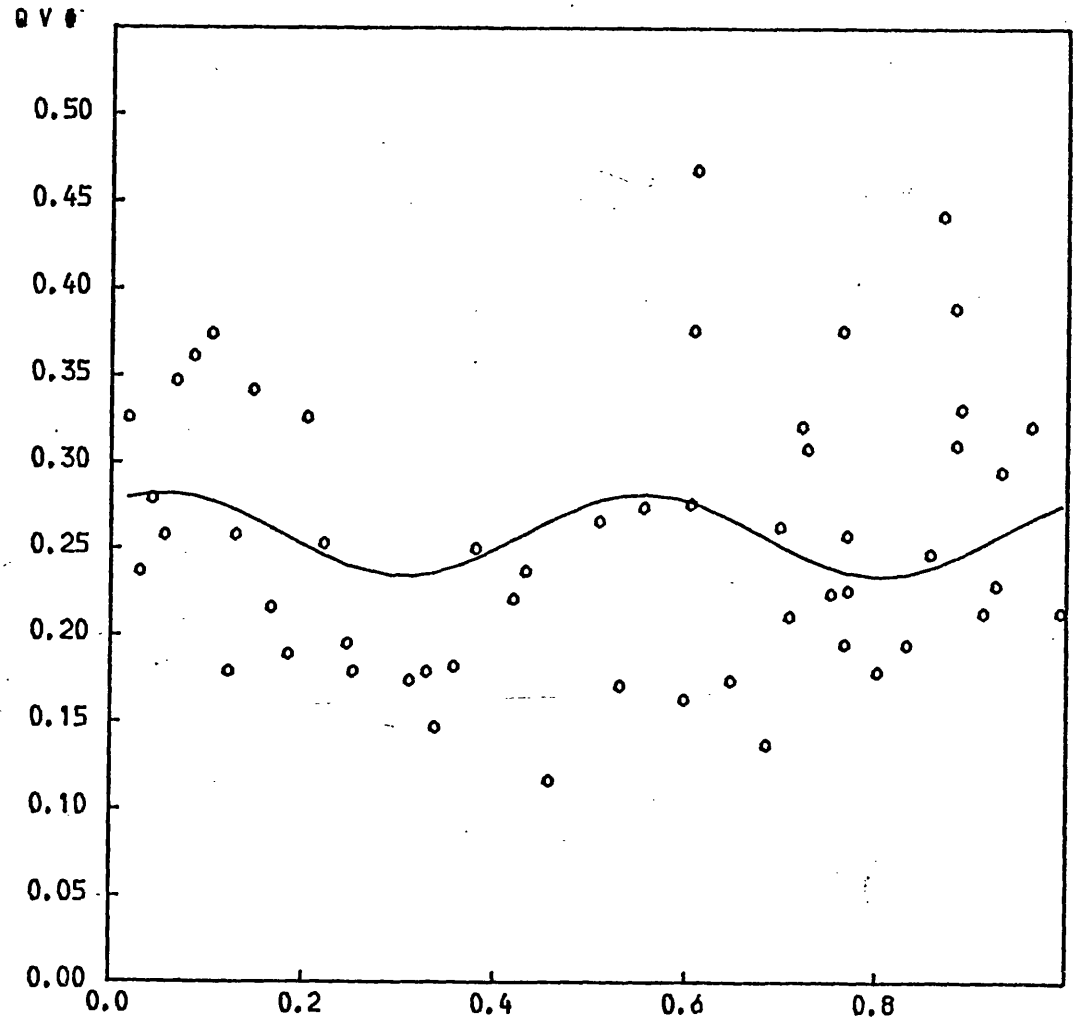

FIGURE 8.5d

Plot of raw data and best fit canonical model (2 harmonics only) for the system Ori E (in the U filter).

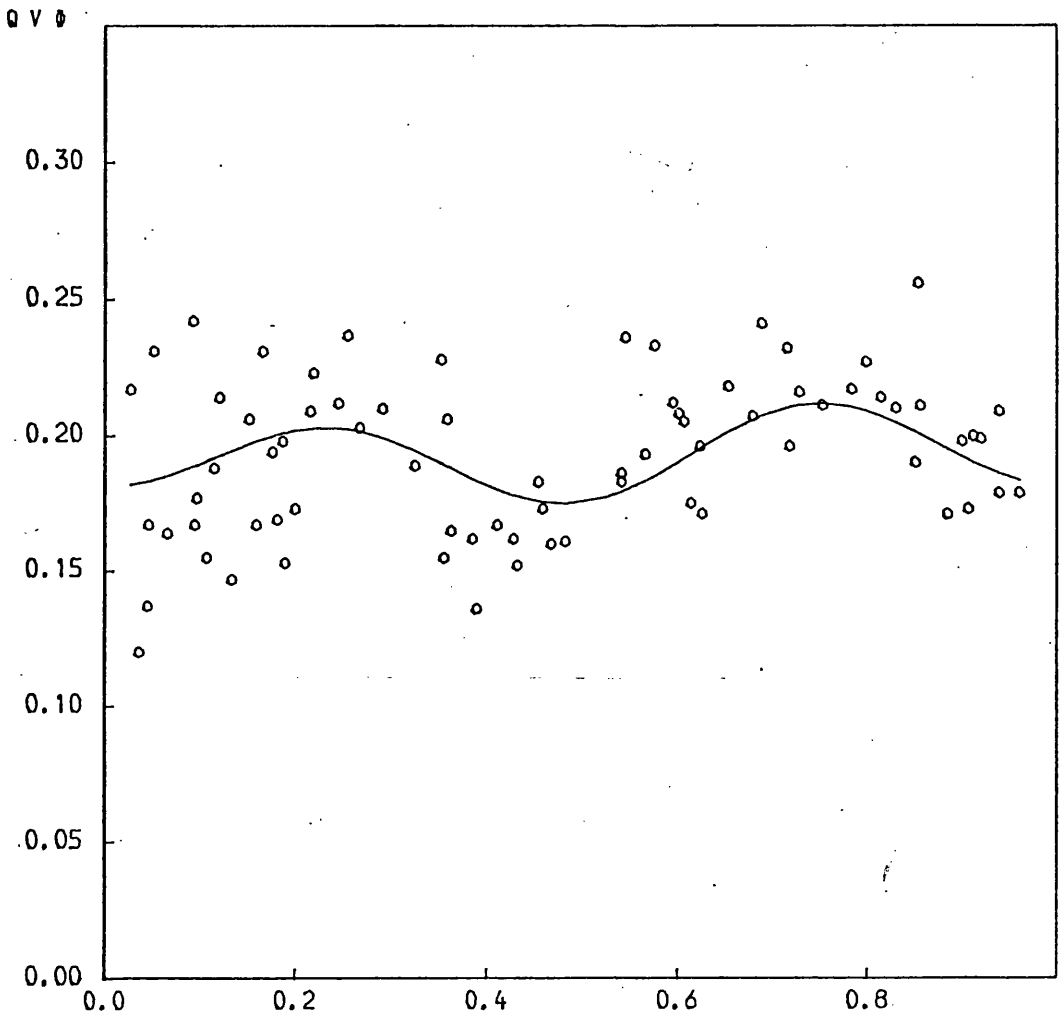

FIGURE 8.6a

Plot of raw data and best fit canonical model (1 and 2 harmonics) for the system U Sge.

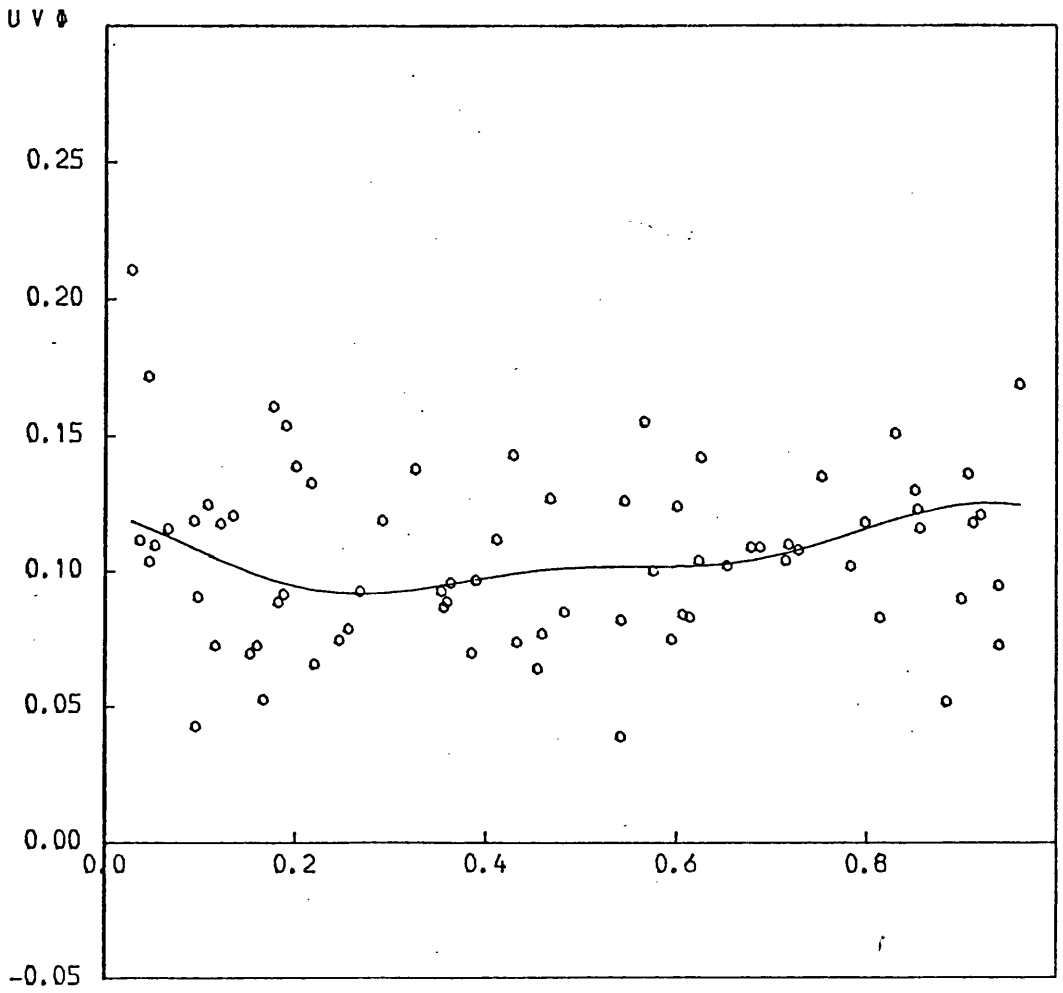

FIGURE 8.6b

see 8.6a

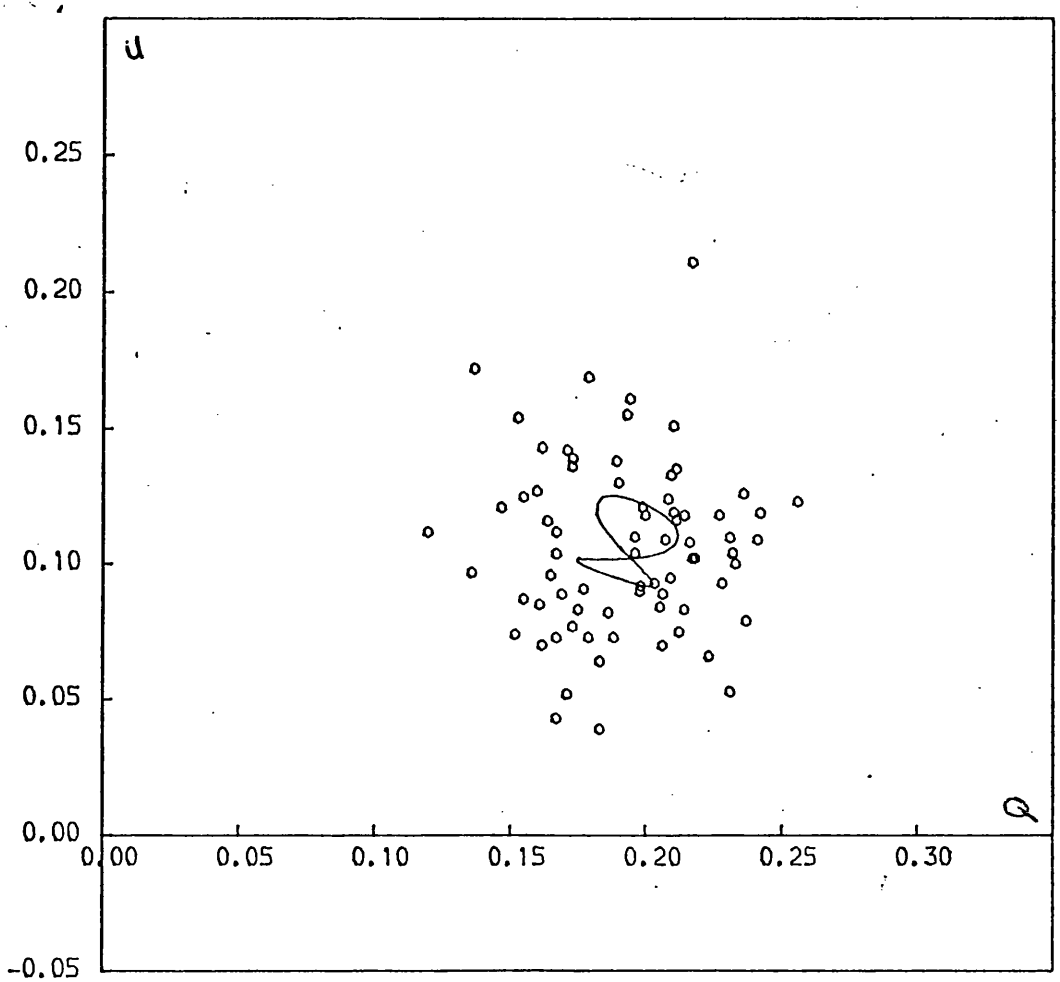

FIGURE 8.6c

see 8.6a

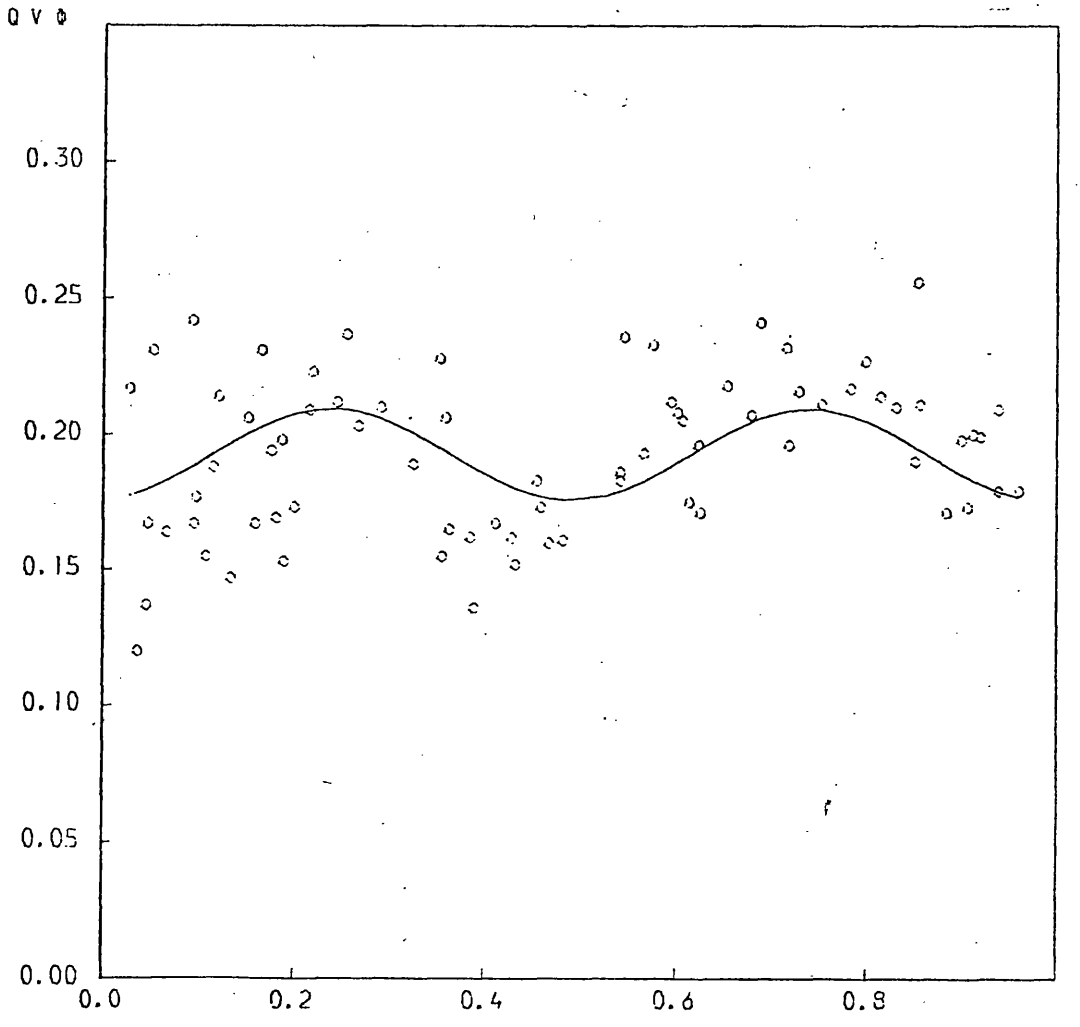

FIGURE 8.6d

Plot of raw data and best fit canonical model (2 harmonics only) for the system U Sge.

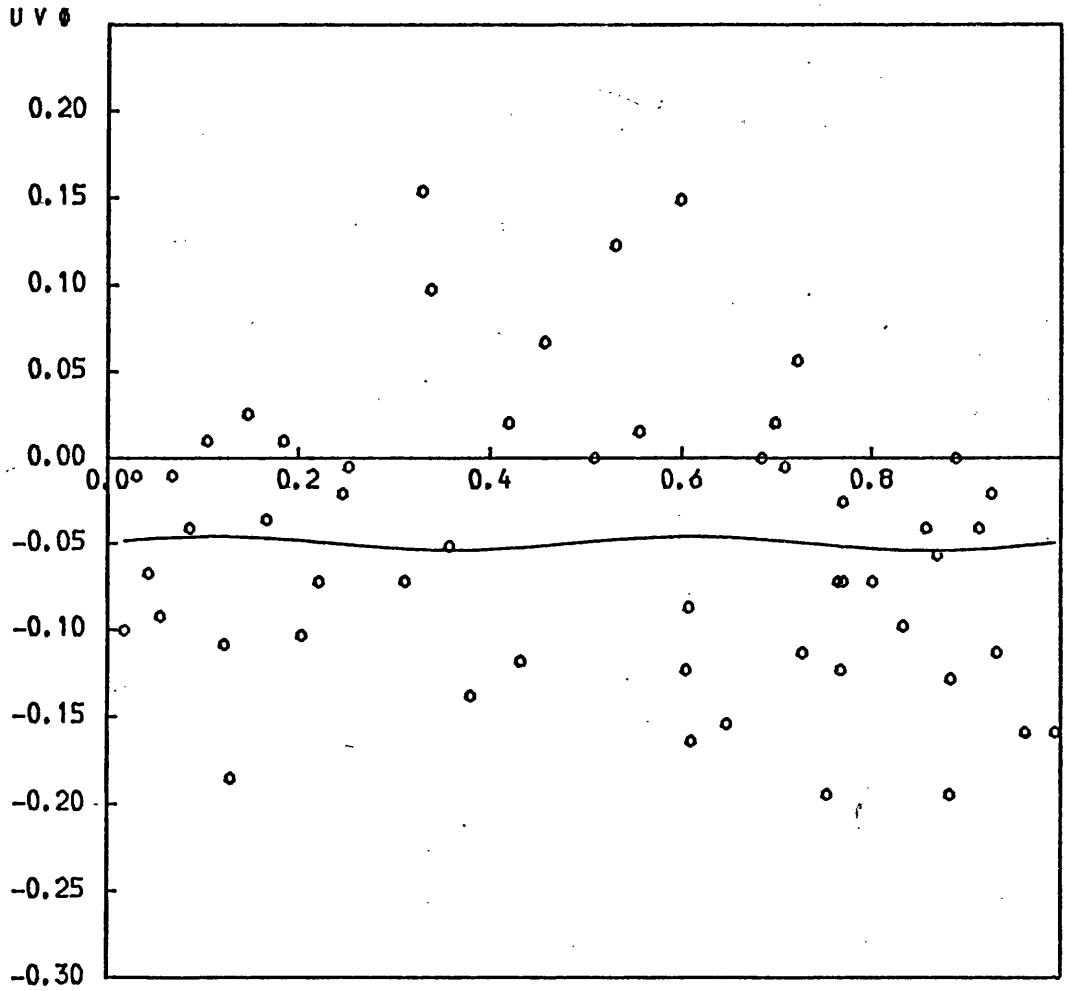

FIGURE 8.6e

see 8.6d

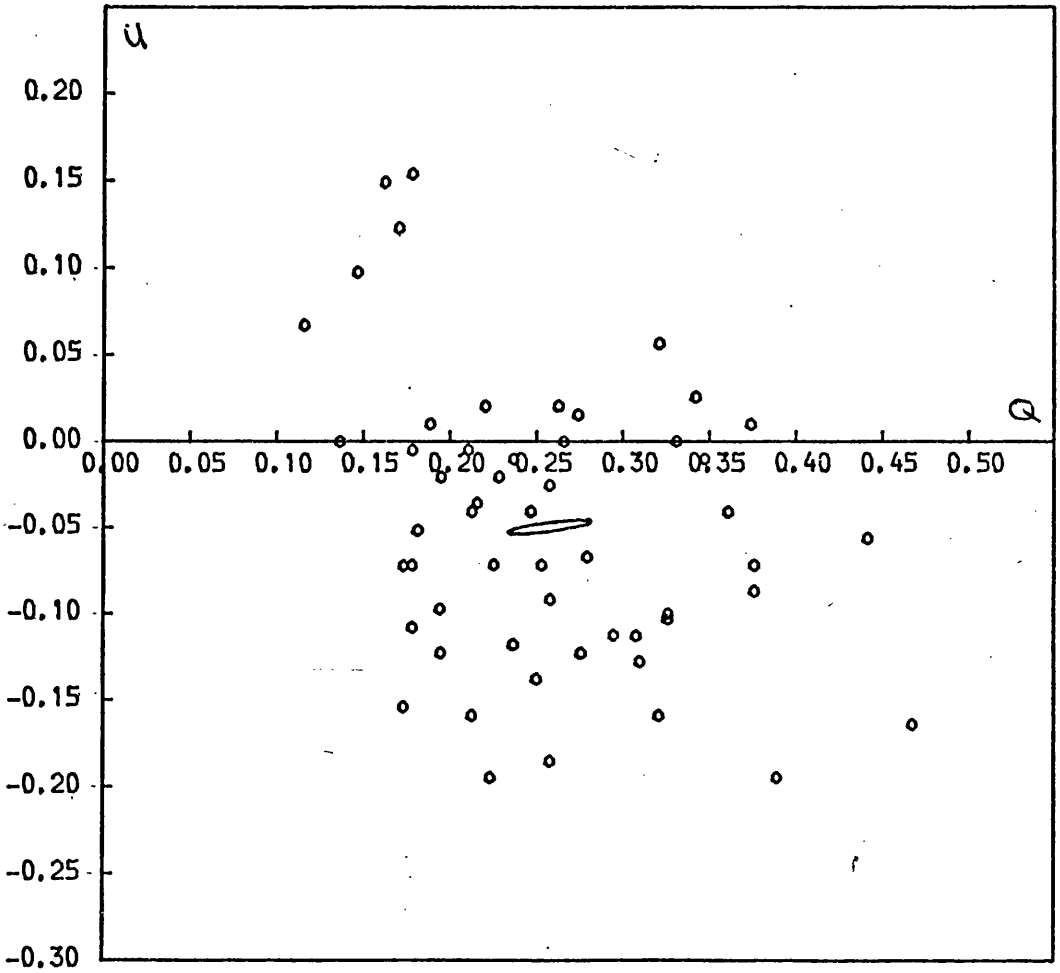

FIGURE 8.6f

see 8.6d

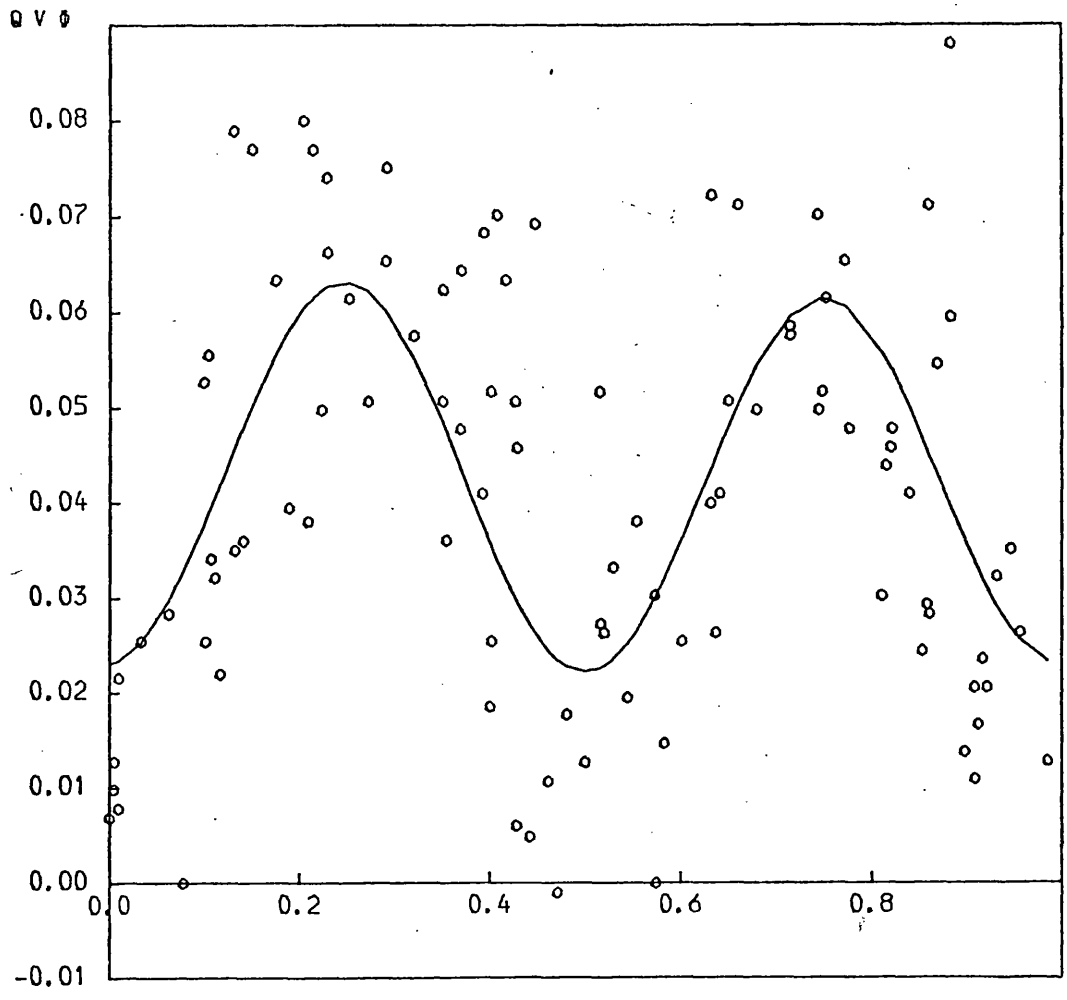

FIGURE 8.7a

Plot of the raw data and best fit canonical model (1 and 2 harmonics) for the system u Her.

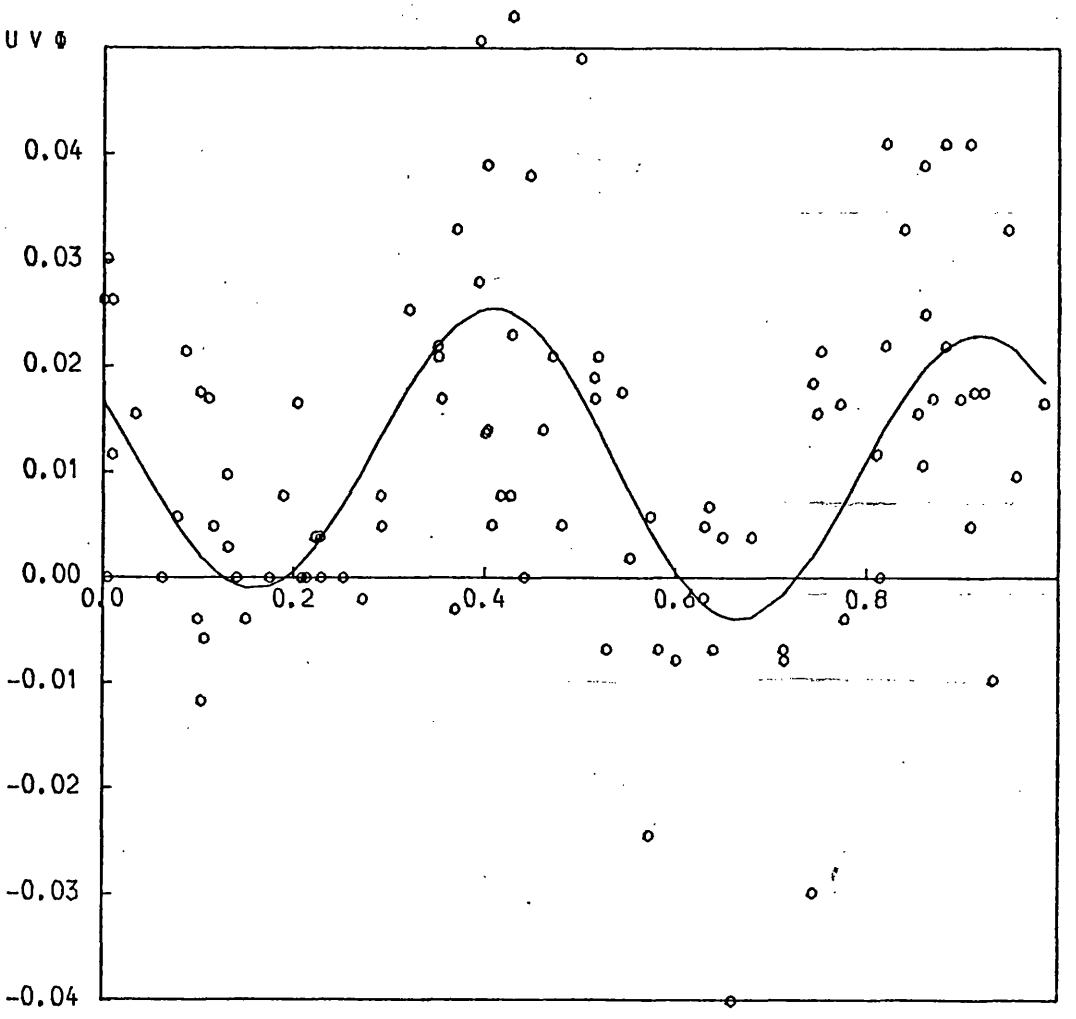

FIGURE 8.7b

seee 8.7a

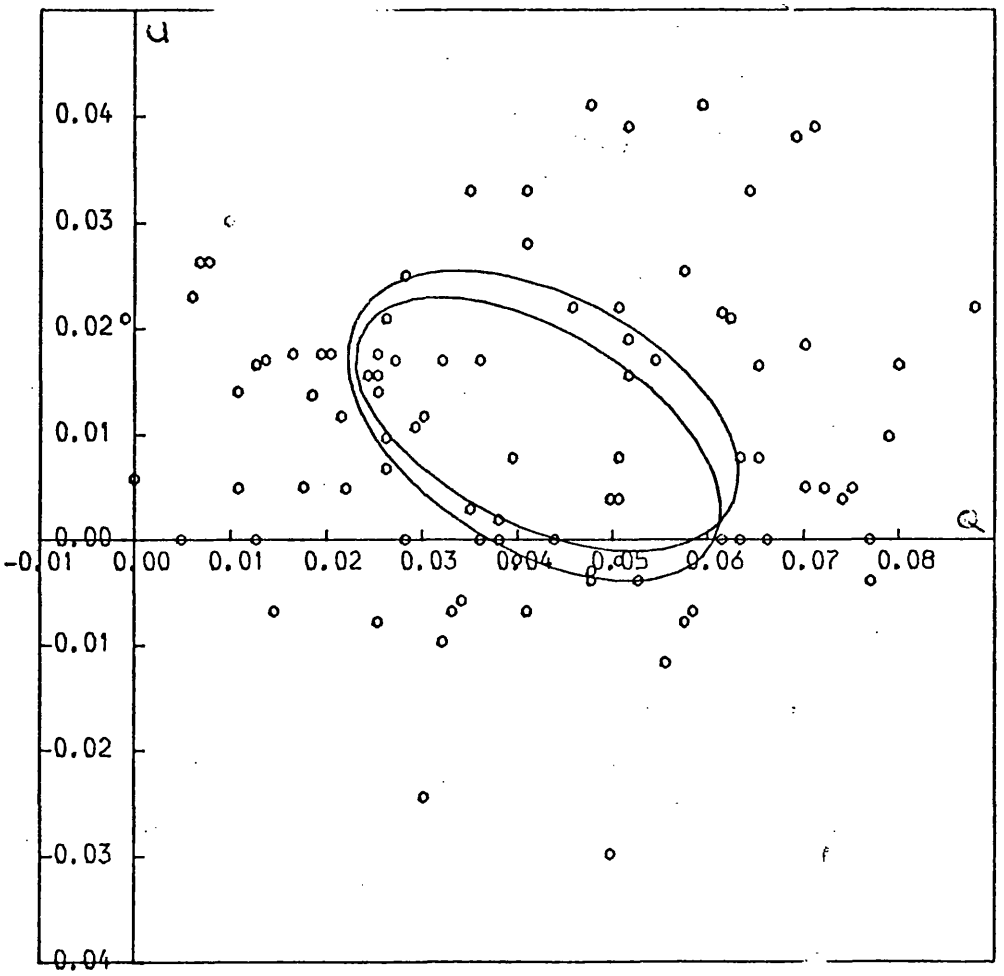

FIGURE 8.7c

see 8.7a

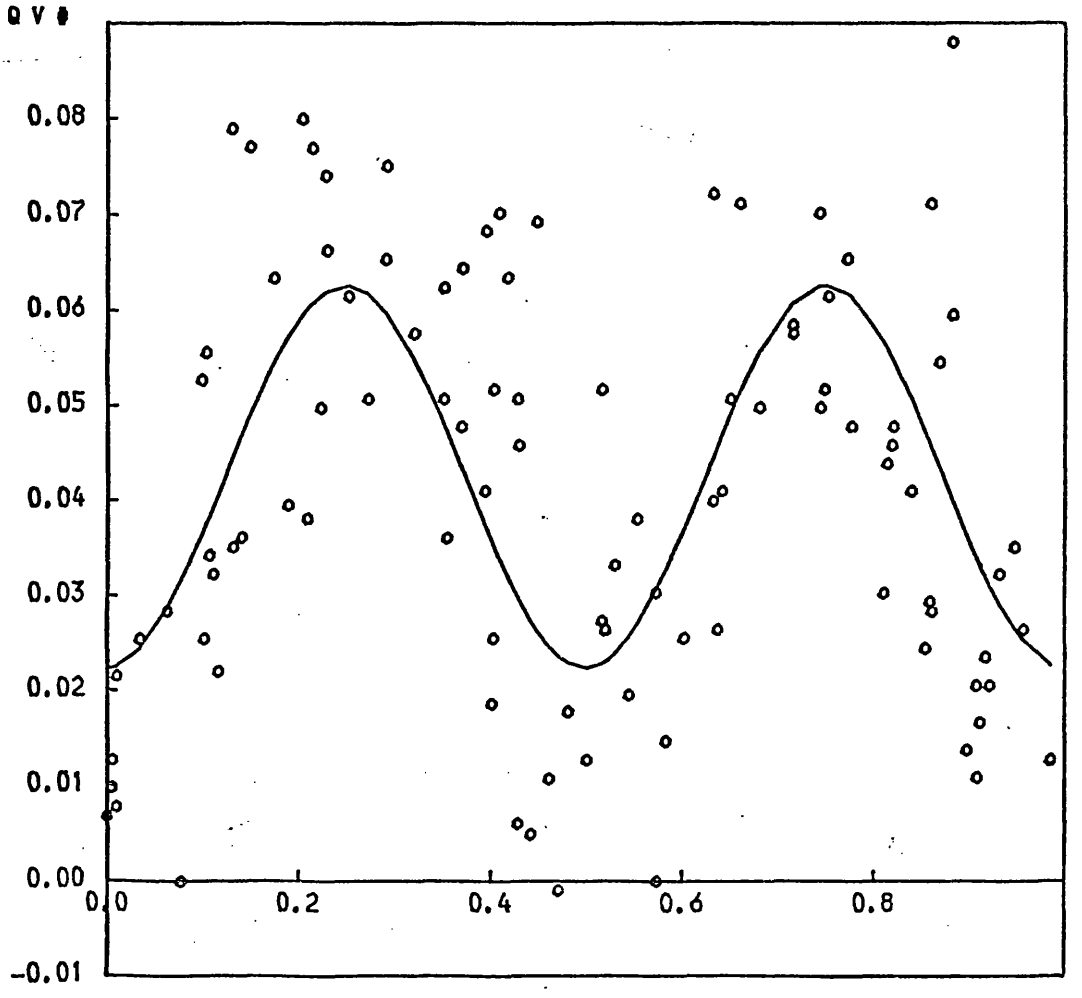

FIGURE 8.7d

Plot of raw data and best fit canonical model (2 harmonics only) for the system u Her.

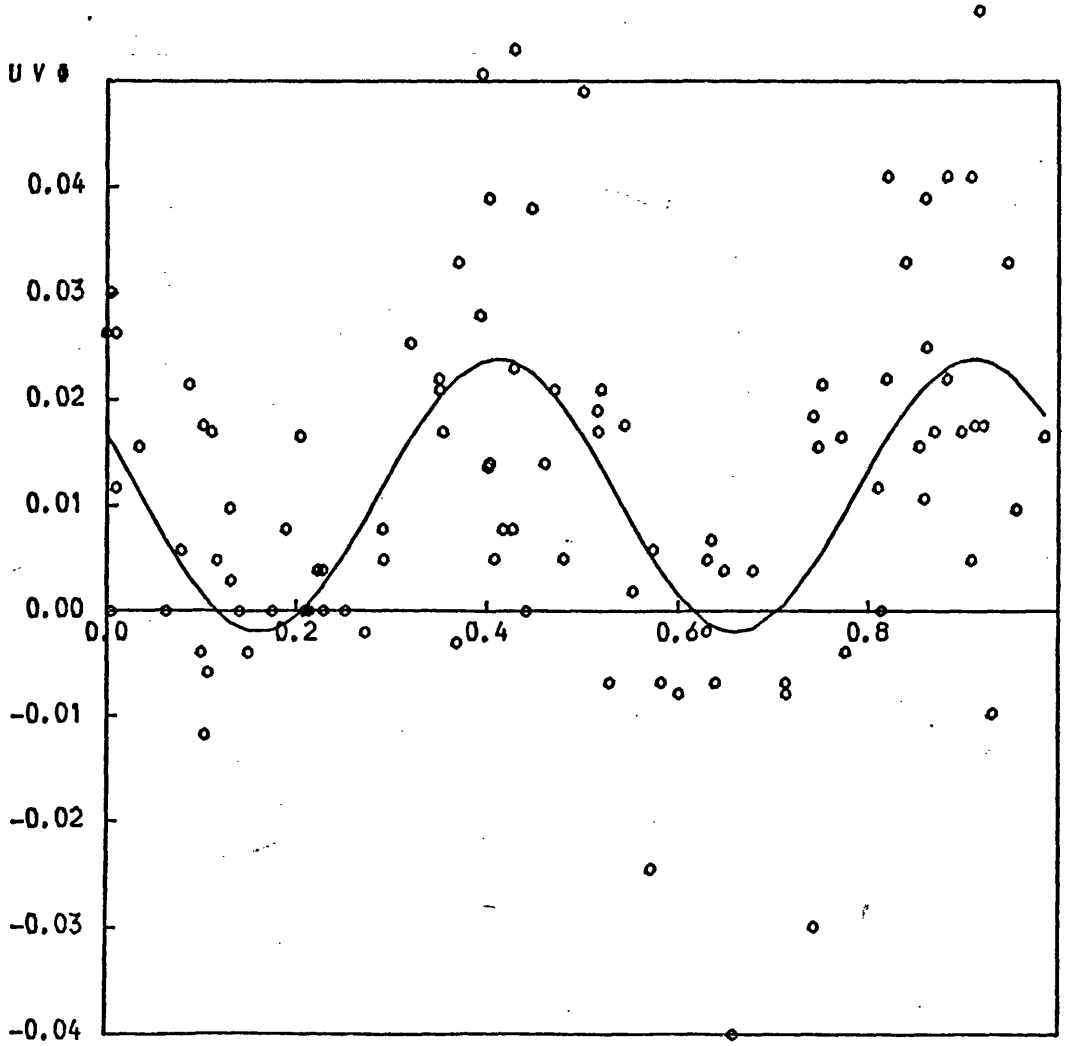

FIGURE 8.7e

see 8.7d

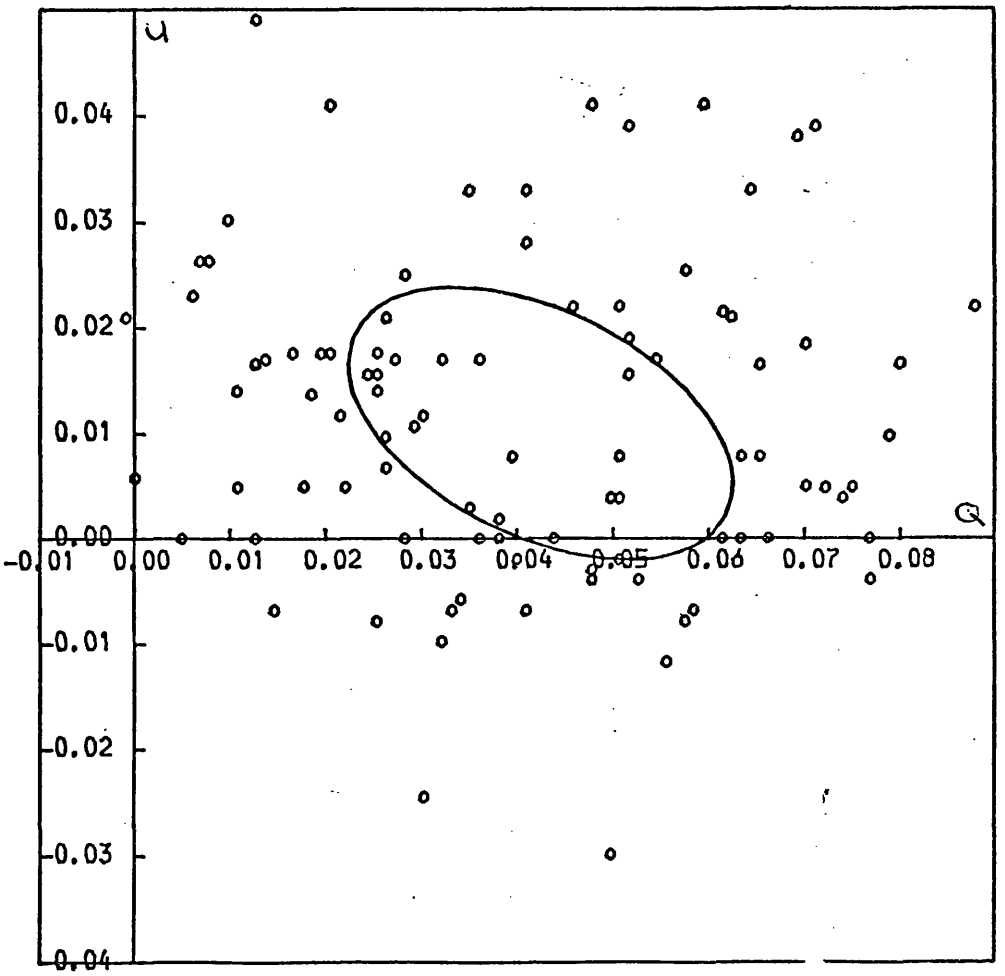

FIGURE 8.7f

see 8.7d

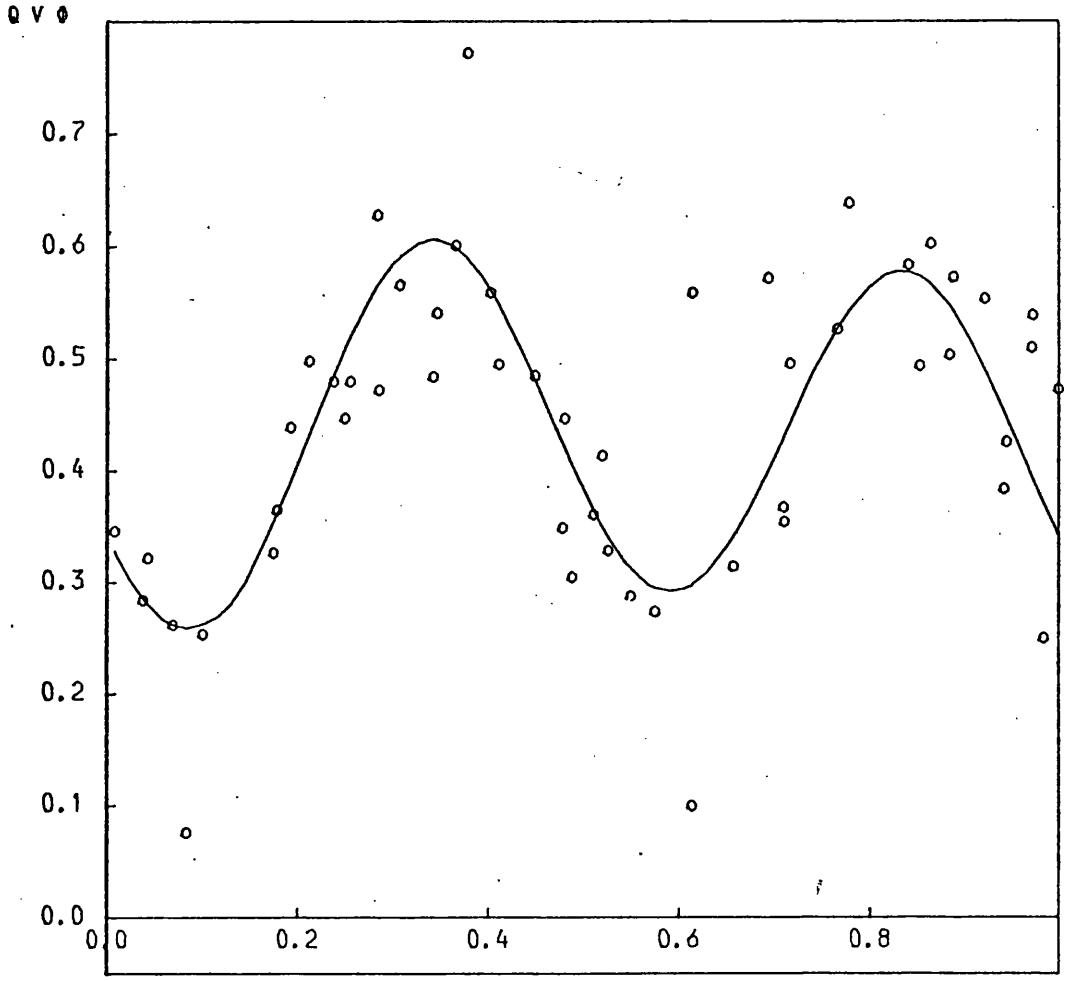

FIGURE 8.8a

Plot of raw data and best fit canonical model (1 and 2 harmonics) for the system V444 Cygni.

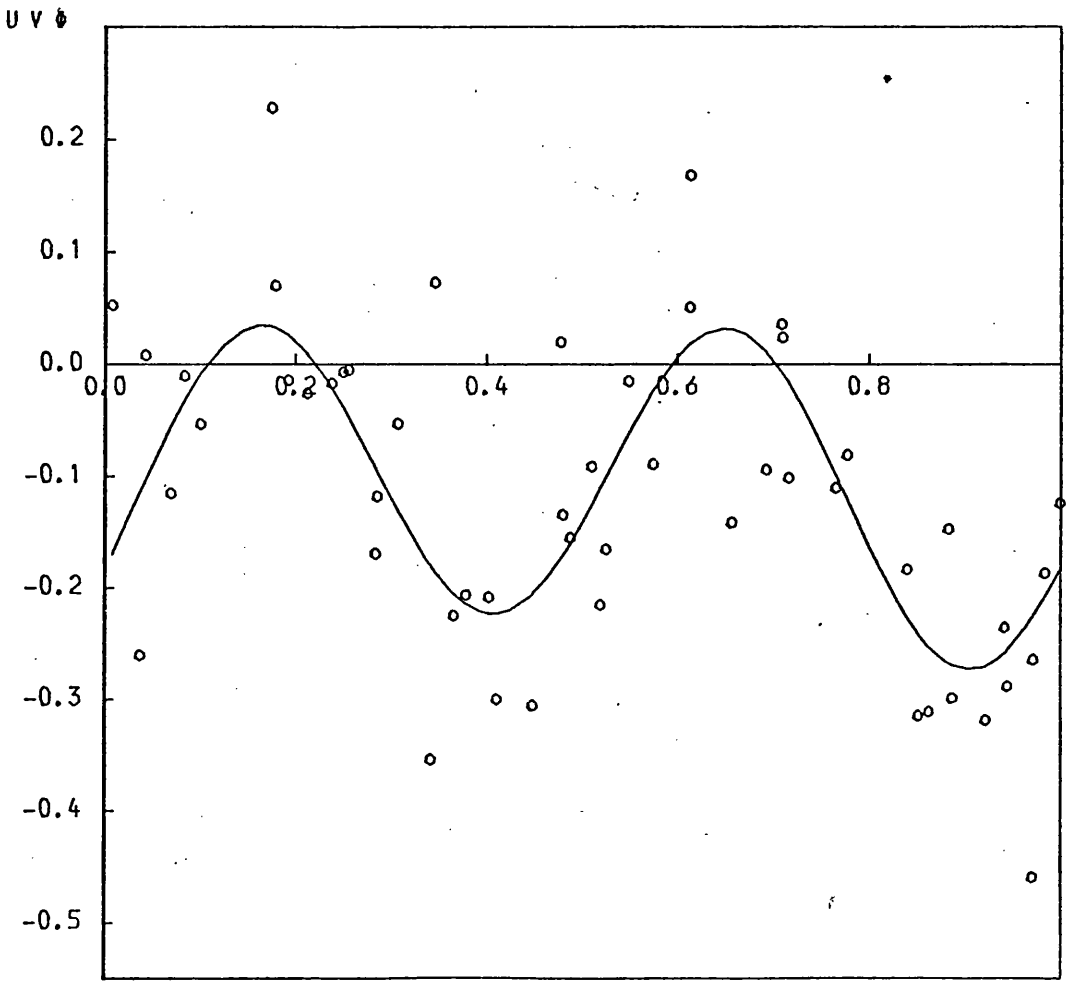

FIGURE 8.8b

see 8.8a

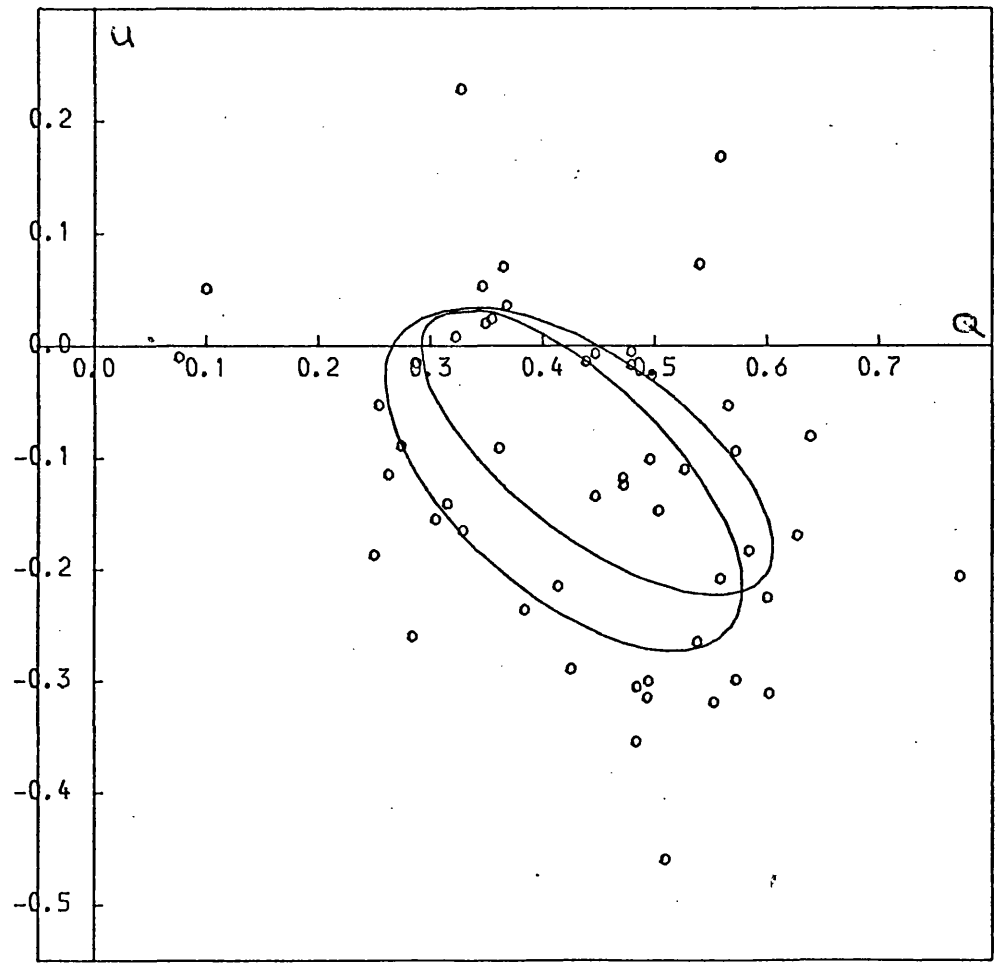

FIGURE 8.8c

see 8.8a

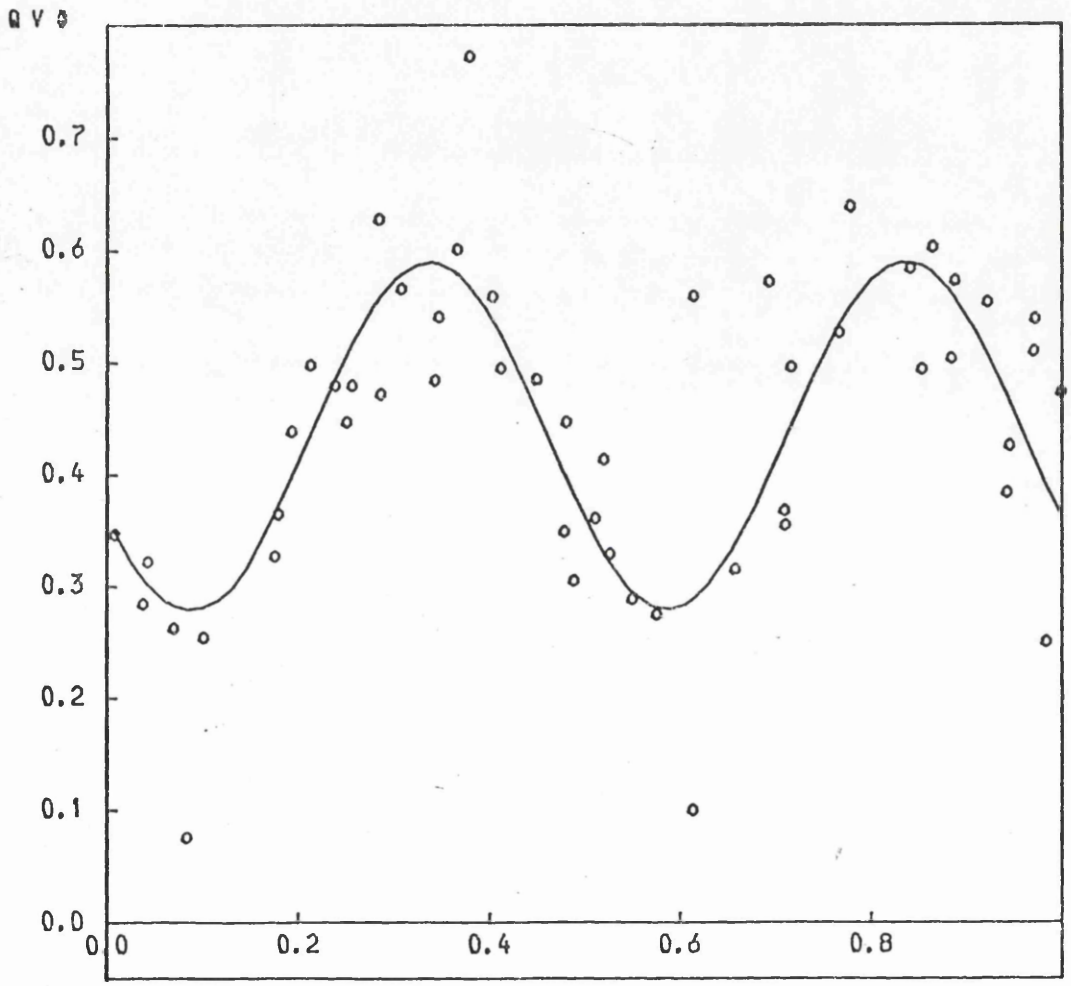

FIGURE 8.8d

Plot of raw data and best fit canonical model (2 harmonics) for the system V444 Cygni.

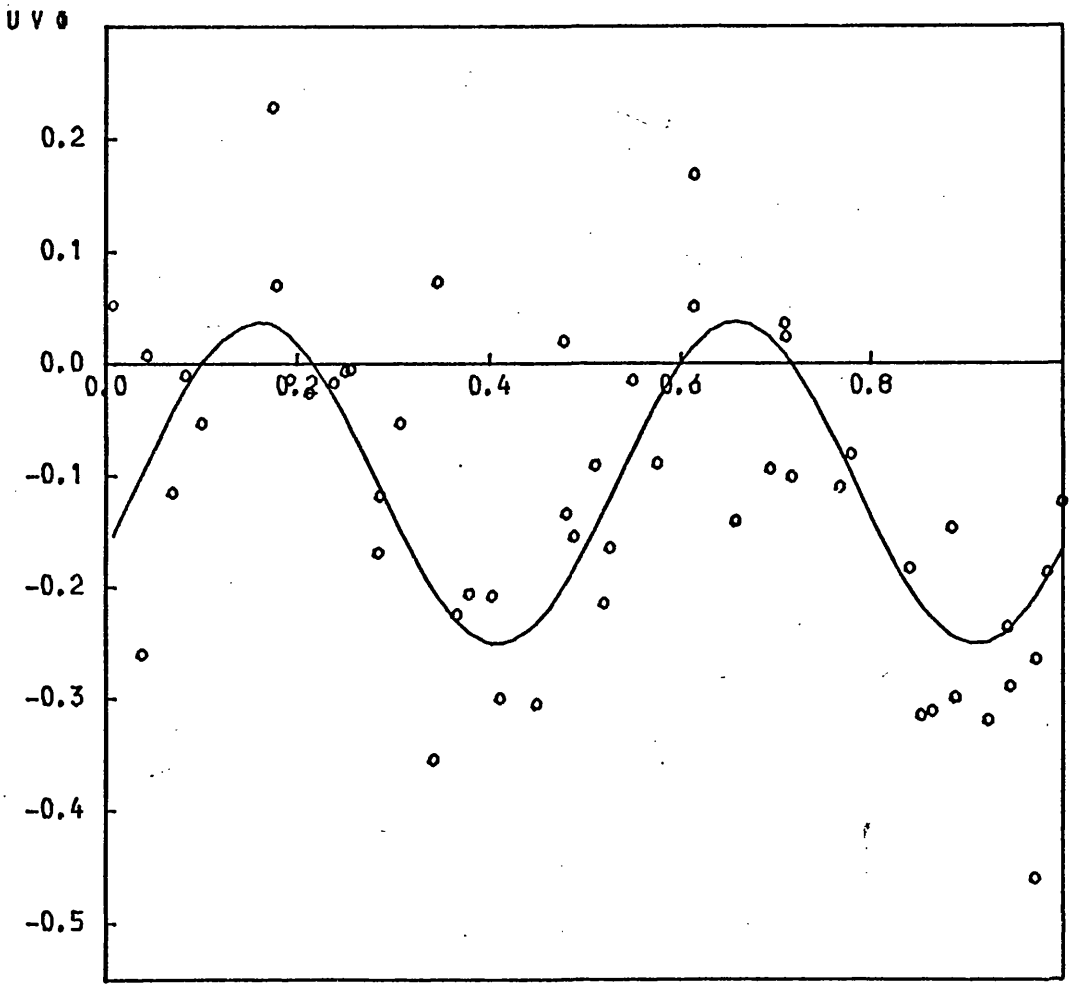

FIGURE 8.8e

see 8.8d

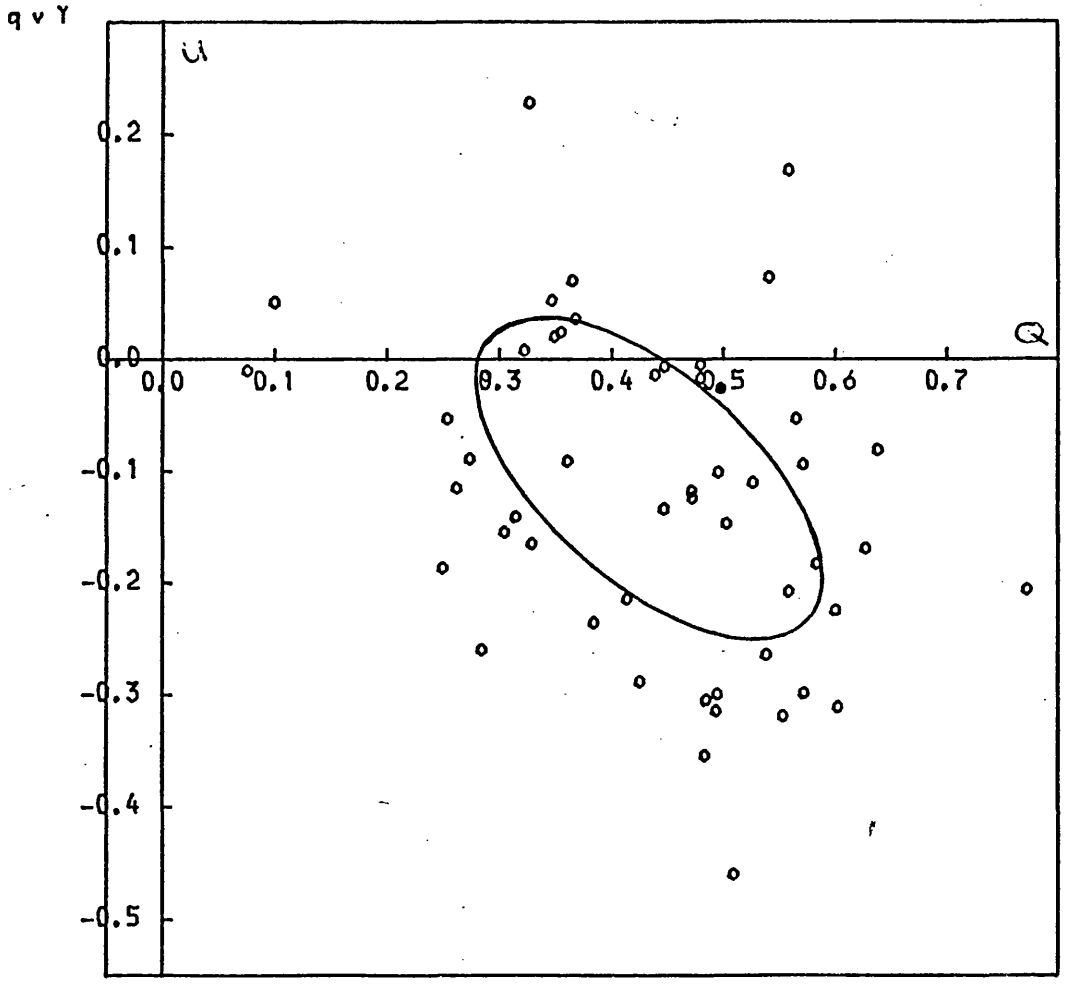

FIGURE 8.8f

see 8.8d

STAR	PRIMARY ECLIPSE	SECONDARY ECLIPSE
ALGOL	0.9,0.1	0.45,0.55
AO CAS	0.85,0.15	0.45,0.55
U HER	0.9,0.1	0.4,0.6
σ ORI E	0.9,0.1	0.3,0.5
U SGE	0.9,0.1	0.42,0.58
V444 CYG	0.9,0.1	0.42,0.58

TABLE IV

ECLIPSE REGION INDICATED IN PHASE

STAR	N	IOPT	MODEL SIG	RCI 10%	X
ALGOL	34	79°	.1%	$0^{\circ},90^{\circ}$	1.3
AO CAS	21	72°	<.001%	$10^{\circ},84^{\circ}$	2.0
U HER	58	74°	<.001%	$0^{\circ},90^{\circ}$	1.4
σ ORI E(B)	30	82°	<.001%	$0^{\circ},90^{\circ}$	2.4
σ ORI E(U)	35	85°	<.001%	$0^{\circ},90^{\circ}$	2.2
U SGE	53	55°	5%	$0^{\circ},90^{\circ}$	1.1
V444 CYG	31	75°	<.001%	$0^{\circ},90^{\circ}$	1.45

N = NUMBER OF DATA POINTS

X = SIGMA(HAT)/SIGMA(DAT)

TABLE V

nature of (Q,U) at some phase is caused by long term systematic variations evolution effects in the scattering region or in fact some other phenomena tending to change the (Q,U) value for a fixed phase over long time intervals. If we divide the long data run into shorter sections and analyse them systematically, perhaps with some overlap between the data sets, then it may be possible to see the effect of these changes reflected in a smooth change in the best fit model parameters as time increases. In this way, with good data, the physical variations occurring in the scattering region may be investigated and some insight may be gained into the polarimetric stability of the system.

One problem encountered with the present data sets was that only that data for Algol, HD47129, U Sge and V444 Cygni was sufficiently complete to allow the application of this technique. For the other systems not enough data was present to allow the sectioning of the data into groups covering small numbers of orbital periods. In the case of [illegible] J.D. time was given for each observation whilst for [illegible] no complete listing of the data (in raw form) was given. (i.e. the data was published ready phased binned).

We impose a constraint that when sectioning the data each group needs to contain more than 15 observations. We divided the data into sections covering 10 and 5 orbital periods and were analysed using the unequal phase interval program (cf. Table V). For Algol 3 overlapping data sets of 10 period coverage and 3 overlapping sets of 5 period coverage were also formed. The optimum inclinations from model fitting were in the range 73° to 81° with, however the model significance being unacceptable at only 0·5% significance (with σ_{dat}) in three cases 1% in one case and at $< 0{\cdot}001\%$ in two other data sets. The values of $\hat{\sigma}$ were larger than σ_{dat} in all cases giving wide confidence intervals i.e. these were still non-phase locked variations present over short 5-10 orbital periods runs of data. Similar results were found for HD 47129 and V444 Cygni. The U Sge data, when sectioned, gave 4 sets covering 10 periods with the optimum inclinations in the range 54° to 81° and a model significance (using σ_{dat}) in all cases $\geq 10\%$ (i.e. 10%, 50%, 10%, 25%). This means that the model fit to the sectioned data was reasonable. The confidence intervals (using $\hat{\sigma}$) were however wide $[\,0^{\circ}, 90^{\circ}\,]$ in all cases (i.e. the 'fit' improved only because of fewer degrees of freedom when comparing χ^2 (i_{opt}) to the tabulated values).

STAR	JD RANGE 2440000+		NO. PERIODS	NO. POINTS	IOPT	MODEL SIG.	X
ALGOL	3012	3032	10	28	80°	.5%	1.25
	3042	3067	10	21	78°	<.001%	1.54
	3027	3053	10	18	73°	1%	1.28
	3012	3026	5	18	78°	.5%	1.35
	3052	3067	5	16	81°	<.001%	1.64
	3020	3032	5	23	77°	.5%	1.28
HD47129	3023	3164	10	34	80°	<.001%	2.6
	3170	3262	10	26	73°	<.001%	3.0
	3100	3262	10	31	81°	<.001%	2.9
	3023	3086	5	21	89°	<.001%	2.6
	3170	3242	5	21	72°	<.001%	3.0
	3133	3192	5	18	83°	<.001%	2.7
U SGE	2941	2974	10	24	61°	10%	1.13
	3002	3031	10	25	81°	50%	1.0
	3041	3068	10	17	54°	10%	1.13
	3018	3051	10	25	79°	25%	1.09
V444 CYG	2947	2989	10	23	79°	<.001%	1.6
	3012	3052	10	25	75°	<.001%	1.6
	2947	2966	5	18	78°	<.001%	1.6

X = SIGMA(HAT)/SIGMA(DAT)

TABLE VI

8·5 Comments on the Results of model fitting

The data for the seven binaries mentioned above have been analysed comprehensively both here (Chapter 8) and earlier (Chapter 5) using both binned forms of the data and the raw unequal phase interval data, with the general (1st and 2nd harmonic) canonical model. In both, the results are comparable in that the σ's used in calculating the model acceptability and confidence intervals are too large to produce good definition of the optimum parameters (i, θ, p) with narrow error bounds. Sequential analysis of the data for Algol and U Sge produced optimistic results, even though a large improvement in data quality is needed before we can be confident about the value of such parameters as the orbital inclination. Likewise, treatment of out-of-eclipse data proved useful but with a similar conclusion being drawn. The optimum inclinations presented here and in Chapter 5, are mostly high ($i > 70^{\circ}$) and when compared to the information on the nature of the systems (i.e. eclipsing) would seem to be reasonable. However, in the presence of the large σ_{dat} (and $\hat{\sigma}$) we have shown in Chapters 3 and 4 that the polarimetric estimator for inclinations is biased and tends to yield high i values (for large σ levels) and wide confidence intervals. This, together with the lack of signififance of the model fit to the observations found in most cases, (and the high σ_{dat}, $\hat{\sigma}$) means that we must consider i_{opt}, for all the systems unreliable.

To be fair, the data analysed here was not taken with the canonical model in mind. We therefore present a more efficient procedure for observing polarimetric binaries with the aim of analysing them in terms of the canonical model.

8·6 Polarimetric observations and analysis in terms of the canonical model

As we have seen, previous polarimetric observations of binaries have been taken over many orbital cycles. This could result in the multivalued nature of (Q,U) if physical variations are present causing the breakdown of phase locking over this timescale. The observed spread in the values of (Q,U) at similar phases indicate this possibility. New data may well have to be taken over shorter periods of time (i.e. smaller number of orbital periods) to minimize this behaviour. We propose therefore that the following technique of observing and analysing polarimetric observations

of binaries be employed in further work when attempting to fit the variations by means of the canonical model of Chapters 2 and 8.

(1) Observations should be made using a large telescope. This would reduce integration times (for constant noise levels i.e. the photon shot noise limited case) and increase the number of observations possible in one night and over the whole observing session.

(2) Continuous observations over a short timescale ($\sim$ few orbital periods - preferably one). This would produce approximately 'smooth' loci in the (Q,U) plane.

(3) Repeated observations as(2) to produce numerous sets of data for a sequential analysis and subsequent comparison. We cannot assume the γ's of the canonical model to be constant between each observing session. The short timescale of observations would help to minimize the non-phase locked variations (longer periods) and establish the nature (i.e. short term phase locked) of the variations. Investigation of the evolution of the scattering region would also be possible if this was achieved.

(4) The choice of binary system to observe. One thought to behave in a manner predictable to be the canonical model i.e. no eclipses, no significant light variations, approximately circular orbits (unless modelled in terms of the eccentric model of Brown et al (1981) and Chapter 6), and the polarization approximately independent of wavelength (i.e. Thomson scattering).

(5) Analysis using the unequal phase interval technique of this chapter (Section 8·2) with model significance tests and full account taken of the error on each observation when calculating the uncertainty in the 'best fit' parameters.

(6) Both sequential analysis and analysis of all the data together may be attempted if the nature of the system indicated by polarization observations is reasonably constant (i.e. phase locked, approximately single valued Q,U measurements).

If this procedure is followed then improvement in model testing and parameter definitions should occur. If the canonical model was found to be unsatisfactory then the comprehensive observations gained by this method would enable more detailed modelling to take place to great accuracy.

CHAPTER 9: RE-ANALYSIS OF CYGNUS X-1 DATA

9·1 Introduction

Polarimetric observations of Cygnus X-1 by Kemp et al (1979) consist of some 358 (Q,U) values covering a period of ~ 3 years (1975 to 1978). These were analysed in terms of the canonical model in Chapter 2 (also Simmons et al 1980) where we phase binned the data to obtain the average behaviour of Cygnus X-1 over the observing period. A problem encountered when attempting this however was that the data error on each phase bin was too large to enable a satisfactory determination of the binary inclination, i. The resulting χ^2 test of model fit depends strongly on this value, σ^2, and hence a large σ^2 would give a wide region of acceptable inclinations when forming the Relative Confidence Interval on i. For Cygnus X-1 an optimum inclination of $i_{opt} \sim 78^\circ$ with a R.C.I. of $[30^\circ, 85^\circ]$ at 10% significance was found by this procedure (Chapter 2). Previous optimum inclinations and errors had been given by Kemp of $i_{opt} \sim 76^\circ \pm 10^\circ$. The error was however 'formal' in nature and did not take into account the fit of the model to the data (a fact that our method tests by the statistic χ^2).

We concluded, an inspection of the folded data (i.e. the time of each observation reduced to the orbital phase) and with the results encountered that the multivalued nature of (Q,U) at certain phases, probably due to incomplete or lack of phase locking of the observations was increasing the bin error value to an unacceptable level and giving a poor determination. The lack of phase locking (or the incomplete nature of it) could be caused by long term evolution effects in the envelope mentioned in Chapter 8. This non-random variation of (Q,U) would tend to be 'smoothed' out by the binning technique but the reliability of the bin mean would be in question especially since a large σ_{bin} would be encountered. Only random fluctuations could be expected to be reduced by binning of the observations which was the incentive in attempting this in the first place.

With the generalization of the canonical model optimization procedure to allow analysis of data to unequal phase intervals (as opposed to analysis of binned data at equal phase intervals)

(cf. Chapter 8) we can apply the sequential analysis technique there described, (and applied to data for 7 other binaries in Chapter 8) to the long run of Cygnus X-1 observations. This would allow sections of data, taken from the whole, to be analysed individually and on investigation of the changes occurring in the structure of the scattering region to be undertaken. Comparison of the results from each section of data would tell us something about the nature of these variations given new data.

9·2 Sequential Analysis of the observations

We here analyse sections of data, taken from the whole run, covering no more than 10 orbital periods. We limit the coverage of each section to 10 periods in order to (a) obtain enough observations for analysis and (b) to stand some chance of reducing the effect of non-random fluctuations present in the data. Ideally the data sections should cover no more than one orbital period and repeated numerous times. The results would then indicate more accurately the variations present in the scattering region from cycle to cycle and allow satisfactory testing of the phase-locking hypothesis. It may be however, that significant non-random variations occur over these short timescales invalidating the use of the canonical model as a diagnostic of Cygnus X-1. In fact the variable X-ray nature of Cygnus X-1 indicates that variations may well occur in the scattering region over short time scales (Rothschild et al 1972).

In Table I we detail the sections of data removed, for analyses, from the whole run. We form 17 overlapping sets of data (each of length 10 orbital periods i.e. 56 days) from the 1275 days of data available. Also given in Table I is the number of points N, and the Julian dates of the start and end of section.

We follow the procedure outlined in Chapter 8 when testing the model fit to the observations and forming Confidence Intervals on the optimum inclinations. This involves use of the data error on each (Q,U) value, σ_{dat} in obtaining a χ^2 value and hence the model acceptability at the optimum inclination and $\hat{\sigma}$, defined by Equation (8·27) in forming the R.C.I's. We again chose the 10% significance level as our acceptability level when testing the model and forming

NUMBER OF SECTIONS	JD 2,440,000+ (START, END)		N
01	2572.9	2628.8	24
02	2600.9	2654.8	25
03	2629.8	2682.7	35
04	2657.8	2699.6	30
05	2682.7	2728.6	13
06	3321.0	3375.9	48
07	3349.8	3400.7	49
08	3377.8	3431.8	43
09	3433.7	3619.9	44
10	3455.7	3597.0	24
11	3626.9	3677.9	35
12	3653.9	3708.9	50
13	3678.8	3728.7	51
14	3709.9	3764.8	44
15	3729.7	3791.7	39
16	3766.7	3819.7	37
17	3792.8	3847.7	31

TABLE I.

the R.C.I. (this gives the 90% confidence interval).

The value of σ_{dat} for Kemp's data is $\sim 0{\cdot}036\%$ (Kemp et al 1979). To find the phase of each observation we fold the (Q,U) values onto the 5·6 day orbital period using the epoch value:- JD ϕ = 244 2552·276 (Kemp et al 1979). Table II gives the resulting 'best fit' inclinations, Model Significances (if > 0·001%) and Relative Confidence Intervals for the 17 data sets analysed. Also, Figures 9·1 to 9·3 show the resultant best fit Q,U vs λ curves and (Q,U) loci for 3 of the data sets considered. It is obvious that the model is not a good representation of the variations present in the data (since all model significances are $< 0{\cdot}001\%$) and that the residuals between the predicted and observed (Q,U) values alter all phase points are large (hence a large R.C.I.). On inspection of the variation of F (the sum of the squares of the residuals) with inclination i it is found that for all of the data sets the range of F is small. This implies the resultant $\sigma^2\ \chi^2$ versus inclination curves are shallow and that almost all inclinations are as significant as each other. This is also indicated in Table II where we give the values of $\sigma = \bar{\sigma}$ necessary when forming confidence intervals to obtain the R.C.I. (at 10% sig.) to $\sim \pm 5^\circ$. We look at the $\sigma^2\ \chi^2$ value at $i_{opt} + 5^\circ$ and $i_{opt} - 5^\circ$ obtain $F(\pm 5^\circ)$ and define $\sigma^2 = F(\pm 5^\circ)/\chi^2_{10\%,2N}$. The ratio $\hat{\sigma}/\bar{\sigma}$ is also given and is always in the range 1·1 to 1·3 for all the sets of data. This means that very little improvement is necessary in the quantity $\hat{\sigma}$ before the R.C.I. reduces from $[0^\circ, 180^\circ]$ to $\sim [i_{opt} - 5^\circ,\ i_{opt} + 5^\circ]$ and is far from the ideal situation. For a good determination of i a sharp minimum in F would be needed making the difference in fit over the i range significantly better at i_{opt} than at any other value.

9·3 Conclusions

Upon reanalysis of the Cygnus X-1 data utilizing the general canonical model optimization procedure with data at unequal phase intervals, we see that the resultant 'best fit' model parameters do not give a good representation of the variations present in the data over timescales of at most 10 orbital periods.

We conclude therefore that the polarimetric nature of Cygnus X-1 is ill defined over such timescales and that shorter observing periods may be necessary to investigate the time variation of the polarization

NO.	IIOPTI	MODEL SIG. IF > .001%	RCI 10% IF<0,180	$\bar{\sigma}$	$\hat{\sigma}/\bar{\sigma}$
1	74^{o}	--	--	0.294	1.205
2	76^{o}	--	--	0.236	1.198
3	87^{o}	--	--	0.204	1.152
4	86^{o}	--	--	0.192	1.148
5	88^{o}	--	--	0.102	1.324
6	78^{o}	--	--	0.168	1.125
7	70^{o}	--	--	0.154	1.117
8	80^{o}	--	--	0.154	1.136
9	85^{o}	--	--	0.153	1.131
10	80^{o}	--	--	0.156	1.206
11	85^{o}	--	--	0.137	1.153
12	61^{o}	--	--	0.111	1.120
13	70^{o}	--	--	0.094	1.126
14	73^{o}	--	--	0.105	1.133
15	54^{o}	--	--	0.149	1.148
16	89^{o}	--	--	0.161	1.145
17	72^{o}	--	--	0.159	1.170

TABLE II

Figures 9.1 to 9.4.

Here we show the best fit canonical models (1st and 2nd harmonics) produced by the unequal spacing analysis of Chapter 8 for four sets of Cygnus X-1 data (1, 2, 6 and 9) See Table I and II for more details.

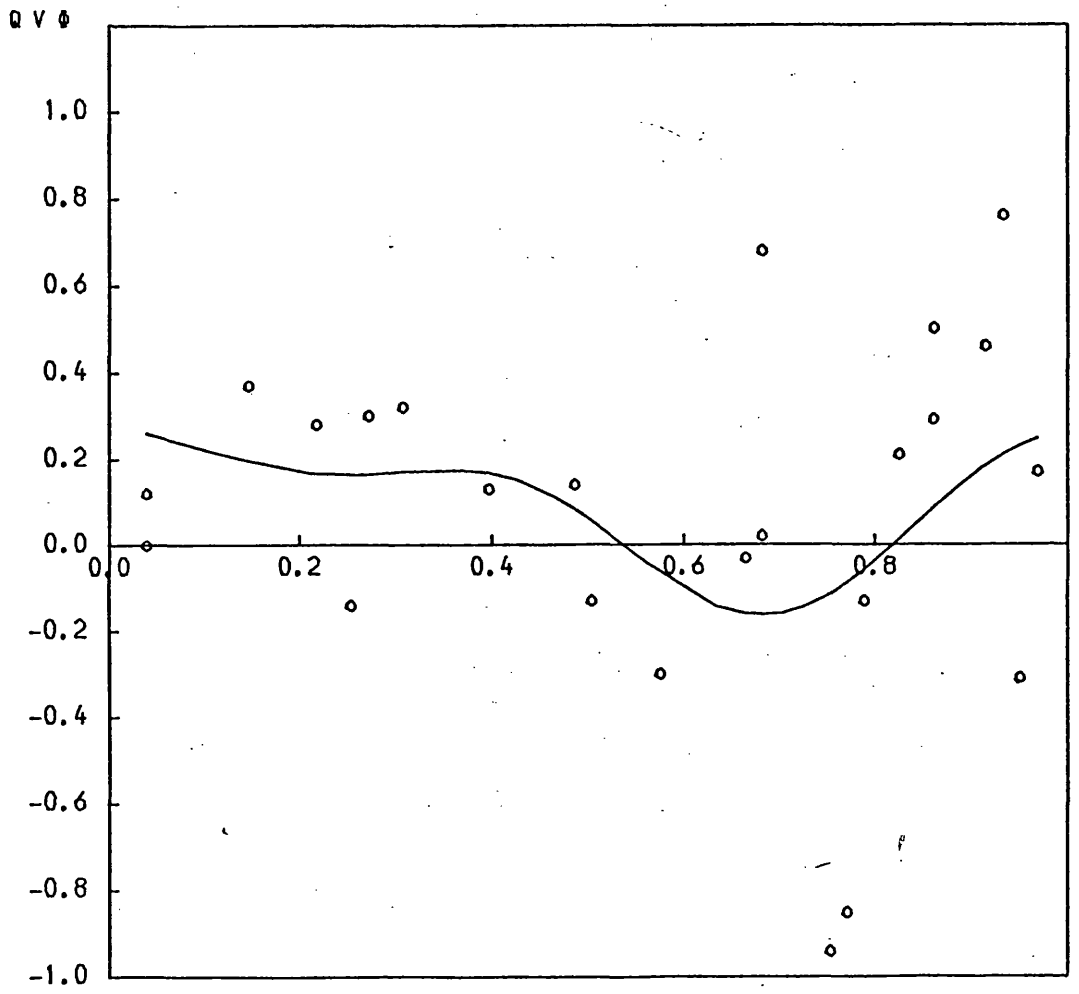

FIGURE 9.1a

Plot of section 1 of the Cyg X-1 data with best fit canonical model.

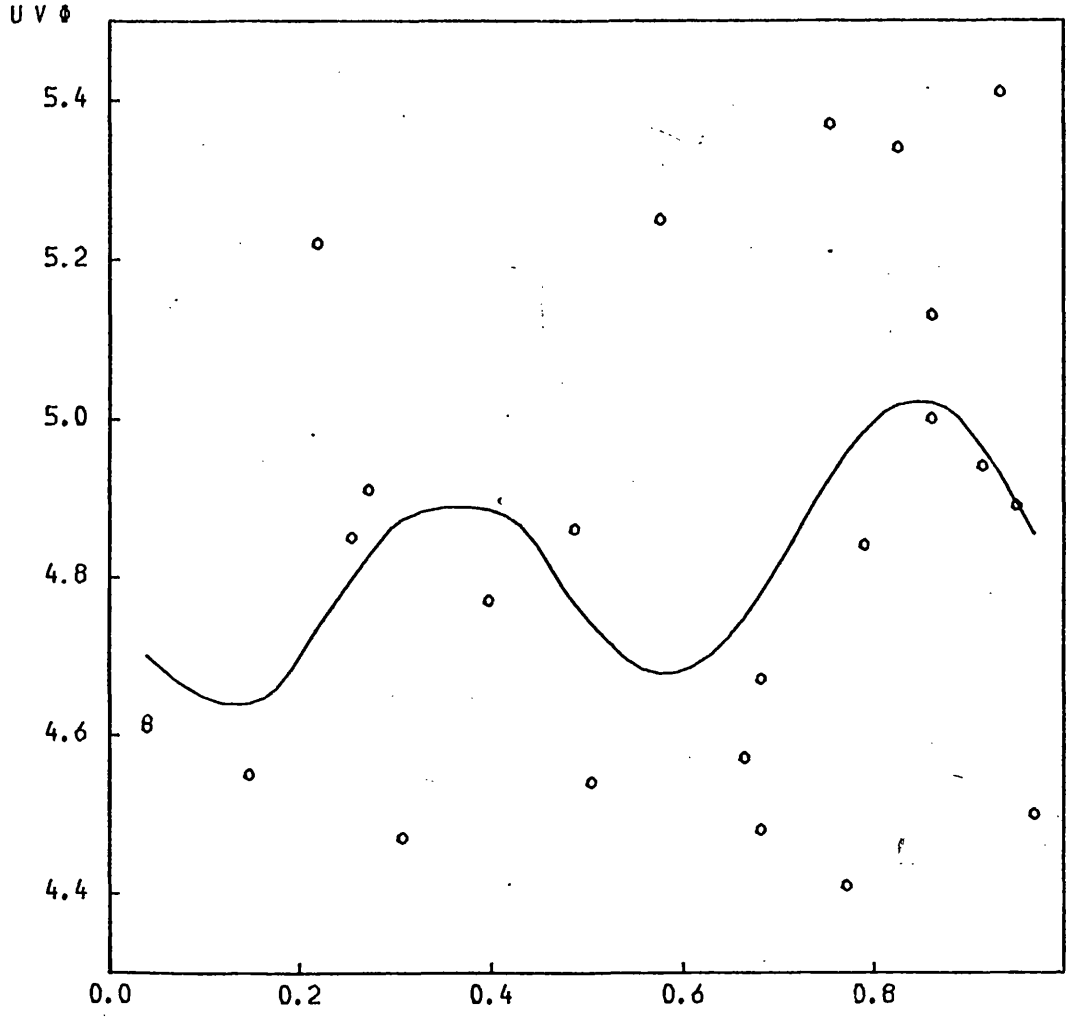

FIGURE 9.1b

see 9.1a

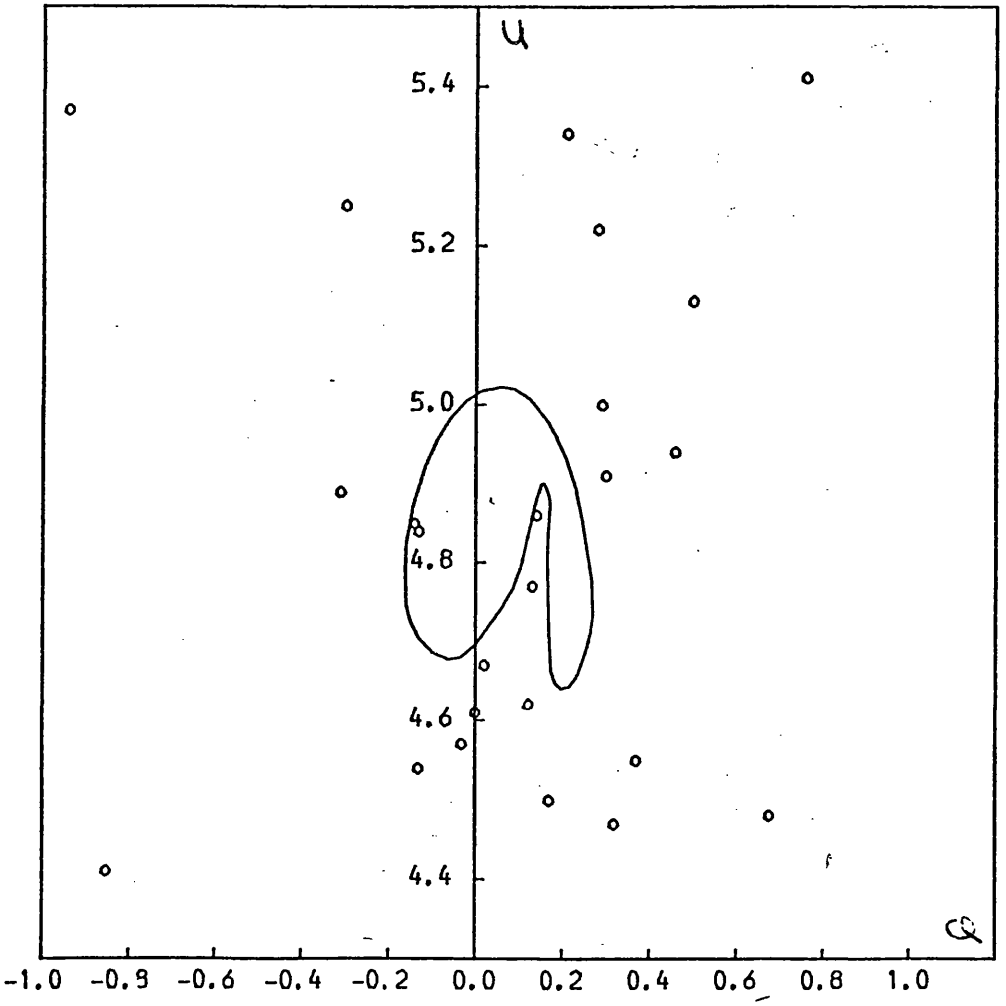

FIGURE 9.1c

see 9.1a

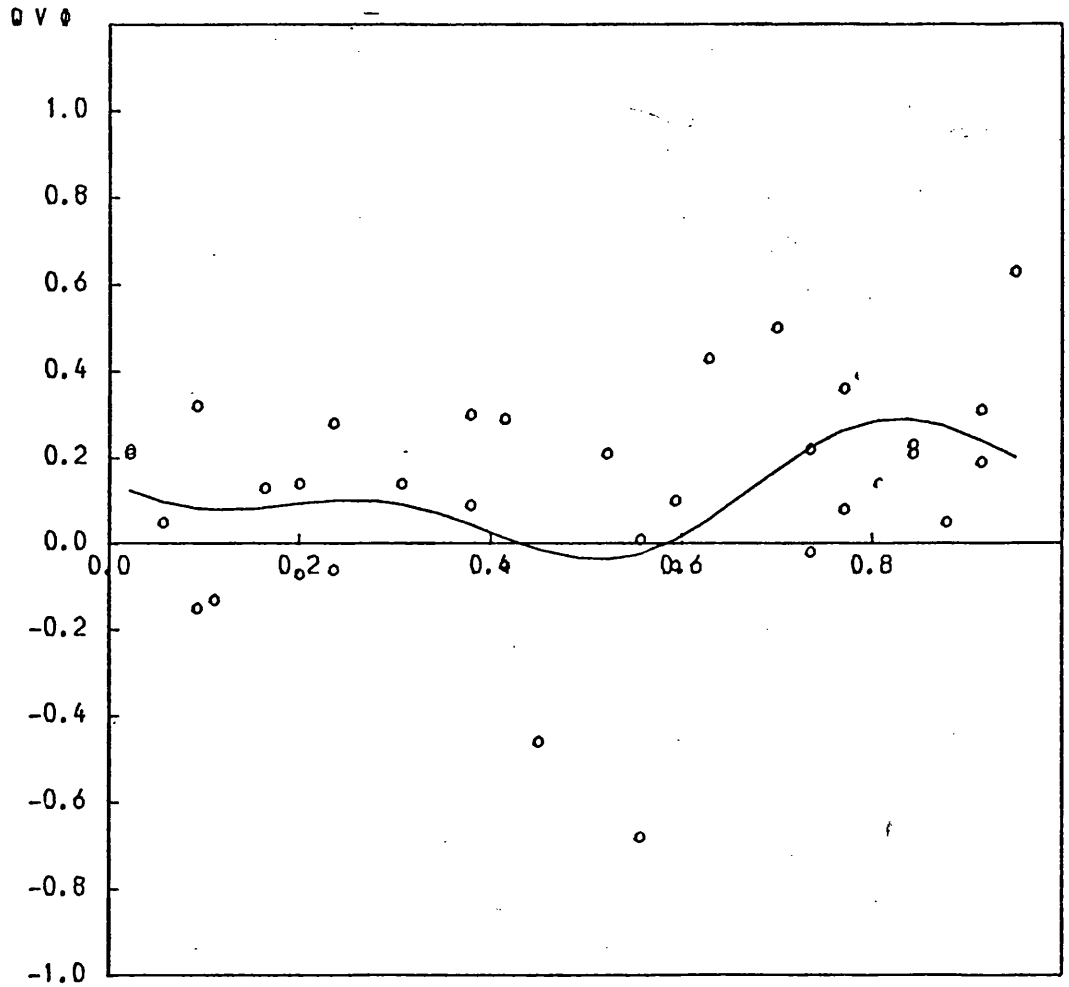

FIGURE 9.2a

Plot of section 2 of the Cyg X-1 data with best fit canonical model.

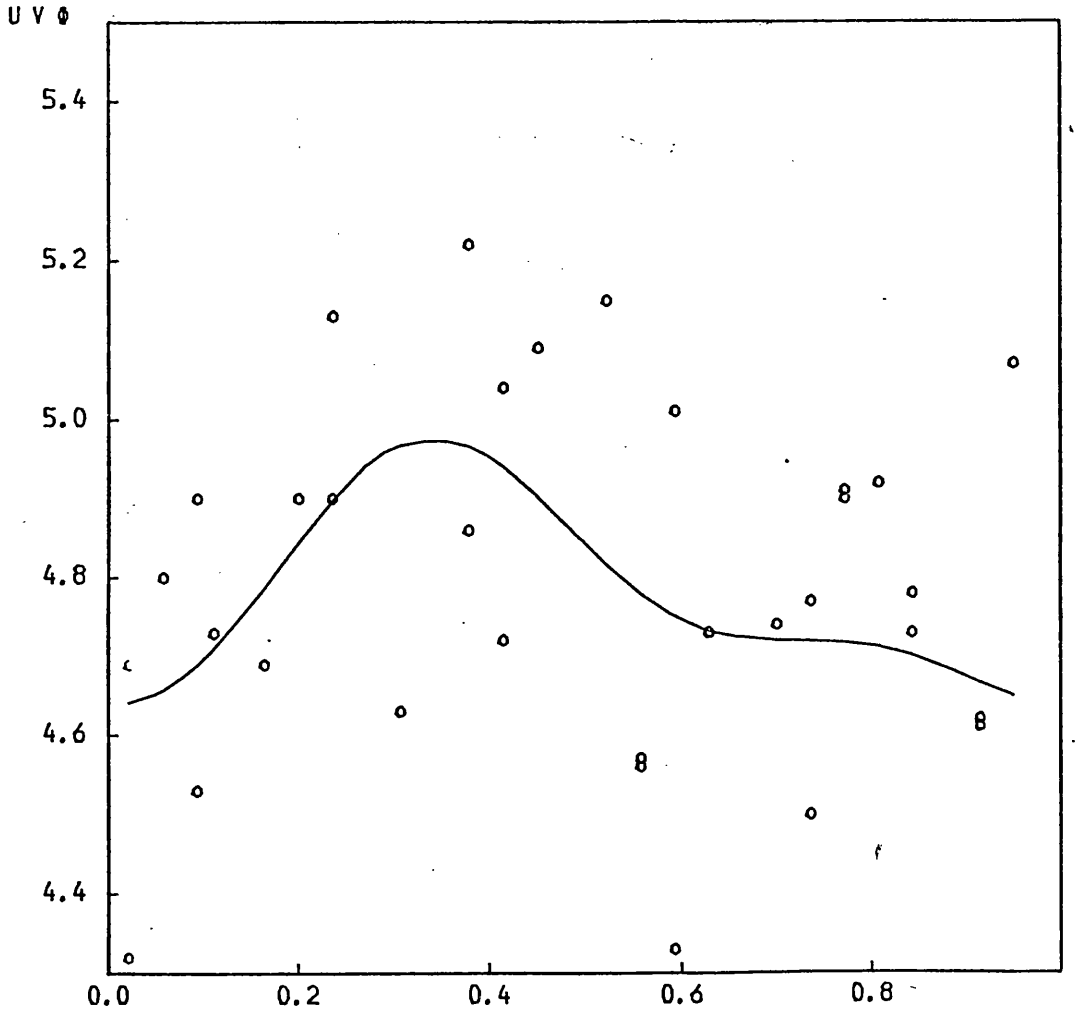

FIGURE 9.2b

see 9.2a

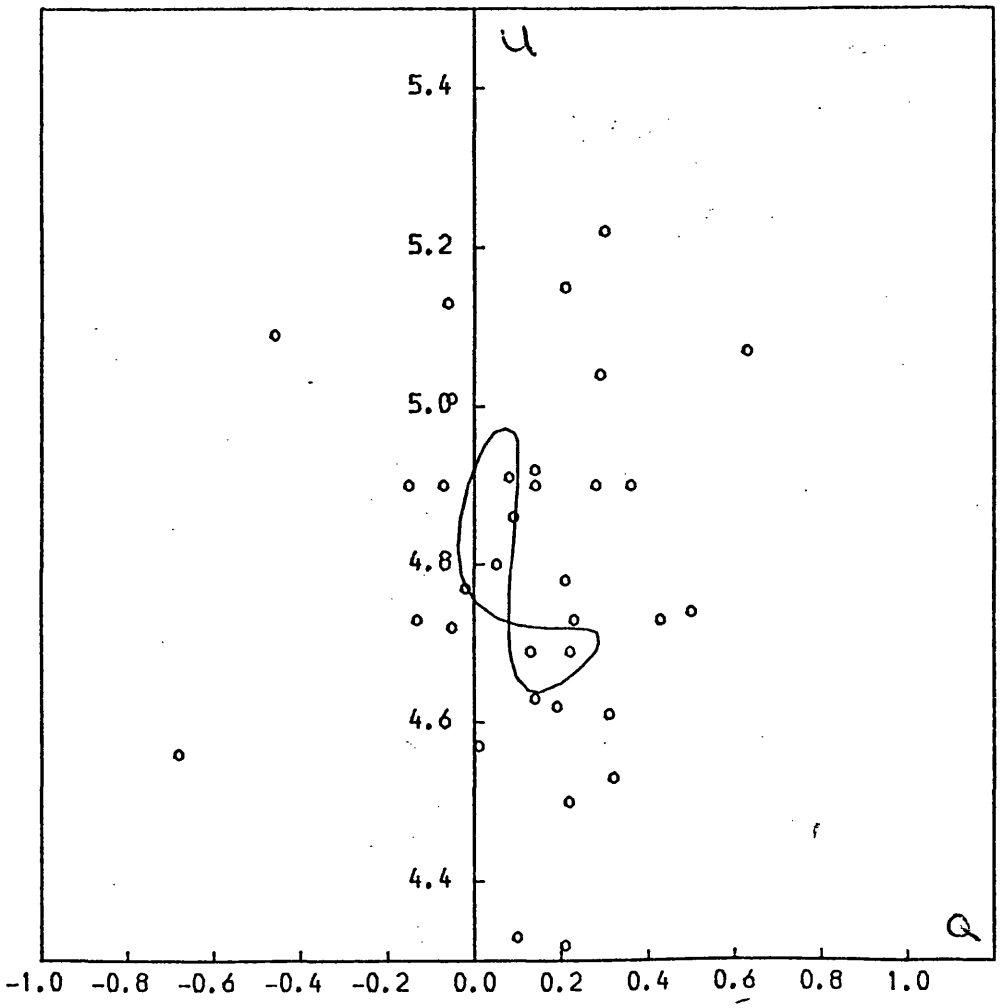

FIGURE 9.2c

see 9.2a

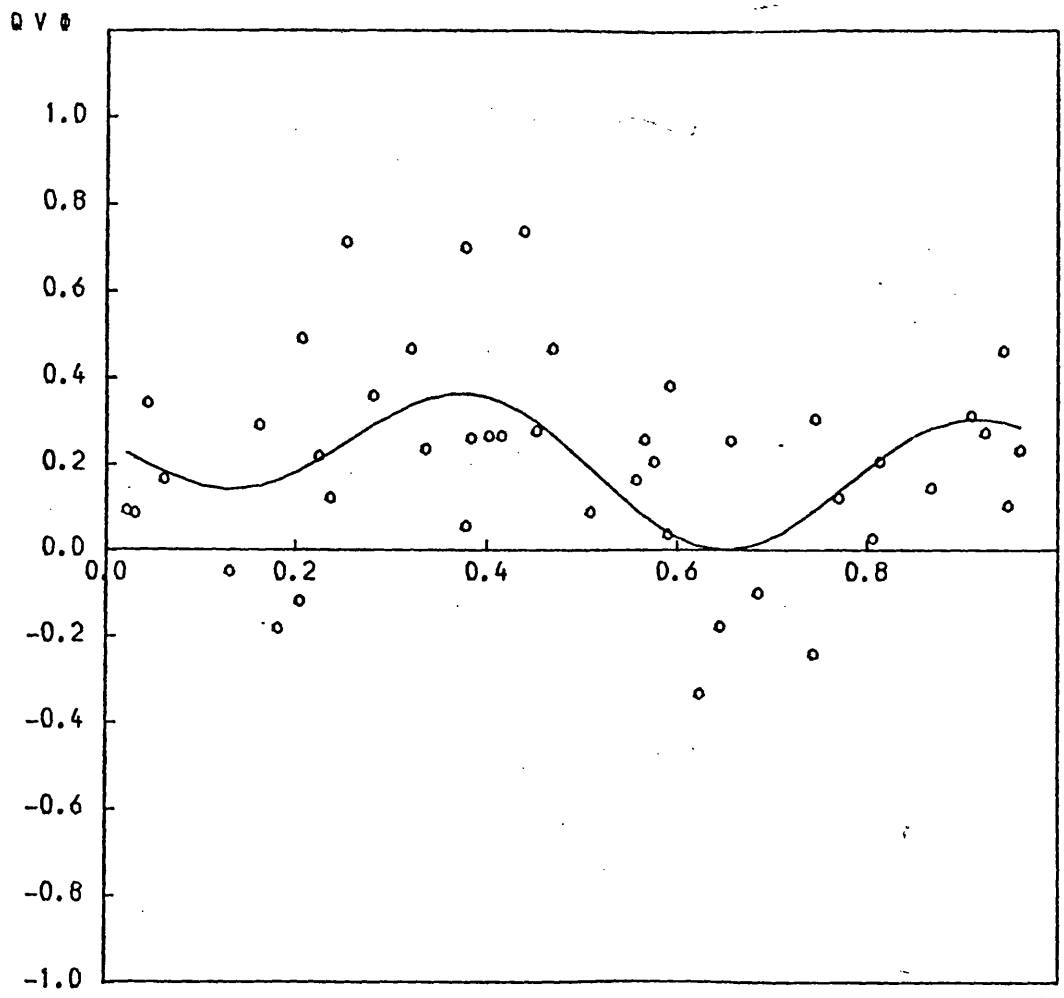

FIGURE 9.3a

Plot of section 6 of the Cyg X-1 data with the best fit canonical model.

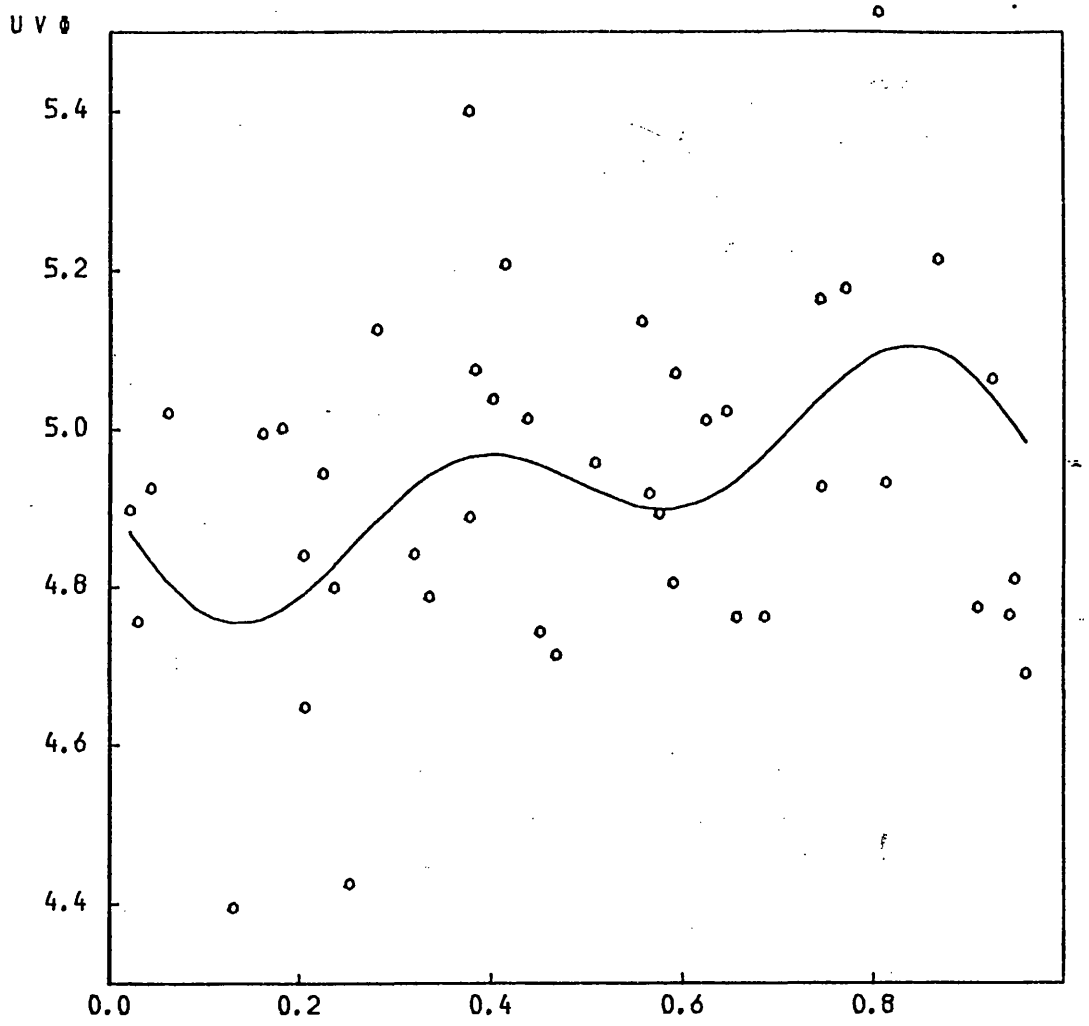

FIGURE 9.3b

see 9.3a

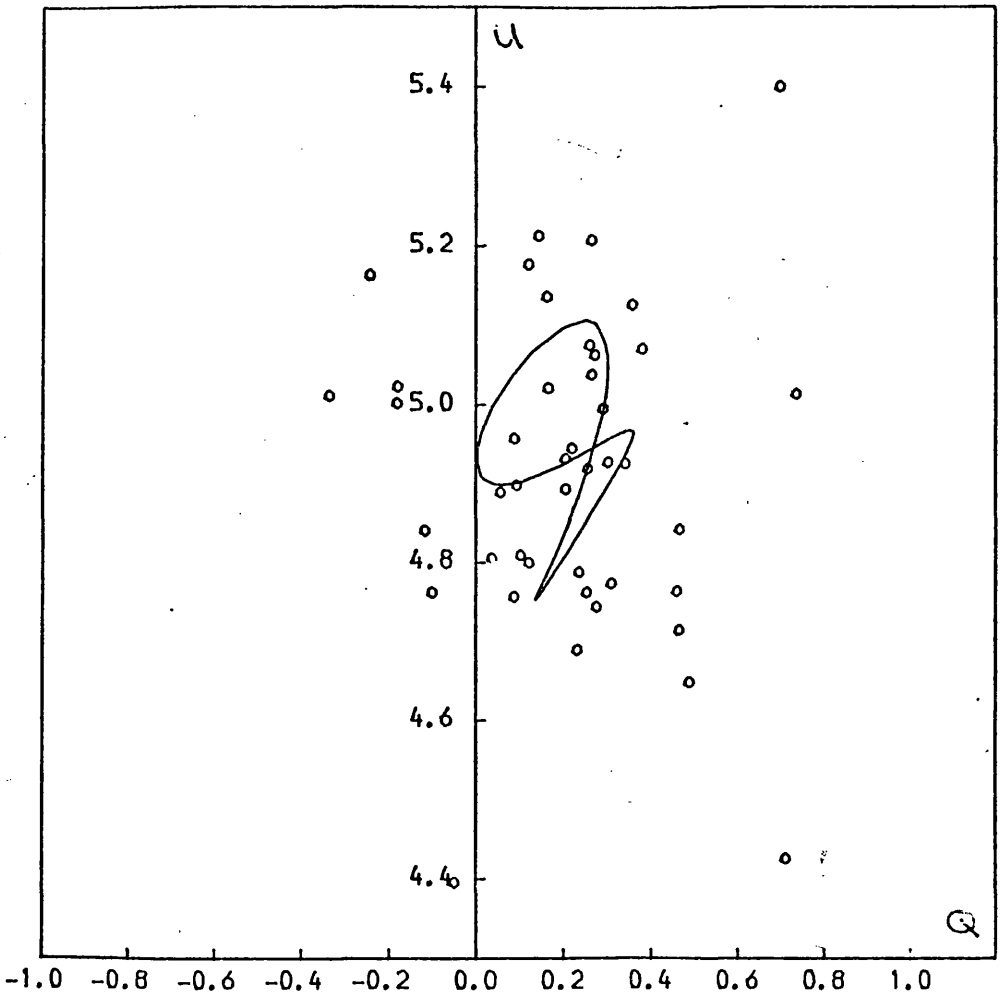

FIGURE 9.3c

see 9.3a

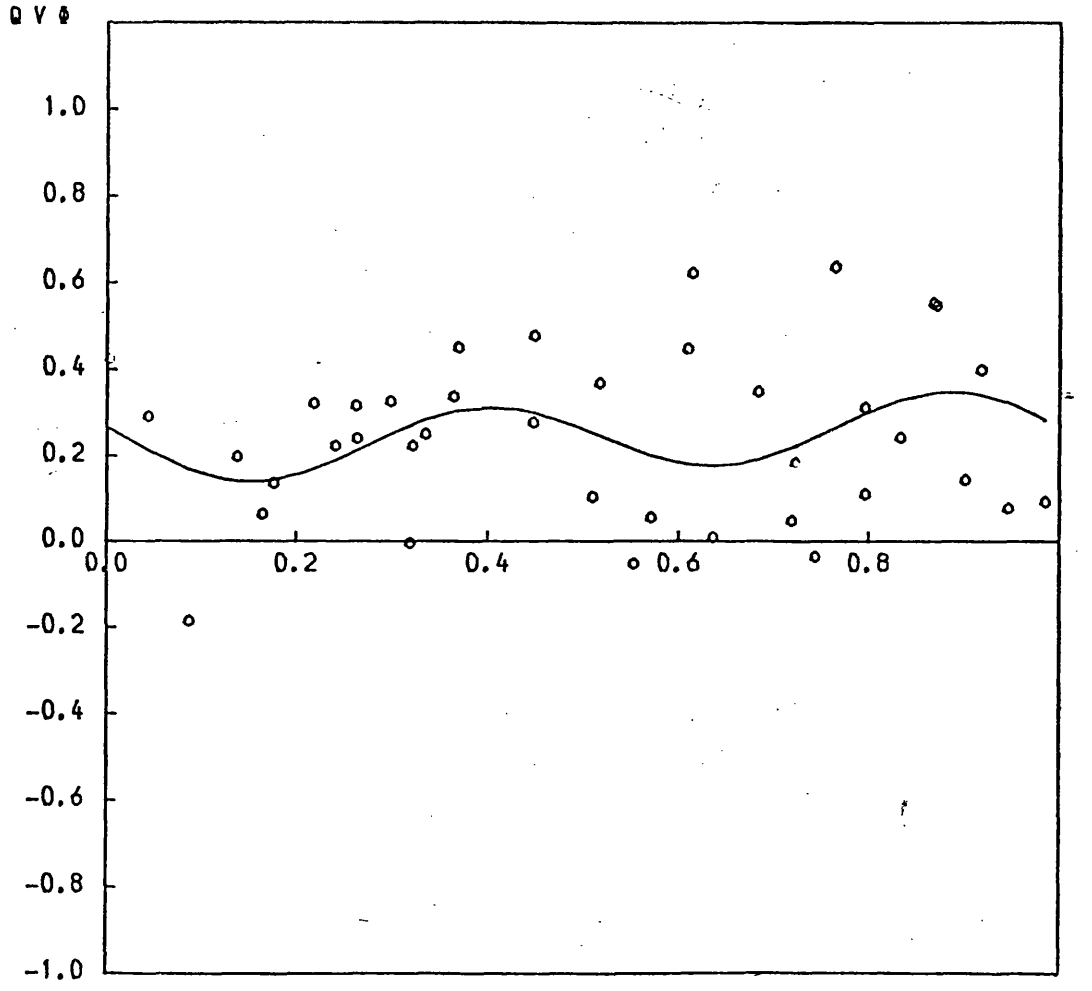

FIGURE 9.4a

Plot of section 9 of the Cyg X-1 data with the best fit canonical model.

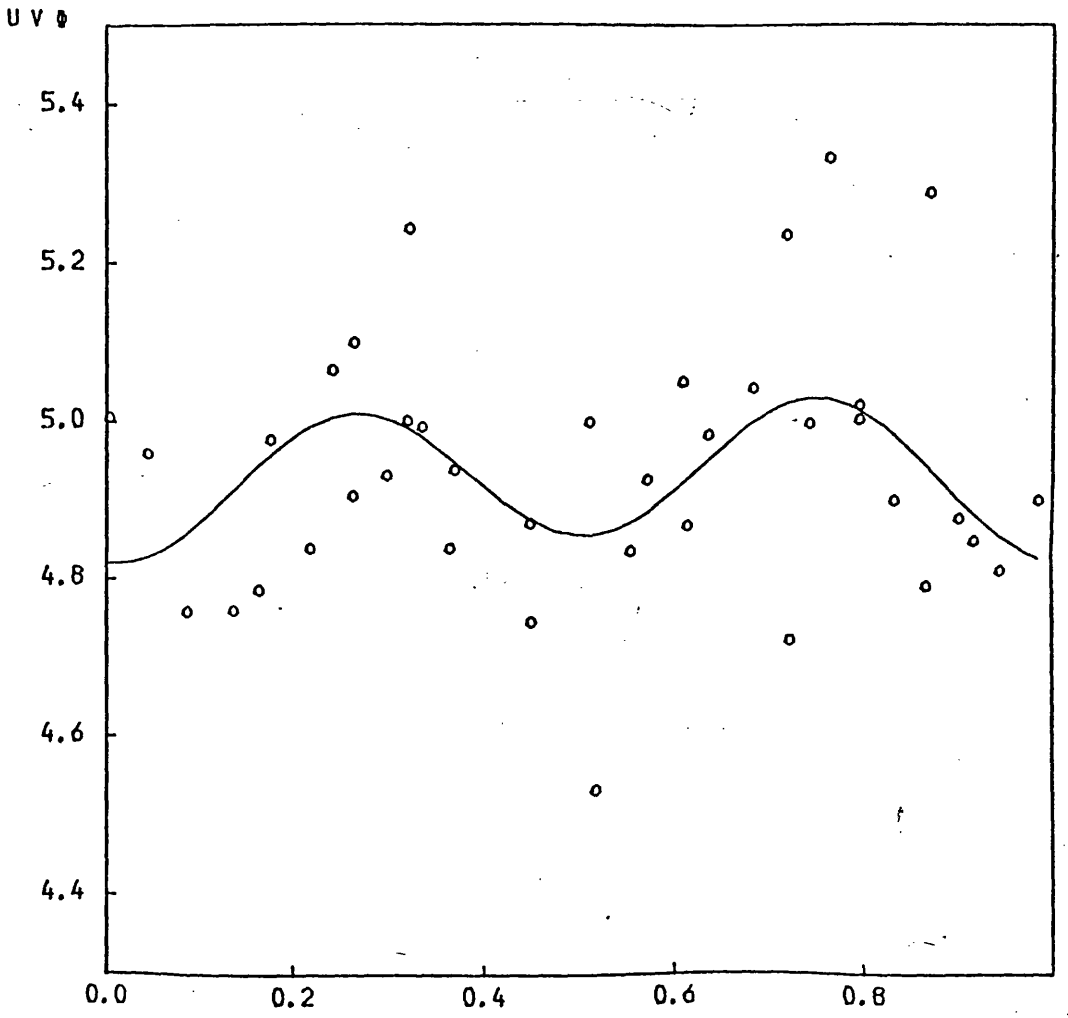

FIGURE 9.4b

see 9.4a

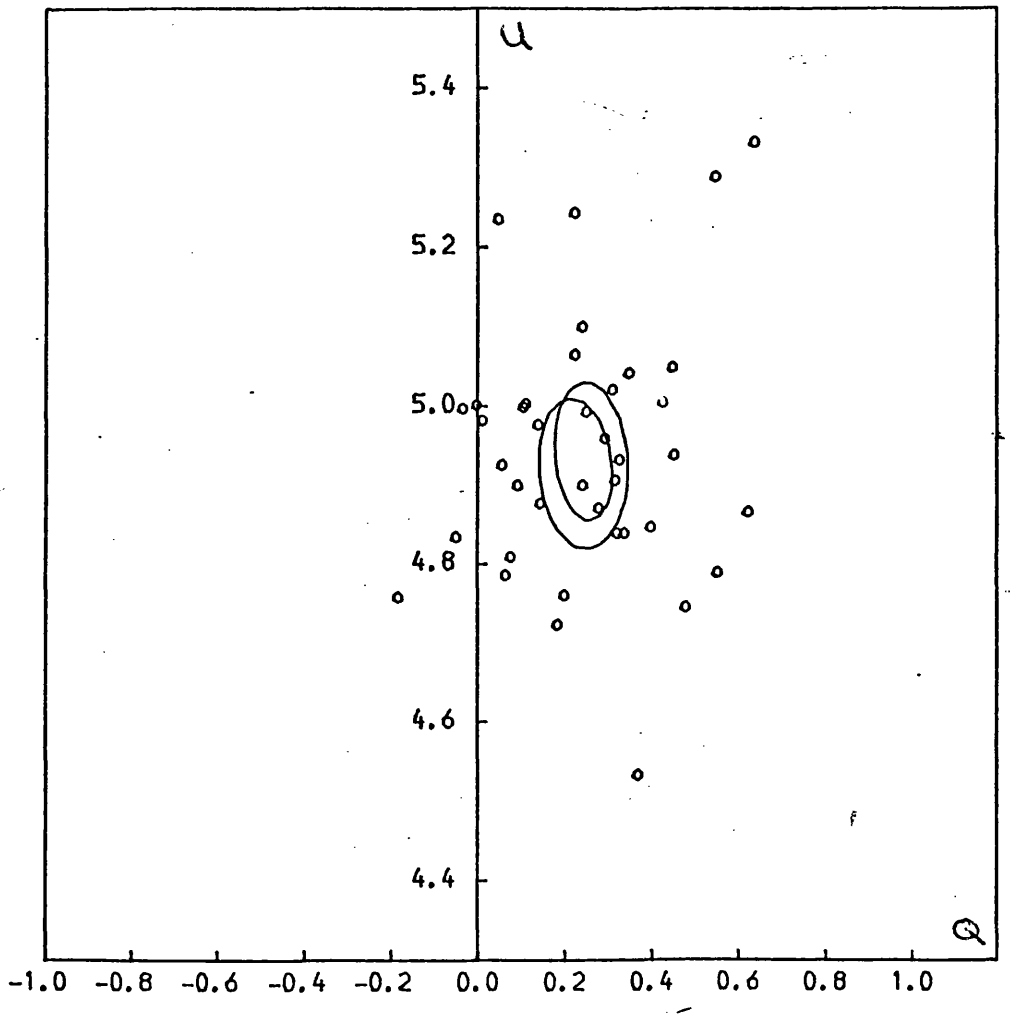

FIGURE 9.4c

see 9.4a

structure. Ideally as mentioned above, data taken over only one orbital period would be needed to provide insight into the nature of such variations.

CHAPTER 10 HD 50896 - ANALYSIS OF POLARIMETRIC OBSERVATIONS

10.1 Introduction

The binary system HD 50896 was observed polarimetrically by McLean (1980) during the 1979 season in the B, U and G filters regions of the spectrum. Spectrophotometric details of the binary are given in Appendix 1 with the observations detailed in Appendix 4. The system believed to consist of a Wolf-Rayet-compact object was observed to exhibit variable linear polarization with peak to peak amplitude of $\sim 0.36\%$. The raw observations are plotted in Figure (10.1) which includes all the observations.

We here attempt to analyse the observations in three separate ways. Firstly we use the optimization procedure (for the canonical model) with binned data (Chapter 2) to investigate the average behaviour of the system over the observing period. Secondly we used the generalized optimization procedure with the raw data (at unequal phase intervals to investigate the detailed structure and evolution of the data by analysing sections of the total observations available (cf. Chapter 8). Thirdly we apply the eccentric model (Chapter 6) to the observations to attempt to improve the fit of the canonical model and hence establish an eccentricity of the orbit of the system. (already suspected - Fermani et al 1980).

10.2 Analysis in terms of the Canonical Model (Binned Observations).

Some 10 sets of observations were detailed from the complete data for analysis namely B filter - Jan-April 1979, B filter - Oct - Dec. 1979, B filter - Jan - Apr. 1979 and Oct - Dec. 1979 similarly for U and G together with all the data (Jan - Apr 1979 + October → Dec. 1979 for B, U and G filter). These were analysed separately using both the general (1st and 2nd harmonic) and symmetric (2nd harmonics only) canonical models. The results are given in Table I where we show the number or bins used, the optimum inclinations obtained (for both model fits), the Relative Confidence intervals on each i_{opt} (at both 10% and 25% significance). Also Figure (10.2) shows the resultant best fit Q versus phase and U versus phase curves produced on the departmental PET computer for both general and symmetric

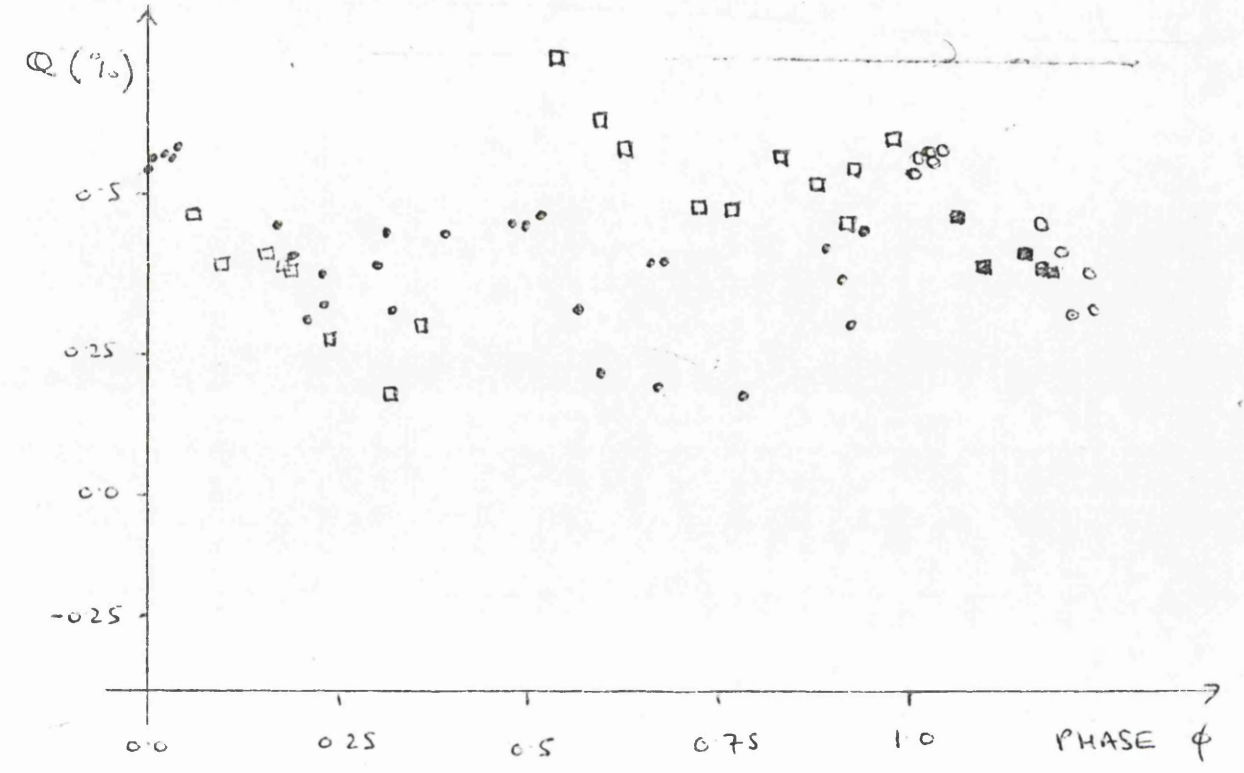
Q (%)
0·5
0·25
0·0
-0·25
0·0
0·25
0·5
0·75
1·0
PHASE φ

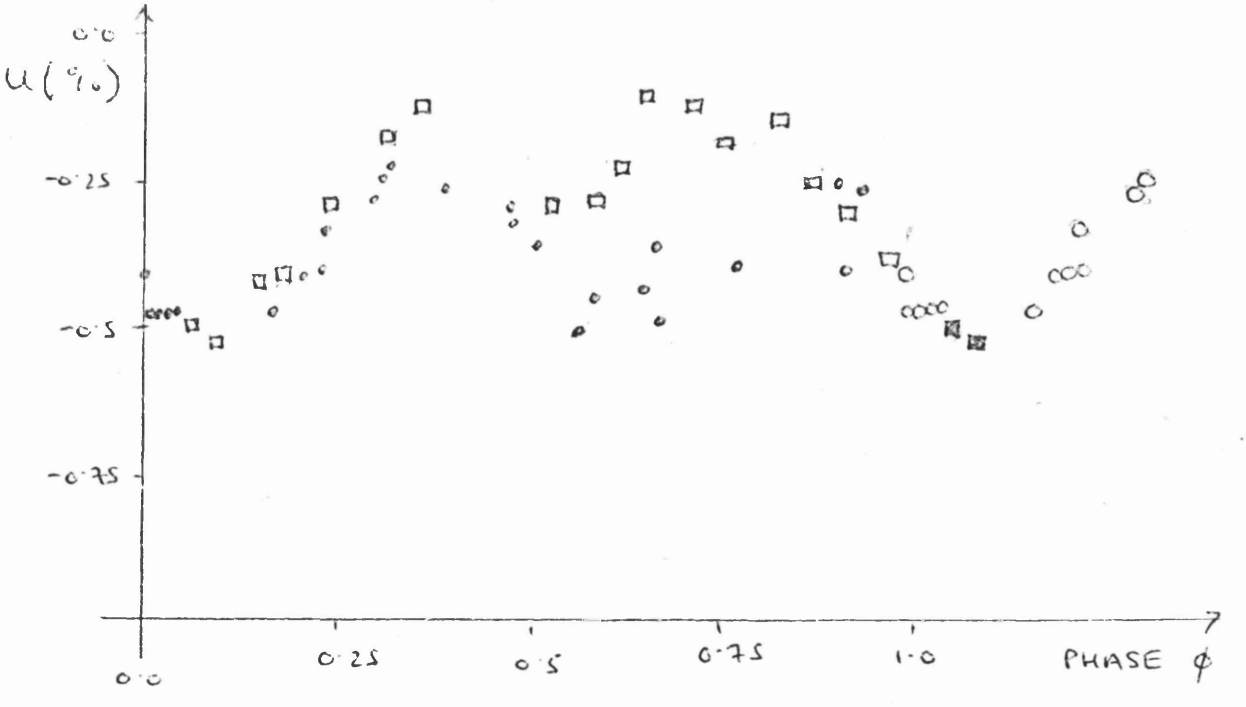
U (%)
0·0
-0·25
-0·5
-0·75
0·0
0·25
0·5
0·75
1·0
PHASE φ

P = 3·76 days

TABLE I

DATA	N	IOPT 1+2	IOPT 2	RCI 10% 1+2	RCI 10% 2	RCI 25% 1+2	RCI 25% 2
B1	20	70°	60°	[0°,86°]	[0°,85°]	[52°,82°]	[53°,81°]
B2	20	72°	83°	[44°,90°]	[45°,90°]	[59°,86°]	[61°,85°]
U1	15	70°	80°	[0°,90°]	[0°,90°]	[0°,87°]	[0°,86°]
U2	15	76°	72°	[34°,83°]	[36°,82°]	[52°,80°]	[54°,80°]
G1	20	79°	74°	[0°,90°]	[0°,90°]	[0°,85°]	[0°,84°]
G2	15	80°	83°	[0°,90°]	[0°,90°]	[0°,90°]	[0°,90°]
B	30	81°	79°	[0°,90°]	[0°,90°]	[0°,90°]	[0°,90°]
U	30	79°	77°	[0°,90°]	[0°,90°]	[0°,90°]	[0°,90°]
G	30	82°	80°	[0°,90°]	[0°,90°]	[0°,90°]	[0°,90°]

Figures 10.1 to 10.9.

Here we show the best fit (burned) canonical model curves (Q and U) for the nine sets of HD50896 data of McLean (1980). See Tables I and II for more details.

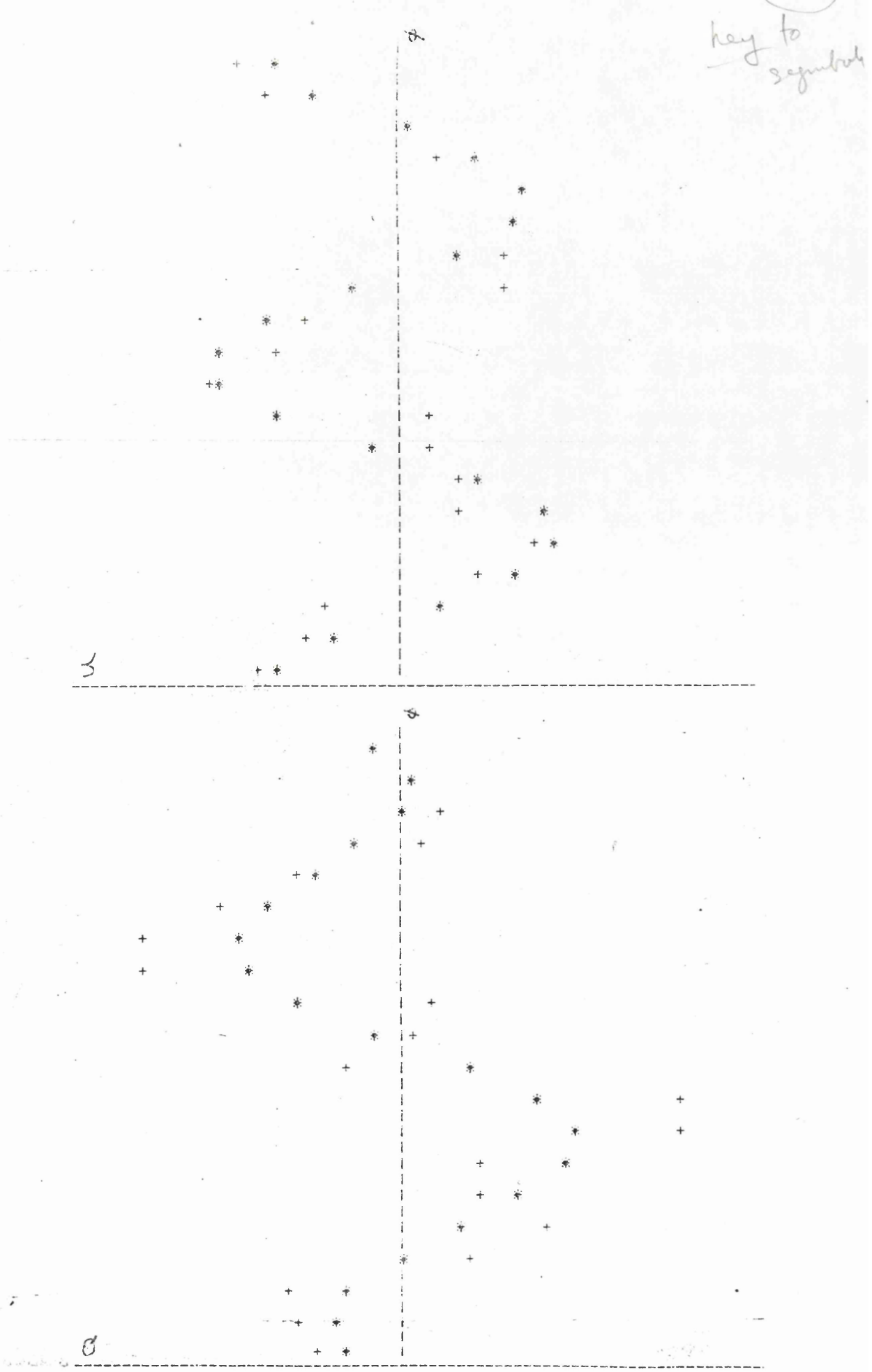

Figure 10.1 - Plot of binned HD50896 data set B-J/A79 with best fit canonical model.

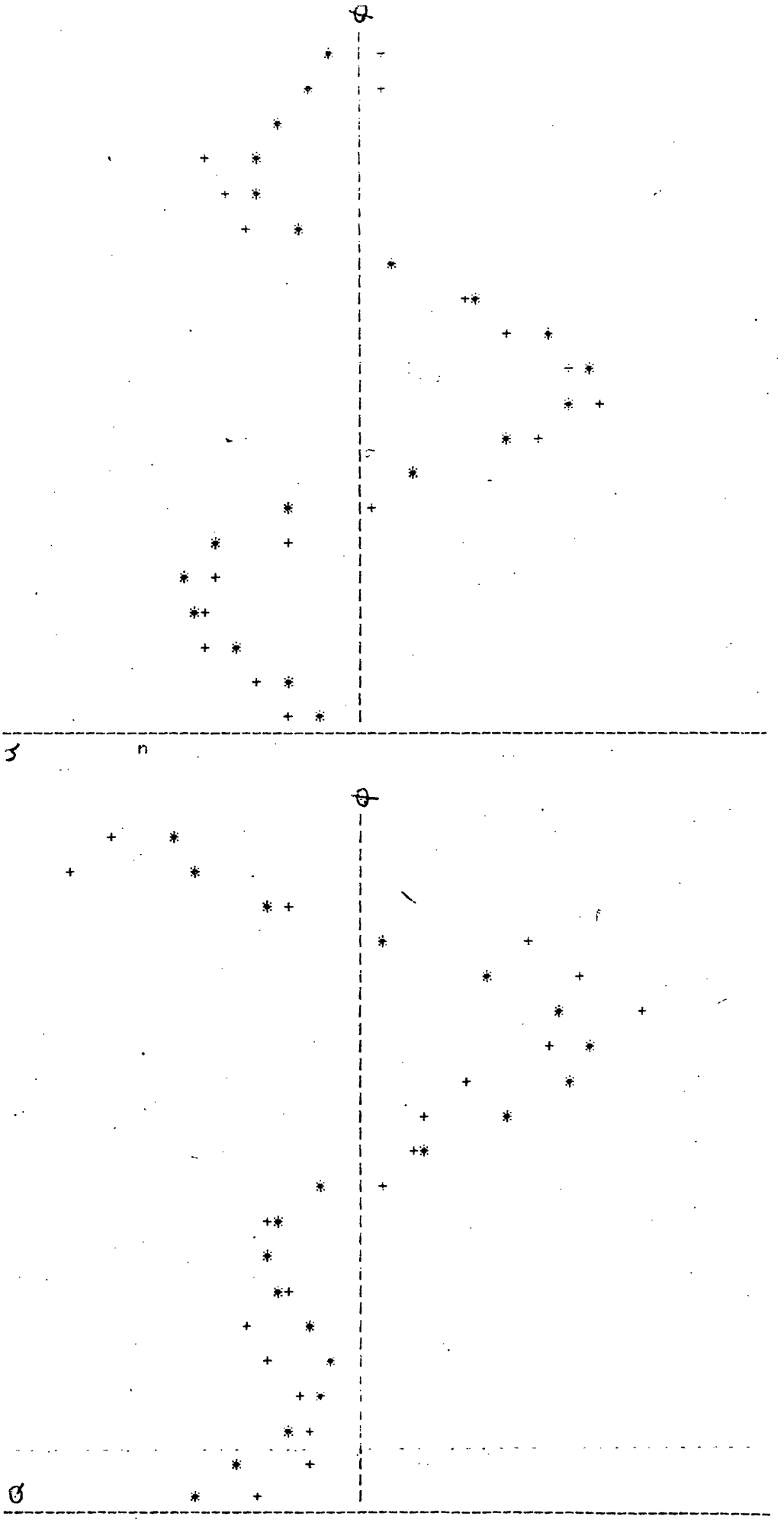

Figure 10·2 - same as 10·1 but for B 0ID 79 data

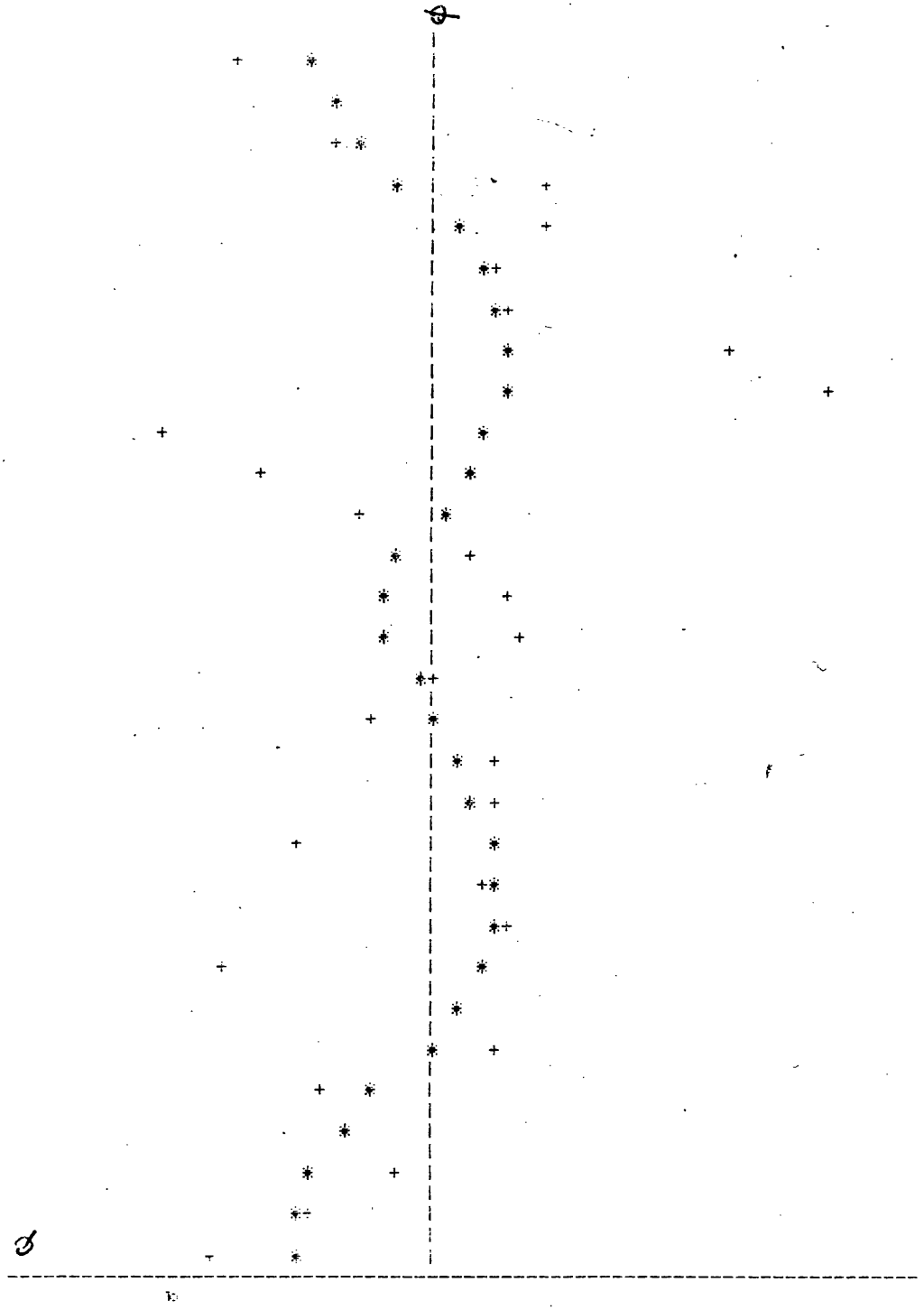

Figure 10·3a same as 10·1 but for all B data.

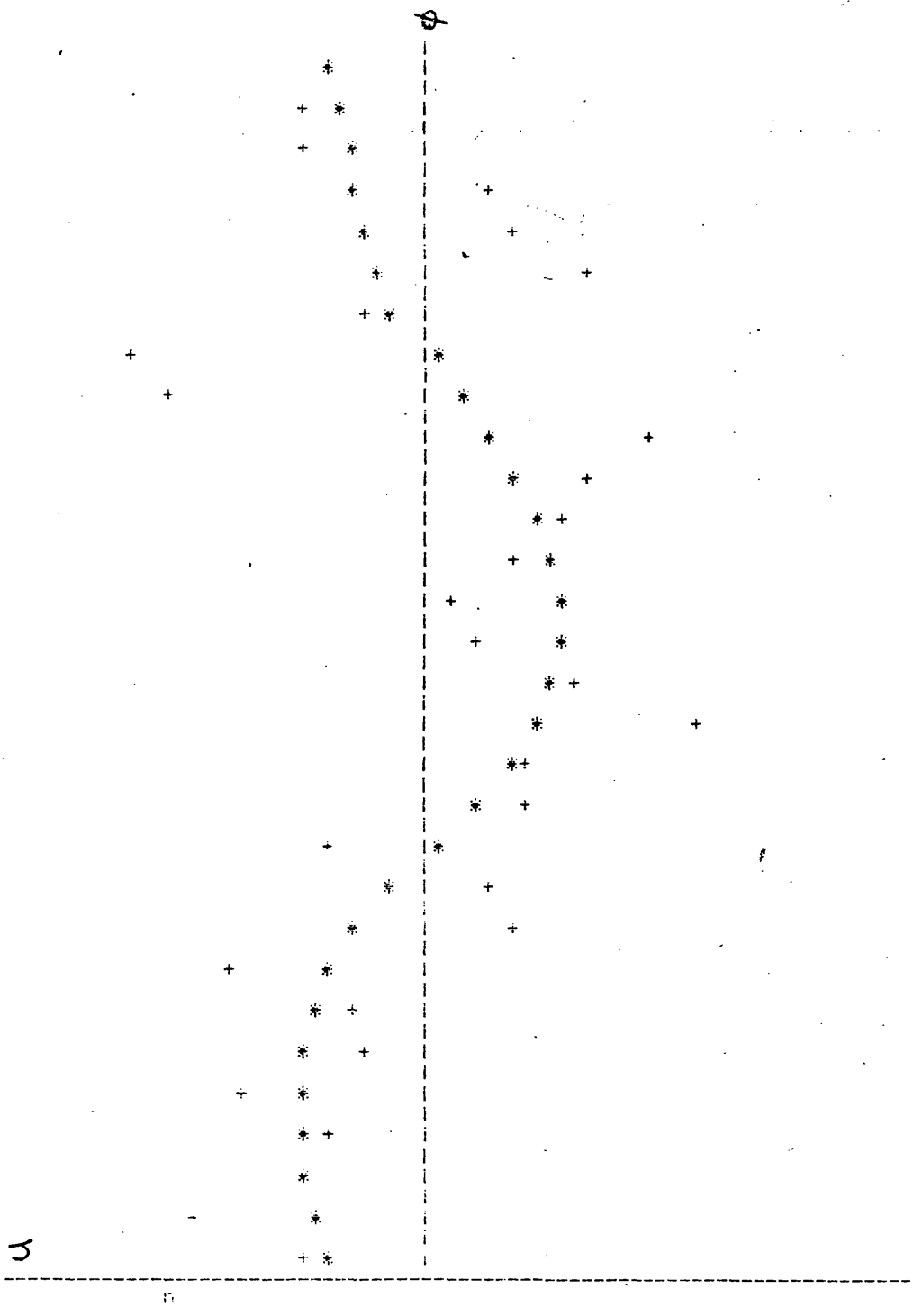

Figure 10.3b see 10.3a.

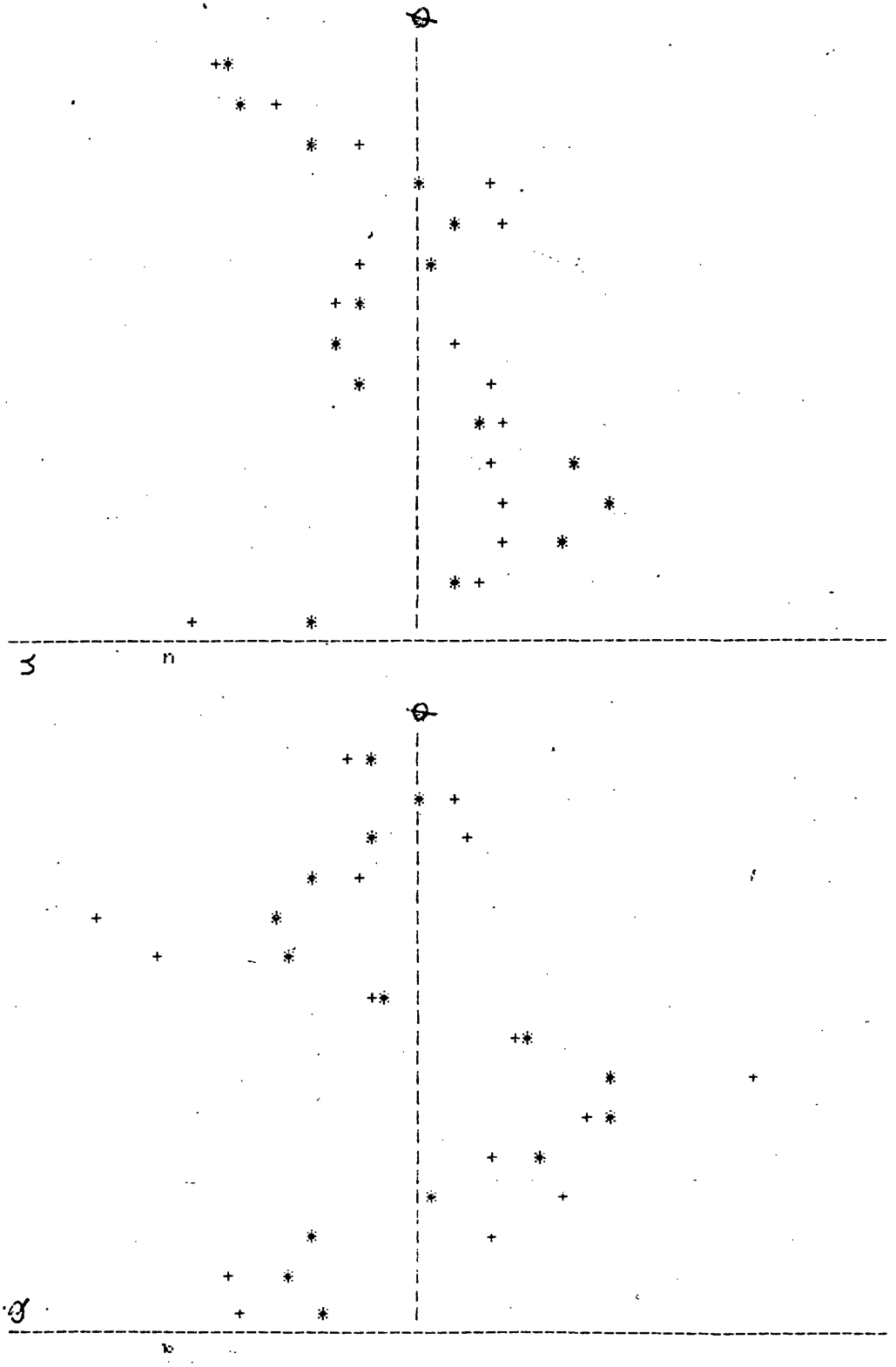

Figure 10.4 Plot of HD50896 data - U J/A 79 (binod) with best fit canonical model.

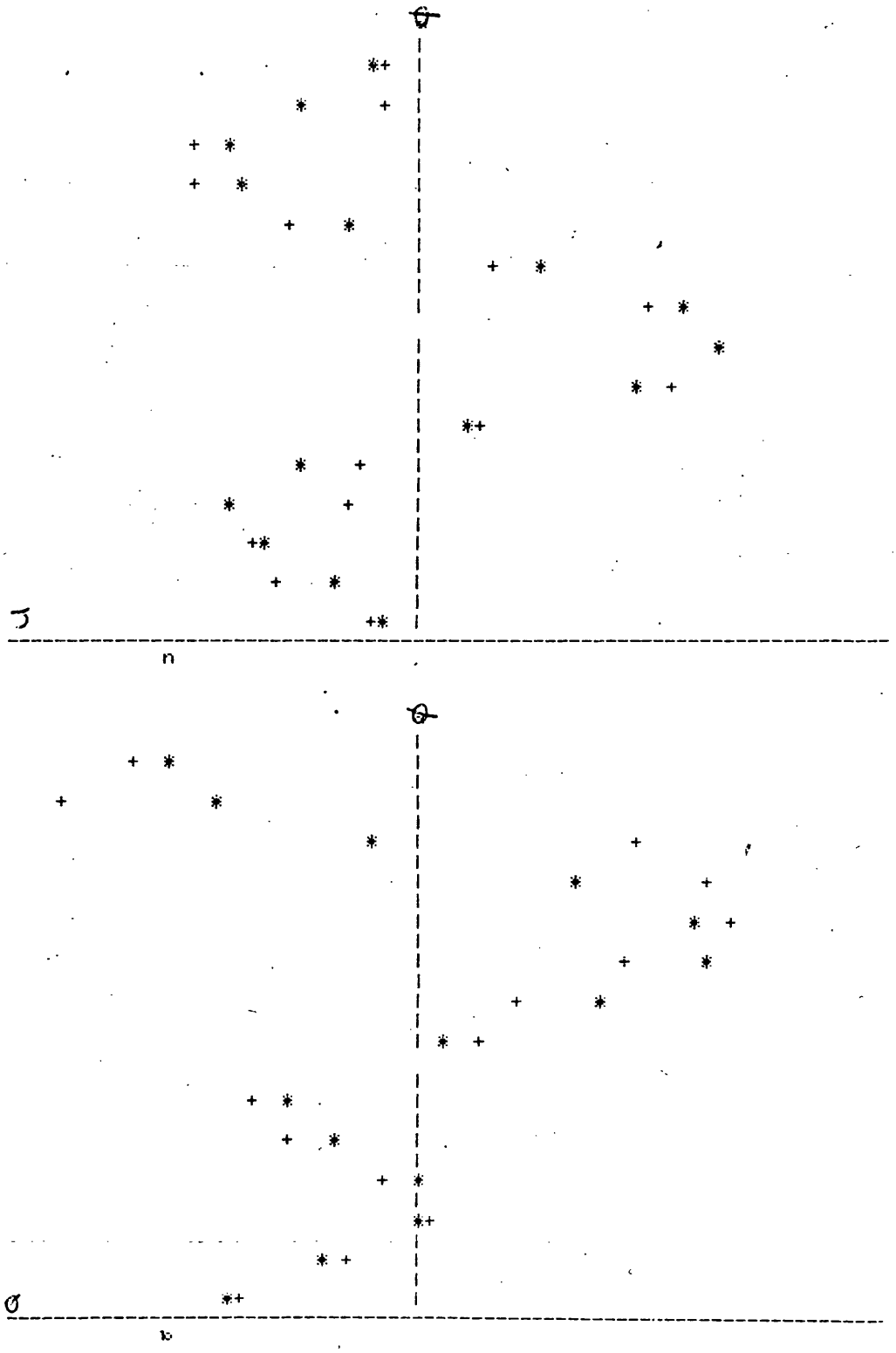

Figure 10·5 - same as 10·4 but for U 0/D 79 data.

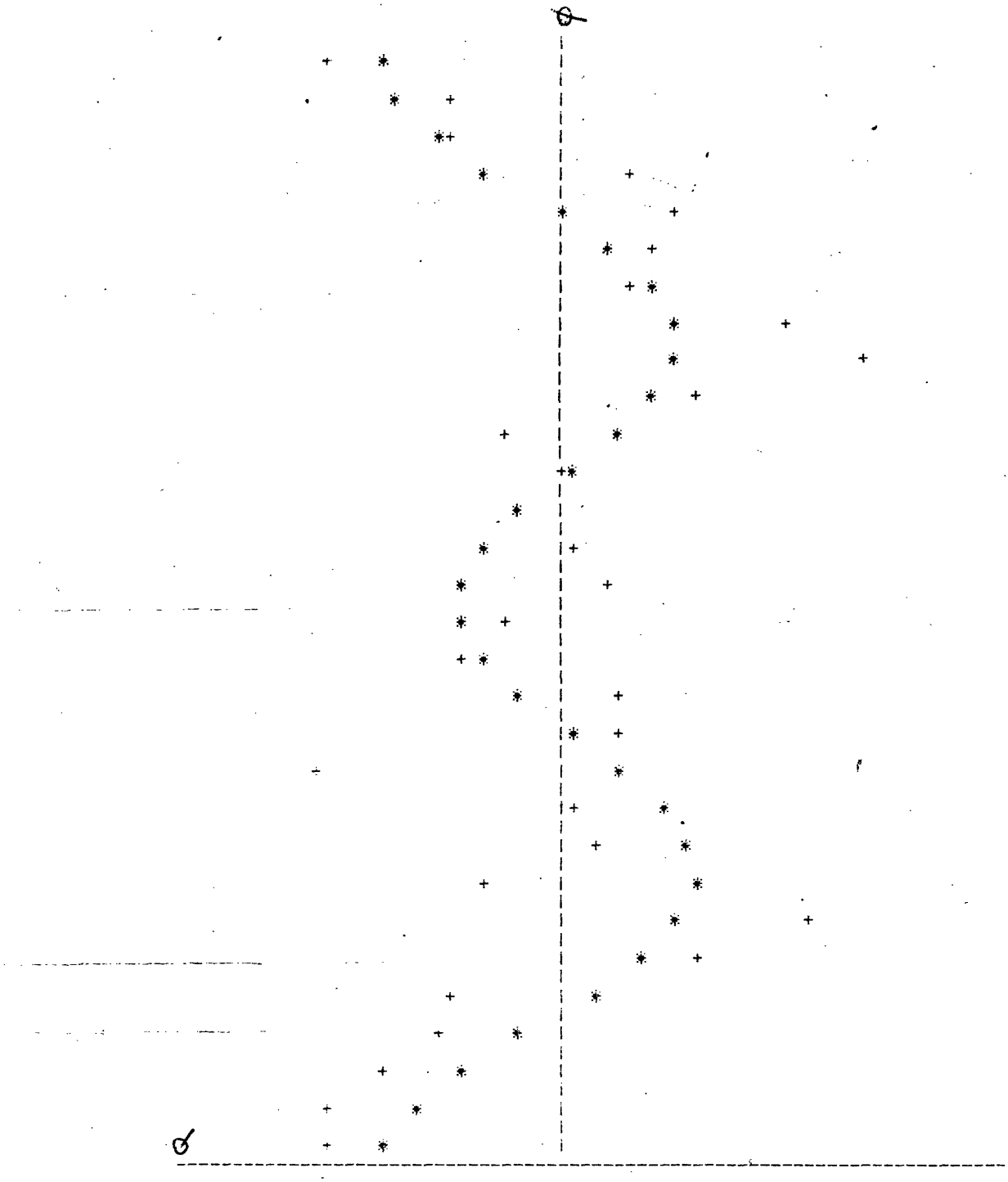

Figure 10.6a same as 10.4 but for all U data. (a Stokes parameter)

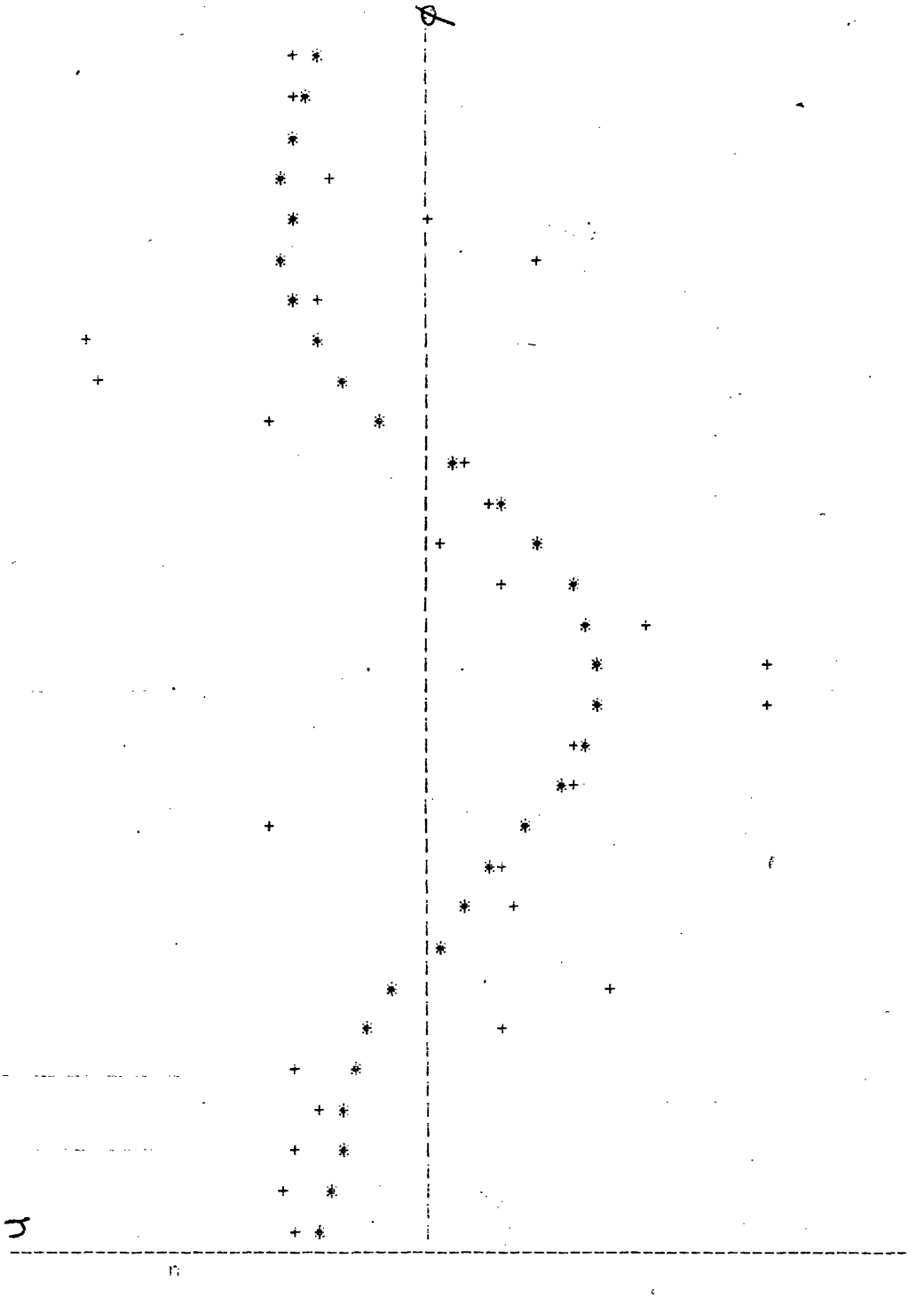

Figure 10.6b same as 10.4 but for U Stokes parameter.

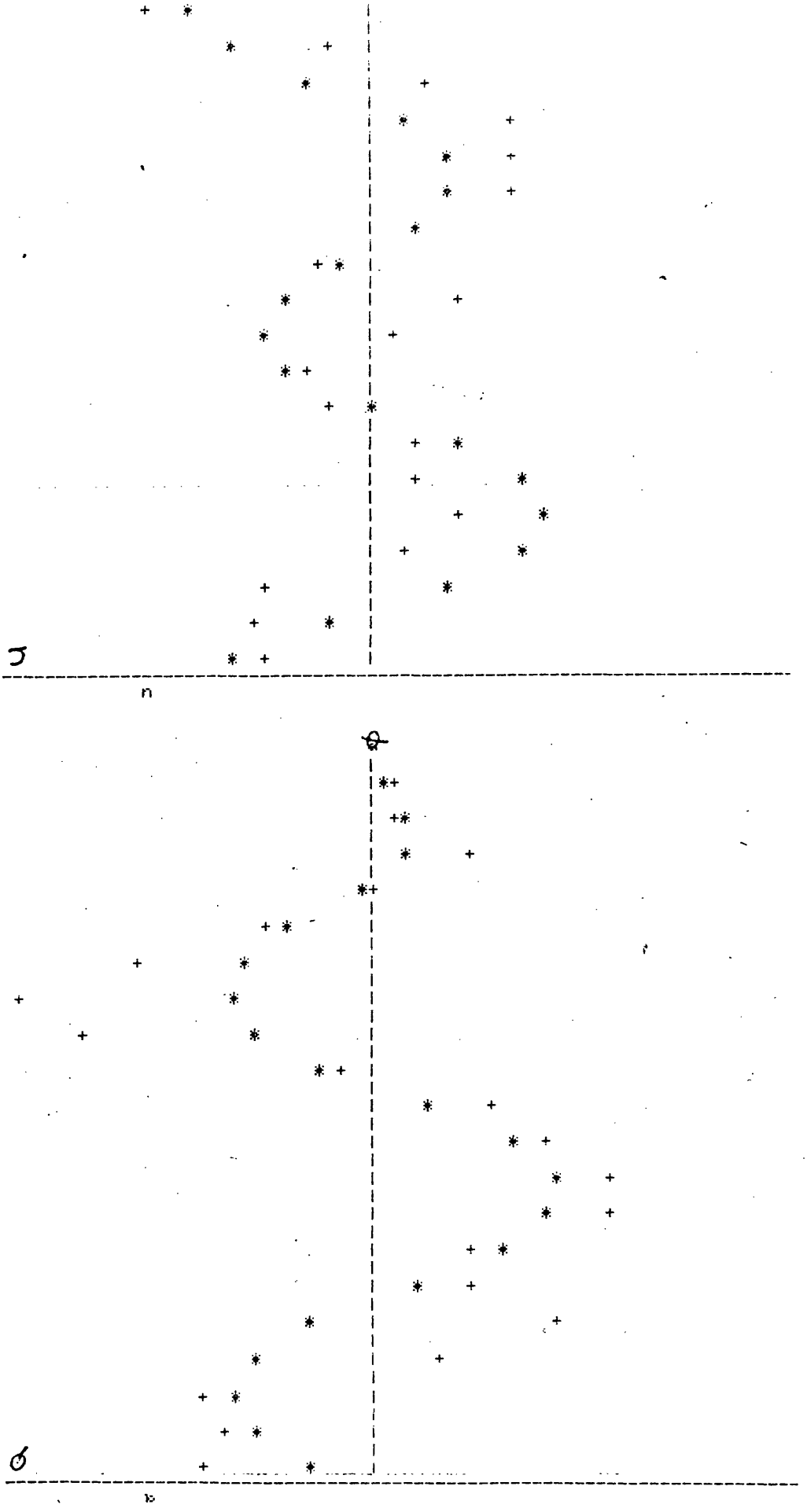

figure 10·7 same as 10·4 but G-J/A 79 data

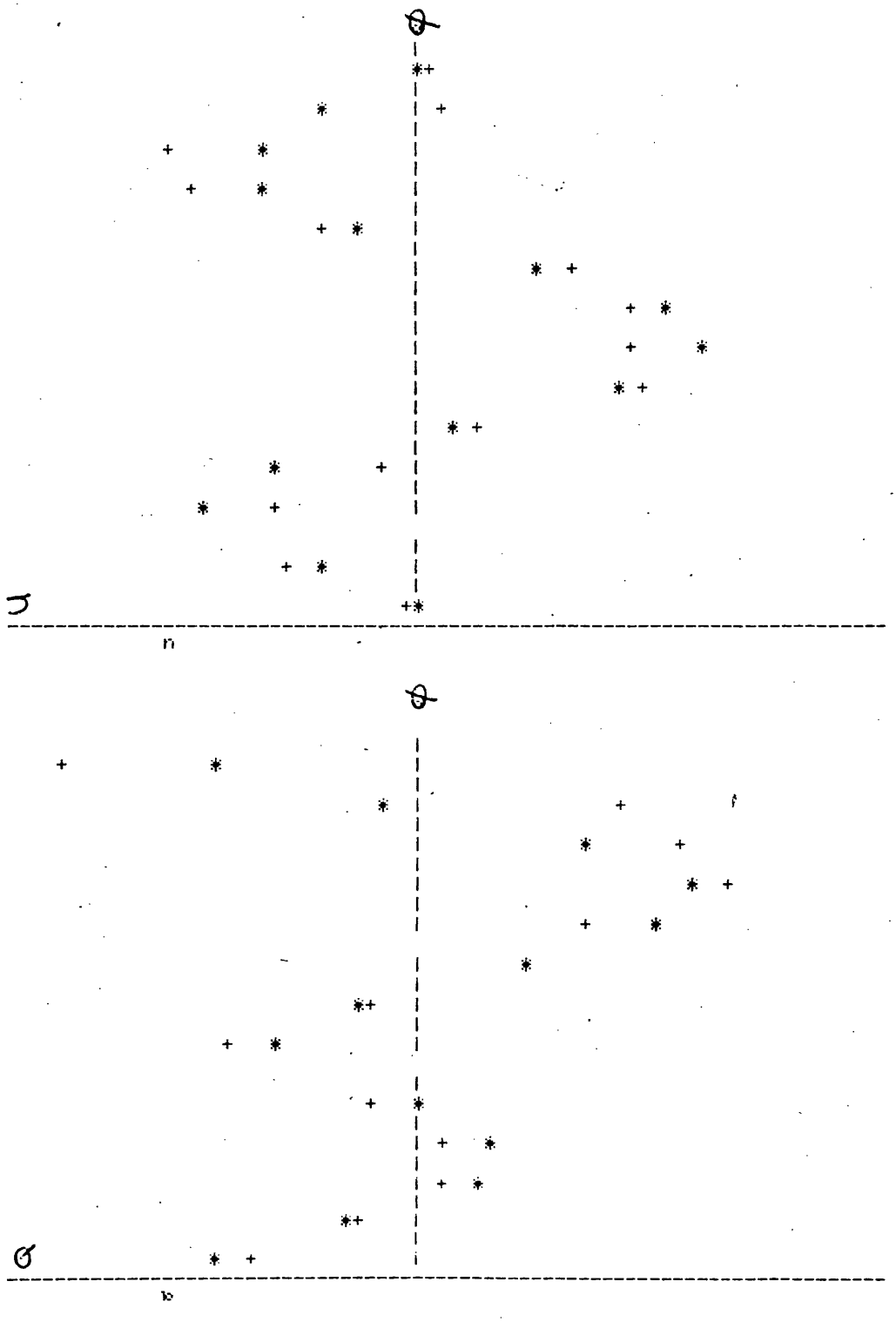

Figure 10.8 same as 10.4 but

G OLD 79 data

bt old

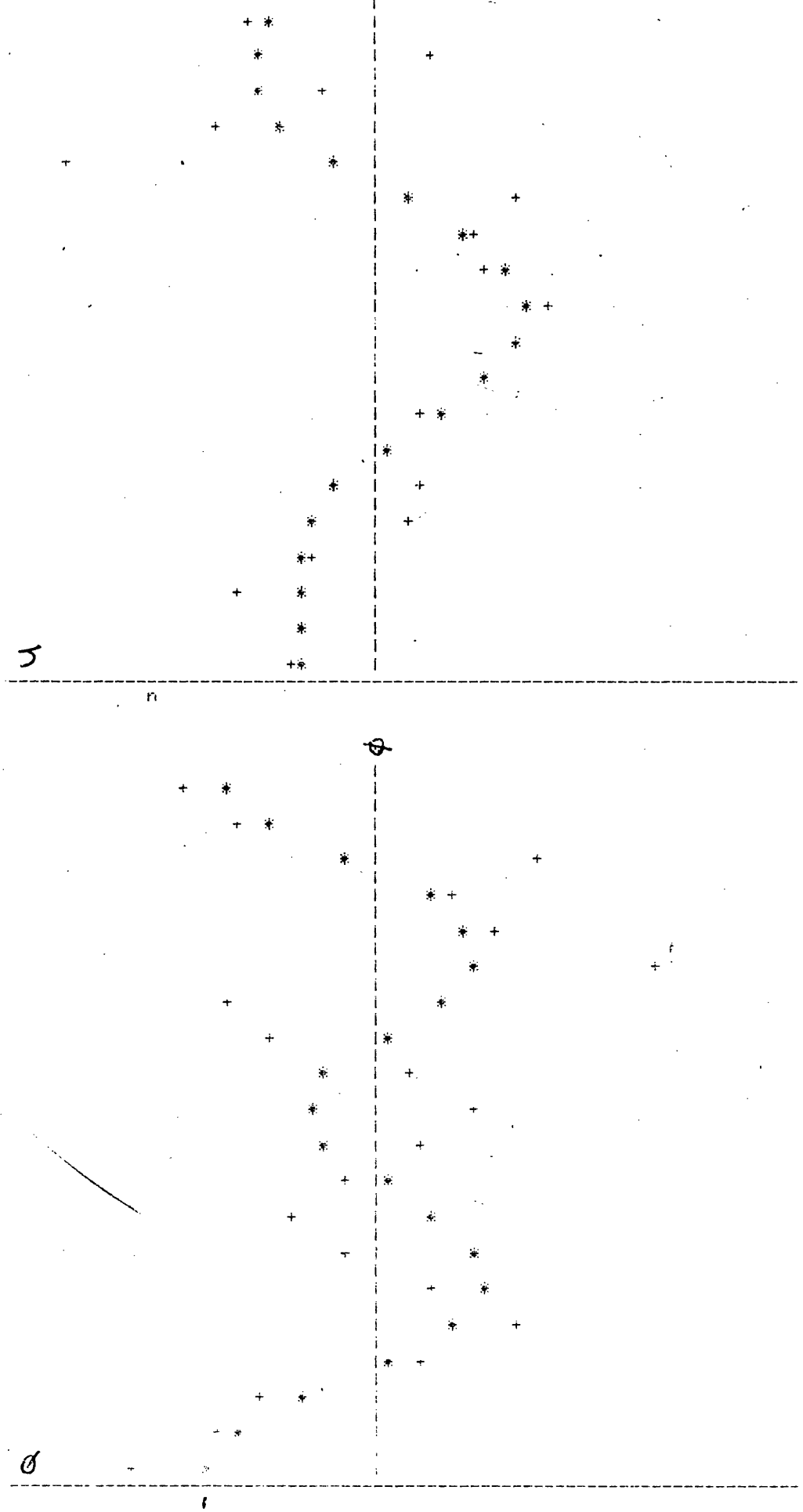

Figure 10·9. same as 10·4 but all G data.

canonical models. We note that in most cases the confidence intervals on i_{opt} are wide and hence the data error (on the binned data) is too large to obtain acceptable model testing and confidence interval formation.

10.3 Analysis in terms of the canonical model with unequal phase interval data.

We proceed to analyse the HD 50896 data sets (10 of them) using the generalized canonical model of Chapter 8 whereby data at unequal phase intervals is considered. The results of the optimization procedure are shown in Table II. The measure of acceptability of model fit and the formation of the Relative Confidence Intervals are as outlined in Chapter 8 whereby the data error σ_{dat} is used to test the goodness of fit of the model at i_{opt} and the residual variance $\hat{\sigma}^2$ is used when forming Confidence Intervals. We take $\sigma_{dat} = 0.0158\%$ from McLean (1980). We see that the model fits are all unacceptable (all significance $<.1\%$) with the Confidence Intervals are broad for seven of the data sets and smaller for the remaining three sets (at both 10% and 25% significances). In the case of the data set B2 (i.e. Oct. to Dec. 79) the R.C.I. on i_{opt} (of 76°) was $[47^\circ, 89^\circ]$ and $[61^\circ, 85^\circ]$ at 10% and 25% signifiances respectively. These would be reasonable limits on the acceptable i values if the model significance (tested using $\sigma_{dat} = 0.0158\%$) was satisfactory (i.e. > 10% say). Data sets B1, B2 and U2 gave these reduced confidence regions on i_{opt}. The reliability of these results is however uncertain since U2 (for example) contained only 15 data points.

10.4 Analysis in terms of the eccentric model

As with the two versions of the canonical model used in (10.2) and (10.3) we analyse the HD 50896 data (the same 10 sections) using the optimization procedure of Chapter 6 of eccentric orbit model and data. In this model we have sixteen free-parameters namely the 12 harmonic coefficients (four for each of the 1st, 2nd and 3rd harmonics predicted), τ_*, the mean optical depth of the scattering region, e, λ_p and i the eccentricity, longitude of perihelion, and

TABLE II.

DATA	N	IOPT	X	SIGMA HAT	RCI 10%	RCI 25%
B1	28	72°	0.215	0.062	[0°,86°]	[51°,89°]
B2	20	76°	0.128	0.056	[47°,89°]	[61°,85°]
U1	18	68°	0.350	0.099	[0°,90°]	[0°,90°]
U2	15	71°	0.114	0.062	[30°,83°]	[51°,81°]
G1	16	68°	0.235	0.086	[0°,90°]	[0°,90°]
G2	13	77°	0.054	0.064	[0°,90°]	[0°,90°]
B	48	88°	1.150	0.110	[0°,90°]	[0°,90°]
U	33	89°	1.439	0.148	[0°,90°]	[0°,90°]
G	29	89°	0.909	0.125	[0°,90°]	[0°,90°]

$X = SIGMA^2.CHI^2$

inclination of the orbit respectively. We adopt the simple optimization technique of chosing e, i and λ_p and hence determining the best fit coefficients as in Chapter 6. This is an extremely protracted computation even though we are restricted to small e (here < 0.4) on implicit assumption of the analyses involved. We therefore best fit the available data for HD 50896 for a range of parameters $0 < e < 0.4$ (in steps of 0.01); $0^\circ \leq \lambda_p \leq 360^\circ$ (in steps of 10°) and $0^\circ \leq i \leq 180^\circ$ (in steps of 1°). This involves for the ten data sets, some 2.6×10^6 numerical optimizations of the eccentric model parameters.

We here summarise the results obtained (cf. Table III). It is clear from the values of the model acceptability (all < 0.1%) that the model is not a good representation of the data and the optimum values of e, λ_p and i are unreliable.

10.5 Conclusions

After applying the three models to the HD 50896 data it is seen that in most cases the data exhibits variations not of a sort representable by the canonical model. The error on each observation is sufficiently small ($\sigma_{dat} \sim 0.0158\%$) to allow reasonably accurate determination of parameters (i.e. the inclination) provided the model fits were satisfactory. The data set best suited to analysis by the general canonical model is the B2 (Oct - Dec 1979) run where, with the binned data (i.e. the smoothed data set), Confidence Intervals on i_{opt} were $[59^\circ, 86^\circ]$ at 25% significance. When the same data set was analysed in raw form (with the generalized model of Chapter (8) the confidence interval at the same significance was $[61^\circ, 85^\circ]$, the two optimum inclinations being 72° and 76° respectively. However it is the model acceptability at i_{opt} that is in error where again, the significance of the model fit at i_{opt} is < 0.1%.

Under development at the moment is a technique and associated program to analyse the departures of a set of data from the canonical form. This involves obtaining the 'best fit' binned canonical model Q,U curves and subtracting the binned theoretical (Q,U) value at each raw data phase point from the observation at that phase. This should

DATA	EOPT	IOPT	LPOPT	X
B1	.25	86°	220°	.4241
B2	.23	81°	260°	.6821
U1	.28	87°	240°	.3834
U2	.38	83°	230°	.7423
G1	.29	84°	240°	.3067
G2	.15	65°	260°	.6727
B	.23	85°	240°	.9273
U	.29	84°	230°	.8748
G	.18	87°	210°	.6347

X = SIGMA↑2.CHI↑2

ALL MODEL FITS AT < .1% SIG.

TABLE III

indicate something about the nature of the departures from canonical model structure the randomness of these departures can also be tested. This would indicate whether the variations present in the data are random or due to some systematic evolution effects tending to change the (Q,U) value, at a certain phase, over relatively short time intervals.

Conclusions and Future work.

The work presented in this thesis has provided analysis concerned with obtaining a set of 'best fit' canonical model parameters, including the orbital inclination i, from any set of polarimetric observations of close binaries. The ability of the optimization procedures derived here to obtain values of these quantities with a satisfactory level of uncertainty (measured for the inclination by the Relative Confidence Interval) has been throughtly investigated. Data error values significantly smaller than those found on previous observations were seen to be necessary to enable this, and when combined with the fact that when noise is present on the observations the optimum inclination from model fitting is biased towards high inclinations, we concluded that the values of the parameters obtained were unreliable. In the limit as the error on the data tends to infinity it was seen that the inferred inclination value tended towards 90^{o}. This behaviour could well explain, or at least contribute to the fact that the polarimetric inclinations determined previously (by other authors) agreed well with values estimated fromphotometric and spectroscopic methods (i.e. within the formal error quoted) in all cases. Most binaries observed polarimetrically have been those exhibiting eclipse behaviour (e.g. Algol, U Sge, u Her) and hence their inclinations were known to be high. This also would lend support to the accuracy of the polarimetrically determined values. Whether the bias is sufficient at the levels of noise encountered to account for the good agreement is not easily estimated. All that can be ascertained is that smaller errors are needed with data taken as outlined in Chapter 8 before conclusions can be drawn as to

the acceptability of the canonical model as a diagnostic of close binaries. Such an observing program is currently being planned. Binary systems with physical and orbital parameters of a suitable sort are given in Table I. The suitability of these is taken as a) those binaries exhibiting no significant light variations (and hence not violating the canonical model assumption of constant light output from the system)i.e. no eclipses, b) those showing no appreciable orbital eccentricity and hence probably corotating,and c) those with orbital periods short enough to allow the interaction of the stars and hence cause free gaseous material in the system and long enough to give good phase coverage,with a reasonable integration time, over one (or at most two) orbital periods. If these conditions (amongst others) are met and variable polarization is established then data suitable for analysis by the generalized canonical model (i.e. the model optimized to accept data at unequal phase intervals) of Chapter 8 should be obtained. Whether the variations encountered will be of a simple nature as predicted by the canonical model is ,of course, a priori unknown. If this is not the case however precise detailed modelling would be considerably easier due to the complete nature of the coverage. This would be justified after rejection of the simpler 'canonical' model.

Also under development at present are numerous techniques to firmly establish the phase locked nature of new,as well as old, observations. These involve the search for periodicities in the data. If phase locking is dominant in the Q,U values obtained then some harmonic of the binary period would be evident in the structure of the data. A comparison of a number

STAR	m(VISUAL)	PERIOD	Sp.T
πCas	4.99	1.96	A5
ϱTuc	5.38	4.82	F5
νAnd	4.52	4.28	B3
δTria	4.87	9.9	G0
HD16769	5.79	2.53	A2
πAri	5.21	3.85	B5
HD21912	5.8	0.917	A0
ο Per	3.83	4.42	B1III
29Tau	5.36	2.41	B3V
biPer	4.65	1.52	A2
41ν^{4}Eri	3.55	5.01	B9
60Tau	5.72	2.14	Am
HD28204	5.88	4.19	A5
88dTau	4.26	3.57	Am
94Tau	4.29	2.96	B5
HD30453	5.88	7.05	A3
π^{4}Ori	3.67	9.51	B3
π^{5}Ori	3.73	3.70	B3
γCam	4.47	3.88	A2
66Eri	5.16	5.52	B9
14Ari	5.06	3.79	A2
ηOriAab	3.32	7.99	B1
136Tau	4.61	5.97	A0
HD40372	6.0	2.74	A5
μOriA	4.14	4.40	A2
1Gem	4.15	9.65	G8
45Aur	5.35	6.50	F5
α^{1}Gem	2.85	2.92	A2
1Hyd	5.62	1.56	F1
ζUMa	4.87	3.98	G0

TABLE I.

STAR	m(VISUAL)	PERIOD	Sp.T
HD102660	5.97	2.78	A2
95 Leo	5.47	6.62	2A2
θ^2Cruc	5.77	3.42	B3
4HDrac	4.95	1.27	Am
32Caml	5.81	3.28	A0
HD118216	5.01	2.61	F0
ν Cen	3.40	2.67	B2
HD124425	5.93	2.69	F5
πSco	2.92	1.57	2B1V
θ Drac	4.06	3.07	F8
σ^2CorB	5.76	1.14	F8
39Her	5.9	2.31	F2/5
ε Her	3.92	4.02	A0
HD157978	5.9	3.75	2A0
HD158261	5.86	5.90	A2
ζ Ser	3.52	2.29	A5
ωDra	4.8	5.27	F5
HD161783	5.9	3.17	B3/5
108Her	5.5	5.51	A2
59dSerbc	5.21	1.85	2A0
δ'Lyr	4.35	4.299	Am
50Drac	5.36	4.11	2A0
18Y Aqu	5.16	1.302	B8
2Sgtr	5.96	7.39	A3
201G Sgt	5.90	4.60	A3III
ϕ Aqu	5.23	3.32	A2
θ'Sgtr	4.35	2.10	B3
18Vul	5.48	9.3	A2
77Cyg	5.48	1.72	A0
32Aqr	5.32	7.8	A3
2 Lacr	4.56	2.61	B5/6

of techniques (here we are considering 4) is considered necessary to distinguish between such effects as aliasing amongst other problems encountered that tend to give false results. We are developing computer programs to find periodicities by the phase dispersion minimization method of Stellingwerf (1978), the phase binned Fourier analysis of Kemp et al (1979), the generalized Fourier technique of Grey and Desicachary (1978) and by Maximum Entropy methods(Gull and Daniels (1977). Once this aim is achieved the suspect phase locked nature of the polarimetric variations in the light of some binaries considered here together with new observations can be comprehensively tested.

Other diagnostic techniques, associated with the application of the canonical model are also under development. We consider it necessary when data sets spanning many orbital periods are available (cf Chapter 9 - Cygnus X-1 data) to consider the average structure (i.e. phase binned nature of the variations) in the data in relation to the detailed nature of the Q,U values by subtracting out the average behaviour of the data over the observing period . It may then be possible to map the deviations in the polarization with other events occurring at specific times. For example if the average behaviour of the Cygnus X-1 data were subtracted out of the raw observations it may become evident that at certain phases of particular periods the deviations were significantly larger than at other times. These periods of 'activity' may well agree with periods of intense X-ray emmision or a similar disturbing

phenomenon. Information regarding the nature of the changes occurring in the scattering region could well be gained by such an analysis.

It is also possible to extend the eccentric orbit model to accept a more general distribution of scatterers. At present the scattering region is constrained to be at the secondary star and hence is a reasonable interpretation of say an accretion disk. If the eccentric model is needed to give better diagnostics of certain systems the extra flexibility of a scatterer at any position in the obbit of the system would allow a more reasonable picture to be formed of the binary.

In conclusion therefore we note that various extensions to the canonical model are clear to enable a more complete and clear treatment of observations when combined with the analysis presented in this thesis.

APPENDIX I - Spectrophotometric Details of Nine Binaries

In this appendix we relate the photometric and spectroscopic observational evidence on the nature of the ten binaries observed polarimetrically, data from which has been re-analysed in this thesis. Also included are the details of the system BETA LYRAE which was the first binary found to exhibit variable linear polarization phenomenon.

i) AO Cassiopeiae

a) Alternative Names: BD+56 46; HD 1337; Boss 46; HR 65; PD 134; Groomb 35.

b) Spectroscopic variations discovered by Adams and Strombers (1918)

c) Photometric variations discovered by Guthnick (1919) and stebbens (1920) with detailed study by Pearce (1926). AO Cas was thought, at this time, to be an eclipsing type binary.

d) More detailed photometric observations were made by Wood (1947) and Koch (1960) - B,V light curves.

e) Spectroscopic studies made by Abyankhar (1959) indicated a mass ratio $q = .85$.

f) Currently accepted elements of AO Cas are given by Hutchings and Hill (1971) and Shneider and Leung (1978):

	M1	M2
Spectral Type	08.5III	08.5III
Mass [M(Sun)]	18	22
Radius [R(Sun)]	11.5	9.5
log Te (K)	4.591	4.556
log [L/L(Sun)]	5.57	5.3
K1,K2 (km/s)	223.4±1.8	178.8±6.1
Period (days)	3.523487	
Epoch (days)	JD 2424002.579	
i (phot)	51 .2+0 .17	
e (orbit)	0.037+0.008 (?)	
w (orbit)	20 .8+13 .3 (?)	
G1 (km/s)	-31.1+1.3	
m(visual):(dm)	6.05 (0.2)	
Period Change (days) (30 yr. interval)	.00035	
Envelope	Gas Stream	

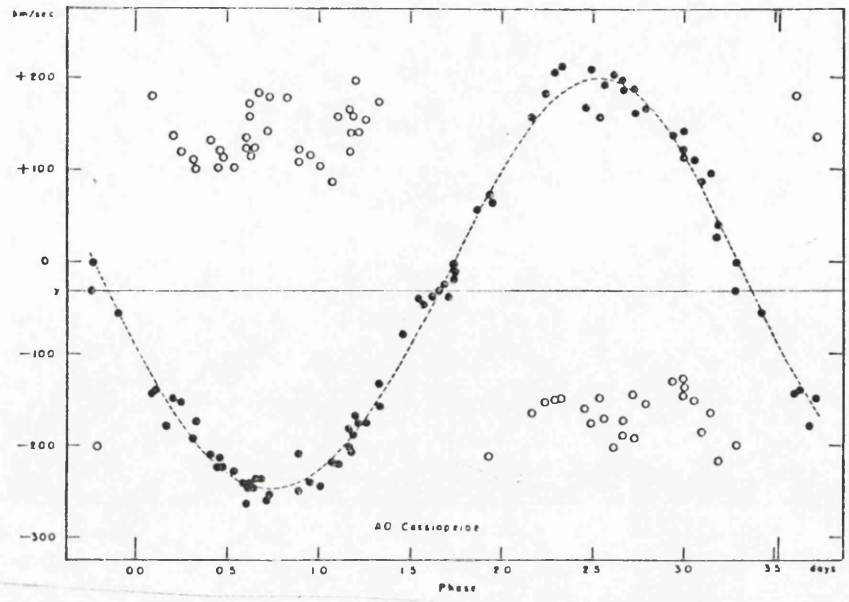

FIG. A1—The radial velocity-curves for AO Cassiopeiae

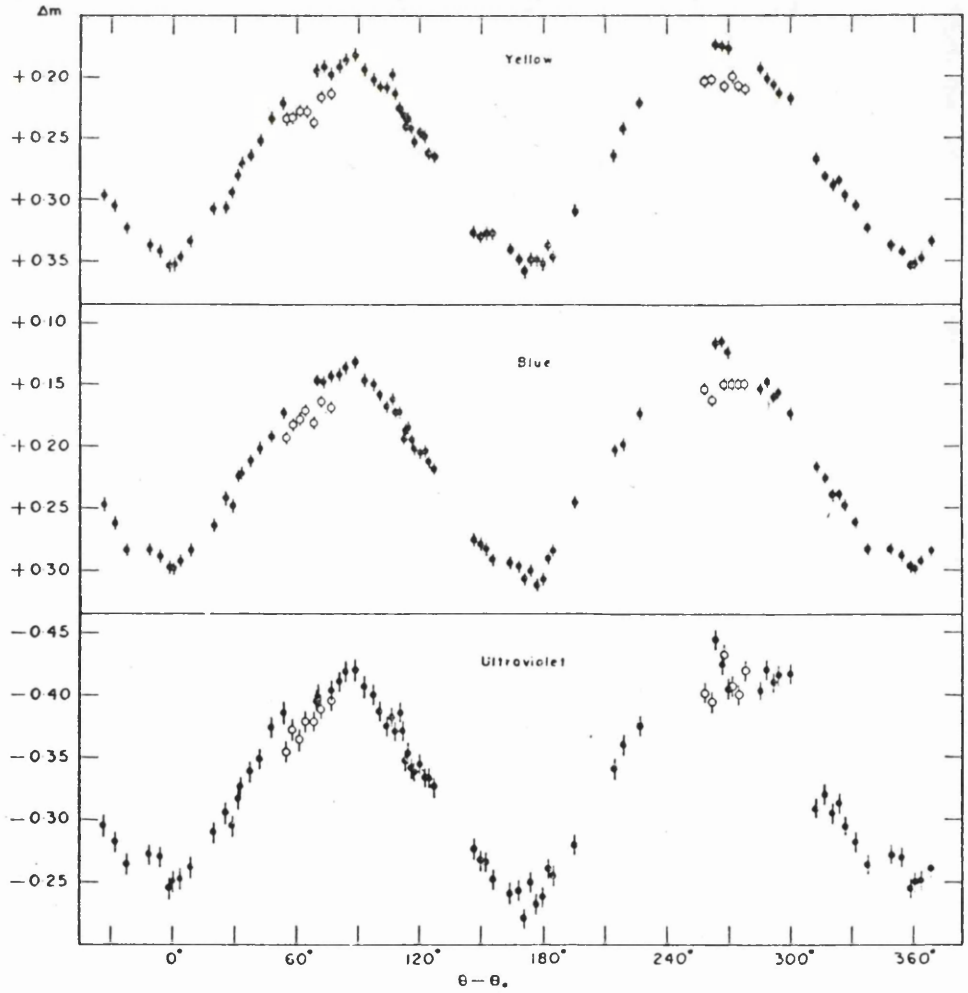

FIG. A2—The light-curves for AO Cassiopeiae. The open circles at phases 60° and 270° represent observations of September 7 and September 16, 1957, respectively.

ii) BETA Persei

a) Alternative Names: ALGOL

b) Prototype eclipsing binary - studied for >150yrs. ~200

c) Triple system - AlgolAB and AlgolC van de Kamp(1960)

d) AlgolC - Am type period 1.862 yrs.

e) Spectrophotometric studies by Frieboes-Condes etal(1970) Hill etal(1971) Guinan etal(1976) and Soderjelm(1980)

	M1	M2
Spectral Type	B8	G-K
Mass [M(Sun)]	3.6	0.79
Radius [R(Sun)]	2.89	3.53
log Te (K)	4.09	3.69
log [L/L(Sun)]	2.26	0.84
K1,K2 (km/s)	44.1+0.4	12.0+0.4
Period (days)	2.86730807	
Epoch (days)	JD 2428487.739	
i (phot)	82.3+0.3	
e (orbit)	0.0	
w (orbit)	-	
m(visual)	2.2 - 3.5	
Period Change (days)	significant	
Envelope	Gas Stream	

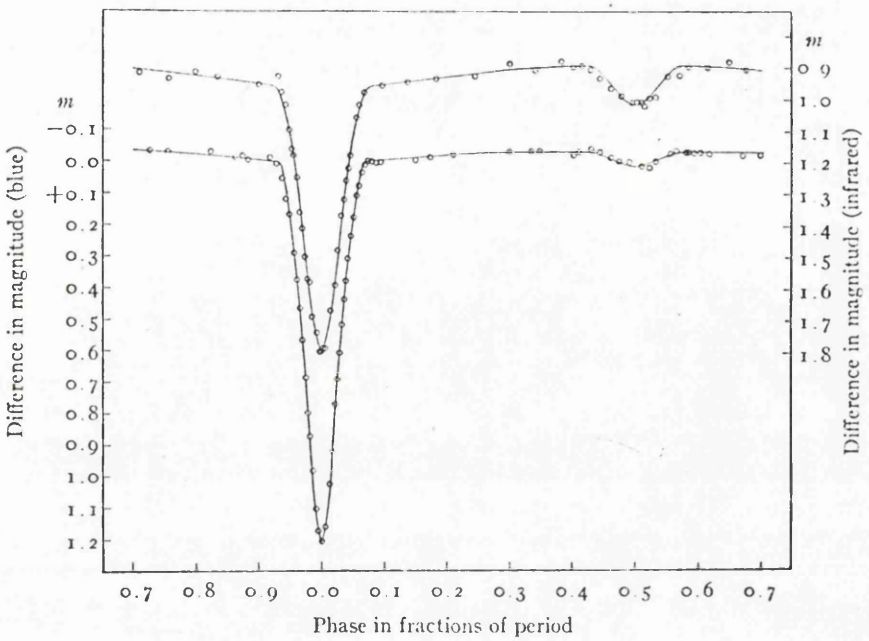

Light curve for Algol.

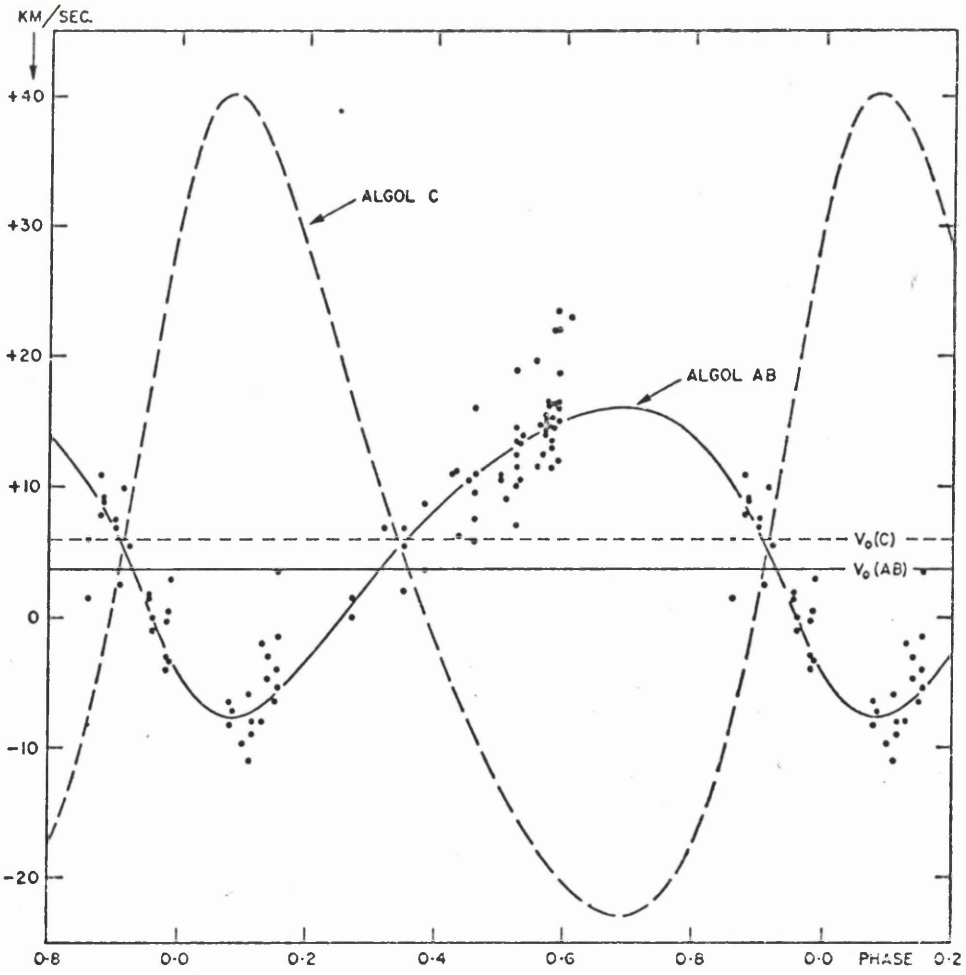

Radial velocity curves for Algol.

iii) HD47129

a) Alternative Names: Plasketts Star

b) Observed spectroscopically Plaskett (1922)
Struve etal(1958) and Abyankhar (1959)

c) Photometric variations of 0.08 mag. - no eclipses
Abyankhar and Spinrad(1958)

d) Most massive binary known

	M1	M2
Spectral Type	O7	-
Mass [M(Sun)]	>55	>55
Radius [R(Sun)]	-	-
log Te (K)	-	-
log [L/L(Sun)]	-	-
K1,K2 (km/s)	205.2+1.0	-
Period (days)	14.414	
Epoch (days)	JD 2423039.94	
i (phot)	-	
e (orbit)	0.011	
w (orbit)	22.4	
m(visual)	6.04	
Envelope	Cloud	

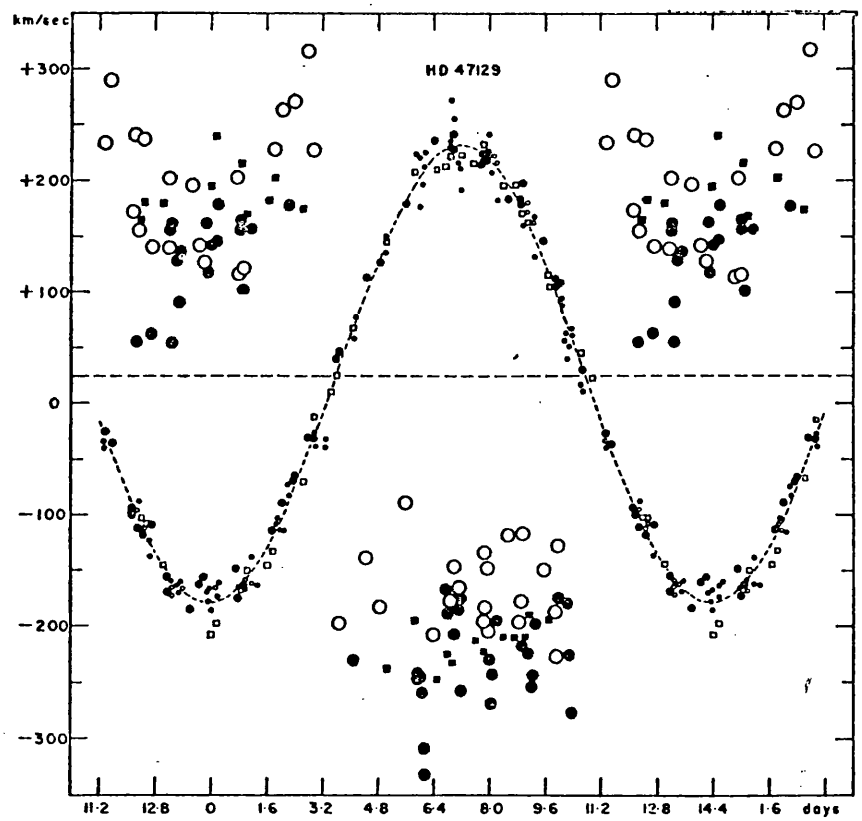

Radial velocity curves.

for HD 47129

iv) U Sge

a) Alternative names: HD181182

b) Eclipsing Binary : Schwabe (1901); Joy (1930); McNamara (1951). Algol type variable

c) Non-synchronous rotation of stars and orbit. Struve (1949)

	M1	M2
Spectral Type	B2	G2
Mass [M(Sun)]	6.7	2.3
Radius [R(Sun)]	4.4	5.6
log Te (K)	-	-
log [L/L(Sun)]	-	-
K1,K2 (km/s)	~~120~~ 84	-
Vrot (km/s)	135	82
Period (days)	3.3806184	
Epoch (days)	JD 2417130.4151	
i (phot)	90	
e (orbit)	0.0	
w (orbit)	-	
m(visual)	0.5-9.8	
Envelope	Cloud/Ring	

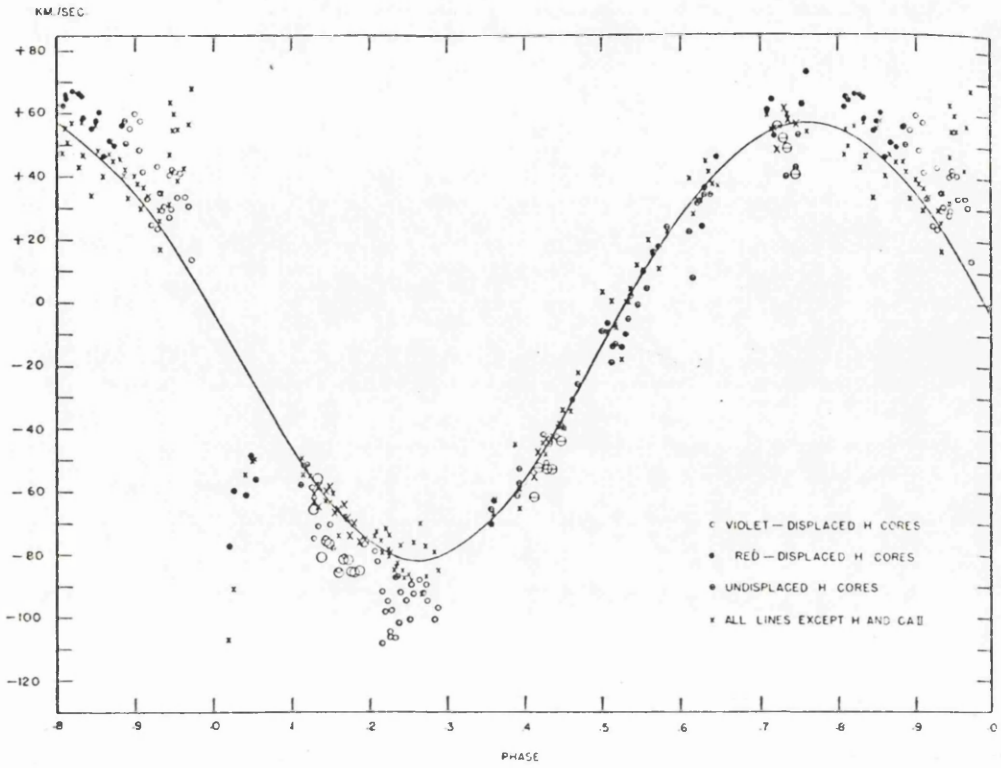

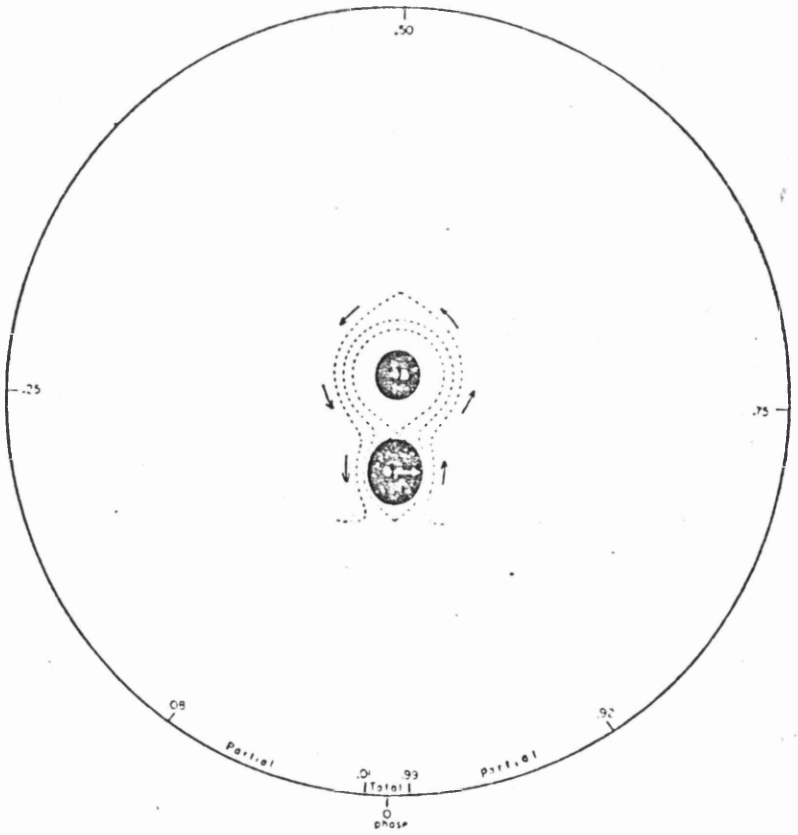

Radial velocity curve and proposed model for USge (Struve 1949).

v) V444 Cygni

a) Wolf-Rayet Binary with young O companion.

b) Eclipsing Binary

c) Photometric studies - Kron and Gordon (1950); Cherepashchuk (1975).

	M1	M2
Spectral Type	WNS	O6
Mass [M(Sun)]	26.4	20.4 (core 2.6)
Radius [R(Sun)]	9.3	2.1
log Te (K)	-	4.87
log [L/L(Sun)]	-	-
K1,K2 (km/s)	-	-
Period (days)	4.21238	
Epoch (days)	JD 2428771.379	
i (phot)	80	
e (orbit)	-	
w (orbit)	-	
m(visual)	8.04	
Mass loss	.000001 (M(Sun)/yr)	
Envelope	Extended Envelope /Disk	

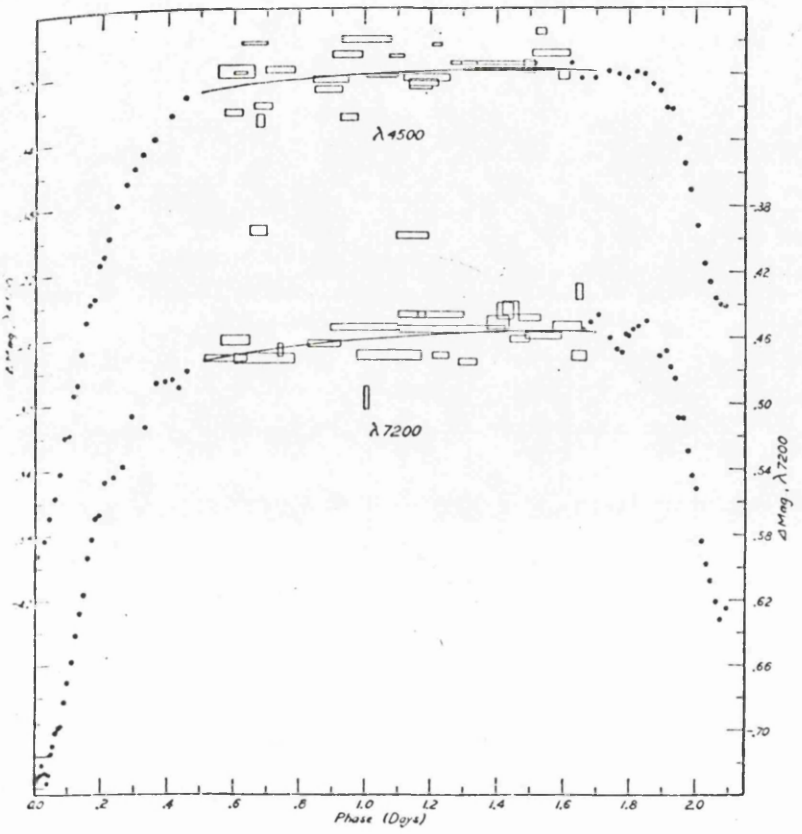

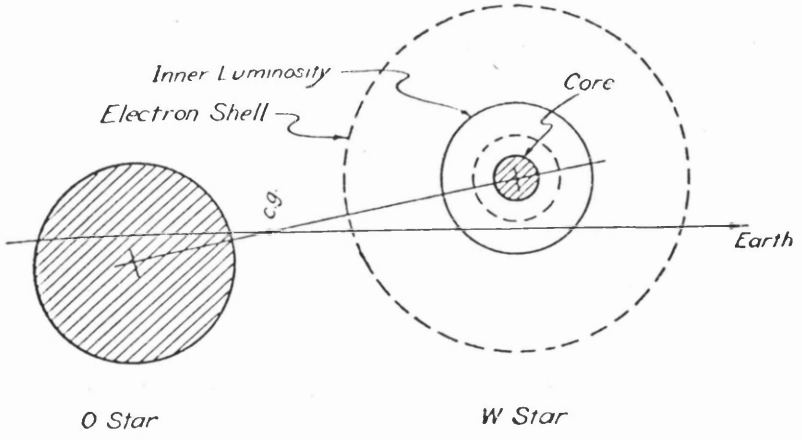

Light curve and model for

VV44 Cygni.

vi) σ Ori E

a) Alternative name: HD37479

b) Peculiar He-rich member of trapezium - first to be discovered.

c) Photometric variations - Hesser et al. (1976,1977).

d) Binary nature queried by Groote and Hunger (1977) - oblique rotator.

e) Landstreet et al. (1978) B 3000 G - period 1.19d

	M1	M2
Spectral Type	B2Vp	-
Mass [M(Sun)]	8	<0.1 M(Sun)
Radius [R(Sun)]	-	-
log Te (K)	-	-
log [L/L(Sun)]	-	-
K1,K2 (km/s)	<4 km/s	-
Period (days)	1.1908 d	
Epoch (days)	JD 2442778.819	
i (phot)	>45 (?)	
e (orbit)	-	
w (orbit)	-	
m(visual)	+6.8	
Envelope	Disk (?)	

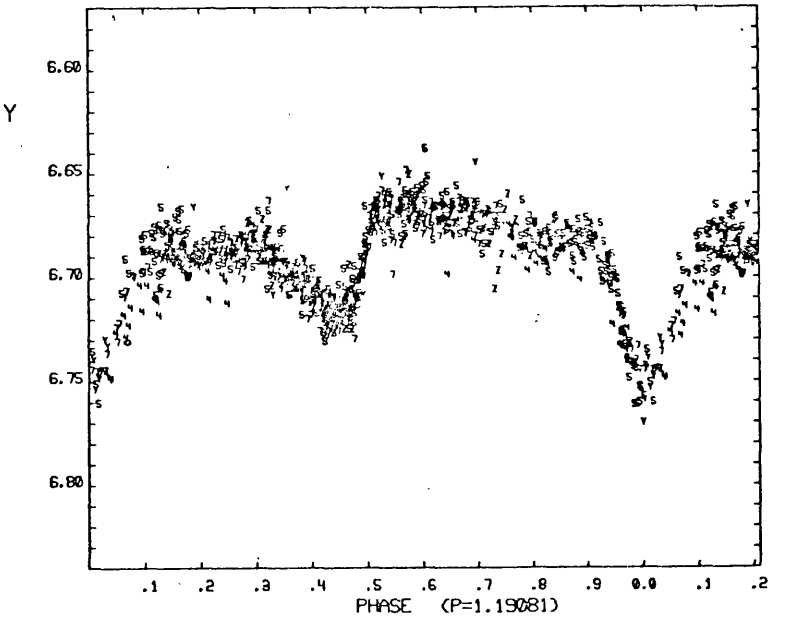

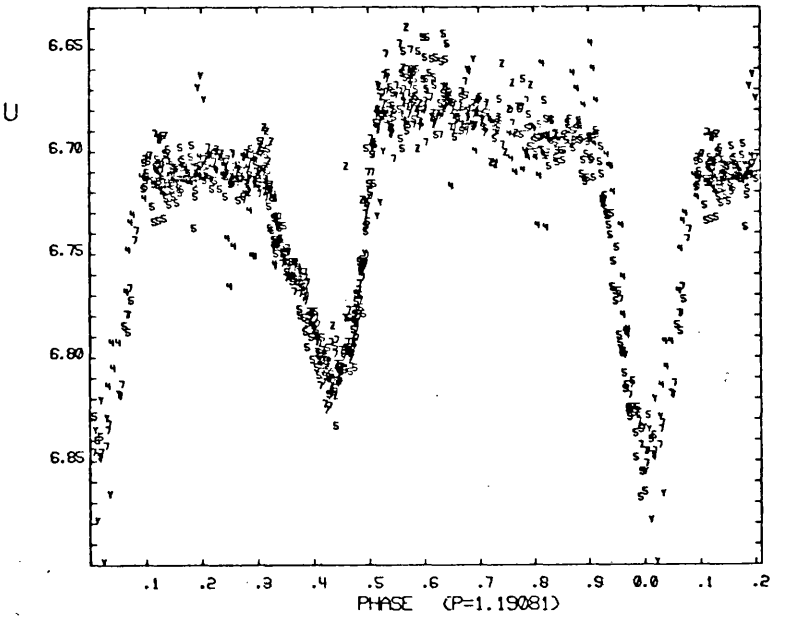

Y and U light variations for the system σ Ori E.

vii) νHer

a) One of the first binaries to be studied photometrically and spectroscopically - Kovachev and Reinhardt (1975).

b) (Partial) eclipse - Soderhjelm (1978).

c) Beta Lyrae type system

	M1		M2
Spectral Type	B2.5V		B5
Total Mass [M(Sun)]		0.174	
Radius [R(Sun)]	0.3		0.34
log Te (K)	4.1		4.34
log [L/L(Sun)]	-		-
K1,K2 (km/s)	93.8		-
Period (days)	2.051027		
i (phot)	78		
e (orbit)	0.058		
w (orbit)	168		
m(visual)	4.5-5.2		
Envelope	(?)		

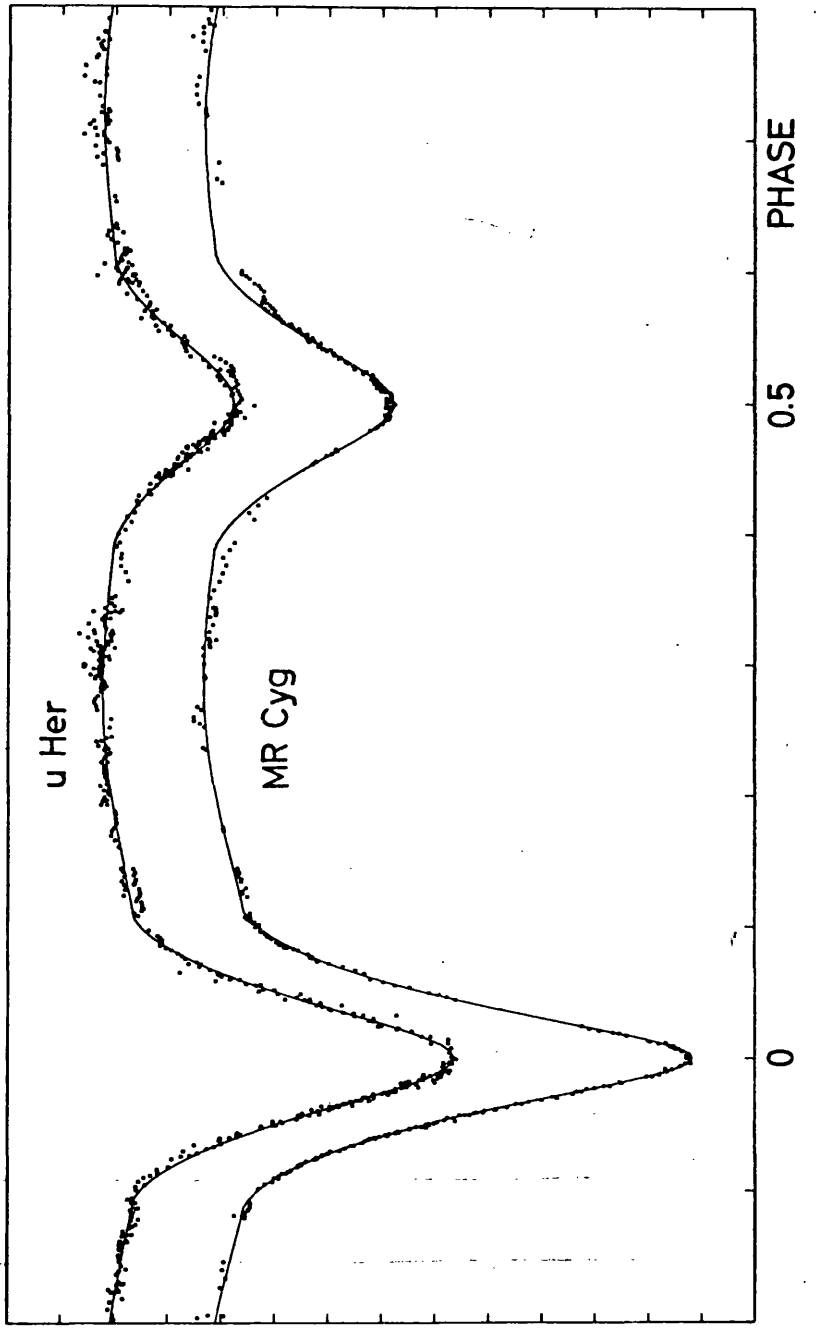

Light curve for u Her.

viii) β Lyrae

a) Alternative name: Sheliak

b) Variability discovered by Goodricke (1784) Pickering (1891) - spectroscopic.

c) Prototype/ cataclysmic type of eclipsing binary systems - Guthnick and Fraser (1917); Smart and Green (1935); Struve (1941).

d) First binary shown to have variable linear polarization - Ohman (1922).

	M1	M2
Spectral Type	B9	F5(?)
Mass [M(Sun)]	3.80	15.0
Radius [R(Sun)]	-	-
log Te (K)	-	-
log [L/L(Sun)]	-	-
K1,K2 (km/s)	185	-

Period (days)	12.93
Rate of change of Period	19 s/yr
i (phot)	70 (?)
e (orbit)	0.014
w (orbit)	-
m(visual)	3.4-4.5
Envelope	Cloud/Disk/Stream

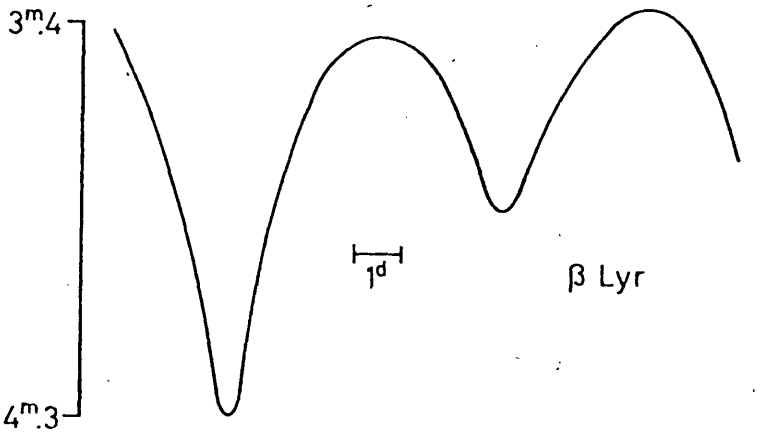

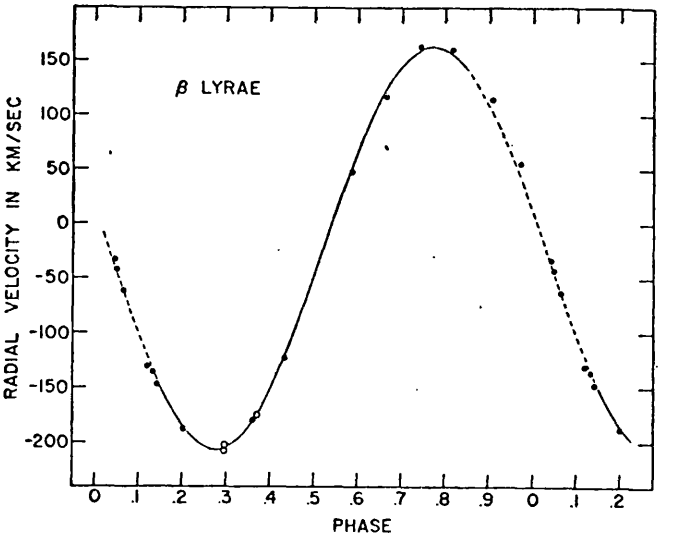

Light curve and radial velocity curve for β Lyrae.

ix) Cygnus X-1

a) Alternative name: HD226868 ; V1357 Cygni; BD + 34 3815.

b) Optical variability discovered by Bolton (1971) and Webster and Murdin (1972).

c) Associated with galactic X-ray source and radio soource.

d) Prime candidate for black hole binary - Rothschild et al. (1974).

	M1	M2
Spectral Type	O9.7Iab	-
Mass [M(Sun)]	20-30	(?)
Radius [R(Sun)]	-	-
log Te (K)	4.48	-
log [L/L(Sun)]	-	-
K1,K2 (km/s)	72.2	-
Period (days)	5.6000	
Epoch (days)	JD 2443252.372	
i (phot)	30 (?)	
e (orbit)	0.06	
w (orbit)	330	
m(visual)	9.0	
Envelope	Stream/Disk (?)	

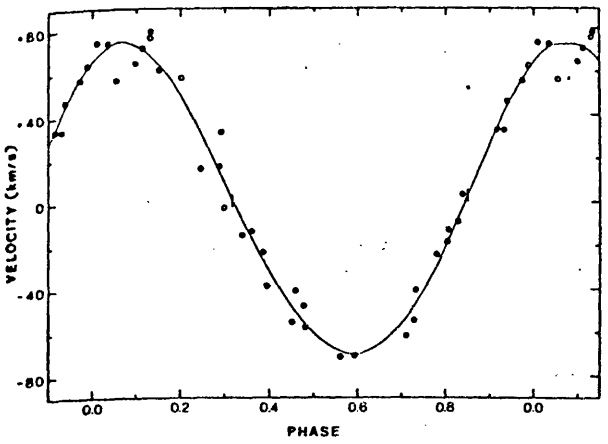

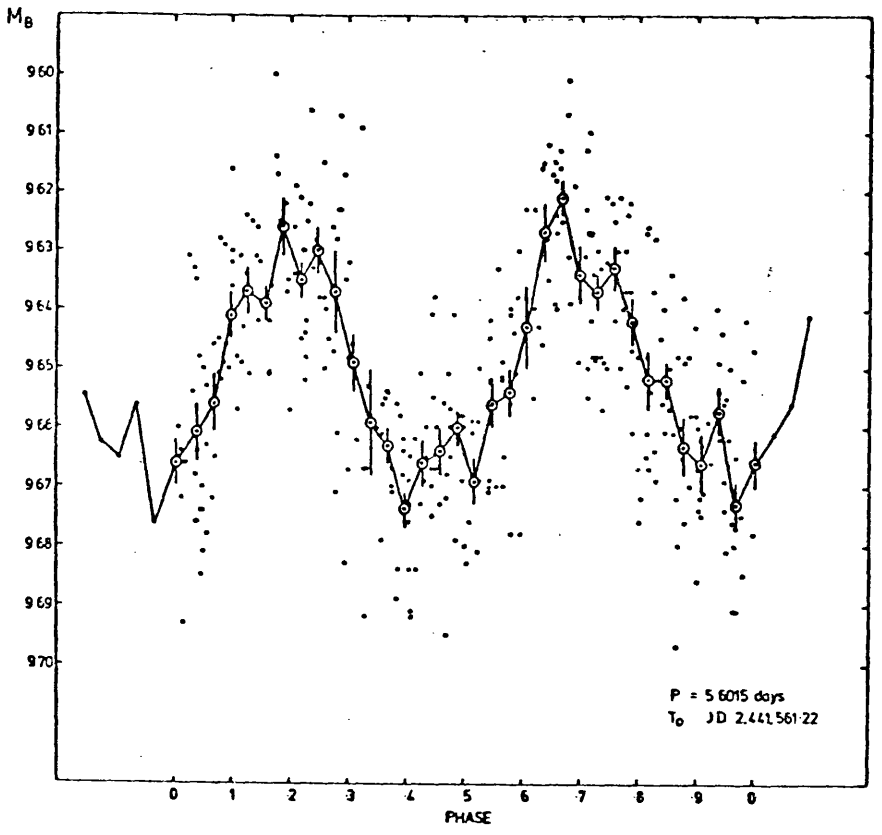

Cygnus X-1 light and radial velocity curves.

x) HD50896

a) Alternative name: MR6; EZ CMa

b) At first thought to be single Wolf-Rayet star.

c) One of brightest WR type systems.

d) Spectroscopic observations - Smith (1968,1973) appears as central object of faint ring nebula S308.

e) Variable emission lines - Ebbets (1980).

f) Thought to be WR star and compact companion - van den Heuvel (1976) ; Moffat and Seggewiss (1979).

	M1	M2
Spectral Type	WN5	-
Mass [M(Sun)]	10	6.9
Radius [R(Sun)]	-	-
log Te (K)	>4.6	-
log [L/L(Sun)]	-	-
K1,K2 (km/s)	-	-
Period (days)	3.76 (?)	
i (phot)	-	
e (orbit)	0.34 (?)	
w (orbit)	-	
m(visual)	6.9	
Envelope	Extended atmosphere	

APPENDIX II - (Q,U) Loci predicted by the Eccentric Model

Shown overleaf are examples of the Stokes parameter loci predicted by the canonical model when generalized to allow for a scattering region in an eccentric orbit.
This non-zero eccentricity violates the corotation assumption of the canonical model. The analysis involved is given in Chapter 6 of the main text.
Also shown are the subsidiary data sets (Q_+,U_+) and (Q_-,U_-) formed as described in Chapter 6 for each of the eccentricities shown. They indicate the growth of the odd and even harmonics respectively as e increases from zero.

Shown are the loci for :

a) i = 75°, lambda p = 0°
b) i = 75°, lambda p = 75°
c) i = 135°, lambda p = 75°

a) b) and c) include figures for e = 0.0 to 0.55 step .05

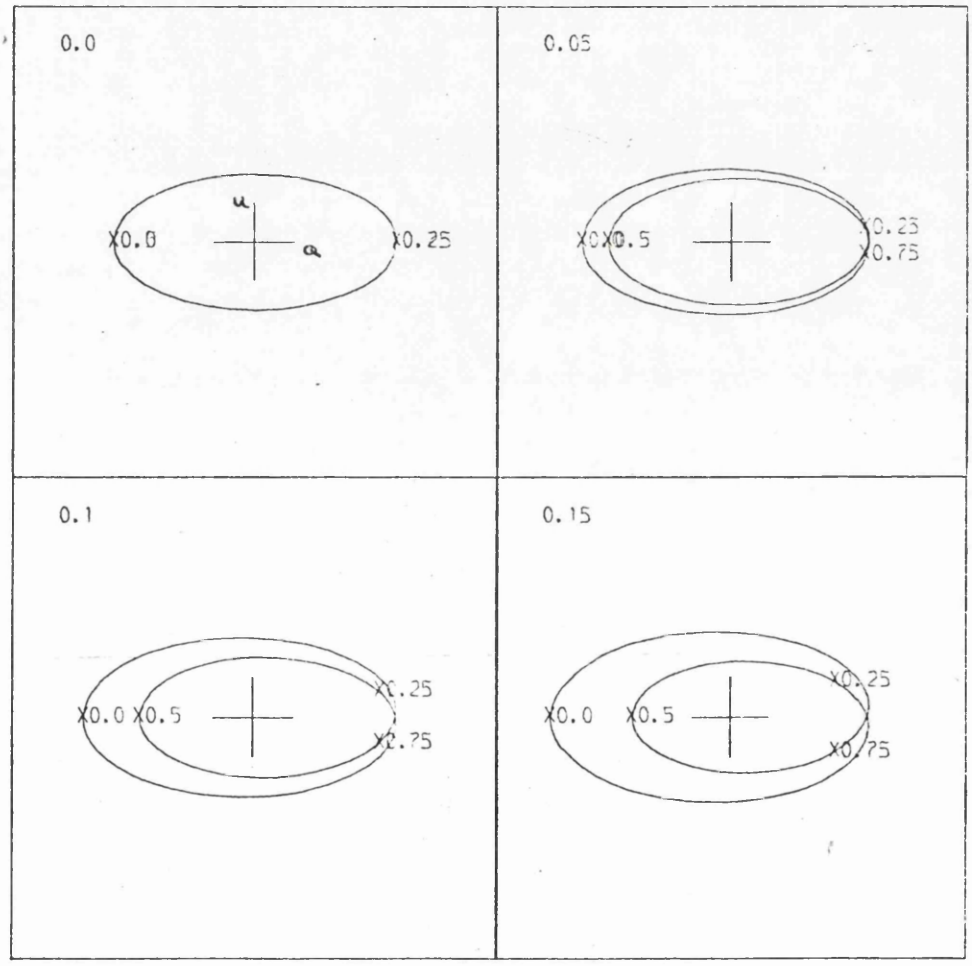
0.0
u
X0.0
a
X0.25
0.05
X0
X0.5
X0.25
X0.75
0.1
X0.0
X0.5
X0.25
X0.75
0.15
X0.0
X0.5
X0.25
X0.75

a)

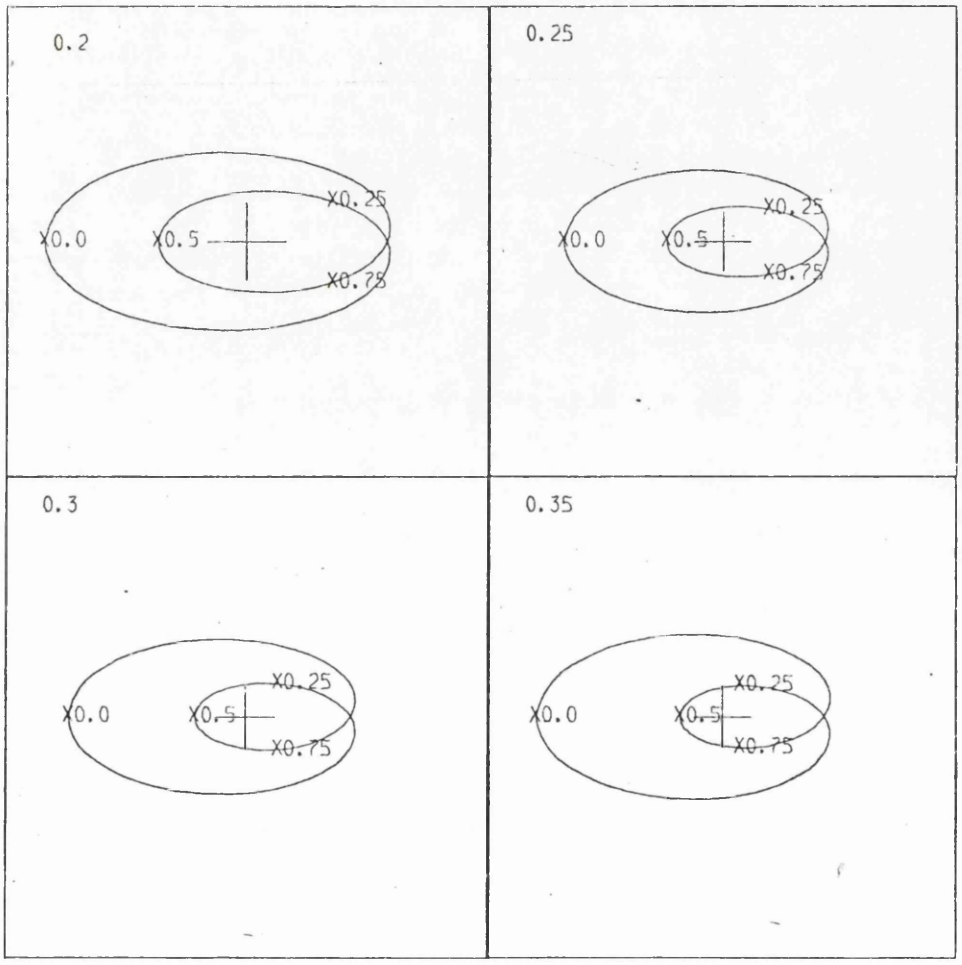
0.2
X0.0
X0.5
X0.25
X0.75
0.25
X0.0
X0.5
X0.25
X0.75
0.3
X0.0
X0.5
X0.25
X0.75
0.35
X0.0
X0.5
X0.25
X0.75

a)

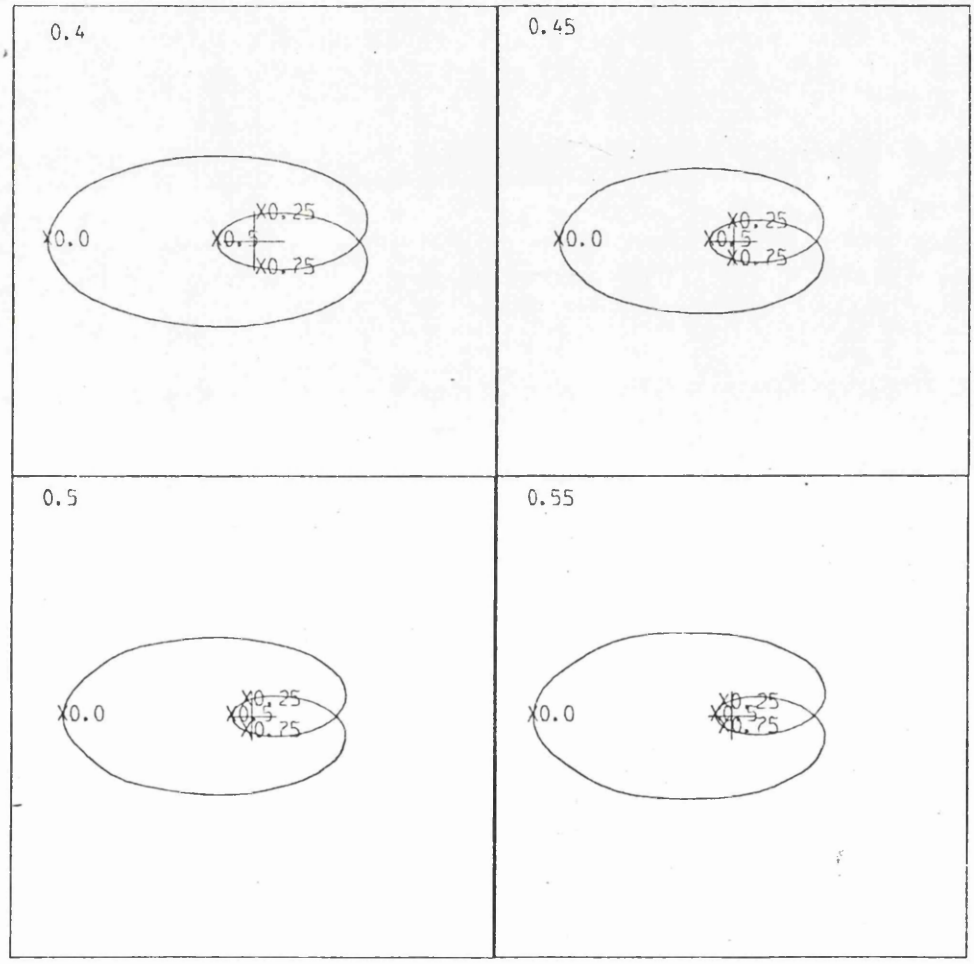
0.4
X0.0
X0.25
X0.5
X0.75
0.45
X0.0
X0.25
X0.5
X0.75
0.5
X0.0
X0.25
X0.5
X0.75
0.55
X0.0
X0.25
X0.5
X0.75

a)

a)

0.0
u_+
X0.85
a_+
0.0
X 0.375
u_-
X0.0
a_-
X0.25
0 X125
0.05
X 0.25
X0.0
X.75
0.05
X 0.375
X0.0
X0.25
0 X125

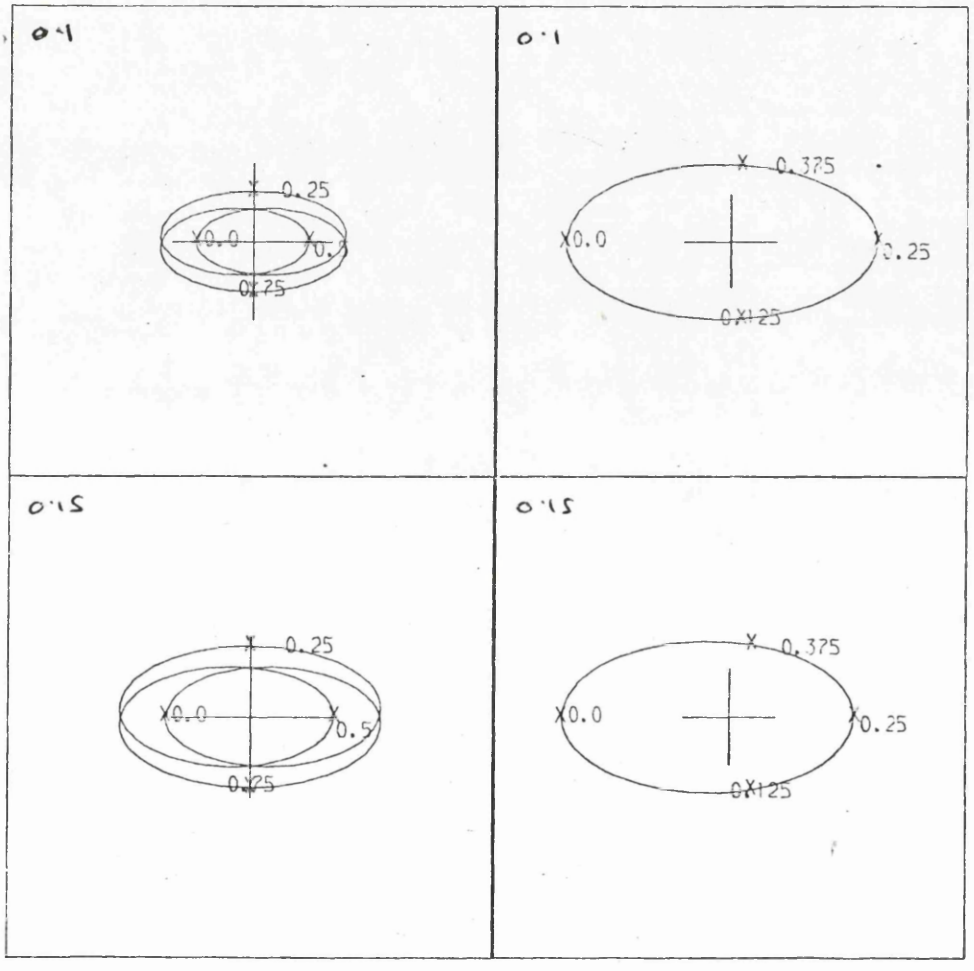
0.1
0.25
0.0
0.5
0.25
0.1
0.375
0.0
0.25
0.125
0.15
0.25
0.0
0.5
0.25
0.15
0.375
0.0
0.25
0.125

a)

0·2 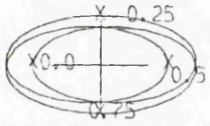	0·2 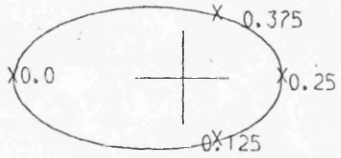
0·25 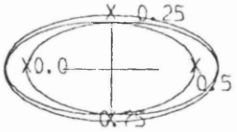	0·25 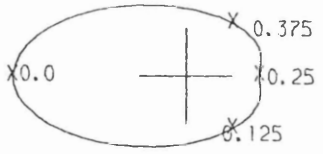

a)

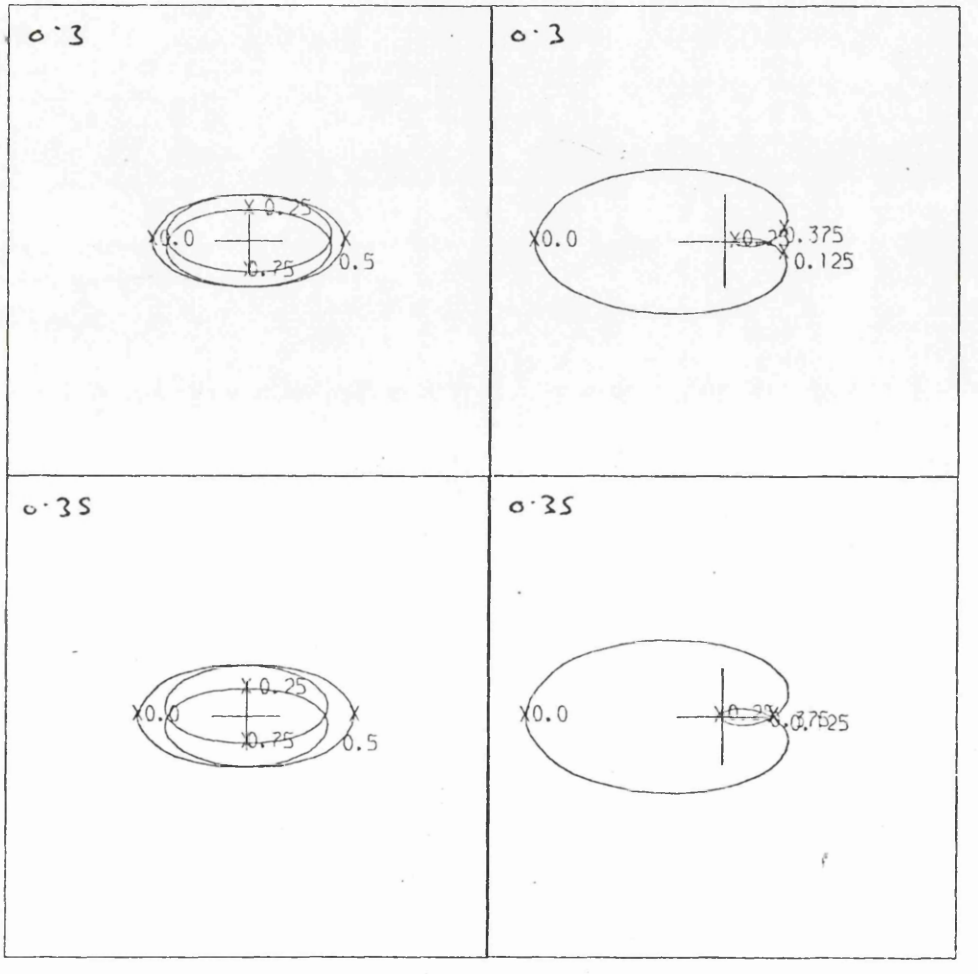

a)

0·4 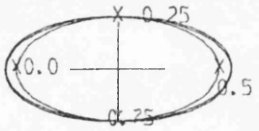	0·4 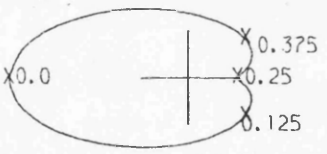
0·45 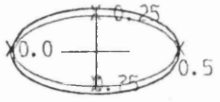	0·45 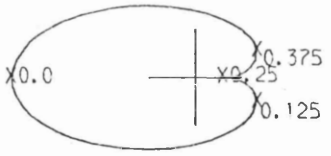

a)

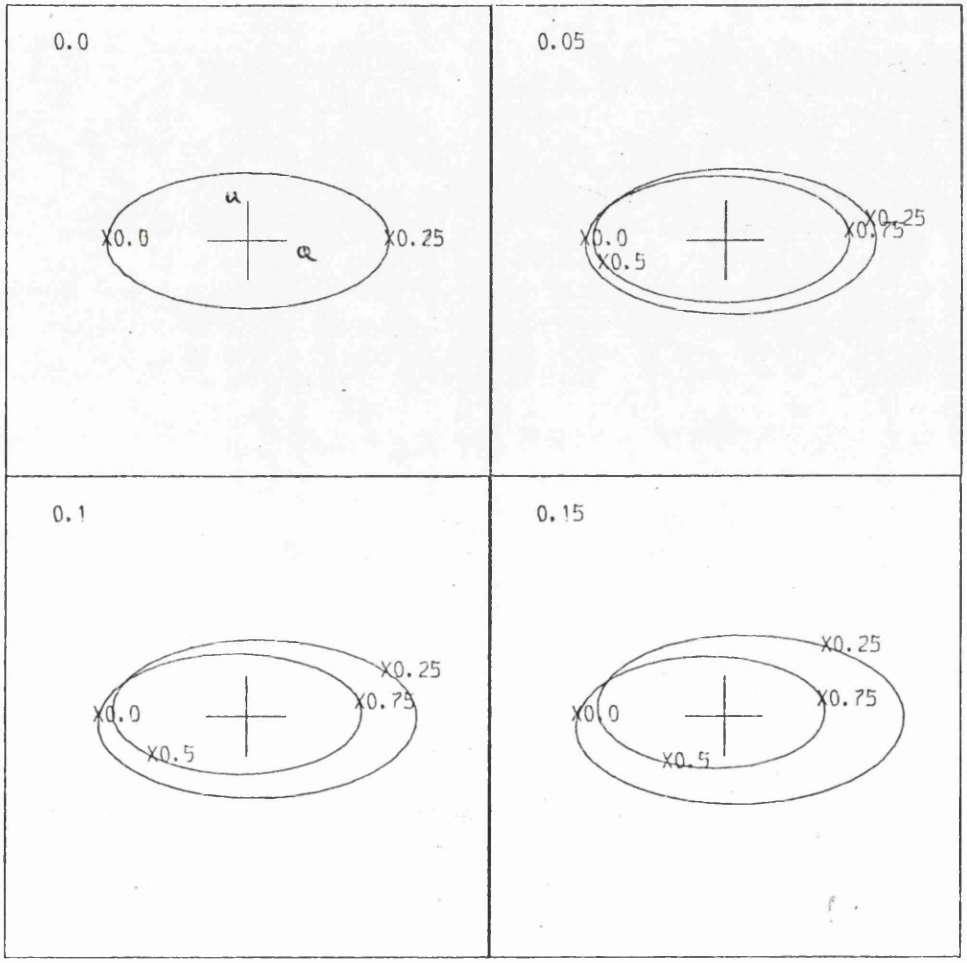
0.0
X0.0
X0.25
0.05
X0.0
X0.5
X0.75
X0.25
0.1
X0.0
X0.5
X0.75
X0.25
0.15
X0.0
X0.5
X0.75
X0.25

b)

b)

0.2

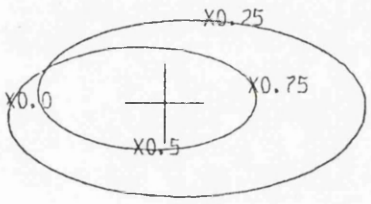

0.25

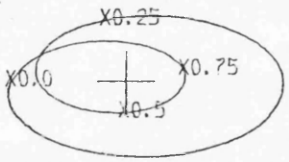

0.3

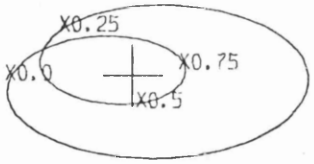

0.35

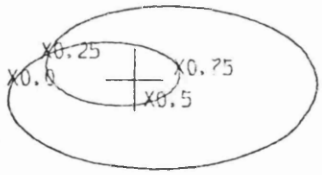

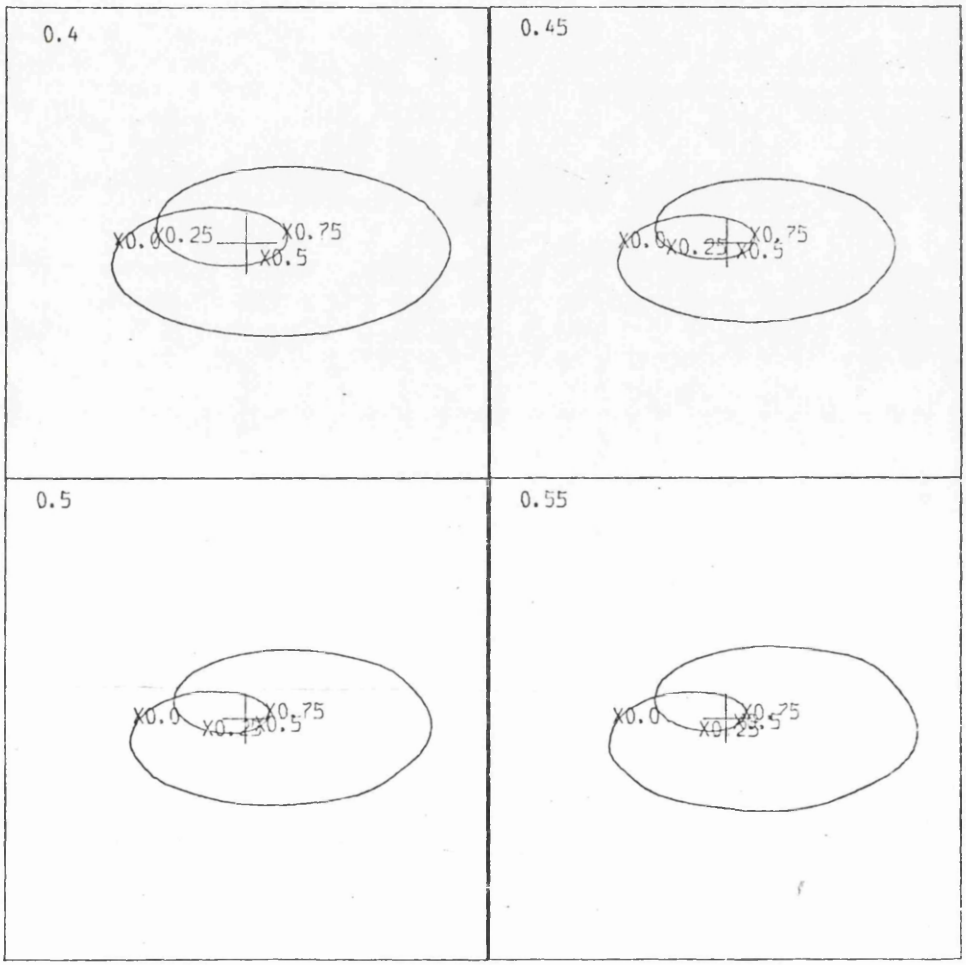
0.4
X0.0
X0.25
X0.5
X0.75
0.45
X0.0
X0.25
X0.5
X0.75
0.5
X0.0
X0.25
X0.5
X0.75
0.55
X0.0
X0.25
X0.5
X0.75

b)

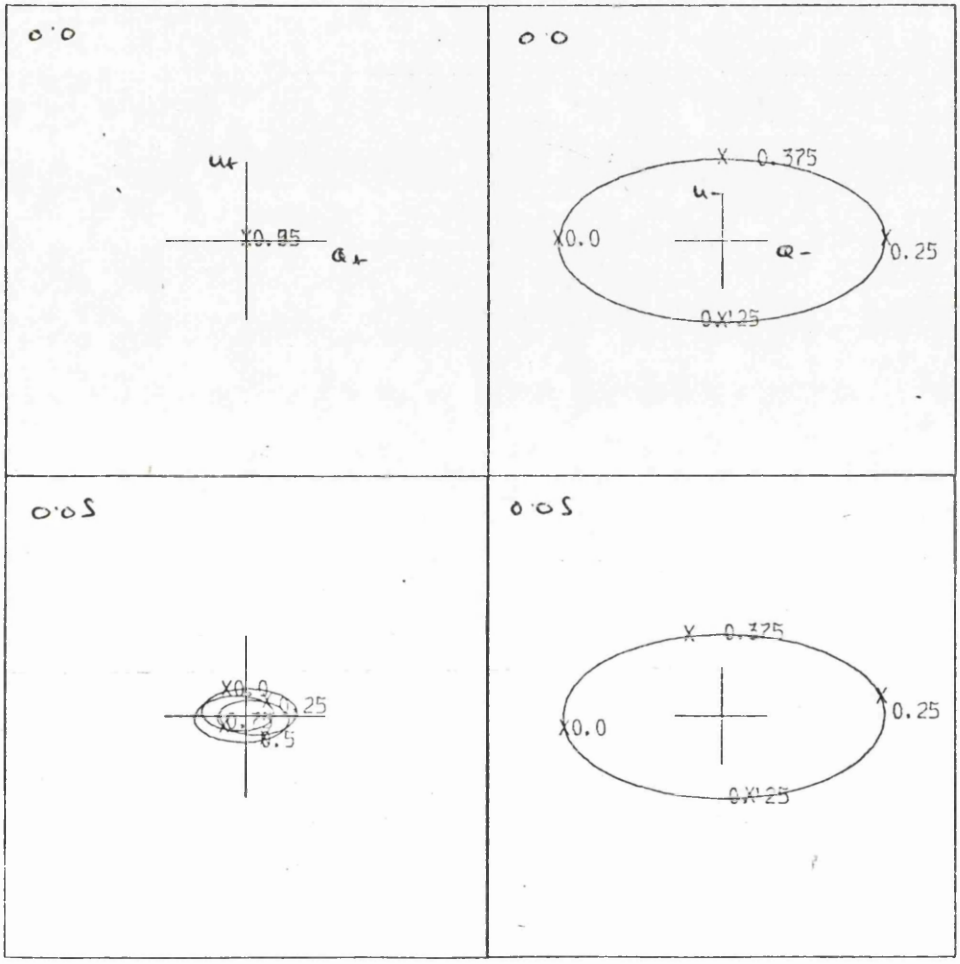
0·0
u+
X0.25
Q+
0·0
X 0.375
u-
X0.0
Q-
X0.25
0X125
0·05
X0.0
X0.25
X0.75
0.5
0·05
X 0.375
X0.0
X0.25
0X125

b)

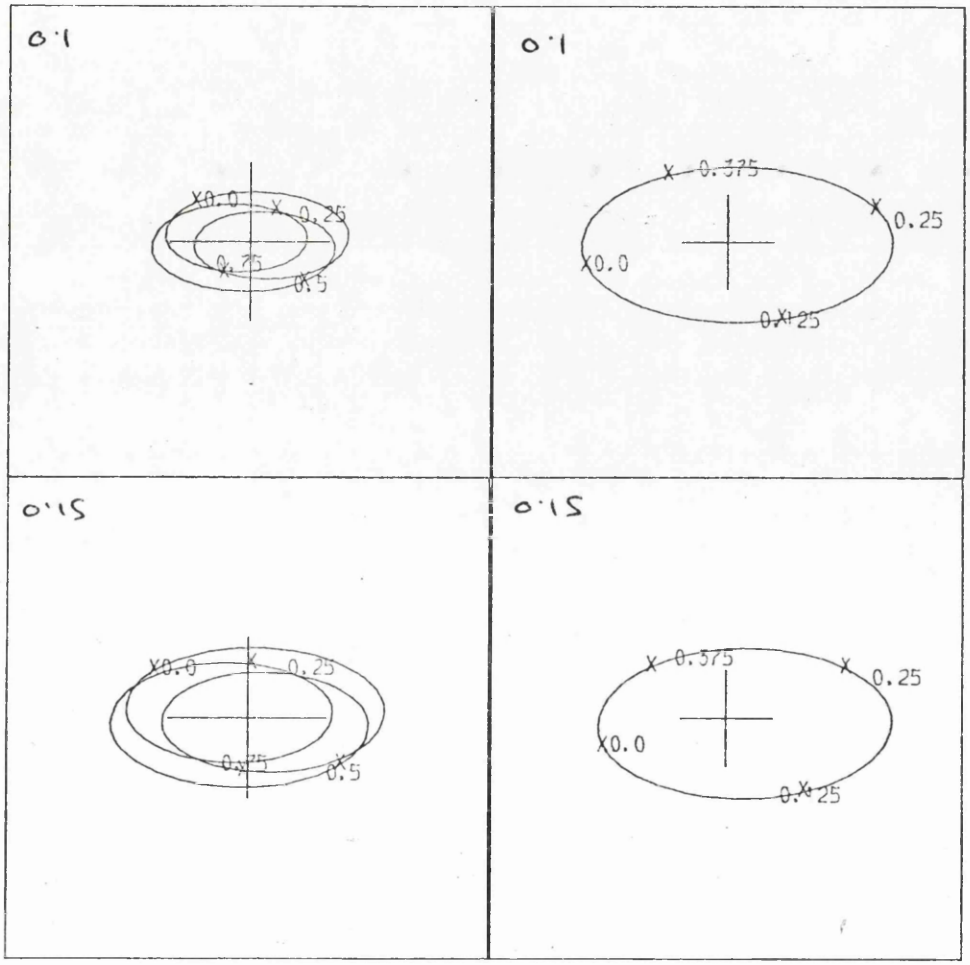
0.1
0.0
0.25
0.375
0.5
0.1
0.375
0.25
0.0
0.25
0.15
0.0
0.25
0.375
0.5
0.15
0.375
0.25
0.0
0.25

b)

0·2 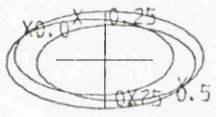	0·2 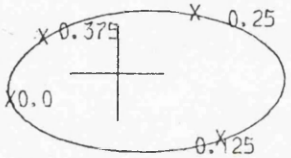
0·25 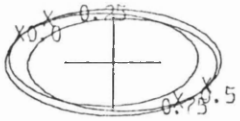	0·25 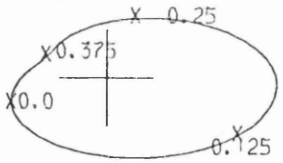

b)

b)

0·3 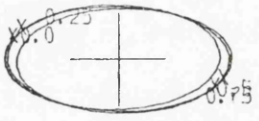	0·3 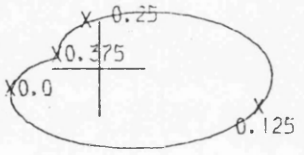
0·35 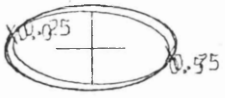	0·35 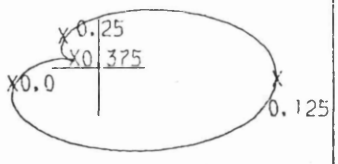

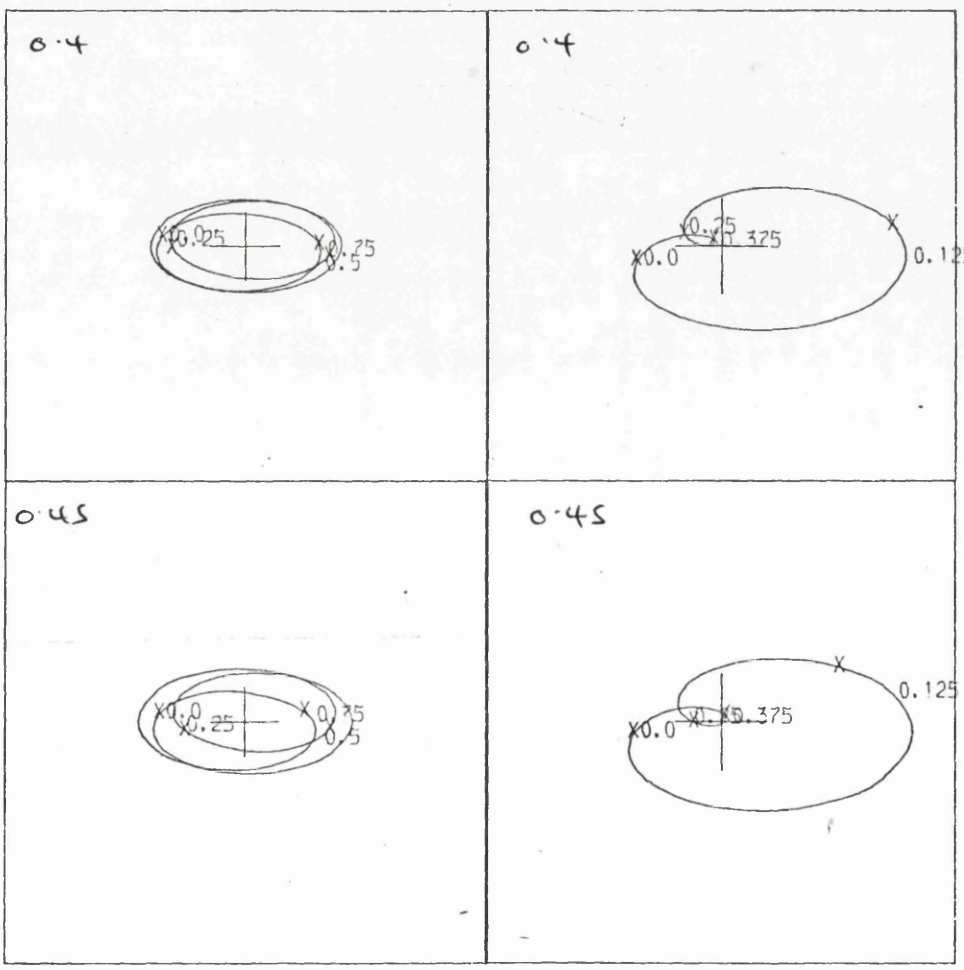
0.4
0.025
0.25
0.5
0.4
0.25
0.375
0.0
0.125
0.45
0.0
0.25
0.375
0.5
0.45
0.125
0.0
0.375

b)

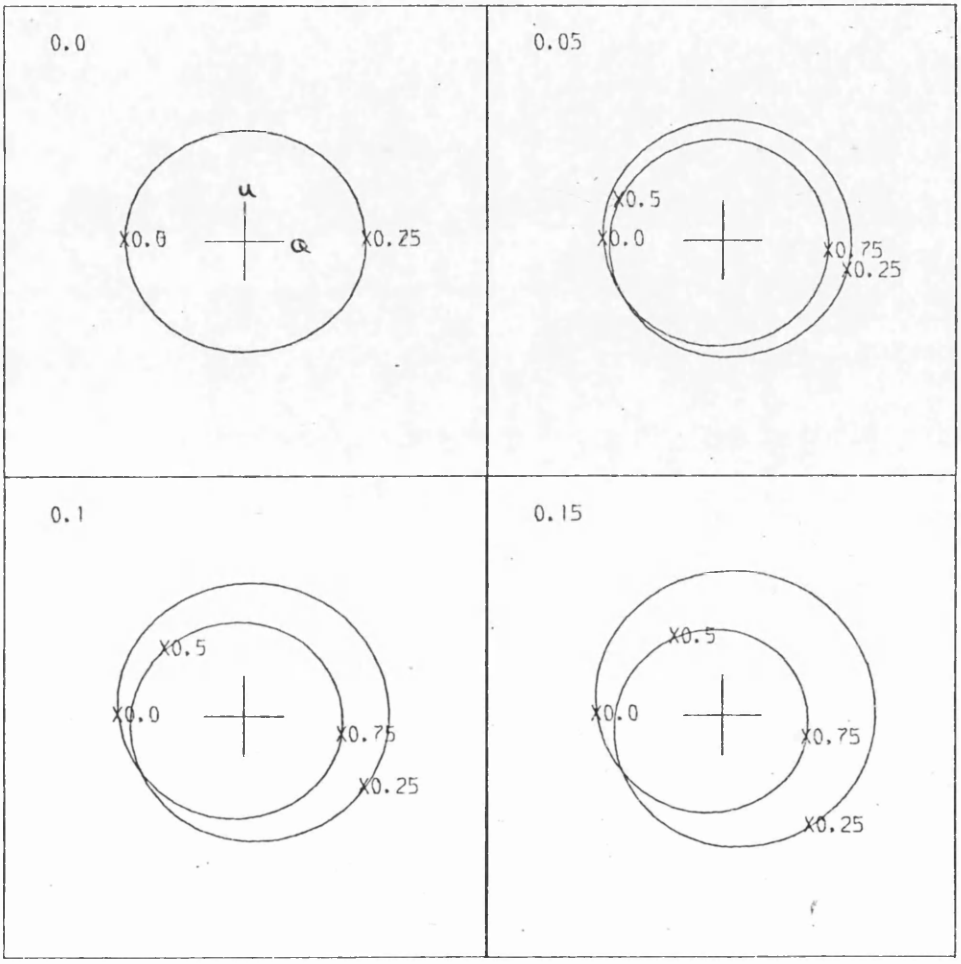
0.0
u
X0.0
Q
X0.25
0.05
X0.5
X0.0
X0.75
X0.25
0.1
X0.5
X0.0
X0.75
X0.25
0.15
X0.5
X0.0
X0.75
X0.25

c)

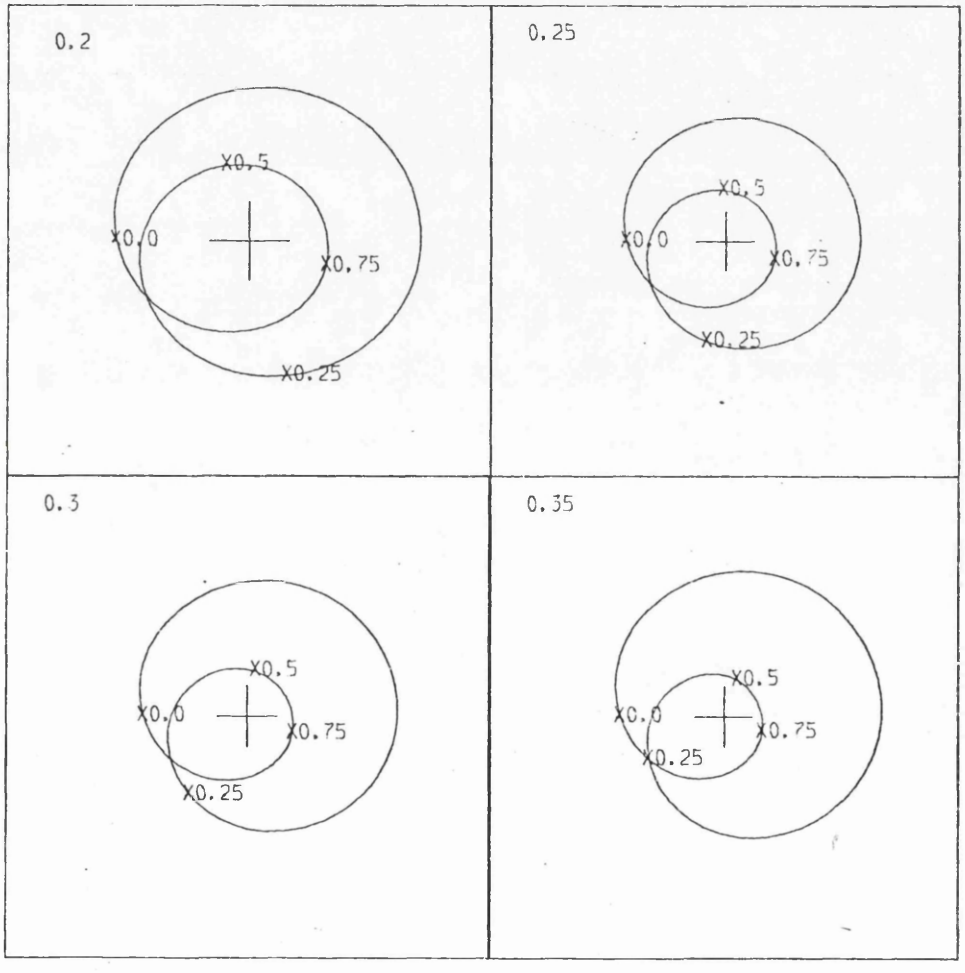
0.2
X0.5
X0.0
X0.75
X0.25
0.25
X0.5
X0.0
X0.75
X0.25
0.3
X0.5
X0.0
X0.75
X0.25
0.35
X0.5
X0.0
X0.75
X0.25

c)

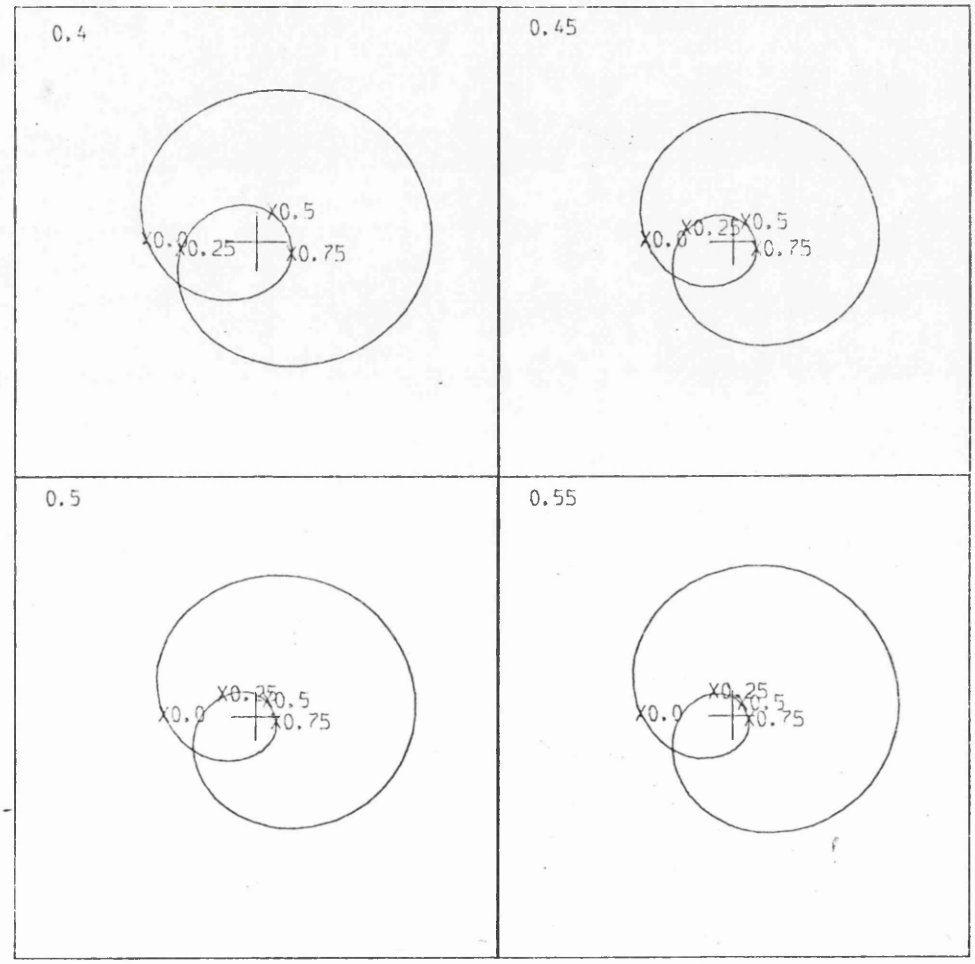
0.4
X0.5
X0.0
X0.25
X0.75
0.45
X0.25
X0.5
X0.0
X0.75
0.5
X0.25
X0.5
X0.0
X0.75
0.55
X0.25
X0.0
X0.75

c)

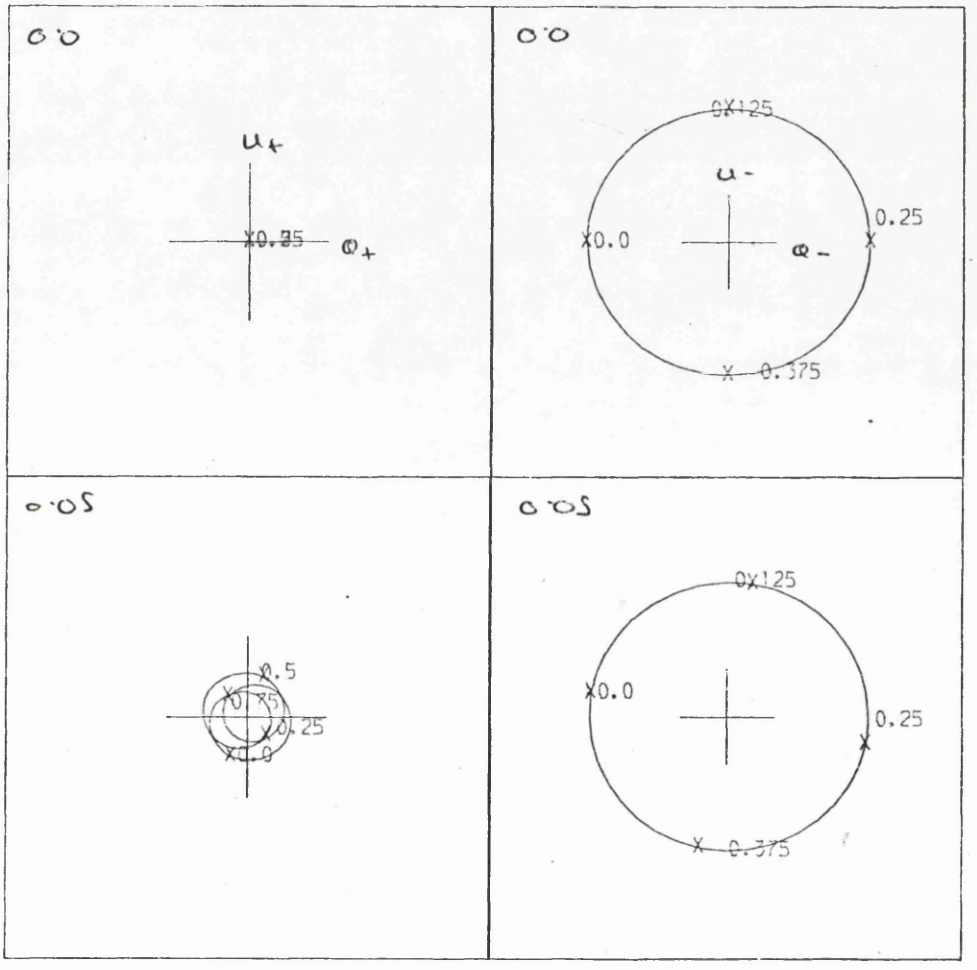
0.0
u+
0.375
Ω+
0.0
0X125
u-
0.25
0.0
Ω-
0.375
0.05
0.5
0.375
0.25
0.0
0.05
0X125
0.0
0.25
0.375

c)

c)

0.1
0.5
0.25
0.0
0.1
0.125
0.0
0.25
0.375
1.0
0.5
0.375
0.0
0.25
1.0
0.125
0.0
0.25
0.375

c)

0.2

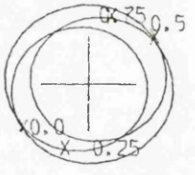

0.2

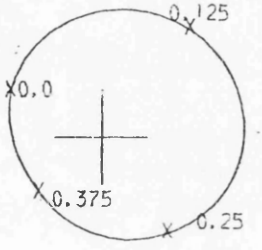

0.25

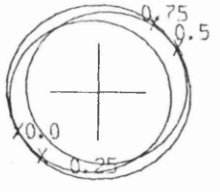

0.25

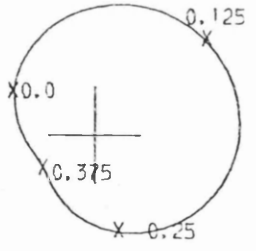

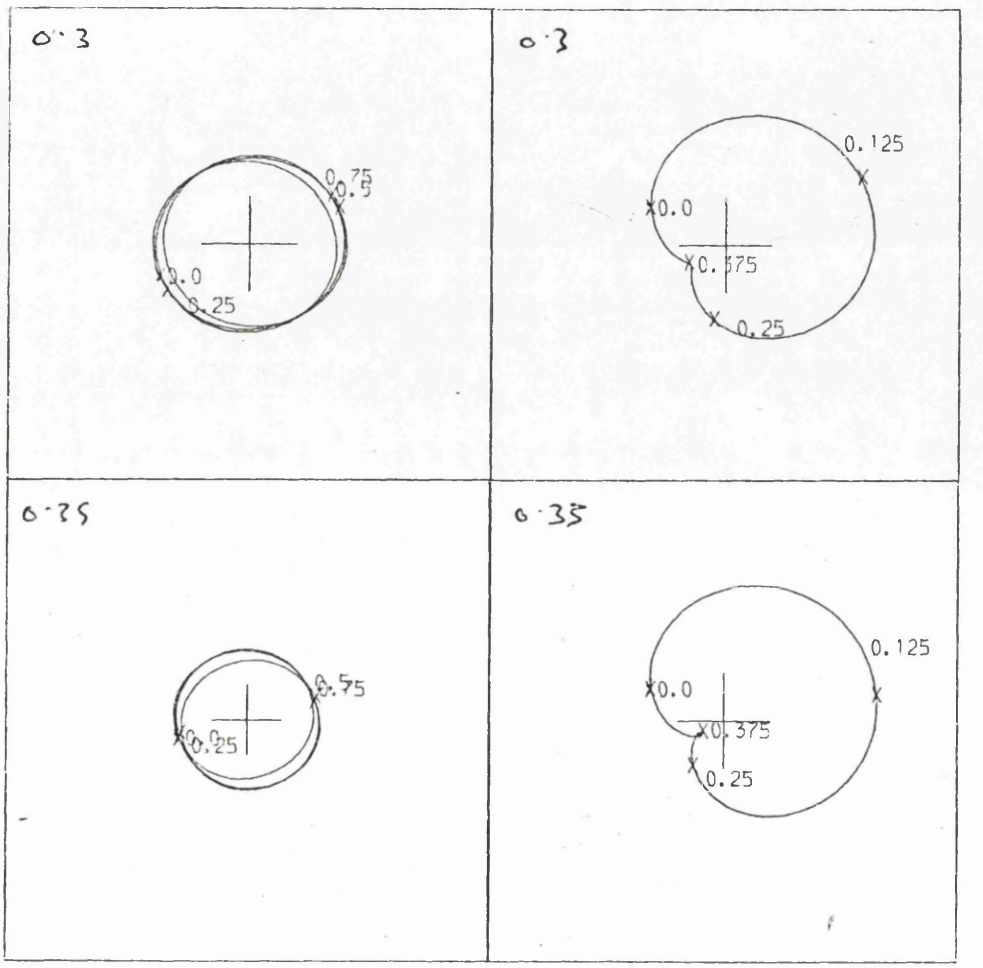
0.3
0.75
0.5
0.0
0.25
0.3
0.125
0.0
0.375
0.25
0.35
0.75
0.0
0.25
0.35
0.125
0.0
0.375
0.25

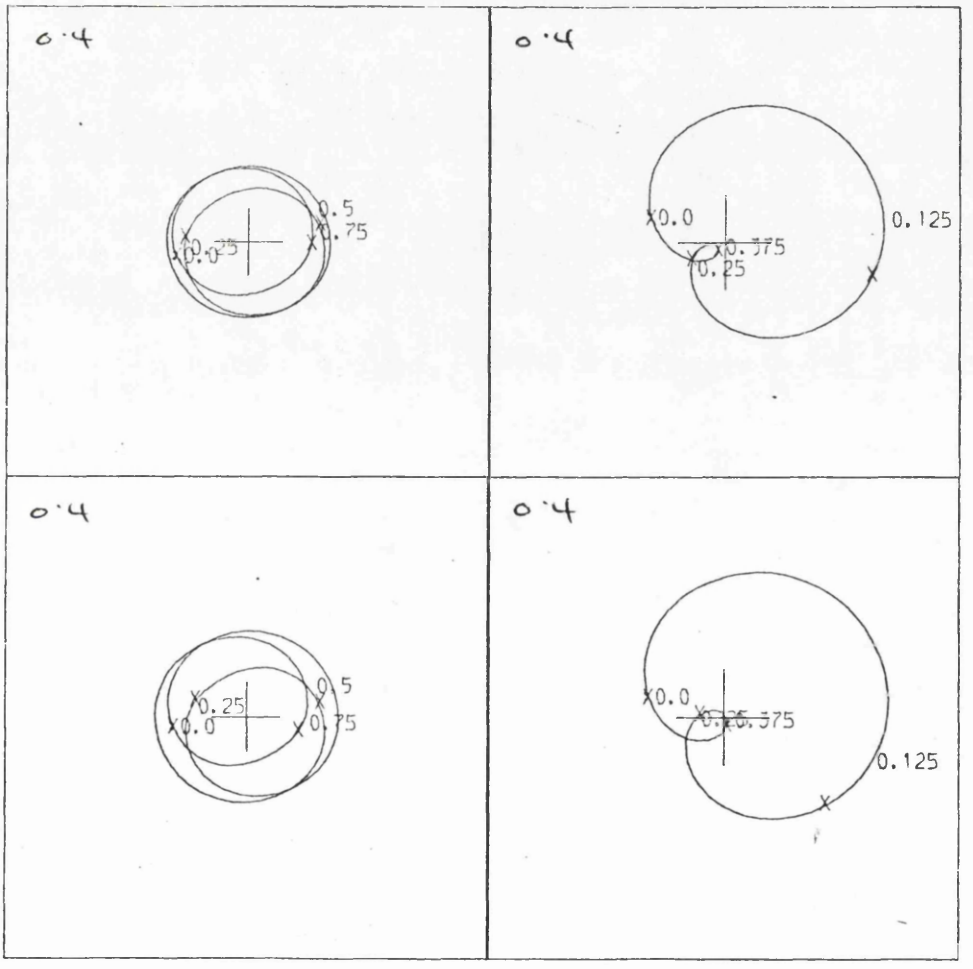
0.4
0.5
0.75
0.0
0.25
0.4
0.0
0.125
0.375
0.25
0.4
0.5
0.25
0.0
0.75
0.4
0.0
0.375
0.125

c)

APPENDIX III - Data used in Thesis

Here we present the data analysed in Chapters 2,5,8 and 9. Both the phase binned data and the raw observations as, in some cases, presented by Rudy and Kemp (1978) for example.

Data is given for :

AO Cas, Algol, u Her, HD47129, Ori e (both and filter), U Sge, V444 Cyg.

Also given are the data for the system HD50896 of McLean (1980) analized in chapter 10.

ALGOL Phase Binned Data

PHASE	Q	U
+.0000	-.0055	+.0090
+.0250	-.0036	+.0037
+.0500	-.0040	+.0035
+.0750	-.0053	+.0070
+.1000	-.0090	+.0055
+.1250	-.0090	+.0070
+.1500	-.0080	+.0080
+.1750	-.0097	+.0103
+.2000	-.0090	+.0167
+.2250	-.0095	+.0130
+.2500	-.0070	+.0180
+.2750	-.0045	+.0190
+.3000	-.0060	+.0175
+.3250	-.0045	+.0180
+.3500	-.0050	+.0125
+.3750	-.0022	+.0095
+.4000	-.0022	+.0097
+.4250	-.0045	+.0085
+.4500	-.0047	+.0090
+.4750	-.0040	+.0040
+.5000	-.0050	+.0040
+.5250	-.0050	+.0020
+.5500	-.0060	+.0015
+.5750	-.0080	+.0030
+.6000	-.0060	+.0012
+.6250	-.0050	+.0167
+.6500	-.0045	+.0115
+.6750	-.0010	+.0220
+.7000	-.0006	+.0206
+.7250	-.0005	+.0202
+.7500	-.0005	+.0160
+.7750	-.0020	+.0147
+.8000	-.0025	+.0115
+.8250	+.0035	+.0105
+.8500	+.0007	+.0085
+.8750	-.0015	+.0065
+.9000	-.0020	+.0020
+.9250	-.0015	+.0035
+.9500	-.0040	+.0027
+.9750	-.0065	+.0020

AO Cas Phase Binned Data

PHASE	Q	U
+.000	+.072	+.644
+.050	+.089	+.726
+.100	+.107	+.727
+.150	+.159	+.737
+.200	+.198	+.730
+.250	+.219	+.735
+.300	+.237	+.681
+.350	+.153	+.631
+.400	+.146	+.632
+.450	+.096	+.613
+.500	+.063	+.630
+.550	+.052	+.620
+.600	+.026	+.760
+.650	+.056	+.815
+.700	+.078	+.819
+.750	+.318	+.762
+.800	+.315	+.704
+.850	+.230	+.598
+.900	+.070	+.557
+.950	+.064	+.561

HD47129 Phase Binned Data

PHASE	Q	U
+.0000	+.1885	+.7170
+.0250	+.1910	+.6950
+.0500	+.1940	+.7060
+.0750	+.1885	+.7530
+.1000	+.1390	+.7520
+.1250	+.1710	+.7730
+.1500	+.2010	+.8140
+.1750	+.1780	+.7930
+.2000	+.1330	+.7510
+.2250	+.1860	+.7820
+.2500	+.2050	+.8060
+.2750	+.2070	+.7770
+.3000	+.2000	+.7620
+.3250	+.1870	+.7390
+.3500	+.1870	+.7390
+.3750	+.1910	+.7270
+.4000	+.2230	+.7190
+.4250	+.2690	+.7040
+.4500	+.2710	+.7200
+.4750	+.2140	+.7520
+.5000	+.1780	+.7060
+.5250	+.1590	+.6610
+.5500	+.1860	+.6660
+.5750	+.1750	+.6780
+.6000	+.1750	+.6810
+.6250	+.1620	+.7140
+.6500	+.1720	+.7570
+.6750	+.1980	+.7760
+.7000	+.1710	+.7260
+.7250	+.1770	+.7840
+.7500	+.1860	+.8010
+.7750	+.1850	+.7520
+.8000	+.2180	+.7410
+.8250	+.1910	+.7740
+.8500	+.2030	+.7890
+.8750	+.2350	+.7490
+.9000	+.2480	+.7430
+.9250	+.2100	+.7560
+.9500	+.2340	+.6930
+.9750	+.2500	+.6990

u HER Phase Binned Data

PHASE	Q	U
+.0000	+.0117	+.0189
+.0250	+.0140	+.0184
+.0500	+.0179	+.0071
+.0750	+.0232	+.0082
+.1000	+.0345	+.0061
+.1250	+.0414	+.0034
+.1500	+.0581	+.0017
+.1750	+.0600	+.0013
+.2000	+.0603	+.0046
+.2250	+.0642	+.0040
+.2500	+.0631	+.0047
+.2750	+.0632	+.0027
+.3000	+.0660	+.0013
+.3250	+.0569	+.0228
+.3500	+.0523	+.0180
+.3750	+.0448	+.0228
+.4000	+.0466	+.0180
+.4250	+.0437	+.0208
+.4500	+.0226	+.0248
+.4750	+.0100	+.0225
+.5000	+.0271	+.0220
+.5250	+.0285	+.0195
+.5500	+.0303	+.0101
+.5750	+.0217	+.0063
+.6000	+.0176	-.0083
+.6250	+.0426	-.0002
+.6500	+.0503	-.0055
+.6750	+.0575	-.0107
+.7000	+.0541	-.0023
+.7250	+.0576	-.0022
+.7500	+.0594	+.0058
+.7750	+.0576	+.0114
+.8000	+.0431	+.0142
+.8250	+.0417	+.0215
+.8500	+.0415	+.0234
+.8750	+.0433	+.0234
+.9000	+.0537	+.0252
+.9250	+.0208	+.0207
+.9500	+.0312	+.0110
+.9750	+.0247	+.0198

ORI E (B) Phase Binned Data

PHASE	Q	U
+.00	+.3560	-.0710
+.05	+.3240	-.0450
+.10	+.3110	-.0330
+.15	+.3120	-.0070
+.20	+.3000	-.0010
+.25	+.2820	-.0270
+.30	+.2980	-.0840
+.35	+.3000	-.0960
+.40	+.2930	-.1030
+.45	+.3050	-.1000
+.50	+.3270	-.1190
+.55	+.3270	-.1210
+.60	+.3010	-.0900
+.65	+.3120	-.0270
+.70	+.2990	-.0060
+.75	+.2840	-.0250
+.80	+.3000	-.0410
+.85	+.3140	-.0430
+.90	+.3080	-.0550
+.95	+.3150	-.0570

ORI E (U) Phase Binned Data

PHASE	Q	U
+.00	+.2750	-.0990
+.05	+.3010	-.0540
+.10	+.3030	-.0570
+.15	+.2600	-.0560
+.20	+.2360	-.0440
+.25	+.2380	-.0500
+.30	+.1700	+.0430
+.35	+.1860	-.0020
+.40	+.2230	-.0720
+.45	+.2050	-.0100
+.50	+.2320	+.0630
+.55	+.2190	+.0720
+.60	+.2890	-.0200
+.65	+.2820	-.0440
+.70	+.2480	-.0080
+.75	+.2650	-.0690
+.80	+.2360	-.0940
+.85	+.2990	-.0740
+.90	+.3070	-.0740
+.95	+.2540	-.0980

U SGE Phase Binned Data

PHASE	Q	U
+.00	-.1768	-.1177
+.05	-.1897	-.1179
+.10	-.1859	-.1095
+.15	-.1948	-.1069
+.20	-.2096	-.1006
+.25	-.1988	-.1072
+.30	-.1793	-.0953
+.35	-.1703	-.0957
+.40	-.1664	-.0956
+.45	-.1825	-.0854
+.50	-.2030	-.0943
+.55	-.1991	-.1084
+.60	-.2026	-.1071
+.65	-.2183	-.1070
+.70	-.2165	-.1132
+.75	-.2172	-.1095
+.80	-.2067	-.0990
+.85	-.1974	-.1086
+.90	-.1850	-.1071
+.95	-.1540	-.1200

V444 CYG Phase Binned Data

PHASE	Q	U
+.00	-.0129	+.3528
+.05	+.0482	+.4218
+.10	-.0570	+.5008
+.15	-.0904	+.5169
+.20	-.1530	+.5928
+.25	-.2437	+.6227
+.30	-.1748	+.4162
+.35	-.1819	+.4200
+.40	-.1305	+.3775
+.45	+.0287	+.3052
+.50	-.0040	+.3865
+.55	-.0552	+.4212
+.60	-.0307	+.4773
+.65	-.0815	+.5572
+.70	-.2510	+.5516
+.75	-.2662	+.4973
+.80	-.2927	+.4438
+.85	-.1945	+.4097
+.90	-.0363	+.2938
+.95	-.0592	+.2780

HD50896 - BINNED DATA

bs = start of bin (phase)

be = end of bin (phase)

qb = binned Q

ub = binned U

iq = no. points in bin

iu = " " " "

bs	be		ab		ub	ia	iu	ii
.950	.050	+	.469	-	.252	03	03	00
.000	.100	+	.421	-	.220	02	02	00
.050	.150	+	.420	-	.161	01	01	00
.100	.200	+	.430	-	.163	03	03	00
.150	.250	+	.455	-	.173	03	03	00
.200	.300	+	.476	-	.243	02	02	00
.250	.350	+	.438	-	.305	03	03	00
.300	.400	+	.461	-	.346	03	03	00
.350	.450	+	.462	-	.471	02	02	00
.400	.500	+	.363	-	.540	02	02	00
.450	.550	+	.332	-	.505	02	02	00
.500	.600	+	.327	-	.445	03	03	00
.550	.650	+	.280	-	.403	03	03	00
.600	.700	+	.198	-	.329	01	01	00
.650	.750	+	.112	-	.209	01	01	00
.700	.800	+	.169	-	.186	02	02	00
.750	.850	+	.227	-	.164	01	01	00
.800	.900	+	.443	-	.240	01	01	01
.850	.950	+	.660	-	.316	01	01	00
.900	1.000	+	.612	-	.315	02	02	00

HD50896 - B filter JIA 79 (binned)

bs	be		ab		ub	ia	iu	ii
.950	.050	+	.369	-	.303	01	01	00
.000	.100	+	.387	-	.342	02	02	00
.050	.150	+	.391	-	.357	03	03	00
.100	.200	+	.270	-	.463	03	03	00
.150	.250	+	.205	-	.502	02	02	00
.200	.300	+	.261	-	.449	03	03	00
.250	.350	+	.261	-	.449	03	03	00
.300	.400	+	.106	-	.421	01	01	00
.350	.450	+	.106	-	.421	01	01	00
.400	.500	+	.348	-	.266	01	01	00
.450	.550	+	.311	-	.320	04	04	00
.500	.600	+	.299	-	.338	03	03	00
.550	.650	+	.504	-	.484	05	05	00
.600	.700	+	.504	-	.484	05	05	00
.650	.750	+	.447	-	.490	01	01	01
.700	.800	+	.390	-	.496	01	01	00
.750	.850	+	.306	-	.429	05	05	00
.800	.900	+	.286	-	.410	05	05	00
.850	.950	+	.309	-	.311	04	04	00
.900	1.000	+	.329	-	.286	04	04	00

HD50896 - B filter all data. (burned)

bs	be		ob		ub	iq	iu	ii
.966	.033	+	.482	-	.292	03	03	00
.000	.066	+	.421	-	.220	02	02	00
.033	.100	+	.368	-	.289	03	03	00
.066	.133	+	.398	-	.308	04	04	00
.100	.166	+	.412	-	.257	03	03	00
.133	.200	+	.320	-	.333	04	04	00
.166	.233	+	.340	-	.325	04	04	00
.200	.266	+	.476	-	.243	02	02	00
.233	.300	+	.309	-	.410	04	04	00
.266	.333	+	.328	-	.393	05	05	00
.300	.366	+	.429	-	.311	02	02	00
.333	.400	+	.316	-	.419	02	02	00
.366	.433	+	.316	-	.419	02	02	00
.400	.466	+	.399	-	.525	01	01	00
.433	.500	+	.358	-	.449	03	03	00
.466	.533	+	.301	-	.384	04	04	00
.500	.566	+	.309	-	.367	04	04	00
.533	.600	+	.337	-	.409	04	04	00
.566	.633	+	.389	-	.440	06	06	00
.600	.666	+	.453	-	.458	06	06	00
.633	.700	+	.512	-	.494	02	02	00
.666	.733	+	.112	-	.209	01	01	00
.699	.766	+	.169	-	.186	02	02	00
.733	.799	+	.308	-	.330	02	02	00
.766	.833	+	.317	-	.457	03	03	00
.799	.866	+	.286	-	.410	05	05	00
.833	.899	+	.289	-	.392	03	03	00
.866	.933	+	.401	-	.290	04	04	00
.899	.966	+	.401	-	.290	04	04	00
.933	.999	+	.466	-	.309	02	02	00

HD50896 - U Filter OLD +9 (binned)

bs	be		ob		ub	iq	iu	ii
.933	.066	+	.542	-	.302	02	02	00
.000	.133	+	.429	-	.194	02	02	00
.066	.200	+	.370	-	.179	02	02	00
.133	.266	+	.425	-	.271	02	02	00
.200	.333	+	.492	-	.282	02	02	00
.266	.400	+	.535	-	.389	02	02	00
.333	.466	+	.463	-	.590	02	02	00
.400	.533	+	.319	-	.632	03	03	00
.466	.600	+	.276	-	.568	03	03	00
.533	.666	+	.174	-	.397	02	02	00
.600	.733	+	.062	-	.216	02	02	00
.666	.800	+	.087	-	.116	02	02	00
.733	.866	+	.163	-	.109	01	01	00
.800	.933	+	.728	-	.308	01	01	00
.866	1.000	+	.659	-	.316	02	02	00

HD50896- U filter J/A 79 (binned)

bs	be		ob		ub	iq	iu	ii
.933	.066	+	.409	-	.261	01	01	00
.000	.133	+	.418	-	.509	01	01	00
.066	.200	+	.183	-	.534	03	03	00
.133	.266	+	.118	-	.531	03	03	00
.200	.333	+	.193	-	.518	03	03	00
.266	.400	+	.097	-	.526	03	03	00
.333	.466	-	.064	-	.522	01	01	00
.400	.533	+	.163	-	.491	01	01	00
.466	.600	+	.279	-	.394	02	02	00
.533	.666	+	.472	-	.412	02	02	00
.600	.733	+	.549	-	.526	01	01	00
.666	.800	+	.297	-	.515	01	01	00
.733	.866	+	.216	-	.416	04	04	00
.800	.933	+	.225	-	.334	06	06	00
.866	1.000	+	.298	-	.278	04	04	00

HD50896- U filter all data (binned)

bs	be		ab		ub	iq	iu	ii
.966	.033	+	.498	-	.288	03	03	00
.000	.066	+	.495	-	.281	01	01	00
.033	.100	+	.443	-	.294	01	01	01
.066	.133	+	.391	-	.308	02	02	00
.100	.166	+	.386	-	.289	03	03	00
.133	.200	+	.169	-	.448	03	03	00
.166	.233	+	.066	-	.547	02	02	00
.200	.266	+	.349	-	.395	02	02	00
.233	.300	+	.263	-	.462	04	04	00
.266	.333	+	.288	-	.443	03	03	00
.300	.366	+	.509	-	.273	01	01	00
.333	.400	+	.248	-	.513	02	02	00
.366	.433	+	.248	-	.513	02	02	00
.400	.466	+	.366	-	.675	01	01	00
.433	.500	+	.330	-	.677	02	02	00
.466	.533	+	.252	-	.571	03	03	00
.500	.566	+	.285	-	.443	03	03	00
.533	.600	+	.315	-	.391	02	02	00
.566	.633	+	.299	-	.440	03	03	00
.600	.666	+	.331	-	.418	02	02	00
.633	.700	+	.171	-	.270	01	01	01
.666	.733	+	.011	-	.123	01	01	00
.699	.766	+	.087	-	.116	02	02	00
.733	.799	+	.230	-	.312	02	02	00
.766	.833	+	.212	-	.447	03	03	00
.799	.866	+	.189	-	.383	03	03	00
.833	.899	+	.229	-	.325	01	01	00
.866	.933	+	.378	-	.290	04	04	00
.899	.966	+	.378	-	.290	04	04	00
.933	.999	+	.499	-	.292	02	02	00

HD50896 - G Filter 01D79 (binned)

bs	be	ab	ub	ia	iu	ii
.933	.066	+ .538	- .295	02	02	00
.000	.133	+ .446	- .207	02	02	00
.066	.200	+ .391	- .167	02	02	00
.133	.266	+ .396	- .198	01	01	00
.200	.333	+ .458	- .288	02	02	00
.266	.400	+ .492	- .358	03	03	00
.333	.466	+ .560	- .497	01	01	00
.400	.533	+ .440	- .489	01	01	01
.466	.600	+ .321	- .482	02	02	00
.533	.666	+ .271	- .432	03	03	00
.600	.733	+ .153	- .244	02	02	00
.666	.800	+ .190	- .131	02	02	00
.733	.866	+ .247	- .106	01	01	00
.800	.933	+ .697	- .321	01	01	00
.866	1.000	+ .634	- .316	02	02	00

HD50896 - G Filter J1A79 (binned)

bs	be	ab	ub	ia	iu	ii
.950	.050	+ .412	- .349	01	01	00
.000	.100	+ .394	- .341	02	02	00
.050	.150	+ .407	- .353	02	02	00
.100	.200	+ .250	- .443	03	03	00
.150	.250	+ .157	- .478	02	02	00
.200	.300	+ .222	- .447	02	02	00
.250	.350	+ .222	- .447	02	02	00
.300	.400	+ .118	- .382	01	01	00
.350	.450	+ .118	- .382	01	01	00
.400	.500	+ .164	- .431	01	01	01
.450	.550	+ .210	- .480	01	01	00
.500	.600	+ .303	- .391	02	02	00
.550	.650	+ .498	- .450	03	03	00
.600	.700	+ .550	- .524	02	02	00
.650	.750	+ .457	- .521	01	01	01
.700	.800	+ .365	- .518	01	01	00
.750	.850	+ .294	- .459	02	02	00
.800	.900	+ .223	- .400	01	01	00
.850	.950	+ .281	- .266	02	02	00
.900	1.000	+ .281	- .266	02	02	00

HD50896 - G filter all data (binned)

bs	be		ab		ub	ia	iu	ii
.966	.033	+	.496	-	.313	03	03	00
.000	.066	+	.459	-	.314	02	02	00
.033	.100	+	.377	-	.333	01	01	00
.066	.133	+	.400	-	.280	03	03	00
.100	.166	+	.407	-	.235	03	03	00
.133	.200	+	.236	-	.384	03	03	00
.166	.233	+	.157	-	.478	02	02	00
.200	.266	+	.228	-	.435	01	01	01
.233	.300	+	.300	-	.393	03	03	00
.266	.333	+	.340	-	.367	04	04	00
.300	.366	+	.461	-	.290	01	01	00
.333	.400	+	.339	-	.439	02	02	00
.366	.433	+	.339	-	.439	02	02	00
.400	.466	+	.169	-	.219	01	01	01
.433	.500	+	.189	-	.349	01	01	01
.466	.533	+	.210	-	.480	01	01	00
.500	.566	+	.310	-	.422	03	03	00
.533	.600	+	.346	-	.422	03	03	00
.566	.633	+	.439	-	.494	02	02	00
.600	.666	+	.424	-	.460	03	03	00
.633	.700	+	.356	-	.436	02	02	00
.666	.733	+	.134	-	.157	01	01	00
.699	.766	+	.190	-	.131	02	02	00
.733	.799	+	.306	-	.312	02	02	00
.766	.833	+	.294	-	.459	02	02	00
.799	.866	+	.223	-	.400	01	01	00
.833	.899	+	.321	-	.342	01	01	01
.866	.933	+	.419	-	.284	03	03	00
.899	.966	+	.419	-	.284	03	03	00
.933	.999	+	.571	-	.311	01	01	00

RAW OBSERVATIONS.

Included are the raw observations, mostly as published, for the systems Algol, AO Cas, HD47129, ζ Oph E (B and U filter), u Her, USge, V444 Cygni and HD50896

Polarization Observations of Algol in B Filter

JD 2,440,000 +	Q(%)	U(%)	ϕ	JD 2,440,000 +	Q(%)	U(%)	ϕ
3011.96	.000	.003	.936	3030.97	-.008	.003	.569
3012.96	-.009	.018	.285	3031.82	-.004	.011	.861
3013.94	-.005	.012	.627	3041.94	-.004	.006	.371
3014.90	-.005	.003	.963	3042.89	-.001	.021	.723
3018.97	-.009	.010	.383	3044.79	.004	.013	.386
3019.88	-.001	.022	.698	3046.90	-.009	.006	.103
3019.90	.003	.017	.707	3046.91	-.009	.010	.126
3020.84	.000	-.007	.034	3051.86	.002	.007	.853
3020.90	-.002	.000	.054	3051.97	-.002	.002	.894
3021.87	.000	.009	.391	3052.88	-.013	.016	.194
3021.91	-.004	.007	.408	3052.95	-.014	.016	.231
3021.99	-.005	.013	.435	3057.87	-.003	.004	.947
3022.90	.000	.013	.753	3057.92	-.008	.001	.966
3022.97	-.005	.012	.776	3058.80	.000	.020	.275
3024.85	-.002	.007	.433	3059.80	-.006	.012	.623
3024.90	-.007	.007	.450	3059.85	-.004	.011	.640
3024.97	-.004	.004	.476	3063.79	-.005	.012	.015
3025.91	.000	.011	.802	3063.83	-.006	.006	.025
3026.83	-.009	.005	.122	3063.91	-.007	-.001	.056
3028.88	.007	.010	.836	3065.79	-.001	.020	.711
3028.98	-.002	.006	.873	3065.82	-.003	.023	.720
3029.84	-.007	.006	.170	3065.91	-.001	.019	.751
3029.90	-.009	.009	.192	3066.80	-.007	.022	.063
3029.97	-.005	.010	.221	3104.82	-.003	.017	.321
3030.82	-.006	.004	.513	3104.81	-.006	.019	.329
3030.87	-.004	.000	.530				

AO Cas - Raw data.

ϕ	a	u
0.069	0.0613	0.755
0.073	0.0245	0.735
0.089	0.167	0.711
0.097	0.103	0.701
0.121	0.152	0.765
0.126	0.137	0.701
0.15	0.157	0.721
0.178	0.245	0.716
0.202	0.201	0.784
0.219	0.201	0.706
0.227	0.186	0.725
0.259	0.284	0.725
0.348	0.186	0.593
0.36	0.157	0.671
0.365	0.191	0.691
0.373	0.098	0.666
0.389	0.127	0.534
0.405	0.168	0.598
0.474	0.044	0.642
0.502	0.137	0.598

AO Cas Raw data cont.

ϕ	α	u
0.506	0.044	0.671
0.538	0.029	0.608
0.559	0.0	0.603
0.624	0.0196	0.843
0.632	0.0098	0.74
0.64	0.073	0.853
0.664	0.078	0.804
0.664	0.103	0.818
0.689	0.054	0.834
0.753	0.304	0.882
0.802	0.333	0.642
0.818	0.3087	0.588
0.891	0.049	0.564
0.922	0.088	0.524
0.925	0.039	0.495
0.925	0039	0.608
0.948	0.137	0.593
0.98	0.0196	0.583

Polarization Observations of HD 47129 in B Filter

JD 2,440,000 +	-Q(%)	U(%)	φ	JD 2,440,000 +	Q(%)	U(%)	φ
3022.99	.148	.814	.088	3141.83	.215	.751	.343
3025.00	.142	.763	.227	3149.82	.269	.740	.898
3026.00	.205	.699	.297	3150.82	.282	.780	.967
3029.01	.103	.653	.506	3163.67	.195	.765	.860
3030.01	.192	.691	.591	3167.83	.269	.876	.149
3031.01	.151	.742	.643	3169.66	.191	.836	.279
3032.00	.138	.673	.713	3170.67	.142	.710	.346
3042.00	.210	.638	.408	3171.65	.302	.786	.415
3049.02	.241	.655	.896	3172.65	.134	.750	.484
3052.01	.165	.666	.104	3176.68	.179	.741	.764
3057.97	.215	.668	.514	3177.66	.211	.813	.832
3058.92	.158	.665	.584	3178.66	.235	.835	.901
3063.96	.186	.678	.933	3179.61	.263	.670	.972
3064.93	.181	.677	.001	3183.75	.243	.853	.255
3065.95	.252	.720	.071	3185.72	.173	.762	.391
3066.95	.153	.775	.141	3190.65	.136	.793	.734
3067.91	.165	.762	.210	3191.78	.172	.736	.812
3058.96	.213	.779	.281	3213.65	.229	.792	.332
3069.86	.180	.716	.343	3218.74	.204	.779	.685
3071.90	.259	.752	.485	3224.66	.184	.770	.097
3079.89	.168	.703	.04	3225.65	.230	.801	.235
3085.95	.248	.752	.461	3233.68	.258	.887	.73
3099.97	.294	.688	.435	3238.67	.170	.707	.07
3104.88	.279	.736	.776	3239.66	.183	.791	.139
3112.90	.170	.724	.353	3240.69	.101	.774	.21
3113.96	.209	.693	.407	3241.68	.182	.740	.28
3122.00	.206	.646	.965	3248.69	.172	.783	.766
3122.87	.196	.757	.026	3252.68	.218	.643	.044
3133.86	.204	.751	.789	3253.69	.086	.757	.115
3140.90	.208	.757	.278	3260.69	.174	.686	.601
				3261.70	.193	.773	.67

Phase	Q	U
.0120	+ .3540	- .0860
.0190	+ .3440	- .1000
.0220	+ .3190	- .0700
.0310	+ .3850	- .0830
.0440	+ .4110	- .0160
.0530	+ .2990	+ .0440
.0650	+ .3160	- .0030
.0750	+ .3440	- .0540
.0900	+ .3190	- .0480
.0930	+ .2640	+ .0030
.1210	+ .2740	- .0870
.1370	+ .3260	- .0520
.1550	+ .2960	- .0550
.1800	+ .2960	- .0160
.1870	+ .3350	+ .0440
.1930	+ .2640	- .0410
.2110	+ .3510	+ .0760
.2240	+ .3070	- .0060
.2300	+ .2560	- .0190
.2460	+ .2970	- .0048
.2800	+ .2940	- .0430
.3230	+ .2580	- .0630
.3480	+ .2960	- .1210
.3550	+ .3510	- .0250
.3610	+ .2880	- .1270
.3670	+ .2380	- .0790
.3920	+ .2940	- .1110
.4110	+ .3330	- .1140
.4290	+ .2820	- .1020
.4350	+ .3130	- .1350
.4420	+ .2940	- .1250
.4600	+ .3020	- .0270
.5510	+ .3320	- .1130
.5820	+ .3220	- .1240
.6340	+ .3330	- .1170
.6530	+ .2630	- .0670
.6590	+ .3070	- .0870
.6840	+ .3320	+ .0206
.7150	+ .3450	+ .0250
.7160	+ .2550	- .0380
.7170	+ .3130	+ .0510
.7530	+ .2660	+ .0030
.7840	+ .2750	- .0170
.7850	+ .2570	- .0350
.7930	+ .3150	- .0250
.8210	+ .3040	- .1170
.8520	+ .3260	- .0130
.8580	+ .3430	- .0170
.8770	+ .2830	- .1140
.8830	+ .3350	- .0550
.9020	+ .3430	- .0380
.9050	+ .3210	- .0030
.9110	+ .3010	+ .0330
.9210	+ .3150	- .0540
.9270	+ .3050	- .1000
.9460	+ .2850	- .1320
.9800	+ .3130	- .0651
.9830	+ .3790	- .0350

UM1 E (U filter) - Raw Data

Phase	Q	U
.0185	+ .3260	- .1000
.0308	+ .2370	- .0103
.0432	+ .2790	- .0670
.0556	+ .2580	- .0920
.0679	+ .3470	- .0103
.0864	+ .3610	- .0410
.1050	+ .3740	+ .0103
.1230	+ .1790	- .1080
.1296	+ .2580	- .1850
.1480	+ .3420	+ .0256
.1670	+ .2160	- .0360
.1850	+ .1890	+ .0103
.2040	+ .3260	- .1030
.2220	+ .2530	- .0718
.2470	+ .1950	- .0205
.2530	+ .1790	- .0050
.3120	+ .1740	- .0718
.3300	+ .1790	+ .1540
.3390	+ .1470	+ .0974
.3580	+ .1820	- .0513
.3900	+ .2500	- .1380
.4200	+ .2210	+ .0205
.4320	+ .2370	- .1180
.4570	+ .1580	+ .0670
.5090	+ .2260	+ .0000
.5310	+ .1710	+ .1230
.5580	+ .2740	+ .0154
.5990	+ .1630	+ .1490
.6050	+ .2760	- .1230
.6080	+ .3760	- .0870
.6110	+ .4680	- .1640
.6480	+ .1740	- .1540
.6850	+ .1370	+ .0000
.6990	+ .2630	+ .0205
.7040	+ .2110	- .0050
.7220	+ .3210	+ .0564
.7280	+ .3080	- .1130
.7530	+ .2240	- .1949
.7650	+ .3760	- .0720
.7680	+ .1950	- .1230
.7710	+ .2260	- .0718
.8020	+ .1790	- .0718
.8330	+ .1947	- .0974
.8580	+ .2470	- .0410
.8700	+ .4420	- .0564
.8830	+ .3890	- .1949
.8840	+ .3100	- .1280
.8890	+ .3310	+ .0000
.9130	+ .2130	- .0410
.9260	+ .2290	- .0205
.9320	+ .2950	- .1128
.9630	+ .3210	- .1589
.9940	+ .2130	- .1589

Phase	Q	U
.0000	+ .0068	+ .0263
.0050	+ .0098	+ .0302
.0051	+ .0127	+ .0000
.0097	+ .0215	+ .0117
.0098	+ .0078	+ .0263
.0340	+ .0254	+ .0156
.0630	+ .0283	+ .0000
.0780	+ .0000	+ .0058
.0870	+ .0980	+ .0215
.0995	+ .0527	- .0039
.1020	+ .0254	+ .0176
.1040	+ .0556	- .0117
.1070	+ .0342	- .0058
.1110	+ .0322	+ .0170
.1150	+ .0220	+ .0049
.1310	+ .0790	+ .0098
.1320	+ .0351	+ .0029
.1410	+ .0361	+ .0000
.1500	+ .0771	- .0039
.1750	+ .0634	+ .0000
.1890	+ .0395	+ .0078
.2040	+ .0800	+ .0166
.2090	+ .0381	+ .0000
.2140	+ .0770	+ .0000
.2230	+ .0498	+ .0039
.2280	+ .0741	+ .0039
.2290	+ .0663	+ .0000
.2520	+ .0615	+ .0000
.2720	+ .0507	- .0020
.2910	+ .0654	+ .0078
.2920	+ .0751	+ .0049
.3200	+ .0576	+ .0254
.3500	+ .0507	+ .0022
.3510	+ .0624	+ .0210
.3540	+ .0361	+ .0170
.3690	+ .0478	- .0030
.3690	+ .0644	+ .0330
.3790	+ .0302	- .0039
.3930	+ .0410	+ .0280
.3940	+ .0683	+ .0507
.4010	+ .0185	+ .0137
.4010	+ .0517	+ .0390
.4030	+ .0254	+ .0140
.4080	+ .0702	+ .0050
.4170	+ .0634	+ .0078
.4270	+ .0507	+ .0078
.4280	+ .0060	+ .0230
.4290	+ .0458	+ .0530
.4420	+ .0049	+ .0000
.4470	+ .0693	+ .0380
.4610	+ .0107	+ .0140
.4710	+ .0010	+ .0210
.4810	+ .0177	+ .0050
.5000	+ .0127	+ .0490

u Her - Raw Data

Phase	Q	U
.5150	+ .0517	+ .0190
.5160	+ .0273	+ .0170
.5190	+ .0263	+ .0210
.5290	+ .0332	- .0068
.5440	+ .0195	+ .0176
.5530	+ .0381	+ .0019
.5730	+ .0303	- .0244
.5740	+ .0000	+ .0058
.5830	+ .0146	- .0068
.6020	+ .0254	- .0078
.6310	+ .0400	- .0019
.6320	+ .0722	+ .0049
.6360	+ .0263	+ .0068
.6410	+ .0410	- .0068
.6500	+ .0507	+ .0039
.6600	+ .0712	- .0400
.6800	+ .0498	+ .0039
.7140	+ .0585	- .0068
.7150	+ .0576	- .0078
.7430	+ .0702	+ .0185
.7440	+ .0498	- .0293
.7480	+ .0517	+ .0156
.7520	+ .0615	+ .0215
.7720	+ .0654	+ .0165
.7770	+ .0478	- .0039
.8110	+ .0302	+ .0117
.8150	+ .0439	+ .0000
.8200	+ .0458	+ .0220
.8210	+ .0478	+ .0410
.8400	+ .0410	+ .0330
.8540	+ .0244	+ .0156
.8590	+ .0293	+ .0107
.8600	+ .0712	+ .0390
.8610	+ .0283	+ .0250
.8690	+ .0546	+ .0170
.8830	+ .0595	+ .0410
.8830	+ .0880	+ .0220
.8980	+ .0137	+ .0170
.9080	+ .0205	+ .0410
.9090	+ .0108	+ .0049
.9120	+ .0166	+ .0176
.9170	+ .0235	+ .0566
.9220	+ .0205	+ .0176
.9320	+ .0322	- .0097
.9470	+ .0351	+ .0330
.9560	+ .0263	+ .0097
.9850	+ .0127	+ .0166

Polarization Observations of U Sagittae in B Filter

JD 2,440,000+	-Q(%)	-U(%)	ϕ	JD 2,440,000 +	-Q(%)	-U(%)	ϕ
2902.88	.212	.075	.595	3014.72	.207	.109	.679
2920.81	.198	.090	.900	3014.86	.196	.110	~~.024~~
2920.83	.173	.136	.907	3016.71	.203	.093	.268
2921.79	.153	.154	.190	3018.80	.171	.052	.885
2940.86	.210	.151	.831	3019.70	.206	.070	.153
2946.89	.175	.083	.614	3019.75	.231	.053	.167
2947.92	.199	.121	.920	3019.80	.169	.089	.182
2948.83	.198	.092	.188	3020.74	.173	.077	.459
2949.77	.160	.127	.467	3020.81	.161	.085	.482
2951.75	.231	.110	.053	3021.73	.211	.135	.753
2951.94	.155	.125	.108	3021.84	.217	.102	.784
2952.78	.155	.087	.356	3022.69	.120	.112	.037
2953.79	.218	.102	.654	3022.72	.167	.104	.047
2953.90	.241	.109	.689	3024.68	.171	.142	.626
2954.82	.179	.169	.961	3025.81	.167	.043	.960
2955.82	.237	.079	.256	3026.69	.223	.066	.220
2956.78	.183	.039	.541	3026.78	.212	.075	.246
2960.80	.216	.108	.729	3029.72	.188	.073	.116
2961.81	.217	.211	.028	3029.87	.167	.073	.160
2962.82	.189	.138	.326	3030.72	.167	.112	.411
2964.80	.200	.118	.912	3040.69	.165	.096	.411
2965.78	.173	.139	.201	3040.78	.136	.097	.390
2967.85	.214	.083	.815	3044.68	.186	.082	.541
2968.80	.242	.119	.034	3044.69	.236	.126	.545
2968.93	.147	.121	.135	3044.77	.193	.155	.566
2969.78	.162	.070	.385	3047.68	.162	.143	.428
2969.93	.152	.074	.432	3048.65	.232	.104	.716
2972.85	.210	.119	.292	3050.80	.228	.093	.353
2973.80	.233	.100	.576	3051.65	.208	.124	.601
2974.75	.211	.116	.856	3051.66	.205	.084	.607
2982.73	.209	.133	.217	3051.72	.196	.104	.624
2986.91	.183	.064	.454	3052.79	.179	.073	.939
3001.79	.256	.123	.854	3063.65	~~.179~~	~~.073~~	~~.939~~
3011.75	.227	.118	.799	3063.73	.194	.161	.177
3011.92	.190	.130	.851	3066.67	.137	.172	~~.046~~
3012.76	.177	.091	.098	3066.74	.164	.116	.067
3012.84	.214	.118	.122	3067.73	.206	.089	.359

OK ?

Polarization Observations of V 444 Cygni in B Filter

$\phi = \phi + 0.097$.

JD 2,440,000 +	Q(%)	U(%)	ϕ	JD 2,440,000 +	Q(%)	U(%)	ϕ
2946.92	.566	-.053	.307	3012.90	.539	-.265	.972
2947.82	.414	-.215	.520	3014.76	.495	-.300	.411
2950.83	.480	-.005	.256	3016.75	.504	-.147	.884
2951.85	.349	.020	.478	3020.78	.584	-.183	.841
2952.83	.355	.024	.711	3020.88	.603	-.311	.864
2953.82	.426	-.289	.945	3021.80	.076	-.010	.084
2953.93	.510	-.460	.971	3022.91	.541	.073	.346
2954.89	.327	.228	.175	3024.74	.639	-.081	.779
2956.82	.315	-.141	.658	3024.88	.572	-.094	.694
2957.79	.573	-.299	.888	3025.70	.346	.053	.008
2957.94	.554	-.319	.922	3025.84	.322	.008	.043
2960.85	.559	.168	.615	3039.74	.484	-.354	.342
2961.81	.494	-.315	.853	3040.72	.274	-.089	.575
2962.77	.262	-.115	.070	3040.89	.100	.051	.614
2962.92	.254	-.053	.101	3043.84	.628	-.169	.284
2964.88	.288	-.015	.550	3044.89	.329	-.165	.526
2965.79	.527	-.110	.767	3040.72	.473	-.124	.999
2968.79	.559	-.208	.403	3046.70	.284	-.260	.038
2969.81	.496	-.101	.717	3051.83	.498	-.026	.213
2970.83	.250	-.187	.984	3064.63	.447	-.007	.250
2972.79	.485	-.305	.449	3065.63	.305	-.155	.488
2980.92	.772	-.206	.379	3065.73	.361	-.091	.511
2988.96	.472	-.118	.286	3077.89	.480	-.017	.238
3001.93	.601	-.225	.366	3078.74	.447	-.134	.480
3011.80	.368	.036	.710	3081.69	.365	.070	.179
3012.78	.384	-.236	.942	3081.75	.439	-.014	.193

MD50896 - Raw data - B J/A 79.

ϕ	a	u
0.0	0.478	−0.433
0.012	0.504	−0.497
0.02	0.515	−0.501
0.027	0.508	−0.501
0.032	0.516	−0.488
0.661	0.325	−0.46
0.673	0.331	−0.496
0.889	0.348	−0.266
0.909	0.305	−0.283
0.938	0.37	−0.301
0.167	0.39	−0.496
0.195	0.325	−0.445
0.298	0.326	−0.309
0.309	0.369	−0.268
0.567	0.258	−0.529
0.232	0.261	−0.418
0.255	0.29	−0.4
0.444	0.382	−0.332

cent.

ϕ	α	u
0·67	0·127	−0·391
0·230	0·317	−0·359
0·394	0·369	−0·303
0·213	0·237	−0·43
0·483	0·392	−0·353
0·319	0·252	−0·267
0·588	0·153	−0·415
0·917	0·224	−0·432
0·508	0·401	−0·387
0·775	0·106	−0·421

HD50896 - Raw data - B - 01079

ϕ	a	u
0.043	0.33	-0.182
0.310	0.379	-0.336
0.574	0.321	-0.439
0.152	0.415	-0.225
0.922	0.66	-0.316
0.186	0.456	-0.103
0.22	0.496	-0.193
0.45	0.399	-0.88
0.486	0.327	-0.556
0.707	0.112	-0.209
0.75	0.227	-0.164
0.982	0.564	-0.715
0.011	0.513	-0.259
0.266	0.456	-0.294
0.538	0.737	-0.454
0.315	0.48	-0.286
0.572	0.323	-0.443
0.113	0.42	-0.161
0.371	0.526	-0.417
0.632	0.198	-0.329

HD50896*****U FILTER****J/A79***18****

α	u	ϕ
.418	-.509	.1082
.143	-.573	.1773
-.011	-.522	.1911
.224	-.498	.2624
.083	-.442	.2769
.272	-.616	.2891
-.064	-.522	.3694
.163	-.491	.5169
.395	-.298	.5519
.549	-.526	.6154
.297	-.515	.7979
.149	-.405	.8145
.191	-.421	.8313
.229	-.325	.8358
.323	-.291	.9102
.34	-.284	.9163
.121	-.279	.9182
.409	-.261	.9968

MD50896 - Raw data - U - 01079

q	a	u
0.153	0.776	-0.251
0.925	0.728	-0.308
0.453	0.366	-0.675
0.484	0.295	-0.68
0.71	0.011	-0.127
0.748	0.163	-0.109
0.985	0.59	-0.324
0.013	0.495	-0.287
0.263	0.477	-0.292
0.541	0.298	-0.542
0.317	0.509	-0.273
0.57	0.235	-0.484
0.111	0.364	-0.107
0.373	0.561	-0.505
0.631	0.113	-0.31

MDS0896 - Raw data G J/A 79.

a	u	φ
.412	-.349	2.7e-03
.377	-.333	.0824
.438	-.373	.11
.219	-.484	.1796
.095	-.472	.1892
.317	-.496	.2749
.128	-.398	.2793
.118	-.382	.3734
.21	-.48	.5156
.396	-.302	.5546
.56	-.508	.6207
.54	-.54	.6346
.365	-.518	.7999
.223	-.4	.8121
.325	-.301	.9089
.237	-.231	.9219

G O/D 79.

a	u	φ
.506	-.279	.0154
.387	-.136	.1148
.396	-.198	.1555
.455	-.287	.2684
.461	-.29	.3189
.56	-.497	.3747
.324	-.484	.5432
.318	-.481	.5751
.172	-.332	.6375
.134	-.157	.7119
.247	-.106	.7529
.697	-.321	.9312
.571	-.311	.9875

References

Abramowitz,M. and Stegun,I.A. (1972) Mathematical Handbook,Dover
Abt,H.A. (1961) Ap.J. Suppl. 6 37
Abt,H.A.,Hintzen,P. and Levy,S.G. (1977) Ap.J. 128 576
Abyankhar,K.D. (1959) Ap.J. Suppl. 4 157
Abyankhar,K.D. and Spinrad,H. (1958) P.A.S.P. 76 411
Appenzeller,I. (1965) Ap.J. 141 1390
Appenzeller,I. and Hiltner,WA (1967) Ap.J. 149 353

Bailey,M.J. (1971) J. Geophs. Res. 76 7807
Bailey,M.J. (1972) Astron.J. 77 177
Batten,A.H. (1967) P.D.A.O. 13. 162
Batten,A.H. (1973) Binary and Multiple Stars,Permagon
Batten,A.H. (1975) Spectro. Bin. Cat. P.D.A.O.
Batten,A.H.,Baldwin,B.W. and Scarfe,C.D. (1974) IAU Circ. 2701
Beardsley,W.R. (1965) A.J. 70 319
Bethe,H.A. and Johnson,M.B. (1975) Ap.J. 199 741
Bolton,C.T. (1972) Nat.Phys. Sci. 240 124
Bolton,C.T. (1975) Ap.J. 200 269
Boyarchuk,A,A, (1960) Sov. Astr. 3.748
Brown,J.C.,McLean,I.S. and Emslie,A.G. (1978) A.A. 57 141
Brown,J.C. and McLean,I.S. (1977) A.A. 57 141
Budding,E. (1981) preprint
Buerger,R.F. and Collins,G.W. (III) (1970) Ap.J. 161 1025

Cassinelli,J.P. and Haisch,B.M. (1974) Ap.J. 188 101
Chandrasekhar,S. (1946) M.N.R.A.S. 103 361
Cherepashchuk,A.M. (1975) Sov. Astr. 19 47

Cherepashchuk,A.M.,Lyutyi,V.M. and Sunyaev,R.A. (1973) A.Z. 50 3
Chojnacki,W. and Serkowski,K. (1965) Acta Astrom. 16 127
Clarke,D. and McLean I.S. (1975) M.N.R.A.S. 172 585
Collins,G.W.(III) and Buerger,R.F. (1974) Planets ans Stars.. Gerhel
Coyne,G.V. (1970a) Ric.Astr.Spec.Vat. 8 87
Coyne,G.V. (1970b) AP. J. 161 1011
Coyne,G.V. (1972) Ric.Astr.Spec.Vat. 8 311
Coyne,G.V. (1974) Ric.Astr.Spec.Vat. 8 475

Dadaev (1954) Izvestia Pulkovo 19 31
Daniel,J.Y. (1978) B.A. A.A. 67 345
Daniel,J.Y. (1980a) A.A. 86 198
Daniel,J.Y. (1980b) preprint
Davidson, Ostriker (1973) Ap.J. 179 585
Dibai,E.A.,Shakovskoi,N.M. (1967) Soz.Astr. 10 1059
Dolan,J.F. (1972) B.A.A.S. 4 338
Dolan,J.F. (1974) B.A.A.S. 6 325
Dolan,J.F. (1977) A.S.S. 52 201
Dombrovski,V.A. (1966) Phd. Thesis (Leningrad)

Fehenbach,Ch. and Prevet,L. (1961) J.O. 44 83
Fehrenbach,Ch. (1948) Ann d'Ap 11 35

Gehrels,T. (1972) Ap.J. 173 L23
Gnedin,Y.N., Silantev,N.A. and Shibanov,Y.A. (1976) Sov.Astr. 20 530
Gobatskii (1967) Astrofiz. 3 245
Gradshteyn,I.S.and Ryzhik,I.M. (1963) Tables of Integrals,A.P.
Grey,D.F. and Desikachary,K. (1973) Ap.J. 181 523
Groote,D. and Hunger,K. (1977) Astr.Ap. 56 129
Guinan,E.F.,McCook,G.P.,Bachman,P.J.,Bistline,W.G.(1975)A.J. 81 57

Korsch,D. and Walter,K. (1969) Astr. Nachr. 291 231
Kraft,R. (1958) Ap.J. 130 99
Kruzewski,A. (1972) Acta Astron. 22 405

Lafler,J. and Kinman,T.D. (1965) Ap.J. Suppl. 11 216
Lecar,M.,Wheeler,J.C. and McKee,C.F. (1976) Ap.J. 205 556
Lester,D.F. (1974) P.A.S.P. 87 177
Lester,D.F. (1976) Ap.J. 205 855
Lester.D.F.,Nolt,I.G.,Radostitz,J.V. (1973) Nature Phys. Sci. 241 125
Lester,D.F.,Wood,N.E.,Kemp,J.C.,Nolt,I.G. (1979) Ap.J. 200 95
Link,F. (1969) Eclipse phenomena in Astr.,Springer
Long,K. (1974) B.A.A.S. 6 462
Longhurst,R.S. (1973) Geometrical and Physical Optics , Longman
Lyot,B. (1934) Comptes Rendus 198 249

Maeder,A. (1973) A.A. 26 215
Maestone,J.A. and Wright,J.A.(1960) Ap.J. 131 119
Martin,P.G.,Illing,R,Angel,JRP.(1972) M.N.R.A.S. 159 591
Mazeh,T. and Shaham,J. (1977) Nature 270 229
McLean,I.S. (1977) A.A. 55 347
Middelton,D. (1966) Statistical Communication Theory N.Y. MacGraw-Hill
Milgrom.M. (1977) A.A. 26 215
Milgrom,M. and Shaham,J. (1977) Ap.J.(Lett) 213 L17
Milgrom,M.(1979) A.A. 76 338

Nagirner,D.I. (1962) Trudy Leningrad Obs. 19 79
Nekrasova,S.V. POlosukhina N.S.(1960) Perevenge Zveydy 13 31
Nolt,I.R.,Kemp,J.C.,Rudy,R.J.,Southwick,R.G.(1975) Ap.J.(LETT) 99 L27

Hall,J.S. (1949) Science 109 166
Hall,J.S. and Walker,K. (1974) A.A. 31 263
Hansen,H.K. and McNamara,D.H. (1959) Ap.J. 130 791
Harper (1919) P.D.A.O. 2 167
Harper (1922) P.D.A.O. 1 157
Haynes,D. (1975) Ap.J.(Lett) 197 L55
Hegyi,D.J. (1977) Ap.J. 217 244
Heisenberg (1925) Z. S. f. Phys. 31 617
Hemmerle,W.J. (1967) Statistical computations,Waltham-Blaisdall
Hiltner,W.A. (1947) Ap.J. 106 231
Hiltner,W.A. (1949) Science 105 166
Hiltner,W.A. and Mook,D.E. (1965) Ap.J.(Lett) 143 1009
Huang,S-S (1963) Ap.J. 138 347
Hutchings,J.B. (1974) Ap.J.(Lett) 193 L61
Hutchings,J.B. (1977) Ap.J. 217 537
Hutchings,J.B. (1978) Ap.J. 226 264
Holt,S.S.,Kaluzienski,L.J.,Boldt,E.A. and Serlrmitz,P.J. (1974) Nat. 261 214

Inglis, Teller (1939) ApJ 90 439

Jackson,R.B. (1975) M.N.R.A.S. 172 483
Jansen,E. (1946) Ap.J. 103 380
Johnson,H.L. and Morgan,W.W.(1951) Ap.J. 114 522

Katz,J. (1973) Nat. Phys. Sci. 246 87
Kemp,J.C. (1972) Ap.J. 130 99
Kemp,J.C. (1980) A.A. 91 109
Kemp,J.C.,Rudy,R.J.,(1975) P.A.S.P. 87 301
Kemp,J.C.,Herman,L.C.,Barbour,M.S. (1976) A.J. 83 962
Kemp,J.C.,Herman,L.C. (1977) Ap.J. 218 770
Kemp,J.C.,Barbour,M.S.,Herman,L.C. and Rudy,R.J. (1978) Ap.J. 220 L123
Kemp,J.C.,Barbour,M.S.,Parker,T.E. and Herman,L.C. (1979)Apj.228 L1
Korhonan,T. and Piirola,V. (1969) Astr.Nachr. 291 231

Nolt,I.R.,Walker,E.N.(1977) cf Kemp et al (1979)
Novikov,D.,Thorne,K.S. (1972) Black Holes, Gordon Breech,C dd Witt N4.

Oda (1977) Sp.Sci.Rev. 20 755
Ohman,Y. (1929) M.N.R.A.S. 89 479
Ohman,Y. (1934) Nature 134 534
Ohman,Y. (1935) Mellande 12 Stockholm Obs.
Oppenheim,Vlokoff. (1949) Phys.Rev. 55 374

Paczynski (1968) Acta Astrón20 521
Pandharipande,V.R.,pines,D., and Smith,R.A.(1970)Ap.J. 208 550
Pearce (1932) P.D.A.O. 6 60
Peters,G.J. (1980) Close Binaries IAU Symp. 88 287
Pettersen,J.A.(1975) Ap.J.(Lett) 201 L61
Pfeiffer,R.J.(1979) Ap.J. 232 181
Pfeiffer,R.J.,Koch,R.H. (1973) IAU INF. BULL. 780
Pfeiffer,R.J.,Koch,R.H. (1973) B.A.A.S. 5 345
Pfeiffer,R.J.,Koch,R.H. (1977) P.A.S.P. 89 147
Piirola,V. (1973) A.A. 27 387
Piirola,V. (1975a) Ann. Acad. Sci. Fennicae AV1 418
Piirola,V. (1975b) I.B.V.S. 1061
Piirola,V. (1980a) IAU Symp.88 Close Binaries Reidal
Piirola,V. (1980b) in press
Piirola,V. (1980c) inpress
Plavec,M. (1974) IAU Circ. 2707
Popper,D.(1942) Ap.J. 97 394
Predergast,K.H.,and Burbidge,G.R.(1968) Ap.J. (Lett) 151 L83
Predergast,K.H.,Taam,R.E. (1974) Ap.J. 189 125
Pringle,J.E. (1973) Nat.Phys. Sci. 243 90

Rees,M.J. (1975) M.N.R.A.S. 171 457

Rees,M.J. (1972) A.A. 21 1

Rhomb,C.G. and Fix,J.D. (1975) B.A.A.S. 7 267

Rothschild,R.E., Boldt,E.A.,Holt,S.S.,Seleomtsos,P.J.(1972)ApJ.189 13

Roy,A.E. (1978) Orbital Mechanics

Rudy,R.J. (1977) Phd. Thesis Uni. Oregon.

Rudy,R.J. and Kemp,J.C. (1977) Ap.J. 216 767

Rudy,R.J. and Kemp,J.C. (1978) Ap.J. 221 200

Rudy,R.J. and Herman,L.C. (1978) P.A.S.P. 90 1103

Rucinski,S.M. (1966) Acta Astron. 16 127

Sahade,J. Struve,O. (1957) Ap.J. 126 87

Sanford (1939) Ap.J. 89 233

Serkowski,K. (1965) Ap.J. 142 793

Serkowski,K. (1970) Ap.J. 126 87

Shakovskoi,N.M. (1962) Sov.Astron. 6 587

Shakovskoi,N.M. (1965) Sov.Astron. 8 833

Shakovskoi,N.M. and Dimov,N.A. (1967) Izv. Krymsk Astrofiz. 27 291

Shulov,O.S. (1962) Trudy Leningrad Obs. 20 530

Shulov,O.S. (1966) Trudy Leningrad Obs. 24 38

Simmons,J.F.L.,Aspin,C. and Brown,J.C. (1980) A.A. 91 97

Soderhjelm,S. (1980) A.A. 89 100

Stellingwerf I.F. (1978) ApJ 222 476.

Struve,O. (1941) Ap.J. 93 104

Struve,O. (1949) M.N.R.A.S. 109 487

Struve,O. (1958) P.A.S.P. 70 5

Struve,O. and Huang,S-S (1957) Occ. Notes R.A.S. 3 161

Struve,O., Shade,J. and Huang,S-S (1958) Ap.J. 127 148

Struve,O. and Wade,M.J.S. (1960) P.A.S.P. 72 403
Swedlund,J.B.,Kemp,J.C.,Wolstencroft,R.D. Ap.J.(Lett) 193 L11

Thomas,H-C (1977) Ann. Rev. Astron. Astr. 15 127

Udick,P. (1912) Allegeny Obs. 2 191
Underhill,A.B. (1957) P.D.A.O. 10 19

van den Heuval E.P.J., de Loore C. (1977) A.A. Suppl. 30 195
van der Hulst P.J. (1957) Scattering from small particles A.P.
van Paradijs,J. (1980) A.A. 87 210
van Paradijs,J. and Zuiderwijk,E.J., Takens,R.J.,Hammerschlag-
Hensberge,G. and de Loore C. (1977) A.A. 30 195
Vinter and Hansen (1940) Lick Obs,Pub. 19 89

Walker,E.N. (1972) M.N.R.A.S. 160 9P
Walker,E.N.,Nolt,I.R. (1977) cf. Kemp et al (1979)
Walker.E.N.,and Quintanilla,R.A. (1978) M.N.R.A.S. 182 315
Walker,E.N. ans Watson,M.G. and Holt.S.S. (1979) Nature 270 230
Walborn,N.R. (1973) Ap.J. (Lett) 179 L123
Walter,K. (1974) A.A. 42 135
Whelan,J.A.J. and Worden S.P. (1973) Ap.J. 183 133
Wilson,R.E. and Devinney,E.J. (1971) Ap.J. 166 605
Wood,R.W.,Ellet,Hanle,Keussler (1928) Struktur der Materie P. Pringsheim
Wood,D.B. and Forbes,J.E. (1963) A.J. 68 257
Woolf,N.J. (1965) Ap.J. P.D.A.O. 15 131
Woolf,C.L., Kondo,Y. (1978) Ap.J. 219 605

Young,R.K. (1919) P.D.A.O. 11 131

Zahn (1975) A.A. 41 329
Zellner,B.H. and Serkowski,K. (1972) P.A.S.P. 84 619